

UNCLASSIFIED

AD NUMBER

AD878212

LIMITATION CHANGES

TO:

Approved for public release; distribution is unlimited.

FROM:

Distribution authorized to U.S. Gov't. agencies and their contractors; Critical Technology; APR 1970. Other requests shall be referred to Air Force Rocket Propulsion Laboratory, DPRR/Stinfo, Edwards AFB, CA 93523. This document contains export-controlled technical data.

AUTHORITY

afrpl ltr, 29 sep 1971

THIS PAGE IS UNCLASSIFIED

0210

F20047

71-0210

AFRPL-TR-70-1

POPPET AND SEAT DESIGN CRITERIA FOR
CONTAMINANT-PARTICLE RESISTANCE

G. F. Tellier
J. W. Lewellen

Rocketdyne Division
North American Rockwell Corporation
Canoga Park, California

J F I A
JAN 4 1971

TECHNICAL REPORT NO. AFRPL-TR-70-1

RECEIVED

April 1970

Approved for public release
—Distribution unlimited.
Auth.: AFRPL ltr 29 Sep 71.
Ref: TAB 72-15.

~~only and each time initial~~
~~be made only with prior~~
~~California 00520~~

Distribution Statement A:
Approved for public release;
distribution is unlimited.

AIR FORCE ROCKET PROPULSION LABORATORY
DIRECTORATE OF LABORATORIES
AIR FORCE SYSTEMS COMMAND
EDWARDS, CALIFORNIA

1971-0210

71-0210

AD 878 212

F20047

NOTICES

When U.S. Government drawings, specifications, or other data are used for any purpose other than a definitely related Government procurement operation, the Government thereby incurs no responsibility nor any obligation whatsoever, and the fact that the Government may have formulated, furnished, or in any way supplied the said drawings, specifications, or other data, is not to be regarded by implication or otherwise, or in any manner licensing the holder or any other person or corporation, or conveying any rights or permission to manufacture, use, or sell any patented invention that may in any way be related thereto.

If this copy is not needed, return to AFRPL (RPRPD)
Edwards, California 93523.

~~This document is subject to special export controls and each transmittal to foreign governments or foreign nationals may be made only with prior approval of AFRPL (RPRPD/STINFO), Edwards, California 93523.~~

AFRPL-TR-70-1

POPPET AND SEAT DESIGN CRITERIA FOR
CONTAMINANT-PARTICLE RESISTANCE

G. F. Tellier
J. W. Lewellen

Approved for public release
—Distribution unlimited.
Auth.: AFRPL ltr 29 Sep 71.
Ref: TAB 72-15.

~~code and each transmittal~~
~~made only with prior~~
~~request 0-7523.~~

FOREWORD

This final report was prepared in compliance with Contract F04611-67-C-0085, Project No. 3058, Task 305802, covering a period of performance from April 1967 through January 1970. The initial survey phase was separately reported as "Survey of Contamination in Rocket Propulsion Fluid Systems," AFRPL-TR-67-290, published November 1967 and, therefore, is not included herein except in summary and reference. Copies of the Phase I report may be obtained from Defense Documentation Center (DDC), Cameron Station, Alexandria, Virginia, 22314. The DD accession number is AD829701.

The effort reported herein represents a continuation, with contamination as a primary variable, of previous valve technology investigations conducted under Contract AF04(611)-9712, Project No. 6753, Task No. 675304. Principal Rocketdyne investigators were G. F. Tellier, Principal Engineer, and J. W. Lewellen. Other contributors were H. Standke (dynamic system design), T. Hull (shear seal analysis), and E. Bramblett (particle entrapment probability analysis). Program managers were W. A. Anderson, succeeded by E. B. Monteath. The report was prepared by Messrs. Tellier and Lewellen.

The program was sponsored and administered by the Air Force Rocket Propulsion Laboratory, Edwards Air Force Base, with J. Hartley as Project Engineer, preceded by J. Lawrence, Project Engineer.

Specialized fabrication and preparation of test models and fixtures were contracted with L. A. Gauge Company, Incorporated, Sun Valley, California, whose cooperation and interest is gratefully acknowledged.

Many of the items compared in this report were commercial items that were not developed or manufactured to meet Government specifications, to withstand the tests to which they were subjected, or to operate as applied during this study. Any failure to meet the objectives of this study is no reflection of any of the commercial items discussed herein or on any manufacturer.

This report was given Rocketdyne Report No. R-8126.

This technical report has been reviewed and approved.

J. Hartley
Project Engineer

Begin

one described.

ABSTRACT

A (u)

~~This final report describes~~ Analytical and experimental investigations to establish design criteria for reliable metal-to-metal poppet and seat sealing in contaminated fluid environments. Static evaluation of standard flat 440C models (0.470-inch seat diameter, 0.03-inch land) with placed hard (R_c 62-67) and soft (R_c 17-21) spherical metal particles defined envelopment closure loads and stress-leakage change characteristics. The control condition was nominally 0.01-scim nitrogen leakage at 1000 psig and 40-pound seat load. Envelopment loads, defined by leakage increase less than 10 times control, were determined to be nearly proportional to the particle diameter squared. The 30-micron diameter constituted an approximate upper size limit for the 0.03-inch land, with about 46 pounds required to envelope one to three equally spaced particles. Larger particles created a radial channel leak path necessitating substantial load increase to effect closure. Dynamic tests of four closure configurations in a recirculation liquid system containing a precisely controlled concentration of hard spherical metal particles provided correlation of impact frequency predictions based on a binomial analysis of concentration, cycles, and theoretical seat sampling volume. "Clean" fluids (<1000 particles/liter) produced substantial impacts in 1000 cycles. Very hard closures (440C and tungsten carbide) ejected impacted particles with minimal residual damage, but failure producing entrapments must be expected with normal unfiltered systems. A hard poppet on soft seat combination was capable of sealing with larger particles entrapped. Developed criteria were utilized in design of four seating configurations intended to provide improved low load sealing (shear seal), particle avoidance capability (self-cleaning model), and particle entrapment tolerance (plain flat and grooved copper seat with 440C poppet). The narrow land (0.003 inch) shear seal provided very low leakage (10^{-4} scim gaseous nitrogen) at loads less than 40 pounds but was susceptible to particle damage. The particle avoidance concept was investigated experimentally and is a potentially fruitful approach to particle resistance. The flat groove copper seat was most capable of sustaining numerous particle impacts with minimal leakage increase at low loading. These results established hitherto unknown fundamental data but, also, emphasized the need for additional effort in gathering parametric data on particle effects parameters (size, hardness, land width) and impact frequency influences for the more promising closure designs.

End awf

1890

1890

1890

1890

CONTENTS

Foreword	ii
Abstract	iii
Glossary	xv
<u>Section I--Introduction</u>	1
<u>Section II--Analysis</u>	3
Valve Seating Geometry	3
Particle Envelopment	5
Leakage Flow	9
Particles in Fluid Systems	13
Particle Entrapment	21
<u>Section III--Phase II Test Models</u>	25
Description	25
Model Preparation	34
Model Inspection	34
<u>Section IV--Phase II Static Tests</u>	37
General Approach	37
Data Presentation	39
Model Tests	42
Particle and Surface Deformation	53
Data Analysis	64
Observations	72
<u>Section V--Phase II Dynamic Tests</u>	75
General Approach	75
Data Presentation	78
Flat 440C Test Models	80
Spherical 440C Test Model	100
Shear Seal Test Models	104
Flat Carbide Test Model	109
Observations	112
<u>Section VI--Phase III Demonstration--Concepts and Model Designs</u>	117
Shear Seal Model Design	119
Self-Cleaning Model Design	122
Flat Copper Model Design	124
Flat Grooved Copper Seat Design	125
<u>Section VII--Phase III Model Tests</u>	133
General Approach	133
Data Presentation	133
Shear Seal Test Models	134
Self-Cleaning Test Models	141
Flat Copper Test Models	149
Flat-Grooved Copper Test Models	161
Model Correlation	187
<u>Section VIII--Conclusions</u>	191
Static Particle Envelopment	191
Dynamic Closure Effects	192
Closure Design	194

<u>Section IX--Recommendations for Future Effort</u>	197
Static Test	198
Dynamic Test	198
Closure Design	198
<u>Appendix A</u>	
Particle Entrapment Probability	A-1
<u>Appendix B</u>	
Shear Seal Design Analysis	B-1
<u>Appendix C</u>	
Static Test Fixture	C-1
<u>Appendix D</u>	
Leakage Measurement	D-1
<u>Appendix E</u>	
Static Test System and Model Test Procedures	E-1
<u>Appendix F</u>	
Dynamic Test Fixture	F-1
<u>Appendix G</u>	
Dynamic Test System and Model Test Procedures	G-1
<u>Appendix H</u>	
Helical Vane Tests	H-1
<u>Appendix I</u>	
Flat-Grooved Copper Seat Fabrication and Inspection	I-1
<u>Appendix J</u>	
References	J-1
<u>Appendix K</u>	
Distribution List	K-1

ILLUSTRATIONS

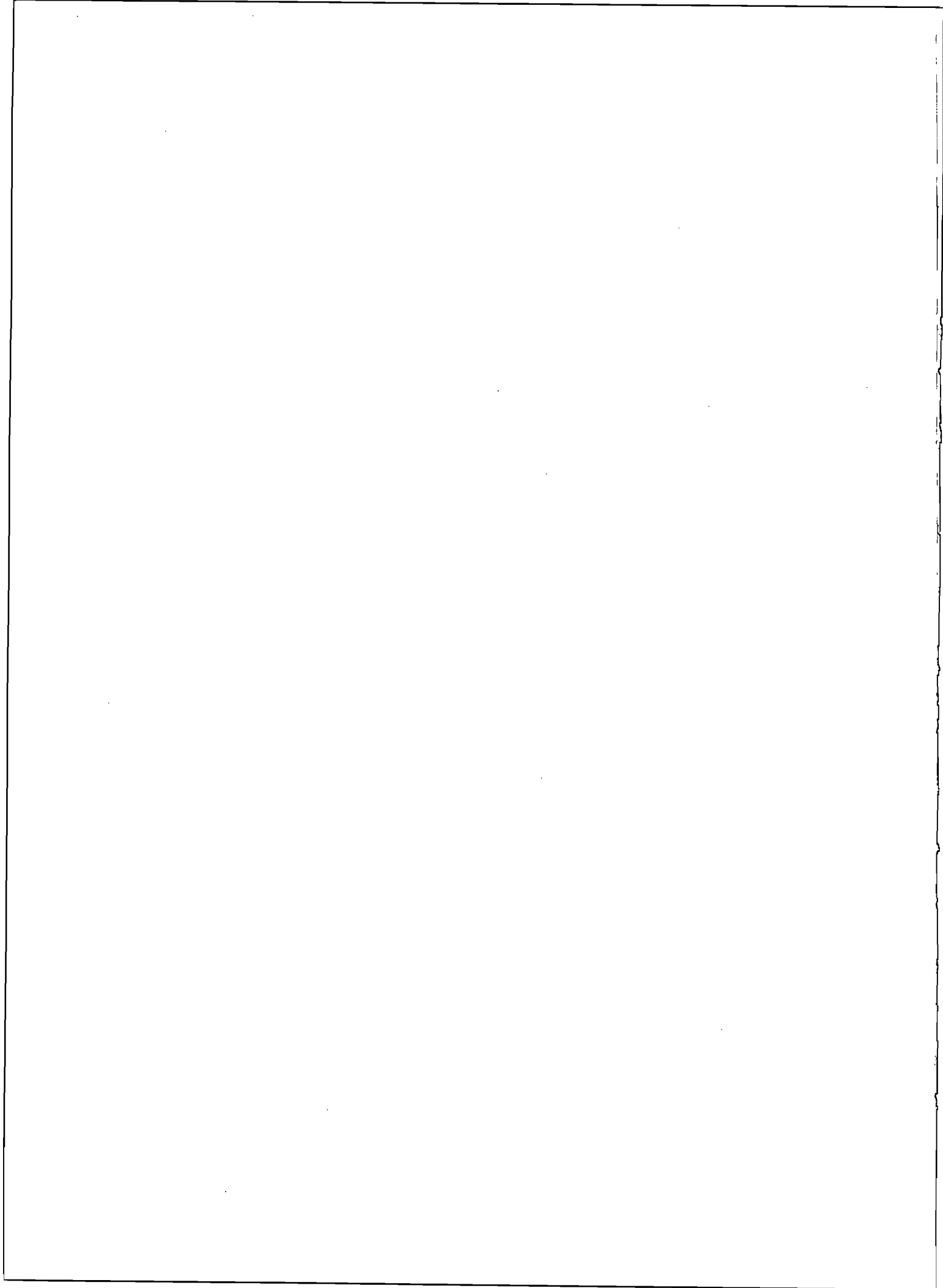
II-1.	Flat, Conical, and Spherical Seating Equations	4
II-2.	Particle Envelopment Model	6
II-3.	Theoretical Seat Leakage, Part 1	10
II-4.	Theoretical Seat Leakage, Part 2	11
II-5.	Theoretical Seat Leakage, Part 3	12
II-6.	Particle Dispersion	17
II-7.	Particle Count Limits for Space Engines per Rocketdyne Specification RA0615-003	18 18
II-8.	Contamination Size Distribution	20
II-9.	Effective Particle Entrapment Land Widths	23
III-1.	Flat Model Poppet	26
III-2.	0.5-Inch Flat Model Seat	27
III-3.	Spherical Model Assembly	29
III-4.	Spherical Poppet Retainer	30
III-5.	Spherical Seat	31
III-6.	Leak Volume Reducing Ring	32
III-7.	Shear Seal Model	33
III-8.	Leitz Interference Microscope With Conical Poppet on Leveling Table	35 35
IV-1.	Stress-Leakage Data for Static Test Model 102, Tests 1, 2, and 3	43 43
IV-2.	Stress-Leakage Data for Static Test Model 103, Tests 1 and 2	44 44
IV-3.	Stress-Leakage Data for Static Test Model 106, Tests 1 and 2	46 46
IV-4.	Stress-Leakage Data for Static Test Model 108, Tests 1, 2, and 3	47 47
IV-5.	Stress-Leakage Data for Static Test Model 112, Tests 1, 2, and 3	48 48
IV-6.	Stress-Leakage Data for Static Test Model 112, Tests 7, 8, 9, and 10	49 49
IV-7.	Stress-Leakage Data for Static Test Model 118, Tests 1 and 2	51 51
IV-8.	Stress-Leakage Data for Static Test Model 119, Tests 1 Through 7	52 52
IV-9.	Stress-Leakage Data for Static Test Model 123, Tests 1 and 2	54 54
IV-10.	Stress-Leakage Data for Static Test Model 124, Tests 1 and 2	55 55
IV-11.	Stress-Leakage Data for Static Test Model 125, Tests 1 Through 5	56 56
IV-12.	Small Glass Handling Probe and Typical Particles	58
IV-13.	Large Glass Probe and Deformed, Soft 50-Micron Particle	58
IV-14.	Model 119; S15 Particle Embedded in Poppet Surface	60
IV-15.	Model 123; Deformed H15 Particle After Removal From Poppet	60
IV-16.	Model 119; S60 Particle Embedded in Poppet Surface	60
IV-17.	Model 119; S60 Particle of Fig. IV-16 and Mating Poppet Depression	60 60

IV-18.	Model 112; Deformed S60 Particle	61
IV-19.	Model 125; Deformed H60 Particle and Mating Depression	61
IV-20.	Model 108; S30 Particle Embedded in Seat	61
IV-21.	Model 108; Seat Depression From S30 Particle of Fig. IV-20	61
IV-22.	Model 108; Poppet Depression From S30 Particle of Fig. IV-20	62
IV-23.	Model 125; H30 Particle Embedded in Seat	62
IV-24.	Model 125; Seat Depression From H30 Particle of Fig. IV-23	62
IV-25.	Model 125; Poppet Depression From H30 Particle of Fig. IV-23	62
IV-26.	Model 112; Poppet Depression From S15 Particle	63
IV-27.	Model 108; Seat Depression From S30 Particle	63
IV-28.	Model 112; Poppet and Embedded S60 Particle	63
IV-29.	Model 125; Seat With Embedded and Fractured H60 Particle	63
IV-30.	Stress-Leakage Data for Static Test Models 112, 118, 119, 123, and 124 With 15-Micron Particles	66
IV-31.	Stress-Leakage Data for Static Test Models 103, 106, 108, 112, 119, and 125 With 30-Micron Particles	67
IV-32.	Stress-Leakage Data for Static Test Models 112, 119, and 125 With 60-Micron Particles	68
V-1.	Stress-Leakage Data for Dynamic Test Model 116, Tests 1, 2, and 3	82
V-2.	Model 116 Load and Displacement Traces	81
V-3.	Model 116 Poppet Showing Damage From HA Particle	84
V-4.	Model 116 Seat Showing Damage From HA Particle	84
V-5.	Stress-Leakage Data for Dynamic Test Model 120, Tests 1, 2, and 3	86
V-6.	Model 120 Poppet Showing Double HA Particle Hits and Fragment Hit Damage	87
V-7.	Model 120 Seat Showing Double HA Particle Hits and Fragment Hit Damage	87
V-8.	Stress-Leakage Data for Dynamic Test Model 121, Tests 1, 2, and 3	89
V-9.	Model 121 Poppet Showing Depression From Double SB Particle Hit	91
V-10.	Model 121 Seat Showing Depression From Double SB Particle Hit	91
V-11.	Model 121 Poppet Showing Depression From SB Particle Hit	91
V-12.	Model 121 Seat Showing Depression From SB Particle Hit	91
V-13.	Stress-Leakage Data for Dynamic Test Model 122, Tests 1, 2, 3, and 4 and Static Tester Preliminary and Final Tests	92
V-14.	Model 122 Poppet Showing HB Particle and Secondary Impact Damage	93
V-15.	Model 112 Seat Showing HB Particle and Secondary Impact Damage	94

V-16.	Stress-Leakage Data for Dynamic Test Model 126, Tests 1, 2, and 3	95
V-17.	Stress-Leakage Data for Dynamic Test Model 126, Tests 4, 5, and 6	97
V-18.	Model 127 Load and Displacement Traces	98
V-19.	Stress-Leakage Data for Dynamic Test Model 201, Tests 1, 2, and 3	101
V-20.	Stress-Leakage Data for Dynamic Test Model 201, Tests 4, 5, and 6	103
V-21.	Load-Leakage Data for Dynamic Test Model 303, Tests 1, 4, and 5	106
V-22.	Model 303 Seat Showing Crowned Condition	108
V-23.	Model 303 Seat With Embedded HB Particle	108
V-24.	Model 303 Seat With Gouge Made by HB Particle	108
V-25.	Model 303 Seat With Embedded HB Particle	108
V-26.	Stress-Leakage Data for Dynamic Test Model 401, Tests 1, 2, and 3	110
V-27.	Stress-Leakage Data for Dynamic Test Model 401, Tests 5, 6, and 7	111
V-28.	Model 401 Seat Showing HB Particle Depression	113
V-29.	Model 401 Poppet Showing HB Particle Depression	113
V-30.	Model 401 Seat Showing HB Particle Depressions and Edge Fractures	113
V-31.	Model 401 Poppet Showing HB Particle Depressions and Edge Fractures	113
VI-1.	Shear Seat Holder Rework	120
VI-2.	Ring	121
VI-3.	Self-Cleaning Model	123
VI-4.	Flat Copper Model	126
VI-5.	Flat Grooved Copper Seating Surface Detail	129
VI-6.	Flat Poppet Rework	130
VII-1.	Model 304 Load and Displacement Traces	136
VII-2.	Load-Leakage Data for Dynamic Test Model 306, Tests 1, 2, 3, 5, 6, 7, and 8	139
VII-3.	Model 306 Seat Land Showing Typical OD Edge Particle Embedment	140
VII-4.	Model 306 Seat Land With Formed Groove	140
VII-5.	Model 306 Seat Land With Formed Ridge	140
VII-6.	Model 306 Typical Seat Land Crown	140
VII-7.	Model 601 Load and Displacement Traces	143
VII-8.	Stress-Leakage Data for Dynamic Test Model 601, Tests 3, 4, and 5	144
VII-9.	Stress-Leakage Data for Dynamic Test Model 602, Tests 2, 3, and 4	145
VII-10.	Model 601 Seat Land	147
VII-11.	Model 601 Poppet Land	147
VII-12.	Model 601 Plug OD Showing Typical Small Gouges	147
VII-13.	Model 601 Plug OD Showing Typical Large Gouge	147
VII-14.	Model 601 Seat Land Bore Showing Typical Gouges	148
VII-15.	Model 602 Seat Land; Poppet of Similar Texture With Duboff Same as Fig. VII-11	148

VII-16.	Model 602 Poppet With Embedded Particle	148
VII-17.	Model 602 Seat Showing Hole From Fig. VII-16 Particle	148
VII-18.	Model 501 Seat Showing Typical Texture and Scratches	150
VII-19.	Model 501 Poppet Showing Typical Texture	150
VII-20.	Model 501 Seat Land Showing Skin Effect; ID on Right	150
VII-21.	Model 501 Seat Land 180 Degrees From Fig. VII-18; ID on Left	150
VII-22.	Stress-Leakage and Seating Structure Deflection Data for Static Tested Model 502	152
VII-23.	Model 502 Seat After 20,000-psi Apparent Stress	153
VII-24.	Model 502 Seat After 60,000-psi Apparent Stress	153
VII-25.	Stress-Leakage Data for Dynamic Test Model 503, Tests 1, 2, and 3	154
VII-26.	Model 503 Seat Land Before Test	156
VII-27.	Model 503 Seat Land Showing Embedded Particle No. 1 and Secondary Damage Below Particle	156
VII-28.	Model 503 Poppet Showing Hole From Particle No. 1 and Secondary Damage	156
VII-29.	Model 503 Seat Showing Embedded Particle No. 6	156
VII-30.	Stress-Leakage Data for Dynamic Test Model 504, Tests 1, 2, and 3	159
VII-31.	Model 504 Seat Showing Single and Double Particle Entrapments, Hits 1 and 2	160
VII-32.	Model 504 Showing Small Double Entrapment of Fig. VII-31	160
VII-33.	Model 504 Seat Showing Particle No. 1	160
VII-34.	Model 504 Poppet Hole From Particle No. 1	160
VII-35.	Model 701 Seat Land No. 4 Showing Typical Lapping Groove Before Test	163
VII-36.	Model 701 Poppet	163
VII-37.	Model 701 Seat Land Before Test	163
VII-38.	Model 701 Seat Land Before Test	163
VII-39.	Model 701 Seat Land With Focus at Base of Grooves	164
VII-40.	Model 701 Seat Land No. 4 Showing Typical Lapping Groove After 5000-psi Apparent Stress	164
VII-41.	Model 701 Seat Land No. 4 Showing Typical Lapping Groove After 10,000-psi Apparent Stress	164
VII-42.	Model 701 Seat Land No. 5 Showing Partially Detached Burr	165
VII-43.	Model 701 Seat Land After 10,000-psi Apparent Stress, Showing Height Reduction of Lands Relative to Outer Land	165
VII-44.	Model 701 Seat Land No. 4 Showing Typical Lapping Groove After 15,000-psi Apparent Stress	165
VII-45.	Model 701 Seat Land Showing 13.3 Microinch Duboff After 15,000-psi Apparent Stress	165
VII-46.	Stress-Leakage Data for Static Tested Model 701, Tests 1 and 2	166
VII-47.	Stress-Leakage Data for Dynamic Test Model 702, Tests 1, 2, and 3	168
VII-48.	Model 702 Load and Displacement Traces	169

VII-49.	Model 702 Seat Land Before Test	170
VII-50.	Model 702 Seat Land No. 6 Showing the Only Lapping Groove Before Test	170
VII-51.	Model 702 Poppet	170
VII-52.	Model 702 Seat Land No. 1 Showing Embedded Particle	170
VII-53.	Model 702 Seat Land No. 1 Showing OD Edge Particle Embedment	171
VII-54.	Model 702 Seat Land No. 6 Showing Typical ID Edge Hit	171
VII-55.	Model 702 Seat Land No. 6 Showing Typical ID Edge Hit, Focused Down on Particle Caused Extruded Metal Hole	171
VII-56.	Model 702 Poppet Showing Typical Particle Damage	171
VII-57.	Stress-Leakage Data for Static Tested Model 703, Tests 1 and 3	173
VII-58.	Model 703 Land Surface Profiles After Test No. 3	175
VII-59.	Stress-Leakage Data for Static Tested Model 704, Increasing Load Only, With Noted Lands Successively Deleted From Sealing Capability	177
VII-60.	Model 704 Formed Seat Land No. 6 After 15,000-psi Apparent Stress	178
VII-61.	Model 704 Formed Seat Land After 15,000-psi Apparent Stress; ID Left	178
VII-62.	Model 704 Seat Land After All Lands Deleted; ID Right	178
VII-63.	Model 704 Seat Land No. 6 Groove	178
VII-64.	Stress-Leakage Data for Dynamic Test Model 706, Tests 1, 2, and 3	182
VII-65.	Stress-Leakage Data for Dynamic Test Model 707, Tests 1, 2, 3, and 4	183
VII-66.	Model 706 Seat Land Before Test	185
VII-67.	Model 706 Seat Land After Dynamic Test; ID Right	185
VII-68.	Model 707 Seat Land Before Test	185
VII-69.	Model 707 Seat Land After Dynamic Test; ID Right	185
VII-70.	Model 707 Seat Land No. 5 Showing Embedded Particle	186
VII-71.	Model 707 Seat Land No. 5 Showing Embedded Particle	186
VII-72.	Model 707 Seat Land No. 1 Showing Embedded Particle	186
VII-73.	Model 707 Seat Land No. 5 Showing Typical 100-Percent Fiber-Type Hit	186
VII-74.	Phase III Model Load vs Leakage Data Comparison	188



TABLES

II-1.	Test Powder Designations	14
II-2.	Particle Entrapment Probability Data for 1000 Cycles of Standard Poppet and Seat	24
IV-1.	Phase II Static Test Model Data	41
IV-2.	Deformed Particle and Model Surface Inspection Dimensions	65
V-1.	Phase II Dynamic Test Model Data	79
V-2.	Model 127 Dynamic Test HB Particle Count Data	99
VII-1.	Phase III Dynamic Test Model Data	135

GLOSSARY

A number of specialized words and terms have evolved in the course of this work. These terms permit presentation of information with minimum verbiage. A brief definition of coined or unusual words and terms is given for ready reference. Particular attention should be made to the definition of terms involving particle encounter, entrapment, event, hit, impact, etc., as they are used somewhat interchangeably in text, but often with different connotations relative to whether or not the particle remains embedded in a sealing surface after separation, and also the degree of damage produced by a particle. Additional definition and discussion may be found in text.

Apparent Seat Stress: seat load divided by design seat land area in contact with the poppet. Real contact area stress and contact pressure distribution due to surface texture and/or angular or curvilinear contacts are neglected.

Background Contamination: unavoidable contamination. An example is the contamination introduced into a sample by the sampling valve. Total background would be that contamination introduced by all undesired sources in the process of handling a fluid. It is analogous to the noise level in an electronic system.

Background Cycle Test: refers to a dynamic cycle test in which the test fluid is unfiltered and the particle population is composed of system-retained and generated contaminants. See ultraclean cycle test.

Balance Pressure: the (hydrostatic) piston control pressure (applied to either dynamic or static tester) required to nullify extraneous closure forces (weight, pressure-area, etc.) to allow precise definition of the net seat load.

Ball Joint: device used in the static tester to provide self-alignment between the poppet and seat.

ccm: cubic centimeters per minute.

Channel Leakage: leakage issuing through a direct radial gap caused by an incompletely enveloped particle. Usually, a land width too narrow relative to the particle size will produce channel leakage.

Classified Particles (powders): particulate matter segregated to a relatively narrow size range. See test particle.

Clean: a qualitative expression for an acceptable contamination level. As used herein, refers to the background contamination level present prior to introduction of specific artificial contamination particulates.

Contamination Level: a quantitative expression of the size, distribution, shape, quantity, and type of particles entrained in the fluid of a system. See particle concentration.

Control Test (or experiment): a datum, or baseline test to ascertain the results of other tests which are performed under identical conditions, except for one varied factor, whose significance can thus be inferred.

cpm: cycles per minute.

Crossover: refers to a stress-leakage characteristic wherein the decreasing (return) stress curve crosses over the initial increasing stress curve to a point of greater leakage, with subsequent stress loops repeating or producing even greater leakage at low stress (attributed to a frictional effect of eccentric loading.)

Duboff: rounding of a sealing surface corner or edge, usually by a polishing action. With a flat seat the net effect is to generate a relatively large radius tangent to the sealing surface which becomes increasing smaller as the edge is approached. Duboff is not a corner radius.

Eccentric Loading: deviation of the poppet-seat actuator load center from the true geometric axis defined by the seat sealing land.

Hit: synonymous with particle encounter.

Hit Frequency: the number of particle encounters occurring between seat and poppet lands for a given number of closure cycles.

Hit Probability: probability of a particle encounter based on the closure configuration, number of closure cycles, and the particle population.

Land Width: a term generally indicating the apparent width (measured radially) of the seat or poppet sealing surface.

Leak Collector: a device that provides a minimum volume in which to collect leakage downstream of a closure.

Leakage Conformance: defined as the seat stress (load) required to reduce particle caused leakage to 10 times that of the clean control test leakage (same as particle envelopment). The factor 10 was chosen as a change in leakage which could be reasonably defined for the range of control test conditions evaluated herein.

Load-Leakage Test: same as stress-leakage test except independent load variable is presented in log-log plot instead of apparent seat stress.

Particle Concentration: the number of particles of a given mean size, or size range, contained in a defined fluid volume (usually 1000 cc, i.e., one liter, as used herein). Defined in a given dynamic test by average readings weighted on a cycle basis (see Appendix G).

Particle Effect: the influence of a particle encounter on the stress-leakage characteristic.

Particle Encounter (event): refers to any general interaction between a dynamically trapped particle and the poppet and seat sealing surfaces (or adjacent areas) during closure.

Particle Entrapment (impact): dynamic closure of the poppet and seat sealing surfaces about a particle. The particle may or may not remain embedded upon subsequent cycles.

Particle Entrapment Frequency: synonymous with hit frequency.

Particle Entrapment Probability: Synonymous with hit probability.

Particle Envelopment: elastic and plastic deformation of particle and/or sealing surfaces to achieve sealing contact in all areas surrounding the particle. A particle is considered enveloped when its effect on leakage is negligible. As defined herein, negligible is 10 times the clean control test leakage. See leakage conformance.

Particle Envelopment Load: the net increase in load over the clean control condition required to obtain particle envelopment.

Particle (cycle) Test: refers to a dynamic cycle test in which the test fluid is unfiltered and the particle population is composed of both background contaminants and purposely introduced particulates.

Particulate Population: a generalization defining the entire range of particle sizes, quantities, and types of particulates within a given system or container.

Residual Damage Effects: sealing surface degradation resulting from a particle encounter after the particle is washed away or removed.

scim: standard cubic inches per minute i.e., cubic inches per minute leakage at 14.7 psia and 70 F; 1 scim is approximately 1000 cc per hour.

Seat Load: the net load applied to the closure interfaces. Definition of the seat load requires compensation for weight, pressure-area, and other forces which must be overcome to effect closure. This is accomplished in the static and dynamic testers by determination of the balance pressure.

Seat Stress: synonymous with apparent seat stress, unless specifically noted otherwise.

Seating Gap: the interfacial separation between closure sealing surfaces resulting from imperfect sealing geometry and/or foreign matter.

Seating Overload: the provision of sufficient load margin (i.e., additional load) to allow for sealing degradation due to particle encounters.

Standard Test Model: refers to the flat poppet and seat test model (depicted in Fig. II-1, III-1, and III-2) with nominal mean seat diameter, $D_s = 0.470$ inch and seat land width, $L = 0.03$ inch, used to establish base line control data.

Stress-Leakage Test: leakage at a constant inlet pressure is measured for incrementally increasing and decreasing seat loads. The test may consist of several successive loops, each of increasing maximum load. Data are presented as a log-log plot of seat stress vs leakage.

Test Model: a closure poppet and seat pair designed and used specifically for evaluating sealing parameters. A test model forms a unique combination of sealing surfaces. It is usually fabricated to much closer tolerances than an operational valve, and also provides for precise load control leakage measurement. As used herein, all test models had inlet flow through the seat.

Test Particle: a defined artificial contaminant; designated herein by hardness (S or H), size ranges (A, B, C, etc.) or specific micron size for single particles (e.g., S30 represents a soft, 30-micron-diameter particle). See Table II-1.

Ultraclean Cycle Test: refers to a dynamic cycle test in which the test fluid is passed through a 0.45-micron membrane element just prior to entering the test model. No particles greater than 12 microns are registered via automatic counter throughout the test. Particles less than 12 microns are not monitored, but, for the model sizes tested, these particles will have negligible effect on model leakage.

Wring: the process of sliding two geometrically matched surfaces together to obtain a very close contact. Strong adherence is provided by a near molecular thickness oil film. Separating pressures near 90 psi have been measured in a vacuum with precision gage blocks.

SECTION I

INTRODUCTION

While much has been accomplished in recent years for sleeve type hydraulic control valves, few data exist on the function and sealing characteristics of valve poppets and seats in contaminated environments. Where environment or fluids allow, most valves use soft seating materials. Because of their elastoplastic nature, large number of contaminant particles can be enveloped by the soft seat configuration without significant leakage increase.

For corrosive or reactive propellants, however, or where cryogenic systems are involved, metal valve sealing is generally required. In a previous program accomplished by Rocketdyne under Air Force Contract AF04(611)-9712, fundamental characteristics of metal poppet and seat closures were established. Evaluation of surface texture and geometry influence on the sealing performance of flat, conical, and spherical configurations was performed and correlated with supporting analyses. These studies provided a basic understanding of the sealing mechanism. Subsequently, the degrading effect of cyclic impact was investigated, with corrosion fretting established as the cause of performance deterioration. Ultimately, these experiments led to the selection of crowned contact at the seating interface as an optimum condition. The results of this program are reported in "Poppet and Seat Design Data for Aerospace Valves," AFRPL-TR-66-147. The experience, knowledge, and hardware resulting from this effort formed the foundation for, and made possible, the extension of metallic valve sealing technology represented by the data presented herein.

In previous investigations, every effort was made to eliminate contamination as a variable. It was recognized, however, that successful application of metal seating in future high-energy propulsion systems would require both a knowledge of the potential contamination environment and the influence of contaminants on valve sealing capabilities. To this end the program described herein was initiated. Its objective was to generate design criteria for valve poppets and seats capable of sealing reliably in the contamination environment experienced in rocket propulsion fluid systems.

Program effort was divided into three phases. In Phase I an attempt was made to describe realistic fluid contamination properties and levels for operating systems, and to define current contamination effects technology. The results were discouraging in that an engineering definition of contamination in rocket fluid systems failed to emerge even though an abundance of contamination "data" was accumulated. The fundamental problem was the lack of a method for accurate, continuous measurement of particulates present in operating fluid systems. Information relating to contaminant influence on valve sealing mechanisms was also singularly lacking, particularly for poppet and seat type closures. However, the data accumulated did provide direction for test system design and established general contamination information from which subsequent experimental effort was initiated. The Phase I survey results are separately published as report AFRPL-TR-67-290, "Survey of Contamination in Rocket Propulsion Fluid Systems."

Phase II effort involved experimental investigations of contaminant effects produced both statically and dynamically. This represented in large part a development effort wherein test method and system requirements were established and proved. Precision test models and classified nickel alloy particles were utilized to explore leakage variations caused by (1) entrapped particles and (2) surface damage effects resulting from particle impacts. In the static test portion, 15 tests with entrapped particles ranging from 15 to 60 microns were performed on 10 flat-seat models.

For dynamic investigations, a 2.5-gpm recirculating Freon TF system incorporating an automatic particle counter was developed. This permitted 1000-cycle model testing under "clean" fluid conditions (on the order of 50 foreign contaminants per liter) and with steady-state test particle concentrations up to 20,000 particles per liter. Sixteen dynamic tests were performed wherein models were cycled in a fluid environment artificially contaminated to levels ranging from 1000 to 10,000 particles per liter. Flat poppet and seat models and examples of spherical and shear seal designs were evaluated. Because this was a low-pressure (about 25 psi) system, erosion effects potential with high-pressure fluid systems were not evaluated.

Phase II investigations established that residual surface damage from particle impacts generally produced tolerable sealing degradation. Entrapped particle effects varied from minimal to gross as a function of particle size and seating dimensions. A significant observation was that, where multiple cycles permitting ejection of trapped particulates is not feasible, a combination of hard-on-soft seating materials is preferable to hard-on-hard. Additionally, analytical prediction of particle entrapment frequency was experimentally correlated within a factor of 2.

In Phase III, the concepts and direction evolving from Phase II investigations were reduced to practice. Designs incorporating particle avoidance (self-cleaning model) and particle envelopment (flat and grooved copper models) were prepared for performance evaluation. Also, the exemplary sealing performance of the shear seal model led to further evaluation of the shear seal design. Eleven models representing these four configurations were tested.

Results of Phase III testing indicated that it may be possible to influence the incidence of particulate encounters through inlet feed geometry and dynamic variations (particle avoidance). The grooved copper model presented the most outstanding results. This concept employed soft seating lands, separated by void annuli to permit particle envelopment with lateral rather than vertical material displacement. It appears to represent an optimum approach to reliable sealing in contaminated environments and warrants further development.

The compilation of program input and output information presented herein is divided into two portions. Sections I through VIII include analyses, test model description, test results, and observations comprising basic test model investigations. Supplementing these sections are particle entrapment probability, shear seal analyses, and a detailed analysis and description of test fixtures and systems presented in Appendixes A through G. In particular, the discussions of test fixture and system capabilities and/or limitations strongly support data presented in test Sections IV, V, and VII.

SECTION II

ANALYSIS

The object of the analytical effort was to provide relationships and analytical approaches for describing the contamination present in fluid systems, the probability of specific particle entrapment, and the effect of entrapment on the closure sealing ability. The analyses and equations presented herein are largely in support of the experimental effort. Theoretical data are presented for a range of conditions for later comparison with test data.

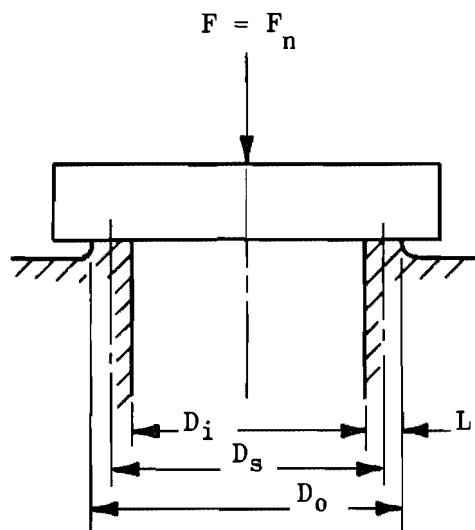
VALVE SEATING GEOMETRY

The performance of a metal-to-metal valve seat is intimately related to the geometrical configuration of the seating surfaces. While a large variety of configurations are employed, the fundamental flat, conical, and spherical geometries can be identified in most cases. This stems from the simplicity of these shapes which are attendant with natural fabrication processes. The three configurations are shown in Fig.II-1 with the parameters and equations combining basic geometry and load for the definition of apparent seat stress (S).

Superimposed upon real valve seating surfaces is a variety of other smaller geometries which often have a greater influence on the closure than the more obvious gross configuration. Most apparent is surface texture. However, often overlooked and of more subtle influence is the geometry of the seat land. While a seat land may be specified by engineering drawing or fabrication process, perfect conformability of mating surfaces is impossible and deviations are difficult to define or prove precisely; hence, the actual contact dimensions may be quite different than planned and also may change with seat load. Because leakage is inversely dependent upon real contact land dimensions, it follows that variation of these dimensions will also have an effect on leakage.

The seating gap under a no-load condition is a result of variation in the above land geometry combined with dimensional and positional errors. In many cases, the real length of land contact is a complex function of the load, being formed elastically with each contact. The seat land may have been developed through plastic flow of an initially sharp edge, with subsequent deformations predominantly elastic. Where the land is plastically formed, the resultant contact shape is largely indeterminate. With defined simple curved shapes, however, a Hertz stress analysis may be used to predict the elastically loaded configuration. In any case, a definite land length does exist under the slightest load, and the term "sharp seat" is a relative generalization.

Dimensional errors result in deviations from true form and nonconformity between poppet and seat lands. Symmetrical errors may create only a taper gap with full contact at the roughness level around the periphery; however, errors of roundness always result in a through-gap. Even with symmetrical errors, as exemplified by differential radii in spherical seating, a finite

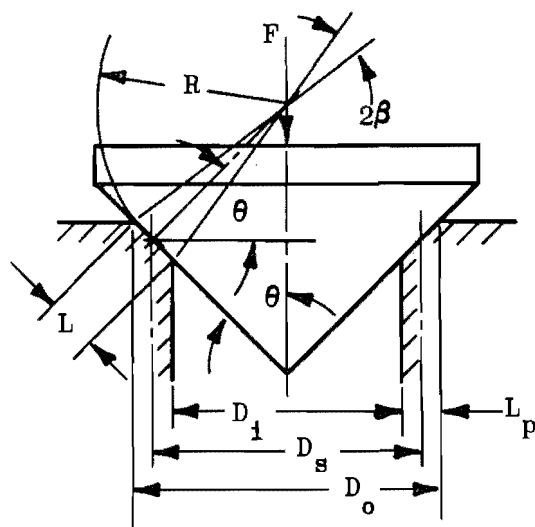


$$L = 1/2 (D_o - D_i)$$

$$D_s = 1/2 (D_o + D_i) = D_i + L$$

$$A_s = \pi D_s L$$

$$S \equiv \frac{F}{A_s} \equiv \frac{F}{\pi D_s L}$$



$$L_p = 1/2 (D_o - D_i) = L \sin \theta$$

$$L = 2R \tan \beta \approx 2\beta R$$

$$D_s = D_i + L_p$$

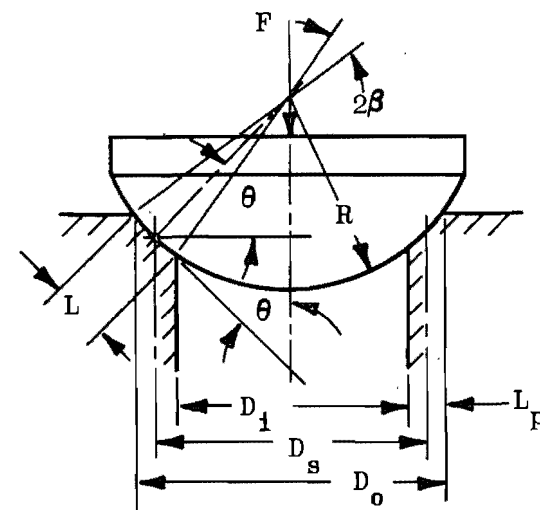
$$A_s = \pi D_s L$$

$$A_{sp} = \pi D_s L_p$$

$$F_n = F / \sin \theta$$

$$F_r = F / \tan \theta$$

$$S \equiv \frac{F}{A_{sp}} \equiv \frac{F_n}{A_s}$$



$$L = 2\beta R$$

$$L_p = 1/2 (D_o - D_i) \approx L \sin \theta$$

$$D_s = 2R \cos \theta$$

$$A_s = \pi D_s L$$

$$A_{sp} = \pi D_s L_p$$

$$S \equiv \frac{F_n}{A_s} \equiv \frac{F}{A_{sp}}$$

Figure II-1. Flat, Conical, and Spherical Seating Equations

load must be applied to establish a minimal land for adequate sealing or else leakage could be in the nozzle regime and, thus, much greater than for the laminar condition.

Superimposed upon the seat land, and causing gaps which may only be reduced but never closed, are the surface textural errors of roughness, waviness, nodules, pits, and scratches. Thus, a variety of geometrical errors cause conformal gaps in seating which must be reduced through load deformation of the "high" material.

These errors were analytically examined and experimentally evaluated in the previous program. The basic test model used was a flat 440C poppet and seat having a nominal 0.470-inch mean seat diameter (D_s) and 0.03-inch land width (L). The complexities of particle envelopment and impact also required an empirical approach. This model geometry was therefore used as a standard to develop baseline control data in Phase II testing for later comparison with Phase III-Demonstration Models.

PARTICLE ENVELOPMENT

Particles entrapped between sealing surfaces subtract from available sealing load. They also cause land damage in the form of local plastic deformation. Due to the extreme complexity of the elastic-plastic deformations involved in the particle deformation process, a very simplified approach has been considered to provide a basis for correlating test data. The purpose of this analysis is to determine the relationship between the particle-enveloping load and the respective properties of particle and seating materials.

A particle may be considered enveloped when its effect on leakage for a given load is negligible. Depending upon the leakage level, "negligible" particle derived leakage could be considered immeasurable to 10 times "clean" leakage. To achieve this condition, the particle and/or sealing surfaces must elastically and plastically deform to achieve contact in areas surrounding the particle. If the particle is too large for accommodation by the sealing land, surface contact will be made circumferentially around the land without achieving radial contact. Leakage will thus issue through a direct radial "channel" path surrounding the particle. Since available load is no longer applied directly to the particle, substantial load increase will be required to close this gap and, unless available, gross leakage will result.

A model of seat land particle envelopment is shown in Fig. II-2. For this analysis it is assumed that (D_c) is much less than (L). For simplification, two extreme cases are considered:

1. Partial plastic deformation of a hard contaminant particle with complete plasticity of the sealing surfaces.
2. Complete contaminant particle plasticity with elastic deformation of the sealing surfaces to envelop the particle.

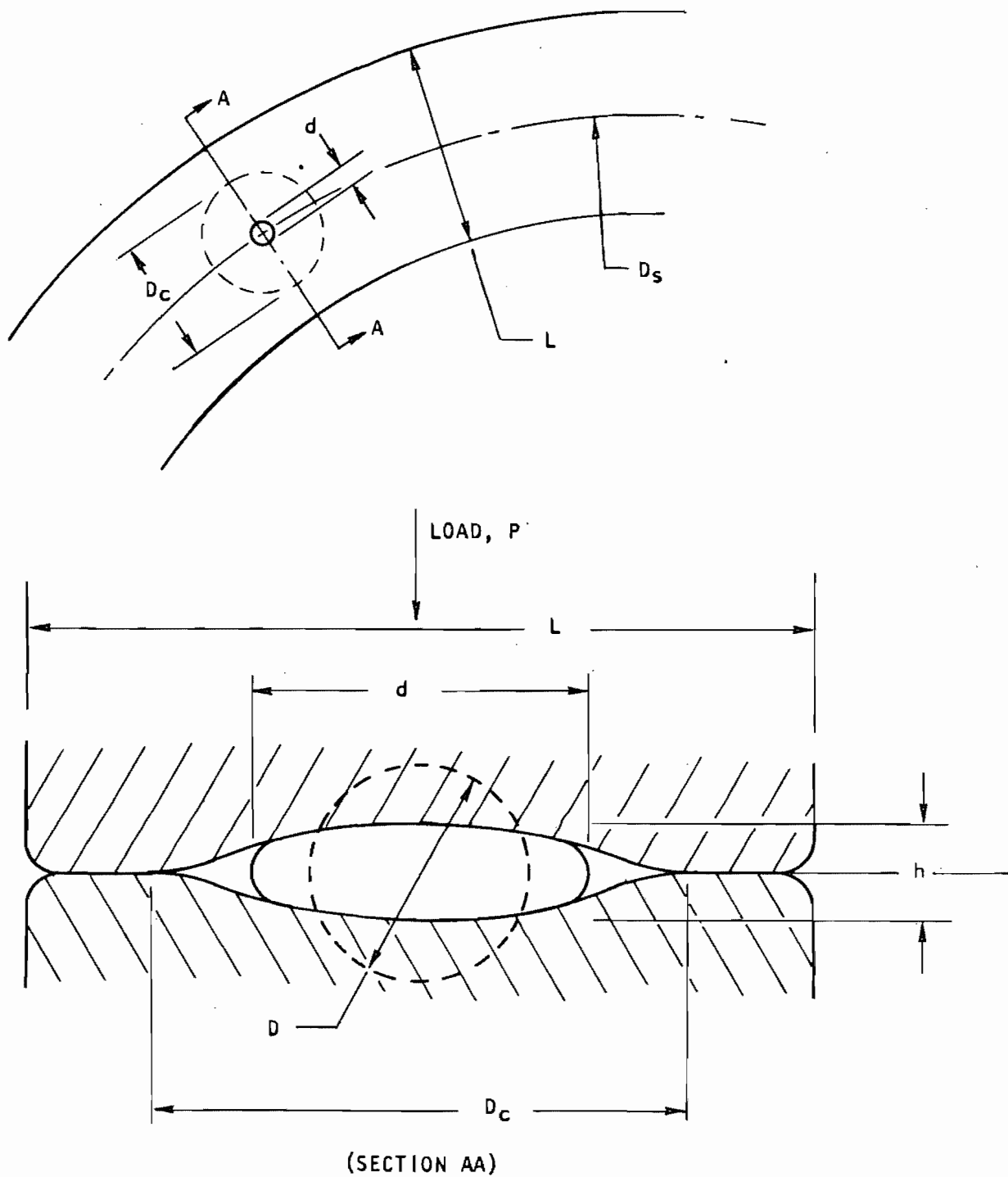


Figure II-2. Particle Envelopment Model

The particle volume is:

$$V = \frac{\pi D^3}{6} \cong \frac{\pi}{4} d^2 h$$

from which,

$$d \cong \left(\frac{2 D^3}{3 h} \right)^{1/2}$$

The contact stress required to develop full plasticity between relatively flat cones or wedges and flat plates has been determined experimentally to be 3 to 5 times the material yield strength (Y) in normal tension, depending upon the cone angle and degree of work hardening (Ref. 1). Denoting this plasticity factor as (γ), the average plastic contact stress is:

$$S \cong \gamma Y$$

and may be applied either to the particle or poppet and seat. The resultant plastic load is:

$$P \cong \frac{\pi}{4} d^2 \gamma Y$$

Case 1

Where the particle is harder than the seating surfaces, some plastic deformation of the spherical particle will take place to support the load. The final particle diameter (d) and height (h) will be a complex function of the plasticity factors of each material which must be experimentally determined; thus,

$$d = K D$$

The correlating load equation is given by

$$P = \frac{\pi}{4} K^2 D^2 \gamma_s Y_s$$

where γ_s and Y_s are properties of the seating material. It is assumed that elastic substrate deformation compensates for the plastically displaced seating material in enveloping the contaminant particles.

Case 2

For the second case, the assumed model is one in which the seating surface deflects elastically to envelop the plastically deformed contaminant particle. The ultimate extent of particle spreading will be limited by the

contacting surfaces remote from the locally deformed area. To determine the elastic deformation, the contact stress acting over the flattened particle will be assumed to be average over the particle surface. The average deformation of the surface across the particle diameter is (Ref. 2):

$$y = \frac{1.08 P_e (1 - \nu^2)}{E_s \cdot d}$$

where

E = elastic modulus

P_e = elastic load

ν = Poisson's ratio (~0.3)

The combined deformation of both surfaces will be twice the foregoing and is equal to h; therefore,

$$h \cong \frac{2 P_e}{E_s d}$$

Combining this expression with the plastic particle load and volume relationship for h and d results in the final load-defining equation:

$$P_e \cong \frac{D^2}{2.25} (\gamma_p \gamma_p E_s^2)^{1/3}$$

This is the load required to close two metal surfaces elastically about a plastically flowed spherical particle of original diameter D.

The corresponding ratio of particle height to original diameter is:

$$\frac{h}{D} = \left(\frac{1.3 \gamma_p \gamma_p}{E_s} \right)^{2/3}$$

Evaluation of this equation allows a consideration of the degree of flattening. For this case, the particle or closure-particle plasticity factor γ_p must be experimentally determined since the envelopment process precludes free lateral plastic flow, and substantial hydrostatic pressures are developed.

By evaluating the subsurface shear stress and combining with previously defined parameters, a criterion for seat elasticity can be established. Elasticity of the seating surfaces at the contaminant contact will be met if:

$$\frac{P_{e \max}}{P_e} = \frac{1.5 \gamma_s}{\gamma_p \gamma_p} > 1$$

where subscript s refers to the seating surface and p the particle;
 $P_{e \text{ max}}$ = seating material yield load.

LEAKAGE FLOW

Leakage was the performance-defining parameter in the particle effects portion of the test program. Based upon previous efforts, leakage data were used to describe equivalent separating gaps and to indicate the relative degree of particle envelopment vs applied load. The leakage parameter also indicated the effect of surface degradation from cyclic impact of particles. Finally, initial leakage and interference inspection was used to define the model surface geometry (such as land width and peak-to-valley roughness) in the "clean" condition as control data for later comparison with effects data.

In the previous program (Ref. 3), parametric test data were obtained for comparison with theoretically predicted flow past a flat, parallel plate poppet and seat model. These investigations included leakage measurement of nitrogen, helium, and argon gases for nozzle, turbulent channel, and transition-molecular flow for the near-seated condition. Close agreement was obtained between theoretical leakage computed from the measured gap and test leakage.

Static particle tests performed herein involved leakage measurement covering all flow regimes. Because of the relatively large gaps caused by entrapped particles, some initial leakage measurements were made at low pressure, with subsequent pressure increase as the particle was plastically enveloped. Correlation of resultant data on a common pressure basis was obtained from theoretical nitrogen leakage curves (Fig. II-3, -4, and -5). These data are computed for the standard flat poppet and seat model and inlet pressures (P_1) defined therein. Equations presented in Ref. 3 were used in preparation of the curves.

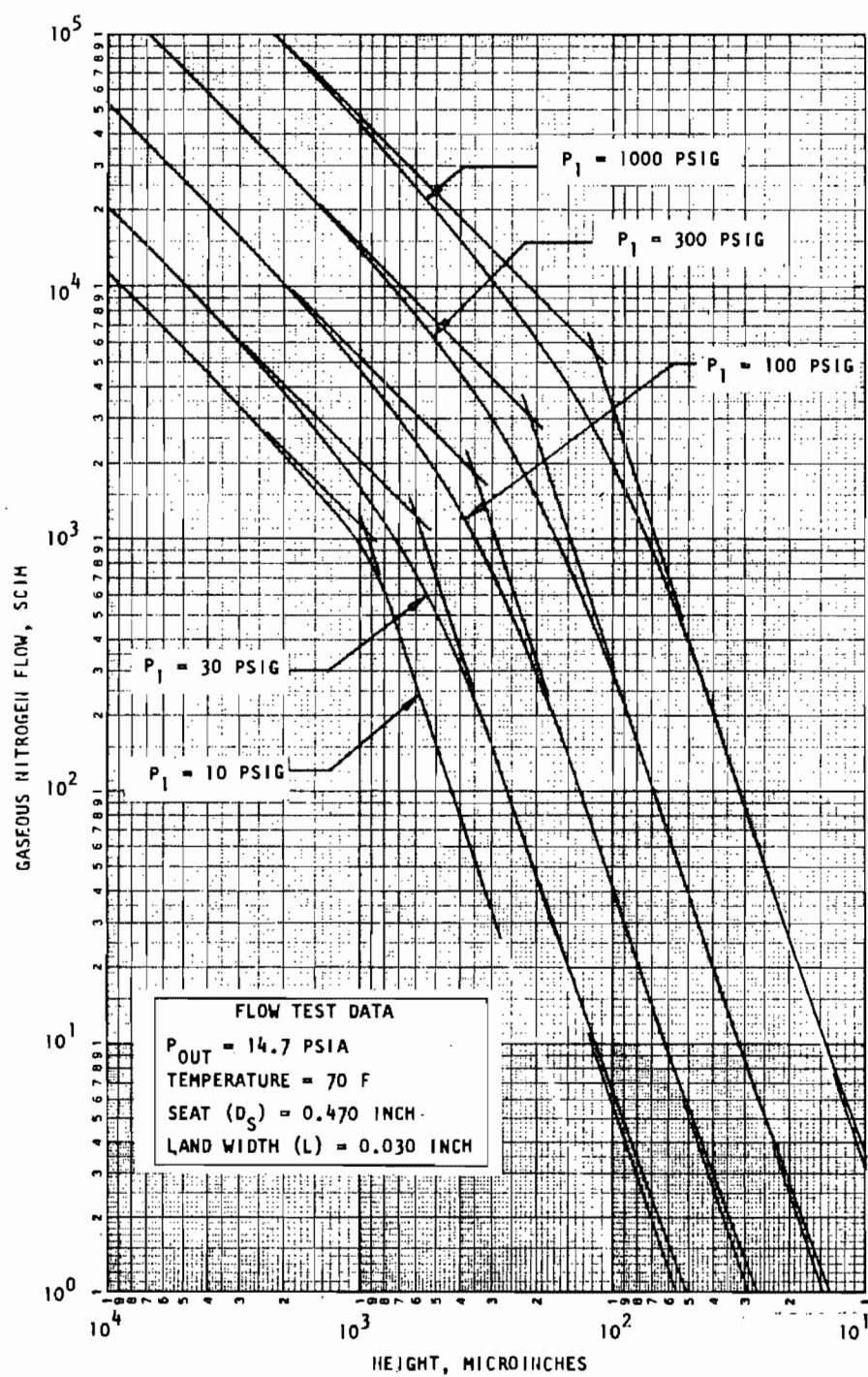


Figure II-3. Theoretical Seat Leakage, Part 1

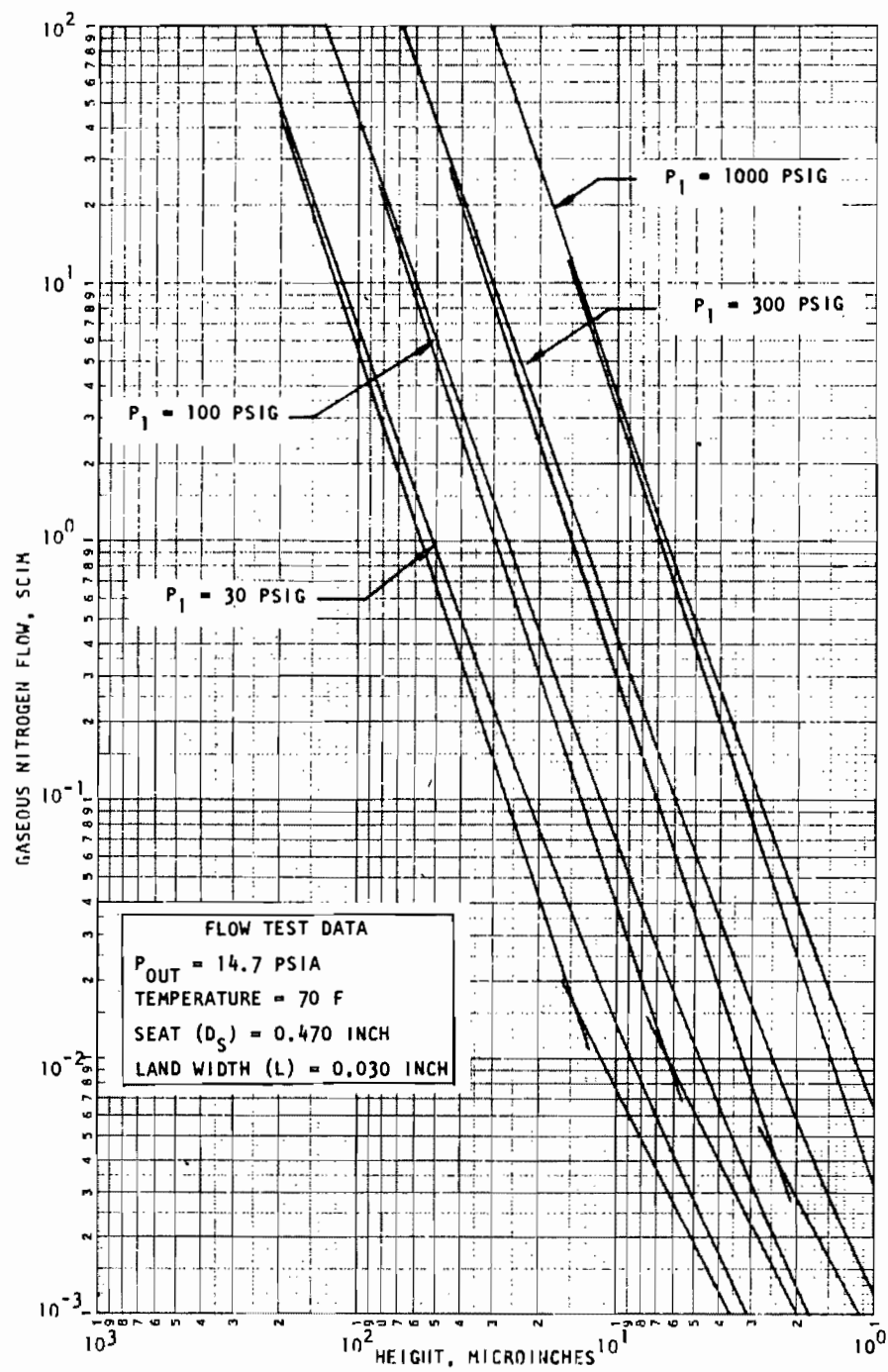


Figure II-4. Theoretical Seat Leakage, Part 2

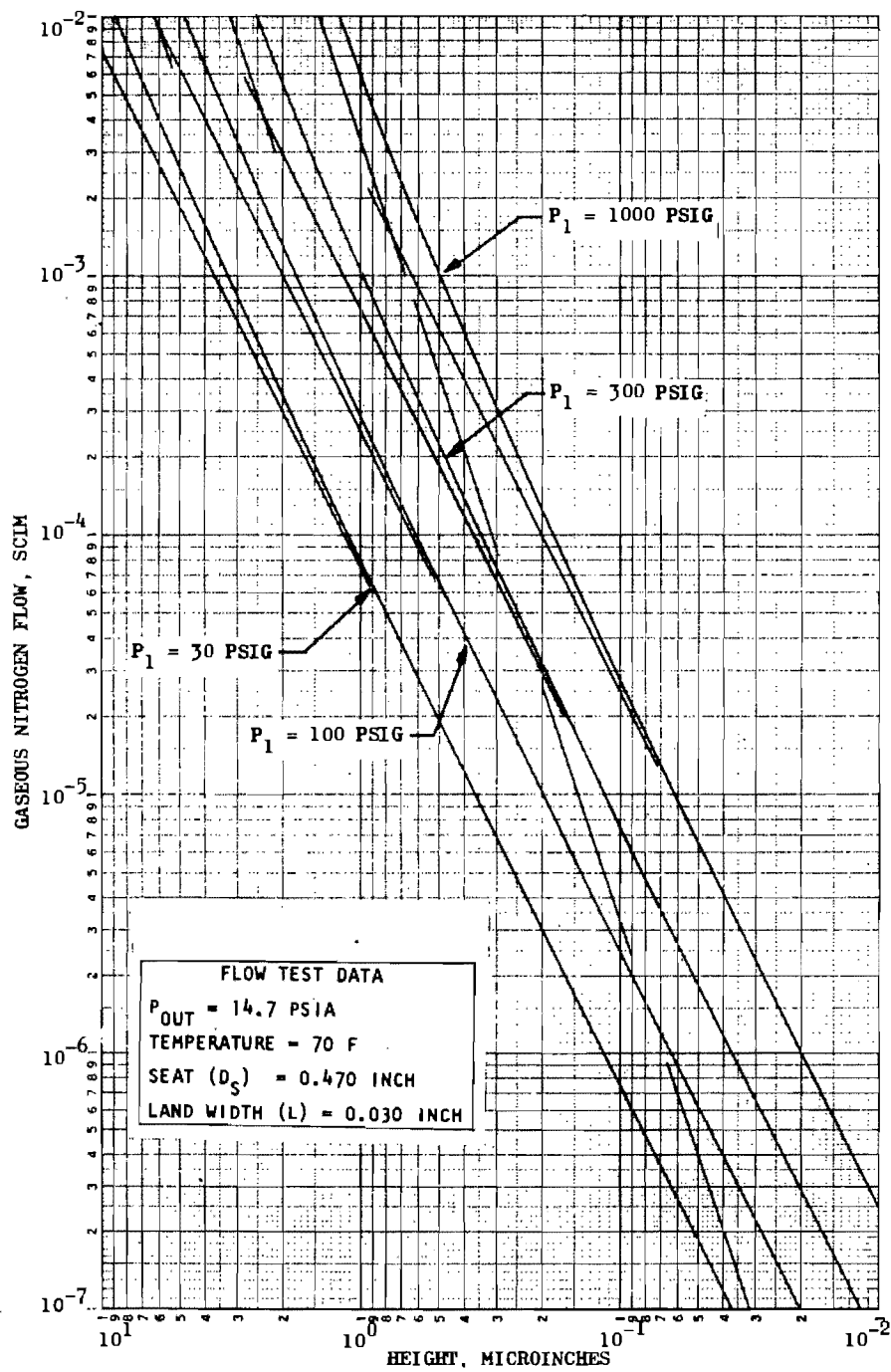


Figure II-5. Theoretical Seat Leakage, Part 3

PARTICLES IN FLUID SYSTEMS

The amount and size of particulate contamination in a fluid system may be described in several ways:

1. Particle counts per sample volume by levels
2. Log-normal parameters
3. Log-log² plot with levels
4. Weight per sample volume
5. ppm - parts per million by volume

These have been presented in detail in the Phase I report (Ref. 4) with definition of contamination levels for a variety of fluids and systems. The purpose of this analysis is to relate these real contamination levels to the artificial contaminant particles used in the subject test program.

Test Particle Definition

A variety of particulates was evaluated before final selection. These included glass beads, road dust (AC Spark Plug Div. of G. M. Corp.), diamond powder, plastic beads, Teflon powder, pollen, and various metallics. Crushed powders such as AC dust and diamond powder were rejected because of irregular shape and excessive fines (very small particles). Glass beads would undoubtedly shatter on impact, and plastic beads would float in Freon TF.

Hoeganaes atomized hard facing nickel powders were chosen because of sphericity, hardness range, cost, and availability. These powders were purchased rough graded between 5- and 100-micron diameter. Additional classification was obtained through Particle Information Service, Los Altos, California, using sieves and a vacuum cyclone separator. While classifying the particles, the separating machine also cleaned them of adhering dirt. In preparing these materials, care was taken to avoid contamination by foreign materials or mixing of the two types of nickel used. New screens were used for each material. The cyclone separating machine was completely dismantled and cleaned prior to its use on each material.

A complete description of the nickel powders is presented in Table II-1. Note that designations "HA," "SB," etc. have been given to classified powders denoting hard or soft material, mean size (d_g) and distribution (σ_g). These letter designations have been used throughout the report. Where individual particles have been selected, the letter prefix indicates the material (hard or soft) followed by the specific size measured; e.g., S30.

Particle Analysis

Particles are described by size, number, and weight. The amount of particulate matter contained in a fluid is specified by number count for several size ranges or by weight, each per a unit fluid volume.

TABLE II-1

TEST POWDER DESIGNATIONS

Hoeganaes Nickel Powder Description	Nominal Size Desired	Particle Information Service Analysis		Program Analysis, Appendix G				Designation
		d _g microns	σ_g	d _g microns	σ_g	5% > Size, microns	95% > Size, microns	
1. Soft Powder (S) Ancor 120 SF, Lot 53-3496	60	59	1.05					SA
a. Size Range: ~5 to 140 microns								
b. Hardness: 17-21 R _C	30	34	1.09	33	1.25	47	23	SB
c. Composition, percent								
C < 0.015	15	15	1.08					SC
Si 2.26								
B 1.35 minimum	7.5	7.7	1.13					SD
Fe 0.42								
Ni Balance								
d. Density = 8.67 gm/cu cm								
2. Hard Powder (H) Ancor 160 SF, Lot 53-4747	60	55	1.07	58	1.09	67	50	HIA
a. Size Range: ~5 to 140 microns								
b. Hardness: 62-67 R _C	30	32	1.12	32	1.25	47	23	HB
c. Composition, percent								
C 0.85	15	18	1.08					HC
Si 3.92								
B 2.91	7.5	8.2	1.07					HD
Cr 16.62								
Fe 3.5								
Ni Balance								
d. Density = 8.09 gm/cu cm								

Defined Terms. The relationship between the above parameters results in the following definitions:

- C_n = number of particles contained in sample volume, particles/liter (p/l)
- C_w = weight of particles contained in sample volume, milligrams/liter (mg/l)
- d_g = number median particle diameter, geometric mean of log-normal distribution, microns
- d_v = mean volume particle diameter by number, microns
- n = number of particles in sample volume, particles (p)
- v = sample volume, liters (l)
- w = weight of particles in sample volume, mg
- γ = number of particles per milligram, p/mg
- ρ = particle material density, mg/cubic micron
(NOTE: 1 gm/cubic cm = 10^9 mg/cubic micron)
- σ_g = geometric standard deviation

Equations. The following relationships are derived from the preceding terms; particle shape is assumed to be spherical.

$$C_n = \frac{n}{v}, \quad C_w = \frac{w}{v}$$

$$\gamma = \frac{1}{\frac{\pi}{6} \rho d_v^3}$$

$$C_n = \gamma C_w$$

Parts per million by volume (ppm) with preceding units is given by

$$\text{ppm} = \frac{C_w}{10^9 \rho}$$

The mean volume diameter, defined as the average volume representing the total particle volume on a frequency basis, is given by

$$d_v \equiv \left(\frac{1}{n} \sum_{i=1}^I n_i d_i^3 \right)^{1/3}$$

Total weight of (n) particles is

$$w = \frac{\pi}{6} n \rho d_v^3$$

For log-normal distribution

$$\ln d_v = \ln d_g + \frac{3}{2} \ln^2 \sigma_g$$

where (σ_g) is most simply obtained from log-normal plot data as

$$\sigma_g = \frac{d_g}{84.13\% > \text{size}} = \frac{15.87\% > \text{size}}{d_g}$$

where

$$d_g = 50\% > \text{size}$$

Contamination in rocket-associated fluid systems is widely dispersed due to relatively low concentration. Numerical estimate of dispersion per inch of line is given by

$$L_c = \frac{61.02}{C_n A}$$

where

A = line area, sq in.

C_n = particles/liter (p/l)

L_c = line inches/particle

Typical values are plotted in Fig. II-6. Familiarity with these data aid in visualizing the amount of contamination in a given system.

Analysis of Engine Contamination Levels and Test Particles

What size and concentration levels should be used in test to best simulate actual contamination levels in operating engine systems? The Phase I Survey partially answered this question; however, no data on operating (firing) systems were available. It was concluded that contamination levels would undoubtedly be greater than indicated by samples taken from static systems.

Engine Contamination Levels. Two particle concentration levels that are estimated to span the expected contamination levels are analyzed. These levels (4 and 8) are taken from the Rocketdyne specification particle count limits for space engines (Fig. II-7); metallics are assumed as the contaminant composition. Level 4 represents a clean condition requiring extreme care in system cleaning and flushing with samples usually obtained from a filtered source.

Level 8 is 10 times the contamination of Level 4 and is assumed to represent the same clean system, but under firing conditions. It is notable that the Level 8 distribution very nearly matches the average of the composite plot of particle count data for flight systems presented in Ref. 4 as Fig. B-20. It follows that the Level 8 assumption is not too rigorous, and may even be optimistic for some systems. However, such data must be obtained from specific systems since, in many cases, contamination results from human failure rather than a repetitive (predictable) process.

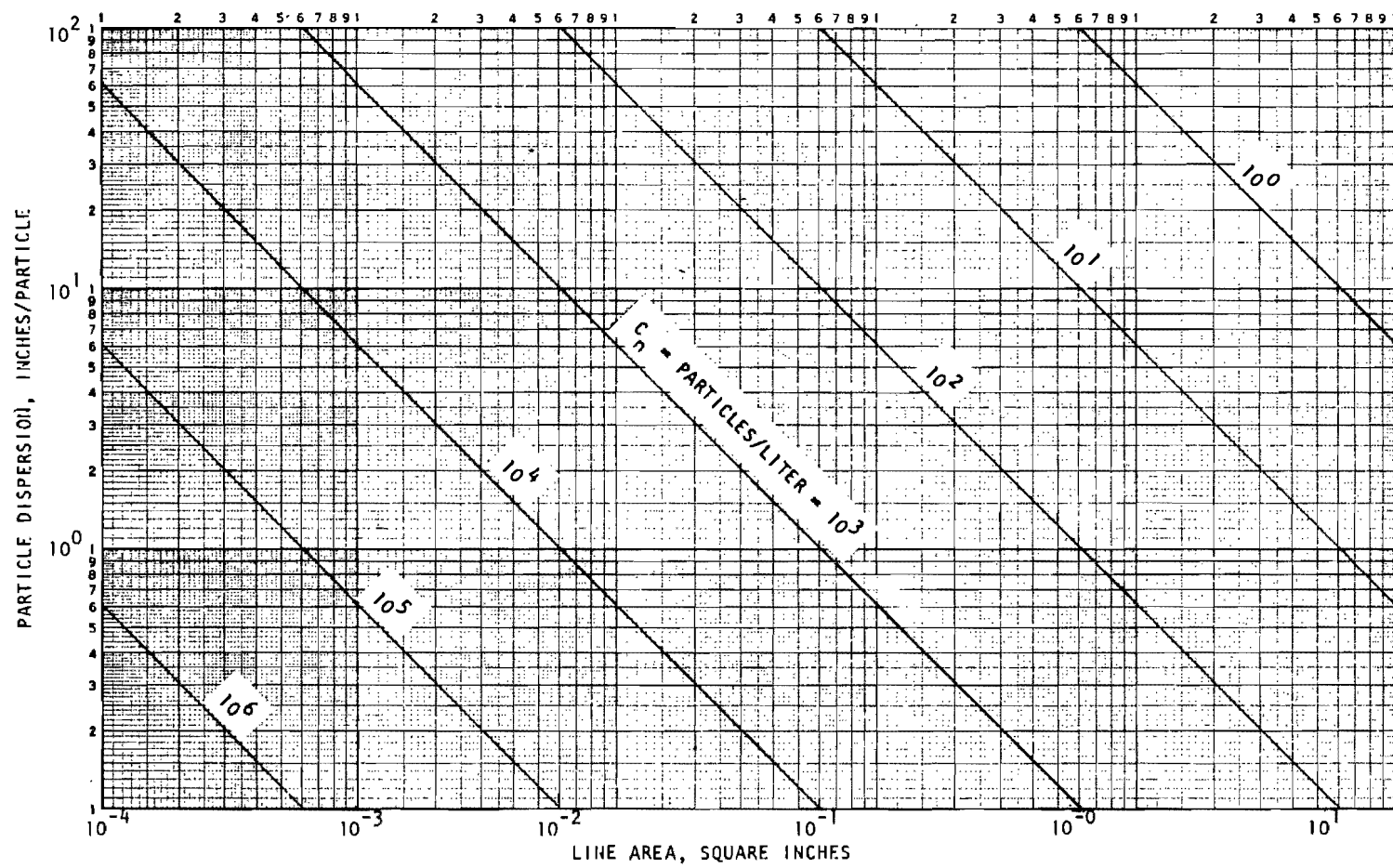


Figure II-6. Particle Dispersion

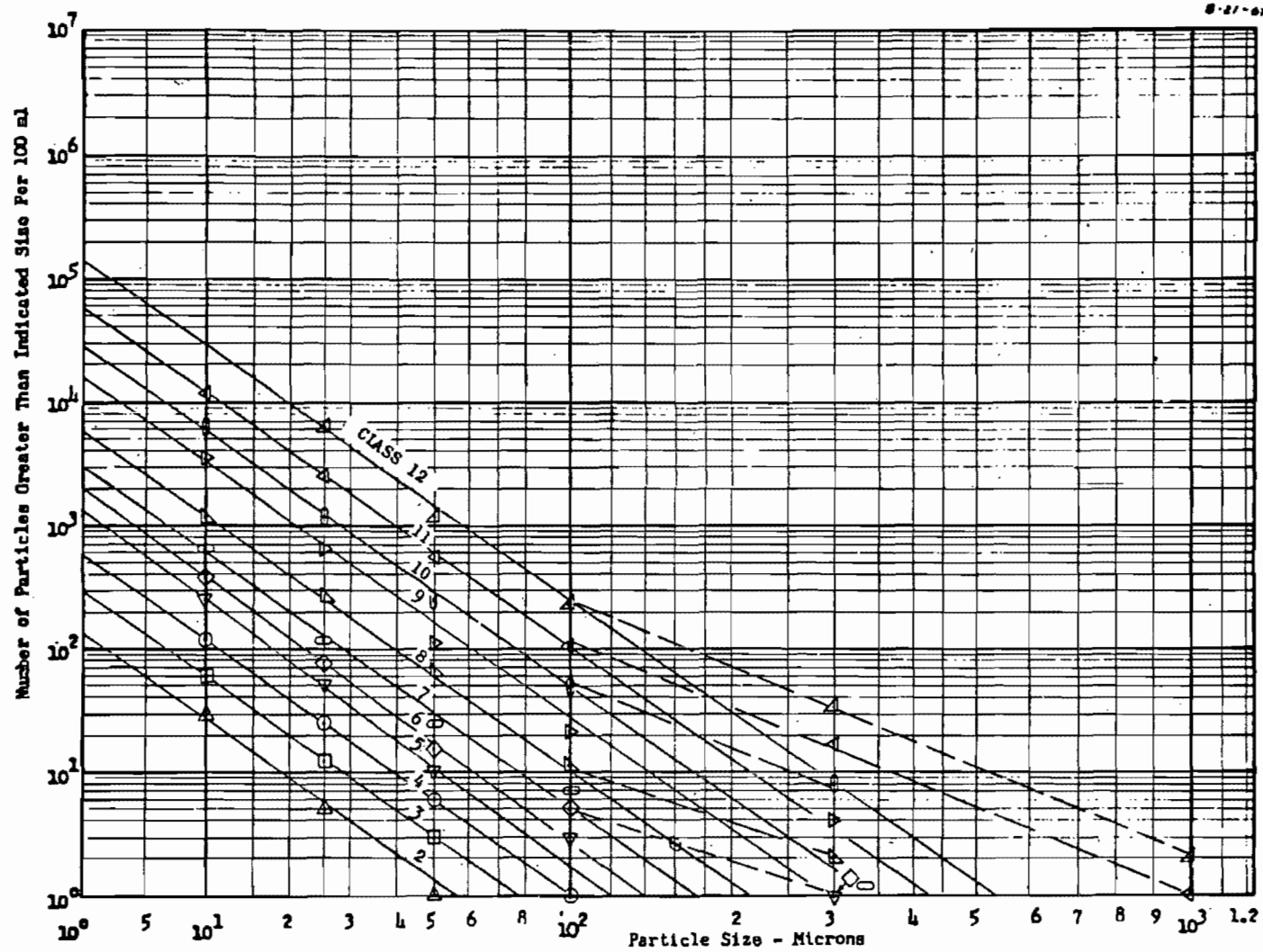


Figure II-7. Particle Count Limits for Space Engines per Rocketdyne Specification RA0615-003

For accurate weight conversion analysis the log-log squared plot for the Level 8 data (Fig. II-7) is converted to eight size intervals below on a liter basis; all sizes are in microns.

Size Range d_{i1} to d_{i2}	d_i	n_i	$\Sigma n_i > d_{i1}$	$\% \Sigma n_i > d_{i1}$
10 to 15	12.5	6,300	12,600	100
15 to 20	17.5	2,400	6,300	50
20 to 30	25	2,100	3,900	31
30 to 50	40	1,200	1,800	14.3
50 to 80	65	410	600	4.8
80 to 120	100	130	190	1.5
120 to 200	160	47	60	0.48
> 200	250	13	13	0.10
		$\Sigma n_i = 12,600$		

The data, with log-normal convert to mean weight (volume) distribution, are plotted in Fig. II-8. As shown, the mean size by count is 14.2 microns, and by weight is 38.0 microns (36.1 was obtained by the definition for d_v). Corresponding weight concentration (C_w) based on hard test-particle density (8.09 gm/cc) are 0.293- and 2.93-mg/l for Levels 4 and 8, respectively.

HB Test Particles. Most Phase II and III dynamic tests were performed with HB particles. They are therefore analyzed for comparison with the preceding Level 8 data as follows:

$$\begin{aligned} d_g &= 32 \text{ microns} \\ d_v &= 34.4 \text{ microns} \\ \gamma &= 5800 \text{ p/mg} \end{aligned}$$

Additional data covering the test (C_n) range are tabulated below with L_c computed for noted areas of (1) the standard flat seat at HB size gap (1.86×10^{-3} sq in.) and (2) a 0.194-inch ID line (0.0296 sq in.).

C_n , p/l	C_w , mg/l	ppm	L_c , in./p	
			$A = 1.86 \times 10^{-3} \text{ in.}^2$	$A = 0.0296 \text{ in.}^2$
1,000	0.172	0.0212	32.9	2.07
2,000	0.344	0.0424	16.5	1.04
5,000	0.860	0.106	6.58	0.414
10,000	1.72	0.212	3.29	0.207
20,000	3.44	0.424	1.65	0.104

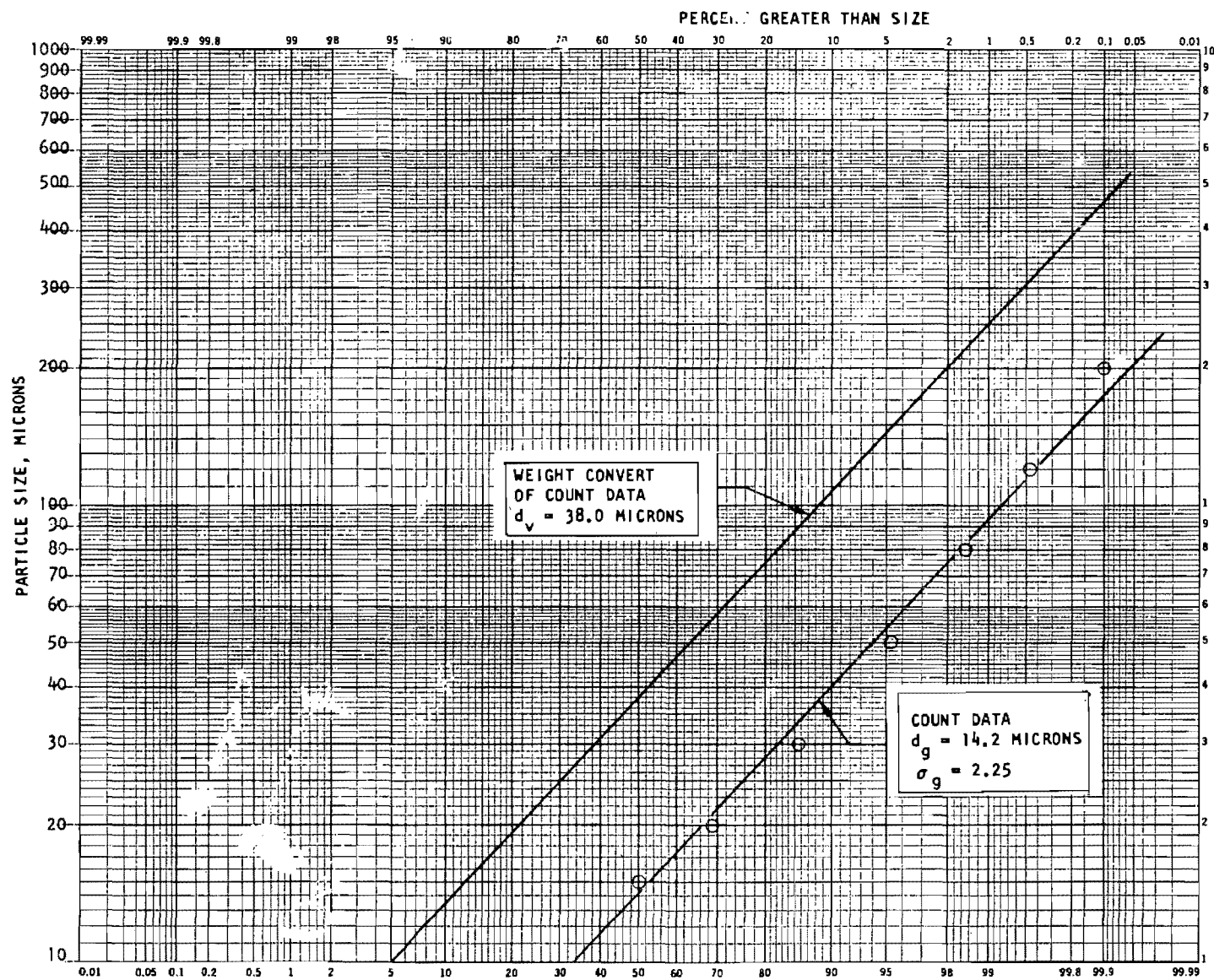


Figure II-8. Contamination Size Distribution

It should be noted that the Level 8 concentration directly comparable with HB particle size is only 3900 p/l (31 percent greater than 20 microns) with 4.8 percent of the concentration (i.e., 600 particles) greater than 50 microns. Test and engine particle size and concentrations are thus comparable. As will be seen later this is of little consequence, since particle impacts and effects are evaluated on a specific basis. Nevertheless, the situation of gross difference between actual and test concentrations has been avoided.

The particle dispersion data reveal the relatively large distances separating particles even at high concentrations. If valve closure is imagined to occur instantaneously to the particle size gap with particles remaining uniformly dispersed (i.e., C_n constant) it can be seen that, for usual valve land widths, the probability of entrapment per cycle is quite low. For the standard seat with 0.03-inch-wide land (L) the probability of entrapment per closure (p') would be

$$p' = \frac{L}{L_c}$$

This concept is further developed in the following paragraphs.

PARTICLE ENTRAPMENT

Evaluation of a computer solution to particle trajectory within changing boundaries by use of a two-dimensional fluid dynamics model led to the conclusion that the effort required for solution was beyond the program scope. Analysis of particle entrapment was limited to simple volumetric considerations to be correlated by test results. In this approach it is assumed that the poppet and seat are exposed to a uniformly distributed particle concentration with each cycle, unaffected by changing boundaries or particle inertia effects. As was previously noted, the probability of entrapment per cycle is quite low, and since particle positions are changing with time, each cycle will represent an independent probabilistic trial. If the seat closure area times the mean particle size is assumed to represent a "sampling volume," then the total number of particles that would be sampled by the seat would be a function of closure cycles and particle concentration.

Equations

Mathematical development of this hypothesis in Appendix A shows that the probability of entrapment for many cycles (trials) is defined by the binomial distribution. The mean of the distribution is given as

$$I = f A d C_n$$

where

- A = particle entrapping "effective" seat area
- C_n = particle concentration
- d = particle diameter
- f = cycles
- I = expected number of particle entrapments

Appendix A presents a table of cumulative values of the binomial distribution for $f = 1000$, the number of cycles used in the test program. These data are useful to evaluate the probability of discrete numbers of entrapments about the mean.

The particle entrapping seat area (A) is determined from the definition of what constitutes a particle "hit" or entrapment. With a seat land that is wider than the particle, entrapment could occur with the particle midpoint just within the land boundary. Effective entrapment length (L_e) is thus logically $(L + d)$. Where the seat land width and particle size are comparable, a damaging edge hit could cause sealing degradation, therefore effective length may be considered as $(L + 2d)$. Conical and spherical seating have additional effective contact length because of the angular geometry. Effective particle entrapment land widths assumed for various geometries are shown in Fig. II-9.

Predicted Entrapments for Standard Seat

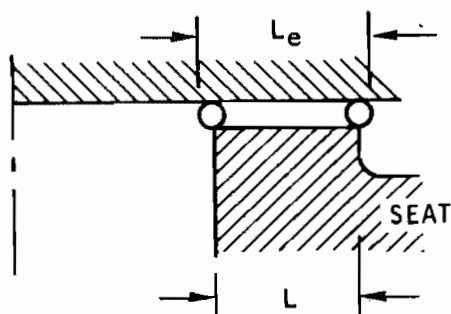
From the preceding analyses a range of data can be computed for typical contamination levels using the standard flat poppet and seat model. The final entrapment equation is given by

$$I = 2.03 \times 10^{-6} f D_s L_e d C_n$$

where

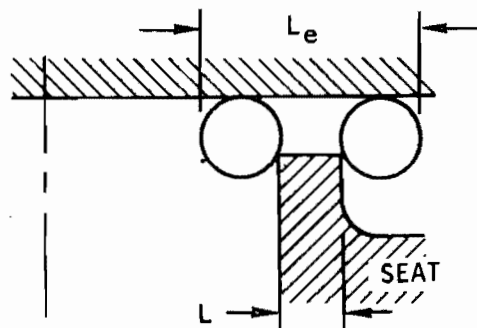
- C_n = particle concentration, p/l
- d = particle diameter, microns
- D_s = mean seat diameter, 0.470 inch for standard seat ($A = \pi D_s L_e$)
- f = number of cycles
- I = number of particle hits
- L_e = effective land width, inches ($L_e = L + d$ where $L = 0.03$ inch for standard seat. This width (L) is total land width including any duboff. Note that d must be converted to inches in computing L_e .)

Table II-2 presents data computed for HB particle size over a range of concentrations and also for the Level 8 concentration over its particle size range. As noted, the data are for 1000 cycles. The salient point from these data is the relatively poor reliability predicted for the Level 8 condition. If particle size greater than 40 microns is considered to be a failure condition (i.e., $C_n = 600$ p/l), the data indicate that there is a 45-percent chance of hitting a failure-producing particle in the 1000 cycles. Even with only 100 cycles of operation, the probability of a single encounter with a particle greater than 40 microns is 5.9 percent. Naturally, as the valve size or land width is increased, the probability of failure would also be increased (but not in direct proportion).



$$L \gg d$$

$$L_e \cong L + d$$



$$L \leq 2d$$

$$L_e \cong L + 2d$$

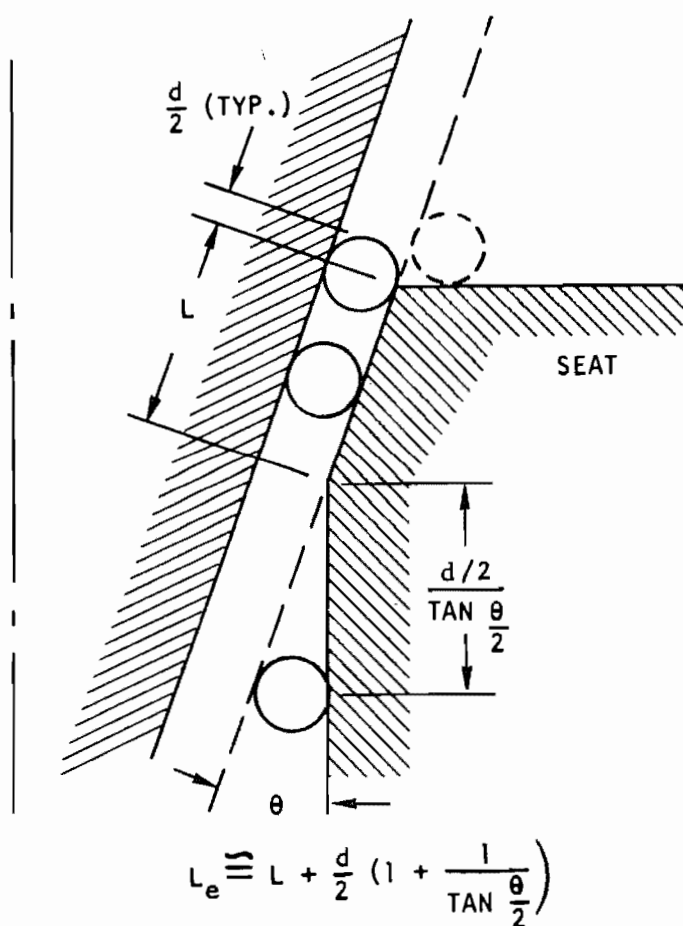


Figure II-9. Effective Particle Entrapment Land Widths

TABLE II-2

PARTICLE ENTRAPMENT PROBABILITY DATA
FOR 1000 CYCLES OF STANDARD POPPET AND SEAT

Particle Size (d_i), microns	Mean Number of Particle Hits, I	Particle Concentration C_m , p/l	Hit Range Probability Computed \rightarrow $X_2 \rightarrow X_1$	Cumulative Probability From X_2 to, and Including X_1
HB Particle $d_g = 32$ microns	0.1	105	1 1	0.0905
	0.5	525	1 1	0.303
	1	1,050	2 1	0.552
	2	2,100	3 1	0.722
	3	3,150	5 2	0.718
	4	4,200	6 2	0.799
	5	5,250	7 3	0.743
	6	6,300	8 4	0.697
	7	7,300	10 4	0.821
	8	8,400	11 5	0.790
	9	9,400	12 6	0.762
	10	10,500	13 7	0.737
Level 8				
12.5	5.85 \cong 6	6,300	8 4	0.698
17.5	2.25	2,400	3 1	0.703
25.0	1.99	2,100	3 1	0.722
40.0	1.16	1,200	2 1	0.575
65.0	0.408	410	1 1	0.271
100.0	0.1347	130	1 1	0.117
160.0	0.0521	47	1 1	0.0494
250.0	0.0158	13	1 1	0.0155

SECTION III

PHASE II TEST MODELS

The basic purpose of Phase II investigations was to produce design data relating the effect of contaminants, or operation in a contaminated environment, on the sealing capability of various closure configurations. Because this effort was experimental and flexible in nature, test fixtures and test models were used in place of real valve mechanisms for the evaluation. Test models fabricated and inspected with extreme precision were required to minimize extraneous influence on sealing performance.

Four test model configurations were utilized in the Phase II investigations. These were flat 440C, spherical 440C, flat carbide poppet on flat 440C seat, and shear seal. The first three versions were initially fabricated and tested in the previous program (Ref. 3) so that basic fabrication, inspection, and performance information was well documented. The shear seal geometry represented a radical departure from previous experience and, therefore, required additional analysis and initial-use experimentation to establish baseline performance.

To provide control and identification of test models, three-digit basic numerical designations were applied to each model configuration, and individual models were sequentially numbered.

DESCRIPTION

Flat 440C (100 Series)

This configuration was the major test vehicle for previous programs. It was readily fabricated and, because of lap finishing ease, had been thoroughly evaluated for sealing characteristics over a wide range of surface roughness conditions (0.1- to 6-microinch AA). The hardened 440C (R 58-62) also represented typical hard seating materials which were demonstrated to have very low leakage capability. With this substantial background, the flat 440C model was used for all static particle deformation tests and the bulk of Phase II dynamic testing.

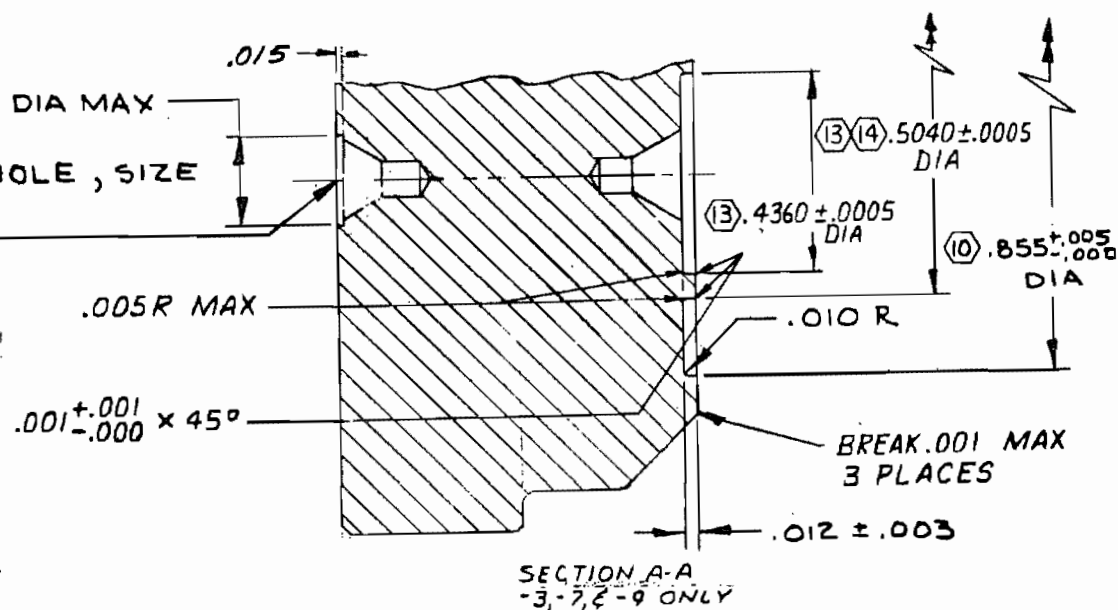
Figure III-1 and III-2 illustrate the flat 440C poppet and seat. Previous program test results indicated that seating land widths for both poppet and seat should be identical, and all 440C poppets were so reworked for this effort. As reported in subsequent test section, however, minimum poppet and maximum seat land chamfers resulted in a difference of several thousandths between poppet and seat lands, with the poppet overlapping the seat.

Spherical 440C (200 Series)

The concept of interfacial scrubbing, or shearing to remove contaminants from sealing surfaces, is directly (or indirectly) employed in many valve designs. Notable among configurations with considerable shearing action are the rotary types, such as ball or blade valves. For poppet and seat

OPTIONAL CENTER HOLE, SIZE
2 OR SMALLER
BOTH ENDS

HEAT TREAT	- 5 & -9 NONE - 3 NOTED (5) - 7 NOTED (6)
FINISH	- 5 & -9 NONE - 3 & -7 PASSIVATE PER RA0110-018
MAT'L	NOTED (1)(2)(3)(4)



14. CONCENTRIC WITHIN .0005 TIR
13. "S" SURFACE LEFT "AS GROUND"
12. FLAT WITHIN ONE HELIUM LIGHT BAND
11. CONCENTRIC WITHIN .001 TIR
10. PARALLEL WITHIN .0003
9. PARALLEL WITHIN .000050
8. PERPENDICULAR TO 1.4948 DIA WITHIN .0003 IN 1.5"
7. -7 HEAT TREAT 40-45 ROCKWELL "C" PER RA0111-014
6. -3 HEAT TREAT PER PR605-14 EXCEPT FINAL TEMPER TO PRODUCE R_c 58-62. MIN FINAL TEMPER 350° F
5. -9 6061-T651 AL ALLOY, QQ-A-325, TEMP T651 1-3/4 x .88 BAR
4. -7 17-4 PH CRES AMS 5643 1-5/7 DIA X .88 BAR
3. -5 TUNGSTEN CARBIDE ROCKWELL "A" 90-93 1-1/2 DIA X .88 BAR
2. -3 AISI TYPE 440C LB0160-151 1-5/8 DIA X .88 BAR
1. 32/ ALL SURFACES EXCEPT HOLE 63/

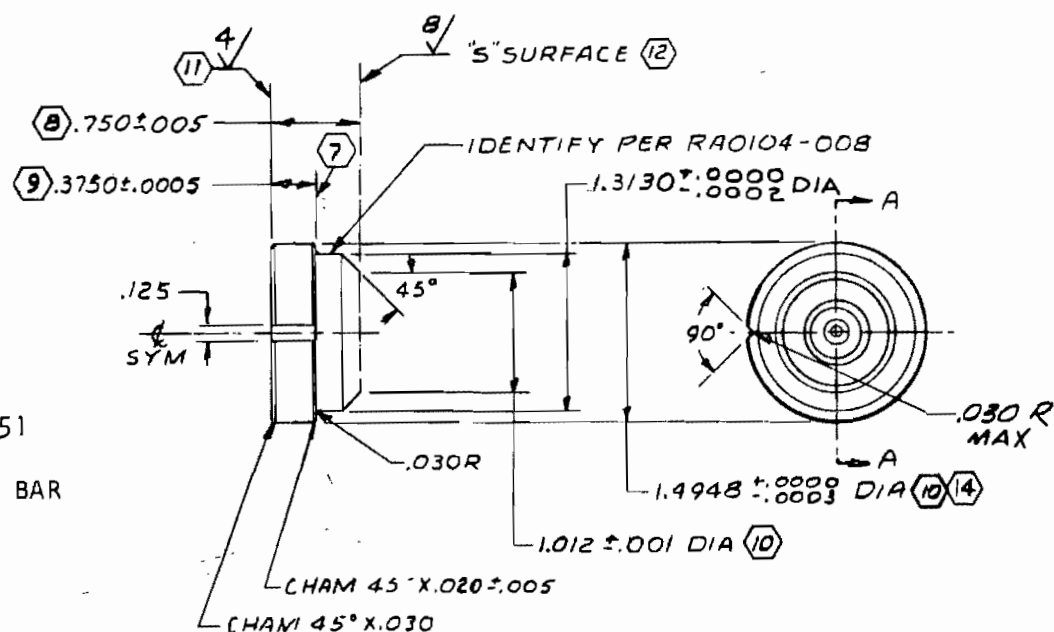


Figure III-1. Flat Model Poppet (Drawing No. 99-556528B1)

12. FLAT WITHIN ONE HELIUM LIGHT BAND
 11. CONCENTRIC WITHIN .0005 TIR
 10. CONCENTRIC WITH .0005 TIR
 9. PARALLEL WITHIN .000025
 8. PERPENDICULAR TO 1.5000 DIA WITHIN .0003 IN 1.5"
 7. -7 HEAT TREAT 40-45 ROCKWELL "C"
 6. -3 HEAT TREAT PER PR605-14 EXCEPT FINAL TEMPER TO PRODUCE $R_c 58-62$. MIN FINAL TEMPER 350°F
 5. -9 6061-T651 AL. ALLOY, QQ-A-325, TEMP T651 1-3/4 X .88 BAR
 4. -7 17-4 PH CRES AMS5643 1-5/8 DIA. X .88 BAR
 3. -5 TUNGSTEN CARBIDE ROCKWELL "A" 90-93 1-1/2 DIA. X .88 BAR
 2. -3 AISI TYPE 440C LB0160-151 1-5/8 DIA. X .88 BAR
 1. 32/ ALL SURFACES EXCEPT HOLE 63/

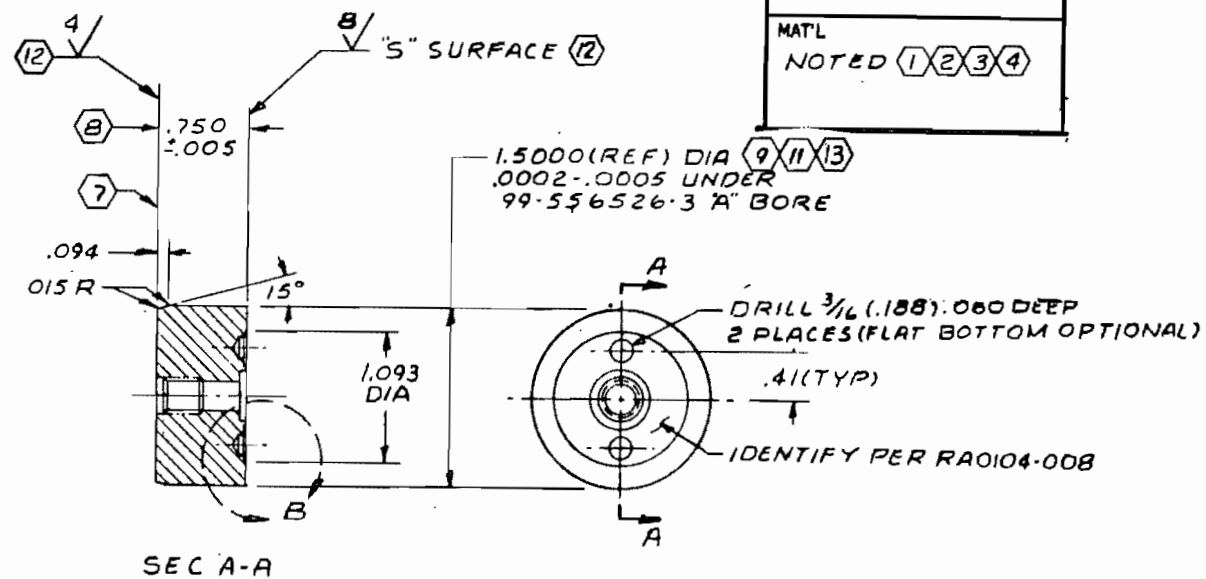
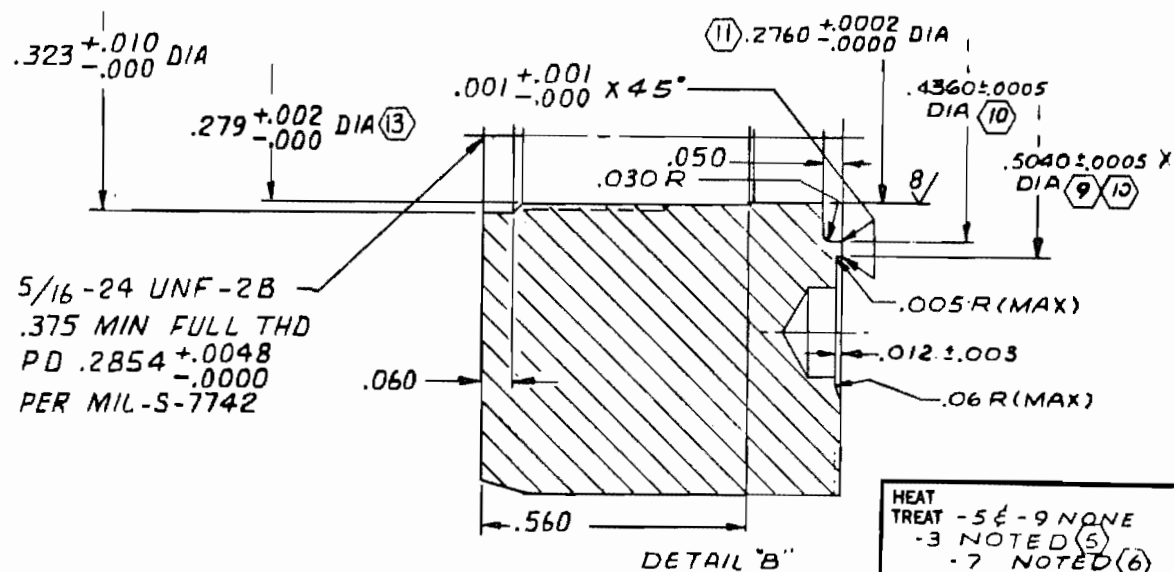


Figure III-2. 0.5-Inch Flat Model Seat (Drawing No. 99-556529B)

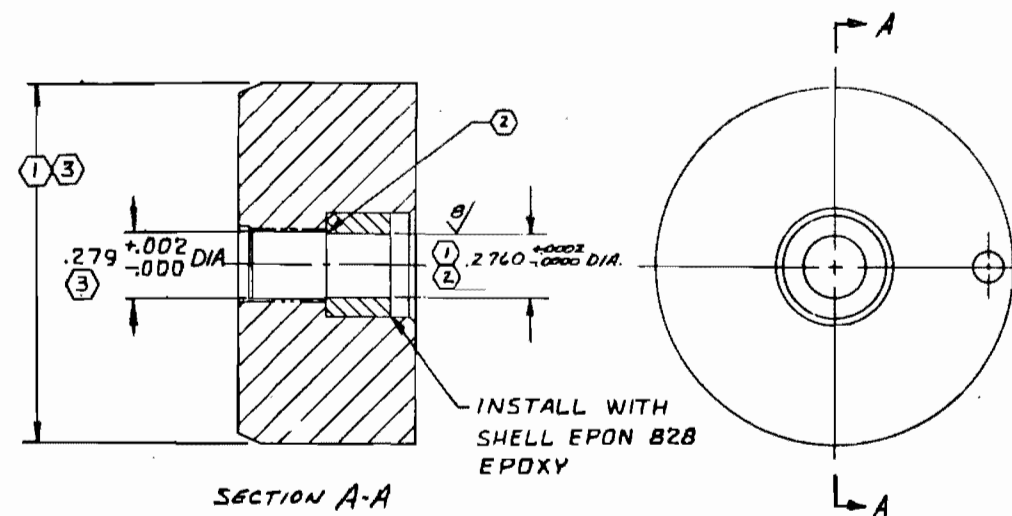
designs, a steep entrance angle is required to allow a type of shearing action to occur. As a means of evaluating this parameter for hard materials in a contaminated environment, and relating it to flat model performance, a spherical configuration was used (Fig. III-3 through III-6). This model employed a 20-degree seating angle and had been static tested in the previous program as model C_S. The seat was modified with a plug to eliminate an inlet counterbore void and for adaptation to the dynamic tester retaining bolt.

Shear Seal (300 Series)

While the deep entry spherical geometry provided a shearing feature, interfacial scrubbing resulted primarily from misalignment. Previous efforts with a male conical poppet entering a lip-type copper seat had indicated superior sealing ability, but contamination resistance was questionable (Ref. 5). This sealing approach was considered for Phase II to explore further the "shear sealing" principal for superior sealing and contamination resistance.

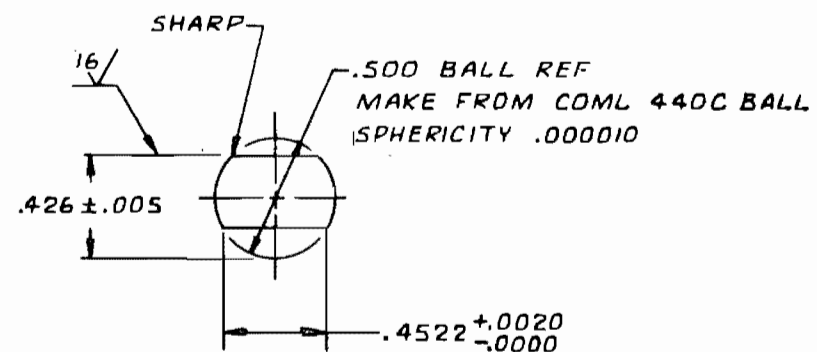
Various design approaches were considered for use with program testers. Because of the requirement for inlet flow through the seat, an inverted version of the usual conical poppet design was required to achieve lip seal pressure loading. The design finally resolved is detailed in Fig. III-7. In this version, the soft copper seating interface is initially plastically formed, and subsequent sealing loads result from elastic deformation of the copper tube. The seat (-4) and nut (-2) are retained in the tester by the bolt shown in phantom in Fig. III-7. Very small spots of either Loctite or Eastman 910 adhesive were applied 180 degrees opposed to the seat OD and nut cone for torque retention. Bottoming was ensured by a preassembly operation in which the seat was locked to the holder base with a 5/16 bolt and nut while the adhesive cured.

The closure design provides several advantages over the conventional conical poppet approach. The most notable advantage is the integral positive stop that is provided with a minimum of tight tolerances. This feature precludes significant seat impact. The conventional design (with male poppet) cannot be made practically with a positive stop because of excessive lengths resulting in tolerance problems and temperature change sensitivity. Because seat impact cannot be avoided and the sealing surface is plastically formed, splitting of the sealing lip is a potential failure mode. This cannot happen with the seat tube compressed by the external spherical poppet. The design shown in Fig. III-7 resulted from the elastic-plastic stress analysis presented in Appendix B. This analysis indicates that with 1000-psig inlet pressure, a load of about 52 pounds is required to form the seat and place the poppet against the seat stop. The developed land width is 0.0064 inch, with about 0.0004-inch axial springback predicted.

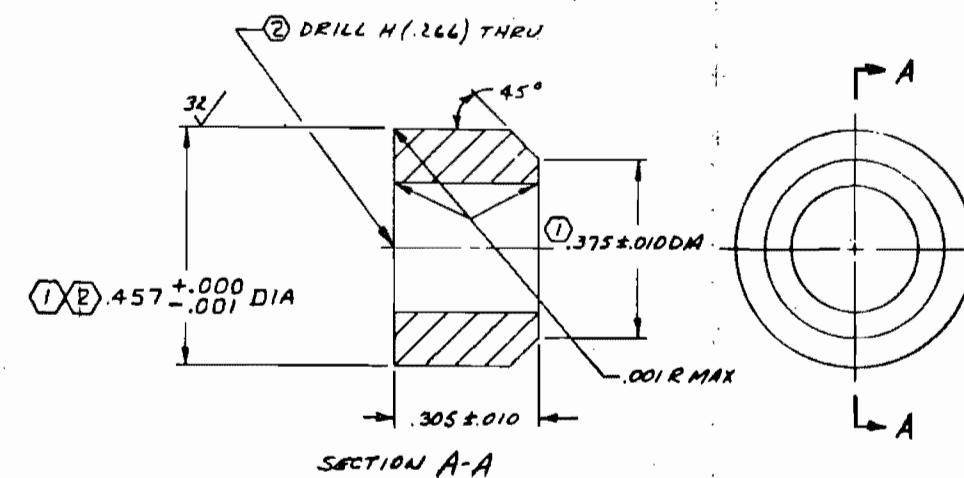


- SECTION A-A
1. MAKE FROM 99-557783-2 SEAT (REF. FIG. III-5) AND SK 6075 PLUG
 2. CONCENTRIC WITHIN .0005 TIR
 3. POLISH

SKETCH NO. 6076 SEAT & PLUG

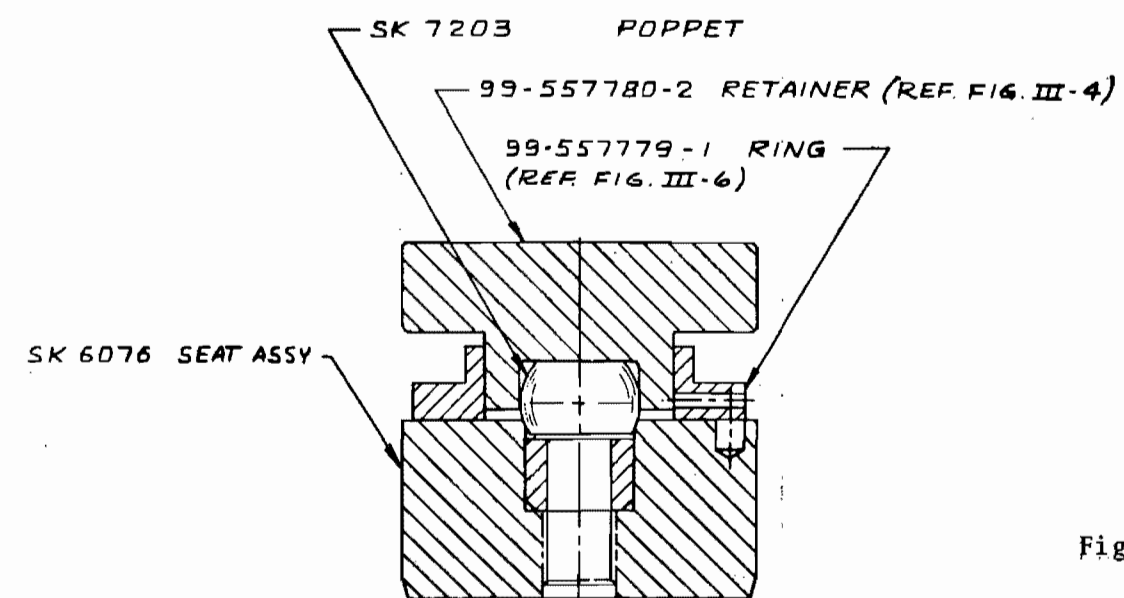


SKETCH NO. 7203 POPPET



- SECTION A-A
1. CONCENTRIC WITHIN .005 TIR
 2. MATL: A131 TYPE 440C CRES BAR (L60160-151)
 3. HEAT TREAT PER RADII-CN7 R_c 58-60

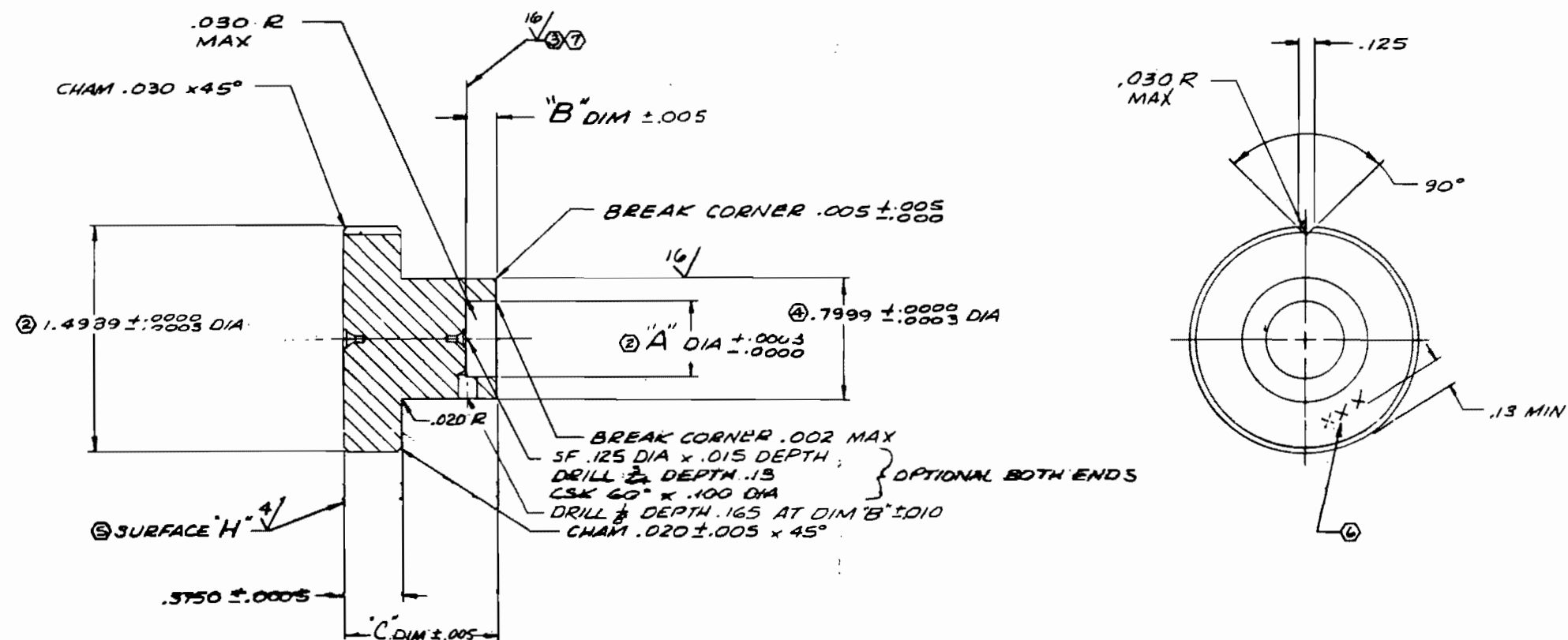
SKETCH NO. 6075 PLUG



SPHERICAL MODEL ASSEMBLY

Figure III-3. Spherical Model Assembly

DASH N°	"A" DIA	"B" DIM	(REF) FOR USE WITH SEAT ANGLE	"C" DIM
- 2	.5003	.200	39° 54'	.704
- 4	.5628	.250	66° 40'	.727
- 6	.6253	.400	82° 28'	.770



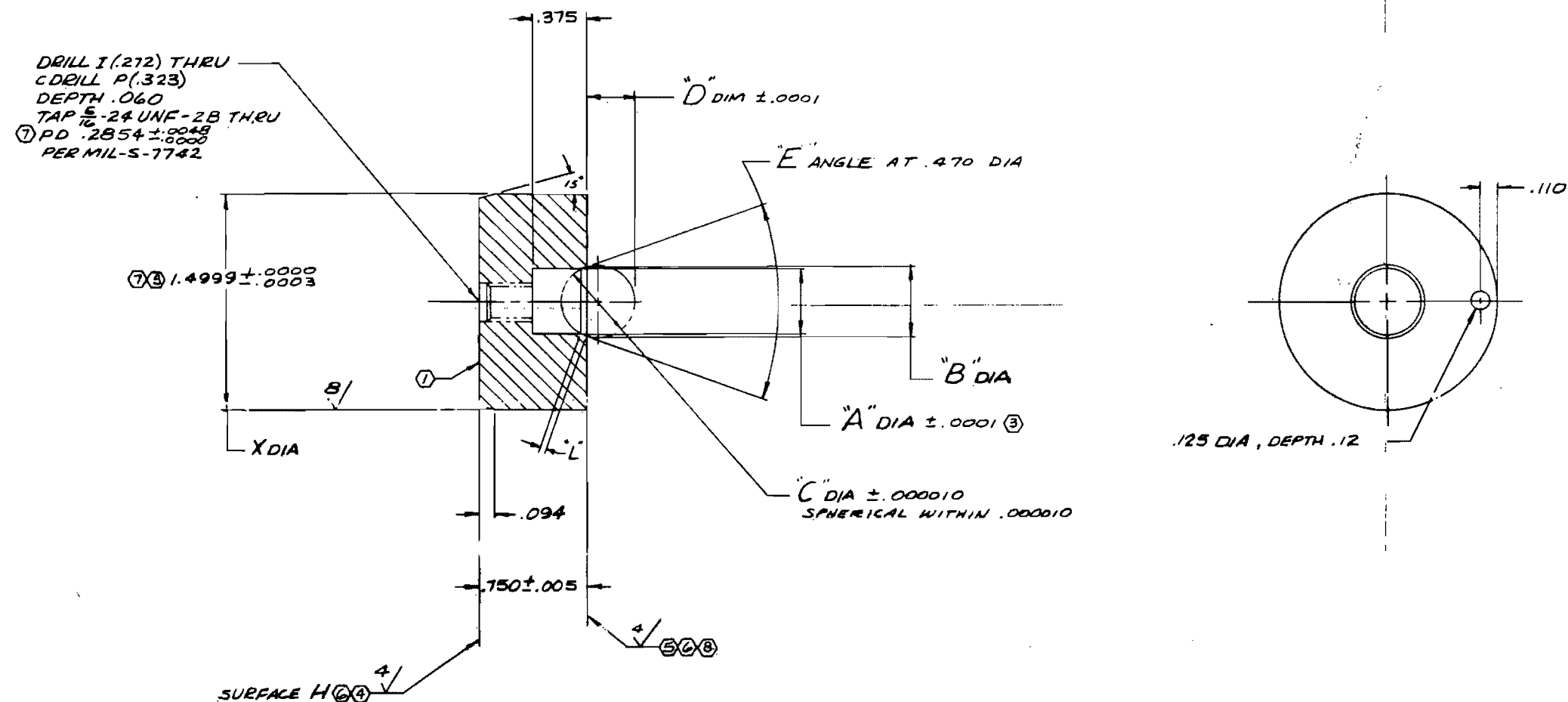
- ⑧ 8. FLAT WITHIN .0001 TOTAL
- ⑦ 7. IDENTIFY PER RA0104-008
- ⑥ 6. FLAT WITHIN .000010
- ⑤ 5. NORMAL TO SURFACE "H" WITHIN .0005 TOTAL
- ④ 4. MACHINE PER RA0103-002
- ③ 3. PARALLEL TO SURFACE "H" WITHIN .001 TOTAL
- ② 2. CONCENTRIC WITHIN .0002 T.I.R.
- ① 1. HEAT TREAT PER PRG05-14 EXCEPT FINAL TEMPER TO PRODUCE R_c 58-62. MINIMUM FINAL TEMPER 350 °F

NOTE: UNLESS OTHERWISE SPECIFIED

HEAT TREAT	⑦
FINISH	
MATL 440C CRES BAR 1 1/8 DIA x 1.12 L80160-151	

Figure III-4. Spherical Poppet Retainer
(Drawing No. 99-557780)

DASH N°	"A" DIA	"B" DIA (REF)	"C" BALL DIA	"D" DIM	"E" ANGLE (REF)	SEAT LAND "L" (REF)
-1	.4683	.4717	$\frac{1}{2}$ (.500)	.3330	39°54'	.005
-2	.4589	.4794	$\frac{1}{2}$ (.500)	.3211	39°54'	.030
-3	.4672	.4727	$\frac{3}{16}$ (.5625)	.4337	66°40'	.005
-4	.4531	.4858	$\frac{3}{16}$ (.5625)	.4231	66°40'	.030
-5	.4667	.4733	$\frac{3}{8}$ (.625)	.5166	82°28'	.005
-6	.4500	.4892	$\frac{3}{8}$ (.625)	.5070	82°28'	.030



8. 9. NORMAL TO "A" DIA WITHIN .0001 TOTAL
 7. 8. CONCENTRIC WITHIN .005 T.I.R.
 6. 7. FLAT WITHIN .000010
 5. 6. PARALLEL TO SURFACE H WITHIN .00010 TOTAL
 4. 5. NORMAL TO X DIA WITHIN .0003 TOTAL
 3. 4. CONCENTRIC WITHIN .0002 T.I.R.
 2. 3. HEAT TREAT PER PRGOS-14 EXCEPT FINAL TEMPER TO PRODUCE R_c 58-62. MINIMUM FINAL TEMPER 350 °F.
 1. 2. IDENTIFY PER RAD104-008.
 1. MACHINE PER RAD103-002.

NOTE: UNLESS OTHERWISE SPECIFIED

HEAT TREAT	②
FINISH	VAPOR DEGREASE
MAT'L 440C CRES	
BAR 1 5/8 DIA x .81	
LBO160-151	

Figure III-5. Spherical Seat (Drawing No. 99-557783)

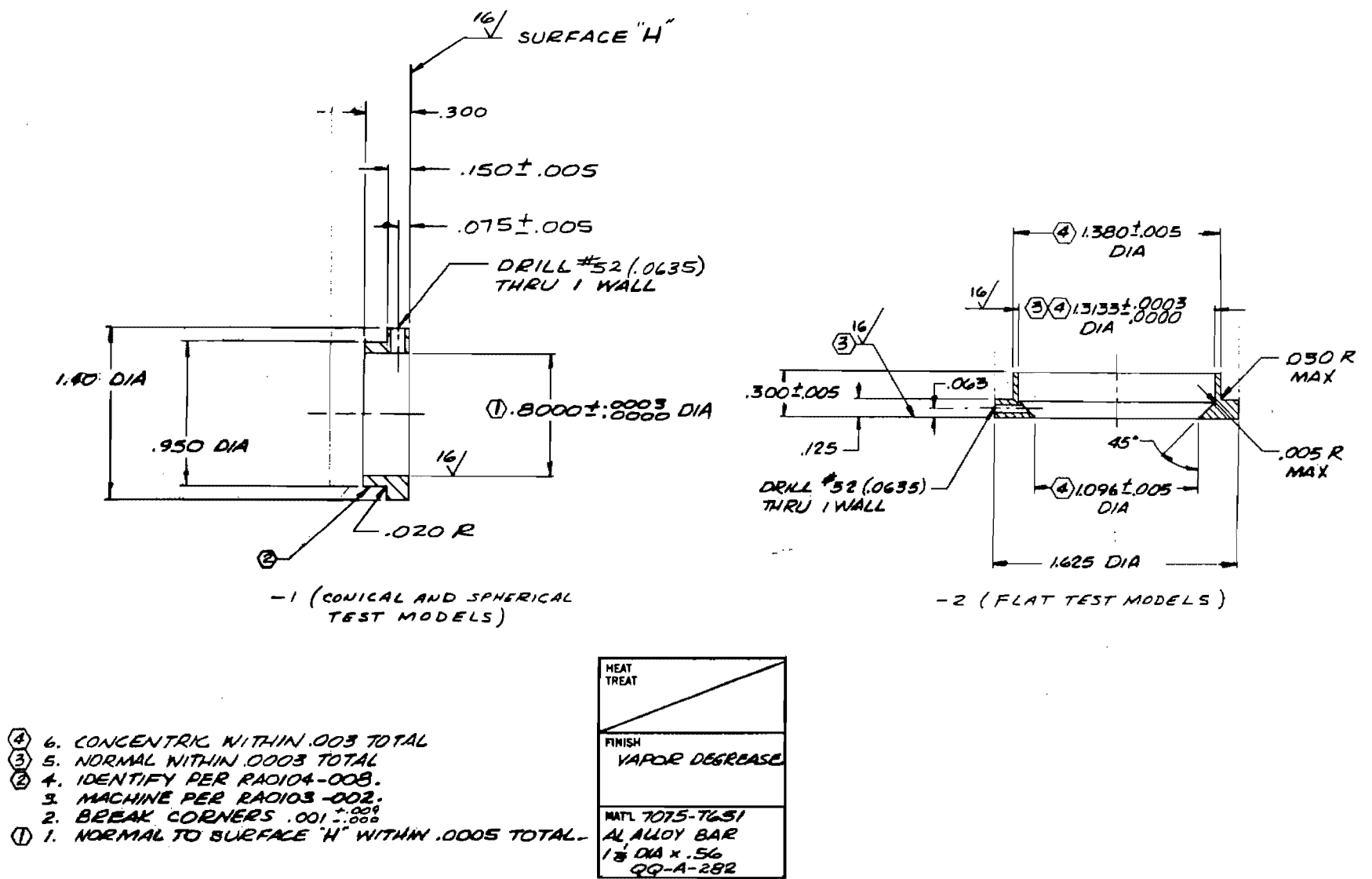
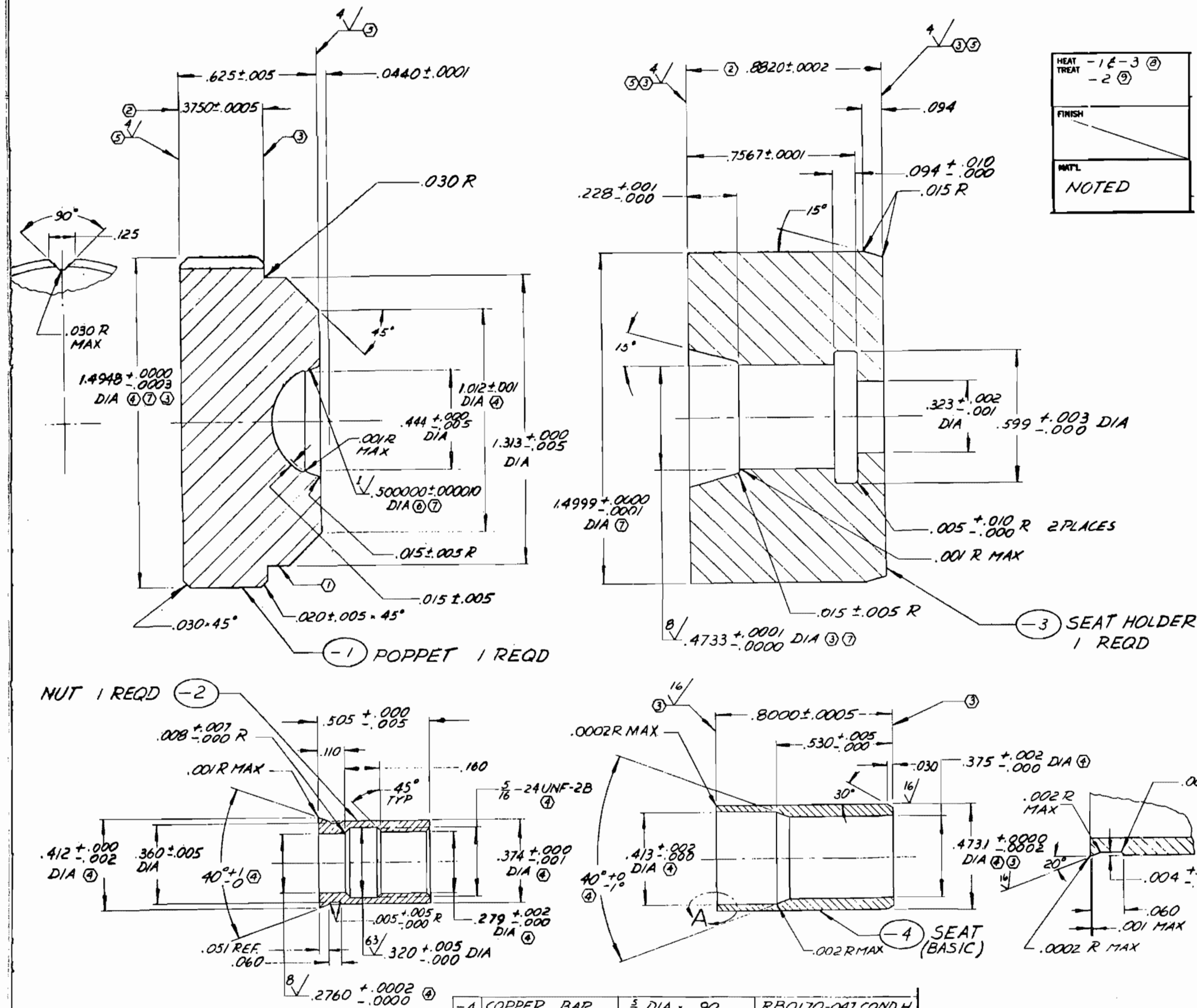


Figure III-6. Leak Volume Reducing Ring (Drawing No. 99-557779)



HEAT TREAT	-1 & -3 (2)
	-2 (9)
FINISH	
MATL	NOTED

- (9) 11. HEAT TREAT TO 180,000 TO 215,000 PSI (Rc 40-47) PER RA0111-016 COND. H 900
 (8) 10. HEAT TREAT PER PR605-14, EXCEPT: FINAL TEMPER TO PRODUCE Rc 58 to 62, MINIMUM TEMPERATURE DURING FINAL TEMPER 350°F.

9. ALL CORNER RADII .002 TO .008 IN.
 8. CONCENTRIC WITHIN .0001 T.I.R.
 7. SPHERICAL WITHIN .000010 IN.
 6. FLAT WITHIN ONE HELIUM LIGHT BAND
 5. CONCENTRIC WITHIN .001 T.I.R.
 4. PERPENDICULAR WITHIN .0003 IN.
 3. PARALLEL WITHIN .0003 IN.
 2. IDENTIFY PER RA0104-008
 1. ALL SURFACES ³²

NOTE: UNLESS OTHERWISE SPECIFIED

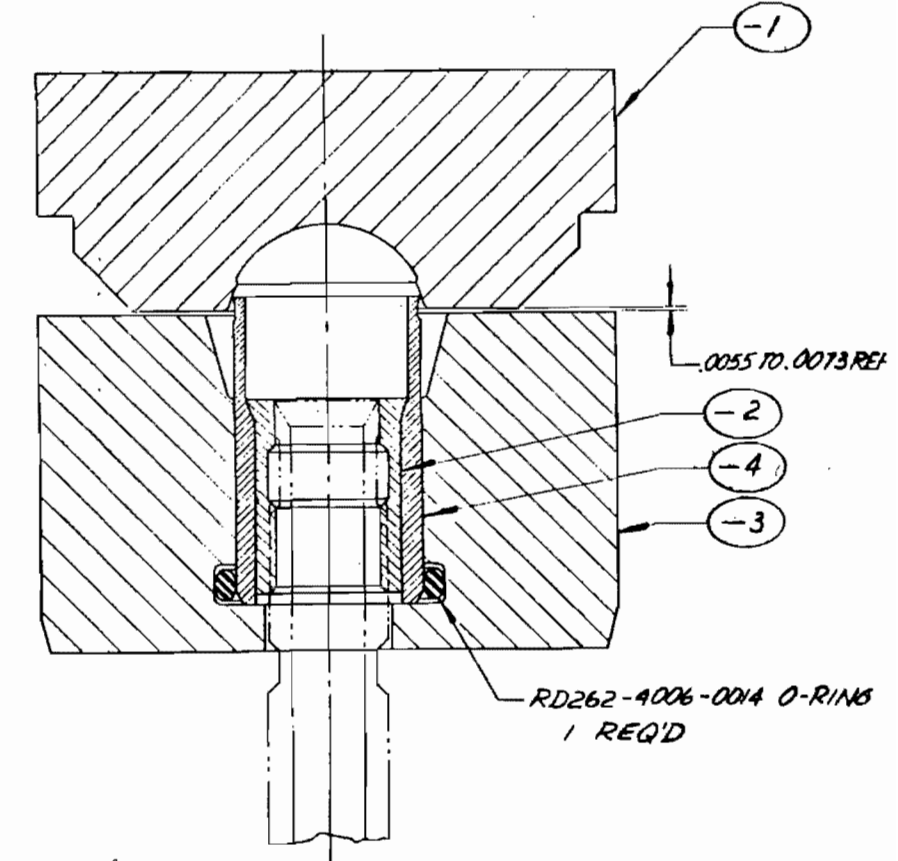


Figure III-7. Shear Seal Model (Sketch No. 6181)

Flat Carbide Poppet (400 Series)

This model employed a flat carbide poppet and a 440C seat for evaluation of contaminant effects on sealing performance where differential hardness between relatively hard seating materials existed. The seat was the same type used for the 100 series models (Fig. III-2). The poppet, while similar to the 100 series geometry (Fig. III-1), reflected the initial configuration where the seating face had no reliefs to produce a defined poppet land.

MODEL PREPARATION

The flat 440C, flat carbide, and spherical models used for Phase II testing all had been fabricated for previous program (Ref. 3) tests. Except for the seat land modifications to some flat 440C poppets, only refinishing of sealing lands was required for testing in this program.

Flat model surfaces were lapped with 1- to 5-micron diamond compound using the techniques described in Ref. 3. Polishing with 1- to 5- or 0- to 1-micron diamond compound on paper to dub (slightly radius) seating land corners completed the process and produced surface roughnesses ranging from about 0.3 to 0.6 microinch AA. Flat lapping operations were performed at the static test facility site where inspection equipment also was located.

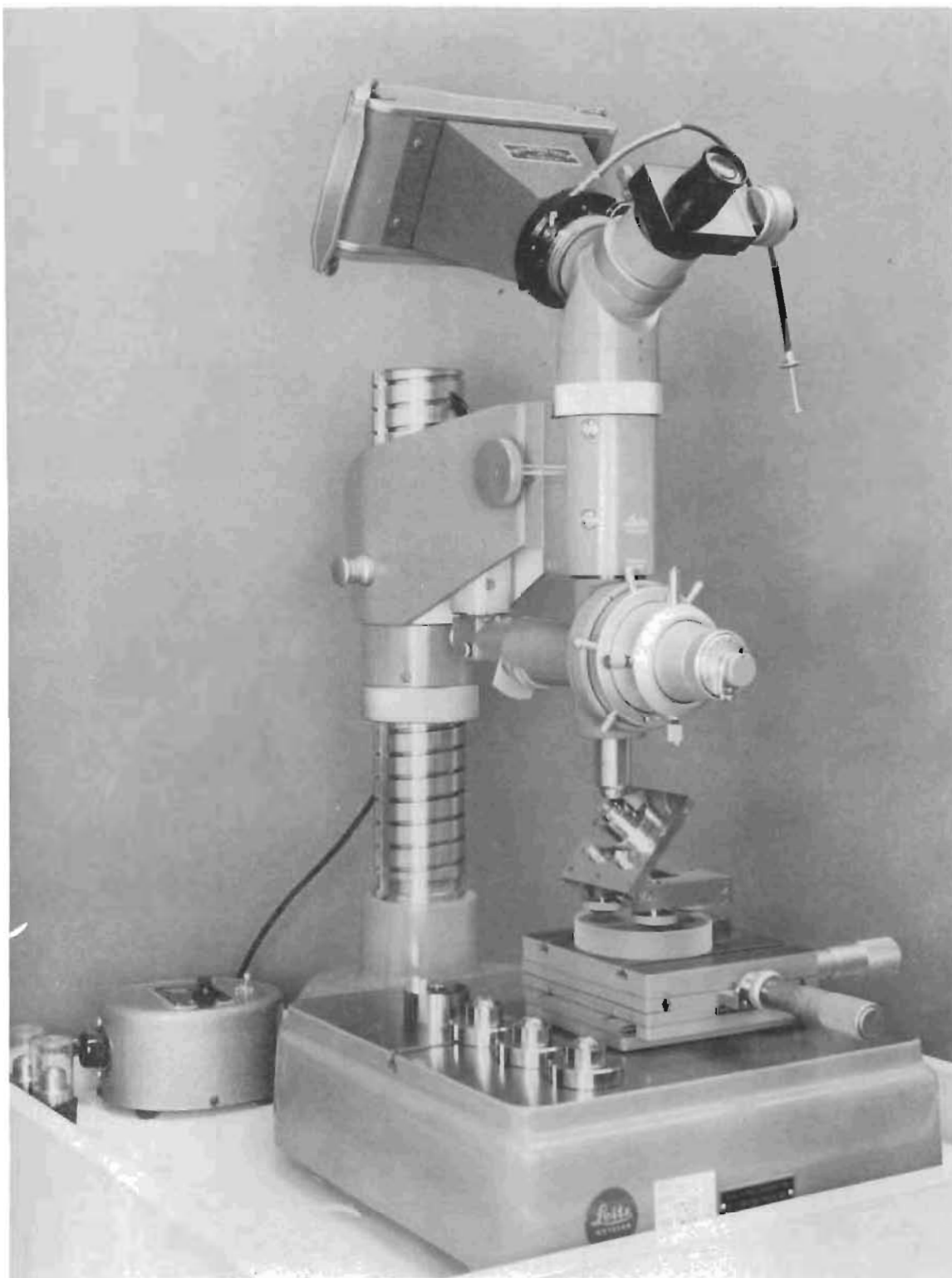
The spherical model seat (as well as the shear seal poppet) was refinished with 0- to 1/4-micron diamond using the lathe ball lapping sequence reported in Ref. 3. The poppet (ball) required no finish preparation other than cleaning.

No lapping or polish finish operations were used for the shear seal seat inserts. Smooth, nearly burr-free seating corners were generated by the intersection of diametral and face-turning finishes of better than 16 microinches AA and left as is. The resultant burr was less than 0.0002 inch. Ultimate seat land finish was developed from plastic deformation of the seat corner by the less-than-1-microinch AA poppet.

MODEL INSPECTION

Deduction of model seating geometry and surface characteristics was accomplished primarily with a Leitz interference microscope and techniques described in Ref. 3. This microscope, shown in Fig. III-8, was the basic inspection tool used for all model surface and damage assessments. Supplementary equipment, such as the Johansson Mikrokator comparator (for parallelism measurements), was used as required; operation and capabilities of this and other auxiliary items also are reviewed in Ref. 3.

Specific posttest inspection techniques and procedures unique to certain models and requirements are discussed in applicable test sections.



CAD41-3/16/66-C11

Figure III-8. Leitz Interference Microscope With Conical Poppet on Leveling Table

SECTION IV

PHASE II STATIC TESTS

The purpose of Phase II static tests was to determine what effect the entrapment of specific particulate material would have on the sealing performance of given poppet and seat closures. This information had a twofold application. It would establish fundamental, controlled data relating particle envelopment loads, influence of entrapped particulates on closure leakage, sealing degradation resulting from particle-caused surface damage, and characteristics of the deformed particle and sealing surface disturbances. Also, from a review of the results, design criteria leading to improved closure designs for contaminated environment service could be developed and applied in Phase III--Demonstration design and testing.

To isolate and separate sealing influence variables, precision model closures of known geometry and dimensions were utilized. Evaluation of these models required, in turn, a test fixture of commensurate precision. This device provided for mounting and loading the test models with concurrent leakage measurements.

Static test problems involving both procedures and the test fixture were encountered. These, together with lengthy dynamic system development, precluded performance of numerous repeat tests wherein statistical confidence could be established. Three particle sizes, in two hardness ranges were ultimately investigated with a flat poppet and seat configuration. To a great extent, therefore, the static tests constituted a developmental rather than experimental effort.

Even though somewhat limited, Phase II static testing did produce data applicable to the intended goals. Furthermore, in the course of the experiments, additional parametric influences on sealing performance were uncovered.

GENERAL APPROACH

The evaluation of a poppet and seat model with test particles involved both the test equipment and a sequence of operations and procedures which are reviewed on a general basis in the following subsections. Detailed descriptions of the test fixture, system, and operating procedures are presented in Appendixes C, D, and E.

Test Model

All Phase II static testing utilized the flat 400C poppet and seal model described in Section III (Fig. III-1 and III-2). "Flat" land width and diameters were measured interferometrically at 500X magnification. This was necessary because all lands were dubbed (slight radius) by polishing

to preclude excessive stress concentration at the edges. The flat land was defined as extending to the point where the amount of duboff equalled the peak-to-valley surface roughness. In lieu of detailed surface assessment, model seating lands were inspected for gross flaws and general conformance to approximately a 0.5-microinch AA roughness. Stress-leakage testing then established the model's sealing characteristic and, ultimately, dictated acceptance for subsequent testing.

Test Fixture

The static test fixture provided for application of seat inlet and loading pressures and the collection of leakage. It consisted essentially of a hydrostatic bearing which permitted accurate loading of model surfaces by pressurization of the resultant free-floating piston. The model seat was clamped to the tester base while the poppet was mounted on a piston ball joint to permit nonrestrained conformance with the seat.

During the static test effort, a potential center-of-load misalignment in the ball joint mechanism was discovered. This problem, termed eccentric loading, resulted in small but significant torque loads being applied to the seating surfaces and influenced test data to varying degrees. After the problem was initially considered, a 0.001-inch shim was installed around the ball joint to reduce radial excursions. While this did not solve the problem entirely, it significantly curtailed eccentric loads during later model testing. A detailed analysis of the eccentric load phenomenon and its influence on test results, together with other potential error inputs, is presented in Appendix C.

Stress-Leakage Test

Test model performance, with or without contaminant particles, was determined by stress-leakage testing. This consisted of incrementally loading the pressurized poppet and seat, and measuring leakage at each load (stress) level. Seat stress was based on the flat land projected area; hence, it is apparent and not real contact stress. Seat stress varied from approximately 300 psi to 30,000 psi with data taken at intervals of increasing and decreasing load. The initial stress leakage test of a new model was considered the control test and provided baseline data from which sealing performance with entrapped particles were evaluated.

Particle Size, Quantity, and Placement

Both hard and soft spherical nickel alloy test particles of the types described in Section II were employed for static tests. Three sizes (15, 30, and 60 microns) were used to approximate the nominal sizes obtained with the classified material. As described in Appendix E, test particles were individually selected at 100X magnification with an estimated maximum sizing error of ± 2 microns.

To ensure that test loads were applied directly to the particles, and could be considered on a unit basis, three particles were generally used. These were placed at 120-degree intervals, on center, around the seating land circumference. A remote-operated handling fixture was employed for the selection and placement operation. This also is described in detail in Appendix E.

Test Sequence

Each test model was subjected to a series of operations which constituted the data acquisition sequence for that model and a given particle size. The following tabulation lists the general test sequence.

1. Finish and inspect test model.
2. Clean and assemble into tester with volume-reducing leak collector ring, Fig. III-6.
3. Perform control stress-leakage test; evaluate for acceptability.
4. Remove poppet from tester and add test particles.
5. Reinstall poppet in tester and perform particle stress-leakage test.
6. Remove model from tester, inspect deformed surfaces and particles, and remove particles.
7. Clean model and reassemble into tester; perform final stress-leakage test.
8. Review stress-leakage data for particle and surface damage influence on model sealing capabilities.

DATA PRESENTATION

Several forms of data presentation are employed in ensuing discussions of test results. The following describes format, source, and interpretation procedures used in compiling these data.

Stress-Leakage Data

The stress-leakage characteristic curves obtained with each model constitute the primary output data for Phase II static testing. Actual data points are shown and the interconnection of these points represents a best-fit plot of the information. Arrows on the curves indicate the direction of recorded data, i.e., increasing or decreasing stress levels similar to hysteresis loops. In the case of control data, the plot represents stabilized performance characteristics. For particle deformation testing, first-load data are presented.

Test numbers indicate the testing sequence with each new number representing a surface separation, partial or complete model removal from the tester, and subsequent reinstallation. All control tests, initial and after particle removal, were performed at 1000-psig supply pressure. Some of the

early models, however, were particle tested at one or several reduced inlet pressures. To permit consistent data presentation and facilitate comparison, all stress-leakage curves are plotted for 1000-psig inlet pressure conditions. Conversion of reduced-pressure leakage data to 1000 psig was done on a laminar, laminar-molecular, or turbulent flow basis, as described in the leakage flow analysis of Section II.

In conjunction with the aforementioned eccentric load problem and analysis, all control test data were reviewed for evidence of eccentric load influence. Except where specifically noted in test model discussions, these data are considered representative down to, at least, the 600-psi stress level, particularly for reduced pressure tests.

Stress-leakage data taken after particle removal usually indicated sealing degradation. This may have been solely attributed to surface damage or might include some eccentric load input. However, because all adverse effects are included, the data conservatively indicate worst conditions. Particle test stress-leakage results may also reflect eccentric load influence. In most cases such potential input, if any, may be considered submerged by particle effects.

Model Inspection and Performance Data

Table IV-1 presents a summary of pertinent model description, inspection, and comparative performance data. Introduction of the 0.001-inch tester ball joint shim is indicated by data separation into eccentric and concentric loading groups. The omitted sequential model numbers represent test failures and models used either for specialized investigations or Phase II dynamic testing. Test failures were declared when control data indicated inadequate model surface preparation or excessive eccentric loading effects and when model damage, invalidating its worth, occurred during a test sequence.

The test particle information following model description is denoted by specific size and letter-coded to indicate material type. Thus, an S15 particle is the soft (R_C 17-21), 15-micron size while an H30 particle is hard (R_C 62-67) and 30 microns in diameter. A complete description of the test particles used is presented in Section II.

Selected leakage information at three stress levels is presented in Table IV-1 for comparison purposes. These data are taken from the increasing load portion of the appropriate stress-leakage curves.

Concluding Table IV-1 are data relating control and particle test conformance characteristics. Leakage conformance is defined as that stress (load) at which particle-caused leakage is reduced to 10 times that of the control condition. It is subsequently referred to as 10:1 conformance.

TABLE IV-1
PHASE II STATIC TEST MODEL DATA

Model Designation and Description								Test Particle Data		1000-psig Nitrogen Leakage, scim at Noted Conditions and Stress Levels									Control vs Particle Conformance Data			
Model ⁽¹⁾	Poppet			Seat						Initial Control Data			With Particles			After Particle Removal			10:1 Leakage Ratio		Inte Con	
	Serial No.	Mean Diameter (D _s), inches	Flat Land Width (L), inches	Serial No.	Mean Diameter (D _s), inches	Flat Land Width (L), inches	Seat Area (A _{sp}), sq in.			Type ⁽²⁾ and Size	Quantity ⁽³⁾	300 psi	1000 psi	3000 psi	300 psi	1000 psi	3000 psi	300 psi	1000 psi	3000 psi	Load, pounds	Stress, psi
Tests With Potential Eccentric Loading																						
102	07	0.4710	0.0322	03	0.4696	0.0284	0.0418	S50	3	0.06	0.040	0.022	15,000	5,000	1.6	0.15	0.042	0.021	309	7,400	125	
103	06	0.4688	0.0325	04	0.4689	0.0253	0.0373	S30	1	0.10	0.039	0.023	220	0.12	0.039	--	--	--	19	500	22	
106	01	0.4697	0.0335	011	0.4695	0.0291	0.0429	S30	2	0.064	0.032	0.02	80	0.084	0.029	--	--	--	25	580	34	
108	04	0.4699	0.0299	06	0.4691	0.0264	0.0390	S30	3	0.07	0.011	0.0042	110	0.18	0.019	0.029	0.011	0.004	59	1,500	31	
112	08	0.4688	0.0319	08	0.4692	0.0275	0.0405	S15	3	0.032	0.016	0.0082	0.07	0.022	0.0090	0.057	0.019	0.0088	--	--	12	
112								S30	3	--	0.020	0.0090	3,000	66	0.032	0.088	0.022	0.0085	61	1,500	61	
112								S60	3	0.088	0.022	0.0085	12,000	2,400	4.3	--	--	--	607	15,000	81	
118	010	0.4712	0.0300	01	0.4686	0.0277	0.0408	S15	3	--	0.014	0.0068	--	0.015	0.0068	--	--	--	--	--	12	
Tests With Concentric Loading (0.001-Inch Ball Joint Shim)																						
119	06	0.4687	0.0304	04	0.4689	0.0238	0.0351	S15	9	0.05	0.018	0.0078	270	0.10	0.12	0.60	0.021	0.0080	31	880	35	
119								S30	3	0.60	0.021	0.0080	--	0.23	0.042	0.11	0.024	0.0086	39	1,100	25	
119								S60	3	0.11	0.024	0.0086	--	--	6.80	0.39	0.032	0.011	597	17,000	70	
123	02	0.4688	0.0309	06	0.4690	0.0279	0.0411	H15	9	0.037	0.0066	0.0036	--	0.017	0.0042	--	--	--	25	600	41	
124	08	0.4695	0.0332	011	0.4696	0.0279	0.0411	H15	9	0.095	0.035	0.019	--	0.052	0.021	--	--	--	--	--	41	
125	02	0.4688	0.0319	06	0.4689	0.0269	0.0396	H30	3	0.047	0.0035	0.0015	--	2,400	0.80	0.18	0.0041	0.0014	174	4,400	32	
125								H60	3	0.18	0.0041	0.0014	--	6,100	550	1.42	0.012	0.0018	752	19,000	99	

⁽¹⁾ Flat lapped 440C models; poppet P/N 556528B-3, seat P/N 556529B-3
⁽²⁾ Nickel alloy spheres sized to ±2 microns. Letter prefix indicates hardness S(R_C 17-21) and H(R_C 62-67), numerals indicate size, microns
⁽³⁾ On land center equally spaced except 2 particles (103) placed 120 degrees apart

TABLE IV-1
PHASE II STATIC TEST MODEL DATA

Model Designation and Description						Test Particle Data		1000-psig Nitrogen Leakage, scim at Noted Conditions and Stress Levels									Control vs Particle Test Conformance Data				Computed Particle Envelopment Data		Model
Poppet		Seat																					
Mean Diameter (D _s), inches	Flat Land Width (L), inches	Serial No.	Mean Diameter (D _s), inches	Flat Land Width (L), inches	Seat Area (A _{sp}), sq in.			Initial Control Data			With Particles			After Particle Removal			10:1 Leakage Ratio		Interface Contact				
								Type ⁽²⁾ and Size	Quantity ⁽³⁾	300 psi	1000 psi	3000 psi	300 psi	1000 psi	3000 psi	300 psi	1000 psi	3000 psi	Load, pounds	Stress, psi	Load, pounds	Stress, psi	
Tests With Potential Eccentric Loading																							
0.4710	0.0322	03	0.4696	0.0284	0.0418	S50	3	0.06	0.040	0.022	15,000	5,000	1.6	0.15	0.042	0.021	309	7,400	125	3000	128.0	3060	102
0.4688	0.0325	04	0.4689	0.0253	0.0373	S30	1	0.10	0.039	0.023	220	0.12	0.039	--	--	--	19	500	22	600	46.2	1240	103
0.4697	0.0335	011	0.4695	0.0291	0.0429	S30	2	0.064	0.032	0.02	80	0.084	0.029	--	--	--	25	580	34	800	46.2	1080	106
0.4699	0.0299	06	0.4691	0.0264	0.0390	S30	3	0.07	0.011	0.0042	110	0.18	0.019	0.029	0.011	0.004	59	1,500	31	800	46.2	1180	108
0.4688	0.0319	08	0.4692	0.0275	0.0405	S15	3	0.032	0.016	0.0082	0.07	0.022	0.0090	0.057	0.019	0.0088	--	--	12	300	11.5	284	112
						S30	3	--	0.020	0.0090	3,000	66	0.032	0.088	0.022	0.0085	61	1,500	61	1500	46.2	1140	112
						S60	3	0.088	0.022	0.0085	12,000	2,400	4.3	--	--	--	607	15,000	81	2000	184.0	4540	112
0.4712	0.0300	01	0.4686	0.0277	0.0408	S15	3	--	0.014	0.0068	--	0.015	0.0068	--	--	--	--	--	12	300	11.5	282	118
Tests With Concentric Loading (0.001-Inch Ball Joint Shim)																							
0.4687	0.0304	04	0.4689	0.0238	0.0351	S15	9	0.05	0.018	0.0078	270	0.10	0.12	0.60	0.021	0.0080	31	880	35	1000	34.5	985	119
						S30	3	0.60	0.021	0.0080	--	0.23	0.042	0.11	0.024	0.0086	39	1,100	25	700	46.2	1320	119
						S60	3	0.11	0.024	0.0086	--	--	6.80	0.39	0.032	0.011	597	17,000	70	2000	184.0	5250	119
0.4688	0.0309	06	0.4690	0.0279	0.0411	H15	9	0.037	0.0066	0.0036	--	0.017	0.0042	--	--	--	25	600	41	1000	34.5	840	123
0.4695	0.0332	011	0.4696	0.0279	0.0411	H15	9	0.095	0.035	0.019	--	0.052	0.021	--	--	--	--	--	41	1000	34.5	840	124
0.4688	0.0319	06	0.4689	0.0269	0.0396	H30	3	0.047	0.0035	0.0015	--	2,400	0.80	0.18	0.0041	0.0014	174	4,400	32	800	46.2	1170	125
						H60	3	0.18	0.0041	0.0014	--	6,100	550	1.42	0.012	0.0018	752	19,000	99	2500	184.0	4650	125

models; poppet P/N 556528B-3, seat P/N 556529B-3

eres sized to ±2 microns. Letter prefix indicates hardness S(R_c 17-21) and
erals indicate size, microns

qually spaced except 2 particles (103) placed 120 degrees apart

Interface contact indicates the loads at which particles are sufficiently deformed and enveloped to permit general contact of seating surfaces. This is presumed to be represented by a change in the stress-leakage curve where leakage sensitivity to load change diminishes noticeably. Computed particle envelopment loads are derived from the analysis of Section II and review of pertinent stress-leakage data and are discussed in a subsequent subsection (Data Analysis).

Particle Damage Data

The final form of data presentation is photographic evidence of deformed particle and surface damage characteristics. All models and virtually all particles were photographed in the course of posttest inspection. Typical photos of pertinent characteristics are presented in various following subsections. The summarization of particle and surface dimensions later discussed was prepared from study of similar photographs and notes taken during microscopic inspection.

MODEL TESTS

A description of Phase II static tests and their purpose and the resulting stress-leakage data are presented herein on a model basis. Correlation and discussion of the data and conclusions derived therefrom follow in a subsequent subsection.

Test Model 102

This model constituted the initial entrapped particle test. In the course of establishing procedures, three S50 particles instead of the S60 size were mistakenly selected. Because the test was successful, with all three particles retained and no particular evidence of eccentric loading effects, it is presented for comparison with S30 and S60 results. Figure IV-1 illustrates the stress-leakage data.

Test Models 103, 106, and 108

These models represented attempts to test a single model surface with three particles and presented the first static test problem, that of particle loss. With Model 103, Fig. IV-2, only one particle was found in posttest inspection with no evidence (surface damage) of the other two particles having been trapped. As there was no previous test experience with 30-micron particles, the stress-leakage data, as acquired, appeared reasonable and the test ran its course.

Model 103 and previous Model 102 were inspected after poppet installation into the tester to verify particle placement. With the aid of a fiber optics "light pipe" for side lighting, the S50 particles were plainly viewed with the naked eye. Similarly, it was believed that the S30 particles of Model 103 had been seen. This might not have been the case and a dust particle may, by a sparkling appearance, have been misinterpreted as a test particle. Therefore, a 40X magnification microscope and adjustable base arrangement was set up for later model inspections.

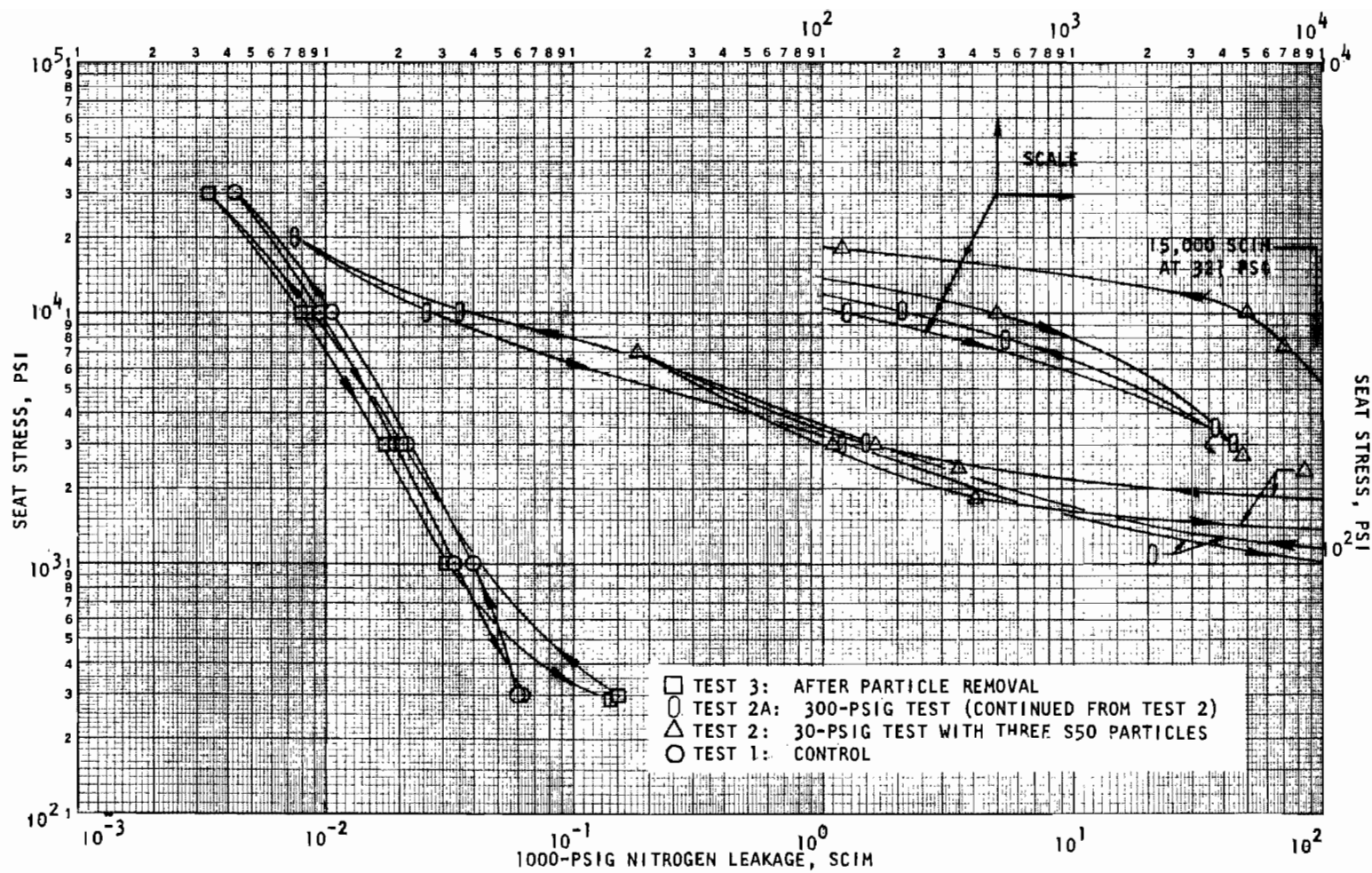


Figure IV-1. Stress-Leakage Data for Static Test Model 102, Tests 1, 2, and 3

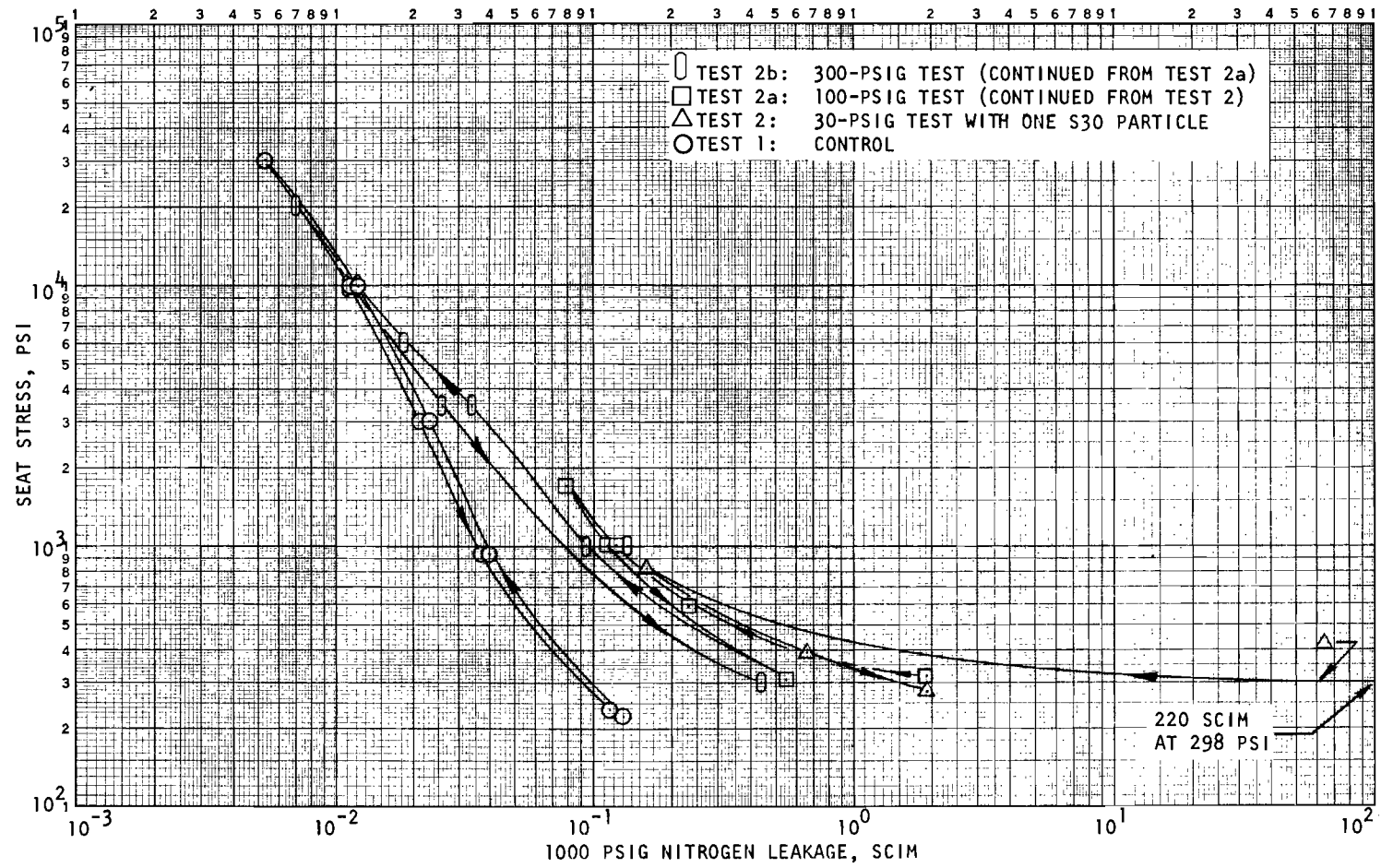


Figure IV-2. Stress-Leakage Data for Static Test Model 103, Tests 1 and 2

With the microscope, three S30 particles were verified in place on Model 106 prior to closure. As with Model 103, a marked leakage increase above control values indicated particles in place and Model 106 test was completed (Fig. IV-3). Inspection indicated that only two particles had ultimately been trapped.

Because of the particle loss phenomenon, Models 103 and 106 were initially termed failures because the three-particle-test intent had not been fulfilled. Thus, no final stress-leakage test after particle removal was performed. When later recognized as contributing useful data, the models had already been refinished and the residual effects test information could not be acquired.

Model 108 was the last in this series of early tests and proved to be successful from a particle standpoint with all three found entrapped after test. The particle stress-leakage data of Fig. IV-4 is extrapolated above 3000 psi because the reduced volume leak collector was omitted and the large tester leak volume resulted in potential measurement error (Appendix D, Leakage Measurement). Control stress-leakage data indicated potential eccentric load influence below 1000-psi stress. This was further substantiated by data obtained after particle removal where leakage at low stress was less than that of the control test.

Test Model 112

This model represented a procedural change point wherein several test method innovations were adopted. Preceding test results indicated that minimal residual effect (after particle removal) was evident from comparison control tests. This indicated that particles of several sizes could be tested on one model surface with residual influences submerged by the larger particles' effect. As this approach would facilitate comparison of particle size data without a variable surface roughness parameter, it was tried with Model 112.

The particle loss problem noted with preceding models also led to procedural changes. The O-ring leak collector was supplanted by an aluminum version. Remote model closure with entrapped particles by piston pressurization was replaced by mechanical closure with handwheel adjustment. (Detail procedures for the preceding are described in Appendix E.) After these changes were adopted, no further instance of particle loss prior to, or during, closure occurred.

Model 112 was tested with three each S15, S30, and S60 particles in ascending size order. Control data for each successive size was obtained from the post-particle removal test of the preceding size. For clarity, stress-leakage data are presented in two plots, Fig. IV-5 (S15) and IV-6 (S30 and S60). It will be noted that Tests 4, 5, and 6 have been omitted. This series was negated by a procedural error and is not presented. Some surface degradation occurred, however, and caused the difference in control

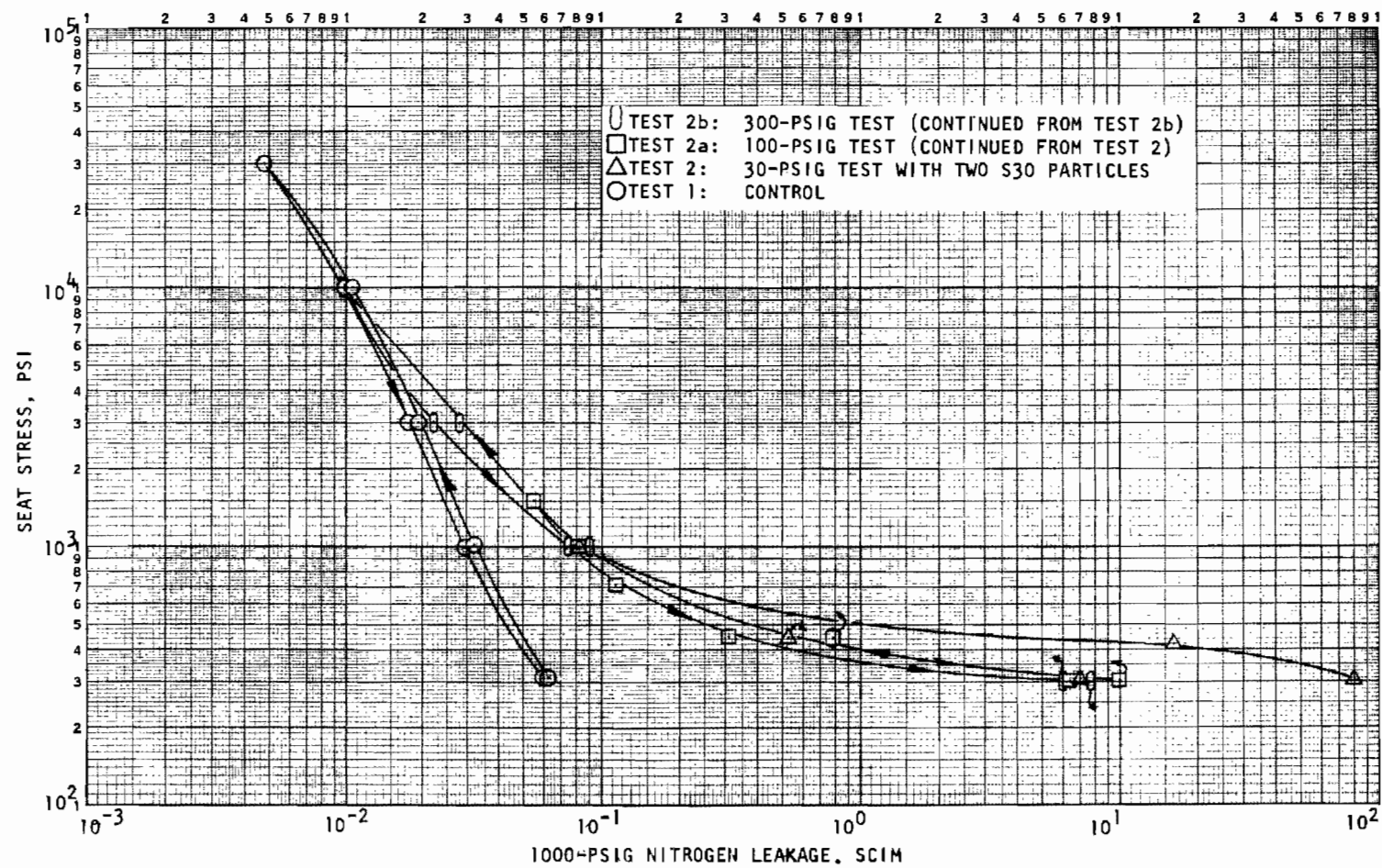


Figure IV-3. Stress-Leakage Data for Static Test Model 106, Tests 1 and 2

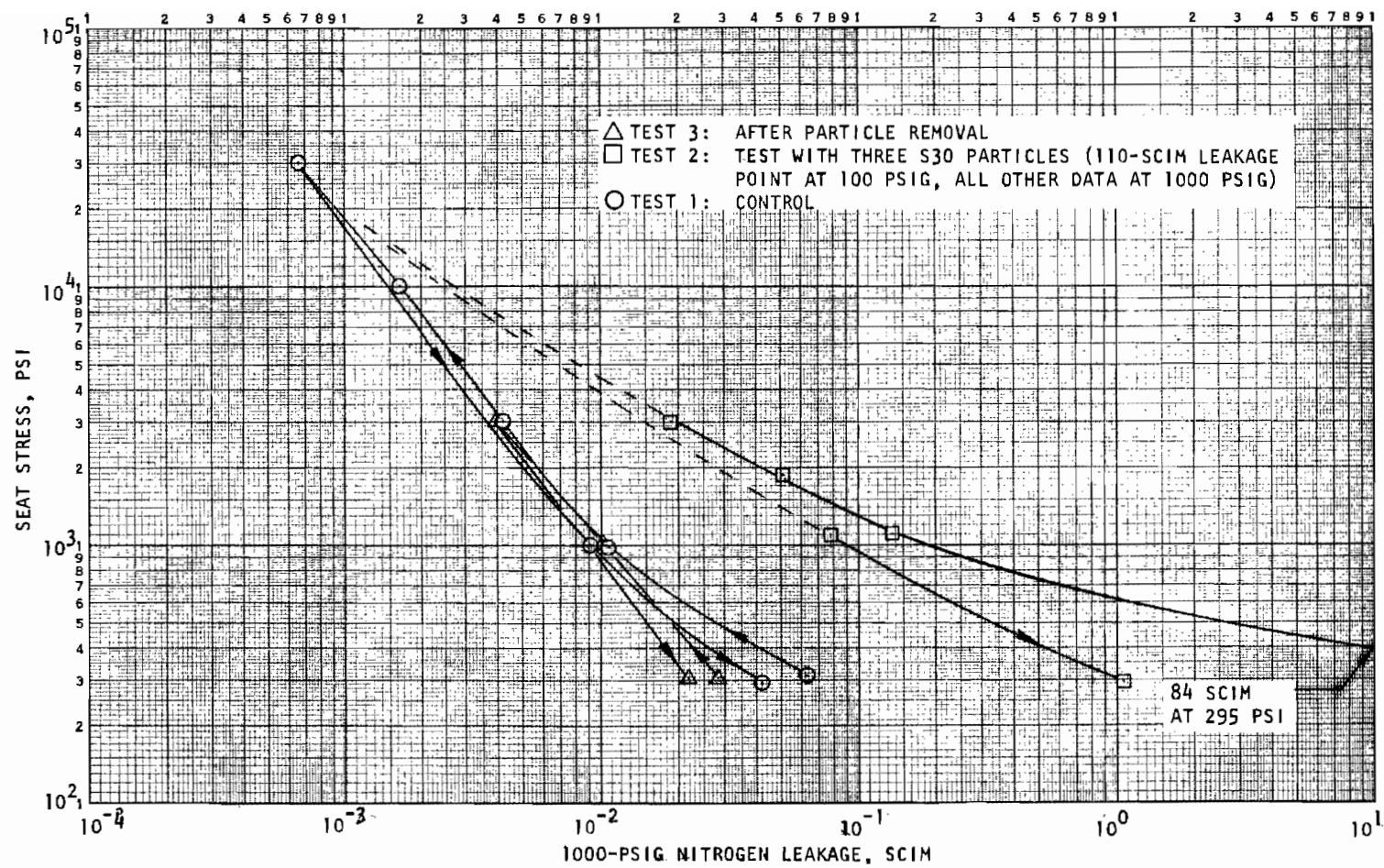


Figure IV-4. Stress-Leakage Data for Static Test Model 108, Tests 1, 2, and 3

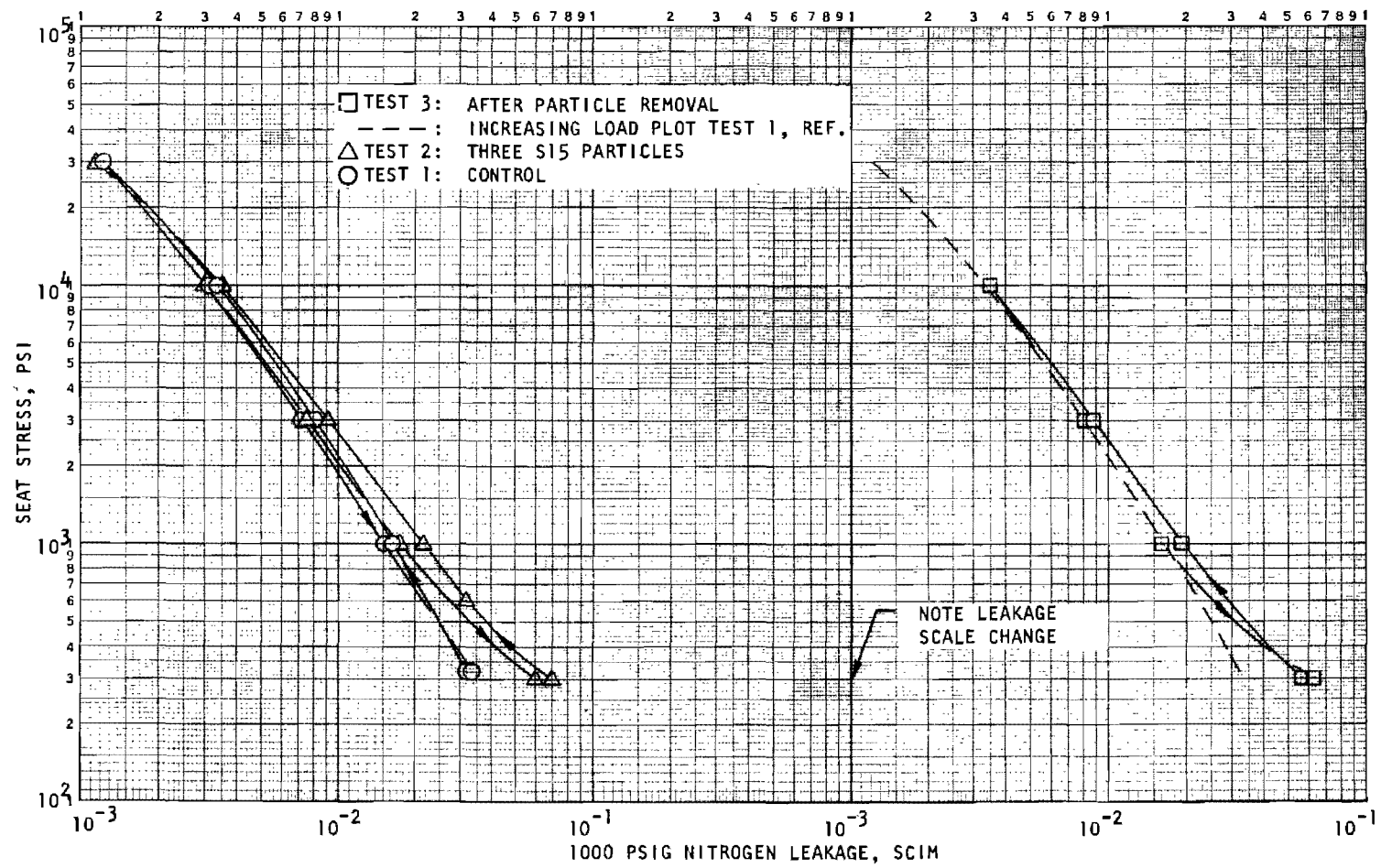


Figure IV-5. Stress-Leakage Data for Static Test Model 112, Tests 1, 2, and 3

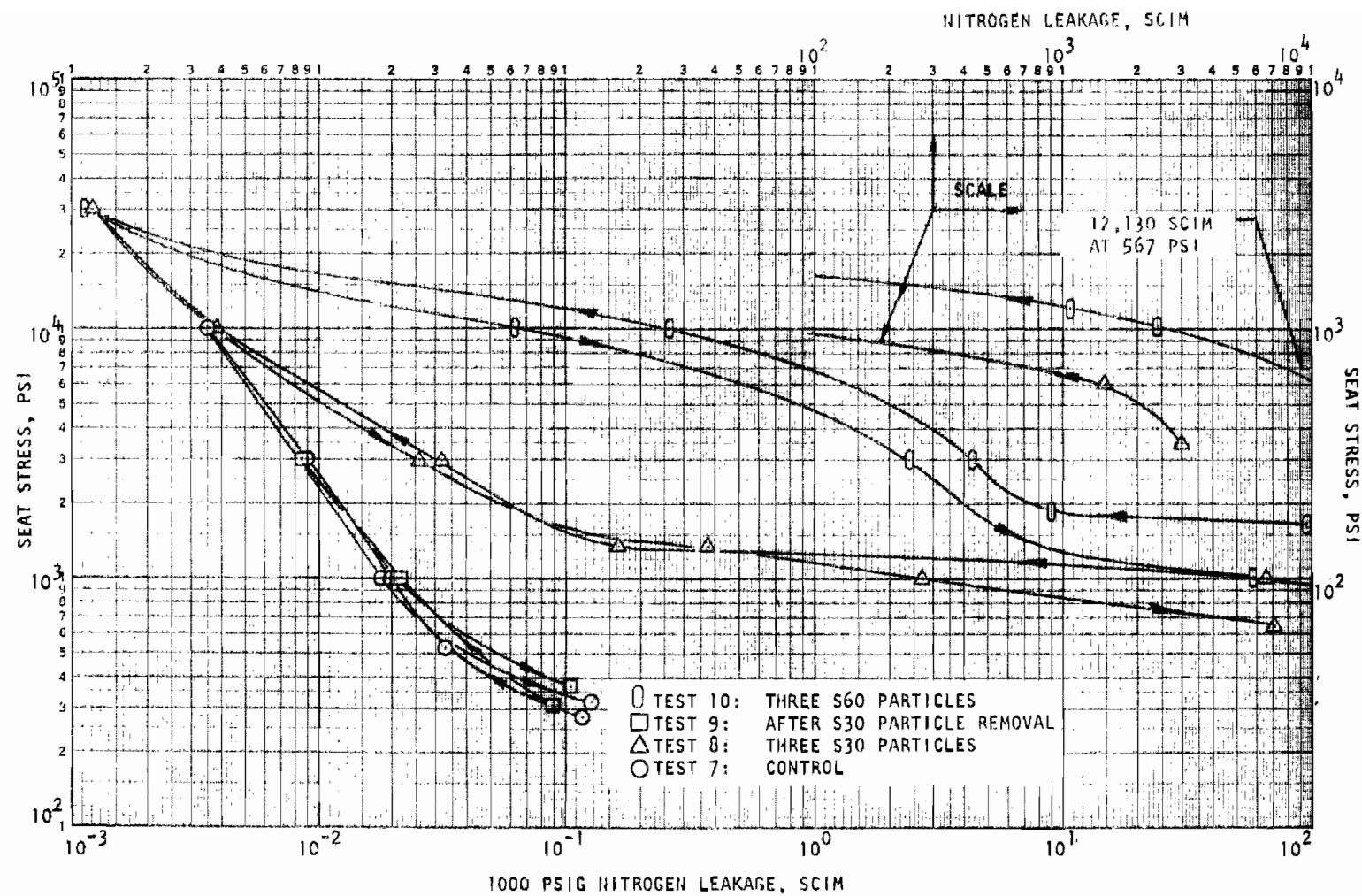


Figure IV-6. Stress-Leakage Data for Static Test Model 112, Tests 7, 8, 9, and 10

test data shown by Tests 3 and 7. The final test, after removal of S60 particles was not performed as the model was prematurely refinished. From the results of Model 102 and subsequently described models, however, little change from previous control performance data would be expected in this case.

Test Model 118

This model was slated for multiple size particle testing similar to Model 112. However, the stress-leakage data for three S15 particles showed less leakage than the control test (Fig. IV-7). After this occurred, further effort was stopped and the eccentric load concept was first considered. Model 118 data (as with Model 112) did indicate that, for the surfaces involved, three 15-micron particles caused only minor change in sealing performance. Consequently, the data are included here for later correlation.

Test Model 119

Model 119 was the first model tested after adoption of the 0.001-inch ball joint shim to reduce tester eccentric load influence on stress-leakage results. The balance of Phase II static testing utilized this tester correction.

Prior to particle testing, Model 119 was stress-leakage tested at 1000-psig inlet pressure to evaluate the shimmed tester configuration. Three separate tests were performed with model surfaces separated and reoriented each time. Comparison of 12 cycles of data to 3000-psi stress indicated data repeatability within 9 percent at a stress level as low as 160 psi. The final loop of this series constituted the initial control data, presented as Test 1 in Fig. IV-8.

Even with this apparent reduction of eccentric load influence, previous Model 112 and 118 results indicated that three S15 particle effects might still be obscured. Accordingly, Model 119 was tested with nine SC particles. Also, larger stress variation during pressure adjustments to operating levels were planned. (Formerly, seat stress was maintained between 100 and 300 psi during this operation.) With 100 to 150 psi as the lower stress level, the modified procedure targeted 500, 1000, and 3000 psi as first data points for S15, S30, and S60 particles, respectively, using 1000-psig operating pressure.

Model 119 leakage with nine S15 particles was large enough to permit a 390-psi stress data point at 300 psig during pressure adjustments. The test was then concluded with 1000-psig inlet pressure. Following the S15 test sequence, three S30 and S60 particles were tested to conclude static evaluation of the soft contaminants.

Test Models 123 and 124

Evaluation of the hard R_c62-67 particles was initiated with these models. It had been intended that three particle sizes would be evaluated on each model. However, two problems occurred to preclude attainment of this goal.

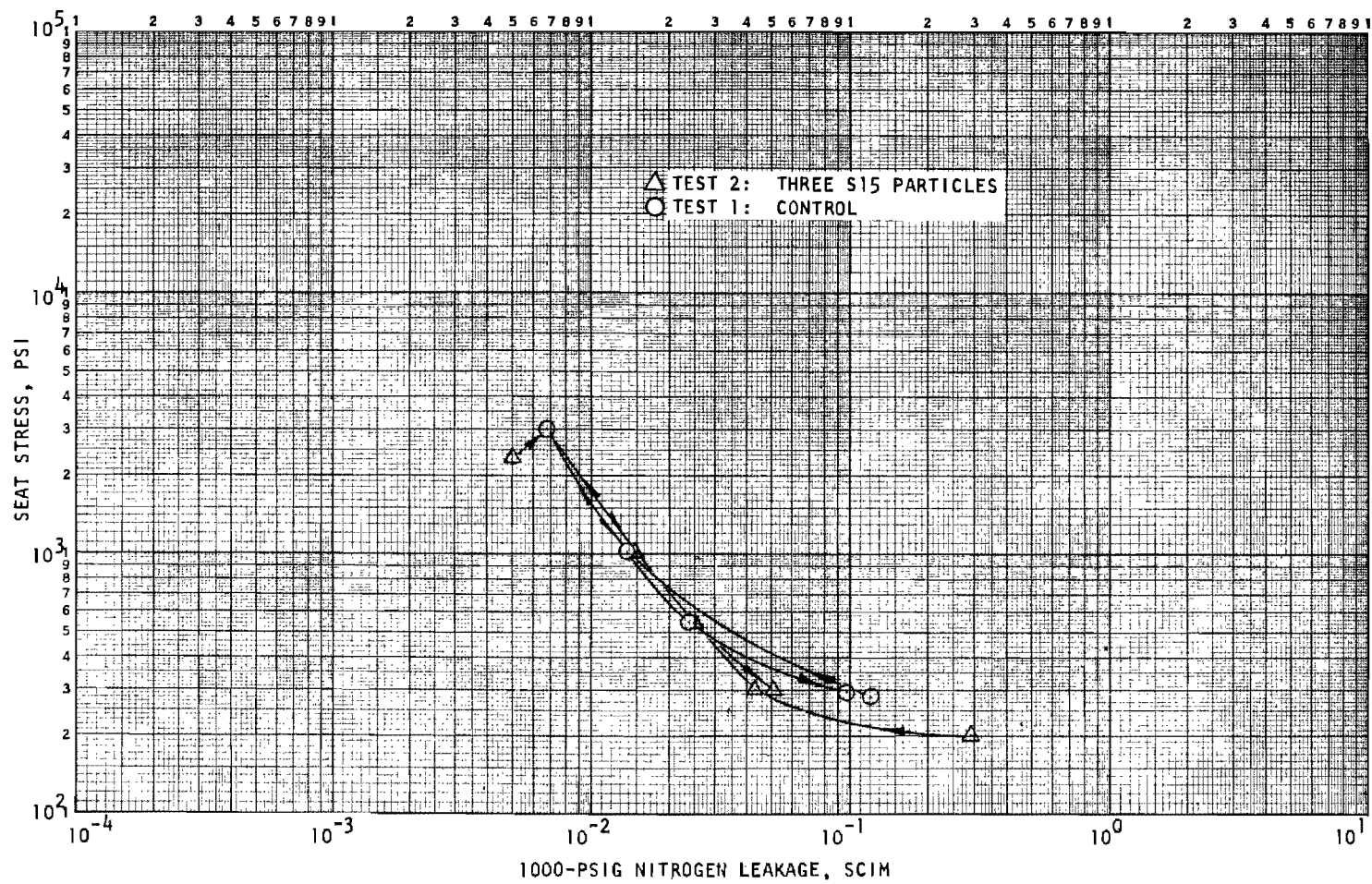


Figure IV-7. Stress-Leakage Data for Static Test Model 118, Tests 1 and 2

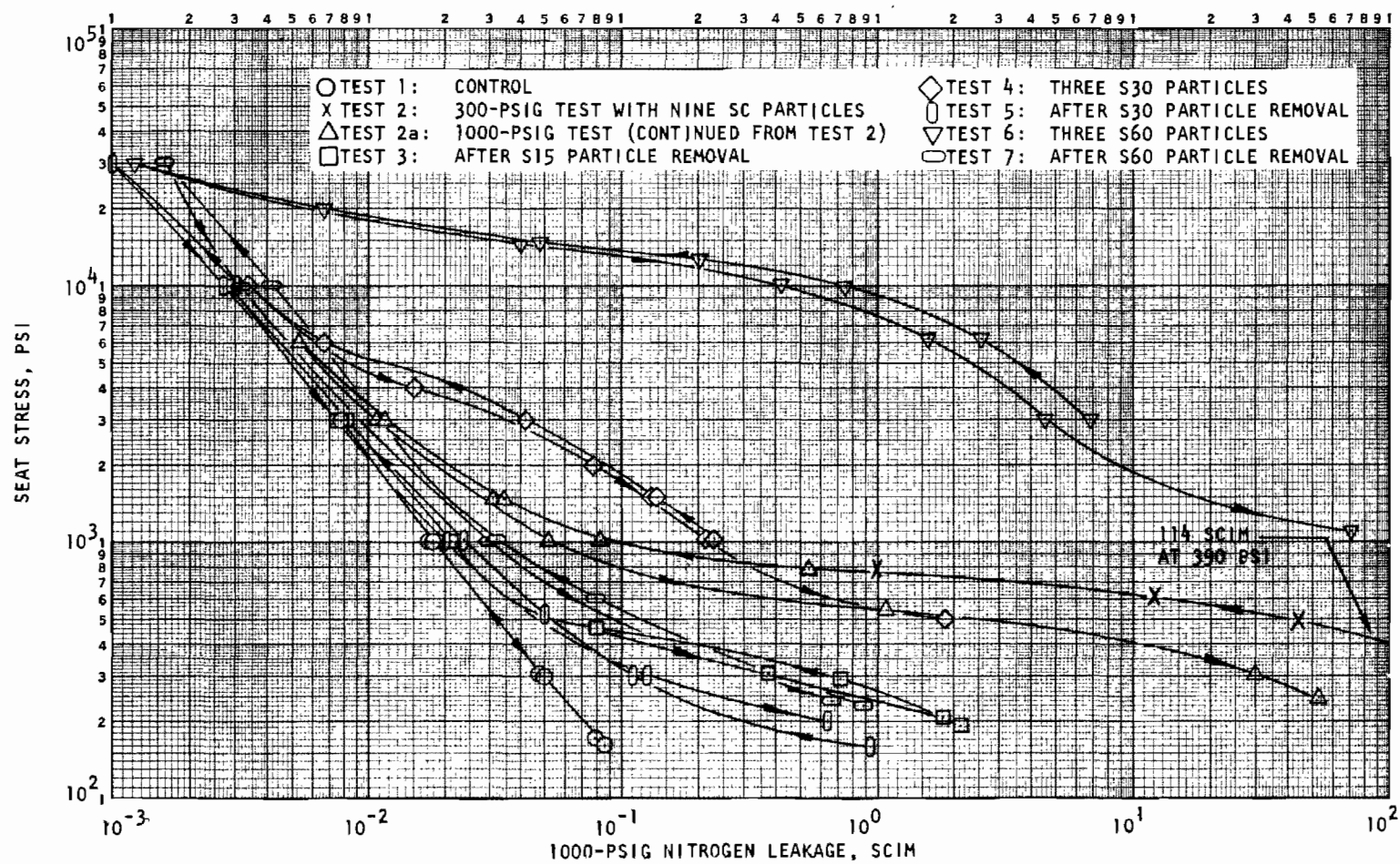


Figure IV-8. Stress-Leakage Data for Static Test Model 119, Tests 1 Through 7

Model 123 initially exhibited an unusually load sensitive control characteristic below 800-psi stress. It was removed from the tester, recleaned, and reassembled with little improvement noted (Test 1, Fig. IV-9). Thus, the effect may have been caused by eccentric loading even with the 0.001-inch ball-joint shim. Nevertheless, because nine H15 particles were expected to produce a significant leakage increase, the test was performed (Test 2, Fig. IV-9).

Retest after particle removal, however, was negated by contamination which yielded leakage not much less than with H15 particles. The contamination was so severe that polishing with 1- to 5-micron diamond compound was required to remove it. This, in turn, sufficiently improved the surface (leakage at elevated stress was halved) to preclude further comparative testing. The static tester gas inlet fitting was believed to be the source of the aforementioned contamination and was recleaned.

Model 124 control stress-leakage data (Fig. IV-10) produced a relatively flat curve with little apparent eccentric load influence. Leakage level, however, was relatively high compared with other models. This characteristic in conjunction with the following problem produced the minimal effect data for nine H15 particles shown in Fig. IV-10.

Posttest inspection indicated that all particles were so deeply embedded in the seat that only five could be removed, even with steel probes. Average particle hole depth in the poppet was about 40 microinches while seat penetration was on the order of 140 microinches, indicating the poppet to be harder than the seat.

As later discussed, both hard and soft particles could be removed from all other 440C flat models without much effort. Also, the particles generally were lodged in the seat, indicating most model poppets were harder than the seat. With Model 124, however, the hardness differential was more pronounced. Further hard particle tests were continued with Model 125.

Test Model 125

Model 125 was tested with three H30 and H60 particles to conclude the Phase II static test effort. Figure IV-11 presents the stress-leakage results which indicate possible eccentric load effect below 1000 psi for the control tests. However, the relative magnitude of residual or post-particle removal damage is still evident at 1000 psi.

PARTICLE AND SURFACE DEFORMATION

Following each particle test, model surfaces were inspected to verify entrapment, assess particle deformation and surface damage characteristics, and remove the particles for subsequent test.

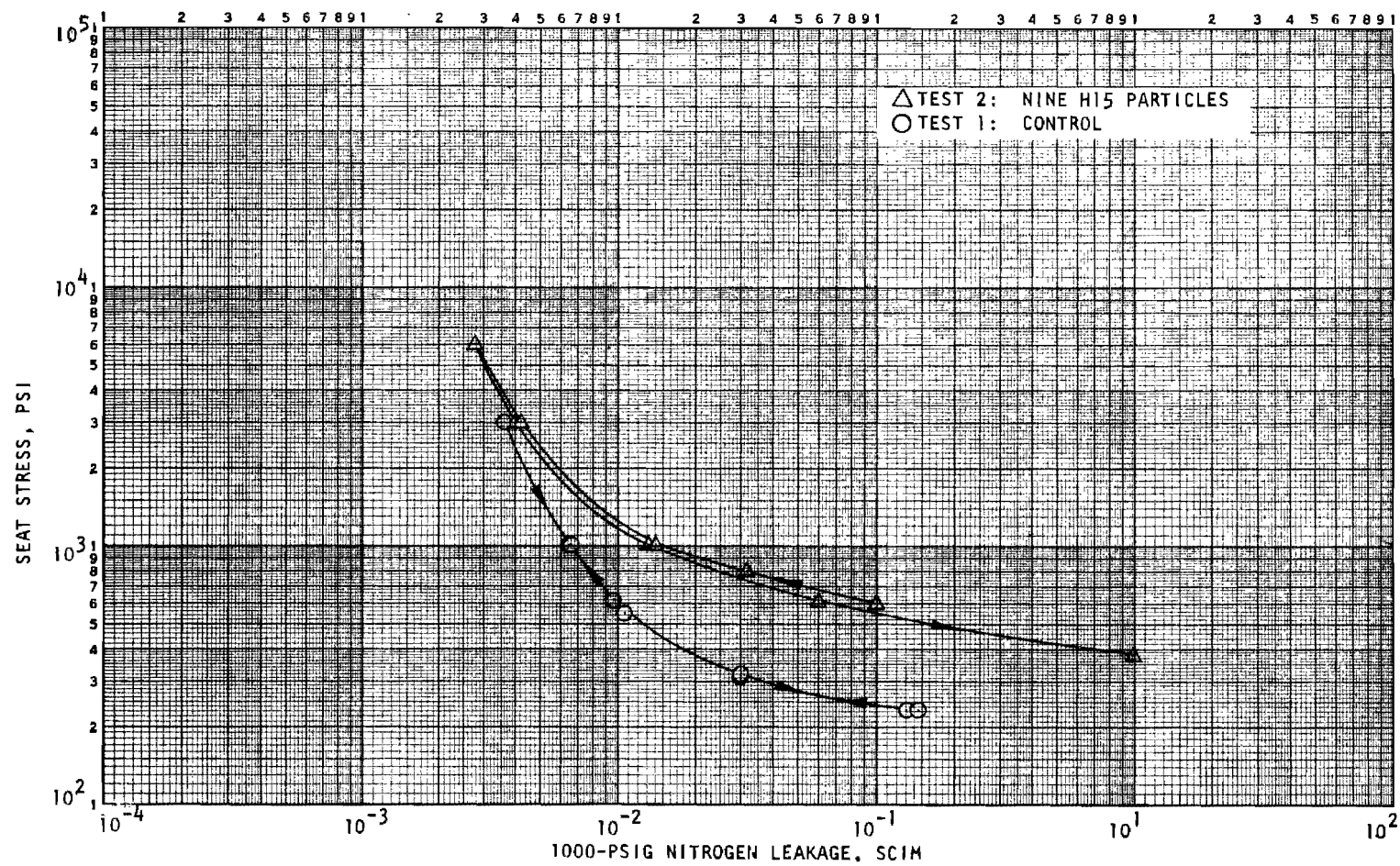


Figure IV-9. Stress-Leakage Data for Static Test Model 123, Tests 1 and 2

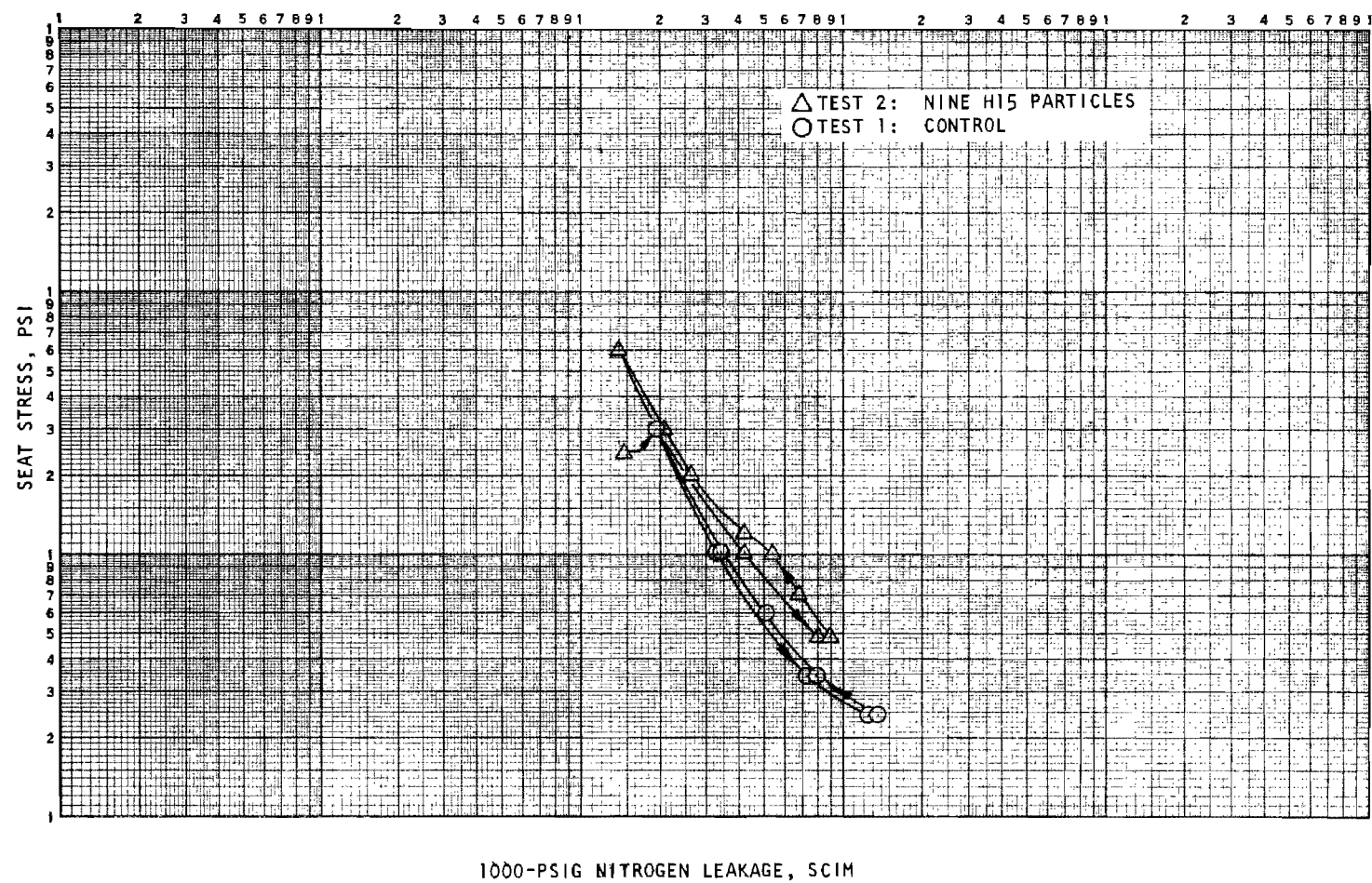


Figure IV-10. Stress-Leakage Data for Static Test Model 124, Tests 1 and 2

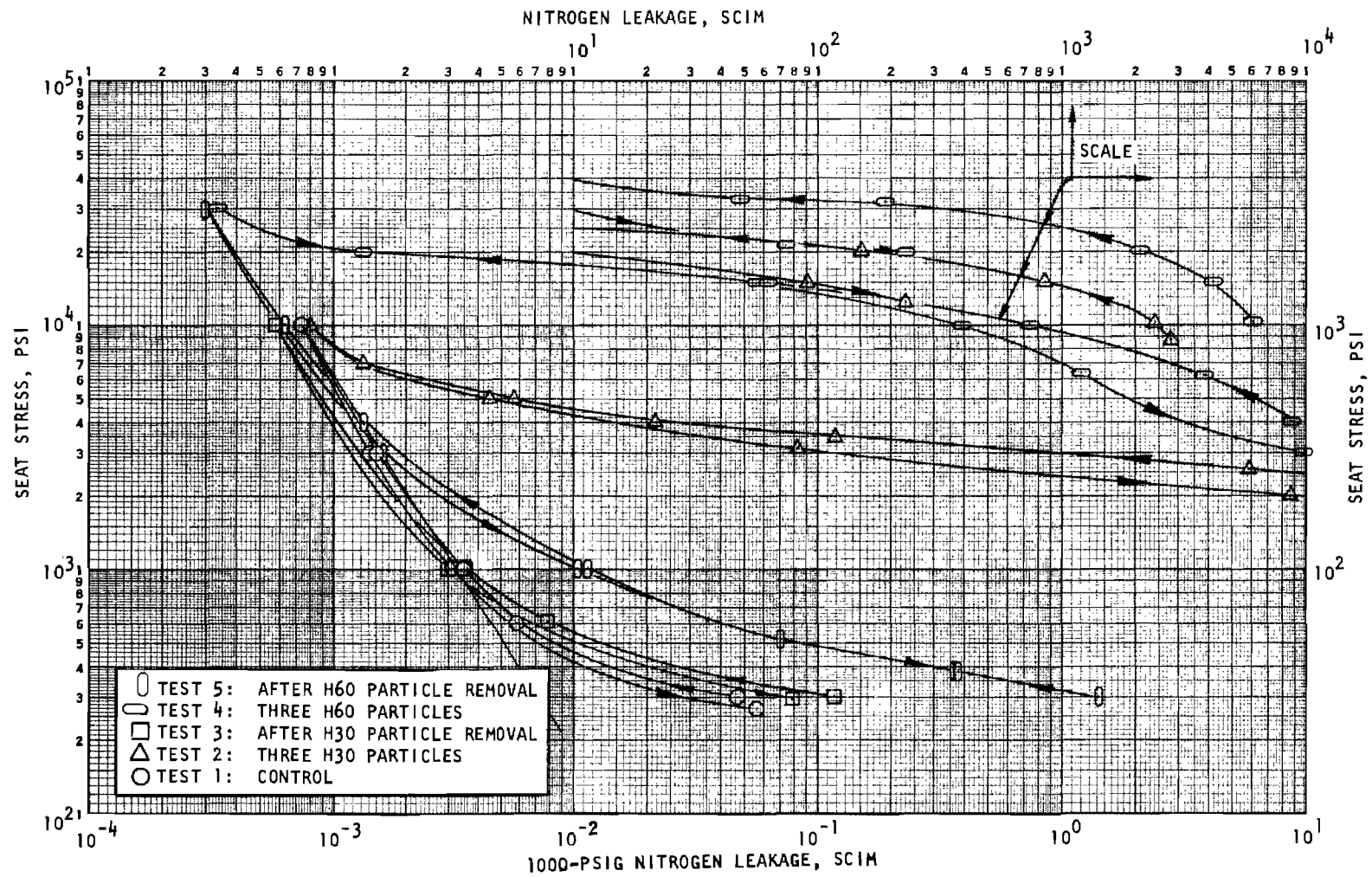


Figure IV-11. Stress-Leakage Data for Static Test Model 125, Tests 1 Through 5

Inspection Methods

The interference microscope at 100X-, 200X-, and 500X nominal magnifications was the primary tool used for model inspection. Trapped particle location on the poppet and seat was seldom readily apparent by plain viewing and interference inspection was required to establish this information. This was accomplished by slightly reducing focal length with circumferential interference bands visible on the particle or hole and noting the direction of band motion. Bands diverging from the center indicated a protuberance (particle) while converging bands revealed a depression, or hole.

Hole depth, trapped particle height, and upset metal height was determined by a combination of green and white light interference bands and, on occasion, an electronic indicator. For uniform holes typical of those formed by soft particles, green light (providing black interference bands) was used and elevation changes determined by directly counting bands (10.6 microinches per band). This type measurement was accurate to within fractional bandwidth estimation, say $\pm 1/4$ band, because bands were viewed as uninterrupted lines.

Measurements of deformed particle height (where boundary geometry made band transition from adjacent surfaces impossible to trace) and irregular hole depth (typical of hard particles) were taken with white light interference. In this mode, interference bands are displayed as a color spectrum, with the central band being nearly black and, thus, useful as an identifier. The black band was focused on the adjacent model surface, centered on the hole or particle in question and simultaneously on an eyepiece reticle line for reference. The band was then pinpoint focused on the low or high point being measured and the corresponding black band displacement on the adjacent surface noted. With selection to green light, the number of bands displaced was then counted. For large displacements, an electronic indicator probe was set on the objective lens case and the focal displacement established by the identifier black band procedure was directly read in microinches. Measurements taken using white light interference are judged accurate within about ± 1 band.

Particle Removal

Removal of embedded particles was accomplished with the particle handler and probe arrangement used for particle placement (described in Appendix E). No particular problems were encountered with the soft particles which were pushed out of their depressions with glass probes of appropriate size. Figure IV-12 illustrates one of the smallest probes used together with typical 10- to 50-micron size particles while Fig. IV-13 shows a deformed 50-micron particle removed with a larger probe.

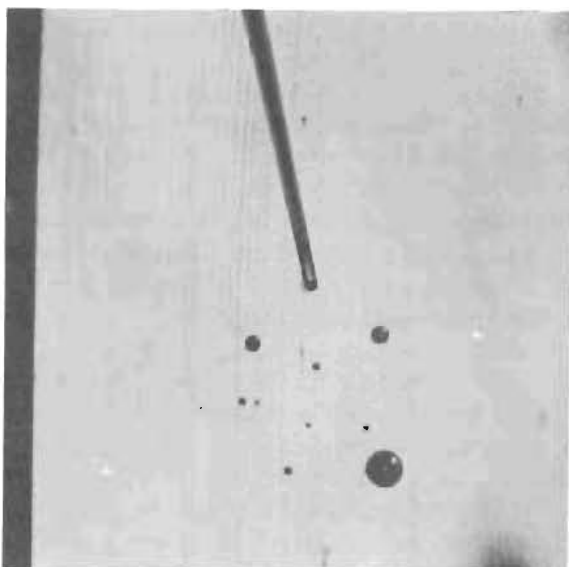


Figure IV-12. Small Glass Handling Probe and Typical Particles (91X Plain Photo)

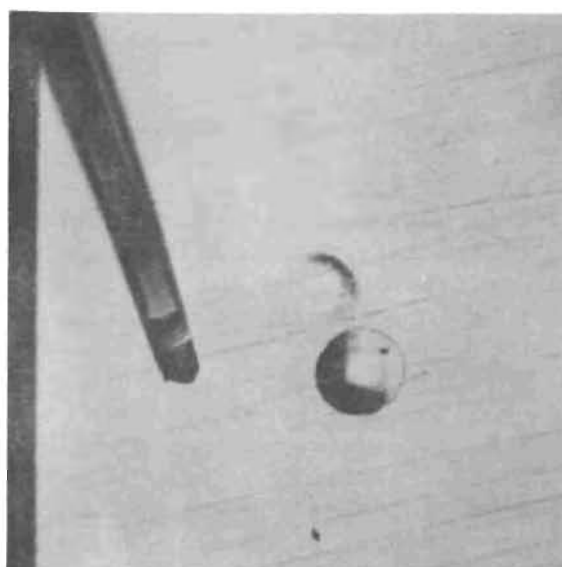


Figure IV-13. Large Glass Probe and Deformed, Soft 50-Micron Particle (91X Plain Photo)

In general, particles were dislodged by axial probe motion. Some were removed by loading the probe normal to its axis but, as the particle broke loose, probe elastic springback propelled it off the surface, usually not to be found again.

Ease of removal is attributed to the elastic springback of both particle and retaining surface after unloading which creates forces tending to eject the particle. This was not true with the purely plastic lead particles formerly tested (Ref. 3). In that case, the lead had to be scraped from the surface even though both poppet and seat had deformed in a predominantly elastic manner.

The fracturing characteristic of the hard particles made their removal more difficult because the irregularities were plastically formed in the mating surfaces. Fifteen-micron particles could be removed with glass probes except for Model 124 where embedment of H15 particles was so deep that even a steel probe (0.02-inch sewing needle, sanded and lapped to about 0.0005-inch tip diameter) was unsuccessful. The steel probe was required for H30 and H60 particle removal. It will be later noted that, even though fracturing, the hard particles remained in one piece. The only exception was the H60 test of Model 125 where one particle fractured during closure and caused several secondary depressions.

Deformed Particle and Surface Geometry

Figures IV-14 through IV-29 show deformed particle and surface geometry for soft and hard particles on flat 440C poppets and seats. These typical photographs illustrate the uniformity attendant with soft particles and

the fracturing or irregularity common to the harder material. Figures IV-14 through IV-19 picture hard and soft 15- and 60-micron sizes at various magnifications and indicate that characteristics are similar for these extreme conditions. For comparison at a single magnification, the family of figures (IV-20 through IV-25) show particle and mating poppet and seat depressions for hard and soft 30-micron particles. Figures IV-26 through IV-29 illustrate deformed particle and land width relative dimensions.

Soft particles were flattened into crowned or pillow-shaped platelets tapering to an edge about 1/10 to 1/4 of the overall thickness. Usually the flattened geometry was circular although, on occasion, oval shapes resulted from nonparallel closure and/or poppet-seat relative motion during closure. Hard particles took an irregular shape. For inspection purposes they were treated as circular forms with an equivalent diameter defined by averaged dimensions taken in several directions.

The hard particle fracturing appeared to have taken place after some seating surface deformation had occurred. This was indicated by a relatively circular "knob" appearing at the high point of the particle and at the bottom of the poppet and seat depressions. Because of the discontinuous surfaces, particle height and seating surface depressions were measured from these readily detected extreme points. Crumbling or fracturing after this initial indentation produced surface discontinuities which could not be measured. The aforementioned general lack of surrounding residue indicates that fracturing occurred after elastic-plastic seating surface deformation had caused hydrostatic envelopment of the particle.

Poppet and seat surfaces evidenced a crater-like appearance with some upset metal at the rim protruding above the surrounding plane. It was this upset metal which formed the surface degradation termed residual damage and produced the changes in control stress-leakage data after particle removal. Upset metal height was relatively easy to measure when uniformly formed by soft particles. When skewed by poor closure (oval shape), however, it was predominant on only one side of the crater. The discontinuities caused by hard particle fracture precluded accurate upset height in this case. There was some evidence that minute protuberances considerably higher than the general appearance did exist. The relative insignificance of surface upset in general, however, indicates little influence from these peaks.

Most particles, soft and hard, were lodged in the seat after separation. Seat depressions were deeper than those of the poppet indicating that the latter parts were harder. This is typically evident from a comparison of Fig. IV-21 and IV-22. The aforementioned problem with Model 124 where H15 particles were so deeply embedded that all could not be removed was an extreme case. However, even with Model 124 only a two-point R_c hardness differential existed between poppet and seat. Thus, penetration and deformation characteristics may be influenced by small variations in poppet and seat materials and certainly is a complex function of the elastic-plastic and work-hardening properties of all materials involved.

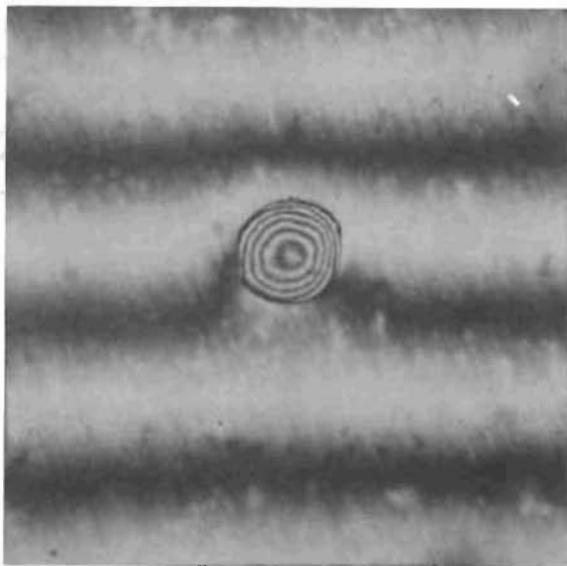


Figure IV-14. Model 119; S15 Particle Embedded in Poppet Surface (462X Interference Photo)

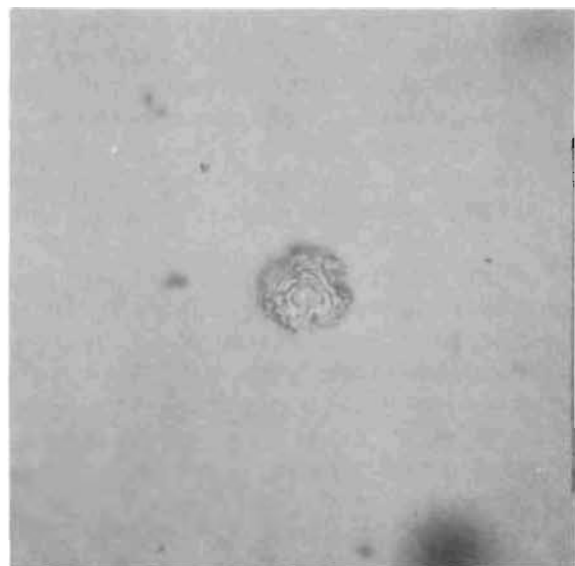


Figure IV-15. Model 123; Deformed H15 Particle After Removal From Poppet (462X Interference Photo)

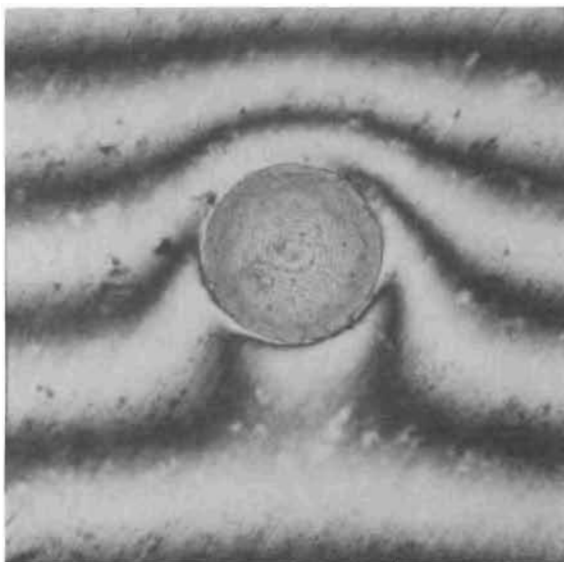


Figure IV-16. Model 119; S60 Particle Embedded in Poppet Surface (187X Interference Photo)

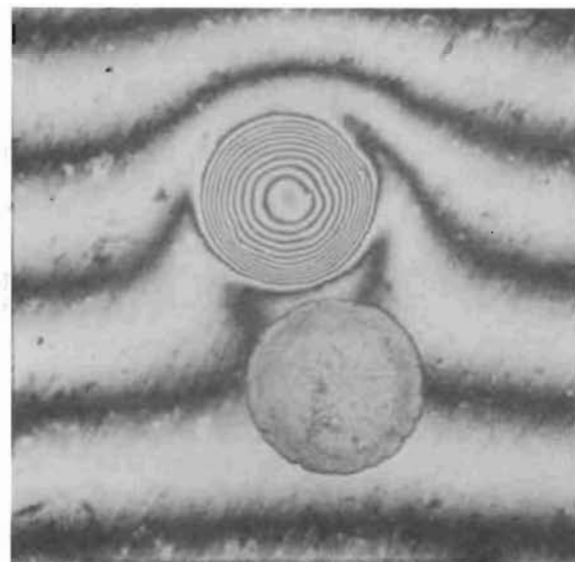


Figure IV-17. Model 119; S60 Particle of Fig. IV-16 and Mating Poppet Depression (187X Interference Photo)

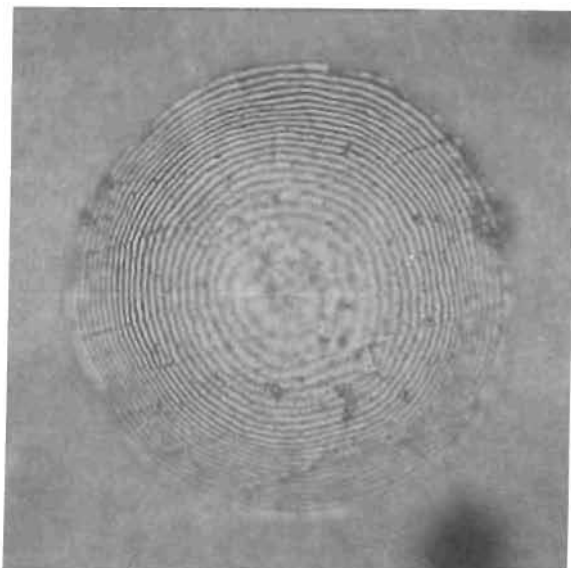


Figure IV-18. Model 112; Deformed S60 Particle (462X Interference Photo)

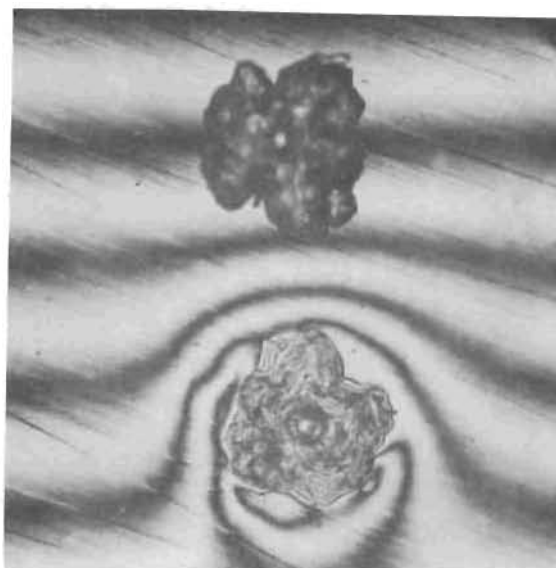


Figure IV-19. Model 125; Deformed H60 Particle and Mating Depression (187X Interference Photo)

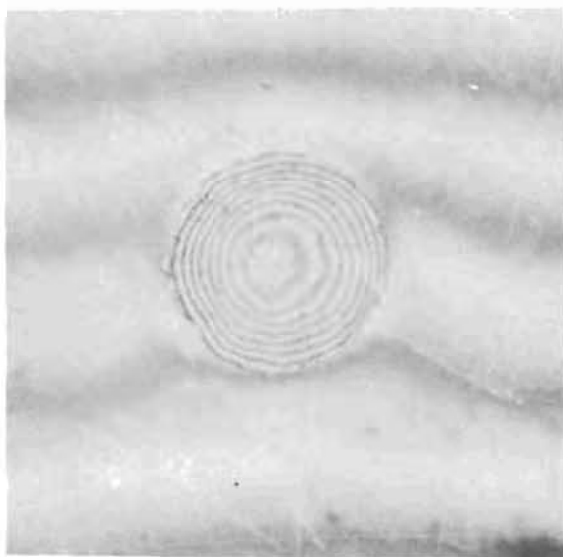


Figure IV-20. Model 108; S30 Particle Embedded in Seat (462X Interference Photo)

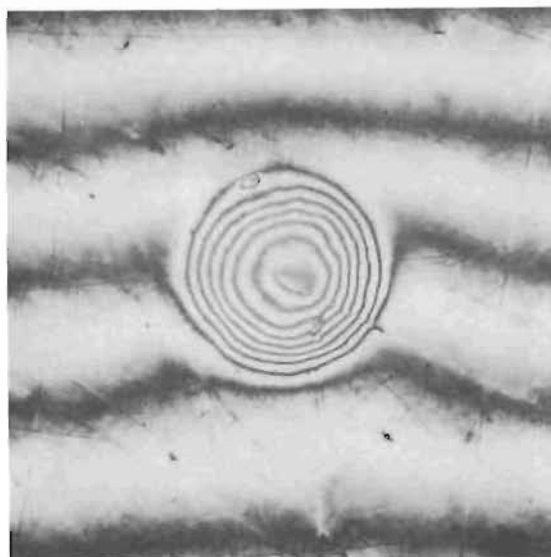


Figure IV-21. Model 108; Seat Depression From S30 Particle of Fig. IV-20 (462X Interference Photo)

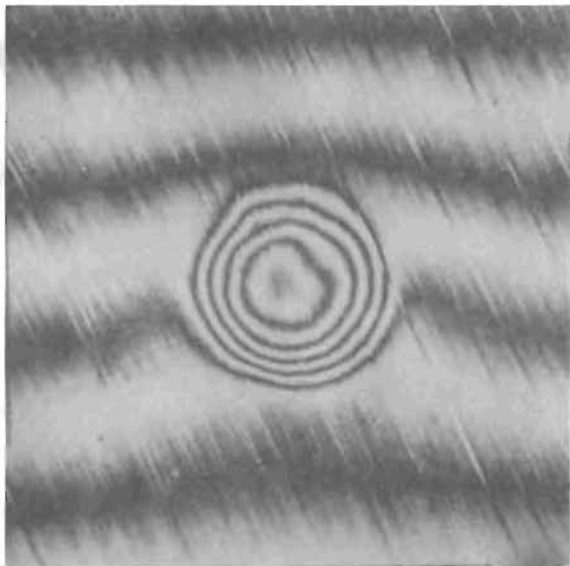


Figure IV-22. Model 108; Poppet Depression From S30 Particle of Fig. IV-20 (462X Interference Photo)

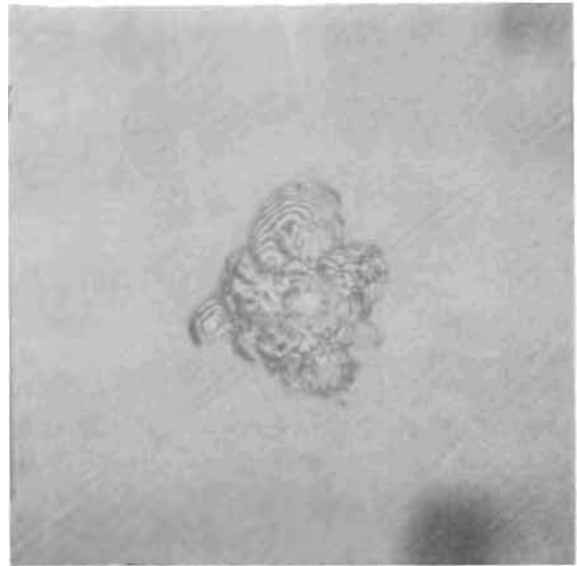


Figure IV-23. Model 125; H30 Particle Embedded in Seat (462X Interference Photo)

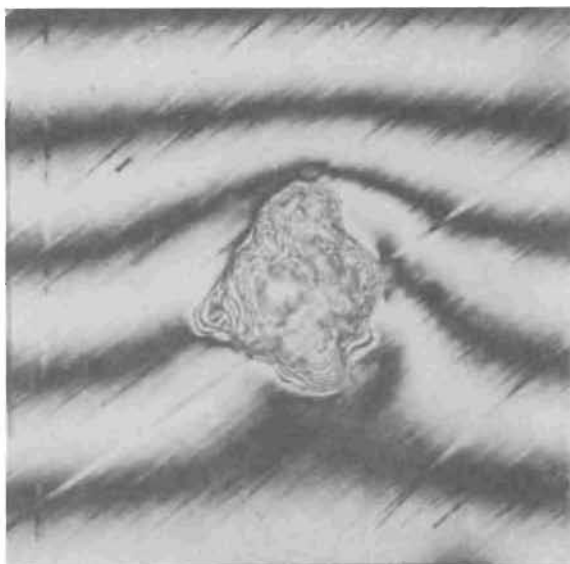


Figure IV-24. Model 125; Seat Depression From H30 Particle of Fig. IV-23 (462X Interference Photo)

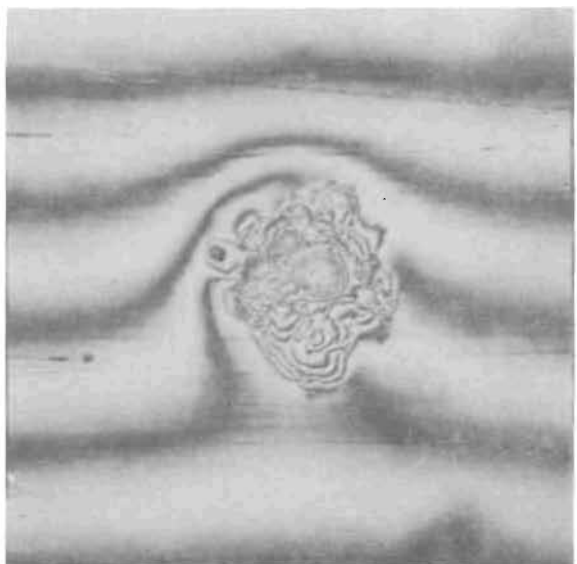


Figure IV-25. Model 125; Poppet Depression From H30 Particle of Fig. IV-23 (462X Interference Photo)

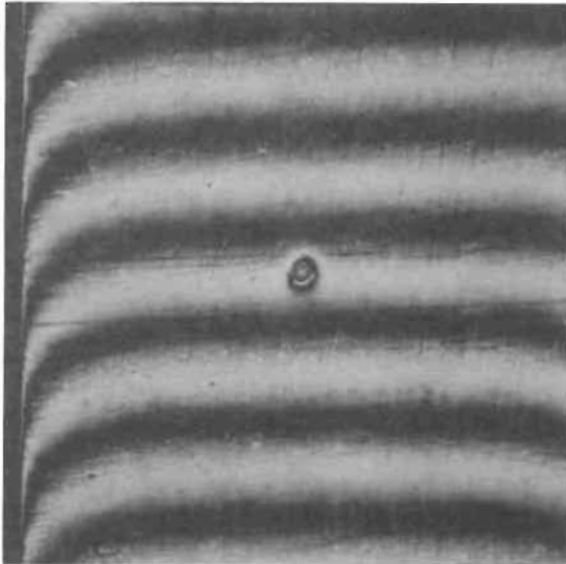


Figure IV-26. Model 112; Poppet Depression From S15 Particle (91X Interference Photo)

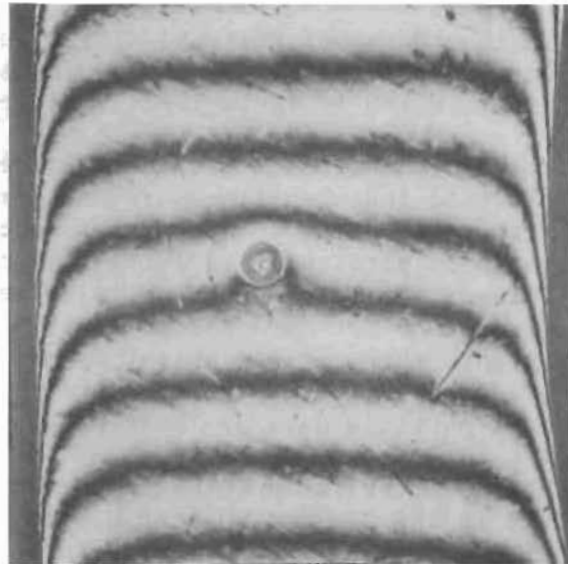


Figure IV-27. Model 108; Seat Depression From S30 Particle. (91X Interference Photo)

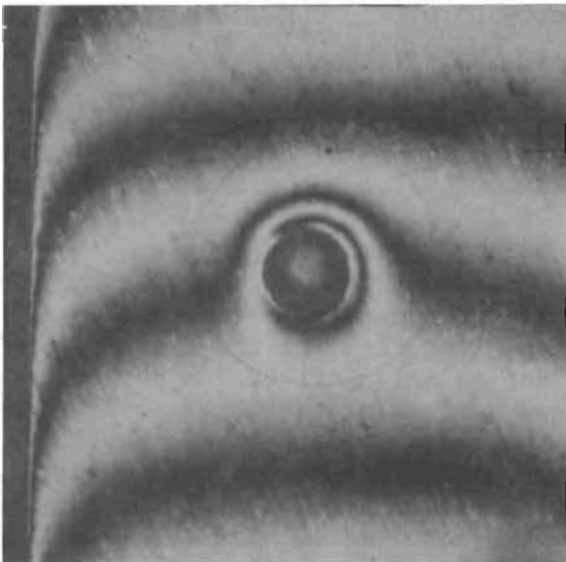


Figure IV-28. Model 112; Poppet and Embedded S60 Particle (91X Interference Photo)

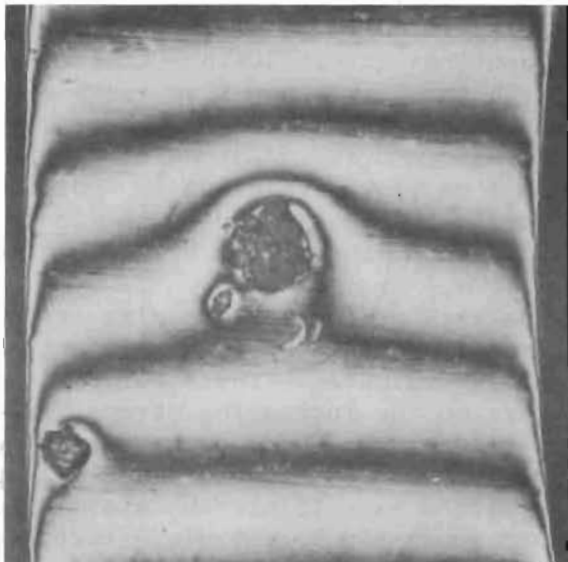


Figure IV-29. Model 125; Seat With Embedded and Fractured H60 Particle (91X Interference Photo)

In the course of Phase II static testing, each model was inspected for various deformation-oriented dimensions. A summary of these dimensions is presented in Table IV-2 tabulated as averages of available data.

The aforementioned deformation irregularity of the hard particles made discrete individual measurements impossible and dimensions associated with these particles represent general appearances. The deformation (h/D) ratio in particular reflects this problem by indicating that deformed volumes for like-sized particles were different. The use of "knob" peak dimensions for hard particle overall height measurements in this case weights the particle height upward. Also, the material volume represented by deformed, hard particle voids adds to the overall height. Thus, the hard particle data are most probably in error in this case.

The diameter ratio (d/D) fares somewhat better with close agreement apparent in the 30- and 60-micron sizes. The discrepancy with the 15-micron size is primarily attributed to potential basic diameter sizing deviations (± 2 microns) where large percentage error is possible.

DATA ANALYSIS

The limited data obtained from static testing precluded the preparation of a data matrix and associated parametric curves. Thus, the information gained can best be expressed by discussion and comparison of the results.

In performing the tests, the optimum method would be to control all variables so that the clean (i.e., without particles) control curves had identical stress-leakage characteristics. This technique was approached with the succeeding-size tests of Models 112, 119, and 125. However, because of variations in model roughness and geometry, data variations between models cannot be directly compared on a point-to-point basis but must be viewed relative to individual respective control curves. The data must also be assessed in the context of the test models employed; i.e., 0.03-inch land width, 0.470-inch mean seat diameter.

Analysis of the test results is considered on a particle size basis. Figures IV-30 through IV-32 present composite test data for the three particle sizes evaluated. These curves portray the relative effects of particle size on the increasing stress versus leakage sealing characteristic. Comparison is made for each model between the control and particle test data. Broadly viewed at about 1000-psi apparent stress, the results may be generalized as: 15 micron, minimal to negligible effect; 30 micron, moderate but generally acceptable effect; 60 micron, intolerable effect even with higher loads. Detail discussion of these results and reasons therefore (many hypothesized) follows.

TABLE IV-2

DEFORMED PARTICLE AND MODEL
SURFACE INSPECTION DIMENSIONS

Inspection Parameter	Particle Designation					
	S15	H15	S30	H30	S60	H60
Basic Particle Diameter (D), inches	0.00059		0.00118		0.00236	
Deformed Particle Diameter (d), inches	0.0014	0.0009	0.0025	0.0022	0.0048	0.0049
d/D = K	2.4	1.5	2.1	1.9	2.0	2.1
Deformed Particle Height, (h), microinches	117	240	256	350	549	930
h/D	0.20	0.41	0.22	0.30	0.23	0.39
Deformed Particle Edge Thickness, microinches	10	45	67	100	130	500
Poppet Hole Depth, microinches	22	46	51	86	133	233
Seat Hole Depth, microinches	32	70	78	124	182	308
Surface Upset Height, microinches	4	9	5	15	12	17

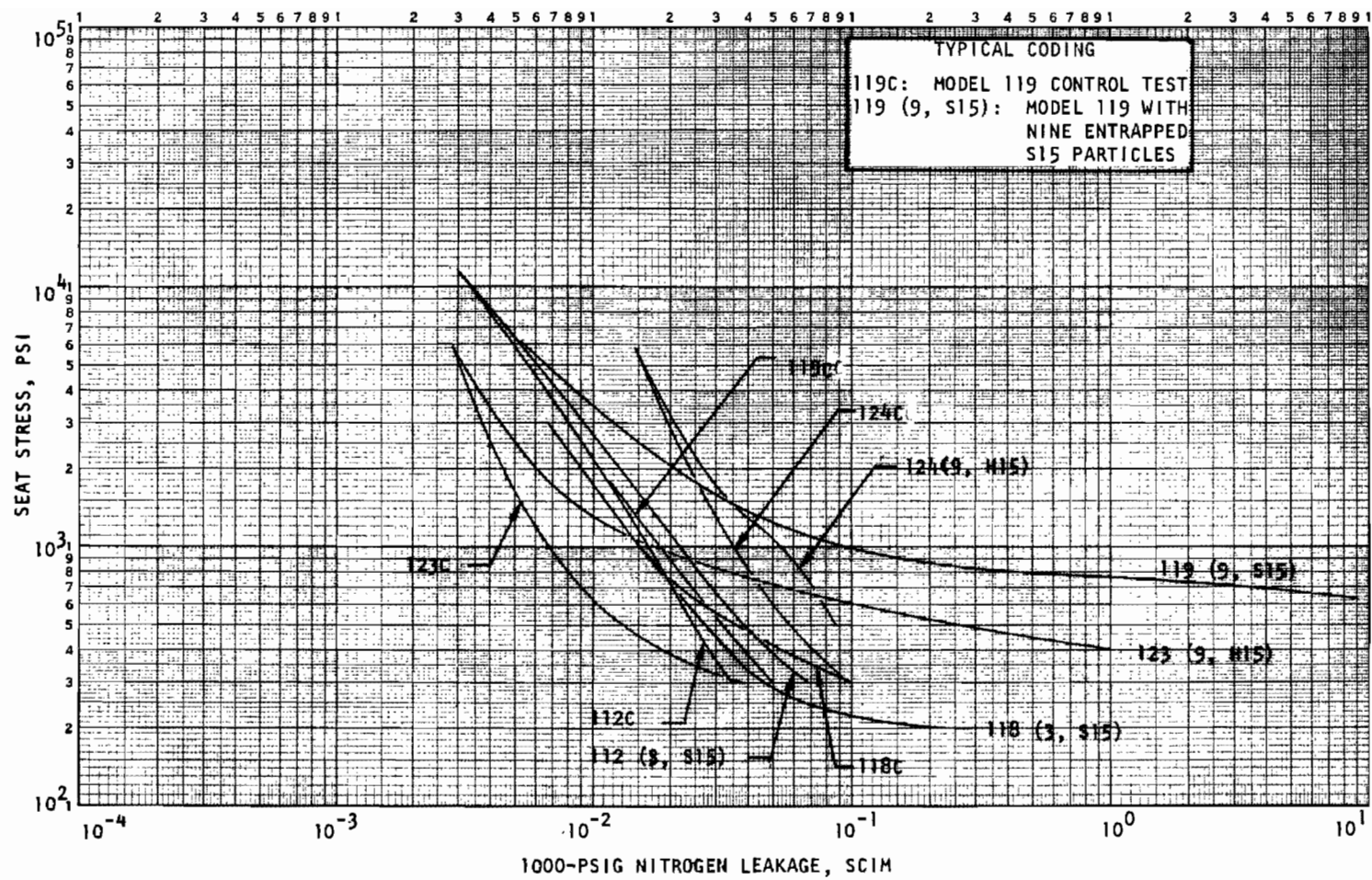


Figure IV-30. Stress-Leakage Data for Static Test Models 112, 118, 119, 123, and 124 With 15-Micron Particles

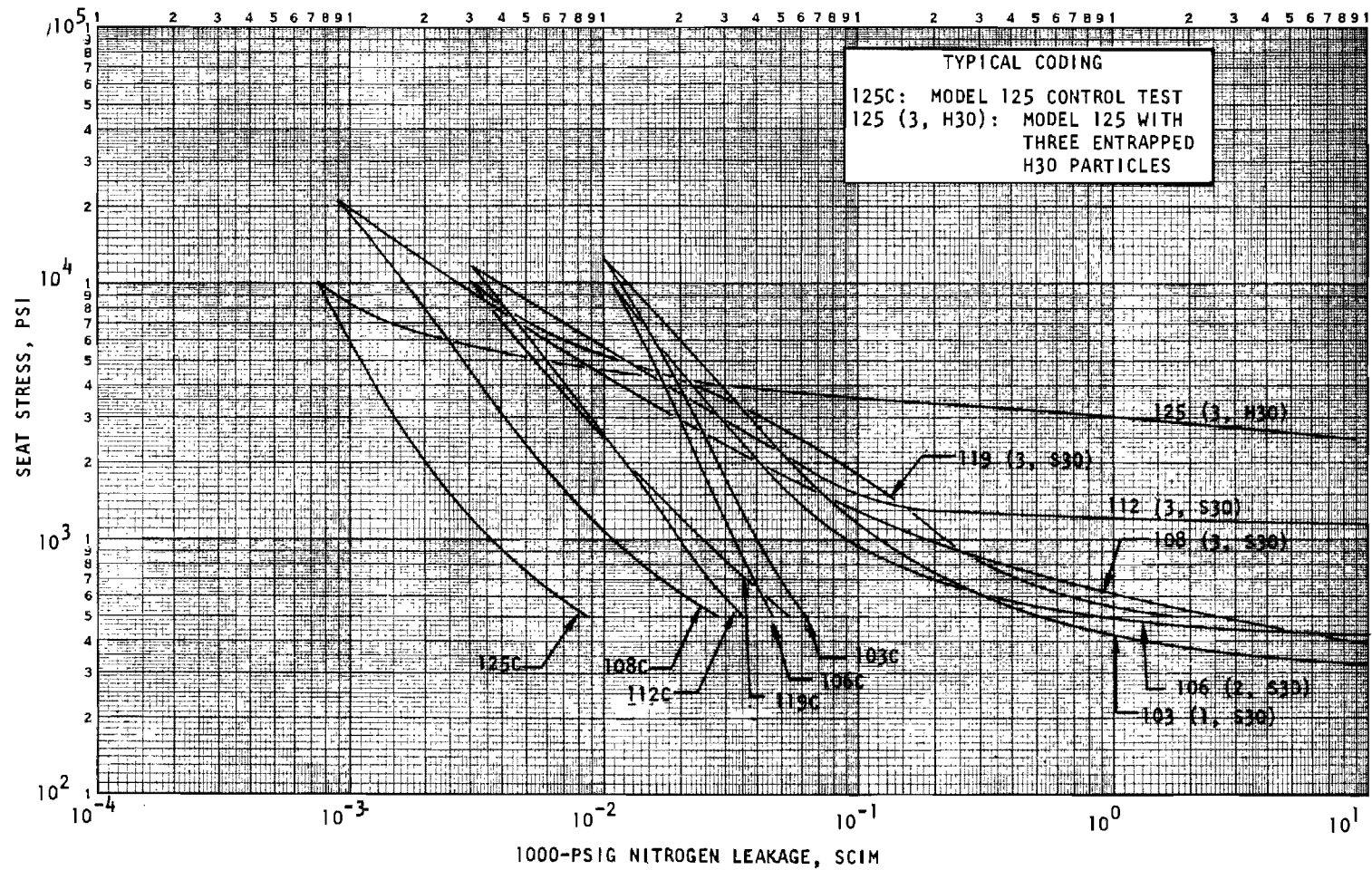


Figure IV-31. Stress-Leakage Data for Static Test Models 103, 106, 108, 112, 119, and 125 With 30-Micron Particles

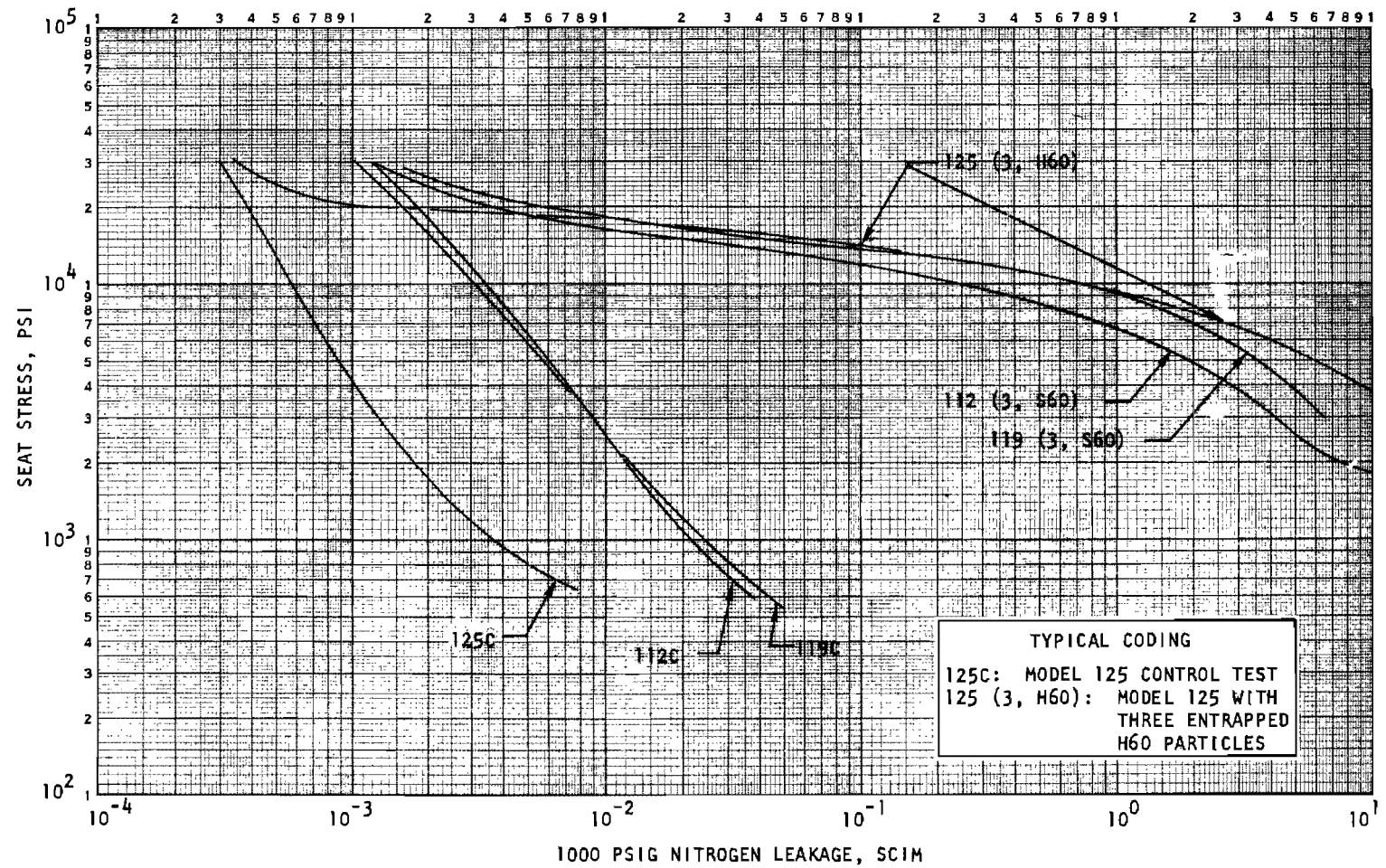


Figure IV-32. Stress-Leakage Data for Static Test Models 112, 119, and 125 With 60-Micron Particles

15-Micron Particle Data

The results of the two tests with three S15 particles (Models 112 and 118, Fig. IV-30) indicate that this type and quantity of contaminant had negligible effect on model sealing performance. At 300-psi apparent stress, corresponding to about 12 pounds seat load for these models, leakage increased less than 2:1. Effects with nine 15-micron particles (both hard and soft) were significantly more pronounced, yielding stress-leakage information similar to that of the 30-micron tests. The hard particles had a lesser effect than the soft material. (This is the case for both hard particle models if an extrapolation of Model 124 data below 1000 psi along the implied slope is imagined.) This may be a function of relative material hardnesses and the surface penetration characteristics of the hard particles.

The deep embedment of H15 particles in Model 124 seat underscores the material parameter which was not considered or controlled to the degree to which it is apparently involved. The minimal leakage influence indicated by deep embedment also suggests that, for some conditions, one seating member softer than the other may be advantageous.

30-Micron Particle Data

The stress-leakage data for Models 103, 106, 108, and 119 (Fig. IV-31) indicate that one, two, or three particles (120-degree separation in the latter two cases) produce similar sealing degradation. This important observation substantiates the selection of three equally spaced particles for test. With one particle entrapped, the seat load is divided between the seating surfaces on one side and the particle on the opposite. Laminar flow through the out-of-parallel surfaces will be 5/16 of that for parallel surfaces at the maximum gap (Ref. 3). With three equally spaced particles, 1/3 of seat load will be concentrated on each particle. The differences between one, two, and three particles are thus somewhat compensating. As the particles are flattened and pressed into the seating surfaces, load will be distributed to the seating surfaces between particles. The interrelationship of these effects is unknown; however, it is hypothesized that the above noted differences are negligible compared with model surface roughness effects at the sealing gaps of interest, i.e., less than 10 microinches. It is therefore concluded that the particle envelopment load for one, two, or three equally spaced particles is about the same. Naturally, particles in close proximity will require proportionally greater envelopment load.

Inspection data for Model 112 indicates deformed particle size and hole depths to be commensurate with other soft particle models. The significant deviation in sealing performance (with particles) up to 1500-psi stress exhibited by this model is attributed primarily to eccentric loading, although hardness-volume factors may also be involved.

All soft particle models attained 10:1 leakage conformance at or below 1500-psi stress. For the contaminant trapped, a factor of 10 leakage increase could be considered tolerable for most valve closures. However, with the nominal model (0.030-inch land, 0.470-inch mean diameter), 1500-psi stress represents 66.5 pounds seat load. For a closure to operate successfully in an environment where such contamination could be encountered, additional load must be provided to compensate for entrapped particles (i.e., particle envelopment load).

In consideration of previous 15-micron test results, Model 125 with hard 30-micron particles would reasonably be expected to produce a stress-leakage characteristic similar to its counterparts tested with like-sized soft material. This was not the case and the gross difference exhibited introduces another variable which has pronounced influence on trapped contamination sealing, that of channel leakage.

Model 125 interface contact is estimated to have occurred at approximately 800 psi (curve "knee", Fig. IV-11). Some 142 additional pounds force was required just to attain 10:1 leakage conformance. It is believed that a channel condition existed wherein the seat material immediately surrounding the particle had not been appreciably loaded and direct radial (channel) leakage paths existed. This was caused by a combination of relatively narrow land (0.0269 inch) and the particle resistance to deformation. The land width parameter may also explain the atypical "bulge" (after interface contact) evidence in the stress-leakage plot for Model 119. This model had only a 0.0238-inch flat land width, smallest of all the models tested.

60-Micron Particle Data

Test results with 60-micron size particle (Fig. IV-32) represents gross sealing degradation where 10:1 leakage conformance required 600 to 750 pounds seating force. Even at interface contact (2000- to 3000-psi stress region), leakage increase from control conditions of three to four orders of magnitude indicates that closures intended for low leakage cannot tolerate channel leakage. Similar results would be expected with one 60-micron particle.

The large load increase required to attain 10:1 conformance after surface contact is believed directly attributable to channel leak paths. The typical photographs of Fig. IV-26 through 29 show relative particle effects on the seating land and illustrate the channel leakage potential of the larger sizes. The S15 particle damage, Fig. IV-26, indicates little surface disturbance or "area of influence" adjacent to the depression. Thus, low load 360-degree envelopment of the particle could be expected and did occur as 15-micron particle stress-leakage data illustrate.

The S30 particle of Fig. IV-27 has created a disturbed area of about 0.006 inch on the flat land width of approximately 0.026 inch or nearly one-fourth of the effective sealing land. It is apparent that, from the amount of plastic deformation shown, a significantly larger elastic

depression surrounding a trapped particle would exist during closure. Should this elastic area of influence overlap the land edge, channel leakage would result. It is probable that some channel leakage occurred with 30-micron particles, especially Model 125.

The illustrations of 60-micron particle surface disturbance, Fig. IV-28 and IV-29, leave no doubt about channel leakage potential with this size contaminant. A plastically deformed area about 0.014 inch in diameter is evident in both cases. With the channel path established by a trapped particle, it is surprising that the 60-micron model leakage ultimately did conform with the control condition.

The preceding information has established land width versus particle size as a vital parameter in sealing consideration. While a fiber bridging the land or particles equal to land width obviously will produce channel leakage paths, the explicit relationship between particle size and corresponding land width required to achieve tolerable load closure has not been established. When the land width parameter is combined with particle and material properties, the magnitude of the contamination sealing problem begins to materialize. Adding closure size and configuration to these variables, it can be seen that these data must be used as a guide. Tests of specific closures must be performed to prove resistance to specific particles.

Particle Envelopment Loads

The analyses of Section II included the development of an expression relating particle size and loads required for envelopment, or seating surface contact:

$$P = \frac{\pi}{4} K^2 d^2 \gamma_s Y_s$$

From Table IV-2, a value for $d/D = K$ of approximately 2.0 was determined. The load equation then reduces to

$$P \cong 3 D^2 \gamma_s Y_s$$

However, values for (γ_s) and (Y_s) could not be explicitly defined. The term (γ_s) , for example, has been experimentally determined as ranging from three to five, but for a condition where plastic flow is unrestrained. This is not the case with enveloped particles. The stress-leakage data were therefore reviewed for information from which an empirical constant relating the unknown factors could be established.

As noted earlier in this section, the region of the stress-leakage curve where leakage sensitivity to load change indicated pronounced reduction was interpreted as indicating interfacial contact. This, however, is a somewhat nebulous value requiring subjective interpretation. Conversely, the 10:1 leakage conformance data, while resulting from an arbitrary

definition, were explicitly established for many model tests. As Table IV-1 data indicate, 10:1 leakage and interface contact loads were similar. Furthermore, leakage at the 10:1 point was generally in the 10^{-1} scim region which is indicative of an interfacial parallel plate gap of about 2 to 5 microinches (Section II, leakage data). These data all generally correlate to indicate interfacial contact and, thus, particle envelopment. As the 10:1 leakage conformance represented the best defined data, this parameter was utilized as an initial approach to establishment of an envelopment load constant (β).

Fifteen and 30-micron leakage conformance data were selected from Models 108, 112, 119, and 123 and per-particle loads were computed. These, in turn, were used to compute values of (β) where,

$$\beta = 3 \gamma_s Y_s = \frac{P}{D^2}$$

Values of (β) ranged from 7.9×10^6 to 14.6×10^6 psi and yielded an average of 11×10^6 psi. Using this constant, envelopment loads were computed for the four particle sizes involved, as shown in the following tabulation.

Particle Size, microns	Envelopment Load, pounds	
	Single Particle	1 to 3 Particles
15	3.84	11.5
30	15.4	46.2
50	42.7	128.
60	61.5	184.

These values are listed in Table IV-1 along with associated stress levels for appropriate model conditions. From the previous discussion it is assumed that the load required to envelop 1, 2, or 3 particles is the same. However, proportionately greater load would be required for more than three particles (e.g., four 30-micron particles would be 46.2 plus 15.4 = 61.6 pounds).

It will be noted that, for those models having no channel leakage influence, the computed loads correlate well within a factor of two with 10:1 leakage and interpreted interface contact data. Even where channel leakage occurs, the calculated loads reflect interface contact although somewhat conservatively. Envelopment to 10:1 leakage within predicted loads would require a larger land width for this case.

OBSERVATIONS

Many variables enter into the evaluation of particle effects on valve closure performance. Moreover, quantitative effects have to be specifically applied for accurate prediction of results. Almost nothing can be quantitatively defined for closures which do not closely approximate

the particles and models tested herein. It is quite evident from the limited data presented that this effort has just set the stage for gathering the matrix of data initially planned. On the other hand, a significant amount of qualitative information has been generated which spotlights the more subtle variables. This information is itemized below as a list of generalities. As before, these must be considered in the context of the specific models tested herein.

1. Envelopment load was empirically correlated. The resultant equation indicates that cermet closures will require much greater load for envelopment than the tested models whereas a hard on soft combination should require much less load.
2. One, two, or three particles require about the same load for envelopment.
3. From consideration of the land width channel leakage parameter, it may be concluded that particles of about 30 microns constitute an upper size limit for envelopment by a 0.03-inch-wide hard metal seat land.
4. Particles larger than 60 microns will cause gross leakage with most hard seat valves, even with high loads.
5. Residual damage effect is minimal with hard sealing surfaces. In this respect, many leakage failures have probably been attributed to various surface minutiae which are incomparable in size (and effect) with the disruptions revealed in the previous photomicrographs. It was this observation which indicated that "contamination" thought to have caused the noted stress-leakage crossover phenomena was incorrect and led to the eccentric load analysis (Appendix C).
6. Particles and sealing surfaces of similar hardness will tend to eject particles because of elastic springback energy. Soft metal particles may smear and be interlocked into surface porosity or pits, especially with the more porous cermets.

SECTION V

PHASE II DYNAMIC TESTS

This portion of Phase II investigations was performed to explore the parameters of dynamic closure and contaminant flow as they apply to poppet and seat sealing performance. As with static tests, fundamental information applicable to Phase III design and testing effort was required. With few precedents to draw from, numerous questions were posed during dynamic test planning and preliminary stages. Predominant among these were:

1. Is dynamic particle hit damage more or less severe than obtained in static envelopment?
2. Will impacted particles shatter or become embedded?
3. With a known particulate population, can impact events be predicted?
4. What influence will particle-induced erosion and background contaminants have on sealing capabilities?

Finally, continued reliability and performance characteristics of the dynamic test system remained to be proved. Thus, the Phase II dynamic tests were to serve as a developmental effort in establishing a firm foundation for particle effects testing. It was expected that correlation of model sealing degradation with cycles, particle hits, and surface geometry for specific model designs would provide both performance limitation data and understanding of particle effects leading to design improvements.

GENERAL APPROACH

The general approach for the dynamic tests was similar to that employed for static evaluation except for model exposure to particulates. Models were stress-leakage tested in the dynamic tester to determine initial acceptability. Further leakage testing after cycling in clean fluid established baseline or control performance from which subsequent effects of particle impacts should be assessed. Finally, the models were cycled in a controlled particulate population environment. The resulting sealing degradation and number of impact events provided the test output data.

The following subsections summarize Phase II dynamic test models, test fixture, and system and sequential operating procedures. Appendices F, Dynamic Test Fixture, and G, Dynamic Test System, present a more detailed description of these features, documenting their usage and limitations.

Test Models

Four model types were evaluated during Phase II dynamic tests. The flat 440C version was the primary test vehicle from which the bulk of effect and hit frequency data was acquired. Two tests were performed with a similar configuration, flat carbide poppet and 440C seat, to explore a differential hardness parameter for the very hard materials. Interfacial scrubbing in relation to wear, and particle-induced damage were investigated with two configurations, deep entry spherical and the more novel

shear seal. Detailed drawings and fabrication and inspection procedures for these models were presented in Section III.

Test Fixture

The dynamic test fixture was similar to the previously discussed static version in the concepts of precision model retention and hydrostatic bearing piston loading. Additional features included solenoid valve-controlled piston pressurization, hydraulic dashpot velocity control, built-in poppet position transducer for velocity indication, and piezoelectric load cell for impact load measurement. The dynamic tester could be used for both cyclic and static (stress-leakage) testing.

In the dynamic tester, the poppet was clamped to the piston. Adjustment of three clamp ring screws provided a means of minimizing poppet-seat interfacial nonparallelism prior to nitrogen static control tests. Cycle tests were performed after switching the tester from a gaseous supply source to a recirculating Freon TF system (Appendix G) via specially re-worked hand valves. In this mode, either clean or particle-contaminated fluid could be directed through the poppet and seat interface during cycling.

Except for reservoir ullage, the system was completely filled with the operating fluid. This led to a problem of tester cavity pressure surges during cycling when the nominal 0.030-inch piston stroke momentarily displaced cavity fluid. The resulting pressure rise caused reverse system flow and presented an undefined particle distribution to the poppet and seat interfaces. Addition of a pressurized surge suppression bladder to the tester cavity ultimately resolved this problem.

Stress-Leakage Test

As with static particle tests, the stress-leakage test provided an index of test model performance before and after exposure to contaminants. It was performed in the same general manner as in the static tester. The only problem encountered was occasional model nonparallelism in excess of tester clamp ring adjustment capabilities. (This was ultimately established during Phase III to be on the order of 10 microinches for the model assembly at the 0.470-inch mean seating diameter.) Some models exceeded the adjustment capability and a greater than normal load sensitivity is reflected in these models' data below 1000-psi stress.

Test Particles and Concentrations

Three types of test particle were used for Phase II dynamic tests: HA, HB, and SB. As previously described, the H and S prefix designated hard (R_C 62-67) and soft (R_C 17-21) nickel alloy material. The letter suffix denotes a distribution about a mean size; hence, HA represents hard 58 micron, HB is hard 32 micron, and SB is soft 32 micron for the classified particles used (see Section II Analysis). As subsequently discussed, numerous HA impacts were found to cause relatively massive sealing degradation and, thus, were not representative of real systems. The SB type, being magnetic, resulted in system cleanup problems and poor concentration control. Most of Phase II (and all Phase III) testing, therefore, utilized HB particles.

Two considerations were involved in establishing particle concentration levels. First, sufficient particle impacts or events were required to produce a measurable effect within a reasonable number of cycles. Secondly, using 1000 cycles as a baseline, the particle concentration required to produce the effect should represent a practical population. Accordingly, test concentration levels in the 1000 to 10,000 p/l (particle/liter) realm were employed. These values effectively bracketed the Level 8 concentration described in Section II and are presumed to reflect reasonable rocket engine propellant contamination.

Test System and Sequence

The dynamic test setup was relatively complex with numerous features and subsystems. It basically consisted of a centrifugal pump-operated recirculation circuit fabricated from relatively clean (no contaminant generation) components and having a minimum of low velocity or trap areas. A small portion of total system flow was diverted through the test model interfaces while the balance maintained a steady particle flow during cycling and served a tester flushing function. Selectively operated pitot tube samplers were provided to extract calibrated representative samples of line flow which, in turn, were continuously analyzed for particle size and concentration by an automatic particle counter. Rotary plug selector valves provided for flow diversion through a cleanup filter bank and isolation of the dynamic tester for 1000-psig nitrogen gas stress-leakage tests.

Detailed test operations were necessarily more complicated than with the static test system, and are described along with the entire system in Appendix G. Following is a summary of basic procedures required for a typical dynamic model test:

1. Finish and inspect test model
2. Clean and assemble into tester
3. Perform initial stress-leakage test; evaluate for acceptability
4. Switch tester to liquid system (filter bank in) and preclean
5. Perform 1000 background (filter bank out) or ultraclean (with filter) cycles
6. Switch tester out of liquid system and perform stress-leakage test
7. Switch tester to liquid system (filter bank in) and preclean
8. Switch out filter bank, add test particles to reservoir and monitor particle counter to verify desired, stabilized count
9. Perform 1000 particle cycles with particle concentrations recorded at 0, 100, 200, 500, and 1000 cycles
10. Switch in filter bank; after system cleanup, switch filter bank out and tester to gas system
11. Perform final stress-leakage test
12. Remove model from tester and inspect for number of particle impacts and resulting damage characteristics

DATA PRESENTATION

Stress-Leakage Data

Stress versus leakage results in conjunction with hit-frequency information provided the prime test output data. With one exception, stress-leakage characteristic curves for dynamically tested models are presented in the same format as static model tests. The variable seating contact area of the shear seal configuration precluded plotting on a comparable stress basis; therefore, data for this model are presented as load versus leakage. All data were taken at 1000-psig supply pressure; hence, no reduced pressure leakage conversion was required.

The initial stress-leakage test provided an index of model acceptability for further test. Leakage data after 1000 clean cycles formed the control baseline from which subsequent particle cycle results were assessed.

Particle Count Data

A tabulation of particle count data is included with each model discussion. These data are taken prior to particle introduction and commencement of cycling, and after completion of portions of the cycle test sequence. The particle counts illustrate system background condition and variations in particle concentration during cycling, and were obtained from 1000 cc model seat flow samples (S_p sampler, Fig. G-1). Values for particles in the size range being evaluated form the basic data from which average particle concentration was computed. The lesser-sized ranges are considered the background, comprised of both uncontrolled contaminants (primarily from the pump seal and valves) and that portion of the classified particles falling in these size ranges (approximately 2 percent).

Model Inspection and Performance Data

Table V-1 presents a summary of pertinent inspection, test parameters, and test result information for Phase II dynamic test models.

Model Description. Seating dimensions were obtained from plain and interferometric inspection in the same manner as described in Section IV. It should be noted that, while normal land widths are given for the spherical and shear seal models, seating area for these models is based on projected (axial) land width. Sketch and abbreviated part numbers refer to detail model drawings presented in Section III.

Test Parameters. Dynamic system flow and pressure parameters were established using the flat 440C model as a standard test vehicle at a stroke of 0.030 inch. Additional ΔP associated with the spherical and shear seal models necessitated larger strokes to maintain standard system flows. Net actuation pressure and static seat stress values pertain to the on-seat stabilized load for each cycle. Generally, 169-psig cyclic control pressure was used. Dashpot friction, tester cavity pressure, and bias spring force reduced net seating loads accordingly.

TABLE V-1

PHASE II DYNAMIC TEST MODEL DATA

Model Designation and Description										Test Parameters								Test Results									
Model	Description	Poppet		Seat				Flat Seat Area (A _{sp}), sq in.	Stroke T, inches	Stroke Flow Area A _f , sq in.	Net Actuation Pressure, psig	Static Seat Stress, psi	Impact Velocity in./sec		Approximate Peak Impact		1000 psig Nitrogen Leakage, ⁽¹⁾ scim, at 1000 psi stress			Particle Data							
		Part No.	Serial No.	Part No.	Serial No.	Mean Diameter (D _s), inches	Land Width (L), inches						Axial	Normal	Force, pounds	Stress, psi	Initial	After Clean Cycles	After Particle Cycles	Type	Concentration Particles/Liter						
							Total															Flat					
Prior to use of tester cavity pressure surge damping bladder																											
116	Flat 440C	'28B-3	07	'29B-3	07	0.4687	0.0285	0.0270	0.0397	0.030	0.0415	139	5910	7.1	7.1	830	20,900	0.01	0.005	0.11	HA	3440					
120	Flat 400C	'28B-3	05	'29B-3	05	0.4700	0.0281	0.0250	0.0369	0.030	0.0416	139	6360	6.3	6.3	710	19,300	0.0059	0.0076	0.23	HA	7430					
121	Flat 440C	'28B-3	04	'29B-3	012	0.4697	0.0310	0.0297	0.0439	0.030	0.0413	139	5340	~7.5	~7.5	800	18,200	0.016	0.013	0.055	SB	9480					
122	Flat 440C	'28B-3	03	'29B-3	010	0.4698	0.0308	0.0284	0.0419	0.030	0.0414	139	5590				19,100	0.013	0.021	0.60	HB	6600					
126	Flat 440C	'28B-3	010	'29B-3	01	0.4688	0.0291	0.0268	0.0395	0.030	0.0414	139	5940				20,200	0.0025	0.0031	0.011	HB	2010					
126	← Same as Above (Repeat Test)																	0.013	0.015	0.031	HB	2980					
201	20 Degree Spherical 440C	'80-2	01	'83-2	01	0.4692	0.0308	0.0306	0.0152	0.035	~0.020	70	7770	4.3	1.5	320	21,000	0.013	0.016	0.40	HB	1100					
201	← Same as Above (Repeat Test)																	0.068	0.065	36.	HB	4850					
303	Shear Seal	7190-1	02	7190-4 (Alternate)	03	0.472	0.0029	0.0029	0.00148	0.040	~0.020			5.3	1.8			0.0003	0.0001	0.37	HB	5310					
401	Flat Carbide Poppet, 440C Seat	'28-5	01	'29B-3	02	0.4690	0.0300	0.0269	0.0396	0.030	0.0413	139	5920	4.7	4.7	640	16,100	0.005	0.0067	0.0076	HB	948					
After installation of tester cavity surge pressure damping bladder																											
401	Flat Carbide Poppet, 440C Seat	← Same as Above (Repeat Test)									→								5.9	5.9	1000	25,300	0.0082	0.0076	0.019	HB	5010
127	Flat 440C	'28B-3	010	'29B-3	03	0.4693	0.0293	0.0263	0.0387	0.030	0.0415	139	6060	6.7	6.7	1000	25,800	← ~0.1 →			HB	2120					
127																				HB	3870						
127																				HB	4415						
127	← Same as Above (Repeat Tests for Impact Event Data Only)									→														HB	4630		
127																				HB	10050						

(1) Shear seal model data at 40-pound load

PHASE II DYNAMIC TEST MODEL DATA

79

Poppet and seat impact velocity and peak impact load data were obtained from photographs of poppet position, elapsed time, and load cell information as displayed on a dual-beam oscilloscope. Impact velocity was based on a representative linear slope occurring over the last 0.010 inch of stroke to within 0.003 inch of impact.

Leakage Data. Model leakage initially and after clean and particle cycles is presented for ready comparison of model performance. Nonparallelism and surface texture effects were generally submerged at 1000-psi stress; hence, this stress level was selected as a reference point. For the shear seal model, 40 pounds seat load was utilized as the baseline condition. This load is approximately equivalent to that required for 1000-psi stress on the flat models.

Particle Data. Particle concentration data of Table V-1 resulted from sample counts taken at intervals during cycling as previously discussed. The averaging procedures described in Appendix G were employed to establish the noted concentration values. The predicted number of particle impacts for 1000 cycles was computed from the average concentration, mean particle size and land dimensions. Derivation of these calculations is described in Section II.

It will be noted that the data are grouped according to tests with and without the tester cavity surge suppression bladder. After addition of the bladder, pressures upstream and downstream of the poppet and seat ensured normal fluid flow. These tests provide valid hit frequency data. Former tests with reverse flow indicated a generally higher than expected hit frequency with HB particles, but lesser with the larger HA particles. The cause of this is unknown and may be due to particle flow dynamics.

Photographic Data

Two types of photographic data appear in subsequent model discussions. As with the static test effort, model surface damage was assessed through the use of an interference microscope. Photomicrographs typifying these observations are presented with appropriate models. Oscilloscope displays of poppet position and loads were utilized to establish impact velocity and load data. Photographs of these displays are presented to illustrate typical dynamic closure conditions. As noted in Appendix F, the position trace between 0.003 inch off seat and closure impact is affected by system elasticity producing an apparent time delay.

FLAT 440C TEST MODELS

The majority of Phase II dynamic testing was performed with flat 440C models. The easily refinished seating lands and past experience with assembly and testing made this configuration ideal for initial particle testing. Consequently, it was used to evaluate HA, HB, and SB particle effects. Because of uncertainties relative to system cleanup capabilities with the smaller sizes, HA particles were used in system development and, therefore, for initial model tests.

Models 116 and 120 (HA Particles)

A flat 440C model had been used during system calibration and establishment of general operating procedures. Model 116 was the first such model to be formally tested. The problem of nonparallel closure was encountered and, with Model 116, the procedure of clamp ring adjustment for minimum low-stress leakage was established. As illustrated by Fig. V-1, the resultant control stress-leakage characteristic indicated that adequate parallelism was achieved.

Model 116 was next subjected to a 1000-cycle background test (filter bank bypassed). Periodic checks of system contaminant level during this test were made as shown in the following tabulation:

Cycles	HIAC Count/Liter	
	10 to 30 Microns	>30 Microns
0	10	0
100	118	0
500	179	2
1000	208	4

Impact velocity was approximately 7.1 in./sec and peak impact force about 830 pounds, as shown by the oscilloscope traces of Fig. V-2. Velocity is computed from the upper left displacement trace.

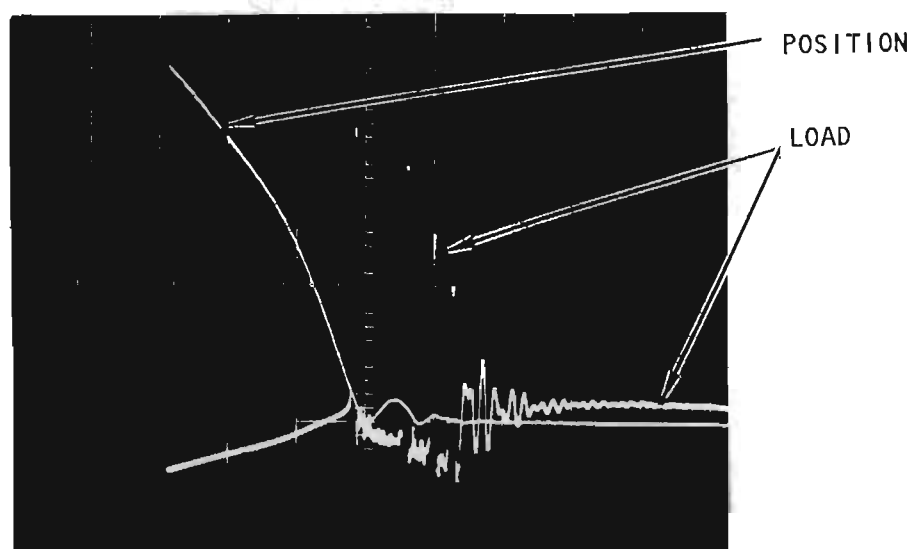


Figure V-2. Model 116 Load and Displacement Traces (0.002 sec/div; 200 lb/div; 0.005 in./div)

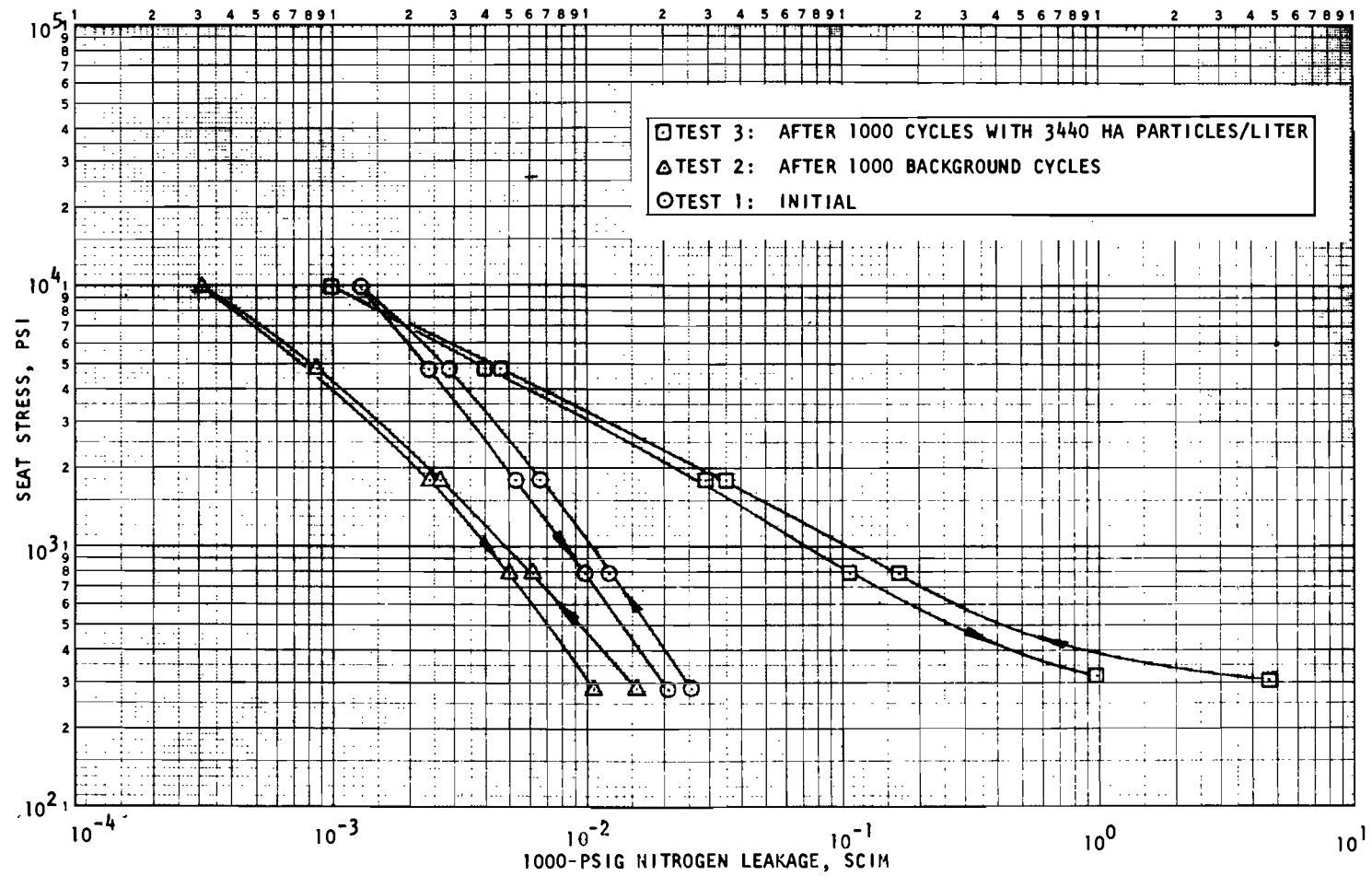


Figure V-1. Stress-Leakage Data for Dynamic Test Model 116, Tests 1, 2, and 3

These traces typify the dynamic characteristics of models tested prior to addition of the tester cavity bladder. The rise in seat load during cavity pressure buildup is evident in the load trace beginning at the lower left. As this load is not applied to the seating surface, it is subtracted from the total indicated value in arriving at net peak impact force.

As shown in Test 2 (Fig. V-1), leakage following background cycles was approximately halved. This trend of improved sealing performance after clean cycles is generally typical of these models. It is primarily attributed to gradual deformation of surface nodules and asperities permitting more intimate interfacial contact.

Model 116 was cycled 1000 times with HA particles. Counts throughout the test are listed in the following tabulation from which an average concentration of 3440 p/l resulted.

Cycles	HIAC Count/Liter	
	10 to 30 Microns	>30 Microns
Background	35	0
0	162	3480
100	987	3400
200	1079	3680
400	1038	3410
1000	1206	3350

The preceding data indicate a final 10- to 30-micron background count amounting to 36 percent of the comparable greater-than-30-micron reading. The excessive background level is attributed to a procedure employed with Model 116 (and Model 120). During these tests, the outboard side of the system pump shaft seal packing was pressurized with filtered Freon TF. This produced a low flow past the seal to prevent test particles from being wedged into the shaft-seal clearance. Particles of seal material in the 10 to 15 micron range were carried into the system and caused the high background counts noted. This problem occurred with subsequently discussed Model 120, and also accounts for the numerous small size counts recorded during background testing of both models. After completion of Model 120 tests, seal pressurization was stopped, background counts dropped, and no further significant seal problems occurred.

As the stress-leakage results of Test 3 (Fig. V-1) indicate, leakage at 1000-psi stress increased by a factor of 20. This performance degradation resulted from four particle hits rather evenly spaced around one third of the land circumference. None of the particles remained trapped, and the upset metal surrounding the impacts (residual damage) was the sole cause for the loss in sealing capability. Height of the upset ranged from 10 to 35 microinches. Figures V-3 and V-4 illustrate the surface damage, which was similar to that noted with Static Test Model 125 (Fig. IV-19).

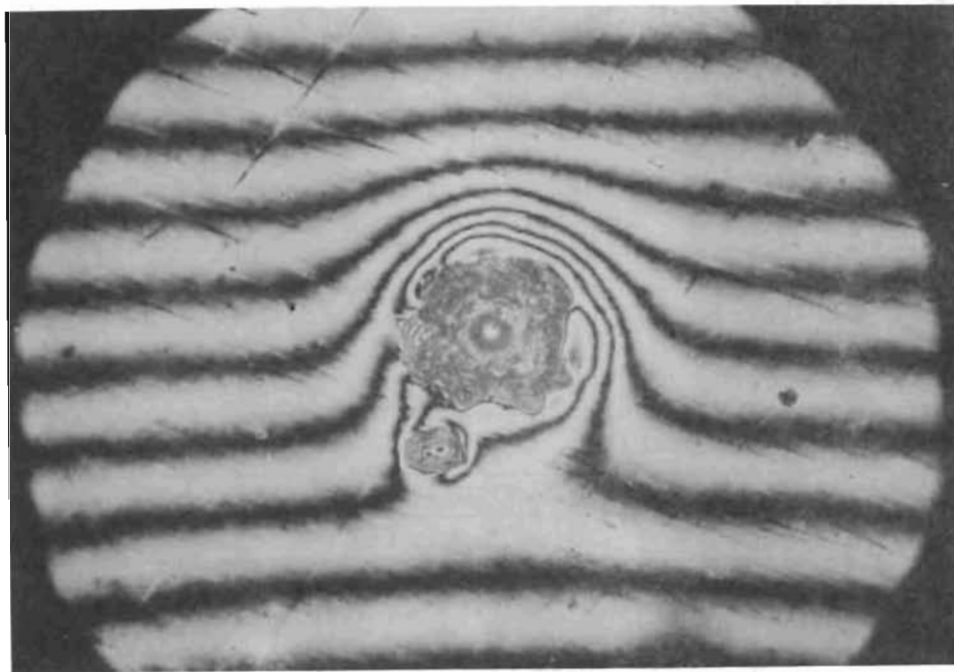


Figure V-3. Model 116 Poppet Showing Damage From HA Particle (187X Interference Photo)

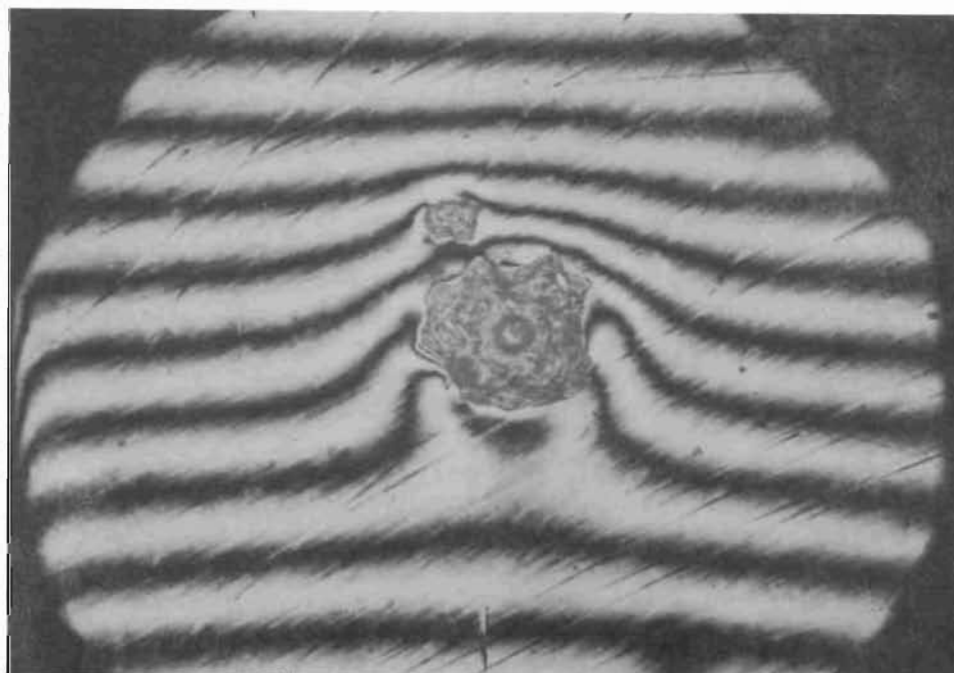


Figure V-4. Model 116 Seat Showing Damage From HA Particle (187X Interference Photo; Same Location as Fig. V-3)

A second test of HA particle effects was performed with Model 120. As shown in Fig. V-5, the initial stress leakage characteristic was similar to that of Model 116, except that some nonparallel influence is evident below 1000-psi stress.

Model 120 was subjected to 1000 cycle background and particle tests. Following are particle count data for these two tests.

Cycles	HIAC Count/Liter	
	10 to 30 Microns	>30 Microns
<u>Background Test</u>		
0	7	0
100	78	4
500	185	1
1000	242	5
<u>HA Particle Test</u>		
Background	8	0
0	178	7200
100	212	7760
200	438	6440
600	686	8270
1000	888	6860

As shown in Fig. V-5, leakage following background cycles improved slightly but not to the extent noted with Model 116. Inspection after HA particle cycles with 7430 p/l revealed 10 "normal" size hits. In addition, approximately 15 encounters of much smaller size were found. It is not known whether these resulted from particulates entrained in the fluid or fragments from larger size impacted particles. Figures V-6 and V-7 illustrate particle-caused surface damage. Upset metal height ranged from 10 to 22 microinches.

A comparison of Fig. V-1 and V-5 indicates that both Models 116 and 120 exhibited similar sealing degradation even though the former incurred much less damage. This is attributed to the hit locations. Model 116 damage occurred on one side of the land while, with Model 120, hits were evenly distributed. Similar to the 1, 2, and 3 particle results of static tests, Model 116 clamshell closure produced leakage equivalent to that of a parallel plate gap of similar height.

Dimensions of surface damage from HA particles resembled those obtained with the H60 static test particles. While the 10 to 20 times increase in 1000-psi stress leakage noted for Models 116 and 120 might be considered tolerable in an actual valve application, this performance loss resulted from residual damage only. In view of the severe degradation attendant with trapped particles noted in static tests, further evaluation of the HA particles with these models was considered impractical.

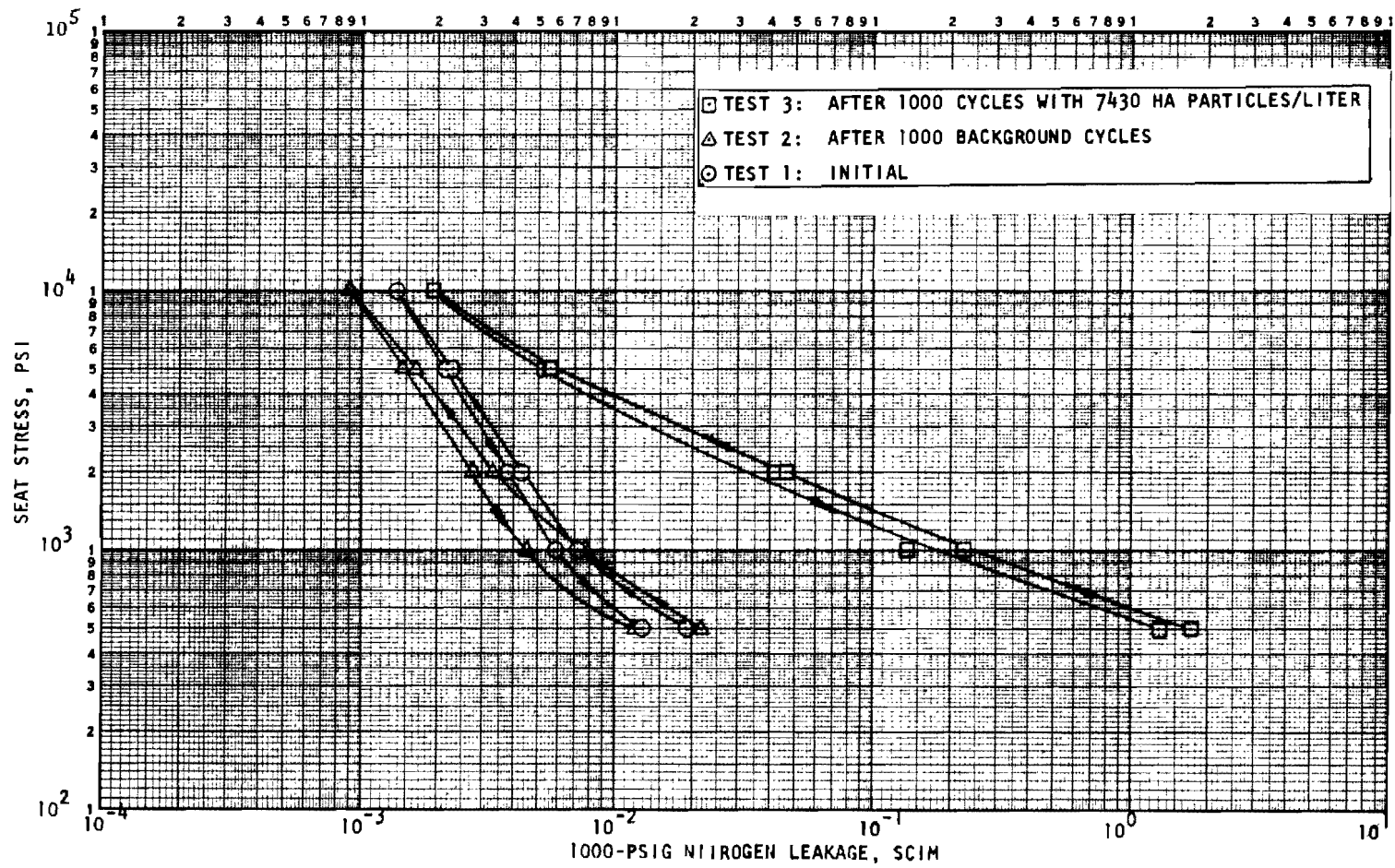


Figure V-5. Stress-Leakage Data for Dynamic Test Model 120, Tests 1, 2, and 3

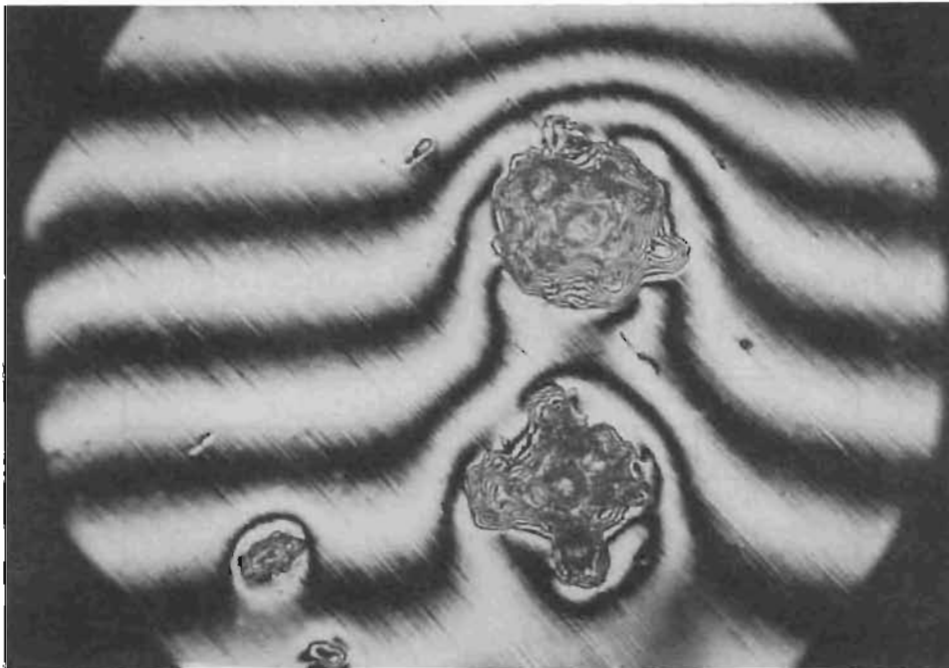


Figure V-6. Model 120 Poppet Showing Double HA Particle Hits and Fragment Hit Damage (187X Interference Photo)

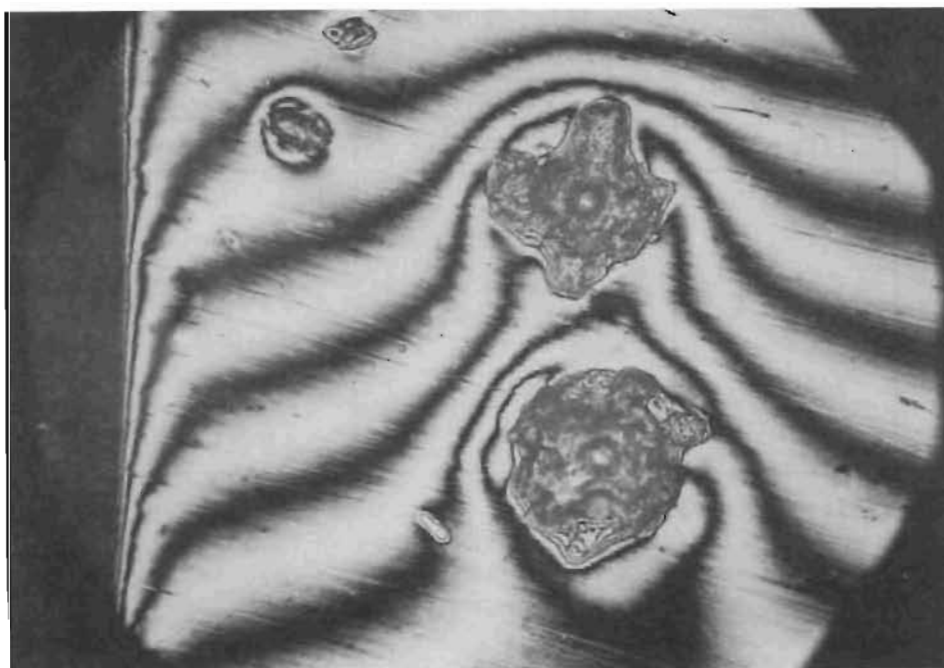


Figure V-7. Model 120 Seat Showing Double HA Particle Hits and Fragment Hit Damage (187X Interference Photo; Same Location as Fig. V-6)

Model 121 (SB Particles)

With the decision to terminate HA particle testing, evaluation of SB particle effects was initiated with Model 121 as the test vehicle. Figure V-8 presents stress-leakage data for the test sequence.

As discussed in Appendix G, the SB particles were magnetic and had a tendency to agglomerate and collect in various portions of the system. At the conclusion of SB particle calibration testing, special attention was directed to system and component cleanup including lengthy filtered run periods. The effect of this effort was reflected in the low 12- to 20-micron counts obtained during Model 121 background cycles shown in the following tabulations:

Cycles	HIAC Count/Liter	
	12 to 20 Microns	>20 Microns
0	2	0
100	18	6
200	25	10
500	20	10
1000	40	18

Following background cycling, which caused little change in leakage characteristics, Model 121 was cycled 1000 times with an average particle concentration of 9480 p/l. As shown in the particle count data following, a significant concentration reduction occurred during these cycles. This problem, attributed to trapping of particles in magnetic areas of the system, ultimately led to cessation of SB particle testing.

Cycles	HIAC Count/Liter	
	12 to 20 Microns	>20 Microns
Background	1	0
0	120	11,900
100	114	10,900
200	123	11,000
500	140	9,420
1000	152	8,270

Inspection after removing Model 121 from the tester revealed that 28 impact events had occurred including two instances of double hits. No particles remained embedded. As shown in Test 3 (Fig. V-8), leakage increase due to residual damage was minimal above 1000 psi.

Considering the results of Models 116 and 120, where predicted impacts were less than the actual, it was thought that the excessive hits of Model 121 were influenced by particle magnetism. Particle concentration was cyclic and closure during passage of abnormally high concentration appeared

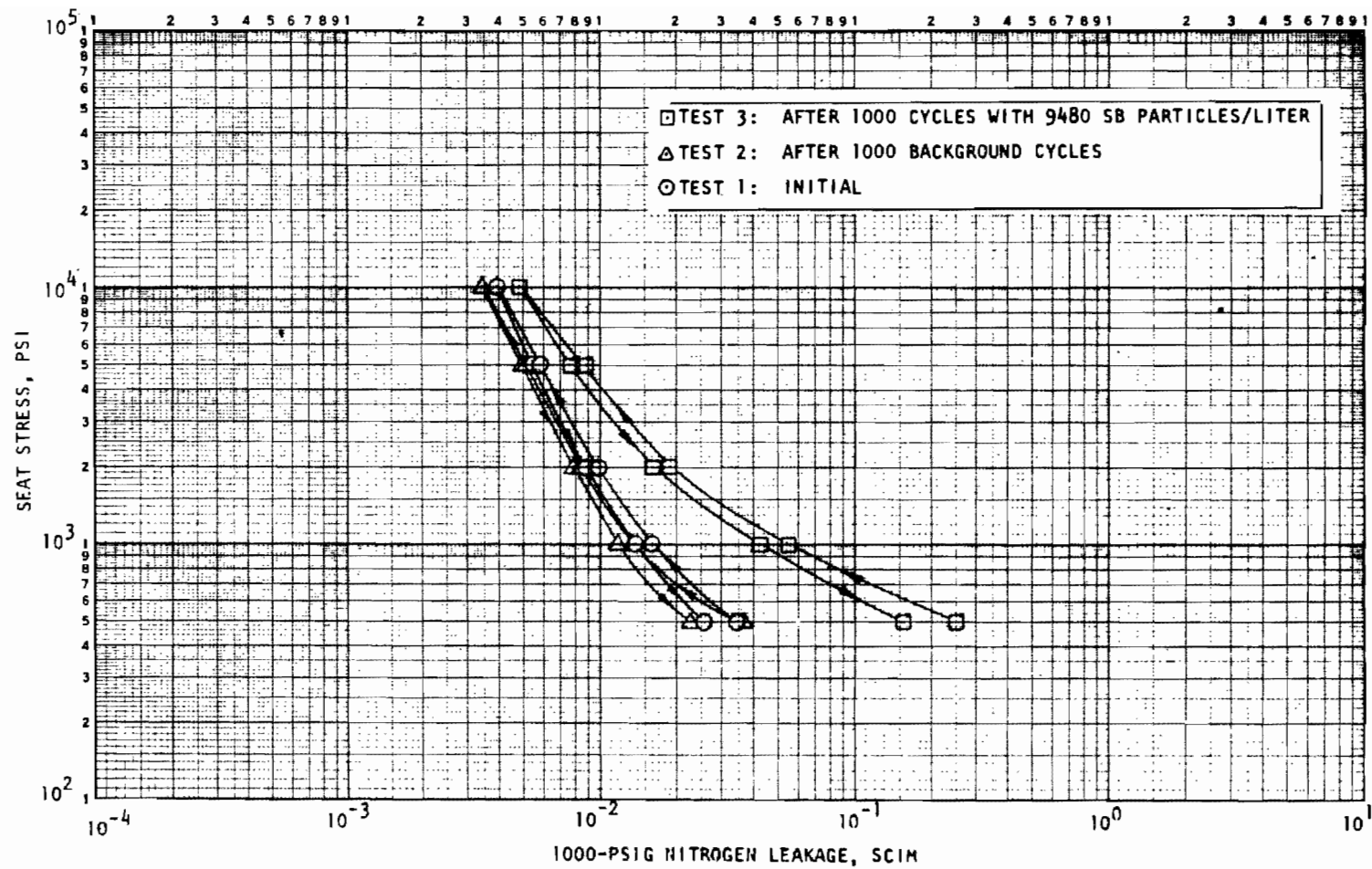


Figure V-8. Stress-Leakage Data for Dynamic Test Model 121, Tests 1, 2, and 3

probable. When subsequent tests using the nonmagnetic HB particles yielded similar results, however, it was eventually concluded that reverse flow and not magnetic effects was the prime cause. In this light, the data for Models 116 and 120 are anomalous and the reason for less-than-predicted hits is unknown.

Surface damage caused by SB particles was similar to that of S30 material except for indications of a relatively soft seat as seat hole depth was about four times that of the poppet. Figures V-9 through V-12 illustrate typical impact characteristics.

Models 122 and 126 (HB Particles)

These models were the first to be evaluated with HB particles and were to serve a twofold purpose: (1) for comparison with the SB particle results of Model 121, and (2) to determine the advisability of further testing with the HB material. Model 122, however, produced anomalous results which greatly negated its worth from an HB particle evaluation standpoint. The stress-leakage data of Fig. V-13 illustrate this problem, which is evident by the high leakage below 2000-psi apparent seat stress.

Model 122 was initially tested for potential use as a static test model. The characteristic curve noted in Fig. V-13 resulted and could not be readily explained. The static tester at that time had been modified with the 0.001-inch ball joint shim and the curve shape did not appear to be that caused by eccentric loading. A surface reinspection offered no explanation and the model was passed over for static testing.

However, because the model was available, it was considered suitable for dynamic hit-frequency evaluation of HB particles. (At this time, the reverse flow influence of dynamic tester cavity pressure surges was not recognized and the bladder had not been installed.) Accordingly, the model was installed in the dynamic tester; initial stress-leakage data closely paralleled the static tester results. The model was then subjected to 1000 background cycles with the following particle counts:

Cycles	HIAC Count/Liter	
	12 to 20 Microns	>20 Microns
0	4	0
100	28	22
200	39	24
500	52	31
1000	59	37

Stress-leakage results after the background test reflected little change. the model was then cycled 1000 times with an average HB particle concentration of 6600 p/l; the following particle counts were recorded:

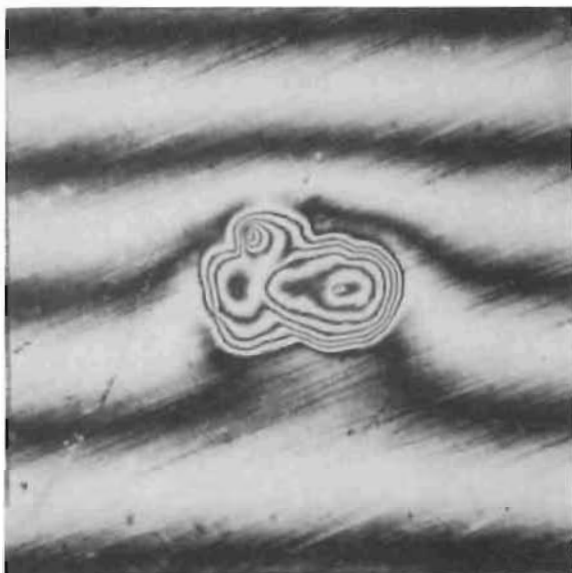


Figure V-9. Model 121 Poppet Showing Depression From Double SB Particle Hit (187X Interference Photo)

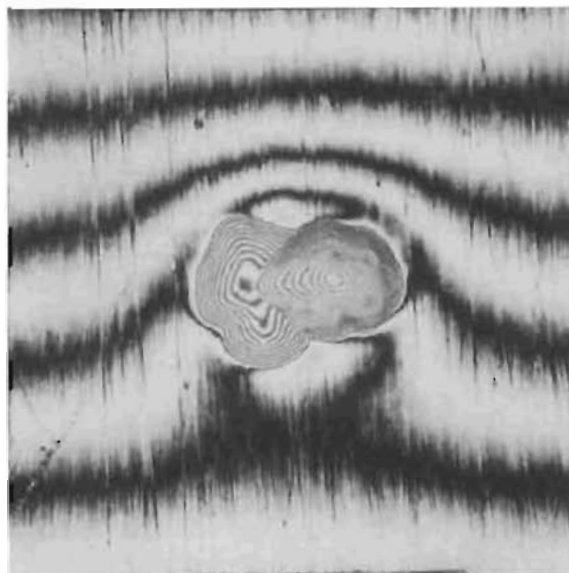


Figure V-10. Model 121 Seat Showing Depression From Double SB Particle Hit (187X Interference Photo; Same Location as Fig. V-9)

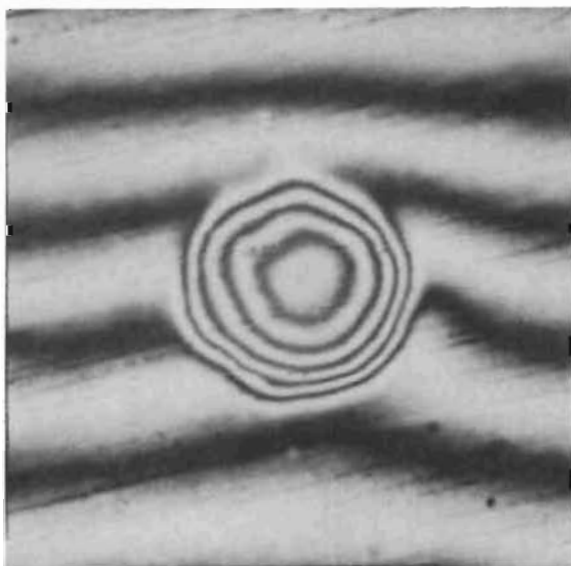


Figure V-11. Model 121 Poppet Showing Depression From SB Particle Hit (462X Interference Photo)

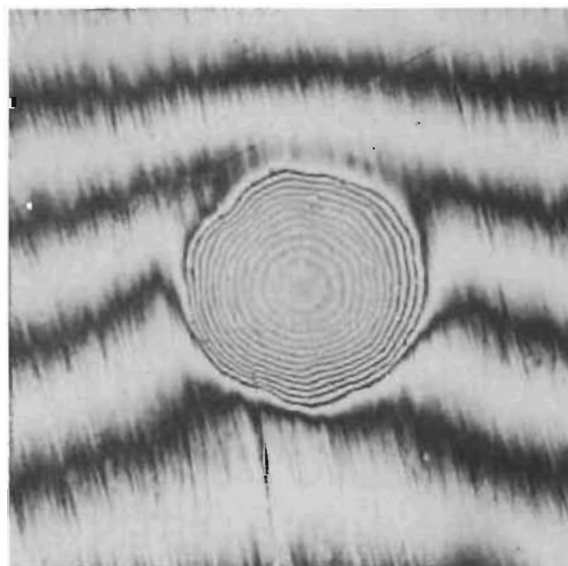


Figure V-12. Model 121 Seat Showing Depression From SB Particle Hit (462X Interference Photo; Same Location as Fig. V-11)

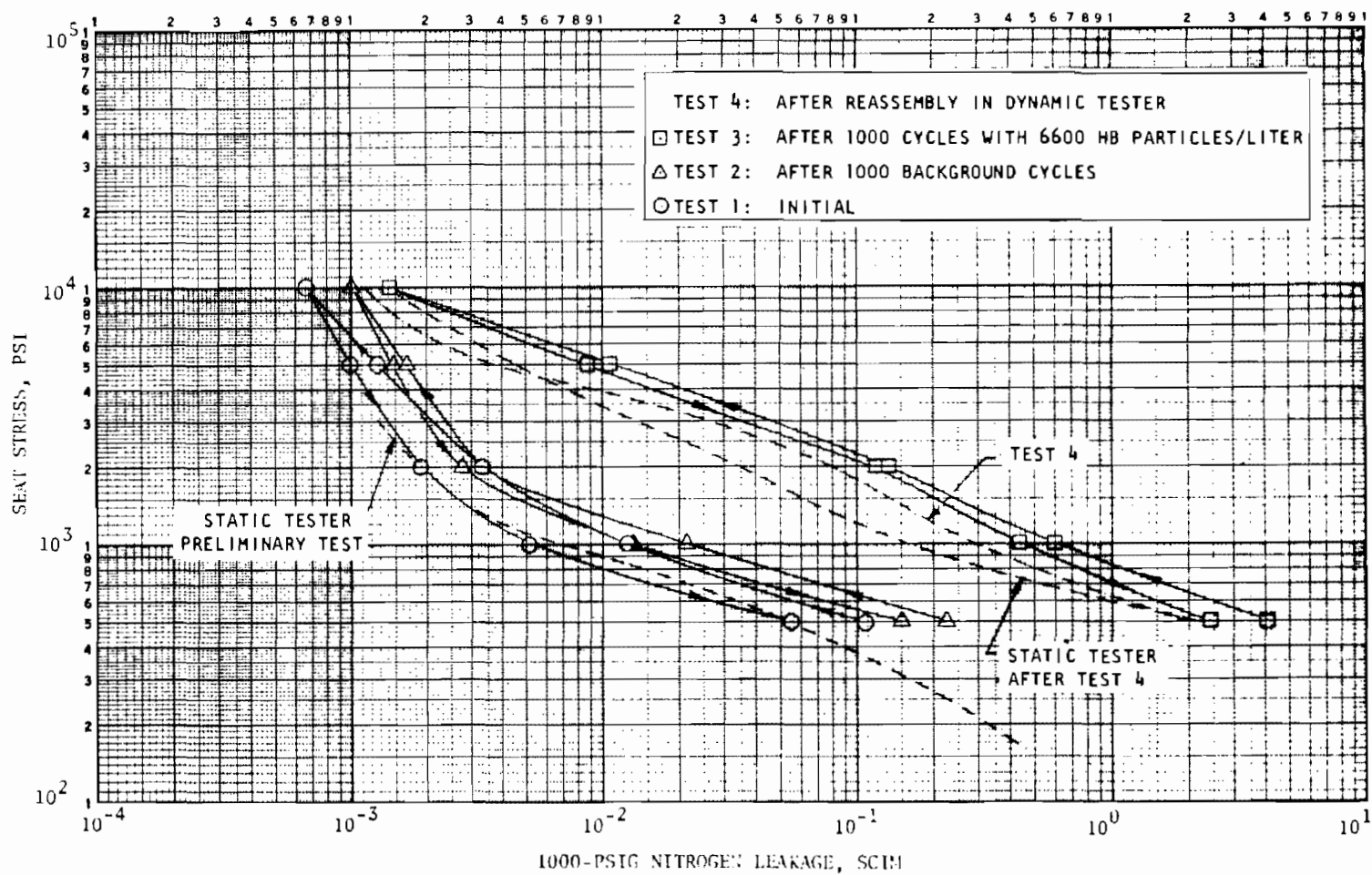


Figure V-13. Stress-Leakage Data for Dynamic Test Model 122, Tests 1, 2, 3, and 4 and Static Tester (Ball Joint Loaded) Preliminary and Final (After Test 4) Tests

Cycles	HIAC Count/Liter	
	12 to 20 Microns	>20 Microns
Background	0	2
0	154	7560
100	175	7080
200	168	6610
500	175	6480
1000	218	6390

Stress-leakage results following particle cycles indicated considerable degradation as shown in Test (Fig. V-13). Inspection following removal from the tester revealed that 20 HB-type hits had occurred. When the subsequently discussed Model 126 was tested and ultimately accumulated 17 impacts, however, sealing degradation was far less than that of Model 122. As a recheck, Model 122 was then retested in the dynamic tester (Test 4) and, finally, in the static tester. As indicated in Fig. V-13, little change was noted.

Detailed interferometric inspection of Model 122 was then performed. In addition to the 20 impacts originally noted with plain microscope viewing, approximately 10 additional apparent impacts of lesser damage were found, as typically illustrated by Fig. V-14 and V-15.

From the inspection, it was concluded that two of the initial HB impacts had resulted in partial retention of particles in the seat. These particles, in subsequent retest, caused secondary damage to the poppet which, in turn, transferred back to the seat even smaller but still recognizable surface blemishes. However, seat reinspection failed to produce evidence of embedded material. It is presumed that it was extracted and lost during final stress-leakage testing.

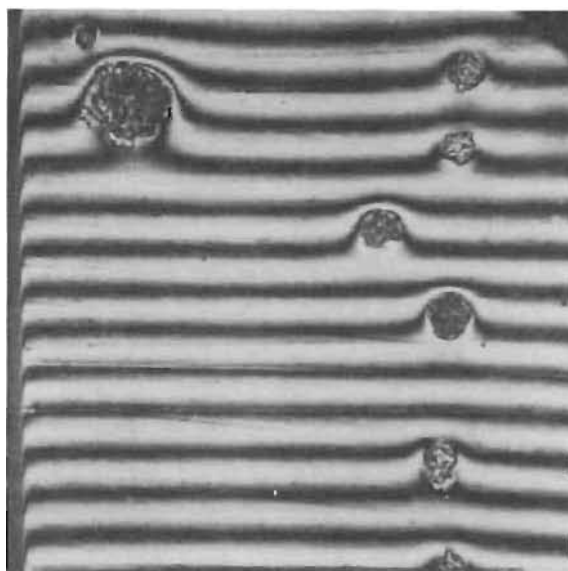


Figure V-14. Model 122 Poppet Showing HB Particle and Secondary Impact Damage (91X Interference Photo)

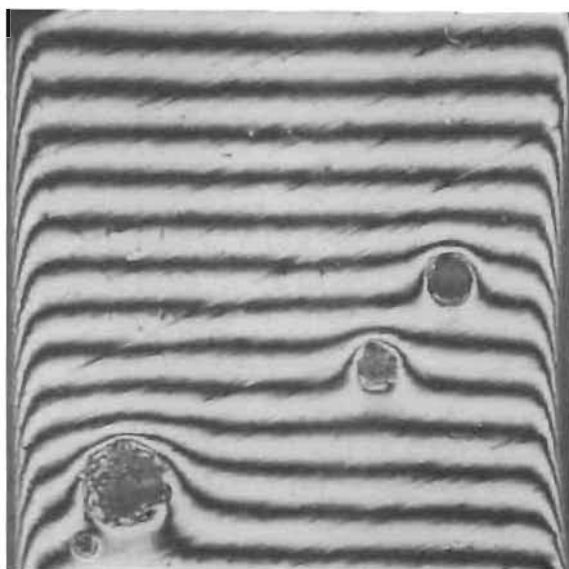


Figure V-15. Model 112 Seat Showing HB Particle and Secondary Impact Damage (91X Interference Photo; Same Location as Fig. V-14)

In contrast to Model 122, tests of Model 126 proceeded without significant event, and two dynamic test sequences were accomplished. Figure V-16 presents stress-leakage data for the first test series. Background and particle test count data for this sequence follow:

Cycles	HIAC Count/Liter	
	12 to 20 Microns	>20 Microns
<u>Background Test</u>		
0	3	2
100	32	11
200	16	10
500	31	22
1000	57	23
<u>Particle Test</u>		
Background	20	0
0	33	1870
100	36	2120
200	118	2040
500	94	2020
1000	142	1910

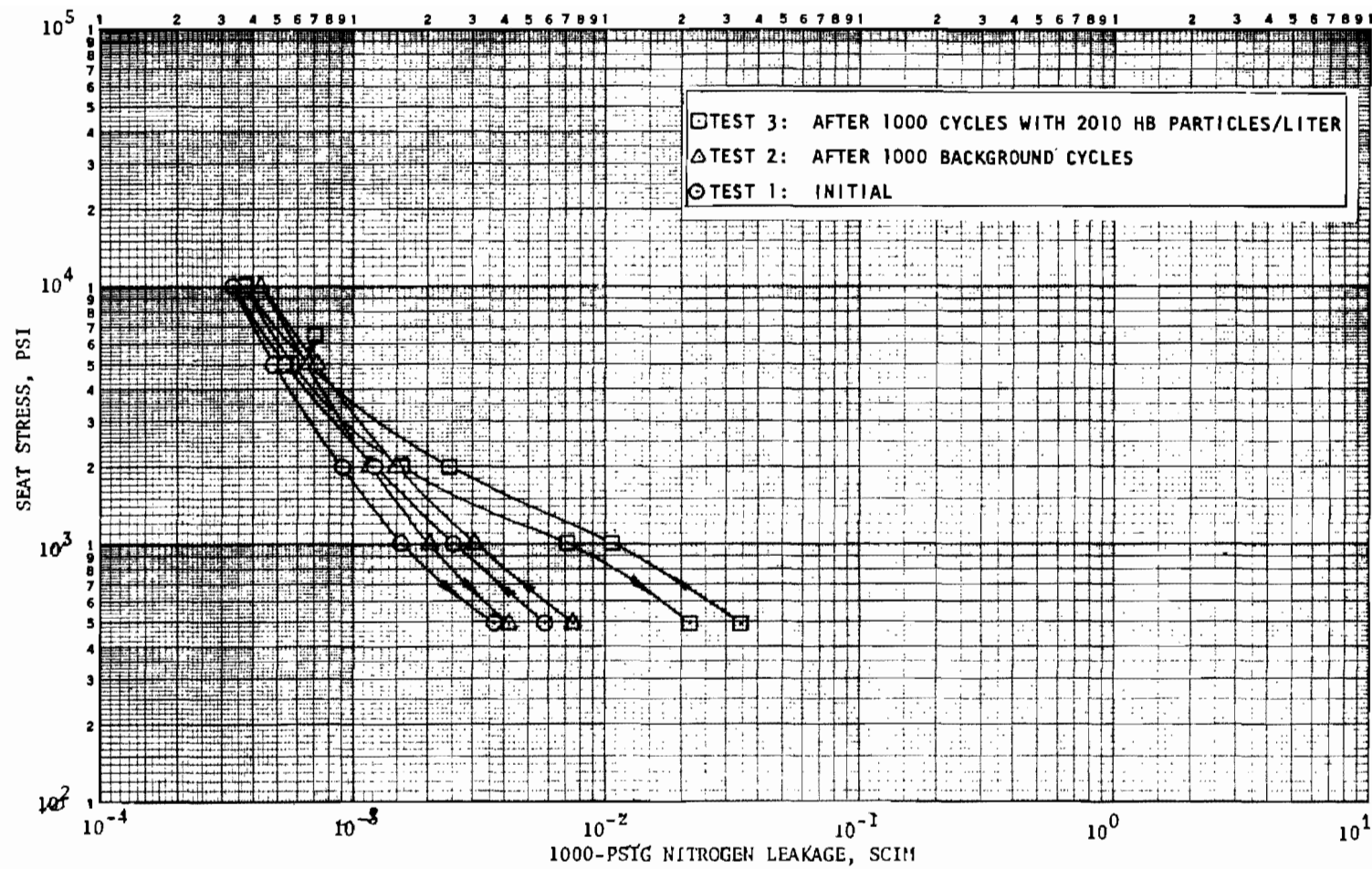


Figure V-16. Stress-Leakage Data for Dynamic Test Model 126, Tests 1, 2, and 3

For an HB particle concentration of 2010 p/l, Model 126 accumulated 8 impacts relatively evenly distributed. As Fig. V-16 indicates, leakage at 1000-psi stress increased approximately by only a factor of three. Accordingly, the model was utilized for a second test. Stress-leakage results are presented in Fig. V-17; particle count data are listed as follows:

Cycles	HIAC Count/Liter	
	12 to 20 Microns	>20 Microns
<u>Background Test</u>		
0	9 (est)	1 (est)
100	9	1
200	12	7
500	17	9
1000	30	17
<u>Particle Test</u>		
Background	0	0
0	49	2960
100	57	3070
200	48	3340
500	88	2920
1000	86	2780

For the second test sequence, the seating surfaces were reoriented 180 degrees from the former condition. Stress-leakage data following reassembly in the tester closely matched the preceding data (Test 3) which permits the model results to be successively compared. As with the first test sequence, background cycles resulted in little change.

After 1000 Cycles with 2980 HB p/l, Model 126 had received nine additional HB hits. Leakage at 1000-psi stress doubled, again a relatively minimal change. For the two test series and 17 impact events, net leakage increase at 1000-psi stress was about one order of magnitude. This indicates that without embedded particles, the 440C model and HB particle combination represents reasonable tolerance to contaminant influence.

As with the previous particles tested, there appeared to be little difference between static and dynamically created surface damage. In view of the relatively constant and predictable flow characteristics of the HB particles, and the problems of heavy damage and poor concentration control associated with the HA and SB material, it was decided to use HB particles exclusively for future tests.

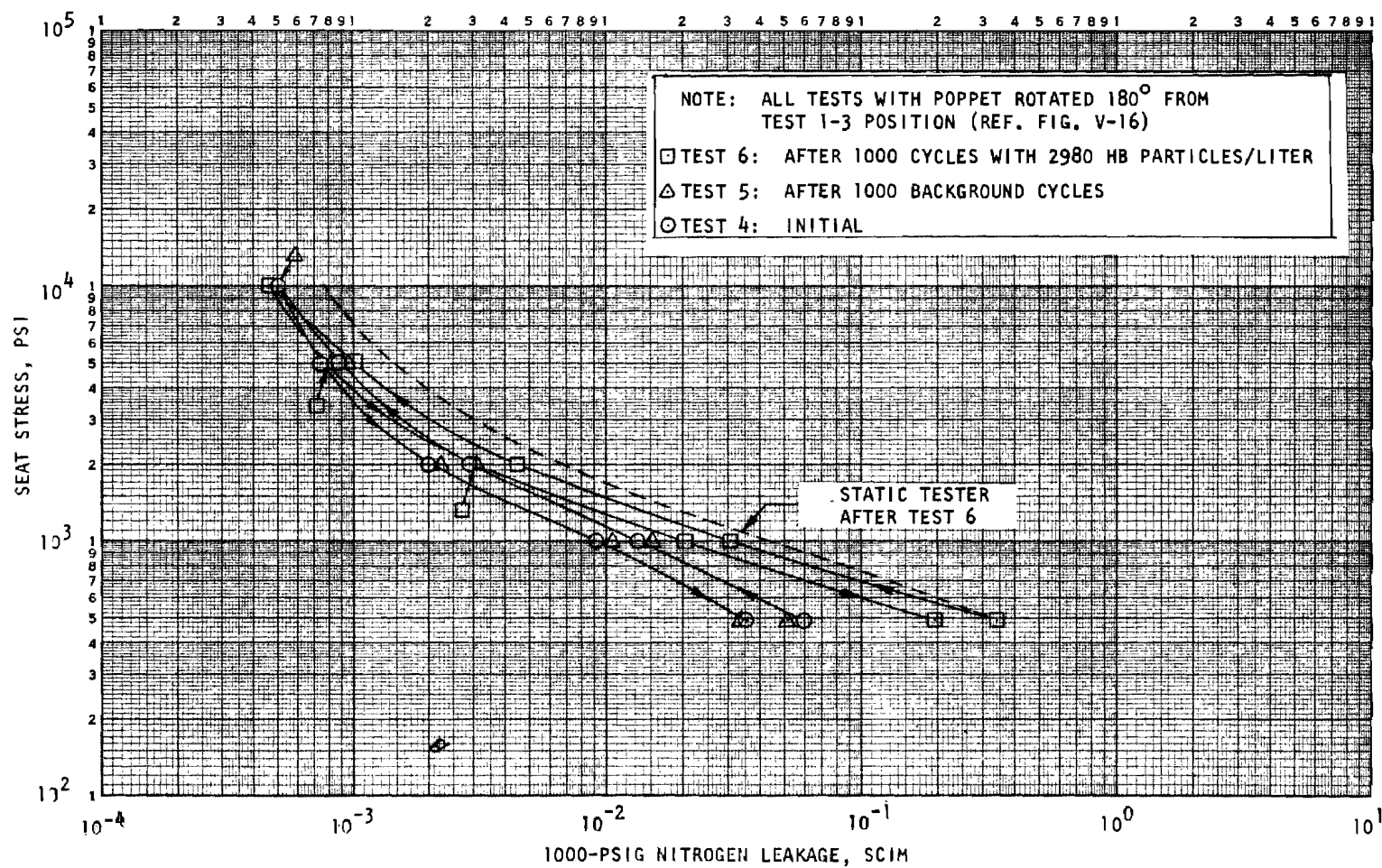


Figure V-17. Stress-Leakage Data for Dynamic Test Model 126, Tests 4, 5, and 6

Model 127 (HB Particles)

Two Phase II dynamic models were tested to evaluate hit-frequency variations after installation of the tester surge suppression bladder. Model 401, (carbide poppet, 440C seat), discussed subsequently, was tested once, but the bulk of this assessment utilized Model 127.

Stress-leakage tests prior to cycling indicated a relatively constant leakage of about 0.1 scim over the 500- to 1000-psi stress range. Later inspection established that the poppet sealing surface had several relatively large lapping scratches. Applying the scratch leakage equation presented in Ref. 3 (page 590), it was determined that two scratches approximately 320 microinches wide by 60 microinches deep produced most of the leakage (0.085 scim). Because HB particle hit-frequency data were the primary requirement, Model 127 was subjected to five particle cycle tests and formal stress-leakage testing was deleted. Spot checks indicated, however, that the aforementioned leakage rate remained essentially constant throughout the test series.

As described in Appendix F, the tester bladder addition made a marked change in dynamic performance. Dashpot velocity control was regained and premature seat load rise was eliminated. Figure V-18 illustrates the improved condition traces which may be compared with the nonbladder characteristics of Fig. V-2 (Model 116).

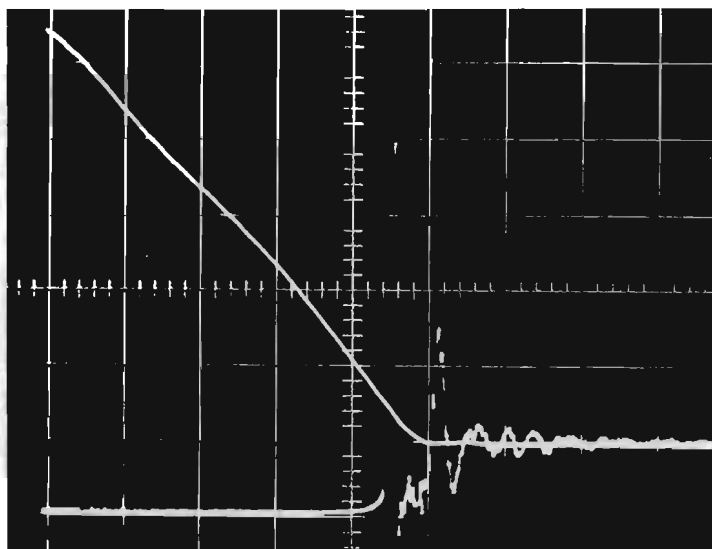


Figure V-18. Model 127 Load and Displacement Traces
(0.002 sec/div; 200 lb/div; 0.005 in./div)

Table V-2 lists particle count data for the five Model 127 tests. The following tabulation summarizes hit frequency information from Table V-1.

TABLE V-2

MODEL 127 DYNAMIC TEST HB PARTICLE COUNT DATA

Particle Test No.	Cycles	HIAC Count/liter, microns	
		12 to 20	>20
1	Background	8	0
	0	62	2185
	100	117	2286
	200	113	2150
	500	161	2120
	1000	163	2025
2	Background	6	0
	0	112	4270
	100	118	4030
	200	158	3985
	500	140	3790
	1000	201	3746
3	Background	5*	0
	0	115	4480
	100	157	4475
	200	202	4600
	500	213	4330
	1000	258	4360
4	Background	4	5
	0	228	4460
	100	220*	4830
	200	222	4700
	500	223	4640
	1000	292	4520
5	Background	1	8
	0	308	10,000
	100	284	10,500
	200	346	10,200
	500	359	9,970
	1000	403	9,880

*Estimated

Particle Test No.	HB Particle Concentration, p/l	Predicted Impacts (I_p)	Actual Impacts (I_A)	I_A/I_p
1	2,120	1.98	4	2.0
2	3,870	3.61	0	0.0
3	4,415	4.11	5	1.2
4	4,630	4.32	1	0.23
5	10,050	9.37	9	0.96

Tests 2 and 4 represent departures from the factor of 2 prediction accuracy apparent from other tests. From the Poisson equation, the probability of no hits (Test 2) and 1 hit (Test 4) is 0.0271 and 0.0576, respectively. These correspond to approximately one test in 37 and one test in 17, which are conceivable conditions.

Prediction of impact events within a factor of 2 represents significant improvement over the 3 to 4 times error noted for previous models without the tester bladder. It is, therefore, reasonably certain that surge pressure did result in reverse flow and influenced the particle concentration. This indicated that additional tests were required to provide statistical confidence and explore hit frequency under a variety of conditions and with both larger and smaller particles.

SPHERICAL 440C TEST MODEL

The 20-degree, deep-entry seating angle of Model 201 provided a configuration having a form of shearing action during closure. Two dynamic test sequences with HB particles were performed to determine impact characteristics and effects with this geometry.

Model 201 had been tested in the previous program as Model C_s. The initial stress-leakage test as Model 201 (Fig. V-19) compared favorably with previous results except that a greater frictional hysteresis effect was evident. This is attributed to the influence of clamped loading and inability to center the seating surfaces as well in the horizontal dynamic tester as in the former vertical static tester.

Model 201 was subjected to 1000 background and HB particle cycles with the following particle counts:

Cycles	HIAC Count/Liter	
	12 to 20 Microns	>20 Microns
	<u>Background Test</u>	
0	3	0
100	6	5
200	6	1
500	11	5
1000	14	10
	<u>Particle Test</u>	
Background	3	0
0	25	1045
100	33	1162
200	58	1182
500	61	1082
1000	64	1041

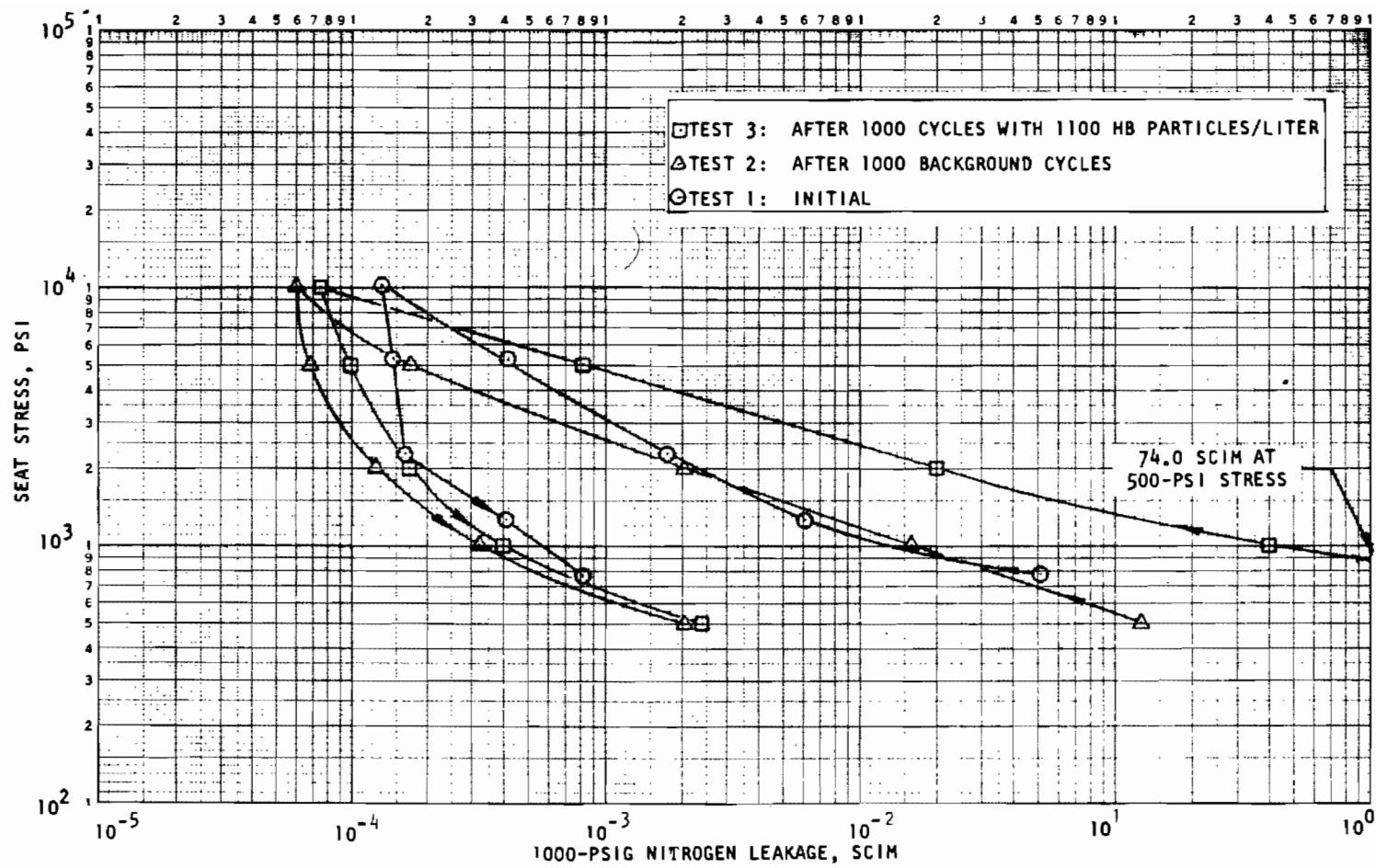


Figure V-19. Stress-Leakage Data for Dynamic Test Model 201, Tests 1, 2, and 3

As testing proceeded, a formidable effect of hysteresis on low-stress sealing was discovered. Stress-leakage Tests 1 and 2 were performed in a sequence that preloaded the sealing surfaces (increasing followed by decreasing load) prior to taking the first (500-psi stress) leakage measurement. This practice was followed also for the initial portion of Test 3. However, when the surfaces were separated at test pressures and then closed so that only nonhysteresis increasing load measurements were recorded, leakage at 500- and 1000-psi stress was considerably more than formerly noted. For example, at 500-psi stress, only 0.838 scim was initially measured as opposed to the 74.0 scim recorded after separation for Test 3. Some difference existed at 1000 psi, but data were unchanged at 2000 psi and greater stress levels. Thus, Tests 1 and 2 can only be compared with later tests from 2000 psi on. All further tests were performed with separation prior to leakage measurement.

In the first dynamic test sequence, Model 201 accumulated three positive impacts and two additional events which, by their location adjacent to other hits, may have been caused by the same particle. However, the effect was notable, as shown in Test 3 (Fig. V-19), with a significant leakage increase evident even at the elevated stress levels. Compared to the flat models, this spherical configuration appeared to be much more sensitive to contaminant-caused surface damage.

Model 201 was subjected to a second dynamic test sequence with the following particle counts; Fig. V-20 presents the stress-leakage data.

Cycles	HIAC Count/Liter	
	12 to 20 Microns	>20 Microns
<u>Background Test</u>		
0	1	1
100	1	0
200	7	2
500	9	1
1000	16	4
<u>Particle Test</u>		
Background	1	0
0	87	4960
100	79	5120
200	89	5120
500	122	4740
1000	166	4700

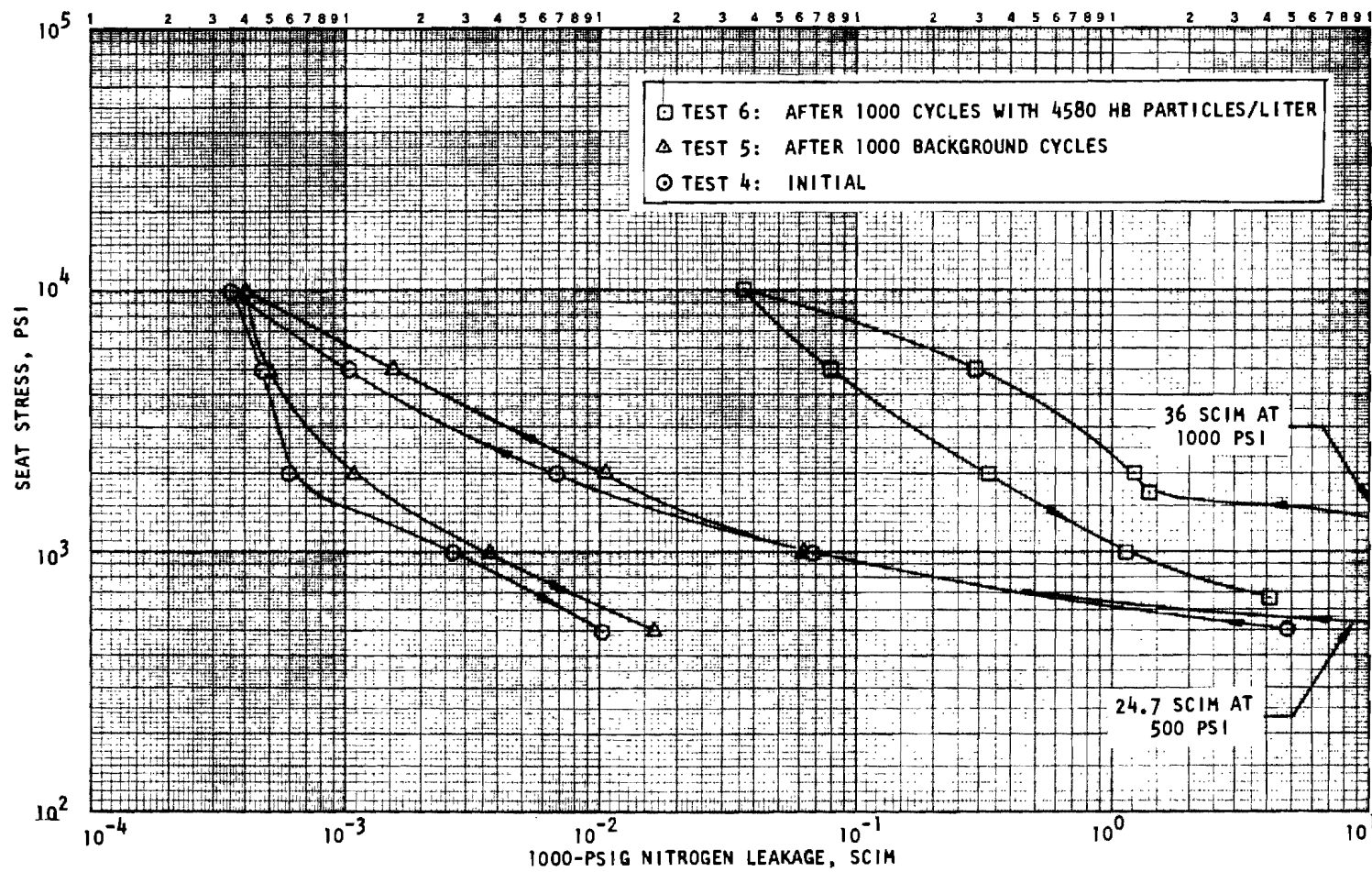


Figure V-20. Stress-Leakage Data for Dynamic Test Model 201, Tests 4, 5, and 6

After the second HB particle cycle test, a very large leakage increase occurred. From the results of Test 6, the curve "knee" suggested that at least one particle had been embedded. Interferometric inspection failed to verify this, although the particle(s) may have been lost. However, there were, in addition to the 25 "primary" hits, approximately 15 additional impacts of secondary nature. These were generally adjacent to the primary hits and appeared to have been caused by repeat impacts of the same particle. Thus, the extensive degradation of Model 201 sealing capability may have been solely due to excessive residual damage.

SHEAR SEAL TEST MODELS

The shear seal configuration represented a radical departure from previously tested models in that plastic seat formation was required. Consequently, all tests were performed in the dynamic tester to avoid seat realignment following formation.

Models 301 and 302

These models were utilized to establish seat forming procedures. Model 301 used the basic straight tube seat insert while Model 302 was tested with the alternate 20-degree undercut configuration (Fig. III-7).

In forming shear seal seats, the dynamic tester 40 pitch thread axial adjustment and electrical contact capabilities were utilized to determine final formed dimensions. After installation in the tester, a reference gap between the seat holder (positive stop) and poppet faces was established and handwheel pointer-scale reading noted. The piston was then advanced until poppet-seat electrical contact was made. Differential scale readings indicated poppet-to-seat holder gap at this condition. Finally, the piston was pressurized to stroke the poppet to the positive stop position and form the seat land with a 1000-psig inlet pressure. A second electrical contact check was made, and the differential gap determined from the two electrical contact readings represented the seat springback (or overtravel) dimension. For Models 301 and 302, these gaps were 0.0022 and 0.0017 inch, respectively. Land widths for the two seats were subsequently measured and found to vary from 0.0024 to 0.0036 inch for Model 301, and 0.0024 to 0.0045 inch for Model 302. In both cases, the variance was fairly uniform, indicating some eccentric alignment influence.

Model 301 had a known land defect and was not tested further. Following land formation, Model 302 leakage at 1000-psig inlet pressure and several pounds load was undetectable (less than 10^{-5} scim). During balance pressure tests, however, surfaces were unloaded to the point where several momentary off-seat cycles occurred similar to relief valve operation. Following this, orifice-type leakage was noted with 6.5 scim at 1000-psig inlet pressure measured.

Disassembly inspection revealed that the seat had been exposed to a blast of HB particles with three found embedded in the seat. Approximately 31 additional spherical impacts were noted in the tube top, adjacent to the

land. It was concluded that the intermittent, high-volume gas flow associated with relief cycles had dislodged particles from inlet valve VN1 and blew them downstream to the seat. With this damage, no further tests were attempted with Model 302. (System fill and flushing procedures were initiated at this time to clean VN1 and an associated filter.)

Model 303 (HB Particles)

Model 303 used the alternate, 20-degree undercut seat tube configuration. Figure V-21 presents leakage data on a load basis for initial and subsequent test conditions.

To assess sealing performance change as a function of cycles only, a 1000-cycle "ultraclean" test was performed with system fluid diverted through the filter bank. (No counts greater than 12 microns from sampler S_b were noted during these cycles.) Leakage was measured twice, after 100 and 1000 cycles. In the latter case 1.4×10^{-4} scim at 7.0 pounds and less than 10^{-5} scim at 15 pounds load were noted, indicating that cycling had significantly improved sealing. (These data are not included in Fig. V-21.)

Following this extraordinary performance, Model 303 was subjected to a 1000-cycle background test with the following particle counts:

Cycles	HIAC Count/Liter	
	12 to 20 Microns	>20 Microns
0	0	0
100	24	1
200	30	7
500	59	23
1000	90	45

Leakage after this test reflected some sealing degradation, but still was in the low 10^{-4} scim region, as shown in Test 4 (Fig. V-21).

Finally, a 1000-cycle HB particle test was performed. Particle count data yielded a 5310 p/l concentration, as follows:

Cycles	HIAC Count/Liter	
	12 to 20 Microns	>20 Microns
Background	1	1
0	72	5130
100	157	5580
200	161	5460
500	210	5320
1000	349	5000

As Fig. V-21 indicates, sealing capability deteriorated significantly with an orifice-type leak resulting.

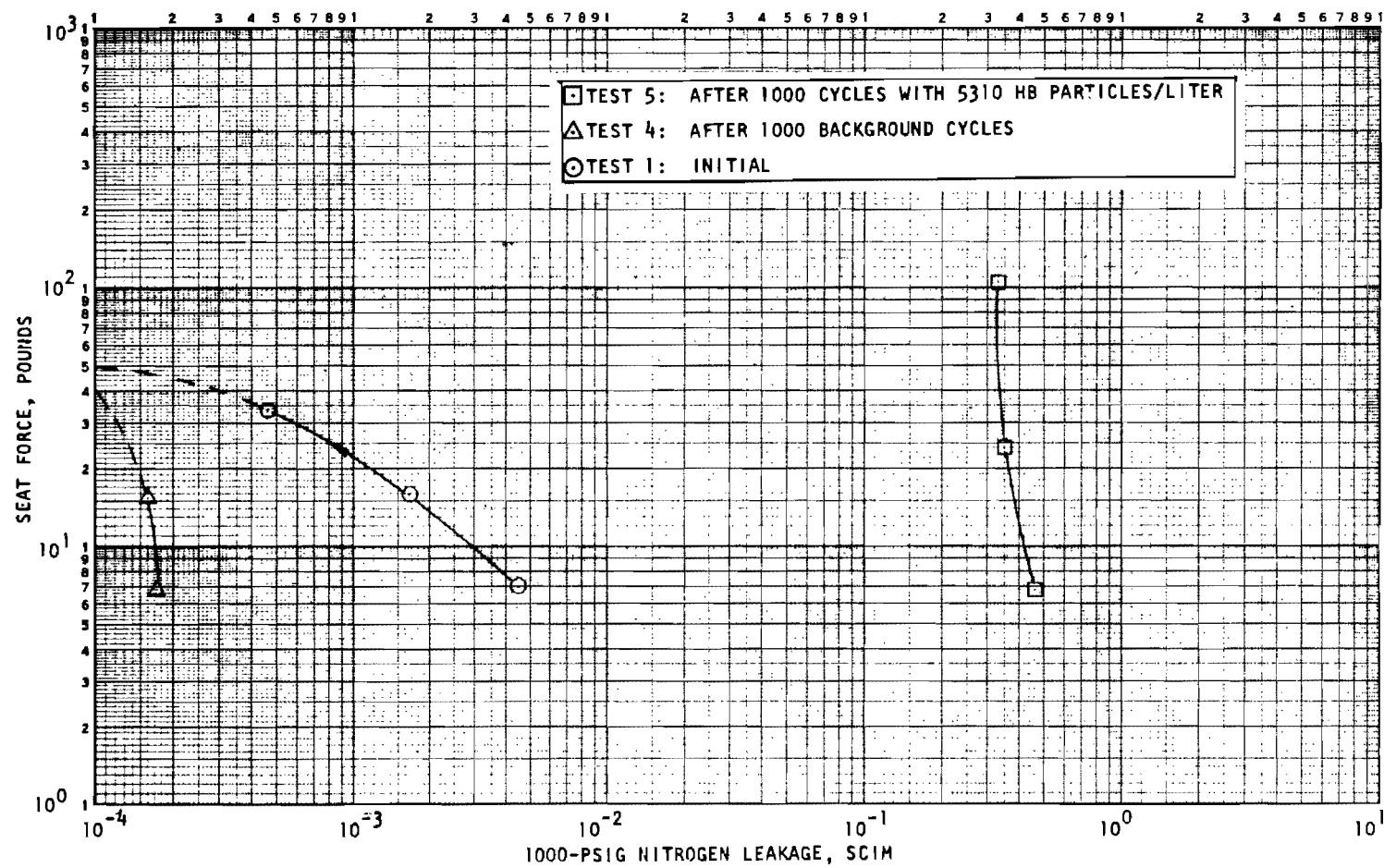


Figure V-21. Load-Leakage Data for Dynamic Test Model 303, Tests 1, 4, and 5

Model inspection revealed that six seat land hits had occurred with three particles remaining embedded. Additionally, approximately 12 "tracks" across the land were noted, apparently from particle contact during closure. Inspection of the poppet sealing surface indicated the seat-embedded particles had worn grooves across the 440C sealing land due to repeated cycle contacts. It is possible that some of the lesser seat damage observed resulted from subsequent leakage tests in which the grooved poppet was reoriented.

Figures V-22 through V-25 illustrate Model 303 seat damage and sealing surface appearance. (The upstream side or tube top is located to the right in these photos.) As shown, the damage from particle impacts is gross. In addition, however, the general surface appearance (in relation to previously tested models) does not appear commensurate with the extraordinary sealing capability. Calculations from typical photo evidence indicated the land crown radius to be on the order of 0.140 inch (compared to the 0.250 inch forming the poppet radius). This indicates considerable elastic springback at land center following general plastic land formation. Thus, it would appear that shear seal low leakage sealing may stem in part from concentrated loading considerably in excess of apparent projected area stress. The circular roughness lay on the poppet is also believed to contribute to low leakage performance.

Like flat Models 121 through 126, Model 303 had been tested prior to adoption of the surge suppression bladder. The actual-predicted hit ratio, however, was significantly greater than for these other models. The reason for this was not known. Several apparent parametric differences between the two models were:

1. Closure velocity
2. Flow direction across the sealing land
3. Shearing closure action
4. Exit configuration
5. Volume flow across the sealing surface during the last 0.002 inch of travel

Considering the above, it was hypothesized that a concentration of particles was being forced back over the seat land due to high pumping pressures generated across the wide positive stop land. A "silting" test was performed to determine if a super-concentration of particles could be trapped in the annular space between the stop and seat land. The system was run for 10 minutes with a concentration of about 20,000 p/l, and the poppet then actuated closed. Approximately 20 particles were trapped within this space of about 0.5 cc, or approximately twice the system concentration. This indicated that the seat holder geometry had some influence on local particle concentration and hit frequency. Thus, while the shear seal configuration demonstrated sealing capabilities warranting further development, the problem of hit sensitivity was yet to be resolved.

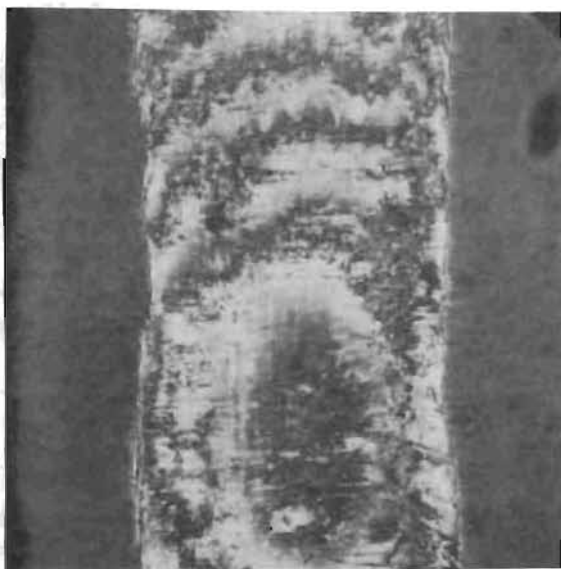


Figure V-22. Model 303 Seat Showing Crowned Condition (462X Interference Photo)



Figure V-23. Model 303 Seat With Embedded HB Particle (91X Plain Photo, Side Lighting)

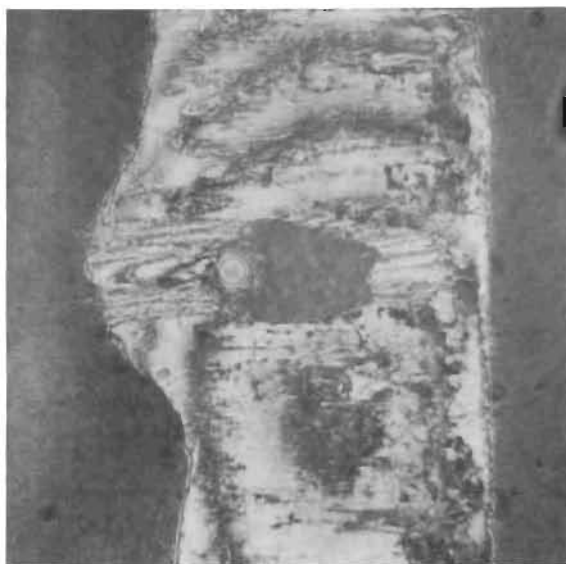


Figure V-24. Model 303 Seat With Gouge Made by HB Particle (462X Interference Photo)

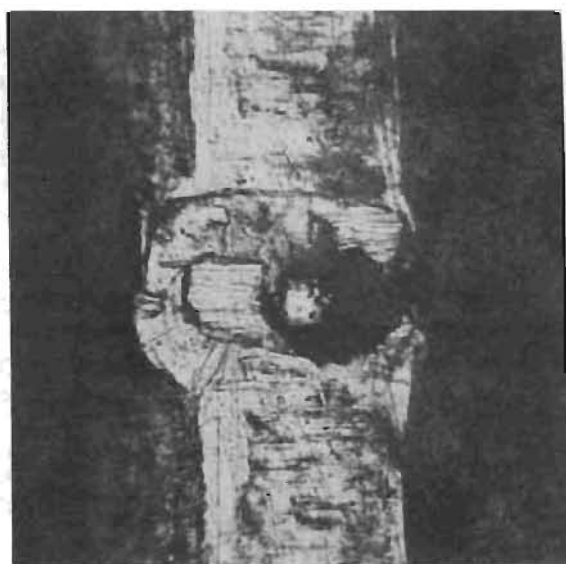


Figure V-25. Model 303 Seat With Embedded HB Particle (462X Plain Photo)

FLAT CARBIDE TEST MODEL

The damage resistance of tungsten carbide was evaluated with flat Model 401. A 440C seat was used as before. The model also marked a change point in test system and procedures. Model 401 was tested initially without the dynamic tester bladder. The second test occurred after adoption of the surge suppression device. Also, the performance of previous models following background cycling indicated that background contaminants had no appreciable effect. Therefore, the exclusive use of filtered fluid cycling to establish control conditions was initiated with Model 401. This procedure reduced cleanup time prior to particle tests by continuously filtering out any foreign contaminants dislodged during clean cycles.

Figure V-26 presents stress-leakage data for the first dynamic test sequence. The degradation noted after ultraclean cycles might be attributed to the influence of numerous seat corner fractures which occurred. Model 401 seat edges had been dubbed over a width of about 0.0015 inch, and ID and OD chamfers were employed. (The dubbing and chamfering practice was adopted in the previous program when corner fractures occurred) However, in the previous program only one cycle test was performed with a tungsten carbide poppet-440C seat combination. In that instance, the seat had a 12-inch crown radius which protected corners from overstress even though the peak impact stress was 96,000 psi compared with only 16,100 psi for Model 401. Thus, the rigid, overlapping carbide poppet produced a failure corner stress condition on Model 401.

The model was cycled with an HB particle concentration of 948 p/l which produced one impact with a secondary mark possibly caused by the same particle. Particle counts during this test are tabulated below.

Cycles	HIAC Count/Liter	
	12 to 20 Microns	>20 Microns
Background	2	0
0	43	923
100	37	1007
200	57	953
500	49	953
1000	47	917

Following surface inspection (discussed subsequently), Model 401 was subjected to a second dynamic test sequence, this time after the tester bladder had been installed. Figure V-27 presents the resulting stress-leakage data. As shown, initial data were nearly identical to the final test of the first series, and ultraclean cycles made little change. Even after HB particle cycles (counts tabulated below), which produced eight hits, leakage increased less than a factor of 10 at stresses as low as 500 psi.

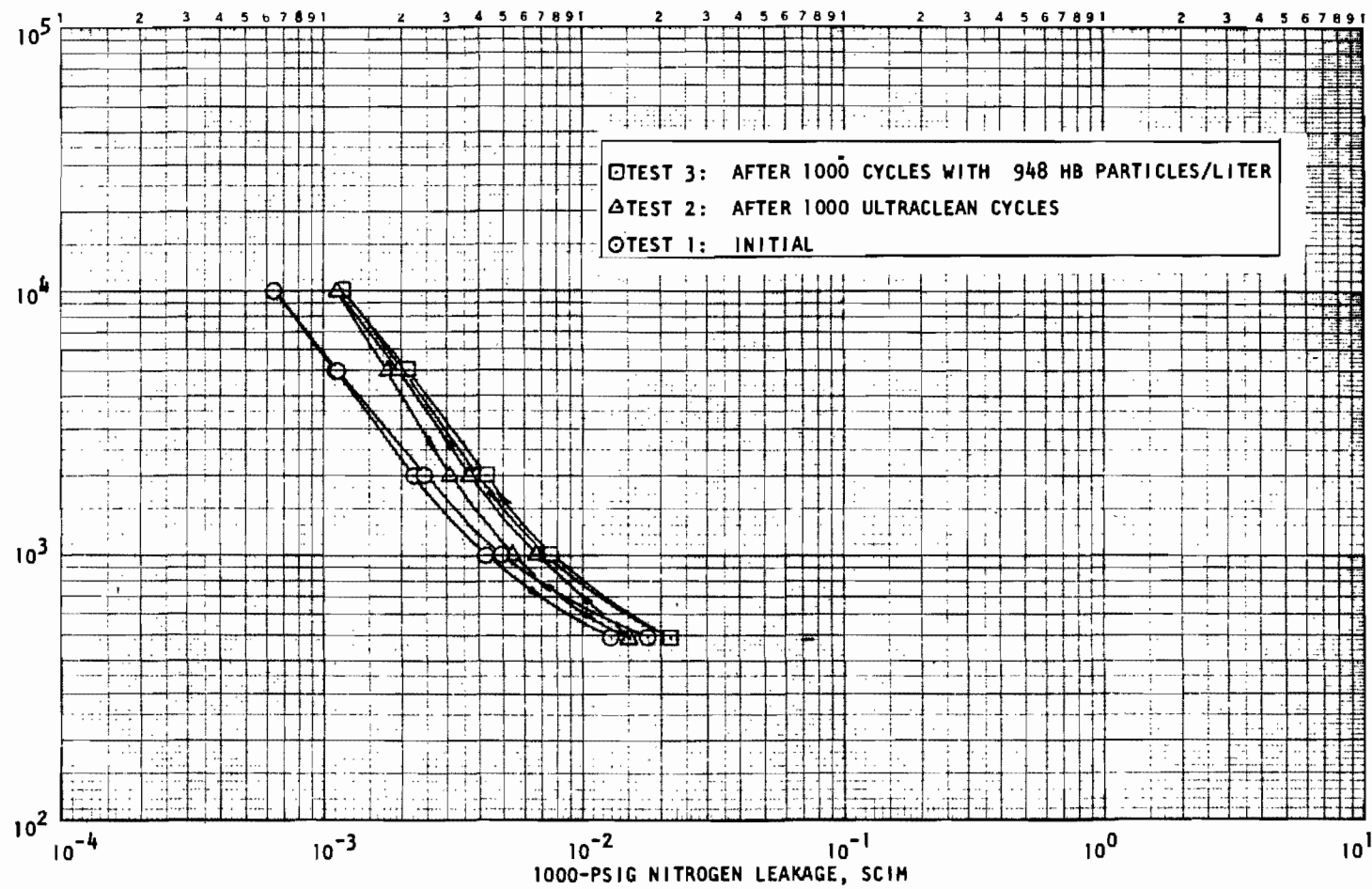


Figure V-26. Stress-Leakage Data for Dynamic Test Model 401, Tests 1, 2, and 3

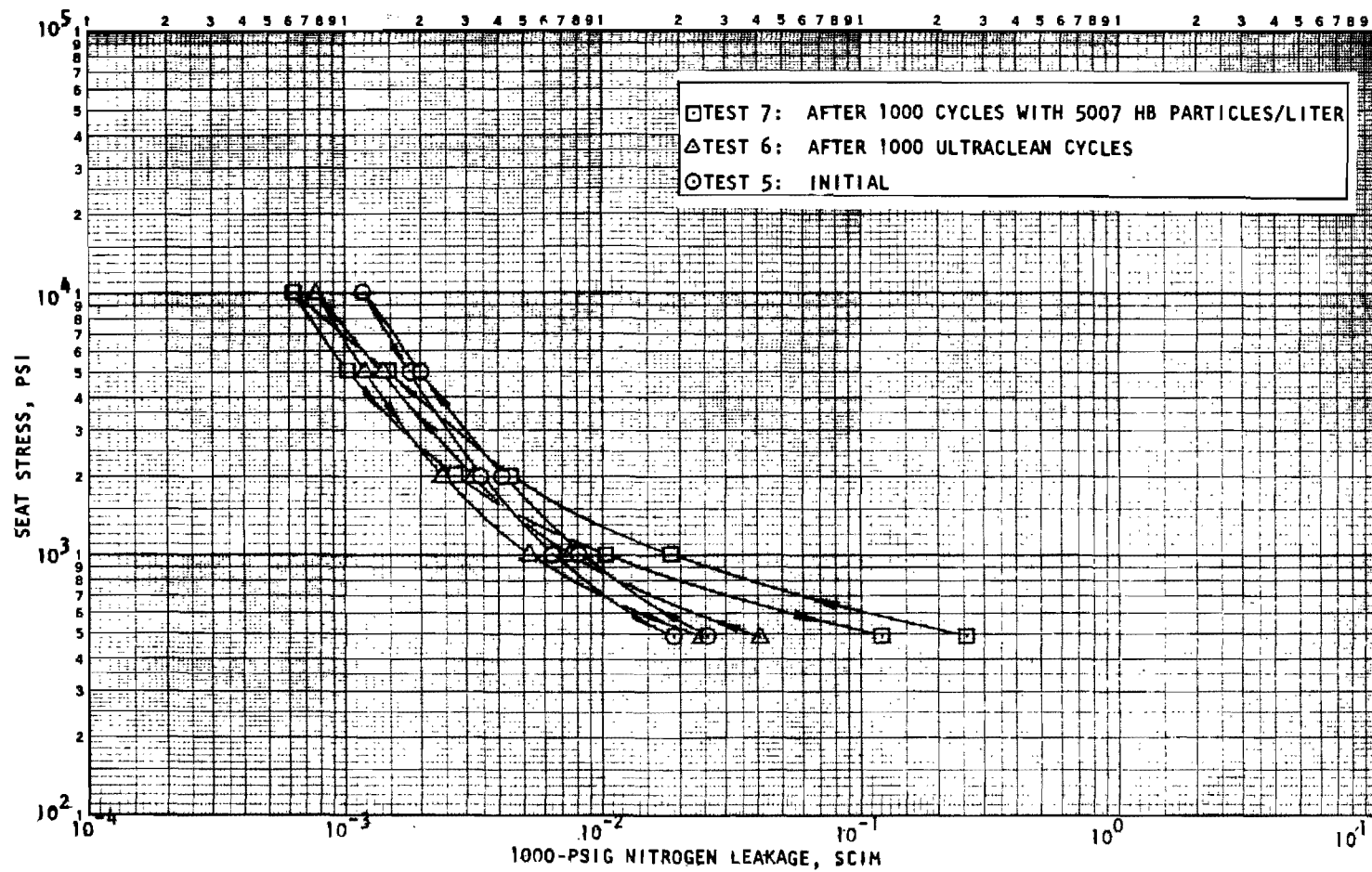


Figure V-27. Stress-Leakage Data for Dynamic Test Model 401, Tests 5, 6, and 7

Cycles	HIAC Count/Liter	
	12 to 20 Microns	>20 Microns
Background	4	3
0	130	5250
100	150 (Est.)	5320
200	163	5110
500	222	4970
1000	188	4810

Particle impact characteristics of Model 401 were interesting. As expected, the 440C seat had sustained the brunt of the damage with deep craters and significant upset metal. However, the tungsten carbide surface, even with depressions 30- to 40-microinches deep, evidenced virtually no sign of raised metal at the hole's edge. Unlike 440C parts, no particular base metal fracture was noted in the carbide depression surface. Figures V-28 through V-31 illustrate poppet and seat damage. This information suggests that carbide on carbide might be a likely candidate for contaminant tolerant closures. However, all test data to date have shown that, at least with 440C, residual effects (after particle loss or removal) are minimal even with large particle hits. Conversely, leakage from an all-carbide closure with a particle entrapped is expected to be much greater than with a hard-soft combination due to the greater resistance to envelopment and, thus, surface conformance. This effect would obviate the low residual effect feature afforded by carbide surfaces unless occasional very high leakage could be tolerated due to an entrapment.

OBSERVATIONS

The extent of Phase II testing was restricted to a relatively few parameters. It is readily apparent that substantial additional investigation would be required to fully explore, with statistical confidence, the numerous variables and questions uncovered in these tests. Nevertheless, certain observations and conclusions have emerged which lead to a better understanding of the problems and indicate the direction for further evaluation.

The test results indicated dynamic particle hit effects to be similar to that produced statically. The major difference appeared to result from multiple impacts on portions of the hard particles which occasionally fractured. This was evident, as shown in Fig. V-3, in about one-half of the particle impacts.

A primary output of Phase II dynamic testing effort was demonstration of the inevitability of particle encounters when practical contaminant levels and cycle life are considered. The capability of reasonably predicting these encounters forms a valuable tool in the closure design process. Once the fact of encounter certainty is accepted, the effects of such encounters may be statistically considered. Static tests can then be employed to positively verify adequate seat loading with particles entrapped.

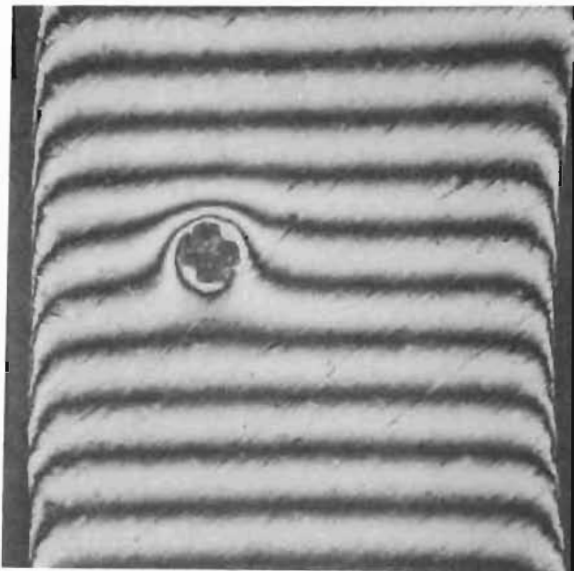


Figure V-28. Model 401 Seat Showing
HB Particle Depression
(91X Interference Photo)

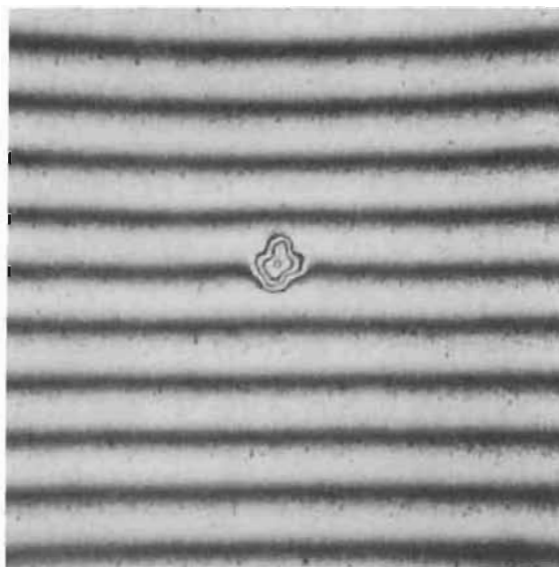


Figure V-29. Model 401 Poppet Showing
HB Particle Depression
(91X Interference Photo
Same Location as Fig. V-28)

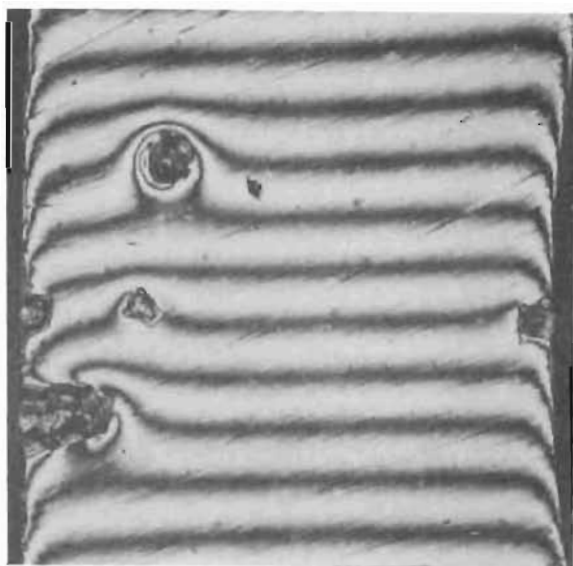


Figure V-30. Model 401 Seat Showing
HB Particle Depressions
and Edge Fractures (91X
Interference Photo)

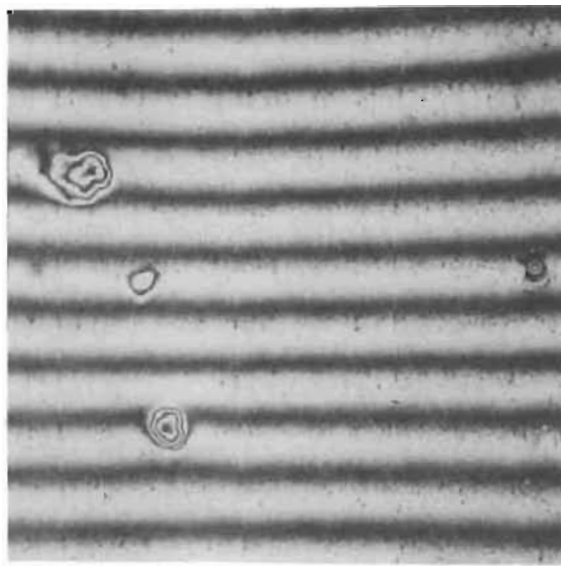


Figure V-31. Model 401 Poppet Showing
HB Particle Depressions
and Edge Fractures (91X
Interference Photo Same
Location as Fig. V-30)

Even with the HA particles, a reasonable number of impacts resulted in residual surface damage which produced tolerable effects. From the test results, hard-on-hard material (such as carbide) would appear to be the best approach for minimal residual damage influence on leakage. This would be followed by 440C on 440C. Hard on semihard would be the most undesirable condition if particulates are harder than the softer surface. While not occurring with Model 401, the likelihood is that retained particles would produce gross leakage with such a combination.

While the harder materials tend to eject hard particles after impact the, question of last-cycle closure on a significant particle can be posed. In this instance, gross leakage could occur. The hard-on-hard concept becomes unattractive if the closure function is such that a subsequent cycle (or cycles) to expell the particle is not possible.

An alternative to the preceding approach is the combination of hard-on-very soft materials, as exemplified by the shear seal model. Contaminant-damaged performance of this configuration was poor. However, for any narrow land geometry, a single-particle encounter may cause excessive leakage. It was apparent from Model 303, though, that deep particle embedment with minimal protrusion above the surface is possible. Thus, a contaminant envelopment or tolerant concept may be considered. With a reasonable number of encounters inevitable, it follows that a hard-on-soft closure would be advantageous in applications where particle ejection cycles are not possible.

In all cases of particle encounters (except carbide), the momentary or permanent particle embedment displaced seating material. Excluding edge hits, this material protruded above the general surface plane to further resist closure. Thus, a design concept to permit lateral rather than vertical material displacement is desirable.

In view of the preceding and Phase II dynamic test results, the flat configuration appeared to offer the best approach to further contaminant effects testing. It was easily fabricated and finished and was amenable to material variations. The spherical 440C geometry was not considered a suitable design due to deep entry scrubbing and apparent sensitivity to contaminant impacts and effects. The shear seal model demonstrated both a propensity for particle encounters and, by virtue of the narrow land, was vulnerable to particle impact damage. Conversely, the remarkable low load sealing capabilities of this configuration certainly warranted further development in Phase III.

Finally, the capabilities of the dynamic test system were proved in Phase II testing. The ability to control and measure both background and introduced particulates for long periods of time produced a unique tool for further investigation of valve closures in contaminated environments.

In regard to particle-induced erosion, the dynamic system did not produce sufficient pressure to create high fluid velocities normally associated with this effect. Only momentary high pumping pressures around the seat were produced during cycling. No erosion effects were noted with any model. With the usual short-term flow typical of liquid rocket propulsion systems, particle-induced erosion is not considered to be a significant problem. (This is not the case with high-pressure pneumatic systems wherein exhaust gases and entrained particles approach sonic velocity.)

SECTION VI

PHASE III DEMONSTRATION--CONCEPTS AND MODEL DESIGNS

The net worth of any research is ultimately proved or demonstrated by a functional design. In the patent field, this is termed a "reduction to practice." The difference between functions claimed for a patented concept and achievements of the working model are often very great. This is especially true of low-leakage valve closure concepts because the fundamental sealing mechanism is seldom understood. The Phase II effort, therefore, represented a "reduction to practice" of the previous research.

The results produced from both Phase I and II were less than planned. A clear definition of rocket system fluid contamination was not available and the matrix of load-leakage data expected from static testing was limited to a few models and test particles. Explicit quantitative data were additionally limited because of extreme difficulties in identifying and controlling numerous variables. Nevertheless, a qualitative understanding of contamination particulates, and effects most damaging to valve seats, did emerge and served to stimulate sealing concepts that might prove to be reliable in such contaminant environments.

The purpose of Phase III Demonstration effort was to develop closure designs that would withstand the fluid system contamination environments defined in the Phase I Survey. To this end, the Phase II investigations provided a thorough and sound background of fundamental experience and test capability absolutely necessary to demonstrate sealing performance in a particulate contaminant environment. This section presents the development of fundamental concepts (with application of Phase II data) resulting in several detail model designs. Test results are presented in Section VII.

FUNDAMENTAL CONCEPTS

The Phase III effort was initiated by defining ways to minimize solid-particle entrapment effects on metal valve seats. Fundamental concepts evolved were:

1. Total filtration
2. Seating design overload
3. Particle avoidance
4. Particle absorption

Total Filtration

The first concept is included because it is a necessary adjunct to clean systems and fluids. As employed herein, total filtration is meant the installation of an element at the entrance to or within a valve that has demonstrated capability to reduce the particulate size level to within the closure tolerance. The purpose of this device, or filter, is not to reduce quantity significantly because this is often not practical due to high flowrates and loading capacity. Consequently, the approach fluid must be clean from a small size and weight standpoint.

Filtration need can be established on a logical basis using the techniques defined in Phase II and further refined in Phase III. To do this the following requirements must be realistically set forth:

1. Closure contaminant tolerance
2. Required cycles
3. Fluid contaminant level under operating conditions

The first item is a function of particulate size, type and closure design. Effects hypotheses may be made from this program data but explicit values must be experimentally determined for most valve designs.

The number of closure cycles should be realistically established for the required mission. A consideration in cycle test evaluation is the improbability of stopping the test on a cycle in which a particle has been entrapped. If the seat design has minimal after effects and tends to eject particles (as with the 440C flat models herein), a valve could ostensibly pass spot leakage tests with flying colors, while actually having had several catastrophic particle encounters. Spot and final leak tests indicate realistic performance only with closure designs that retain entrapped particles.

Some mission requirements may provide for recycle wherein singular encounters with attendant high leakage is not as important as overall average low leakage. A design with an absolute minimum residual effect would thus be required. The Phase II data indicate that the very hard metals and cermets have this feature. However, it must not be overlooked that very soft or "sticky" contaminants may remain on sealing surfaces for many cycles. This was indicated in the previous program tests with lead particles. These particles had to be scraped from the hardened 440C seating surface. In the same program, an unanodized polished aluminum seat was pressed to the plastic stress level by a tungsten carbide poppet. Subsequent microscopic inspection revealed that small particles of aluminum had been plucked from the seat and were plastically flowed into numerous minute pits in the sintered carbide surface.

The fluid contaminant level under operating conditions should be dictated by valve contaminant tolerance, cycles, and hit probability. If the number of encounters and estimated effects exceeds the closure tolerance (i.e., causes excessive leakage), the fluid contamination level must be altered.

While much effort has been expended along these lines with hydraulic controls, very little has been done with propellant systems. This has been due, in large part, to the lack of any realistic measurements and data. This situation is attributed to one fundamental deficiency, i.e., the lack of a method for accurate, continuous measurement of the particulate level within a steady flow system. Without these data, even an empirical comparison between contaminant level and failure cannot be made.

From these observations, the combination of particle removal element and valve closure is considered as a potentially necessary approach to reliable sealing in contaminated environments.

Seating Design Overload

Where filtration is not desired or possible, the second alternative is to provide sufficient load margin to meet requirements. Load margin is determined from a knowledge of contaminant tolerance and closure stress-leakage characteristic. Usual leakage allowances for cyclic degradation are a factor of 1.5 to 2. This concept proposes factors of 10 to 1000 on leakage and is particularly feasible where leakage requirements are not too stringent.

Particle Avoidance and Absorption

The preceding concepts are sound in theory but would require significant advancements in many areas of measurement and test. The most expedient approach to reliable sealing may be through exotic or unusual closure designs which either avoid particle encounters or are able to absorb particles in large sizes and/or quantities. The development and evaluation of these concepts constituted a major part of the Phase III Demonstration effort.

The design approach, theories, and application of design data are presented for each of four contamination-resistant models in following subsections.

SHEAR SEAL MODEL DESIGN

The clean sealing performance of Model 303 in Phase II testing was phenomenal compared with conventional flat models. The promise of low leakage with very low loading warranted further evaluation of the design.

The Phase II results indicated an excessive hit frequency. This was not expected because of the relatively narrow land width. Excessive hits could have been due to: (1) an improbable test result, (2) inlet geometry, or (3) a pumping effect caused by the wide positive stop land.

For Phase III testing, the seat holder was modified to promote free particle flow during closure. The rework (Fig. VI-1) consisted of relieving the holder annular positive stop to provide four stop posts. An additional O-ring seal groove was also incorporated with bleed hole to ensure complete isolation of inlet pressure from downstream leak collection volume. A leakage volume reducing ring (Fig. VI-2) was fabricated to allow use of the leak collection O-ring.

With this change, and elimination of reverse flow with addition of the dynamic tester bladder (Appendix F), it was believed that a reduction in hit frequency would result. Even if particle hit effects were too severe, but clean sealing performance proved repeatable, the design would be an excellent candidate for the particle avoidance or total filtration concepts.

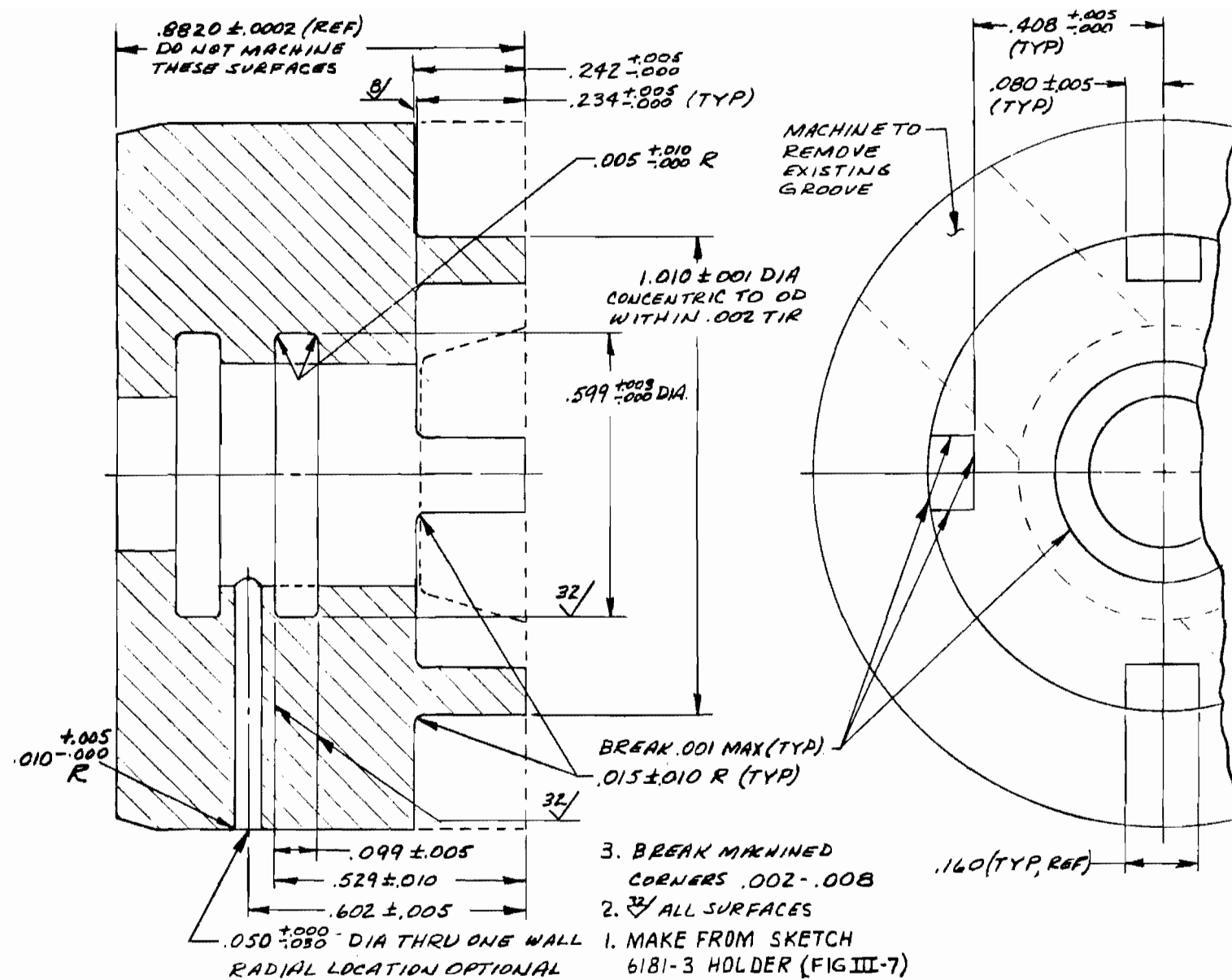
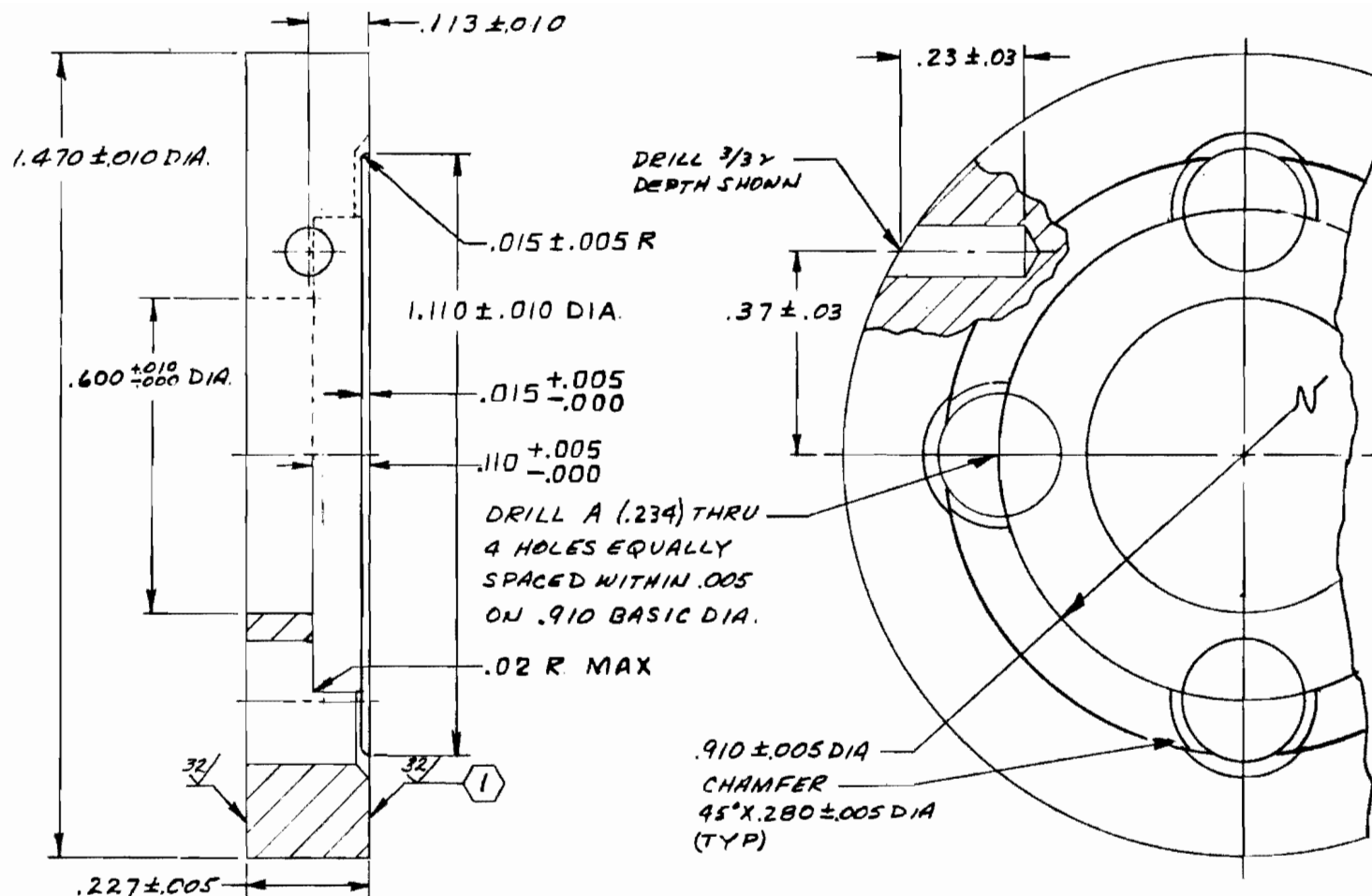


Figure VI-1. Shear Seat Holder Rework (Sketch No. 7191)



- ① 4. FLAT WITHIN .0001 PRIOR TO ANODIZE
3. $\frac{63}{100}$ ALL SURFACES
2. MATL: 6061-T651 OR SIMILAR AL ALLOY
FLASH HARD ANODIZE CONFORMING TO LB0125-103
TYPE I (RAD109-010) COATING THICKNESS .0001-.0002
1. MACHINE PER RAD103-002

Figure VI-2. Ring (Sketch No. 7192)

SELF CLEANING MODEL DESIGN

Considerable thought was given to a means for causing particles to be directed from the sealing interfaces during the last 0.01 inch of closure. Any device that collects particles during open flow was unsatisfactory because the design objective was to pass particulates freely up to the point of closure. This naturally ruled out cyclones or traps because these merely represented a form of filtration.

Design

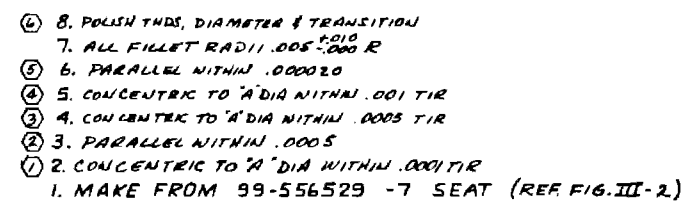
The concept finally chosen was one in which a portion of the mainstream particle concentration was reduced to at least 1/100 of the line concentration and this "clean" fluid was directed across the seat during the last 0.01 inch of closure. From Section II Analysis, this reduction would provide a significant increase in reliability.

The model design prepared for test is shown in Fig. VI-3. Operating theory deduced from development test results follows:

1. Feed flow passes through a helical vane which produces a high rotational fluid velocity.
2. During passage through the vane, flow is turbulent and particles are "mixed" due to unsymmetrical passage shape and surface friction.
3. On exit from the vane, the two flows recombine and continue to whirl in a free vortex which centrifuges the heavier particles to the tube OD.
4. The poppet plug probe is positioned at the optimum distance from the vane to achieve minimum particle concentration.
5. A core of "clean" fluid is thus created which flows through the plug probe and eight passages to the seat annular slot.
6. As the poppet closes on the seat, particle-laden "outer" flow is cut off by the close fit between the plug OD and seat bore. The clean reservoir of fluid contained within the plug is forced across the seat annulus during final closure and impact.

Design Analysis

Plug dimensions were based on steady-state tests of flow, ΔP variation with stroke (at standard flows). Analysis indicated that the relationship between closure timing, plug "clean" volume, and system flowrates was very critical and that little margin existed in which to ensure closure on clean fluid. This was due to the extremely small trapped plug volume and need for reasonable flow volume (and, thus, area) through the plug while open. Subsequent closed flow potential was relatively high and, consequently, the period of clean flow very short. Because the effects of closure surge were unknown, no precise prediction of plug flow was possible. Trial and error was thus required to define the final configuration.



DRILL #36 (104) X .41 ± .03 DEPTH
C'SNK 60° X .138 ± .010 DIA.
THD #6-32 NC-38 X .31 MIN FULL THD.
PD 1177 $\pm \frac{.0027}{.0003}$ PER MIL-S-7742

CHAMFER 45° X .005 $\pm \frac{.0005}{.0005}$

30° ± ½°

BREAK .001 MAX

60° ± ½° (TYP)

.005 $\pm \frac{.003}{.000}$ R.

.030 ± .010 R

15° ± 1°

.002 $\pm \frac{.000}{.001}$

.375 ± .003 DIA

.060 $\pm \frac{.000}{.002}$ DIA

.040 ± .002 DIA

BREAK .001 MAX

.02 R MAX.

.153 $\pm \frac{.0009}{.0009}$ DIA

.050 $\pm \frac{.0009}{.0009}$

.0040 ± .0005

.270 ± .010

.0170 ± .0005

.069 ± .004

.527 ± .010

.1730 $\pm \frac{.0000}{.0001}$ DIA

.300 ± .003 DIA

.029 ± .002 DIA THRU ONE WALL TO & AS SHOWN (TYP 8 HOLES EQUALLY SPACED WITHIN .005)

1. 4330 $\pm \frac{.0000}{.0001}$ DIA.

2. 6. NORMAL TO (3) DIA WITHIN .0001 TOTAL

3. 7. NORMAL TO (3) DIA WITHIN .0005 TOTAL

4. BREAK CORNERS .001-.010

5. CONCENTRIC WITHIN .0001 TIR

6. ALL DIAS CONCENTRIC WITHIN .001 TIR

7. 3/8" ALL SURFACES EXCEPT TND HOLE

8. MATL: 17-4 PHCRS BAR AMS 5843 COND A

9. HEAT TREAT PER RAH11-016 COND H-1150 (R, 28-32)

Technical drawing of a mechanical part with dimensions and callouts:

- Top View:**
 - Overall width: $.725 \pm .005$ FINAL
 - Top chamfer: $45^\circ \pm \frac{1}{2}^\circ$
 - Top surface: MACHINE... .025 FROM ORIGINAL SURFACE TO REMOVE PRESENT LANDS
 - Top hole: $\phi 1.012 \pm .005$ DIA
 - Top hole depth: $.005 \pm .000$ R (TYP 2 PLS)
 - Top hole chamfer: $.001 \pm .001$ X 45°
 - Top hole break: BREAK .001 $\pm .002$ / $\pm .000$
 - Top hole diameter: $\phi 1.85 \pm .005$ / $\pm .000$ DIA
 - Top hole diameter: $\phi 1.5040 \pm .0005$ DIA
 - Top hole diameter: $\phi 1.731 \pm .0001$ DIA
 - Top hole diameter: $\phi 3.10 \pm .001$ DIA X $90^\circ \pm \frac{1}{2}^\circ$
- Side View:**
 - Overall height: $.080 \pm .003$
 - Overall diameter: "A" DIA

Figure VI-3. Self Clearing Model

Figure VI-3. Self Cleaning Model

Construction and Fabrication

There are several ways to centrifuge particles from a fluid. Because the purpose of the design was to prove the concept, a simple and economical means for particle separation was required. The helical vane shown in Fig. VI-3 provided more than the desired 100:1 reduction. Dimensions shown were experimentally determined using the HIAC particle counter. The test results are presented in Appendix H.

The vane was constructed by twisting a flat strip of annealed copper clamped between a lathe chuck and tailstock. The OD was then centerless ground to match the tester bolt ID. Vane tips were hand ground as shown. The indicated pitch was the minimum obtainable without helix distortion.

Closure interface design is similar to the flat 440C model except for the lack of poppet seat ID relief required for smooth clean fluid flow. The poppet and seat were fabricated from 17-4PH to provide an additional flat seat model material data parameter. It was assumed that test particle concentrations would be increased to a level sufficient to cause several hits.

Lapping of sealing surfaces was performed similar to the flat 440C models using 1- to 5-micron diamond with final polish on paper. It was notable that the 17-4PH metal was much more difficult to lap free of deep scratches than the harder materials.

The probe design represented the greatest compromise. As initially conceived, the probe tip was entered by a shutoff plug during closure so that clean flow would be positively expelled across the annulus. The small diameters involved with the standard seat precluded this refinement. Three parts were made for test but two had EDM holes at the 0.04-inch probe hole base. The third part was thoroughly inspected and was within all specified tolerances. The most difficult tolerance stackup was mating parts concentricity because the plug-to-seat diametral clearance was only 0.0010 to 0.0012 inch. As proved in later assembly and test, the plug entered the seat without interference.

FLAT COPPER MODEL DESIGN

The shear seal design indicated the tremendous sealing potential of soft metals. However, these materials have many fabrication, handling, and use problems. This is why their application has been limited to static seals and valving applications having the high loading capability necessary to plastically form a sealing land.

Because soft metals readily undergo plastic flow, the concept of particle envelopment was most easily attained with a flat seat made of copper. The selection of copper for this model was based on previous use, material cleanliness, and properties being similar to other soft, work hardenable metals of potential application with rocket engine propellants (e.g., gold, silver, etc.).

Design

The flat copper model is detailed in Fig. VI-4. The seat is an insert into a holder similar to the shear seal model. This allowed for extreme precision in the holder because only two of these parts were fabricated. The seat is retained by the shear seal nut in the tester assembly. Eastman 910 adhesive was used for torque retention in very small spots 180 degrees opposed on the seat OD and nut cone. Bottoming was ensured by a preassembly operation in which the seat was locked to the holder with a 5/16 bolt and nut while the adhesive cured.

For clamped assembly in the dynamic tester, seat-poppet parallelism was obtained by match lapping the copper seat base to the prefinished seating surface. The required degree of parallelism evolved from model tests. Seat concentricity without affecting parallelism was provided by a close OD fit at the seat base with OD relief over most of the seat length.

The poppet was designed to have a fairly wide seat land overlap. As initially planned, seat impact was to be controlled by positive stops. These were provided by the three poppet pads obtained by relief grinding the poppet face. This feature was not used in final tests and the seat was left protruding from the seat holder, as shown by Fig. VI-4.

Fabrication

The 440C poppet sealing surface was lapped the same as Phase II flat models using 1- to 5-micron diamond compound on a cast-iron lapping plate with final polish on paper.

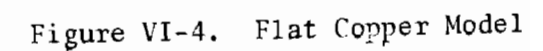
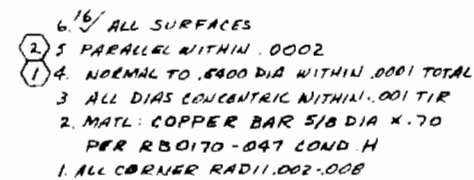
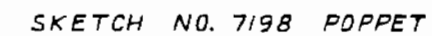
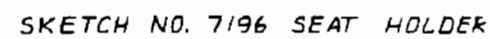
Finishing the copper seat surface proved exceedingly difficult with very deep scratches resulting from use of a cast-iron lap and 1- to 5-micron diamond. A variety of techniques was tried, but only with moderate success. Best results were obtained using a copper lap, 0- to 1/4-micron diamond in water-soluble paste and alcohol or water for lubricant. This was essentially a wet slurry process and produced a minutely pitted texture, but without deep scratches. Later lapping experiments with the flat-grooved model (described next) indicated that somewhat better results might have been achieved using a tungsten carbide lap and 0- to 1/4-micron diamond.

The difficulty in lapping these soft metals is one of the major deterrents to their use. It was this consideration that emphasized the need to plastically develop the sealing surface from a mating hard material having a very fine finish, preferably with circular lay.

FLAT GROOVED COPPER SEAT DESIGN

Design Concept

Consideration of particle effects observed from Phase II tests indicated that raised metal from particle entrapment is minimal when the event occurs near a boundary. This is because the material has access to free space, i.e., can flow laterally with minimal restraint. Conversely, particles



entrapped within a wide seat land must displace their volume through a combination of plastic and elastic deformation, resulting in relatively large amounts of material extruded vertically with the general surrounding plane more gently raised. It follows that a valve seat composed of "all edges" would more readily envelop particles. Conventionally, a narrow land conical seat is thought to have favorable "particle-eating" properties, but just the opposite is true for very low leakage, because a single particle can bridge the land. Combining these concepts, however, a flat or spherical seat land, composed of concentric sealing annuli 0.001- to 0.002-inch wide, separated by grooves of similar width and depth, would appear to be advantageous. The grooves provide a repository for displaced material and, also, particles. Multiple sealing annuli allow for the loss of one or more lands without serious increase in leakage. It was hypothesized that the grooves may also contribute to a flow condition wherein particles are preferentially forced into the grooves rather than remain on the seat land.

The optimum choice of material for this seating concept is problematic in that the softer metals can more easily envelop particles, but are subject to other damage. A very hard, brittle metal is subject to extremely high corner stresses which tend to cause fractures.

Due to these unknown and many fabrication difficulties with harder metals, copper was selected as the seat material. As planned, the plain flat and grooved designs complemented each other, allowing data from the flat test to be used in design of the grooved model.

From examination of the shear seal land using the interference microscope, it was hypothesized that sealing was effected by a combination of: (1) crowned land developed by plastic flow which concentrated high bearing stress at the land center, (2) low elastic modulus of copper, and (3) circular lay poppet which formed a matching surface on the seat land. These speculations led to the following requirements:

1. Initial land width small with respect to the final width so that lateral plastic flow would allow superposition of the flat poppet surface finish onto the lands and close scratches.
2. Total land-forming load well within the elastic limit of the seat insert to maintain lands in the same flat plane after forming.

Several means for groove fabrication were reviewed such as photoetch, electrical discharge machining, ultrasonics, foil lap, and single-point turning. The latter was chosen for three reasons:

1. Proved precision with flat model turning in the previous program (17-4PH Model NN_f, 2 microinch AA and flat with 10 microinch).
2. Wedge-shaped crests required to provide lateral plastic flow believed necessary for sealing.
3. Immediate availability of precision machines and techniques.

Detail Design

The preceding concepts were analyzed and then developed through a combination of fabrication experiments and model tests. The final seat design used in model test is shown in Fig. VI-5. This drawing also delineates detail fabrication processing that was developed by trial using numerous copper seat blanks. Because the grooved seat detail is made from the flat copper model (Fig. VI-4), only the seat land is shown. It is detailed face downward with overlapping poppet land (Fig. VI-6) on the bottom (dash lines). The outermost seat land of 0.0011-inch width was finished along with the six seating lands and served as a reference inspection plane. Complete fabrication processing information for the flat grooved seat is covered in Appendix I.

Wedge Analysis

Plastic flow of a wedge is defined in Ref. 1. These are the same equations used in the shear seal analysis of Appendix B. Individual land width predicted for the design is given by:

$$\ell = \frac{LS}{\frac{P_f}{S_o} \cdot S_o n}$$

where

L = apparent land width (0.031 inch)

S = apparent stress, psi

$\frac{P_f}{S_o}$ = ratio of fully developed plastic flow pressure to yield stress;
2.55 for 60-degree angle (Appendix B)

S_o = yield strength for fully work hardened copper (45,000 psi)

n = number of lands (6)

whence

$$\ell = 4.50 \times 10^{-8} S$$

also

$$F = SA_s = S \cdot \pi D_s L$$

where

D_s = mean seat diameter (0.470 inch)

F = seat load, pounds

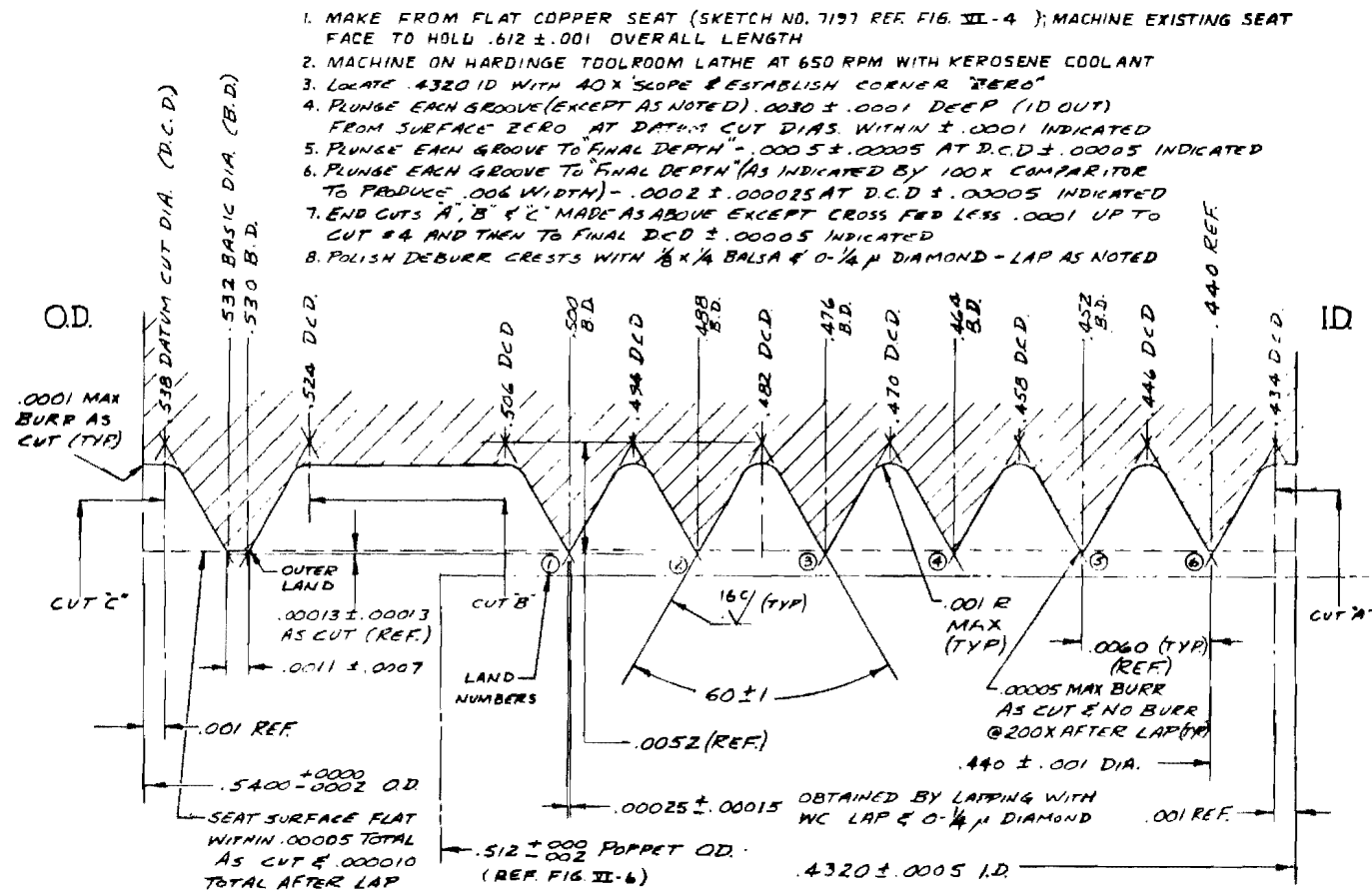
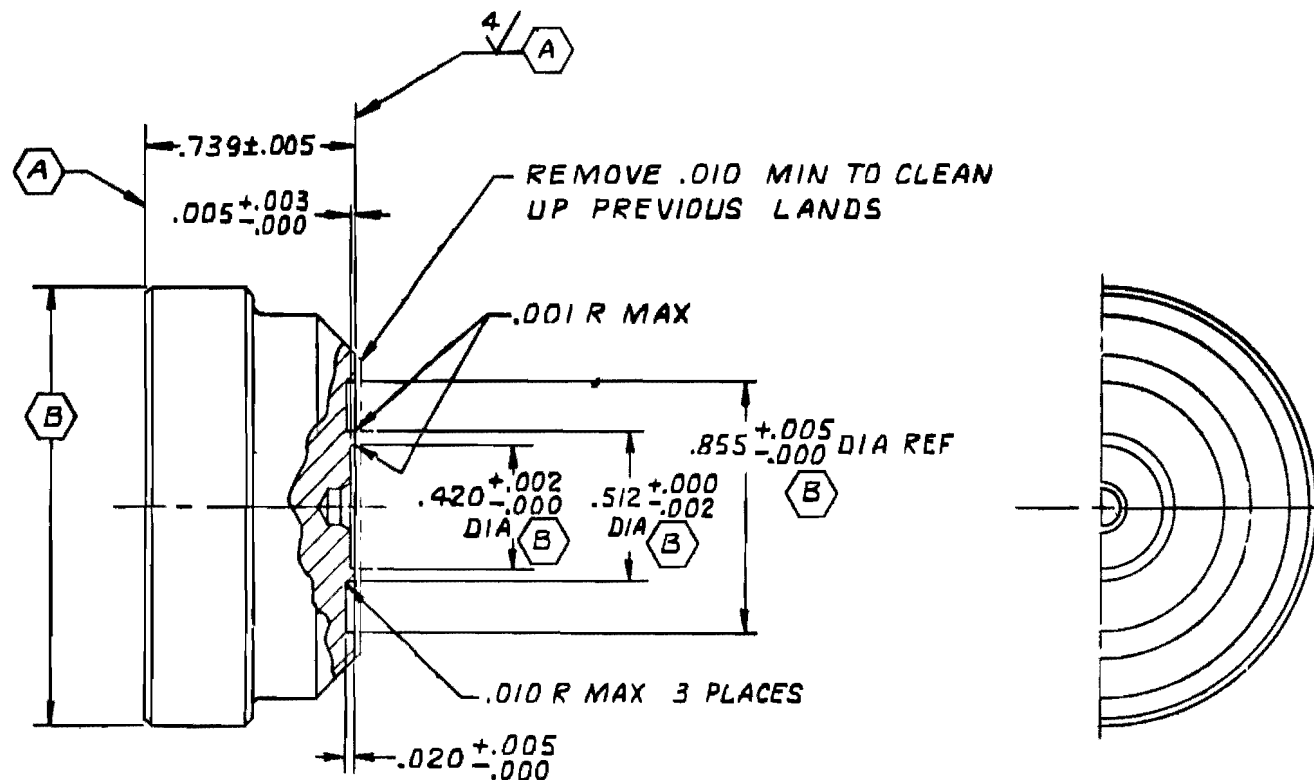


Figure VI-5. Flat Grooved Copper Seating Surface Detail (Sketch No. 7201)



4. BREAK MACHINED CORNERS .002-.008
- A 3. PARALLEL WITHIN .00002
- B 2. CONCENTRIC WITHIN .001 TIR
1. MAKE FROM 93-556528B-3 POPPET (REF. FIG. III-1)

Figure VI-6. Flat Poppet Rework (Sketch No. 7202)

and, thus,

$$F = 0.0458 S$$

which yields the following tabulation:

<u>S,</u> <u>psi</u>	<u>F,</u> <u>pounds</u>	<u>ℓ,</u> <u>in. x 10⁴</u>
5,000	229	2.25
10,000	458	4.50
15,000	687	6.75
20,000	916	9.00
25,000	1145	11.25
30,000	1374	13.50

SECTION VII

PHASE III MODEL TESTS

Phase III model tests were performed on the four previously presented basic model designs listed below:

1. Shear seal model
2. Self-cleaning model
3. Flat copper model
4. Flat-grooved copper model

A specific test objective was to compare sealing ability and contamination resistance with Phase II models. The overall objective was development of design criteria for one or more closure designs offering superior sealing and contamination resistance.

GENERAL APPROACH

A test plan was prepared and approved by AFRPL. The general approach was to perform developmental static tests so as to define a final configuration. Targeted baseline performance leakage was less than 10^{-2} scim at 1000-psi inlet pressure and 1000-psi apparent stress. The finalized version was then evaluated in the dynamic test system using HB particles. Procedures established in Phase II were followed. For a brief description of the static and dynamic test fixtures, systems and operating procedure, the introductory paragraphs of Sections IV and V should be reviewed. Detailed description and performance analyses of the testers, leakage measurement, test systems, and procedures are presented in Appendixes C through G.

A dynamic test of the Phase III models followed the same procedures established in Phase II except for the refinement of latter tests in which poppet-seat rotational orientation was maintained throughout the test series. With soft metal seats, it was found that reorientation following cycle tests produced multiple surface defects because of embedded particles. For these tests, the piston bias spring and leak collection O-ring were not removed until the test sequence was completed. The O-ring was rolled up onto the poppet OD during cycling (see Appendix F).

DATA PRESENTATION

Model data presentation is similar to that followed for Phase II dynamic test models. Specific model data are presented in the form of apparent stress or load versus leakage plots with discussion of results, particle count data, and concluding with typical photomicrographs of poppets and seats with particle hits and entrapments.

Table VII-1 presents a summary of model inspection, dynamic test, and comparative performance data. Static tests were considered developmental and are described in text. Except for the additional "surface reorientation" and "particle embedment" columns, this table is identical with Table V-1 presenting the Phase II dynamic test model data.

SHEAR SEAL TEST MODELS

This model configuration received only limited testing in Phase II. Because of potential superior sealing performance, it was selected for a more complete evaluation test series in Phase III. The purpose of these tests was to: (1) further investigate sealing and land formation using annealed and full-hard copper seats, and (2) evaluate hit frequency without downstream backflow. The latter feature was provided by incorporation of a bladder in the dynamic tester cavity (Appendix F) and previously described modification to the shear seal model seat holder.

As with Phase II shear seal models, all tests were performed in the dynamic tester so that land formation and concentricity could be maintained throughout the test series. However, as indicated in Table VII-1, the poppet and seat were reoriented with each cycle test. This unavoidably induced some eccentricity with each reassembly.

Model 304

This model seat was fabricated and tested to evaluate the possible advantages of annealed copper as opposed to the full-hard copper used with Phase II Models 301, 302, and 303. Following assembly into the dynamic tester the seat land was formed in conjunction with axial deformation measurements using electrical contact for reference. These measurements indicated a poppet-to-holder stop gap of 0.0099 inch prior to formation. The land was then plastically formed with 63 pounds load with 1000-psig inlet pressure. The remaining stop gap at zero inlet pressure was 0.0012/0.0017 inch. A slightly greater gap was probably available at 1000-psig inlet pressure due to tube expansion, but this was not measured.

Seat leakage at 1000-psig inlet pressure and 13.5 pounds seat load was less than 10^{-5} scim. For the nominal 0.0022-inch wide land measured later, this corresponded to an apparent stress of 12,300 psi. The model was then subjected to a 1000-ultraclean (flow through filter bank) cycle test after which leakage at 13.5 pounds was 1.2×10^{-5} scim. No further tests were performed so that the undamaged sealing surface could be inspected. Oscilloscope impact load and position displays typical of all Phase III shear seal model tests are shown in Fig. VII-1.

Posttest inspection indicated the land surface was not as uniform as with previous Phase II models, and several areas of either voids or upset material in the seating plane were noted. The insert tube had plastically deformed radially inward so that an ID reduction occurred. This deformation was noted in removal of the formerly free-fitting retaining nut which shaved a minute copper ring just at the ID exit during extraction. The amount of

TABLE VII-1

PHASE III DYNAMIC TEST MODEL DATA

Model Designation and Description										Test Parameters								Test Results											
Model	Description	Poppet		Part No.	Serial No.	Seat		Flat Seat Area (A _{sp}), sq in.	Stroke T, inches									Stroked Flow Area A _f , sq in.	Net Actuation Pressure, psig	Static Seat Stress, psi	Impact Velocity, in./sec		Approximate Peak Impact		1000 psig Nitrogen Leakage, ⁽³⁾ scim, at 1000 psi stress			Seating Surface Reorientation	
		Part No.	Serial No.			Mean Diameter (D _s), inches	Land Width (L), inches			Axial	Normal	Force, pounds	Stress, psi	Control	After Clean Cycles	After Particle Cycles	Yes				No	Type	Concentration, Particles per Liter						
				Total	Flat																								
304	Shear Seal	7190-1	01	7190-4	X-1	0.472	0.0022	0.0022	0.0011	0.040	0.20			6.7	2.3			< 10 ⁻⁵	< 10 ⁻⁵	--	X								
305	Shear Seal	7190-1	02	7190-4	X-2	0.472	0.0023	0.0023	0.0012	0.040	0.020			7.2	2.5			Event Test Only			X		HB	5,960	1.19				
305	Same as Above (Repeat Test)									Same as Above (Repeat Test)								Event Test Only			X		HB	6,550	1.31				
306	Shear Seal	7190-1	01	7190-4	306	0.472	0.0050	0.0050	0.0025	0.040	0.020			6.5	2.2			9.0 x 10 ⁻⁵	3.0 x 10 ⁻⁴	8.7 x 10 ⁻³	X		HB	2,740	0.784				
306	Same as Above (Repeat Test)									Same as Above (Repeat Test)								--		3.0 x 10 ⁻³	2.5 x 10 ⁻³			HB	3,470	0.993			
306	Same as Above (Repeat Test)									Same as Above (Repeat Test)								--		1.6 x 10 ⁻²	2.7 x 10 ⁻¹	X		HB	5,600	1.60			
601	Self Cleaning	7195	01	7193	01	0.4702	0.0310	0.0200	0.0295	0.030	0.0413	139	7,940	4.9	4.9	600	20,400	0.0064	0.0060	0.016		X	HB	5,190	5.13				
601	Same as Above (Repeat Test)									Same as Above (Repeat Test)								9.1	9.1	1440	48,900	Event Test Only			X		HB	12,100	12.0
602	Self Cleaning	7195	02	7193	02	0.4683	0.0299	0.0146	0.0215	0.030	0.0413	139	10,900	5.1	5.1	680	31,300	0.015	0.017	0.62		X	HB	12,040	11.4				
603	Self Cleaning	7195	01	7193	01	0.470	0.0316	0.0291	0.0430	0.030	0.0413	139	5,450	2.5	2.5	270	6,280	Event Test Only				X	HB	12,370	12.4				
603	Same as Above (Repeat Test)									Same as Above (Repeat Test)								1.0	1.0	100	2,320	Event Test Only			X		HB	13,320	13.4
503	Flat 440C Poppet, Copper Seat	7198	05	7197	4	0.4678	0.0299	0.0272	0.0400	0.030	0.0413	139	5,860	6.7	6.7	600	15,000	0.034	0.022	0.11	X		HB	6,550	6.21				
504	Flat 440C Poppet, Copper Seat	7198	01	7197	5	0.4684	0.0308	0.0254	0.0374	0.030	0.0412	139	6,270	6.5	6.5	570	15,200	0.038	0.0095	0.35		X	HB	8,090	7.91				
702	Flat 440C Poppet, Grooved Copper Seat	7202	06	7201	6	0.470	0.0052 (1)	0.0052 (1)	0.0458 (2)	0.030	0.0413	136	5,000	6.7	6.7	660	14,400	0.0013	0.00048	0.0080		X	HB	8,230	5.10				
706	Flat 440C Poppet, Grooved Copper Seat	7202	07	7201	22	0.470	0.0055 (1)	0.0052 (1)	0.0458 (2)	0.030	0.0413	136	5,000	6.8	6.8	670	14,600	0.0011	0.00085	0.0006		X	HB	5,590	3.52				
707	Flat 440C Poppet, Grooved Copper Seat	7202	07	7201	25	0.470	0.0057 (1)	0.0057 (1)	0.0458 (2)	0.030	0.0413	136	5,000	6.8	6.8	670	14,600	0.00024	0.0011	0.016		X	HB	4,910	3.22				

(1) Summed individual land widths
(2) Assumes solid land from inner land ID to outer land OD
(3) Shear seal model data at 40-pound load

TABLE VII-1

PHASE III DYNAMIC TEST MODEL DATA

Model Designation and Description								Test Parameters								Test Results																
Poppet		Seat														Test Results																
		Part No.	Serial No.	Part No.	Serial No.	Mean Diameter (D _S), inches	Land Width (L), inches		Flat Seat Area (A _{sp}), sq in.	Stroke T, inches	Stroked Flow Area A _f , sq in.	Net Actuation Pressure, psig	Static Seat Stress, psi	Impact Velocity, in./sec		Approximate Peak Impact		1000 psig Nitrogen Leakage, ⁽³⁾ scim, at 1000 psi stress			Seating Surface Reorientation		Particle Data		Particle Impact Data							
Total	Flat						Axial	Normal						Force, pounds	Stress, psi	Control	After Clean Cycles	After Particle Cycles	Yes	No	Type	Concentration, Particles per Liter	Predicted Impacts, I _P	Actual Impacts, I _A	I _A /I _P	No. of Particle Embedments	Model No.					
7190-1	01	7190-4	X-1	0.472	0.0022	0.0022	0.0011	0.040	0.20				6.7	2.3				< 10 ⁻⁵	< 10 ⁻⁵	--	X								304			
7190-1	02	7190-4	X-2	0.472	0.0023	0.0023	0.0012	0.040	0.020				7.2	2.5				Event Test Only			X		HB	5,960	1.19	6	5.0	6		305		
Same as Above (Repeat Test)																Event Test Only			X		HB	6,550	1.31	4	3.0	4		305				
7190-1	01	7190-4	306	0.472	0.0050	0.0050	0.0025	0.040	0.020				6.5	2.2				9.0 x 10 ⁻⁵	3.0 x 10 ⁻⁴	8.7 x 10 ⁻³	X		HB	2,740	0.784	1	1.3	1		306		
Same as Above (Repeat Test)																--	3.0 x 10 ⁻³	2.5 x 10 ⁻³			HB	3,470	0.993	1	1.0	1		306				
Same as Above (Repeat Test)																--	1.6 x 10 ⁻²	2.7 x 10 ⁻¹	X		HB	5,600	1.60	9	5.6	9		306				
7195	01	7193	01	0.4702	0.0310	0.0200	0.0295	0.030	0.0413	139	7,940	4.9	4.9	600	20,400	0.0064	0.0060	0.016			X	HB	5,190	5.13	1	0.20	1		601			
Same as Above (Repeat Test)																9.1	9.1	1440	48,900	Event Test Only			X		HB	12,100	12.0	7	0.58	0		601
7195	02	7193	02	0.4683	0.0299	0.0146	0.0215	0.030	0.0413	139	10,900	5.1	5.1	680	31,300	0.015	0.017	0.62			X	HB	12,040	11.4	6	0.53	2		602			
7195	01	7193	01	0.470	0.0316	0.0291	0.0430	0.030	0.0413	139	5,450	2.5	2.5	270	6,280	Event Test Only				X	HB	12,370	12.4	3	0.24	Not		603				
Same as Above (Repeat Test)																1.0	1.0	100	2,320	Event Test Only			X		HB	13,320	13.4	6	0.45	Determined	603	
7198	05	7197	4	0.4678	0.0299	0.0272	0.0400	0.030	0.0413	139	5,860	6.7	6.7	600	15,000	0.034	0.022	0.11			X	HB	6,550	6.21	7	1.1	7		503			
7198	01	7197	5	0.4684	0.0308	0.0254	0.0374	0.030	0.0412	139	6,270	6.5	6.5	570	15,200	0.038	0.0095	0.35			X	HB	8,090	7.91	9	1.1	9		504			
7202	06	7201	6	0.470	0.0052 (1)	0.0052 (1)	0.0458 (2)	0.030	0.0413	136	5,000	6.7	6.7	660	14,400	0.0013	0.00048	0.0080			X	HB	8,230	5.10	22	4.3	3		702			
7202	07	7201	22	0.470	0.0055 (1)	0.0052 (1)	0.0458 (2)	0.030	0.0413	136	5,000	6.8	6.8	670	14,600	0.0011	0.00085	0.0006			X	HB	5,590	3.52	12	3.4	4		706			
7202	07	7201	25	0.470	0.0057 (1)	0.0057 (1)	0.0458 (2)	0.030	0.0413	136	5,000	6.8	6.8	670	14,600	0.00024	0.0011	0.016			X	HB	4,910	3.22	13	4.0	4		707			

iths
inner land ID to outer land OD
10-pound load

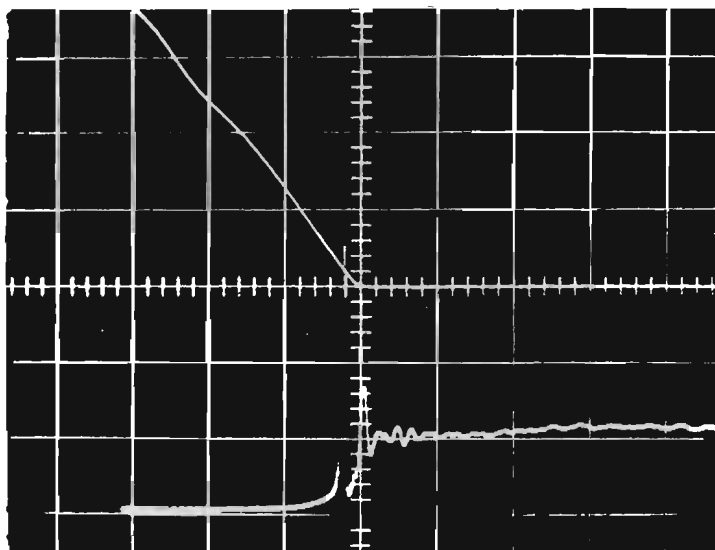


Figure VII-1. Model 304 Load and Displacement
Traces (0.002 sec/div; 200 lb/div;
0.010 in./div)

ID upset was not measured but it accounted for the less-than-expected land width. These results, in conjunction with the nonuniform deformation noted with flat, soft copper Model 501 (discussed later), ultimately led to the cessation of soft copper material testing.

Model 305

Shear Model 305 also used a soft copper insert, but one which had suffered handling damage to the seating corner. As such, it was used only for impact event tests to establish a new hit frequency baseline for the modified tester and seat holder. Formed land width was 0.0020 to 0.0025 inch except in the damaged area. Poppet-stop gap was 0.0082 inch prior to land formation and 0.0011/0.0013 inch afterward. Two 1000-cycle HB particle tests were performed with the following recorded particle count data:

HIAC Count/Liter		
Cycles	12 to 20 Microns	>20 Microns
First Test		
Background	5	5
0	307	6170
100	377	6240
200	400	6120
500	538	5820
1000	557	5910
Second Test		
Background	30	10
0	180	6450
100	423	6800
200	324	6950
500	306	6430
1000	398	6350

With an average count of 5960 p/l six hits occurred, while four hits were noted at 6550 p/l. Predicted impacts for the particle concentrations and normal land width involved were 1.19 and 1.31, respectively. These results, similar to those achieved with Phase II Model 303, suggest that the modifications involved made no marked change in hit frequency.

Model 306

This final model seat was fabricated of fully hardened copper bar having a Rockwell F of about 90. Seat land formation produced a nominal 0.005-inch wide land. Poppet-stop gap prior to formation was 0.0076 inch with 0.0027/0.0030 inch remaining afterward. This was slightly greater than the Phase II models and it was believed that the additional land width and springback was produced by an extremely sharp seat corner not present on previous hard seat models.

Three complete dynamic tests were performed on Model 306 with disassembly and hit inspection between tests. Particle count data are tabulated as follows for each test:

HIAC Count/Liter

Cycles	12 to 20 Microns	>20 Microns
First Test		
Background	10	0
0	67	2710
100	130	2850
200	247	2720
500	222	2720
1000	274	2745
Second Test		
Background	7	0
0	167	3320
100	-	3590
200	218	3420
500	216	3490
1000	271	3450
Third Test		
Background	10	10
0	184	5800
100	179	5690
200	201	5800
500	230	5650
1000	287	5270

A final inspection of each seating surface was performed using the interference microscope. Test results are presented in Table VII-1 and Fig. VII-2 for the entire series. As indicated, each particle test was preceded by a 1000-cycle ultraclean cycle test to provide a control datum. Consequently, this model accumulated a total of 6000 cycles.

Leakage after forming was about 10^{-5} scim at 63 pounds and 1.3×10^{-4} scim at 15 pounds load. The initial 1000 clean cycle test resulted in some sealing degradation with almost a 30 times leakage increase at 40 pounds load following the first HB particle test. Preliminary seat inspection revealed one particle embedment had occurred. The model was then reassembled with poppet and seat reoriented approximately 15 degrees and control tested (Test 4, not shown in Fig. VII-2). Leakage was about 10 times that obtained after the second 1000 clean cycle test (Test 5, Fig. VII-2). This indicated that reorientation caused sealing degradation either from particle damage misalignment or poppet-to-seat eccentricity, but that additional cycling had a wear-in effect.

The second HB particle test also produced one embedment occurring very close to the first. Each particle was located near the land OD, with evidence that the particles had been pushed axially away from the sealing land. Leakage change following this test was negligible, indicating comparable particle damage.

Additional sealing degradation was evident following the third assembly into the tester with initial leakage approximately 10 times greater than the preceding results. Sealing performance after 1000 ultraclean cycles (Test 7) was virtually unchanged. Apparently the aforementioned surface damage, in conjunction with probable eccentric misalignment during installation in the tester, was sufficiently severe to preclude cyclic-induced self-healing. Following the third 1000 HB particle cycles, leakage increased by a factor of 10 (Test 8). Posttest inspection indicated that nine embedments had occurred, with the majority at the land center. This result further supported the conclusion that the model configuration was subject to excessive particle hits.

Typical land photos are shown in Fig. VII-3 through VII-6. Figure VII-3 reveals a characteristic particle embedment (ID on right). The mottled texture is believed caused by oxidation and nonuniform plastic flow. The latter also is portrayed in Fig. VII-4 and VII-5. These photos also show areas where the land was imperfectly formed, resulting in a groove or ridge. Most of the land, however, appeared as shown in Fig. VII-6. Crown radius indicated by the latter photo is 0.186 inch, or less than the 0.25 inch poppet spherical radius. As demonstrated in the previous program, land crown is desirable because it produces a load concentration at the land center. This results in minimum leakage at low loads.

Each particle embedment produced a corresponding pock-mark in the poppet surface. Interference photos could not be obtained because of the 20-degree seating angle. However, the appearance and size of the poppet surface damage was similar to that obtained with the flat copper model. Photos of these parts are discussed later.

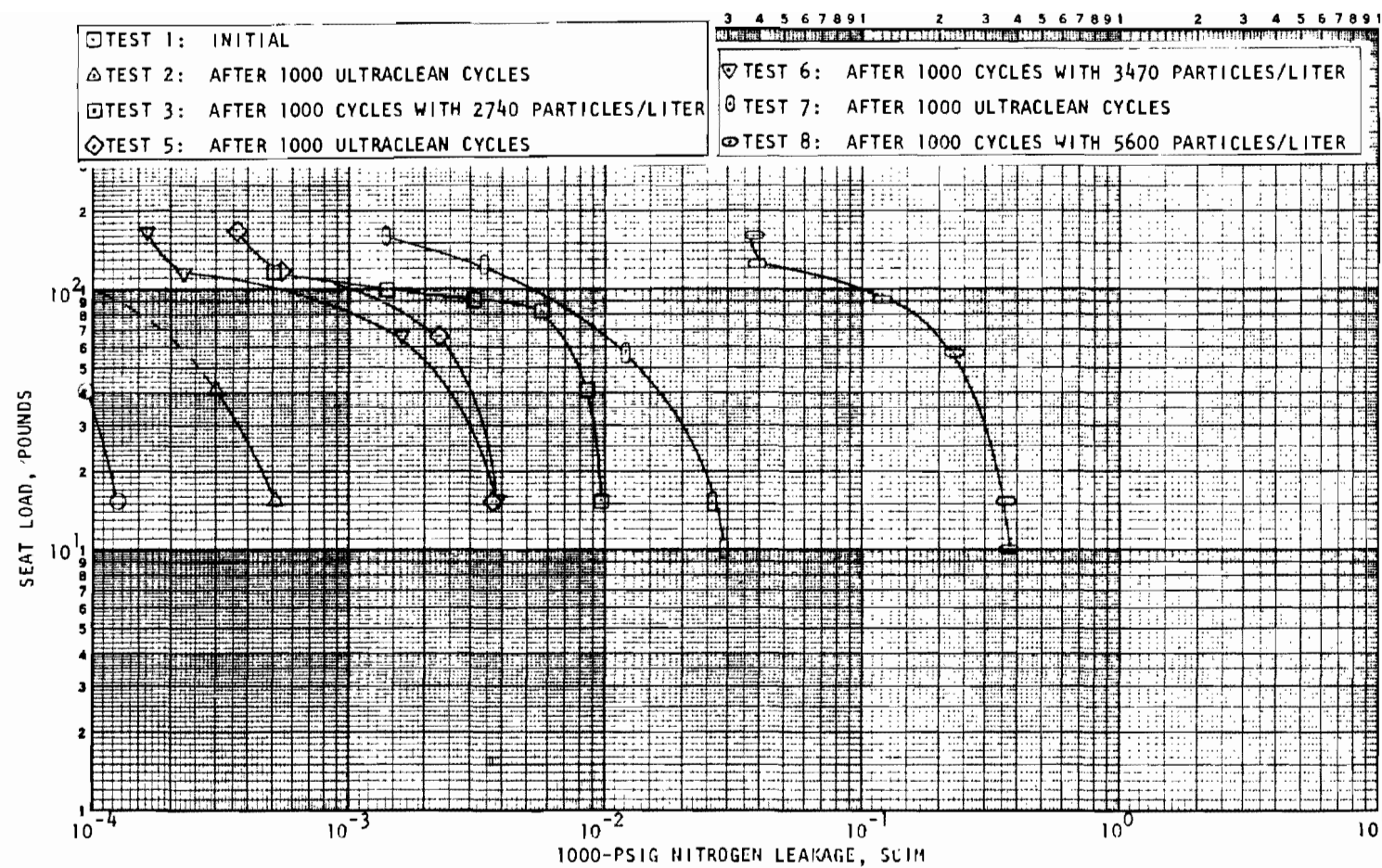


Figure VII-2. Load-Leakage Data for Dynamic Test Model 306, Tests 1, 2, 3, 5, 6, 7, and 8

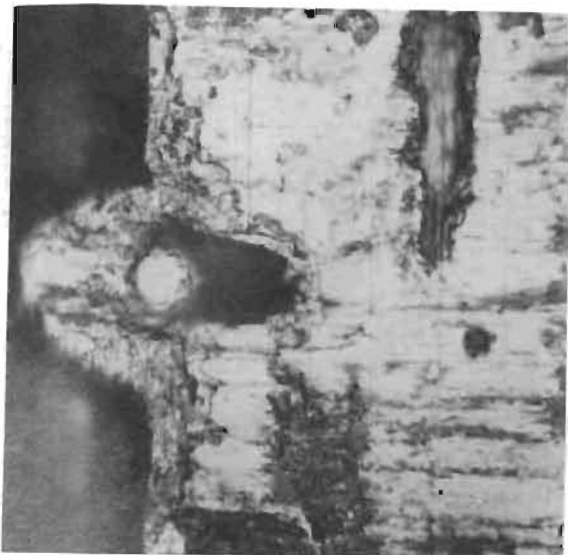


Figure VII-3. Model 306 Seat Land
Showing Typical OD
Edge Particle
Embedment (462X
Plain Photo)

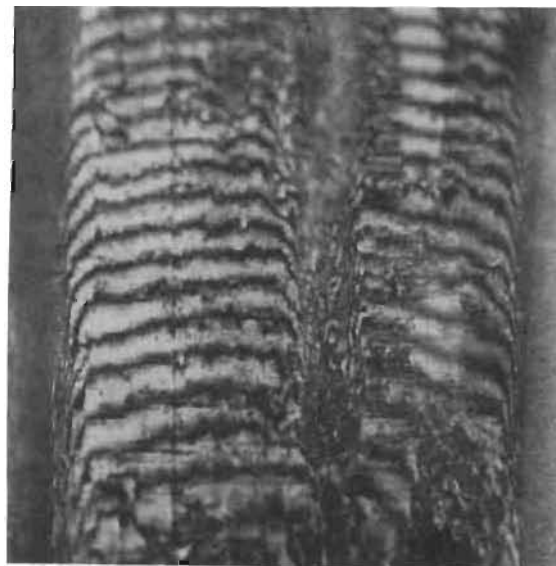


Figure VII-4. Model 306 Seat Land
With Formed Groove
(462X Interference
Photo)

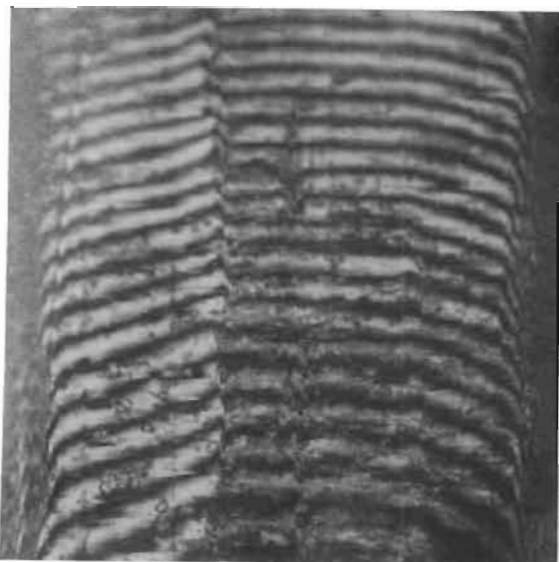


Figure VII-5. Model 306 Seat Land
With Formed Ridge
(462X Interference
Photo)

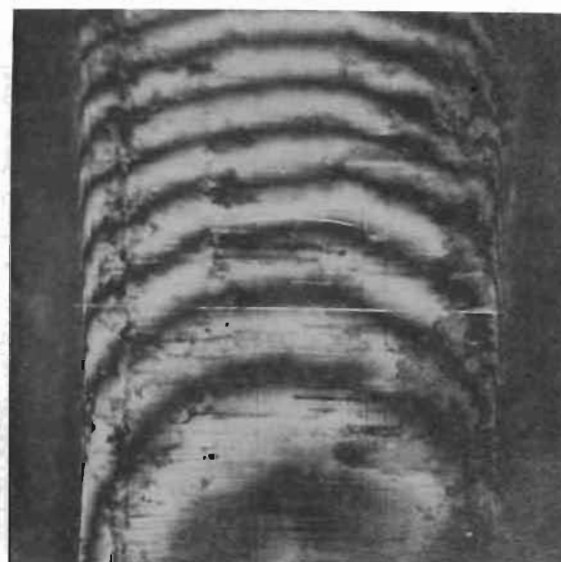


Figure VII-6. Model 306 Typical
Seat Land Crown
(462X Interference
Photo)

Observations

The shear seal model has shown the potential sealing advantage of plastic land formation, but other complex problems also have been revealed. The outer land positive stop provides significant design advantage but flow through the seat results in the necessity for nearly 180-degree turn in flow which may be the cause of excessive hit frequency. A center cone for turning flow might improve this condition.

Uniform land formation is certainly dependent on the initial seat corner condition, but treatment of the relatively soft copper is difficult. This aspect of the design needs additional development to correlate land formation with corner condition. Additionally, the effect of poppet eccentricity should be explored because it is evident that precise control is necessary to achieve the indicated results. A "zero clearance" actuator bearing would probably be required in application to a functional valve design because of tube end resistance to lateral deformation.

Even with these problems, however, it should not be overlooked that Model 306 sustained 3000 clean cycles and 3000 cycles with particles producing 11 embedments. Even then, leakage at 10 pounds load was about 0.4 scim at 1000-psig inlet pressure. It is reasonably certain that several 60-micron particles could be enveloped with comparable performance, particularly if the poppet were harder than the particles. This is substantially better performance than indicated by the 440C and carbide materials with particles entrapped.

SELF-CLEANING TEST MODELS

Five particle tests of this model were performed to demonstrate efficacy of the avoidance concept. As shown in Table VII-1, two tests included particle impact effects with the 17-4PH material. Poppet and seat orientation was maintained throughout these tests to ensure precise mating of poppet and seat particle damage. The remainder of the tests demonstrated hit frequency at various conditions. The model surfaces were refinished for each test to provide definition of impact events.

Static Test Leakage Investigation

Attempts to test the first self-cleaning model were negated by indications of a gross out-of-parallel situation. Even with the best condition possible by clamp ring screw adjustment, leakage at 1000-psi stress was more than an order of magnitude greater than anticipated, and an abnormally steep closure rate was in evidence. It was theorized that plug overtorque had elastically deformed the sealing face of Model 601 poppet. The poppet was subsequently interferometrically inspected with plug screw torques estimated from 2 to >10 inch-pounds. Under the largest load, only a barely discernible deviation in the seating surface plane was noted, indicating that assembly loads were not a significant factor.

Both poppet and seat were then inspected for parallelism. Model 601 was found to be 23 microinches out-of-parallel at the 0.470-inch mean seat diameter. A check of Model 602 indicated a 19 microinch deviation. Apparently, the previously noted problems of producing a reasonably scratch-free finish on the 17-4PH surfaces resulted in the final parallelism correction being neglected. The excessive low stress leakage of Model 601 was attributed to some contamination effects and an out-of-parallel condition too severe for tester clamp ring adjustment to accommodate.

Model 601 and 602 poppets and seats were reworked by lapping the back (mounting) faces to provide a net out-of-parallelism of 5 to 7 microinches at the mean seating diameter. To provide reference stress-leakage data, both models were tested in the static tester with ball joint loading.

Particle Effect Tests

Model 601. Except for a slight (0.005 scim) increase at 500-psi stress, Model 601 stress-leakage results after installation in the dynamic tester were virtually identical to ball joint loading data. A minor improvement in the high-stress region resulted after 1000 ultraclean cycles. The model was then cycled 1000 times with the following HB particle count:

HIAC Count/Liter

Cycles	12 to 20 Microns	> 20 Microns
Background	4	7
0	117	5275
100	120	5330
200	144	5350
500	231	5180
1000	229	5020

Assuming no self-cleaning action, the count average of 5190 p/l would yield a predicted 5.13 hits. Impact velocity was 4.9 inch/sec with 5 inch/sec targeted. (The latter was a design value established to ensure closure prior to exhausting the plug volume of clean flushing fluid.) The impact load and position traces are shown in Fig. VII-7.

Following this test, leakage increased about a factor of 2 at 1000-psi stress (Fig. VII-8). Posttest inspection revealed that one impact event had occurred with the particle remaining embedded in the poppet. Additionally, three plug-seat diametral encounters were noted.

Model 602. Model 602 initial assembly stress-leakage data repeated ball joint results over the entire stress range. (This duplication of data, readily achieved on both Models 601 and 602, indicates that net model surface parallelism on the order of 10 microinches is required for clamp ring adjustment to be effective.) Following 1000 ultraclean cycles, a slight increase in low-stress leakage resulted, as shown in Fig. VII-9.

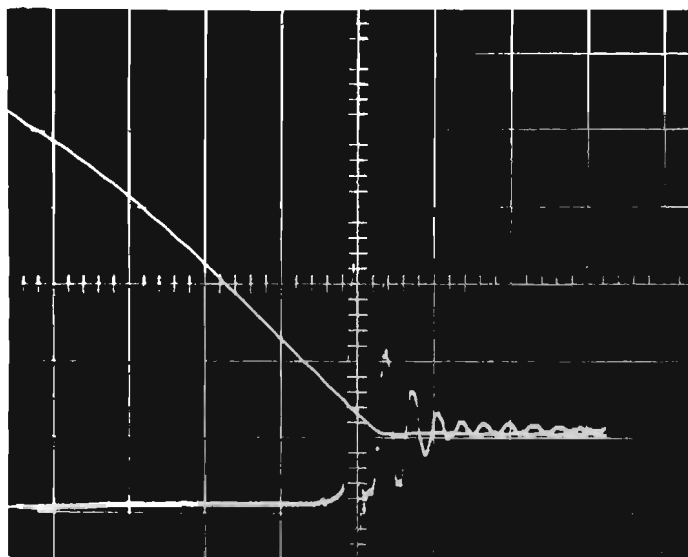


Figure VII-7. Model 601 Load and Displacement
Traces (0.001 sec/div; 200 lb/div;
0.005 in./div)

In reviewing the results of Model 601, the probability of accumulating one event was only 3 percent. Without benefit of multiple test results, it was not known whether this relatively low hit frequency was due to the self-cleaning effect or chance. Particle concentration was, therefore, increased for subsequent tests to reduce the potential influence of the latter. Accordingly, Model 602 was tested with an average concentration of 12,040 p/l, as obtained from the following count data:

HIAC Count/Liter

Cycles	12 to 20 Microns	> 20 Microns
Background	0	0
0	256	12,190
100	286	12,680
200	371	12,640
500	366	11,870
1000	398	11,530

Velocity and impact load parameters were nearly identical to those of Model 601.

As illustrated by Fig. VII-9, leakage following HB particle cycles increased nearly 40 times at 1000-psi stress and was still 2.5 times greater than the control value at 10,000 psi. Posttest inspection revealed six hits had occurred; 11.4 were predicted. Both poppet and seat had one entrapped particle. Approximately 21 encounters at the plug-seat clearance were observed.

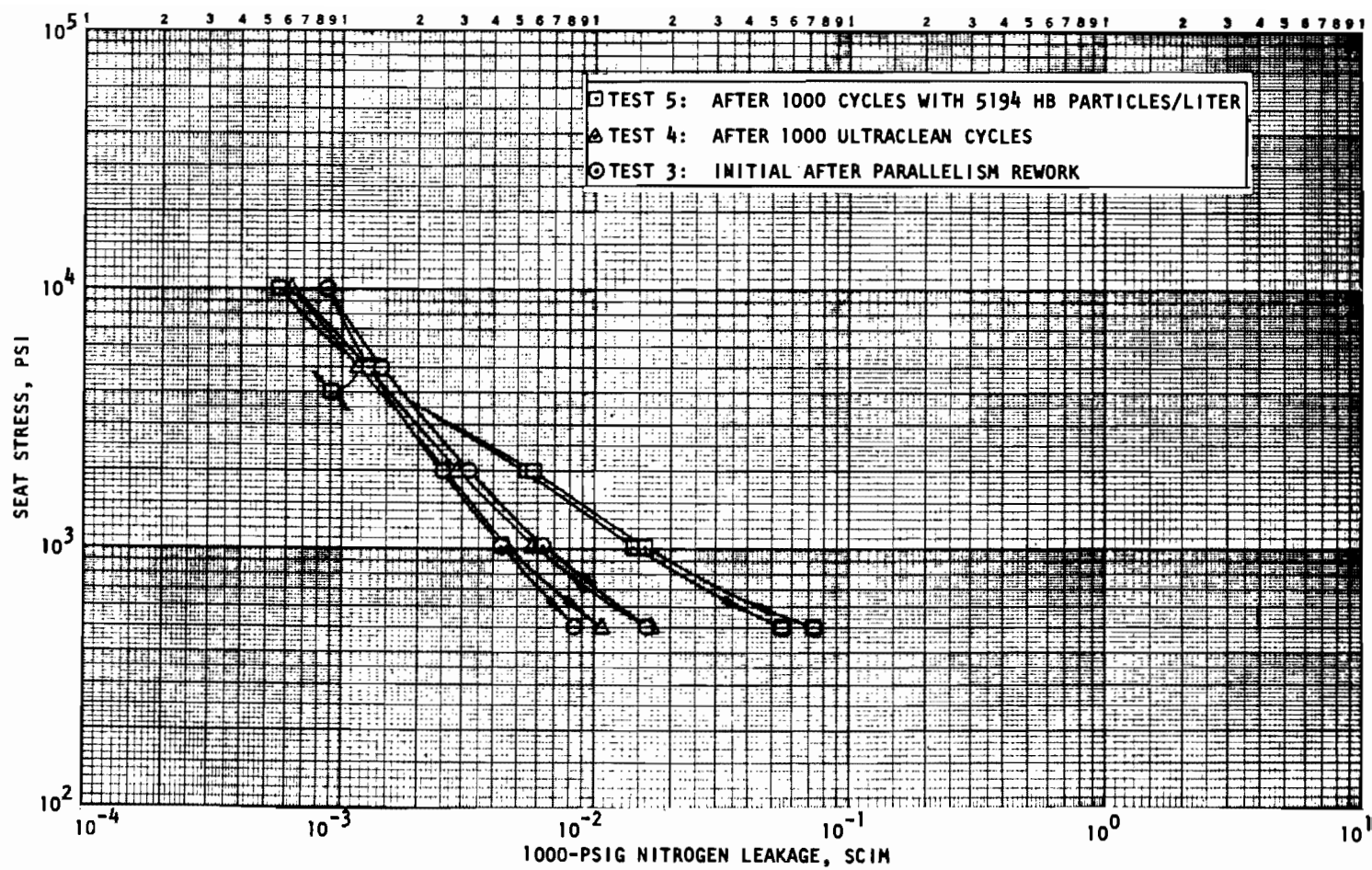


Figure VII-8. Stress-Leakage Data for Dynamic Test Model 601, Tests 3, 4, and 5

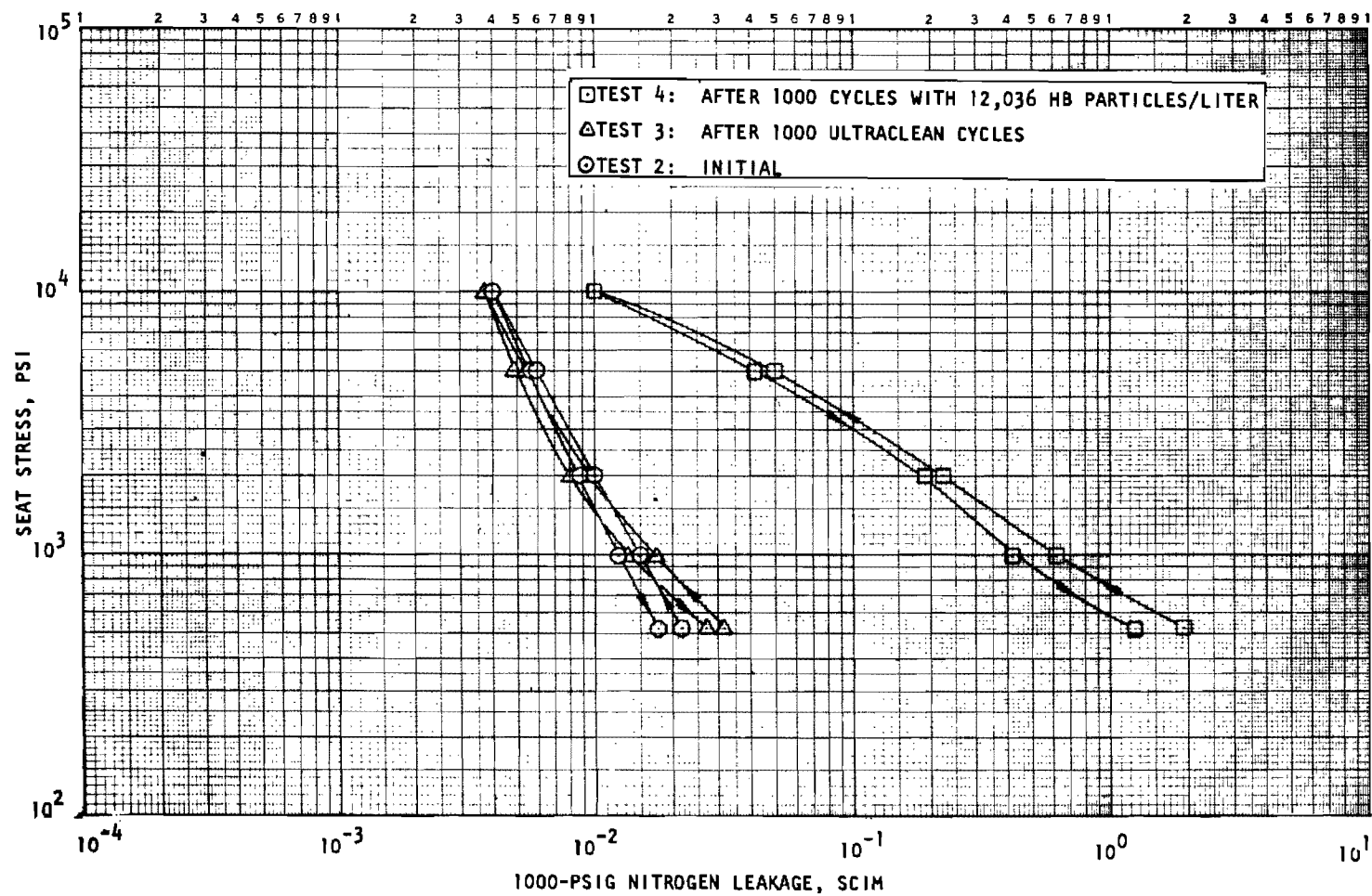


Figure VII-9. Stress-Leakage Data for Dynamic Test Model 602, Tests 2, 3, and 4

Particle Damage

Plain and interference photos of Models 601 and 602 showing land texture, a typical embedded particle, and plug clearance encounters are given in Fig. VII-10 through VII-17. Assessment of these and other photos indicate that the average particle hole depth in the 17-4PH material was 0.0004 inch. Surface upset height was generally on the order of 30 to 40 microinches and the area of disturbed metal approximately 0.004 inch in diameter. Embedded particles protruded above the surface about 0.0004 inch. All but one particle in both dynamic tests remained intact. This particle fractured similar to that obtained with flat 440C models.

There was no evidence that particles caught between the plug and seat radial gap became permanently embedded. Troughs gouged by these particles (at entrance edges only) varied in size, with dimensions of 0.0005-inch wide by 0.0015-inch long and 0.0013-inch wide by 0.0069-inch long representing typical small and large plug damage, respectively. Groove depths ranged from about 0.0001 to 0.0005 inch, and upset metal up to 0.0002 inch above the surface was noted. Although both plug and seat were made from 17-4PH CRES, the plug (R_C 28-32) was softer than the seat and thus sustained deeper grooves. There appeared to be no relationship between plug-seat diametral encounters and those occurring on the seating surface.

Impact Event Tests

Previous Models 601 and 602 were tested at a nominal 5 inch/sec. This value was based on rather inconclusive preliminary test data; specific closure dynamics were unknown. The 5.0-inch/sec velocity was, therefore, bracketed in an attempt to improve effectiveness of the self-cleaning feature.

Using a particle concentration similar to that of Model 602, Model 601 was retested at 9.4 inch/sec. It was subsequently refinished (as Model 603) and, again, with similar concentrations, tested at 2.5 and 1.0 inch/sec. The results, including Model 602, are summarized in the following tabulation. Background and count variation for these tests was similar to that previously presented for Model 602.

Model	Impact Velocity, inch/sec	Particle Concentration, p/l	Predicted Hits	Actual Hits
601	9.4	12,100	12.0	7
602	5.1	12,040	11.4	6
603	2.5	12,370	12.4	3
603	1.0	13,320	13.4	6

In view of previous tests with other flat models, where actual and predicted hits compare very favorably, the data indicate the self-cleaning feature has, to some extent, been effective. It is further indicated that the optimum closure velocity for the geometry and system parameters involved

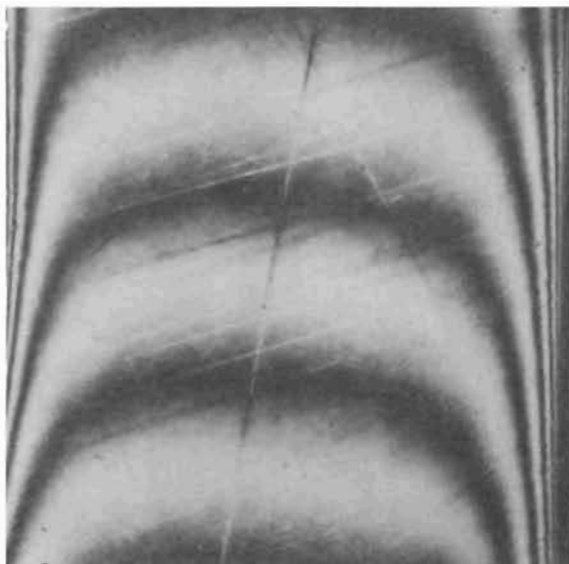


Figure VII-10. Model 601 Seat Land
(91X Interference
Photo)

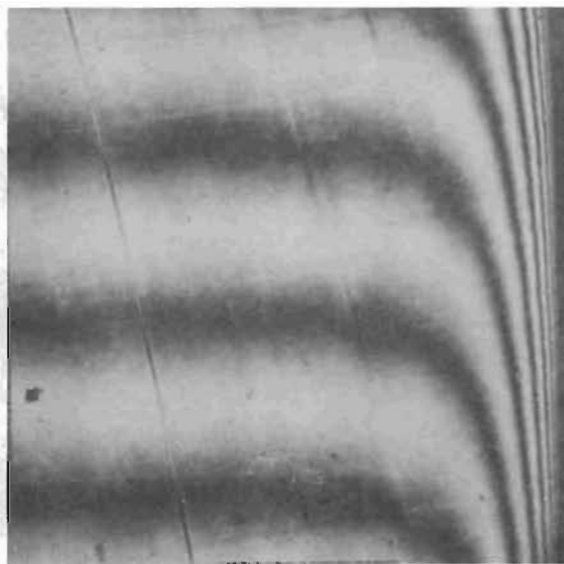


Figure VII-11. Model 601 Poppet
Land (91X Inter-
ference Photo)

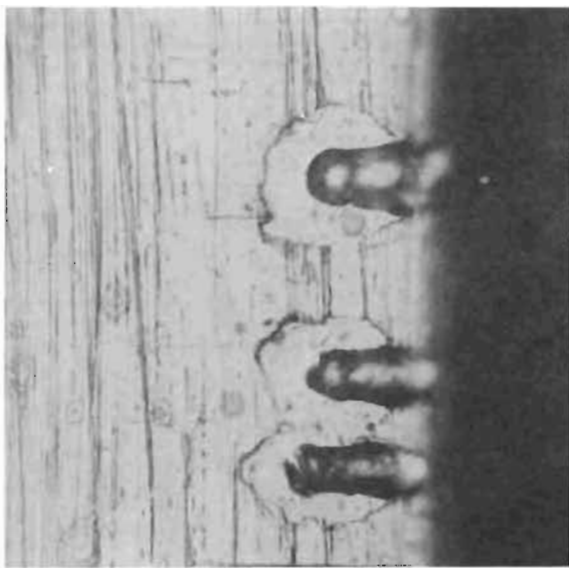


Figure VII-12. Model 601 Plug OD
Showing Typical
Small Gouges (462X
Plain Photo)

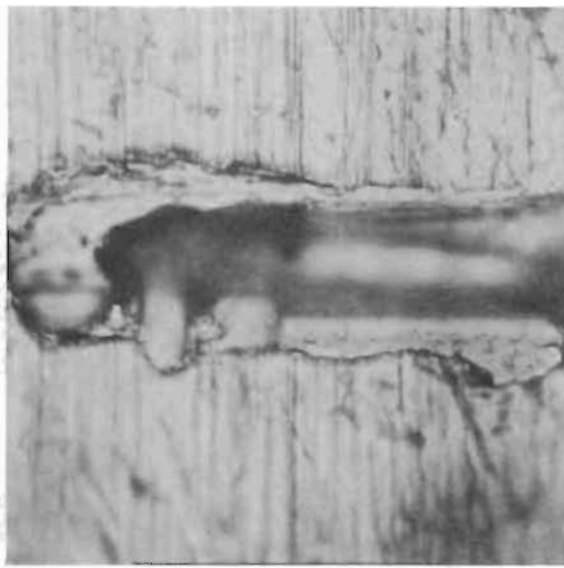


Figure VII-13. Model 601 Plug OD
Showing Typical
Large Gouge (462X
Plain Photo)

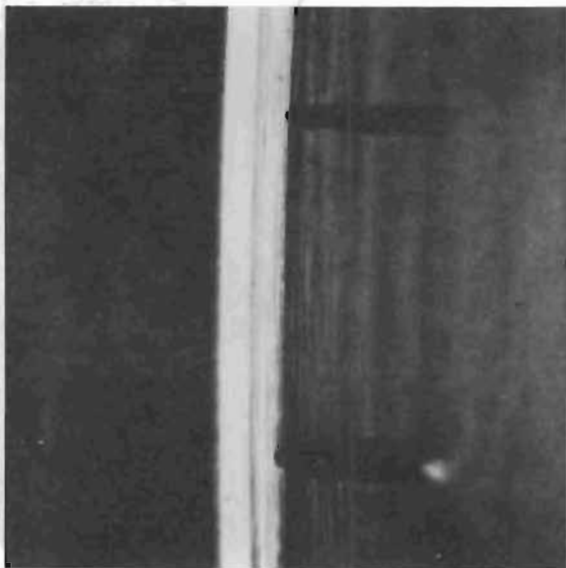


Figure VII-14. Model 601 Seat Land Bore Showing Typical Gouges (91X Plain Photo)

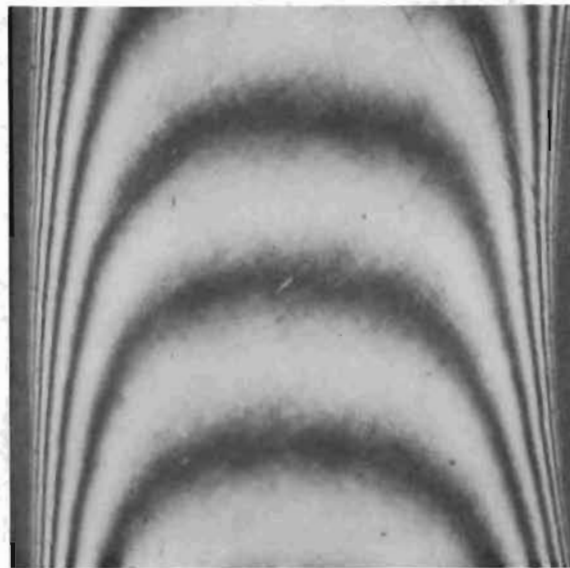


Figure VII-15. Model 602 Seat Land; Poppet of Similar Texture With Duboff Same as Fig. VII-11 (91X Interference Photo).

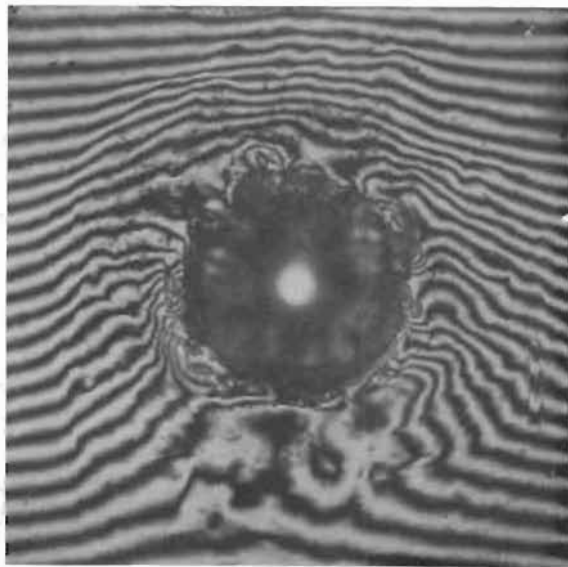


Figure VII-16. Model 602 Poppet With Embedded Particle (462X Interference Photo)

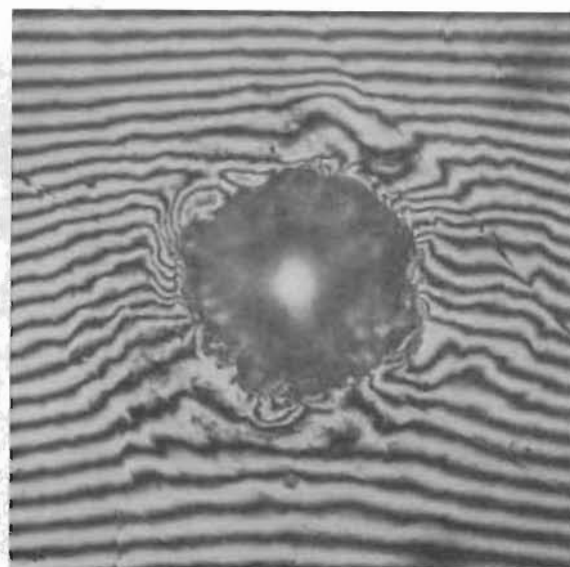


Figure VII-17. Model 602 Seat Showing Hole From Fig. VII-16 Particle (462X Interference Photo)

lies between 5 and 1 inch/sec. However, single test results do not provide a sufficient sample from which firm conclusions can be drawn.

Also, the pressure and flow transients occasioned by plug travel and ultimate entry into the seat bore may have influenced the number of hits in either a greater or lesser direction. The self-cleaning model configuration, therefore, remains a potential but unproved means of significantly reducing poppet and seat particulate impact encounters.

Observations

These tests indicated that local particle concentrations can be drastically altered and significant reduction in hit frequency can be achieved. Refinement of the approach with a thorough fluid dynamics analysis should provide the functional details necessary to obtain much better performance than noted herein.

The particle entrapment effects with this semihard metal suggest that there likely is a combination of seat, poppet, and particle hardness and work hardening properties in which particle embedment depth is sufficient to retain impacted particles. While apparently obvious with very hard particles, such as aluminum oxide or diamond, there is insufficient data to predict this effect with the many other materials. It can be generally stated, however, that particle embedment with the harder seating materials will require greater loads to effect envelopment. Consequently, it is concluded that: (1) both seating surfaces should be very hard, or (2) one surface should be much softer than the other. As previously noted, minimal entrapment effects with the hard combination is dependent on the particle being ejected or washed from between the sealing surfaces.

FLAT COPPER TEST MODELS

Embodying the particle envelopment concept, this model design was tested to compare performance with other models and, also, to establish a foundation for subsequent flat-grooved model design. The initial two models (501 and 502) were static tested to ascertain general performance and sealing surface plastic deformation characteristics. Two dynamic tests were then performed with Models 503 and 504. (Envelopment load data would have best been determined statically for this model, as in Phase II particle placement tests.)

Model 501

This model employed an annealed (soft) copper insert extending 0.0006 inch above the seat holder positive stop face in the initial, unloaded condition. The seat insert reflected the first lapping attempts and, while basic surface roughness was less than 1 microinch AA, a myriad of deep scratches resulted. For this and subsequent reasons, the model was considered a developmental prototype and no stress-leakage data are presented. Interference photos of the model are shown in Fig. VII-18 through VII-21.

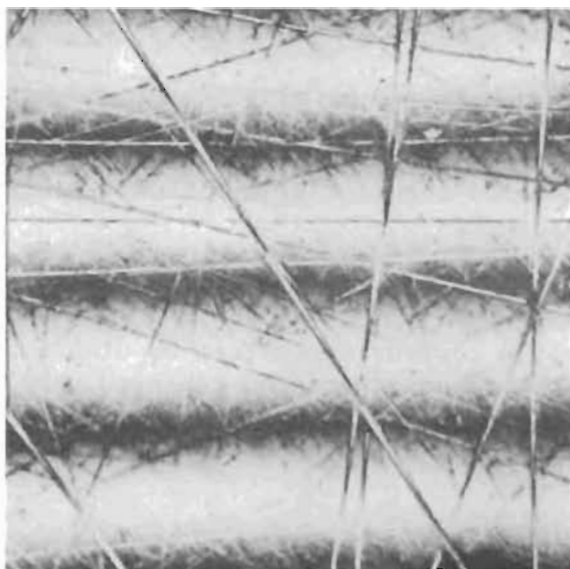


Figure VII-18. Model 501 Seat Showing Typical Texture and Scratches (462X Interference Photo)

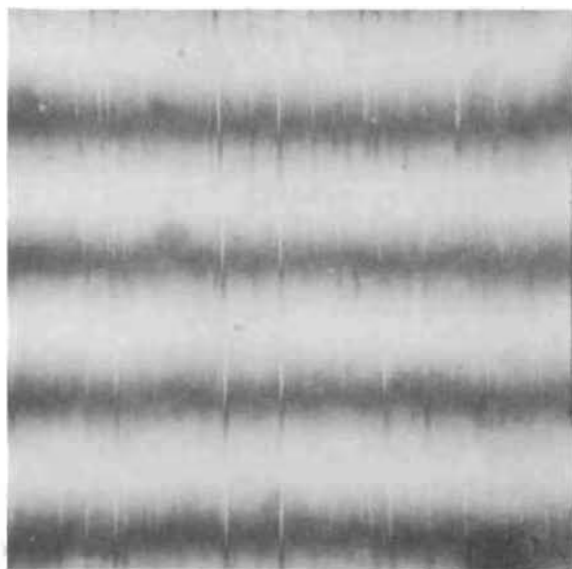


Figure VII-19. Model 501 Poppet Showing Typical Texture (462 X Interference Photo)

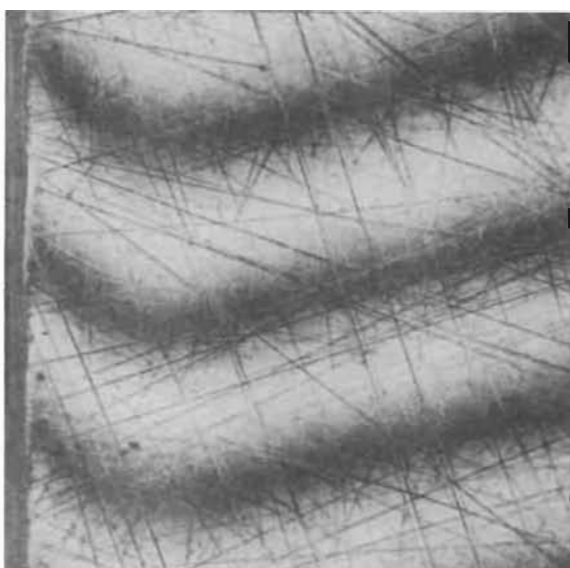


Figure VII-20. Model 501 Seat Land Showing Skin Effect; ID on Right (91X Interference Photo)

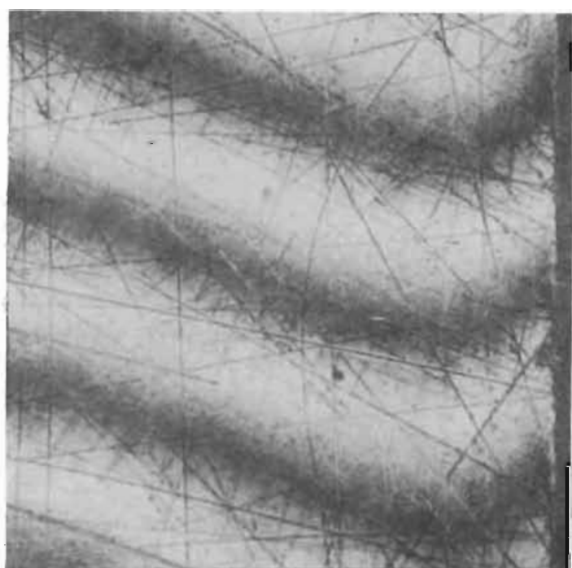


Figure VII-21. Model 501 Seat Land 180 Degrees From Fig. VII-18; ID on Left (91X Interference Photo)

After testing in the static tester to 10,000-psi apparent seat stress, Model 501 evidenced a surface deformation characteristic not previously observed with other test models in this or former programs. A relatively uniform falloff from ID toward OD occurred, terminating in a maximum depression of about 10 microinches at 80 percent of the land width. From this point to the OD, surface height increased about 5 microinches (Fig. VII-20 and VII-21). This surface distortion characteristic is believed due to a "skin effect" of machining-induced work hardening of the annealed seat material. While lapping exposed the annealed substructure on the sealing surface, the adjacent areas were as-machined and thus stronger, preventing uniform surface deformation.

Following a test where seat stress was increased to 60,000 psi, little change to the surface was noted. The overall insert height was reduced 0.0003 inch, however. This indicated that the substructure was weaker than the cold worked (surface deformation) plane and, by collapsing, precluded further significant sealing surface change through poppet contact with the seat holder.

From these results and previously described soft shear seal insert tests, it was decided that soft copper testing would be terminated and future effort expended on the full hard (R_p 90) material. The parts could have been annealed after machining; however, the dubious benefits gained would have been offset by potential handling damage and distortion. Moreover, the weaker substructure appeared to be a deterrent to adequate seat forming.

Model 502

Model 502 used a hard copper seat insert finished with improved procedures so that very few significant scratches existed; however, the surface was generally pitted. Insert height above seat holder surface was 0.0022/0.0023 inch. The model was successfully tested in the static tester to maximum stress levels of 10,000 to 60,000 psi. Figure VII-22 presents stress-leakage data for the first and last tests. Also shown is a composite curve representing insert deflection. While the latter data include poppet, seat holder, and tester deflections, insert deformation accounts for the bulk of the displacement. It will be noted the seat holder surface was not contacted (maximum deflection approximately 0.0014 inch).

Seat surface inspection after 10,000-, 20,000-, and 30,000-psi stress tests showed the surface to be generally crowned with minimal but uniform deformation. However, following a final series of load cycles terminating in 60,000-psi apparent stress, the seat land width was reduced from 0.029 (initial) to 0.022 inch due to a 30-microinch duboff at the land OD. This is shown in comparison of Fig. VII-23 (after 20,000-psi apparent stress) and VII-24 (after 60,000-psi apparent stress).

It was tentatively concluded from these results that seating load should not exceed 20,000-psi apparent stress, or 800 pounds. The following dynamic tests with Models 503 and 504 were, therefore, limited to 15,000-psi apparent impact stress. As will be seen, seat land flatness was maintained by this loading limitation.

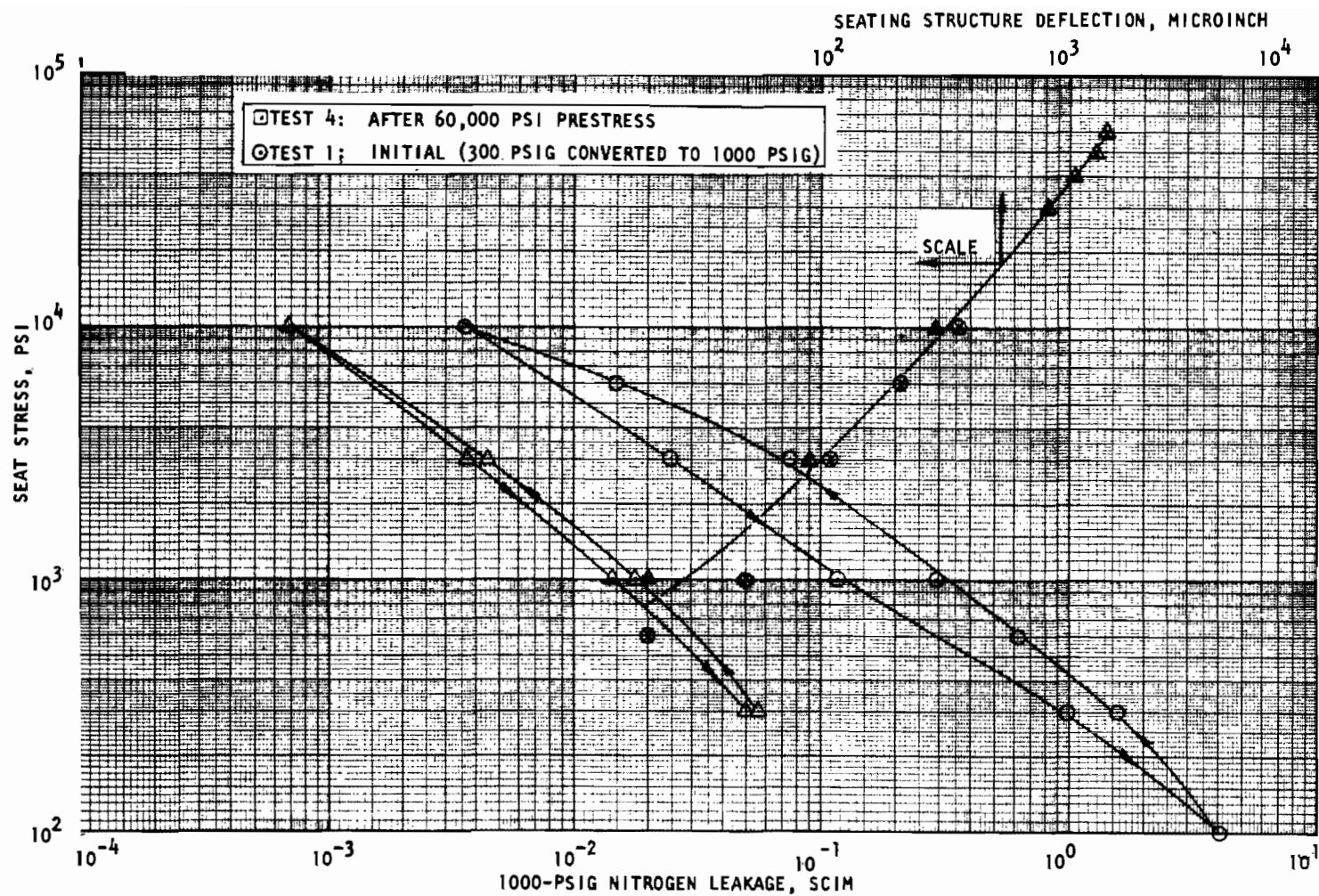


Figure VII-22. Stress-Leakage and Seating Structure Deflection Data for Static Tested Model 502

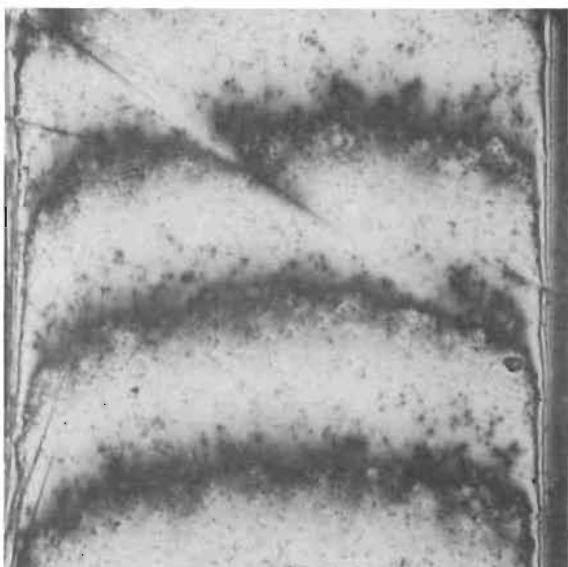


Figure VII-23. Model 502 Seat After 20,000-psi Apparent Stress (91X Interference Photo)

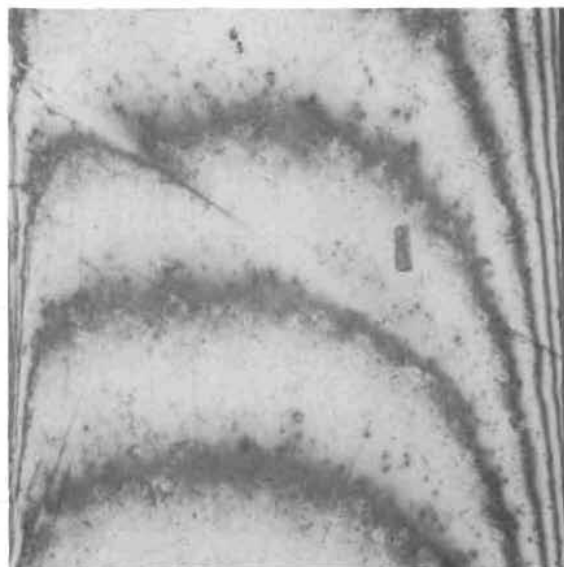


Figure VII-24. Model 502 Seat After 60,000-psi Apparent Stress (91X Interference Photo)

Model 503

Initial assembly in the dynamic tester revealed a sufficiently out-of-parallel condition that the previously employed procedure of selective loading clamp ring screws was ineffective. The seat retaining bolt load was varied from 150 to 600 pounds and, for this model at least, made little difference. Ultimately, by rotating the poppet 180 degrees and, with crude shimming, the condition was adjusted to yield a tolerable stress-leakage characteristic, as shown in Fig. VII-25.

The seat insert face was known to be out-of-parallel with the holder back face by some 20 microinches during initial inspection. It was believed that clamp ring adjustments could accommodate this deviation. However, additional nonparallelism due to poppet, piston feet, and potential assembly contamination combined to preclude such simple correction.

As indicated by Fig. VII-25, 1000 ultraclean cycles resulted in little change to the stress-leakage characteristics. Because this preliminary data existed and entrapped particle potential effects were unknown, it was decided to cycle Model 503 with HB particles to at least provide a frame of reference for further tests. Particle count data for the 1000-cycle test are as follows:

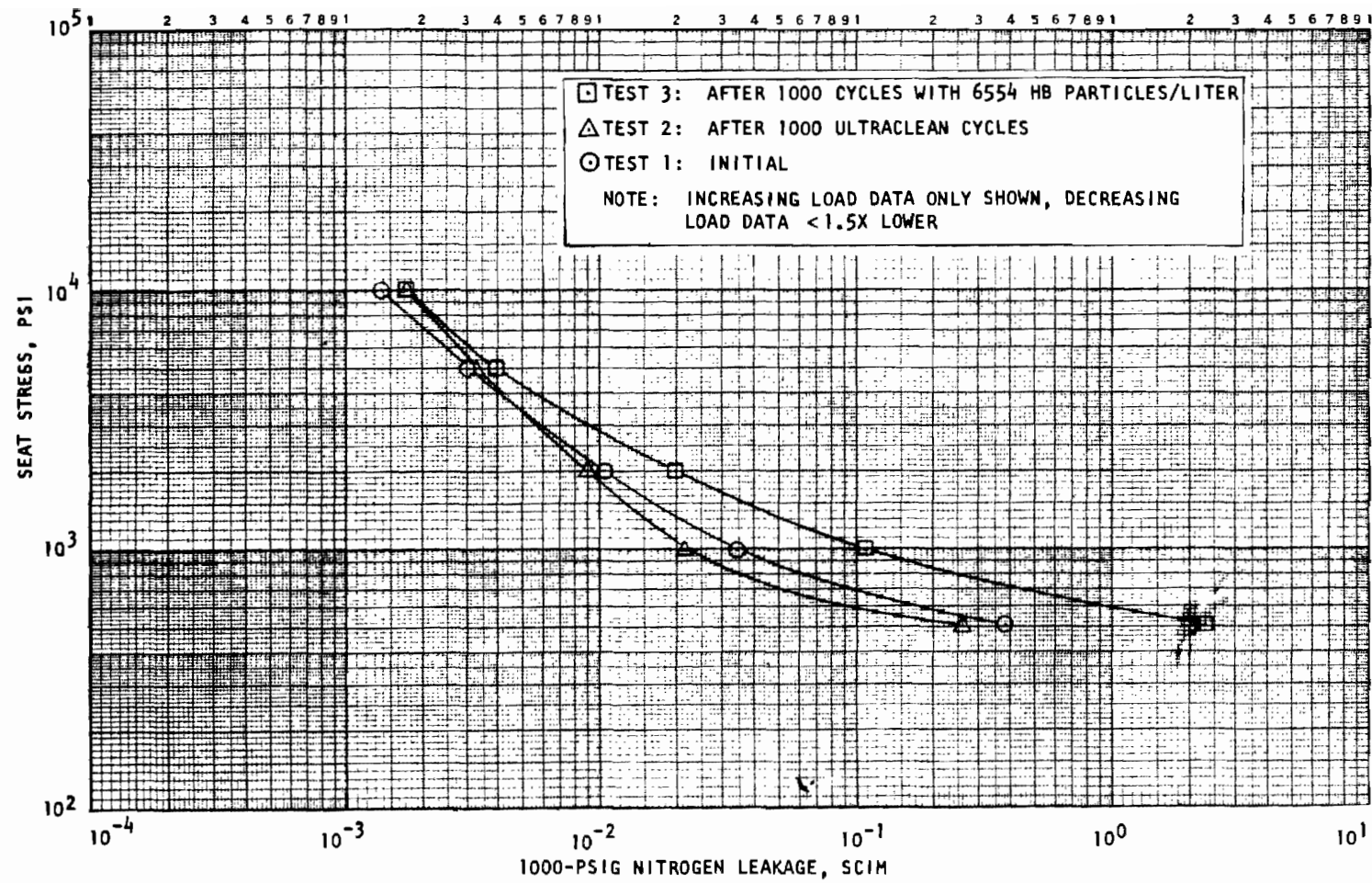


Figure VII-25. Stress-Leakage Data for Dynamic Test Model 503, Tests 1, 2, and 3

HIAC Count/Liter

Cycles	12 to 20 Microns	>20 Microns
Background	10	0
0	164	6740
100	185	6730
200	215	6870
500	250	6530
1000	315	6230

Following 1000 cycles with an average HB concentration of 6550 p/l, the final stress-leakage data of Fig. VII-25 were taken. This test indicated that leakage at 1000-psi stress had increased five times, a relatively insignificant change for seven embedded particles (6.21 predicted). Poppet position and impact load oscilloscope traces for this and subsequent Model 504 were similar to those illustrated for previous models.

In testing 440C flat models where no particle entrapment occurred, and even with the shear seal configuration where minimal poppet damage was noted, realignment of poppet and seat surfaces after cycling was not a major consideration. Because the bias spring was removed to insert the leak collection O-ring, previous circumferential alignment was not maintained. Inspection of Model 503 revealed multiple surface damage from circumferential misalignment. Embedded HB particles had produced secondary holes in the poppet, while poppet upset metal (around initial impact holes) had left circular impressions in the seat. Thus, for seven original hits, 28 seat surface defects resulted. The noted leakage increase in Test 4, therefore, was influenced to an unknown degree by the secondary damage. This effect resulted in the test approach modification to maintain poppet-seat rotational alignment, as previously noted.

Poppet and seat surface texture and particle damage characteristics are illustrated in Fig. VII-26 through VII-29. As-fabricated seat surface texture is typically shown in Fig. VII-26, and by band areas surrounding the particle embedment of Fig. VII-29. The particle causing secondary damage in the poppet (Fig. VII-28) is shown embedded near the seat land ID (Fig. VII-27). Particle size estimate from poppet hole is about 0.0016 inch, or 40 microns diameter. Because it is not known how many cycles followed this entrapment, the resultant characteristic may have been produced by some degree of flattening and wear. Nevertheless, the primary and secondary poppet holes caused by reoriented testing are surprisingly deep (approximately 106 and 53 microinches, respectively). In all cases, the 440C poppet material surrounding the particle-caused hole was raised above the primary poppet plane by about 20 to 100 microinches. It was these disruptions which produced secondary damage in the seat.

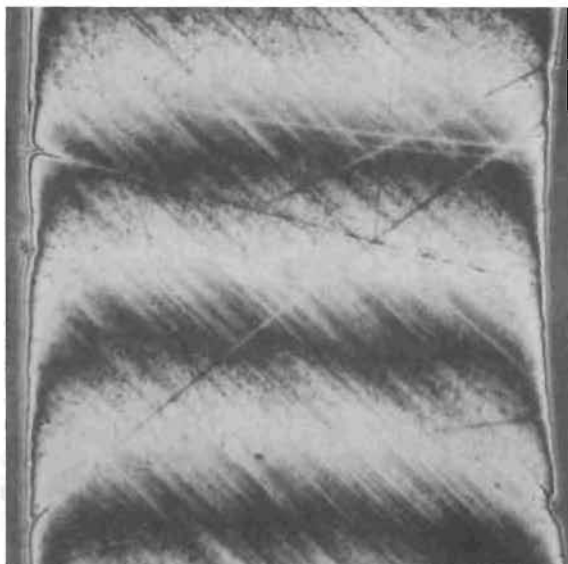


Figure VII-26. Model 503 Seat Land Before Test (91X Interference Photo)

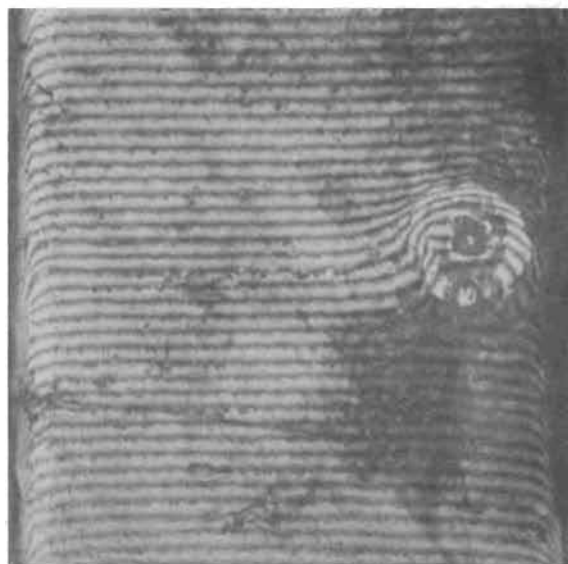


Figure VII-27. Model 503 Seat Land Showing Embedded Particle No. 1 and Secondary Damage Below Particle (91X Interference Photo)

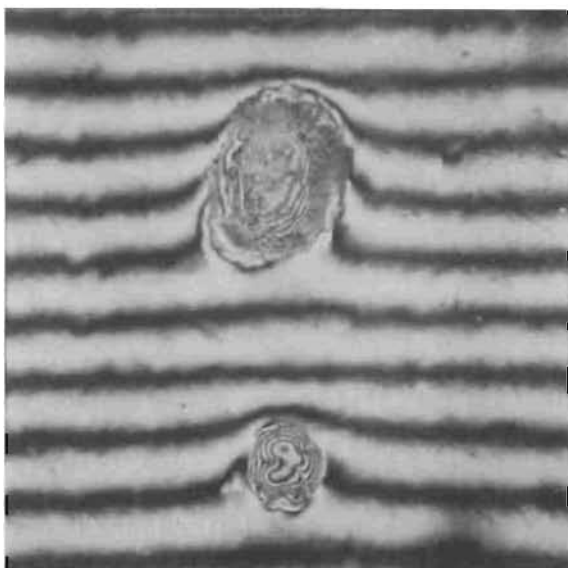


Figure VII-28. Model 503 Poppet Showing Hole From Particle No. 1 and Secondary Damage (462X Interference Photo)

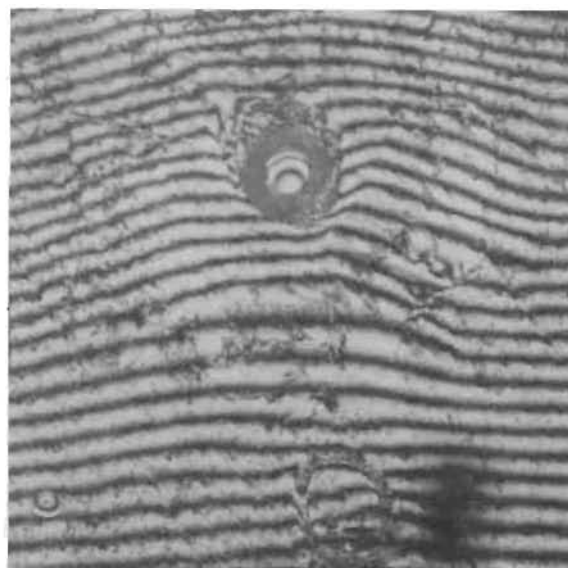


Figure VII-29. Model 503 Seat Showing Embedded Particle No. 6 (462X Interference Photo)

A summary of particle damage for primary entrapments is tabulated as follows:

Particle Number	Poppet Hole Minor Diameter, inch	Particle Height Above Basic Seat Surface, microinch	Seat Upset Above Basic Seat Surface, microinch
1	0.0016	130	42
2	0.0008	53	30
3	0.0014	96	32
4	0.0014	117	42
5	0.0014	106	42
6	0.0011	64	32
7	0.0009	75	32

The seat outer upset diameter, as shown in Fig. VII-27, ranged from 0.007 to 0.011 inch. The ball height above the basic seat surface was about 25 percent greater than that of the corresponding poppet hole. Thus, separating force was provided both by the particle and displaced metal.

Model 504

As previously noted, an out-of-parallel condition greater than poppet clamp ring adjustment could correct, was noted with flat copper Model 503. As a result, low-stress leakage in excess of that normally expected somewhat submerged the effect of entrapped HB particles. Inspection of the seat holder indicated that seat bottoming and back (mounting) faces of the holder were 90 microinches out-of-parallel; the holder was per print but intolerable. Additionally, the seat retention face was tapered 0.00025 inch, high at the ID. The two deviations not only caused the seat insert to cock but made the degree of tilt sensitive to retaining bolt torque.

The seat holder was lap-reworked to correct the deficiencies; ultimately, taper was removed and out-of-parallelism was reduced to less than 10 microinches. In addition, the bore diameter was increased 0.003 inch (except for a short guide portion near the bottom) to promote insert self-alignment during assembly. Final parallelism was determined with the seat locked into the seat holder with a 5/16 bolt and nut. A spare spherical poppet retainer (Fig. III-4, -6 part), lapped parallel within 10 microinches, was used as a base fixture in which the nut was located and the holder and retainer wrung together for parallelism measurements with a Johansson Mikrokator comparator. As subsequently described, these revisions corrected the problem and a satisfactory assembly was achieved, with overall holder and seat parallelism within 20 microinches.

This model was the second and final flat copper configuration subjected to a complete dynamic test series. Stress-leakage results (Fig. VII-30) indicated definite improvement in parallelism after assembly and tester adjustment. The characteristic curve shown was readily achieved indicating the effectiveness of seat holder rework. Initial leakage was

somewhat greater than desirable but, as illustrated, a significant reduction was realized after 1000 ultraclean cycles. A 1000-cycle test with HB particle count was performed as follows:

HIAC Count/Liter

Cycles	12 to 20 Microns	>20 Microns
Background	5	0
0	212	8300
100	221	8270
200	288	8350
500	341	7800
1000	390	8210

Following the 1000 HB cycles, leakage at elevated stress levels was further reduced even though particles had been trapped.

Posttest inspection revealed Model 504 had accumulated seven impact events of nominal size. In addition, two pairs of impacted particles much smaller than the 32-micron nominal HB size were observed. No evidence of poppet-seat misalignment was noted at 200X microscope viewing; thus, the orientation test procedure previously discussed proved satisfactory.

Particle damage for this model was similar to that presented for Model 503. An interesting series of entrapments and effects is shown in Fig. VII-31 through VII-34. The double hit illustrated occurred twice and each was counted as one entrapment. This may have resulted from a dumbbell-shaped particle.

A summary of particle damage is tabulated as follows:

Particle Number	Poppet Hole Minor Diameter, inch	Particle Height Above Basic Seat Surface, microinch	Seat Upset Above Basic Seat Surface, microinch
1	0.0013	148	37
2a, b	0.0006	100	37
3	0.0016	148	37
4	0.0011	127	32
5a, b	0.0013	143	42
6	0.0009	95	26
7	0.0012	112	13 (edge)
8	0.0012	85	26
9	0.0014	100	43

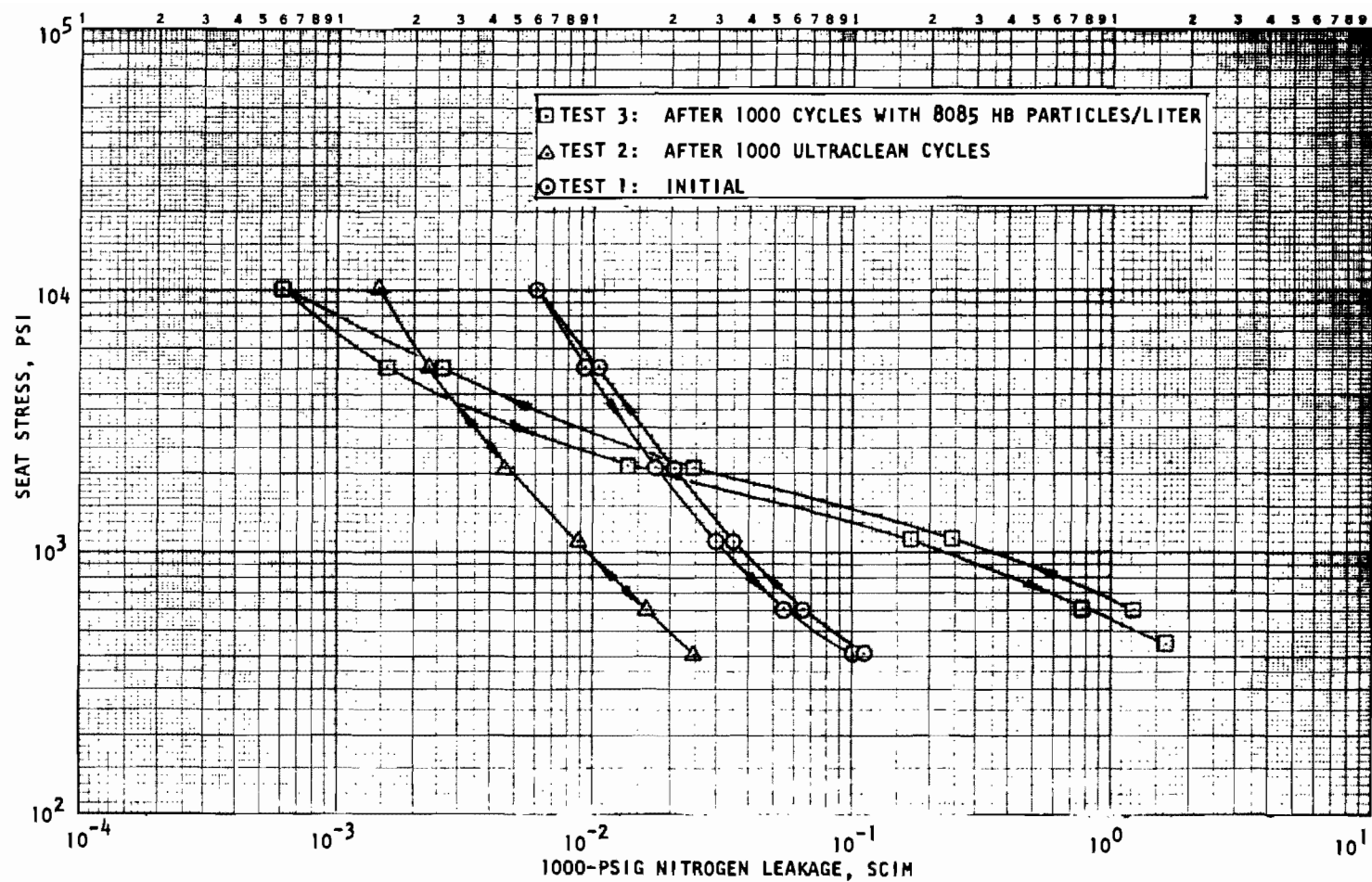


Figure VII-30. Stress-Leakage Data for Dynamic Test Model 504, Tests 1, 2, and 3

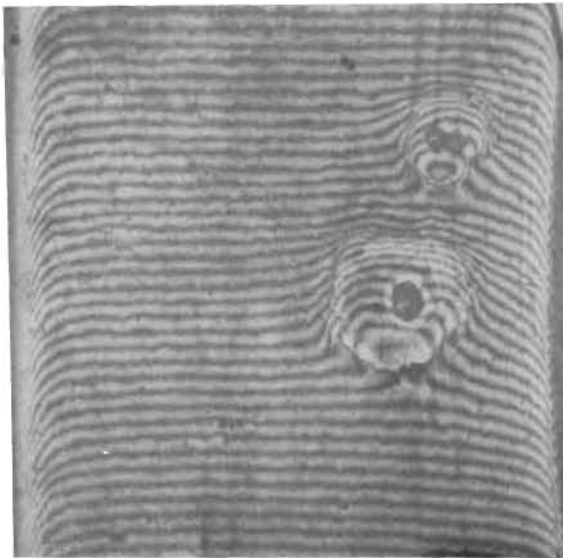


Figure VII-31. Model 504 Seat Showing Single and Double Particle Entrapments, Hits 1 and 2 (91X Interference Photo)

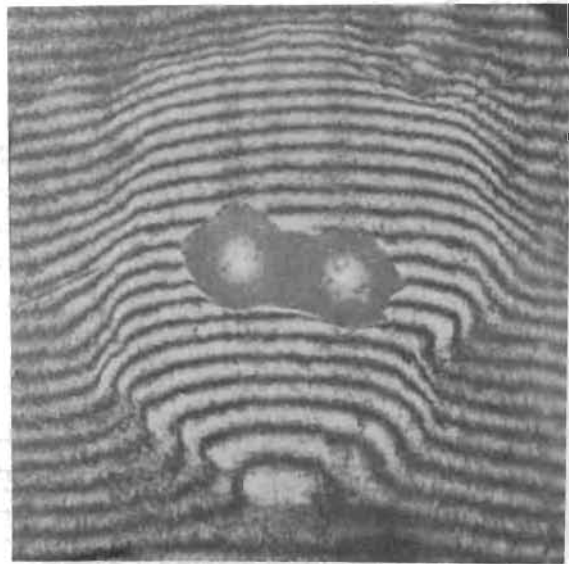


Figure VII-32. Model 504 Showing Small Double Entrapment of Fig. VII-31 (462X Interference Photo)

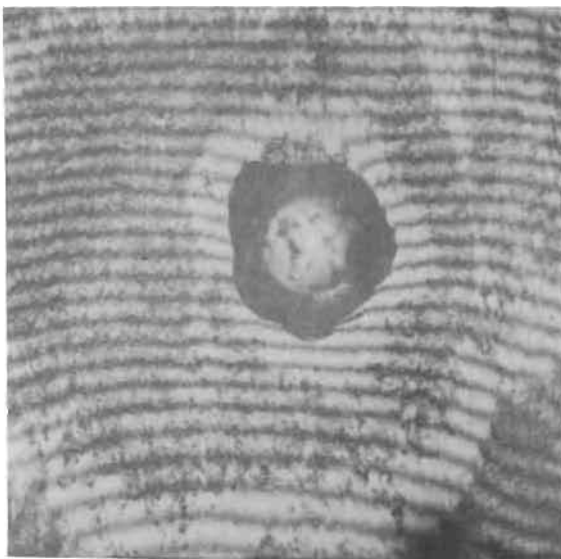


Figure VII-33. Model 504 Seat Showing Particle No. 1 (462X Interference Photo)

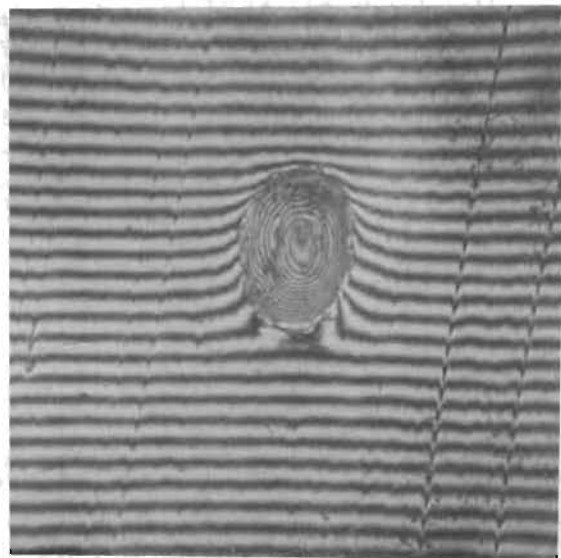


Figure VII-34. Model 504 Poppet Hole From Particle No. 1 (462X Interference Photo)

Observations

These test results illustrate the advantage of plastic flow in particle envelopment. Additional advantage also is provided with cyclic self healing, as was demonstrated with Model 504. This seat had undergone considerable handling and numerous parallelism measurements with a Johansson Mikrokator comparator which caused minute surface tracks. These and other surface defects were reduced by cyclic impact to improve sealing.

A worthwhile development of these sealing examinations was the conclusion that fully work-hardened copper was preferable to annealed because of machining work hardening which created a strong outer shell while leaving a soft substructure that could not sustain seating loads. This illustrates the advantage of a soft outer plate over a hard-base material in allowing a plastic flow smearing of the sealing metal while maintaining loading without substructure failure.

On the negative side, soft metal is easily damaged and can sustain only a limited degree of plastic flow without failure. For repeatability and long life, an extremely precise actuator is required to preclude damaging impact stresses. The determination of these limitations adds a significant degree of complexity to an already complex problem.

FLAT-GROOVED COPPER TEST MODELS

The flat-grooved copper model represented the ultimate design evolved from previous results to meet the program objective. With narrow lands, it was expected that numerous particle hits could be sustained with each land providing partial sealing in the event of direct encounters. With plastic land formation, it was expected also that very low leakage could be obtained at light loads to provide significant seating overload.

A joint static-dynamic model test effort was followed in evolution and evaluation of the grooved seat design. From previous flat copper model tests, it was concluded that the tubular insert seat geometry and land could sustain 15,000-psi seat stress loading (600 to 700 pounds). Preliminary land forming tests indicated development of nominal 0.001-inch-wide lands from initial 0.0003-inch width, with apparent stress between 10,000 and 20,000 psi. Unlike the flat copper seat, however, OD ruboff was about 15 microinches. It was assumed that loading necessary to obtain full poppet contact of all six lands was negligible. These considerations led to the use of 15,000-psi loading for land formation and impact load limitation, as this level was commensurate with many actual valves. Static cycle stress was maintained at about 5000 psi.

Model 701 static tests provided groundwork and data for preliminary dynamic tests performed on Model 702. Model 703 was prepared to evaluate the load necessary to obtain full poppet-seat conformance. However, foreign contamination damaged the seat and it was used to further explore overstress plastic flow. These tests led to important findings relative to seat symmetry requirements. Land conformance tests were successfully performed

with Model 704 with results indicating that flatness on the order of 2 microinches was required for full contact of all lands at low load. This led to a brief exploration of means to achieve this flatness after forming with final results, indicating that the seat tube was too flexible. Final dynamic tests were performed on Models 706 and 707.

Fundamental to this overall effort was the necessity for precise measurements, particularly of surface plastic-flow differentials and parallelism. Because the seat lands could be contacted by only minute loads (i.e., tissue, finger, etc.), all inspection had to be performed optically with the interference microscope. Parallelism, overall flatness, and land duoboff measurements were made with the seat bottomed in the seat holder. The technique and calibration measurements, as described in Appendix I, indicated measurement accuracy within ± 2 microinches.

Data for dynamic test Models 702, 706, and 707 are shown in Table VII-1. For comparison with previous flat models, stress-leakage data have been presented assuming a solid land from inner land ID to outer land OD ($L = 0.031$ inch). Bearing contact stress is, therefore, about six times the values noted. Predicted impacts are based on a summation of land widths plus 12 HB particle diameters (i.e., $L + 0.0151$ inch; see Section II, Analysis).

Model 701

Flat-grooved part number 4 was assembled into the static tester and tested for crest compression deformation and leakage. This part was lapped on cast iron with 1- to 5-micron diamond compound and then with 0- to 1/4-micron diamond compound on carbide. Due to the cast-iron lapping, the part had about 20 scratches measured near 0.001-inch wide and 100-microinches deep. Crest land width before test was nominally 0.00025 inch. This corresponds to a six land bearing area of 0.00222 in.². These seat features and subsequent test effects are illustrated in the photomicrographs shown in Fig. VII-35 through VII-45. The seat OD is on the right-hand side of these photos.

The 440C poppet had nominal 0.5 microinch AA roughness with unidirectional lay and occasional 0.0001- to 0.0003-inch-wide by 2- to 5-microinch-deep scratches (Fig. VII-36). Two of these surfaces would produce between 10^{-2} and 10^{-3} scim GN₂ leakage at 1000-psi apparent stress and 1000-psig inlet pressure.

Results of stress leakage testing are shown in Fig. VII-46. To set the seat and reduce initial leakage, the seat was preloaded to 1920-psi apparent stress (0.0443 in.² apparent area), or 84.4 pounds. Inlet pressure was then applied at 300 psig and apparent stress increased from 690 to 4870 psi and back for the first loop. As shown, the 4870-psi stress was insufficient to close off the noted scratches. These initial data have been converted to 1000-psi inlet pressure based on a straight laminar flow conversion factor of 10.4. Inlet pressure was then increased to 1000 psig and a second loop of data obtained prior to seat separation.

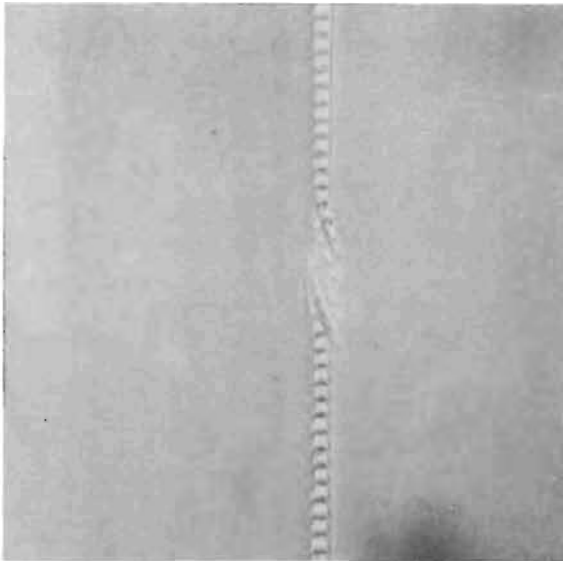


Figure VII-35. Model 701 Seat Land No. 4 Showing Typical Lapping Groove Before Test (462X Interference Photo)

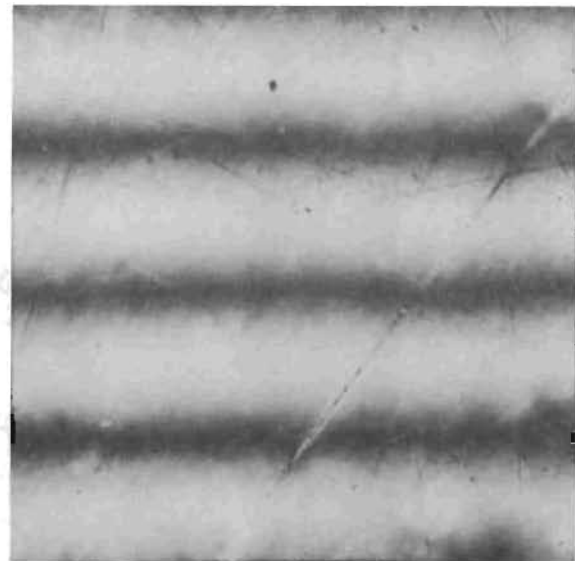


Figure VII-36. Model 701 Poppet (462X Interference Photo)

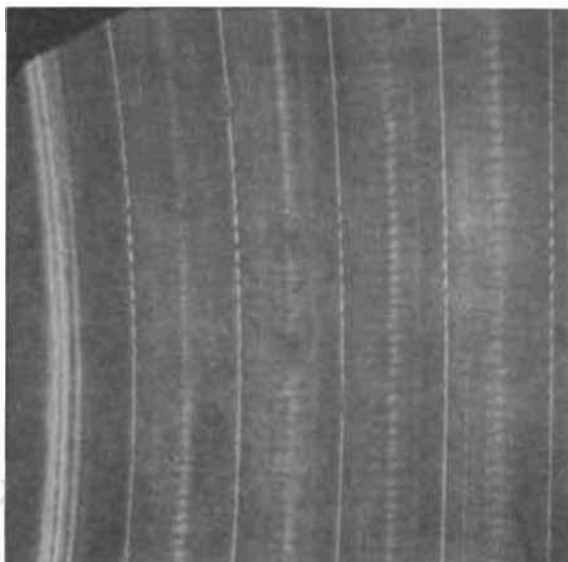


Figure VII-37. Model 701 Seat Land Before Test (91X Interference Photo)

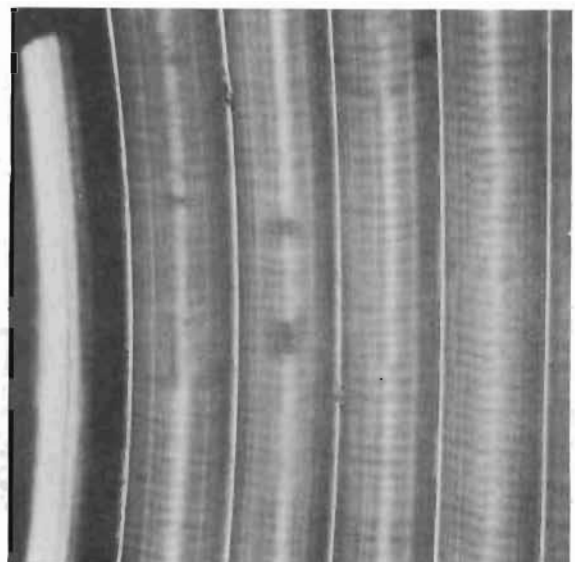


Figure VII-38. Model 701 Seat Land Before Test (91X Plain Photo Same Location as Fig. VII-37)

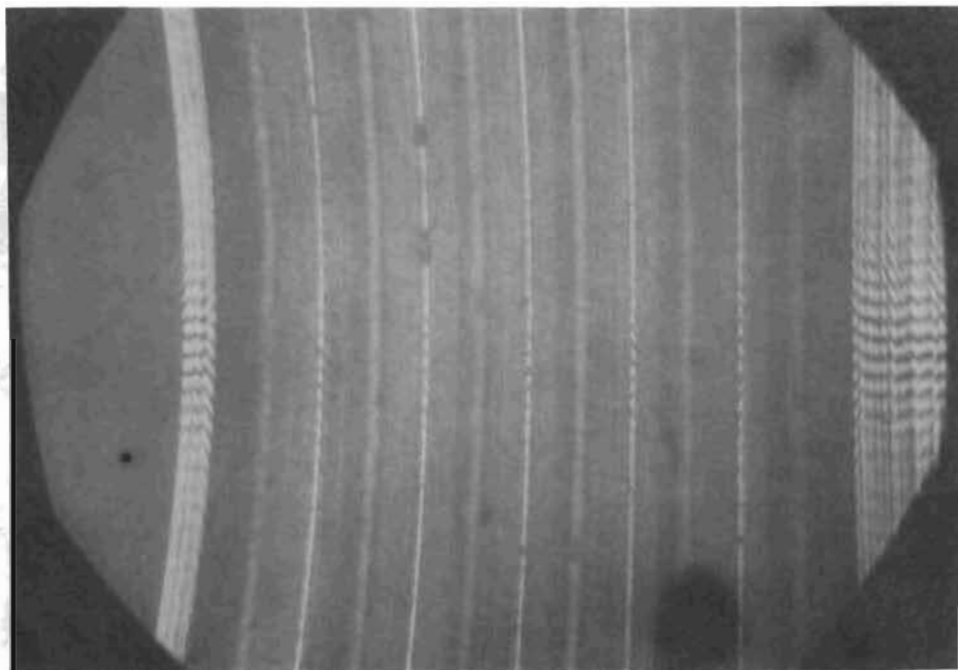


Figure VII-39. Model 701 Seat Land
With Focus at Base
of Grooves (91X Inter-
ference Photo)

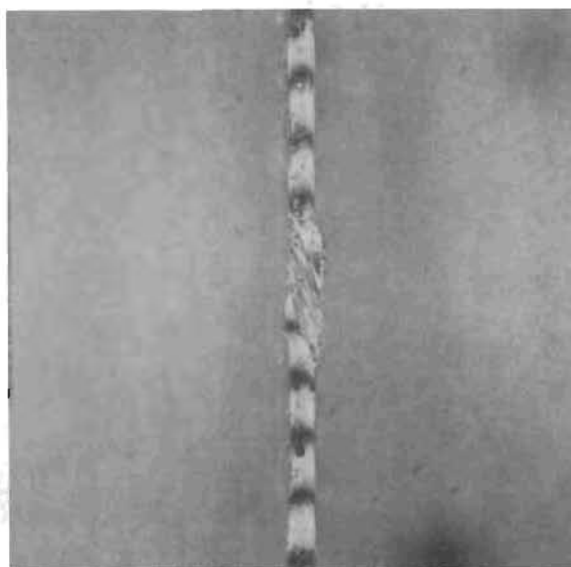


Figure VII-40. Model 701 Seat Land
No. 4 Showing Typical
Lapping Groove After
5000-psi Apparent Stress
(462X Interference Photo
Same Location as Fig.
VII-35)

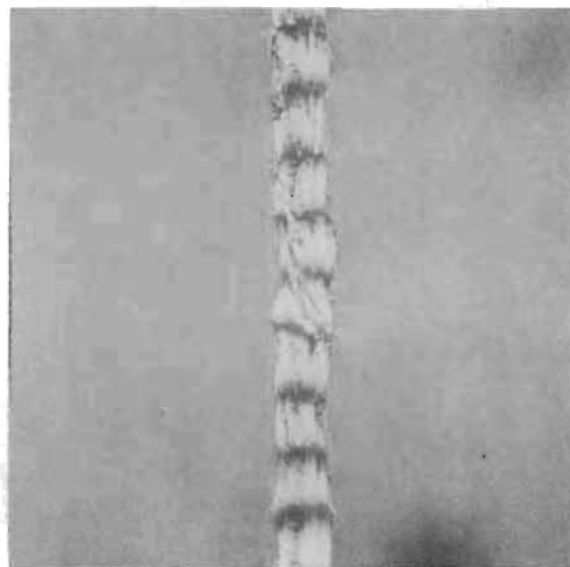


Figure VII-41. Model 701 Seat Land
No. 4 Showing Typical
Lapping Groove After
10,000-psi Apparent Stress
(462X Interference Photo
Same Location as Fig.
VII-35)

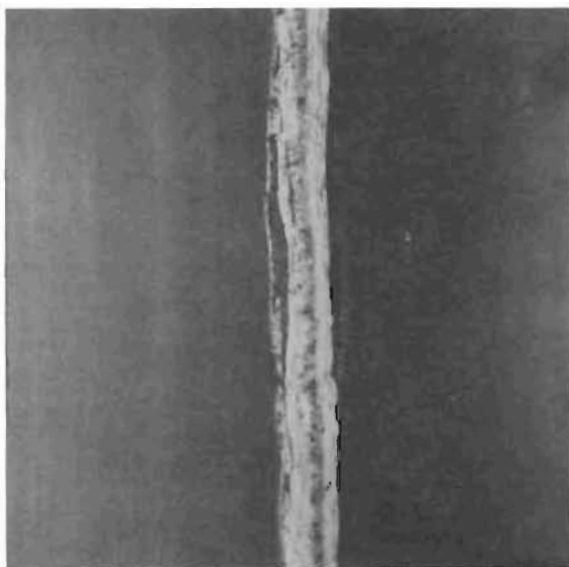


Figure VII-42. Model 701 Seat Land No. 5 Showing Partially Detached Burr (462X Plain Photo)

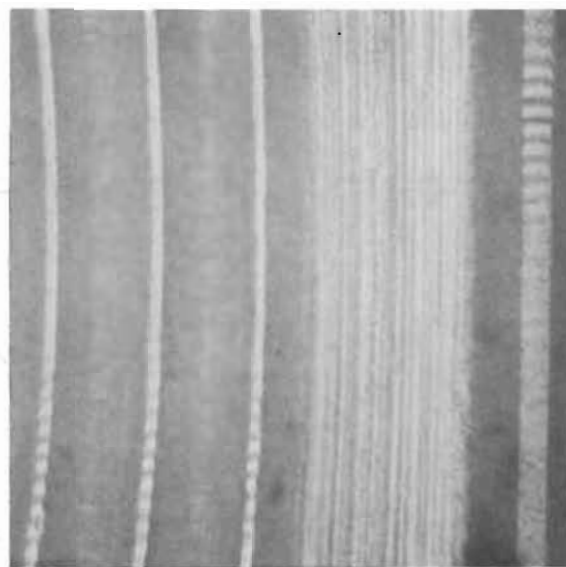


Figure VII-43. Model 701 Seat Land After 10,000-psi Apparent Stress, Showing Height Reduction of Lands Relative to Outer Land (91X Interference Photo)

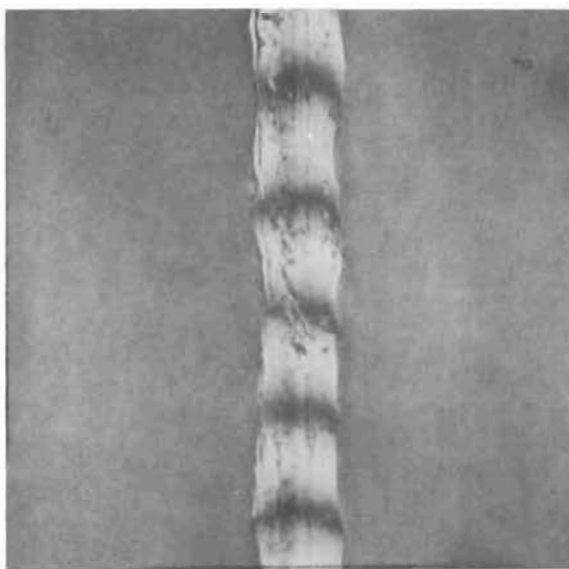


Figure VII-44. Model 701 Seat Land No. 4 Showing Typical Lapping Groove After 15,000-psi Apparent Stress (462X Interference Photo Same Location as Fig. VII-35)

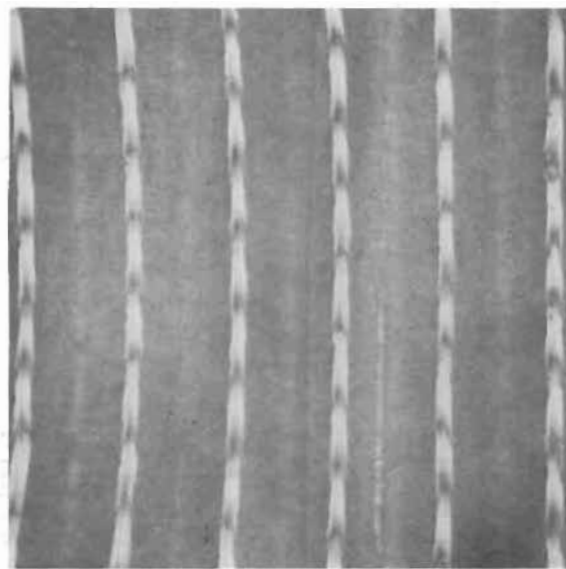


Figure VII-45. Model 701 Seat Land Showing 13.3-Microinch Duboff After 15,000-psi Apparent Stress (91X Interference Photo)

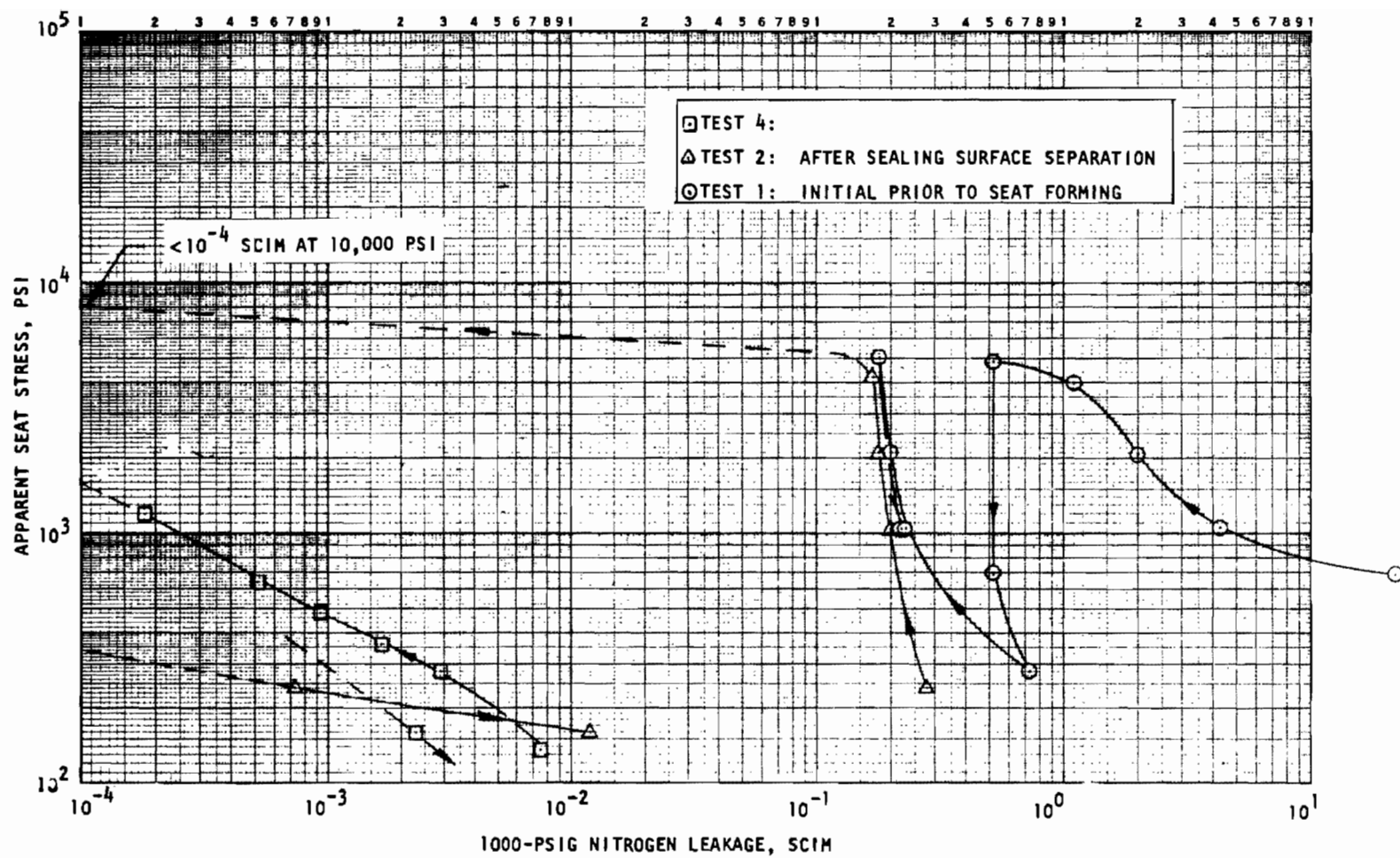


Figure VII-46. Stress-Leakage Data for Static Tested Model 701, Tests 1 and 2

Seat inspection following the second stress loop to 5000 psi indicated a nominal land width of 0.00035 inch for an increase of about 0.0001 inch (Fig. VII-40). The overall land was still essentially flat. Reassembly and test to 10,000 psi was then accomplished. As shown in Fig. VII-46, leakage became undetectable between 5000 and 10,000 psi and, most important, remained so until the seat stress was reduced to less than 1000 psi apparent. Inspection of the seat following this test indicated nominal land widths from OD inward of 0.00060, 0.00056, 0.00056, 0.00054, 0.00064, and 0.00058 inch. Interference inspection of several scratches showed that they had been closed by plastic flow (Fig. VII-41). A partially detached burr is shown in Fig. VII-42. Axial deformation was measured by electronic gage (on objective lens case) and the interference microscope as 0.0002 inch (Fig. VII-43).

A final stress loop was performed to 15,000 psi. In this case, leakage was undetectable above about 2000-psi stress. Seat inspection revealed land widths for OD inward of 0.00088, 0.00088, 0.00091, 0.00090, 0.00098, and 0.00095 inch (Fig. VII-44). The overall seat land was dubbed from ID (high) to OD by 13.3 microinches (Fig. VII-45).

Model 702

This model was 1000-cycle tested both clean and with HB particles. Pretest seat inspection indicated a nominal, lapped land width of 0.00023 inch with only one surface blemish of significance. Seating face-to-holder base parallelism on the order of 20 to 25 microinches was optically measured. Electrical contact leakage results following installation in the dynamic tester indicated poppet and seat faces were out of parallel approximately 56 microinches. Because of potential seat damage, and the relatively large axial plastic deformation which would follow with seat land formation, improved parallelism through clamp ring screw adjustment and initial balance pressure tests were not attempted.

To permit simulation of a possible real valve method of plastically forming sealing lands, it was decided to perform initial stress-leakage tests to only 5000-psi apparent stress. Ultimate land formation was to be accomplished by cycling to an impact stress of 15,000 psi which, from previous model test data, would produce the desired 0.001-inch land widths. Accordingly, Model 702 was initially static tested in successively increased load increments to the 5000-psi stress level. Final stress-leakage data are shown as Test 1 in Fig. VII-47. These data are plotted on the basis of a pressure balance test performed after land formation achieved during the 1000 ultraclean cycles. The tests indicated a balance diameter of 0.452 inch. Because later inspection indicated a significant and variable duboff, the pre-land formation balance diameter was probably nearer the theoretical of 0.481 inch and, if so, the plotted stress points (circles) would be reduced by 470 psi. Consequently, the circle data shown are probably conservative.

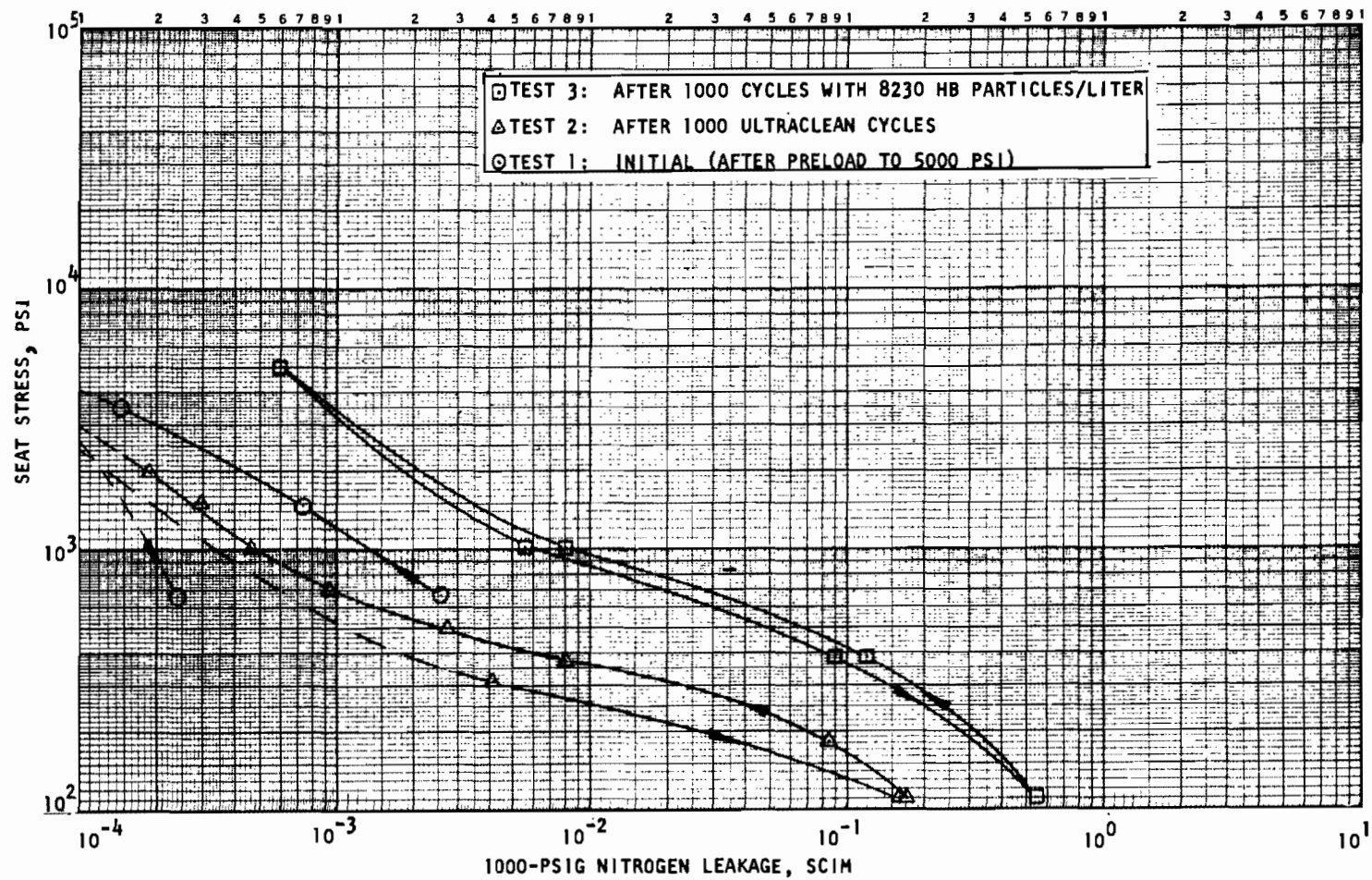


Figure VII-47. Stress-Leakage Data for Dynamic Test Model 702, Tests 1, 2, and 3

As shown in Table VII-1, Model 702 was cycled with an impact load of about 660 pounds to produce 14,400-psi apparent seat stress. Impact and displacement traces are shown in Fig. VII-48; these are typical of all flat-grooved copper models.

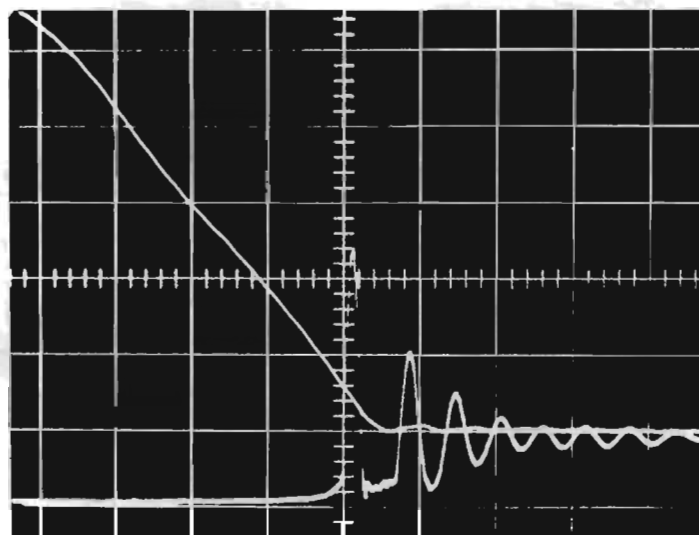


Figure VII-48. Model 702 Load and Displacement Traces (0.001 sec/div; 200 lb/div; 0.005 in./div)

Leakage data after 1000 ultraclean cycles (Test 2) are comparable with Test 1 and; also, subsequently described static tests of Models 703 and 704. A 1000-cycle HB particle test was then performed with the following count data:

HIAC Count/Liter

Cycles	12 to 20 Microns	>20 Microns
Background	20	0
0	242	8300
100	374	8240
200	409	8260
500	481	8260
1000	561	8140

Stress-leakage test results following 1000 cycles with an HB particle concentration of 8230 p/l indicated leakage increased by a factor of 8 to 17 over the 300- to 2000-psi apparent stress range. Subsequent inspection revealed that 22 impact events had occurred with three particles embedded (typical photos of the pre- and posttest seat and poppet are shown in Fig. VII-49 through VII-56). Four lands were damaged so that the entire surface was bridged, two by HB particles and two by fiber-type particulates

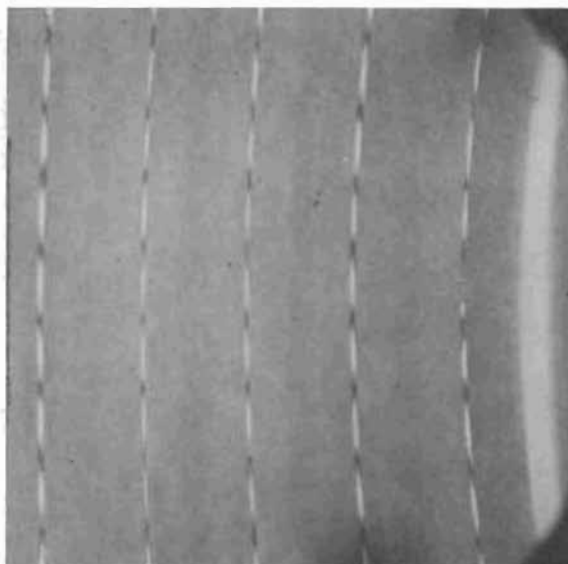


Figure VII-49. Model 702 Seat Land Before Test (91X Interference Photo)

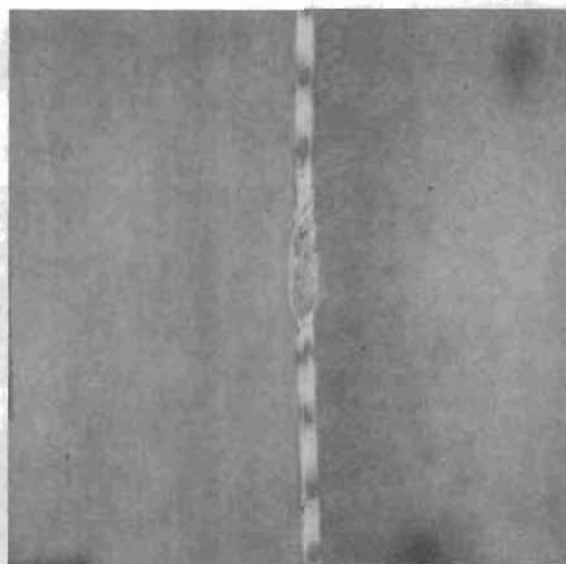


Figure VII-50. Model 702 Seat Land No. 6 Showing the Only Lapping Groove Before Test (462X Interference Photo)

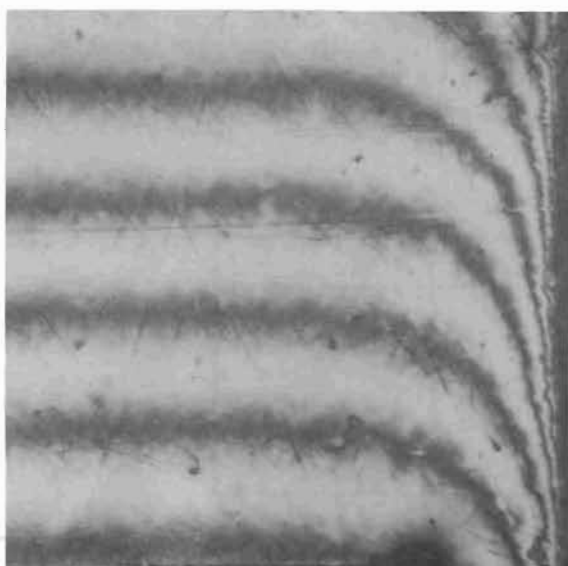


Figure VII-51. Model 702 Poppet (462X Interference Photo)

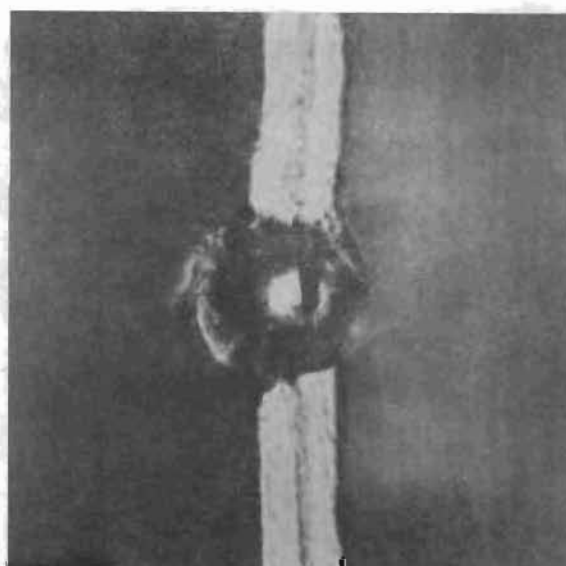


Figure VII-52. Model 702 Seat Land No. 1 Showing Embedded Particle (462X Plain Photo)

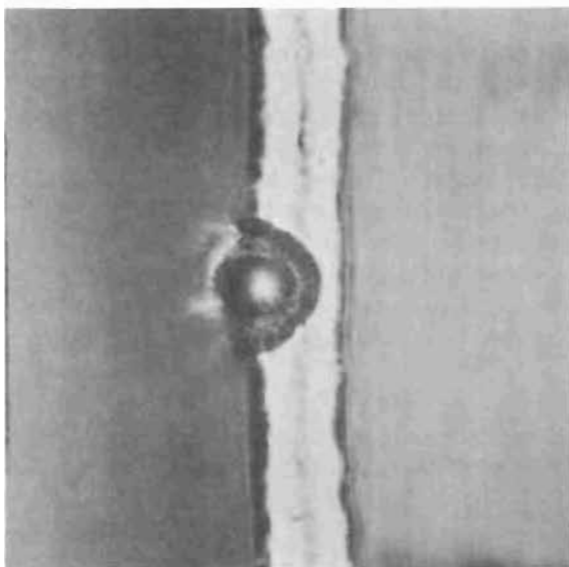


Figure VII-53. Model 702 Seat Land No. 1 Showing OD Edge Particle Embedment (462X Plain Photo)

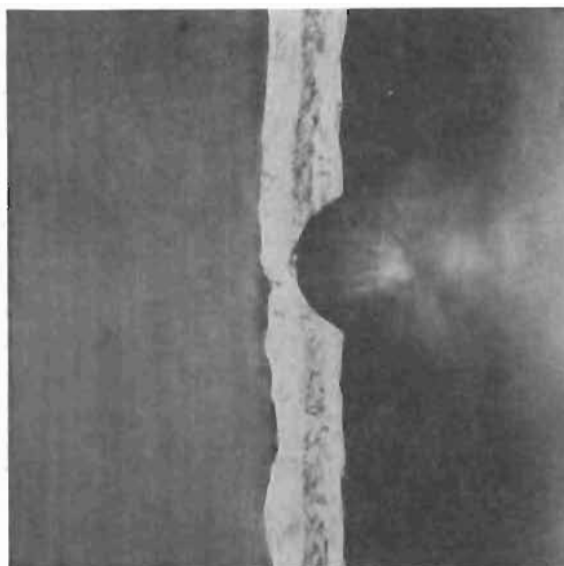


Figure VII-54. Model 702 Seat Land No. 6 Showing Typical ID Edge Hit (462X Plain Photo).

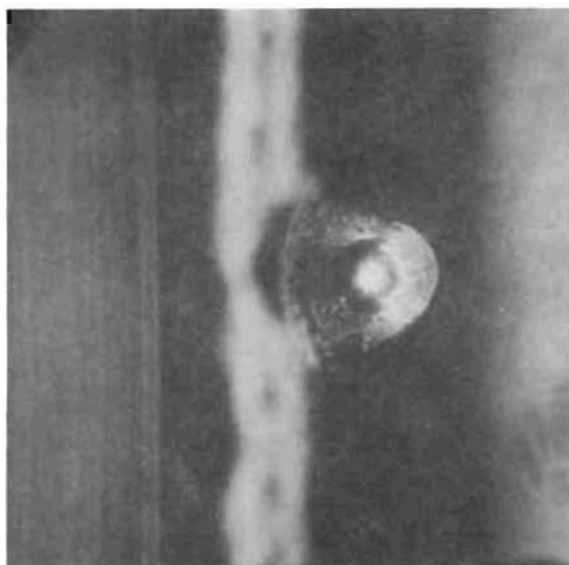


Figure VII-55. Model 702 Seat Land No. 6 Showing Typical ID Edge Hit, Focused Down on Particle-Caused Extruded Metal Hole (462X Plain Photo)

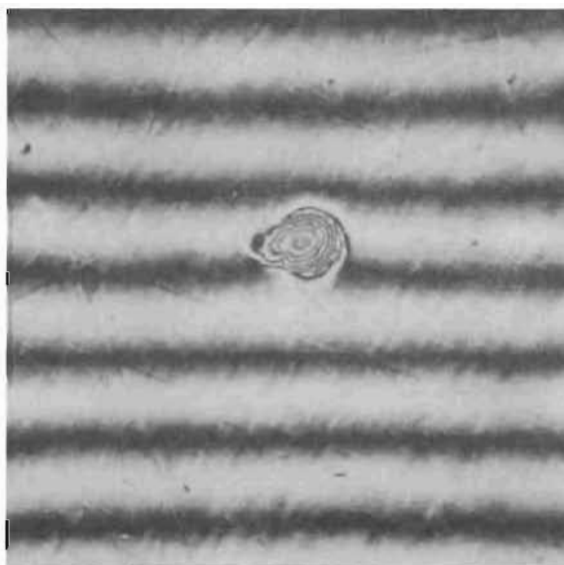


Figure VII-56. Model 702 Poppet Showing Typical Particle Damage (462X Interference Photo)

(probably pump packing material). The innermost (No. 6) land received six hits, while the remainder had between 2 and 4. Significantly, except for two instances (one each at land center and OD), all impacts occurred at the ID edge of the lands. Damage from these hits ranged from 20 to 70 percent of the land sealing width. Land widths varied from 0.0008 to 0.0010 inch, with the average at 0.00087 inch. This compares favorably with static test results and indicates that dynamic cycling did form the desired land width. It is notable that there was no raised metal adjacent to any of the hits, even with particles embedded. This is the advantage of the edge-hit condition. In comparison, previous flat copper Model 504 had an upset metal height about 40 microinches over an 0.008-inch diameter surrounding the embedded HB particle.

With the exception of the shear seal configuration, actual and predicted hits on previous models have correlated very well. The "excessive" number of events noted on Model 702, therefore, is attributed to a fluid-particle dynamic condition which apparently causes particles to collect in the seat grooves. This hypothesis is somewhat supported by the incidence of ID hits observed. The relatively deep (approximately 0.005 inch) grooves produced coincident with land generation were not specifically intended as particle repositories but occurred as a function of convenient tool preparation. As the lands need only be relieved sufficiently to permit lateral (instead of vertical) material displacement in the event of particle impact or entrapment, the groove depth can be significantly less. It is possible that such a design revision (groove depths on the order of 0.001 inch as machined) would materially reduce or eliminate the tendency for particle collection.

Although Model 702 did not perform as well as expected, it should be noted that with 22 hits, leakage at 1000-psi stress was still an order of magnitude less than flat copper Models 503 and 504, each with seven embedded HB particles. Further comparison with 440C static Test Model 108 with three entrapped SB particles also indicates an order of magnitude improvement. Consequently, it is apparent that reduction of hit frequency (by possibly less groove depth) would result in planned performance near 10^{-3} scim at 1000-psi stress. It is also expected that land formation using poppet with circular lay would produce clean-condition leakage less than 10^{-4} scim, comparable with the shear seal model.

Model 703

Flat-grooved Model 703 was intended for evaluation in the static tester to establish the load required to fully contact all six sealing lands; however, inlet gas system contamination resulted in numerous land impressions. The model was then used in a limit static test to 30,000-psi apparent stress.

Stress-leakage test results are shown in Fig. VII-57. Prior to recording Test 1 data, the sealing lands were formed at 15,000-psi apparent stress, and balance pressure was measured as 95.0 psig indicating the fifth land as the effective diameter. Inspection following Test 1 indicated 31 damaged

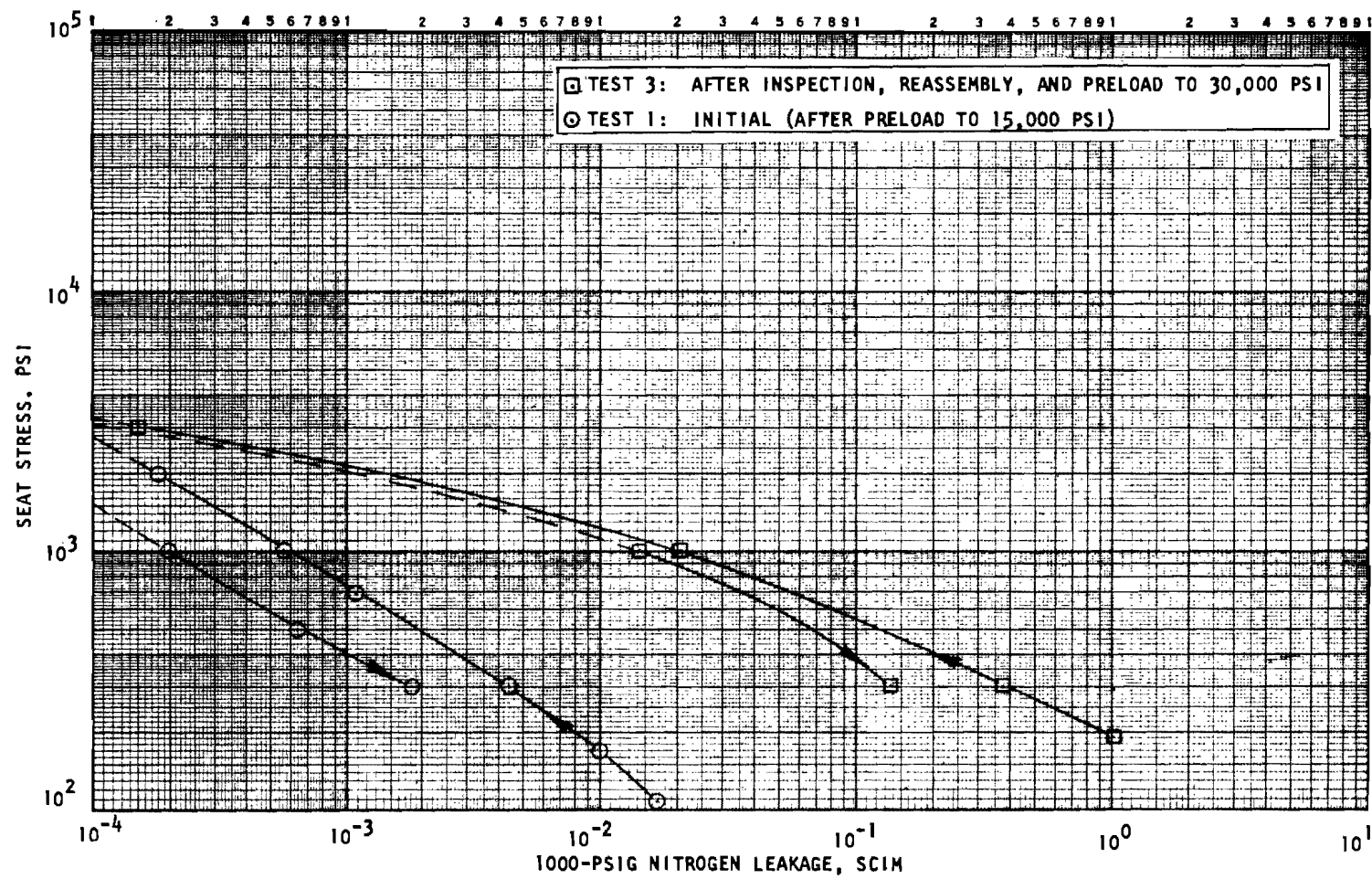


Figure VII-57. Stress-Leakage Data for Static Tested Model 703, Tests 1 and 3

areas resulting from static tester inlet cavity contamination due to improper blowout procedures. These occurred as follows:

Land No.	Number of Damaged Areas	Sealing Affected
1 (OD)	14	Yes
2	8	Yes
3	4	No
4	3	No
5	2	No
6	0	No

Lands 1 and 2 were damaged with particles which had bridged the nominal 0.001-inch-wide lands with impressions about 0.001-inch wide by 15 to 20 microinches deep. Impressions on other lands were of similar size, but did not bridge the land.

The model was reassembled and tested to relate the noted damage with leakage. The results (Test 2) were not significantly different from Test 1 indicating that, at the low stress level, outer lands 1 and 2 were ineffective due to duboff measured as about 29 microinches.

Because the model was not suitable for the intended test, it was decided to perform a 30,000-psi land-forming limit test. The results of this Test 3 were quite informative. As shown in Fig. VII-57, the stress-leakage results were significantly degraded. Disassembly inspection showed that, while additional stress had "healed" the previous damage by increasing the nominal land width to 0.002 inch, the high stress level had produced an unusual egg-shaped, out-of-flat condition. Because this model was initially out of parallel with the holder base by close to 0.0001 inch, the combination assessment of the two deviations proved difficult and led to the calibration measurements of a flat but out-of-parallel surface, documented in Appendix I. Model 703 was similarly measured, with the results plotted in Fig. VII-58. As shown, the outer (lap) land which was initially flat within several microinches was now out of flat by about 14 microinches. This is indicated by the deviation from the datum curve at about 270 degrees. Lands 1 and 6, which were depressed about 0.0008 to 0.0009 inch below the outer land, had greater deviations from flatness. As the errors shown are gross, further assessment was not made because the cause of excessive leakage was determined. The reason for the out-of-flat condition was traced to the use of Eastman 910 contact adhesive applied between the seat tube and holder in two 0.03-inch-wide stripes for about 90 degrees at 110- and 290-degree locations. It was postulated that the adhesive provided support to the tube which produced the excessive plastic flow at these locations. Average duboff of the six lands was 46 microinches between 90 and 270 degrees.

Comparison of land mean diameters as fabricated, and following each test, indicates a general growth in mean diameter of 50 to 100 microinches after 15,000-psi stress and up to 200 microinches following the 30,000-psi stress.

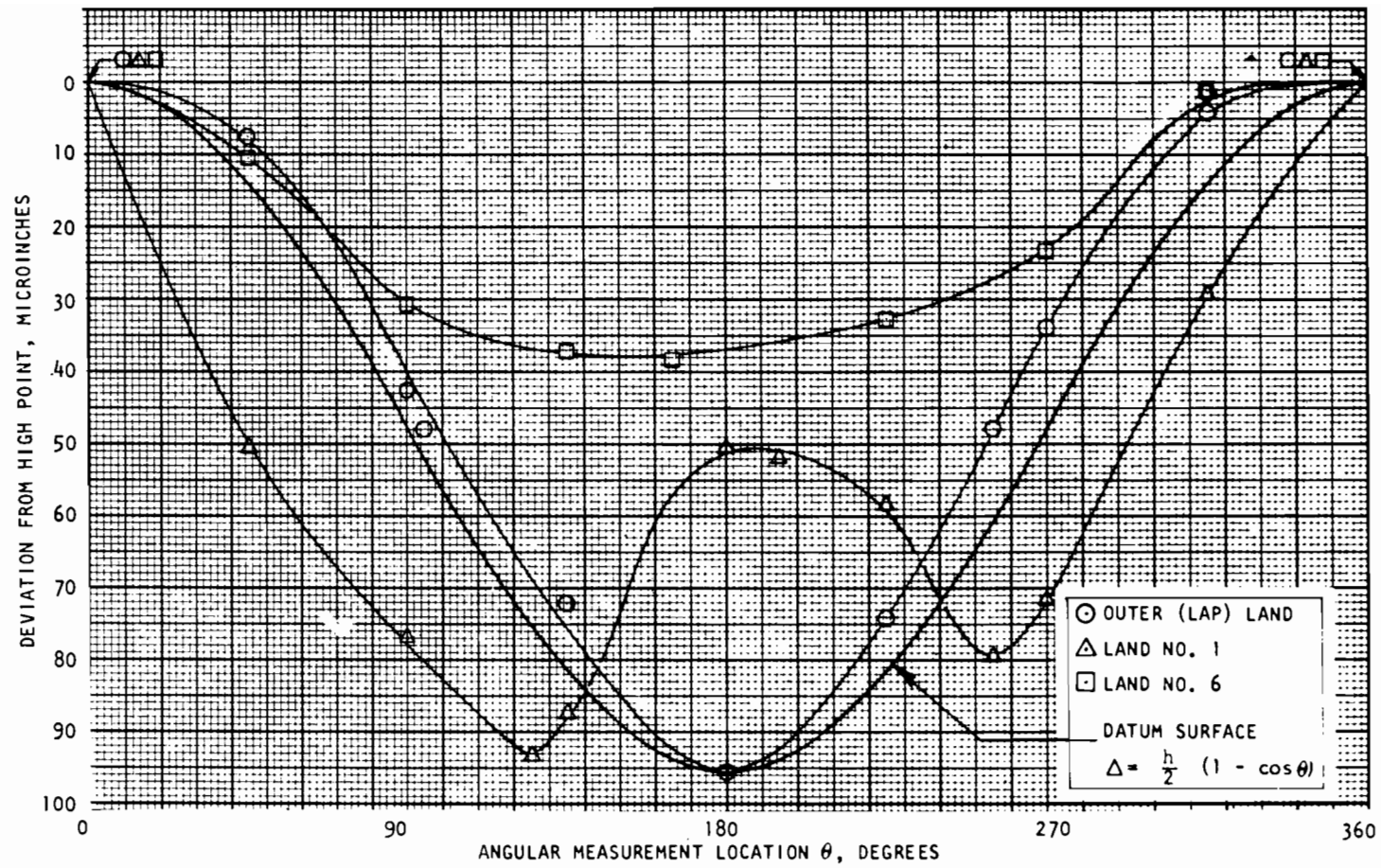


Figure VII-58. Model 703 Land Surface Profiles After Test No. 3 (30,000-psi Loading)

Evaluation of load versus land width formation indicates that, from the average initial land width of 0.000264 inch, the 15,000-psi apparent stress load of 686 pounds produced an average land width of 0.000980 inch. The 30,000-psi apparent stress produced an average land width of 0.00195 inch. These average values correspond to plastic flow pressures of 78,900 and 79,400 psi, respectively. This pressure is considerably lower than previously computed ($2.55 \times 45,000$ psi yield strength = 115,000 psi).

Model 704

Flat-grooved Model 704 was static tested twice in preparation for sealing land versus closure load testing. Eastman 910 was used only between the angled faces of the retaining nut and seat insert. The seat insert base was wrung to the holder bearing surface with a thin film of fluorolube. This retained the insert sufficiently for tester assembly and avoided the diametral restraint previously encountered with insert-to-holder adhesive bonding. The seat land was formed at 15,000-psi apparent seat stress with initial duboff measured at 13 microinches.

To permit sealing land deletion in a controlled manner, a wedge-shaped cutting edge was lapped on the broken tip of a needle. The "tool" was mounted on the particle handling fixture so that it overhung an X-Y micrometer stage on which the test seat was placed. Under 100X magnification, the stage and tool were positioned to machine shape two grooves 180 degrees apart in the land of interest, effectively deleting it from the gross sealing capability of the seat. Groove dimensions were approximately 0.004-inch wide by 0.0005-inch deep. Following each land deletion, the seat was lightly polished with 0 to 1/4-micron diamond lapping compound on tissue and thumb pressure to remove upset metal.

Beginning with "high" land No. 6 (ID), each land was successively deleted followed by a stress-leakage test to define the resultant effect. The data are presented in Fig. VII-59. The seat land is shown in Fig. VII-60 and VII-61 prior to individual land deletion. The 13-microinch duboff shown by Fig. VII-61 was carefully measured to ascertain uniformity around the entire seating circumference. Figures VII-62 and VII-63 show the seat land deletion grooves following the test series.

The test results clearly show the desirability of a nondubbed condition. With the baseline 1000-psi stress leakage as reference datum, an additional 5000 psi (228 pounds) is required to bring the outermost land (No. 1) into sealing contact. This is for a condition of about 11 microinches duboff from lands 5 to 1. The reduction from initial 13-microinch duboff height is believed due to the polishing operation utilized after each land deletion. The loss came primarily from land 6 which ultimately was a microinch or two lower than No. 5, but the entire surface undoubtedly was somewhat improved. As the surface change occurred gradually, however, assessment of duboff effect in the area of concern (lands 4, 5, and 6) was possible. The initial height change from land 6 to 5 and 5 to 4 was approximately 1.6 microinches. From the data of Fig. VII-59, the loss of land 6 made

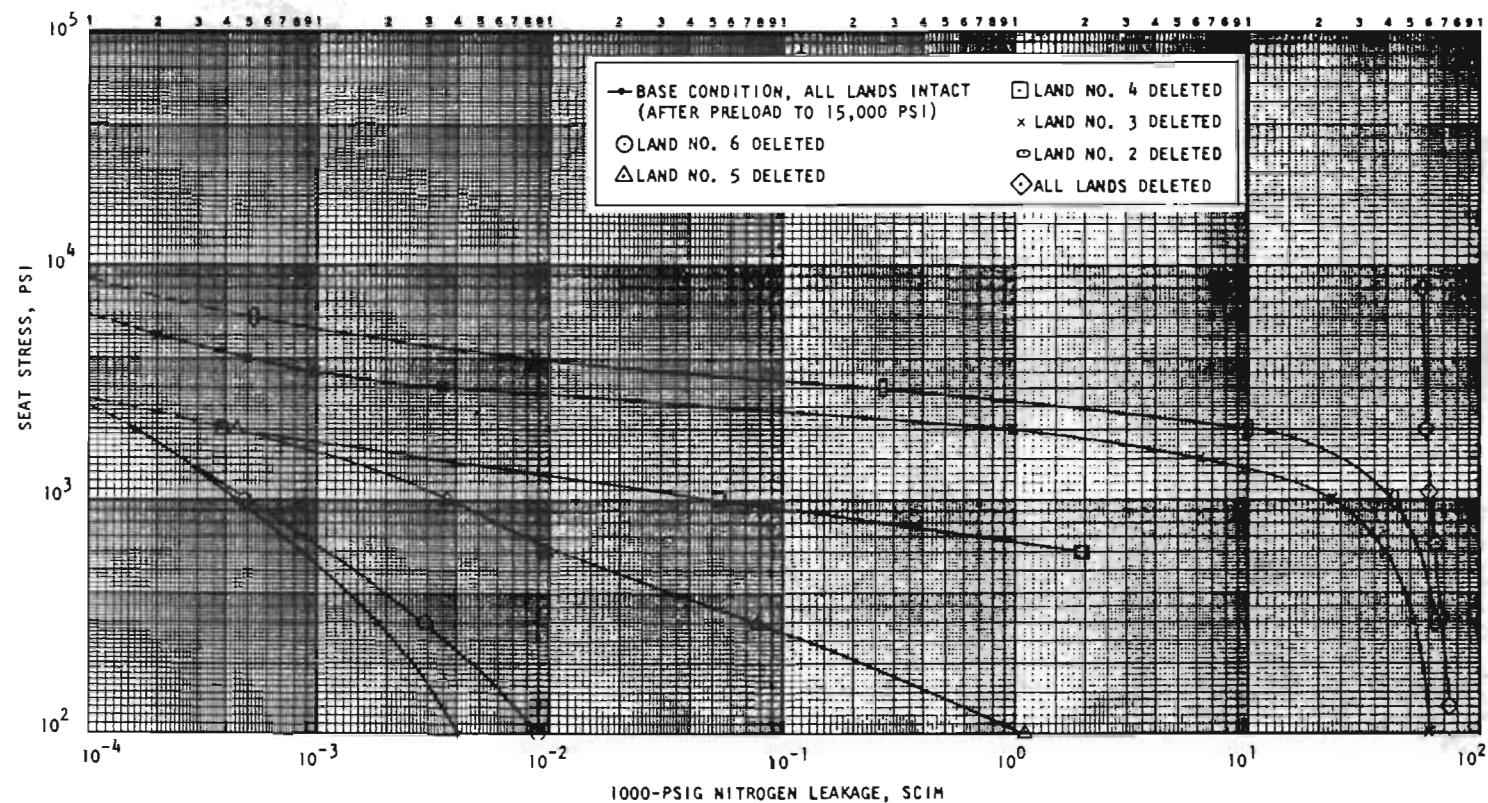


Figure VII-59. Stress-Leakage Data for Static Tested Model 704, Increasing Load Only, With Noted Lands Successively Deleted From Sealing Capability

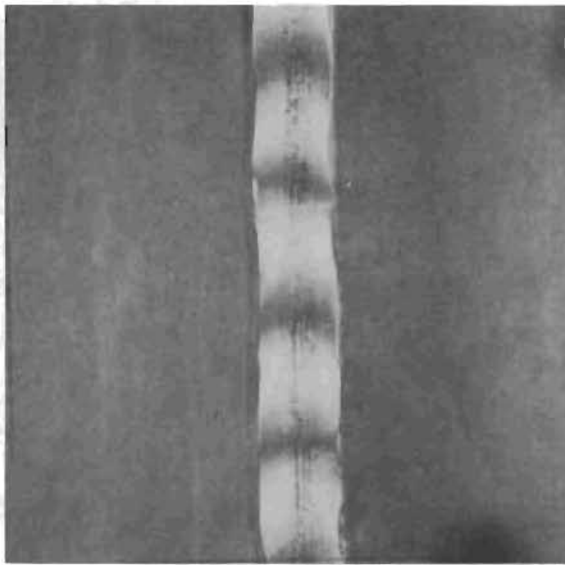


Figure VII-60. Model 704 Formed Seat Land No. 6 After 15,000-psi Apparent Stress (462X Interference Photo)

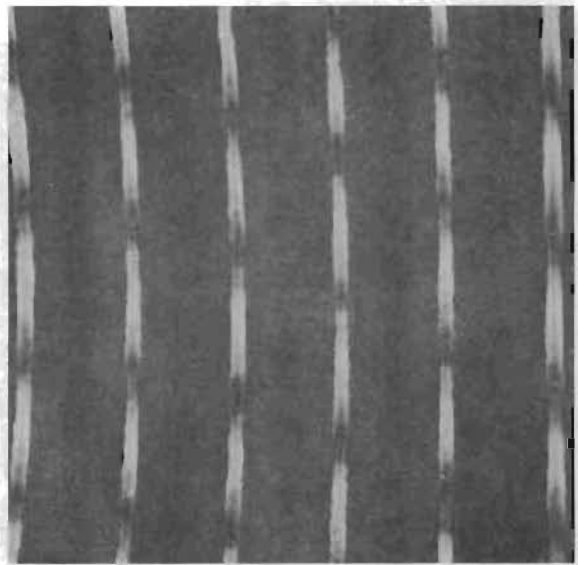


Figure VII-61. Model 704 Formed Seat Land After 15,000-psi Apparent Stress; ID Left (91X Interference Photo)

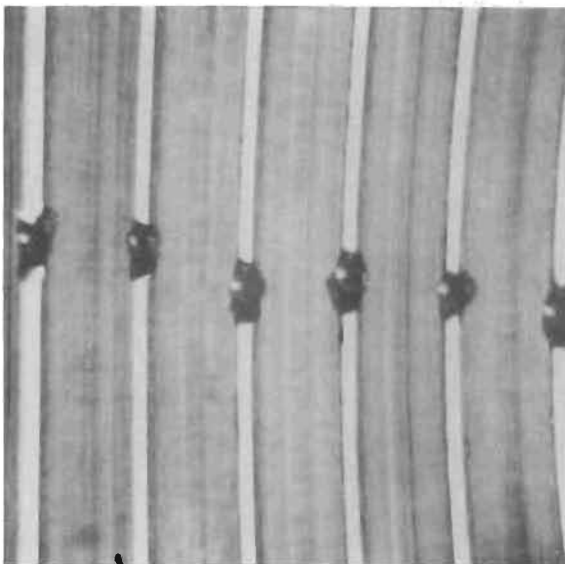


Figure VII-62. Model 704 Seat Land After All Lands Deleted; ID Right (91X Plain Photo)



Figure VII-63. Model 704 Seat Land No. 6 Groove (462X Plain Photo)

minimal change but, with land 5 deleted, the load to achieve initial 1000-psi leakage is nearly doubled. This indicates that, for the particular materials and construction geometry employed, the six sealing lands should be flat within about 2 microinches to ensure conformance with relatively high loads (e.g., 40 to 50 pounds).

Supplemental Tests

Four sample grooved seat inserts were subjected to various static tests to investigate the duboff characteristic and influencing parameters. Pertinent information is presented in the following table and discussion.

GROOVED COPPER SEAT DUBOFF TEST RESULTS

Seat S/N	Configuration	Seat Stress, psi	Inlet Pressure, psig	Seat Characteristic
3A	Standard	15,000	0	18.5 microinches dub; ID high
2A	Tapered base	15,000	0	25.2 microinches dub; ID high
7	0.509 OD	15,000	0	21.0 microinches dub; OD high
		5,000	1000	No change
		12,000	1000	15.9 microinches dub; land 2 high
12	0.525 OD	15,000	0	8.0 microinches crown; lands 3 and 4 high
(Designated Model 705 for stress-leak test)		15,000	1000	23.8 microinches dub; ID high

Sample 3A. This part typified the normal grooved seat inserts tested to this point. It was used to establish a control reference to test procedures to be used for subsequent tests. No Eastman 910 adhesive was used to retain the insert to the holder or to the lock nut. After assembly into the tester, control pressure equivalent to 15,000-psi apparent seat stress was applied momentarily and then reduced to zero to complete land formation. As tabulated, an ID high duboff of 18.5 microinches resulted.

Sample 2A. The results of initial flat copper seat deformation characteristics were utilized in analysis of the grooved version. As noted in Model 503 discussion, however, the seat holder internal shoulder was found to be tapered, a condition subsequently corrected. To investigate how this taper might have influenced flat copper seat land deformation (or lack of it), the base of Sample 2A was machined with a 0.00045-inch taper (0.010-inch ID flat annulus contacting initially) to simulate the original holder condition. After 15,000-psi loading, the noted 25.2-microinch,

ID high duboff resulted. This indicated that elastic springback strongly influences the duboff characteristic. In this case, even though the land ID was highly loaded, it was more free to move radially inward than the relatively well supported OD land could move outward. Elastic springback of the ID-displaced metal thus created an even greater duboff than the initially designed version.

Sample 7. To further evaluate the elastic-plastic hypothesis advanced with Sample 2A, this insert was reworked by machining the OD to 0.509-inch diameter, just outside of the outer land. The resultant seat land was symmetrical with equal support to ID and OD lands, or a simple tube. After 15,000-psi land formation, Sample 7 had a reverse duboff, OD high, of 21.0 microinches. In this case, the ID was more resistant to axial deformation than the OD. Thus, load was concentrated at the ID, increasing its plastic flow relative to the now unsupported OD which, in turn, was free to elastically move outward. The result was an elastic springback-formed, OD high duboff.

Sample 12. With the preceding information and hypothesis established, it was decided to attempt an optimization of the elastic-plastic properties of the grooved insert to minimize duboff. Sample 12 was reworked to reduce the OD support material to one-half the original amount, or 0.525-inch diameter. This produced a relatively uniform deformation condition after 15,000-psi loading with middle lands 3 and 4 high in an 8-microinch crown. Even though uniform, however, the crown height was in excess of that considered necessary for relatively light load conformance as indicated by Model 704 test results.

Inlet Pressure Effect, Samples 7 and 12. Because Sample 12 was crowned a relatively small amount, it was decided to perform a stress-leakage test for comparison with previous models. Stress-leakage results (1000-psig inlet pressure) were not particularly different from other data, but posttest inspection revealed a significant change to the land geometry. The initial crowned condition was eliminated, and a 23.8-microinch, ID high duboff had been produced; an inlet pressure influence was thus established. The insert tube had either been diametrically expanded at the interface or further axially downward in a "barrel" shape to cause a change in load distribution and, ultimately, in the free condition land plane.

In a final test to verify inlet pressure influence, Sample 7 (OD high duboff) was subjected to a retest, this time with 1000-psig inlet pressure. After being subjected to 5000-psi apparent stress with inlet pressure, no duboff change was apparent. Following 15,000-psi loading in the next test, however, the duboff, while still OD high, had been reduced to 15.9 microinches.

Conclusion. These tests clearly illustrated the highly variable contact pressure distribution possible due to elastic substructure deformation. It is concluded that the flat copper model configuration as tested was not sufficiently rigid to permit the designed amount of surface plastic flow. It is possible that a lesser amount of plastic flow, with increased lapping to obtain the desired 0.001-inch-wide lands, would provide the first state flatness required for multiple land sealing at low loads. Along

with other needed changes, however, it is reasonably certain that increased tube thickness or adoption of a single-piece construction similar to the standard flat 440C seat would improve flatness. It may appear obvious that soft metal plating would be advantageous. However, considering the above-revealed complexity, a cautious, experimental approach is warranted.

Models 706 and 707 Dynamic Tests

Because Model 702 test results had established that dynamic land formation was possible, Models 706 and 707 sealing lands were statically formed at 15,000-psi stress initially after assembly into the dynamic tester. This procedure permitted acquisition of baseline data from which cyclic performance could be assessed. Test 1 (Fig. VII-64 and VII-65), represents the baseline information for Models 706 and 707, respectively.

Electrical contact tests of both models indicated that Model 706 was 32 microinches out-of-parallel, while Model 707 was out approximately 65 microinches. It is interesting to note that Model 707, having the greater (indicated) parallelism deviation, yielded one of the best initial stress-leakage characteristics achieved. This indicates that, through plastic land deformation, sealing surfaces were brought into near perfect parallel conformance with minimum elastic springback.

Following 1000-ultraclean cycles, a degradation of low stress (below 1000 psi) sealing performance was noted (Test 2), particularly with Model 707. The latter was so severe that the model was removed from the tester and inspected. Contaminant material (apparently nonmetallic) was found embedded in land 6 with evidence of similar damage to land 5. Polish-cleaning with a cotton swab and 0- to 1-micron diamond lapping compound appeared to remove the bulk of the trapped material and significantly reduced the low-stress leakage, as shown by Test 3 (Fig. VII-65). There was, however, evidence of "minor" contaminant damage to both the primary sealing lands 5 and 6, as well as to other lands. It may be that similar damage contributed to the low-stress performance degradation of Model 706 as well as previous Model 702.

During clean cycles, no particles greater than the monitored low limit of 12 microns were observed. However, the bypass line flowmeter and one selector hand valve are located between the sampling point and seat. Possible discharge of entrapped material from the flowmeter or breakdown of the Rulon seal material in the hand valve could allow unsampled contaminants to reach the seat area. Foreign material might also have been introduced during static testing and balance pressure measurement when a second selector valve (but not the flowmeter) was in the flow stream.

Because Model 702 had accumulated 22 hits with an average HB particle concentration of 8230 p/l, it was decided to reduce the concentration for Models 706 and 707. Particle counts for both models are tabulated at the top of the next page.

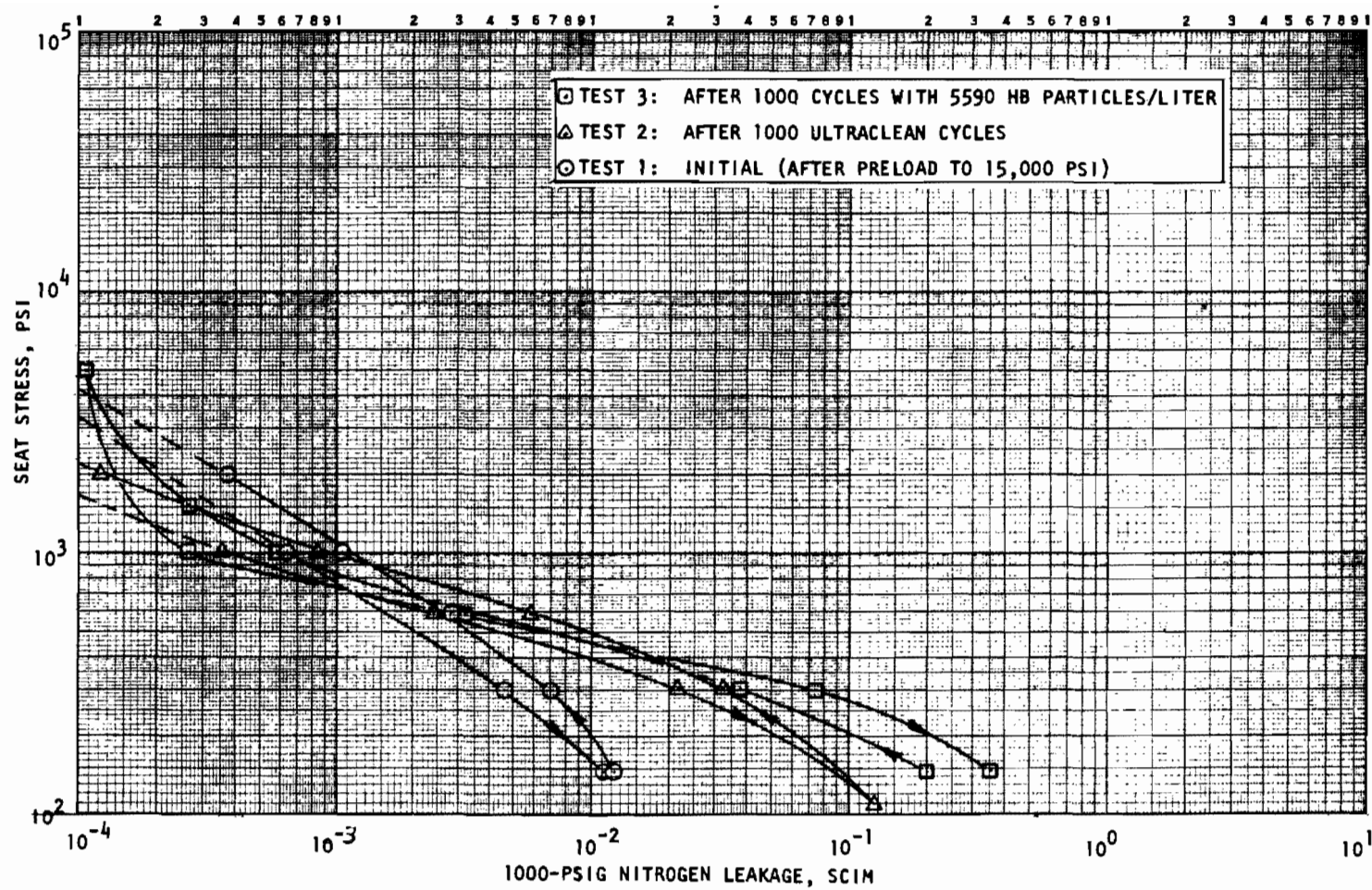


Figure VII-64. Stress-Leakage Data for Dynamic Test Model 706, Tests 1, 2, and 3

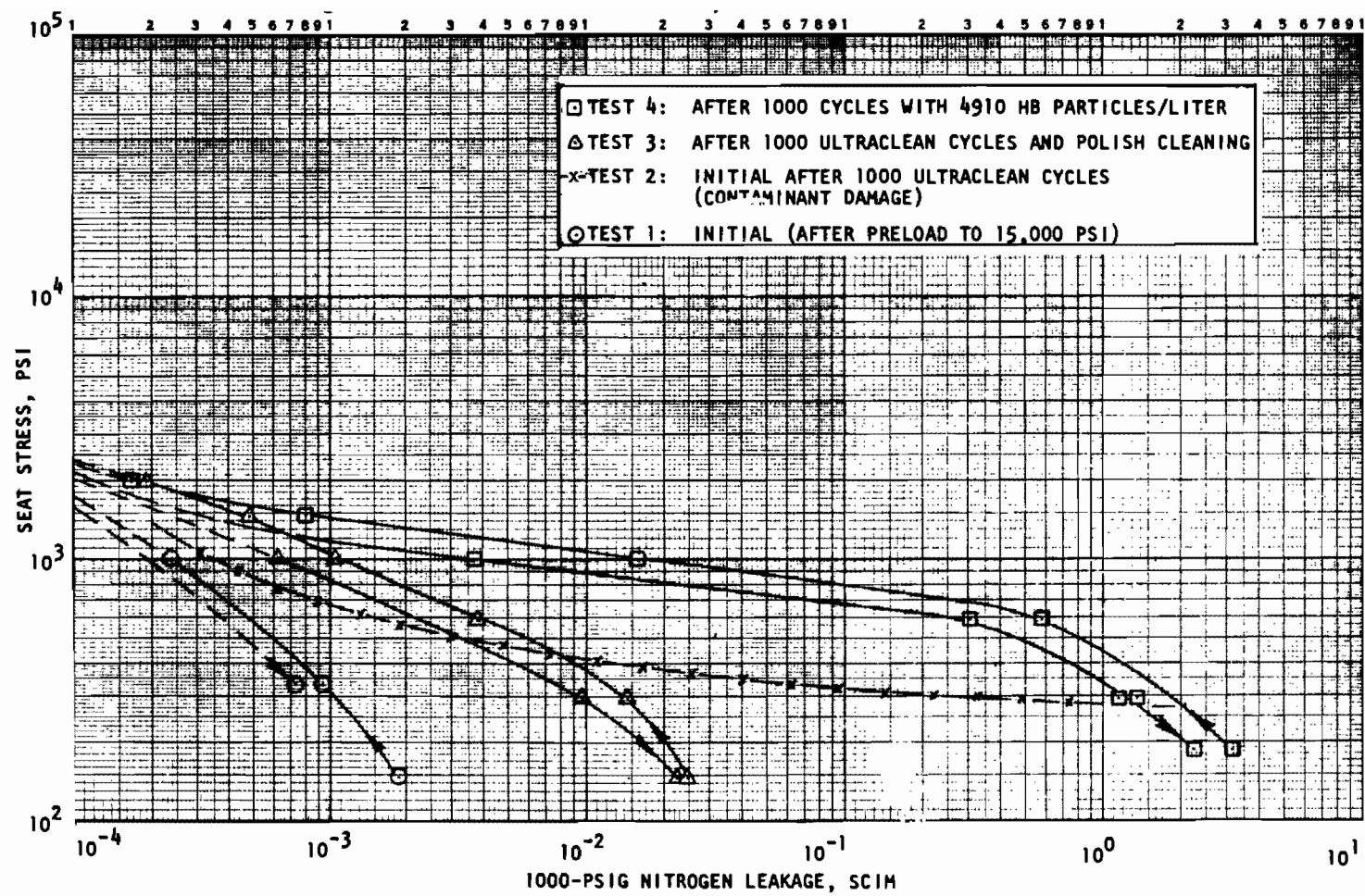


Figure VII-65. Stress-Leakage Data for Dynamic Test Model 707, Tests 1, 2, 3, and 4

HIAC Count/Liter

Cycles	12 to 20 Microns	> 20 Microns
Model 706		
Background	20	0
0	133	5330
100	176	5680
200	208	5630
500	226	5690
1000	266	5400
Model 707		
Background	10	0
0	144	5010
100	144	5010
100	211	5270
200	202	5010
500	258	4880
1000	335	4725

From these data, Model 706 was cycled with an average HB count of 5590 p/l, and Model 707 with 4910 p/l.

Model 706 Inspection. Posttest inspection of Model 706 indicated that 12 impact events had been accumulated. Four HB particles remained embedded in the seat, involving lands 1, 2, 3, and 6. Additionally, primary sealing lands 5 and 6 each evidenced fiber-type hits both bridging the lands and ranging from 20 to 40 microinches deep and 0.001 to 0.002 inch wide.

Duboff measurement indicated lands 4, 5, and 6 were relatively flat, with land 5 higher by about a microinch. Maximum duboff, from land 5 to land 1 (OD), was approximately 17 microinches. Average individual land width was 0.00092 inch.

The fiber-type impact damage to the primary sealing lands apparently had more influence on leakage degradation than particle encounters. This is indicated by comparison of leakage occurring after clean and particle cycles (Fig. VII-64), where the major increase followed clean cycling. As previously noted, unmonitored, nonmetallic contamination was noted with Model 707 prior to HB particle cycles, and the same problem, therefore, is presumed to have occurred with Model 706 as well.

Seat land photos (for Models 706 and 707) with typical particle hits are shown in Fig. VII-66 through VII-73.

Model 707 Inspection. Model 707 had 13 particle encounters. Both primary sealing lands 5 and 6 had an embedded particle at land center; two particles remained in land 1 as well. Three significant fiber-type hits were noted. Land 6 had two, 20 to 30 microinches deep and 0.004-inch-wide depressions, but neither affected more than one-half the land width.

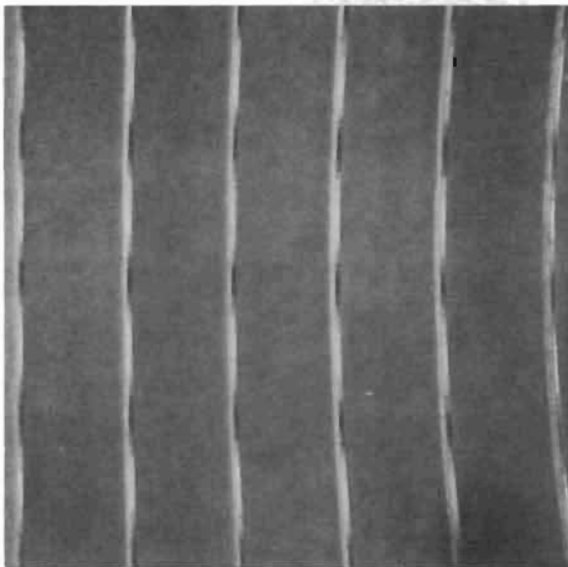


Figure VII-66. Model 706 Seat Land
Before Test (91X
Interference Photo)

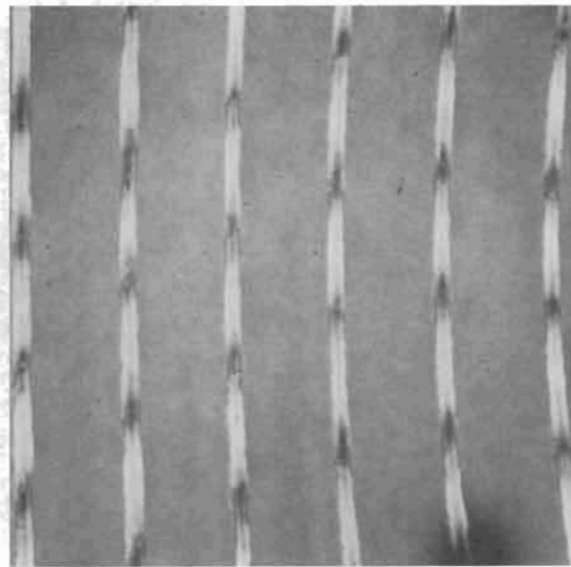


Figure VII-67. Model 706 Seat Land
After Dynamic Test;
ID Right (91X Inter-
ference Photo)

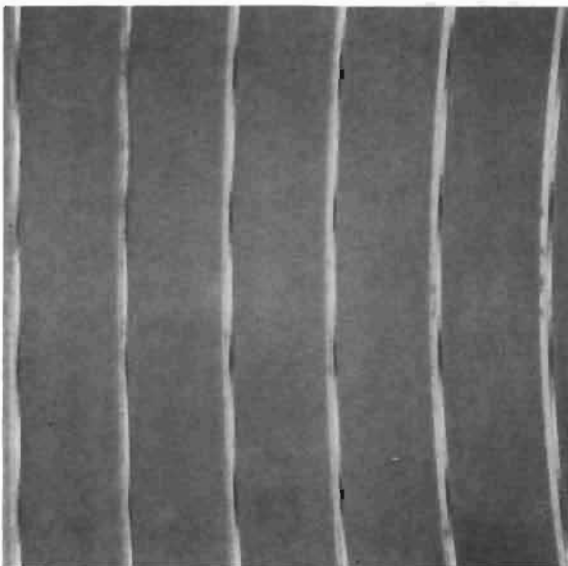


Figure VII-68. Model 707 Seat Land
Before Test (91X
Interference Photo)

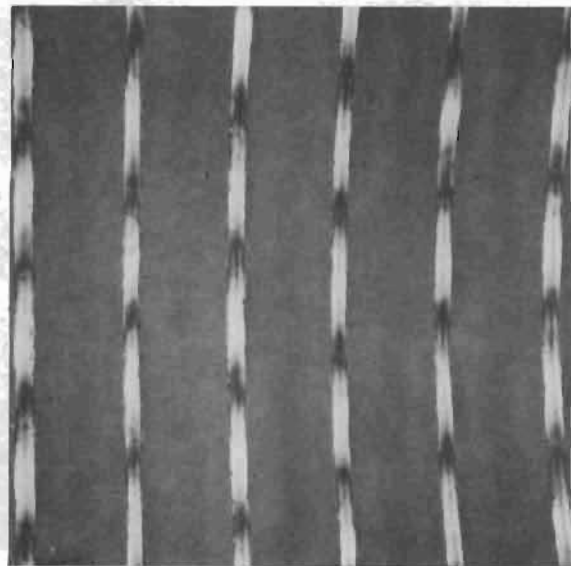


Figure VII-69. Model 707 Seat Land
After Dynamic Test;
ID Right (91X Inter-
ference Photo)

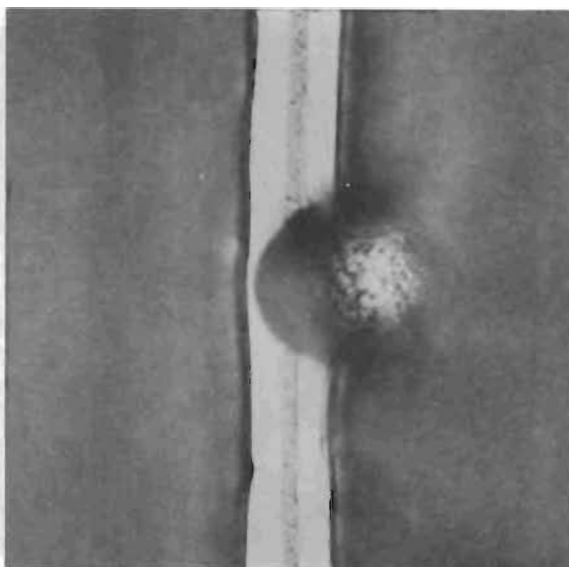


Figure VII-70. Model 707 Seat Land No. 5 Showing Embedded Particle (462X Plain Photo)

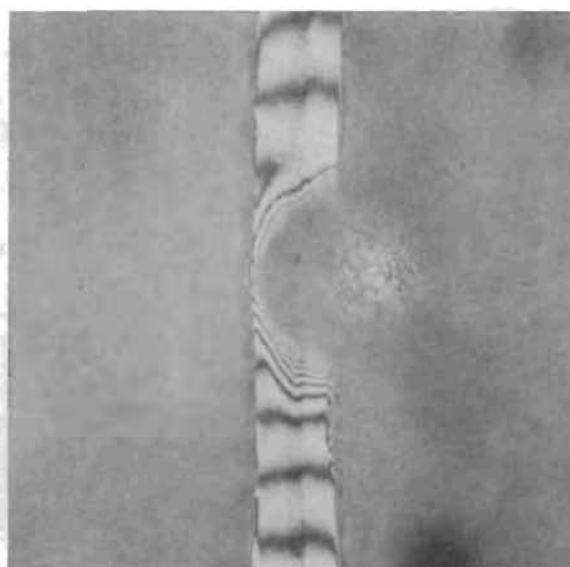


Figure VII-71. Model 707 Seat Land No. 5 Showing Embedded Particle (Note Lack of Raised Metal) (462X Interference Photo Same Location as Fig. VII-70)

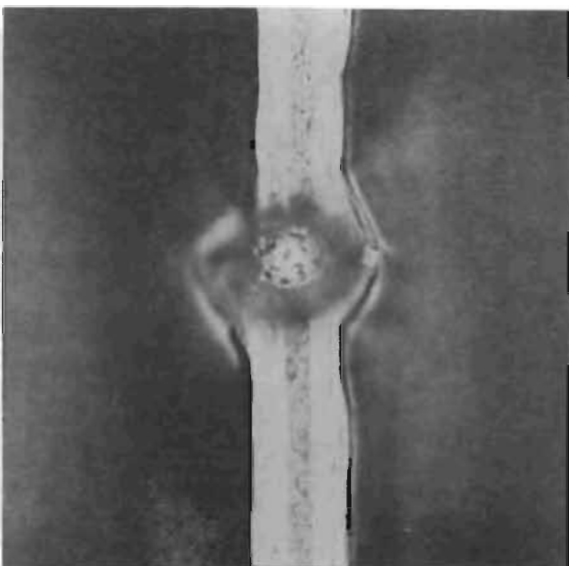


Figure VII-72. Model 707 Seat Land No. 1 Showing Embedded Particle (462X Plain Photo)

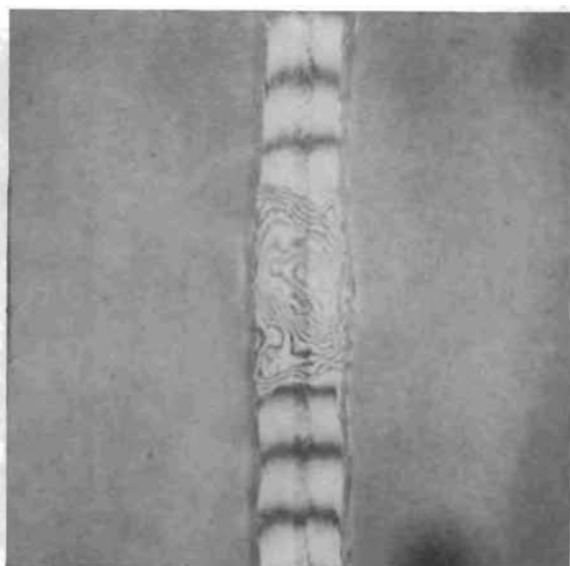


Figure VII-73. Model 707 Seat Land No. 5 Showing Typical 100-Percent Fiber-Type Hit (462X Interference Photo)

Land 5, however, was bridged by a 0.0025-inch-wide by 90-microinch deep depression (Fig. VII-73). A duoboff of about 18.5 microinches from inner land 6 to OD land 1 was measured, and land widths averaged 0.00095 inch.

As illustrated by Fig. VII-65, Model 707 evidenced severe contaminant damage after clean cycles. This, however, was subsequently improved by polish cleaning. It is not known whether the large leakage increase noted after HB cycles was due to particle or fibrous contaminant effects. However, it appears likely that the very deep depression found on land 5 occurred during particle cycles. This assumption follows the observation that particle center hits on primary sealing lands of other models did not result in the large leakage increase as was obtained with Model 707. Thus, the fiber damage may have been the predominant factor in Model 707 sealing degradation, which was almost 27 times that of Model 706 at 1000-psi apparent stress.

Observations

The results of Model 702, 706, and 707 tests reveal the advantage of the grooved configuration in maintaining low leakage at reasonable loads even with sealing surface damage. The grooved model sealing capability at 1000-psi stress is more than an order of magnitude better than flat copper or 440C versions. It is expected that, with a grooved land geometry where all lands are flat within 2 microinches or less, a significant reduction in leakage, particularly in the low (less than 1000 psi apparent) stress region, would be realized both clean and with entrapped particles. This potential, in conjunction with the previously noted consideration of a lesser groove depth to reduce hit frequency, is believed to warrant further development of the grooved concept.

MODEL CORRELATION

The Phase III model designs represented widely divergent approaches to minimize particle effects. Performance relative to the standard flat model also was comparatively different in both load-leakage effects and hit frequency. In general, however, each model design performed as expected, but usually with added (unforeseen) complications which limited planned performance. Typical model performance is reviewed comparatively in the following paragraphs.

Load Versus Leakage

Representative Phase III model data are presented on a load basis in Fig. VII-74 for general comparison. Also shown are the "after particle cycling test plan target curves," flat 440C Model 119, and shear seal Model 303 results from Phase II. All data are taken from individual stress-leakage data previously presented for the increasing load condition. Except for Model 119, which was successively static tested with three 30- and 60-micron SB particles, all "clean" curve data are following a 1000-cycle clean test. The particle effects data result from surface degradation following a 1000-cycle test with HB particles. The number of embedded particles contributing to the observed leakage change are identified with each curve. Total number of hits are defined in Tables V-1 and VII-1 previously presented.

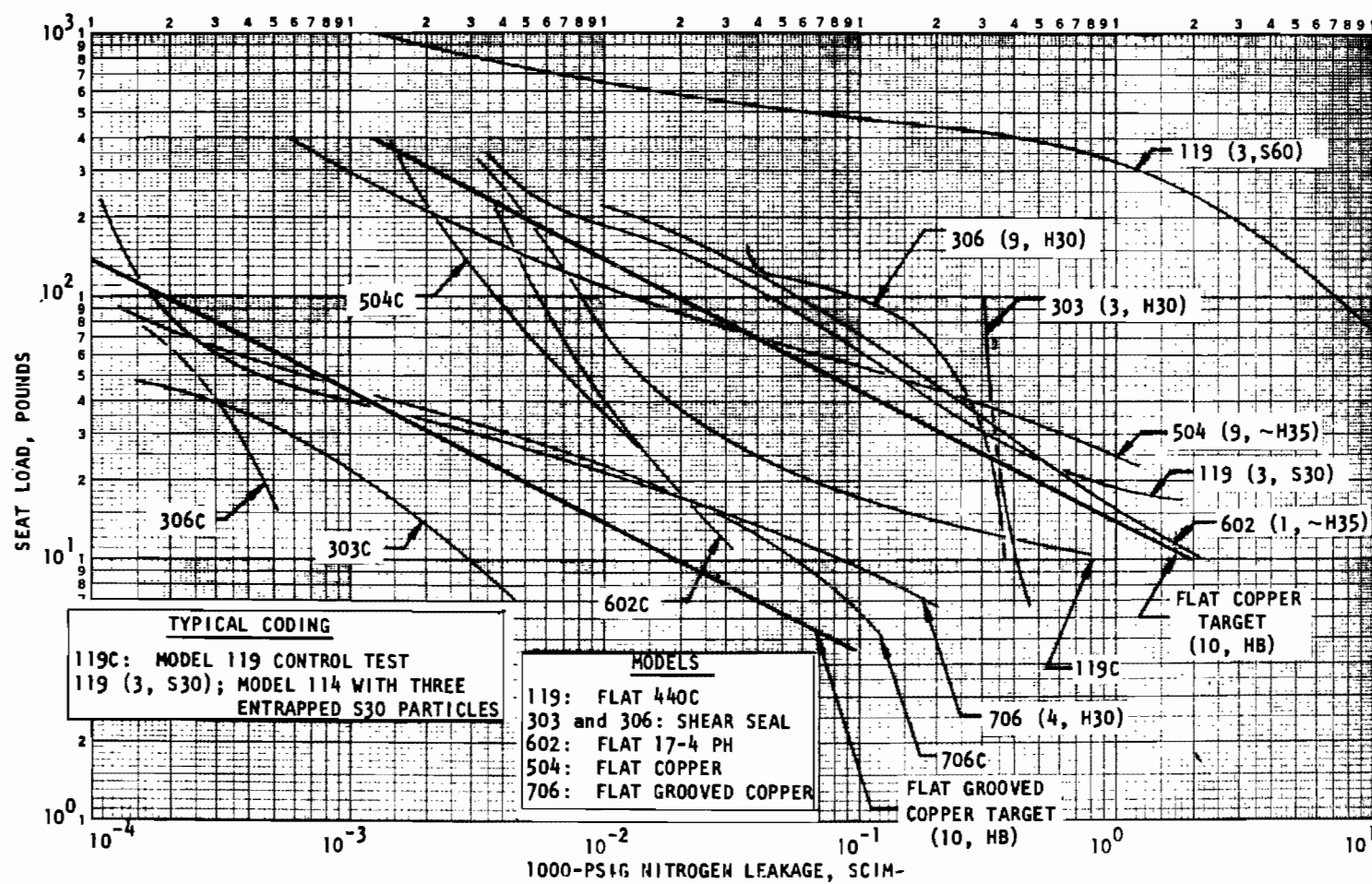


Figure VII-74. Phase III Model Load vs Leakage Data Comparison

Direct comparisons between model configurations are difficult because of the many test variables. Initial clean condition performance is different and so is the particle impact experience. When model design is best?

Considering first the clean curve data, it can be seen that the three plain flat models (119, 602, and 504) have a similar leakage characteristic, differing by no more than a factor of 3 between 20 and 200 pounds seat load. The tolerance of these three models to HB particles is markedly different, however. Flat copper Model 504 had nine HB particles embedded without significantly greater leakage increase than either the 440C Model 119 with three soft particles or 17-4PH Model 602 with only one hard particle. Furthermore, it has been demonstrated that the 440C model most probably would not accumulate particles, whereas the 17-4PH model did have the one hard particle embedded following the 1000-cycle test. From these results, it is concluded that material combinations of this intermediate hardness is the least desirable for best particle tolerance.

Where each cycle must be to a specific low leakage requirement, the particle envelopment design is considered necessary. With the harder materials, even one entrapped particle larger than the land width and load parameters can accommodate will result in a potentially gross leakage increase, as indicated by Model 119 with three 60-micron particles. It should be noted that this result will not be significantly improved even with only one particle trapped. Conversely, where recycle capability exists, the very hard materials have the advantages of producibility, wear resistance with long cyclic life, and particle ejection with minimum residual damage.

Models 303, 306 (shear seal), and Model 706 (flat grooved) are radical departures from conventional valve seating. Outstanding clean performance of these models is directly attributed to the plastically formed sealing geometry resulting in high contact stress. The shear seal design especially has resulted in very low leakage at low loads from a narrow land and the circular lay of the mating 440C spherical poppet. The relatively narrow sealing land (0.002 to 0.004 inch) has extreme susceptibility to particle damage, however. The effect of particle damage bridging the sealing land is shown by Model 303 in Fig. VII-74. The seat damage and embedded particles offer little separating force, as indicated by the flat load-leakage curve. It can thus be concluded that leakage is solely due to nearly fixed leak paths.

The flat-grooved copper model represents the ultimate approach in this program for a valve closure design capable of reliable operation in a highly contaminated fluid system. Clean and after-cycling results shown in Fig. VII-74 indicate the outward advantage of this design concept. The results seem even more remarkable considering that, at the 10^{-2} scim leakage load of about 23 pounds, all sealing is provided by only the two innermost seat lands only 0.001-inch wide each. Furthermore, as was previously reported in the inspection of Model 706, both sealing lands had fiber-type hit damage which bridged these lands. Although the duboff problem was not completely resolved, it is probable that increased flatness would improve the indicated results which are close to the test plan target established for 10 particle encounters. Model 706 had 4 embedded

particles and a total of 12 hits. However, most of these encounters were on lands having no sealing contact at the 23-pound load level. It is, therefore, possible that the sealing characteristics would not be significantly improved with all lands in contact at this load level. As a result of these tests, additional development of the flat-grooved seat is warranted.

Hit Frequency

Review of the Phase III model hit frequency experience has indicated that particle dynamics at closure and/or inlet geometry may have influence on the probability of particle entrapment. The self-cleaning model was a direct attempt to influence this parameter, with only partial success achieved. Results with both the shear seal and flat-grooved models have indicated increased hit frequency compared with plain flat models. Even allowing increased effective width for angular contact and particle edge hits does not produce a satisfactory correlation for these models. A possible explanation may be that particle concentration in the immediate vicinity of the closure is influenced by feed geometry. With both the shear seal and flat designs, a sharp change in flow direction is required adjacent to the seat which may have produced a high particle concentration in this area. This hypothesized high particle concentration may be presented to the sealing interfaces at closure, with additional influence of seating interface geometry. It is possible that streamlining the inlet flow path may reduce the hit frequency. This argument may be taken from the self-cleaning model results if it can be assumed that the significant reduction in particle encounters obtained were produced, not by the cleaning function, but simply by the cleaning plug turning effect. This important observation should be further explored in any future effort.

SECTION VIII

CONCLUSIONS

The results produced by this investigation have served mainly to establish particle handling methods, test procedures and systems, and some experimental data. This information has provided a better understanding of particle effects on closure sealing while defining the scope of the problem and the direction for further effort. Because of the complex nature of particle envelopment and dynamic impact, it is necessary to limit the scope of the observations and conclusions to the test parameters defined herein. Most specifically, this refers to particle size and hardness, closure size and hardness, and dynamic test system variables.

Because much of the static stress-leakage data was based on the previous research, conclusions from this prior effort (Ref. 3) were reviewed. Except as affected by load eccentricity and parallelism, these prior findings on basic sealing phenomena are considered germane to this current effort. Isolation and definition of eccentric load and parallelism effects as defined herein represented significant achievements in stress-leakage testing.

STATIC PARTICLE ENVELOPMENT

Particle envelopment is defined by contact of opposed sealing surfaces which surround a particle. The load necessary to achieve this condition is interrelated with surface contact loads which are developed in areas remote from the particle. Because of this complexity, the particle envelopment load has been defined as the seat force required to reduce particle-caused leakage to 10 times that of the clean control test leakage. This load is a complex function of many variables and must be determined for each closure configuration and contaminant of interest. The following conclusions must be applied only to the extent allowed by configuration, size, and material similarities with models and particles tested herein.

1. Valve closure particle envelopment can be achieved by normally translating closure surfaces (flat poppet and seat) in three ways:
 - a. Total elastic encapsulation of a very soft particle by relatively hard (and, thus, strong) closure surfaces.
 - b. Total plastic flow of one or both closure surfaces about a much harder particle.
 - c. Combinations of elastic and plastic deformation of all members.
2. Minimum sealing surface particle-caused damage is afforded by the flat poppet and seat.

3. For nominal 1/2-inch-diameter, 0.03-inch land width 440C (R_C 60) poppet and seat, envelopment loads were empirically determined for hard (R_C 62-67) and soft (R_C 17-21) nickel particles of 15-, 30-, and 60-micron diameter. Envelopment load is approximately the same for one to three (equally spaced) particles, hard or soft, and varies with the square of the particle diameter. (For more than three particles, or for particles on one side only, the load is proportionately increased.)
4. For 440C material, the 30-micron particle constitutes an upper size limit for reasonable particle envelopment with a 0.03-inch full contact land width. This is due to a radial channel leakage path remaining after remote circumferential sealing surfaces are brought into contact around one or more particles. The channel leak path phenomena established land width versus particle size as a vital parameter in particle envelopment.
5. Particles larger than 60 microns will cause gross leakage with most hard seat valves even with large loads.
6. Residual damage effect is minimal with hard sealing surfaces. (Many leakage failures have probably been attributed to surface minutiae visible under 10X to 100X magnification which are incomparable with seat damage disruptions illustrated herein.)
7. Hard closure surfaces should have equal hardness to minimize particle penetration. (Static testing showed that with particles softer than 440C poppet and seat, elastic springback forces served to eject a previously enveloped particle even though the flattened particle plastically formed holes in each sealing surface. With particles slightly harder than 440C poppet and seat, particle ejection also occurred. However, evidence indicated that with one closure member slightly softer than the other, a permanent embedment could occur.)

DYNAMIC CLOSURE EFFECTS

Dynamic tests served to define the effects of impact entrapment of particles, simulating real systems but with precise control of related parameters. Valuable contributions of this effort were: (1) proof of particle entrapment predictability, (2) definition of entrapment characteristics, and (3) specific residual damage effects on stress-leakage performance for a variety of closure designs. Unless otherwise noted, the following observations and conclusions relate to the effects of 32-micron nominal, hard (R_C 62-67) particles in a liquid environment.

1. Particle hit frequency and the probable distribution of hits can be determined from simple volumetric concentration analysis and the binomial distribution of chance events. (Independence from trajectory effects and resultant particle concentration gradients during closure is assumed and deviation from theory may be taken as the result of these variables. Hit frequency predictability allows a more scientific approach to contaminant tolerance testing because concentration and cycles are directly interrelated.)

2. With average (see Section II Analysis) contamination, the reliability of conventional hard metal closures will be poor, with a 5- to 50-percent chance of a failure-producing contaminant encounter in 100 to 1000 cycles, respectively. (System requirements and closure design criteria must be established through joint compromise to effect a reliable solution so that the contamination level is within the valve closure life tolerance.)
3. Very hard (R_C 60) metal surfaces do not retain semihard (R_C 20) or hard (R_C 64) impacted particles. (This is probably due to elastic ejection forces previously noted combined with impact shock waves. However, more than one cycle may be required to wash out a partially retained particle. With particles retained for more than one cycle, it is mandatory that precise orientation of poppet and seat be maintained between all cycles. This is to preclude multiple damage transfer back and forth between the poppet and seat.)
4. Residual damage effects for impacted particles on flat 440C surfaces are similar to those produced statically. Therefore, static tests should be employed to positively verify adequate seat loading with particles entrapped. (Leakage increase of 10:1 was tolerable at 1000-psi apparent stress with up to five 60-micron and twenty 30-micron hard particle encounters.)
5. Particle hardness substantially greater than the closure material may result in permanent particle embedment. (In this case, the combination of two semihard, R_C 20-40, metals should be avoided in favor of one hard and one very soft metal. Tests with flat tungsten carbide poppet on 440C seat contradicted the preceding conclusion in that no particles were retained in the 440C seat after eight hits over 1000 cycles. This may be a special case due to these very hard materials. Although not proved, it is possible that impact shock pulverized the particles with subsequent washout on subsequent cycles.)
6. Carbide on carbide probably offers the most damage-resistant material combination. (A possible exception to this is that very soft metallic particles may be plastically smeared onto a semi-porous cermet or ceramic surface and, consequently, retained for many cycles. Hard closure materials have very limited particle envelopment capability and leakage is likely to be gross with particles greater than 30 microns entrapped. Direct cyclic evidence of particle entrapment between hard surfaces is difficult to obtain because particles are (thought to be) easily washed out and the probability of stopping a cycle test on a specific entrapment is usually very low. If the flight leakage requirement includes all cycles, then this factor must be considered because the cycle test could indicate success, whereas several gross failures could have actually resulted.)

CLOSURE DESIGN

Closure designs were evaluated in both Phases II and III for characteristics and criteria that would indicate the best design approach to contamination resistance in a liquid medium. Considering the many questions posed by this effort and the variety of results obtained, it is difficult to draw any final conclusions as to the best possible approach to closure design for contamination. It is certainly concluded that for design purposes, specific effects must be obtained with models that duplicate material properties and have a very similar, if not exact, sealing geometry and size.

1. A successful particle avoidance design would rate first consideration if the design were compact and economical. However, this design approach has yet to be proved feasible.
2. A hard-on-soft metal approach should be pursued if low leakage is mandatory for every cycle. Particle concentration versus cycle life must be influenced with cleaning methods and filtration to limit the number of particle encounters according to the design.
3. The results obtained herein indicate significant advantage for the flat-grooved design. However, this approach must be modified to allow full contact seating across all lands at the working load level. Furthermore, the adverse hit frequency record of the design indicates the need for improvement, possibly by reduction in groove depth.
4. The shear seal design has shown an excellent sealing capability. Although the configuration tested indicated an adverse hit frequency, particle effects were limited to orifice-type leaks caused by particle damage bridging the sealing land. The very high leakage associated with hard closures and large particles entrapped is thus avoided. Moreover, this design approach has the advantage of seat deflection isolation from local body deformations. Close concentricity control between the poppet and seat is required, however, because of lateral stiffness.
5. Deep entry spherical seating is considered the least desirable approach for particle resistance, although a dissimilar hardness design may offer better performance than obtained herein.
6. It was demonstrated that a strong vortex could create very high, local particle concentrations. If the closure design were to cause such a high concentration near the seating interfaces, an excessive hit frequency might occur. Moreover, flow reversals at the instant of closure may also contribute to adverse hit frequency. Additional tests are required to verify these hypotheses.
7. Experience with machining and forming the copper seats described herein indicates that a work-hardened metal is preferable for plastically formed seats and seals. Work hardening, resulting from machining annealed metals, produces a hardened skin over a substantially weaker substrate. To obtain sealing plastic flow,

the inner metal must be plastically deformed sufficiently to bring the surface to the plastic flow pressure. With annealed metals, this may not occur due to limited deflection. It is apparent that the most desirable combination would be a soft, annealed surface skin with a harder base metal.

SECTION IX

RECOMMENDATIONS FOR FUTURE EFFORT

Conclusions from the Phase I Survey were that: (1) currently employed quantitative methods for contamination control did not meet design needs, and (2) means should be established for evaluating the contamination level in operating systems and the contamination tolerance level of components used in these systems. The limited data defined herein for Phases II and III re-emphasizes the need for correlation of measured engine contamination levels and corresponding valve performance. Also, much additional effort is required to answer the many questions uncovered in the experimental investigations and to fully develop contaminant-resistant closures to meet the needs of high-performance rocket propulsion systems. Some of the more pertinent questions are:

1. What is basic influence of land width on the stress-leakage characteristic?
2. What minimum land width is required to permit particle envelopment as a function of:
 - a. Closure materials (hard on hard and hard on soft)?
 - b. Particle size (hard and soft)?
3. What is the load required to effect a given leak rate as a function of closure and particle hardness, and closure size (primarily land width) and particle diameter? (A variation of question 2.)
4. Should land structure be of maximum stiffness to cause greatest particle flattening and embedment, or should it be made elastically flexible to allow deflection about a particle?
5. What is roughness parameter effect on the stress-leakage characteristic with particles? Is there a minimum practical roughness for a given particle size and load?
6. How does hit frequency vary with land width, particle diameter, and inlet feed geometry?
7. Can hit frequency be reduced by streamlining feed geometry?
8. Will very soft particles stick to hard and/or porous impacting closure surfaces? What influence has impact level and number of cycles?
9. Are particles ejected from hard closures on first cycle or are additional cycles required?
10. What is the optimum low-leakage, long-life closure configuration for minimum particle effects?

Answers to the preceding questions can be obtained for specific cases by additional model testing as performed and reported herein. A three-part effort is recommended.

STATIC TEST

Additional parametric design data regarding particle envelopment is required. This is best obtained by static test of flat models for the following variables:

1. Interface hardness (hard on hard and hard on soft)
2. Particle hardness
3. Closure size, i.e., land width
4. Particle size (diameter)
5. Surface roughness

DYNAMIC TEST

Hit frequency is a relatively new concept. The defined parameters need more positive verification. This must be accomplished statistically with at least three tests per parameter. With the dynamic test system, a variety of parameters can be evaluated using simple models fabricated explicitly for this purpose. Leakage would not be measured; therefore, the expense of fine sealing surfaces could be avoided. Recommended variables for test with flat models are:

1. Land width
2. Particle diameter
3. Feed geometry

Once a firm basis is established for the flat configuration, additional closure configurations could be similarly evaluated with confidence. In particular, the addition of an inlet feed fairing for the shear seal should be evaluated to ascertain if excessive hits observed with this configuration resulted from the poppet inlet cavity design. Also, reduction of groove depth with the flat-grooved model should be investigated.

CLOSURE DESIGN

The flat poppet and seat configuration remains the best design for most applications. Further pursuit of a material combination and surface structure that can tolerate many cycles and significant amounts of large particles is recommended. This effort will entail both static and dynamic tests to define loading requirements, cyclic life, and particle hit characteristics.

APPENDIX A

PARTICLE ENTRAPMENT PROBABILITY

The process of closing a valve in a fluid system that contains sparsely dispersed particles can be likened to withdrawing colored balls from a jar. The analogy is made by imagining the entire system volume to be divided into unit volumes equal to the volume of a single particle. This is written

$$N = \frac{V}{V_p} = \frac{V}{\frac{\pi}{6} d^3}$$

where

$$\begin{aligned} d &= \text{particle diameter} \\ N &= \text{number of unit volumes in system} \\ V &= \text{system volume} \\ V_p &= \text{particle volume} \end{aligned}$$

A small sample volume (V_s) withdrawn from the system will similarly contain (V_s) unit volumes

$$n = \frac{V_s}{V_p}$$

The sample volume (V_s) is defined by the valve seat closure area (A) and particle diameter (d) as

$$V_s = A d$$

For (f) closure cycles, what is the probability of extracting exactly (x) number of particles from the system containing (M) particles? Since (N) and (M) are very large with respect to (x), entrapment probability (p) is constant. Each trial (closure) is thus independent and the probability of exactly (x) successes in (f) trials is given by the binomial distribution (Ref. 6) as

$$p(x) = C(f, x) p^x (1 - p)^{f-x}$$

for $x = 0, 1, 2, \dots, f$, and the probability of (x) or fewer successes in (f) trials is

$$P(x) = \sum_{i=0}^x C(f, i) p^i (1 - p)^{f-i}$$

where

$$C(f, x) \equiv \frac{f!}{x! (f - x)!}$$

$p(x)$ = density distribution

$P(x)$ = cumulative distribution

p = expected probability for one trial (cycle)

The probability (p) of entrapping a particle in one cycle is determined from

$$p = \frac{n M}{N}$$

Substitution of volumetric terms reduces this to

$$p = V_s \frac{M}{V}$$

and with $M/V \equiv C_n$ (particle concentration in fluid) gives

$$p = A_s d C_n$$

The mean number of particle entrapments in (f) cycles is thus

$$I = f A_s d C_n = f p$$

The computation involved in solution of the binomial distribution for large values of (f) is prohibitive; therefore, computer prepared tables must be used (Ref. 7).

The Poisson distribution equation provides an approximation to the binomial distribution for (f) large and (I) up to five (Ref. 6); the equation is written as

$$p(x) \cong \frac{I^x}{e^I x!}$$

where $e = 2.718...$

The variance (σ^2) for the binomial distribution is

$$\sigma^2 = f p(1 - p)$$

This reduces to $\sigma^2 = I$ for the Poisson and little error is incurred if the same is assumed for the binomial with (I) up to 20.

A table of cumulative values for the binomial distribution is presented in Table A-1 (Ref. 7) for $f = 1000$ and $p = 0.001$ to 0.010 ($I = 1$ to 10). The data answer the question: "What is the probability of (x) or fewer entrapments?" Probability for specific values of (x) are obtained by subtraction from the next lower value for (x); e.g., $p(4)$ for $p = 0.006$ is $0.28425 - 0.15040 = 0.13385$. Similarly, the probability of, say, 3 to 11 entrapments for a mean of 6 would be found as 0.91881 .

TABLE A-1
CUMULATIVE VALUES OF BINOMIAL DISTRIBUTION
($P(x)$ for $f = 1000$)

X	P									
	.001	.002	.003	.004	.005	.006	.007	.008	.009	.010
0	0.36770	0.13506	0.04956	0.01817	0.00665	0.00243	0.00089	0.00032	0.00012	0.00004
1	0.73576	0.40573	0.19870	0.09114	0.04009	0.01713	0.00716	0.00294	0.00119	0.00048
2	0.91979	0.67668	0.42285	0.23752	0.12402	0.06143	0.02925	0.01350	0.00608	0.00268
3	0.98108	0.85730	0.64723	0.43308	0.26432	0.15040	0.08103	0.04181	0.02082	0.01007
4	0.99637	0.94753	0.81551	0.62884	0.44005	0.28425	0.17203	0.09872	0.05420	0.02869
5	0.99941	0.98354	0.91638	0.78545	0.61596	0.44519	0.29981	0.19013	0.11460	0.06614
6	0.99992	0.99551	0.96671	0.88975	0.76255	0.60630	0.44919	0.31239	0.20555	0.12888
7	0.99999	0.99892	0.98822	0.94923	0.86715	0.74439	0.59871	0.45240	0.32284	0.21886
8	1.00000	0.99977	0.99625	0.97888	0.93240	0.84786	0.72955	0.59255	0.45506	0.33169
9	1.00000	0.99995	0.99892	0.99200	0.96854	0.91669	0.83121	0.71712	0.58741	0.45730
10	1.00000	0.99999	0.99971	0.99723	0.98653	0.95787	0.90222	0.81669	0.70653	0.58304
11	1.00000	1.00000	0.99993	0.99911	0.99467	0.98024	0.94728	0.88895	0.80389	0.69735
12	1.00000	1.00000	0.99998	0.99974	0.99804	0.99137	0.97346	0.93698	0.87676	0.79251
13	1.00000	1.00000	0.99999	0.99993	0.99933	0.99648	0.98748	0.96641	0.92706	0.86556
14	1.00000	1.00000	1.00000	0.99998	0.99978	0.99865	0.99445	0.98315	0.95926	0.91758
15	1.00000	1.00000	1.00000	1.00000	0.99994	0.99951	0.99768	0.99202	0.97849	0.95213
16	1.00000	1.00000	1.00000	1.00000	0.99998	0.99983	0.99908	0.99643	0.98924	0.97361
17	1.00000	1.00000	1.00000	1.00000	1.00000	0.99994	0.99965	0.99848	0.99489	0.98616
18	1.00000	1.00000	1.00000	1.00000	1.00000	0.99998	0.99987	0.99939	0.99769	0.99309
19	1.00000	1.00000	1.00000	1.00000	1.00000	0.99999	0.99995	0.99976	0.99900	0.99671
20	1.00000	1.00000	1.00000	1.00000	1.00000	1.00000	0.99998	0.99991	0.99959	0.99850
21	1.00000	1.00000	1.00000	1.00000	1.00000	1.00000	0.99999	0.99997	0.99984	0.99934
22	1.00000	1.00000	1.00000	1.00000	1.00000	1.00000	0.99999	0.99999	0.99994	0.99972
23	1.00000	1.00000	1.00000	1.00000	1.00000	1.00000	0.99999	1.00000	0.99998	0.99989
24	1.00000	1.00000	1.00000	1.00000	1.00000	1.00000	0.99999	1.00000	0.99999	0.99995
25	1.00000	1.00000	1.00000	1.00000	1.00000	1.00000	0.99999	1.00000	1.00000	0.99998
26	1.00000	1.00000	1.00000	1.00000	1.00000	1.00000	0.99999	1.00000	1.00000	0.99999

APPENDIX B

SHEAR SEAL DESIGN ANALYSIS

Previous efforts with a deformable lip-type seat have produced superior sealing ability, although with some indication of contamination sensitivity (Ref. 5). With the contamination environment controlled, the ability of this design concept could be better defined. A closure of similar design was undertaken as a part of Phase II to evaluate the merits of a scrubbing, soft seal closure, as opposed to direct contact sealing. The general task included: (1) basic configuration tradeoff study; (2) detail design analysis relating loads, stresses, and deformations with detail dimensions; and (3) detail drawings suitable for fabrication.

This effort culminated in the design, in elementary form, of a fully elastic shear seal closure and the sketches and analytical data to facilitate detailing an elastic-plastic shear seal poppet and seat. The elastic version was not pursued further as attendant mechanical characteristics (alignment, guiding, tolerances, etc.) required extremely close, although not unobtainable, control. The elastic-plastic poppet and seat, so-called to designate that the seating interface is plastically formed and the seat stress results from elastic deformation of the seat member, appeared to have considerable merit and test units were made for evaluation. This design was finally termed "shear seal."

DESIGN

General design requirements were as follows:

1. Compatibility with dynamic tester (refer to Appendix F)
2. Seat diameter = 0.470 inch
3. Operating pressure = 1000 psig
4. Proof pressure = 1500 psig
5. Static seat loads between 4 and 400 pounds
6. Operating with nitrogen and Freon TF
7. Poppet material, hardened 440C
8. Seat material, copper

A schematic of the final design that evolved from the configuration study is illustrated in Fig. B-1. The dimensions shown are those resulting from the final analysis and detail layout of Fig. B-2. The poppet contacts the tip of the seat with 0.00657 inch of stroke remaining before it reaches the physical stop imposed by the seat holder. As the poppet is forced against the stop, the tip of the seat is plastically formed, producing a land calculated to be 0.0064 inch wide. The cylindrical seat is also radially compressed by the poppet and subject to diametrical expansion from internal pressure; both stresses are within the elastic limit of the material. Calculated seat stress and axial elastic deflection of the configuration is presented in the following paragraphs.

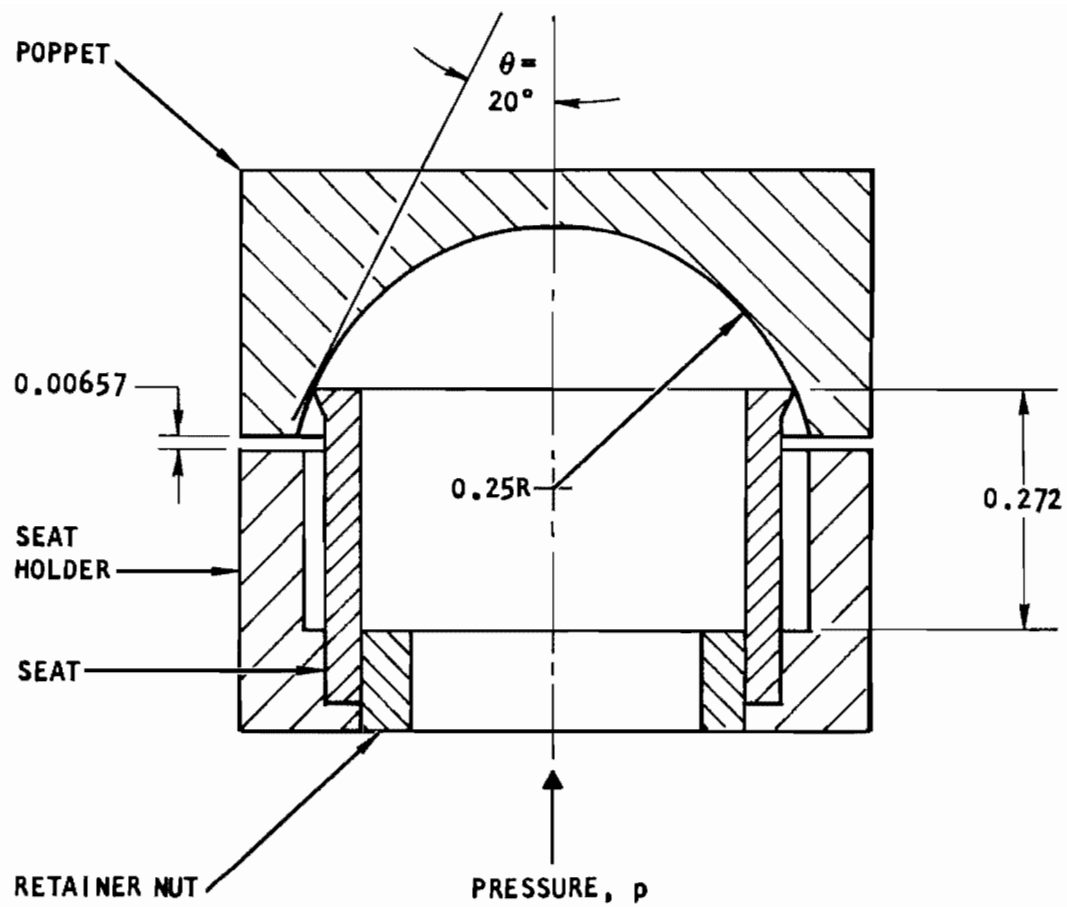


Figure B-1. Elastic-Plastic Poppet and Seat Schematic

B-3

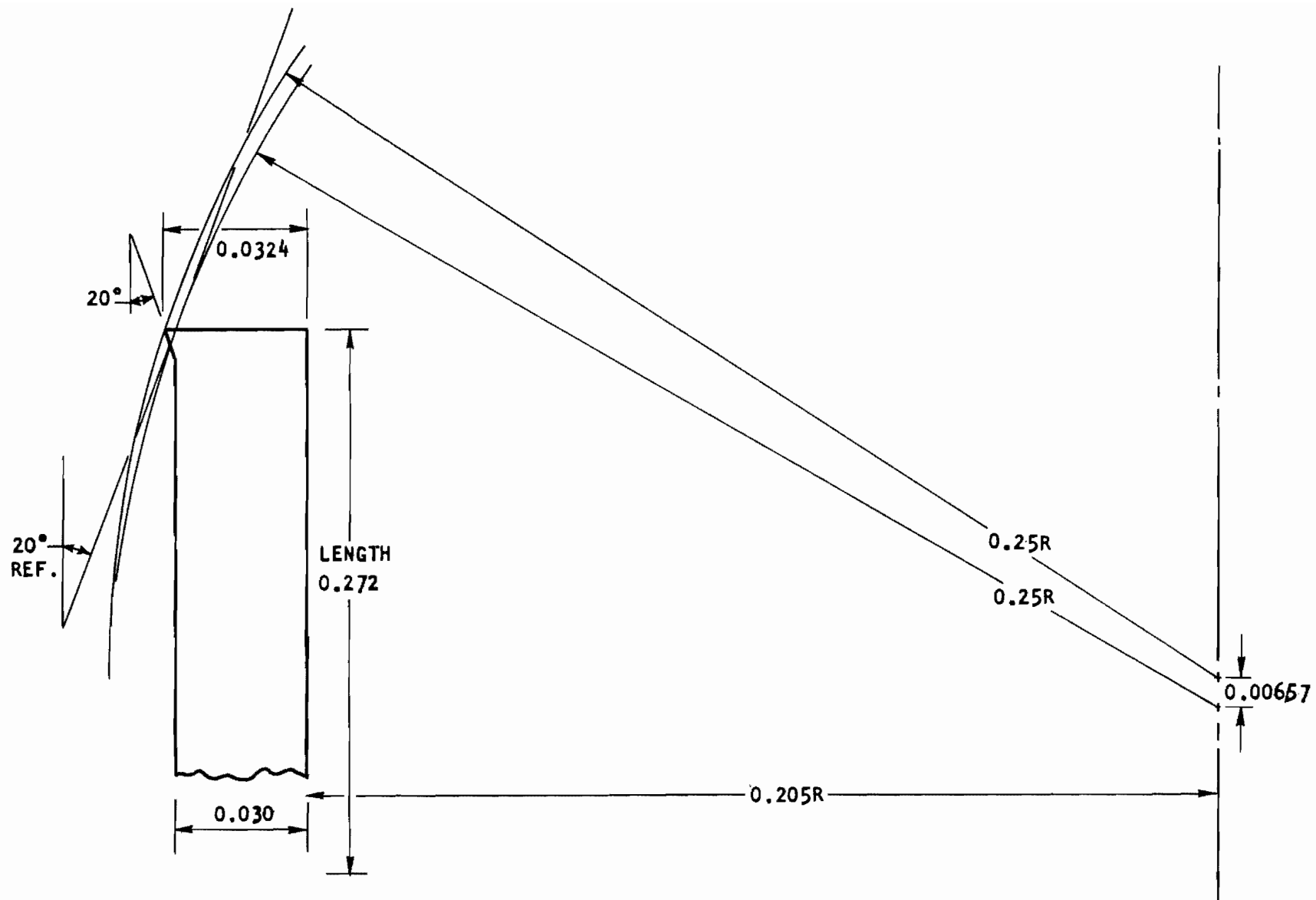


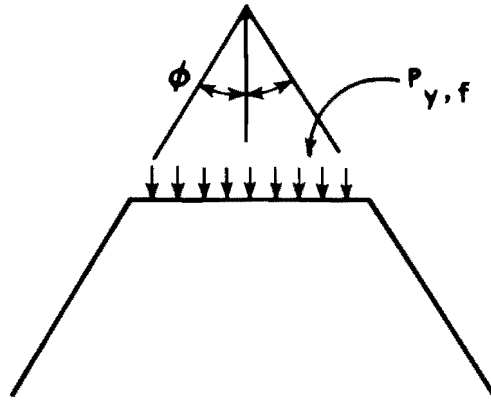
Figure B-2. Seat Detail Layout

WEDGE PLASTIC FLOW

The analysis of the elastic-plastic poppet and seat is predicated on the plastic flow of a wedge. The assumptions involved in this analysis are:

1. The wedge is perfectly plastic.
2. The coefficient of friction is approximately 1/3.
3. The increase in the octahedral shearing stress due to a tangential load increases the ratio of the octahedral shearing stress to the normal stress and alters the location of the stress. For coefficients of friction 1/10 or less, the shear is subsurface; larger tangential loads result in the maximum octahedral shearing stress occurring at the surface (Ref. 8).
4. Wedge flow characteristics are approximately the same regardless of geometric symmetry or cylindrical configuration.

A schematic of the wedge with nomenclature and equations from Ref. 1 are summarized below:



where

$P_{y,f}$ = uniform load (yield or fully plastic), pounds
 ϕ = wedge half angle, degrees
 S_0 = material tensile yield stress, psi

The load required for the initiation of yield is

$$P_y = 1.153 S_0 \left[\frac{(\phi + \frac{\pi}{2}) \sin \phi + \cos \phi}{1 + \sin \phi} \right] \quad (\text{refer to Fig. B-3})$$

The load required for fully developed plastic flow is

$$P_f = 1.153 S_0 \left[1 + (\phi + \frac{\pi}{2}) \tan \phi \right] \quad (\text{refer to Fig. B-4})$$

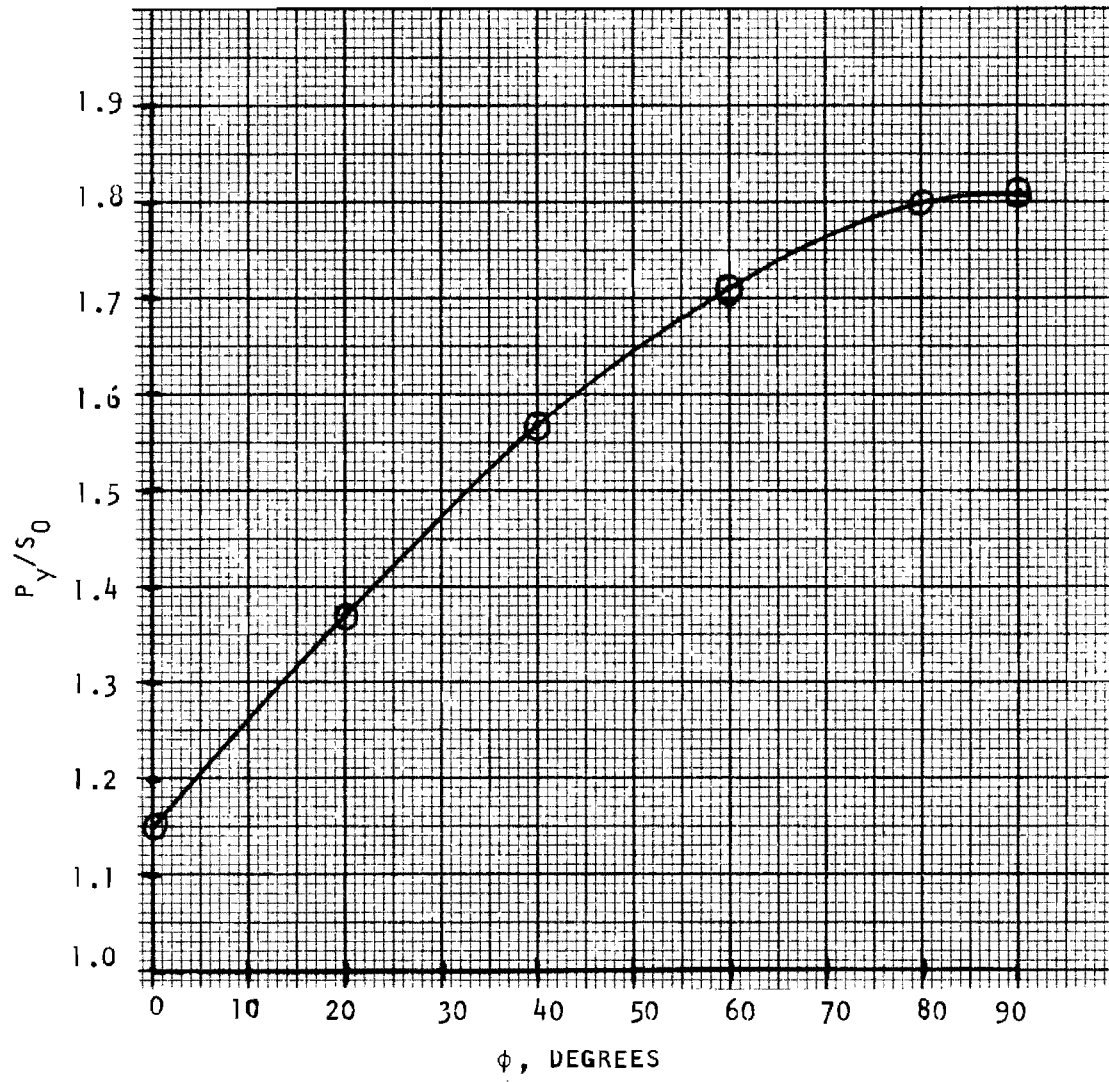


Figure B-3. Yield Stress Ratio vs Wedge Angle

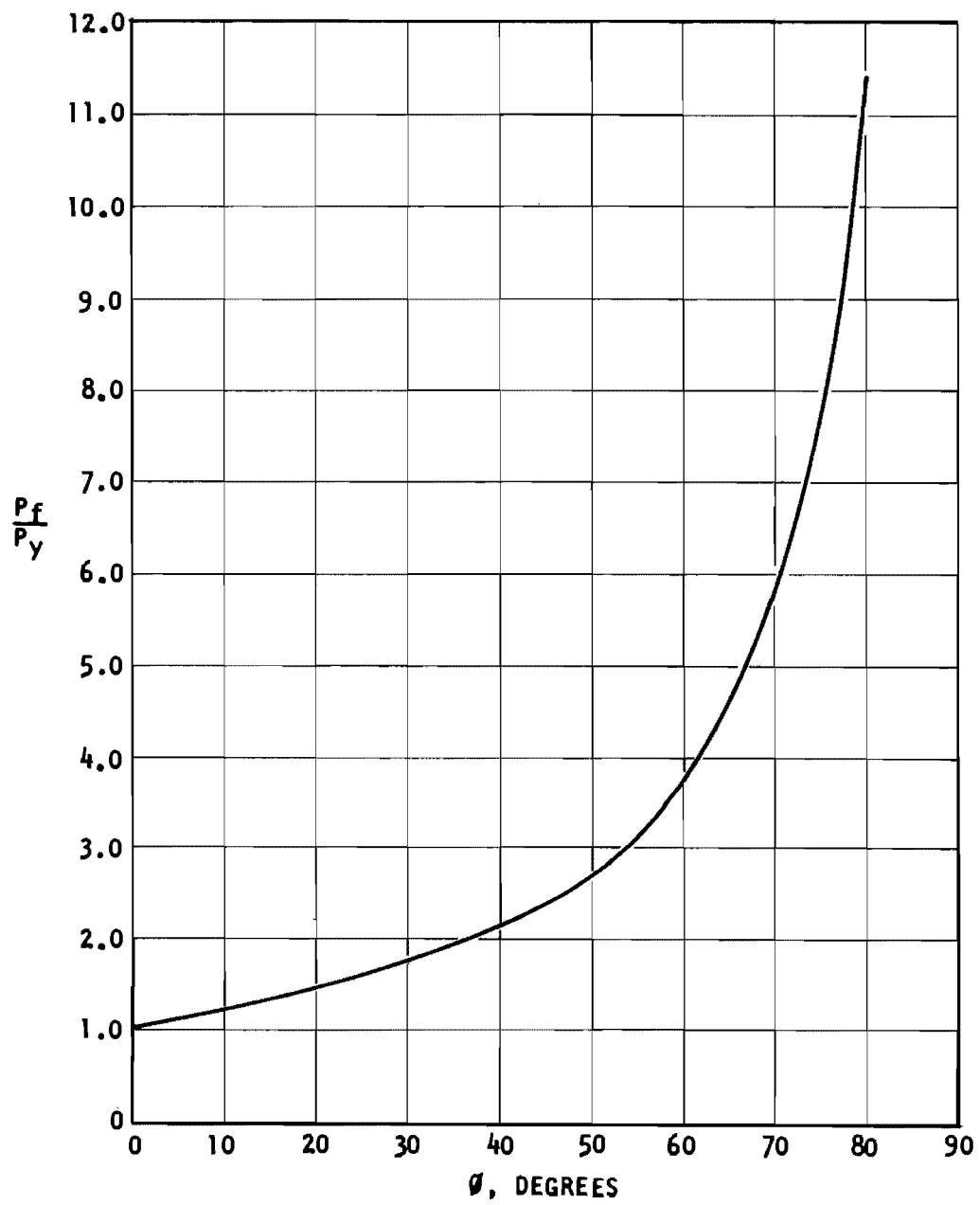


Figure B-4. Plastic Flow Stress Ratio vs Wedge Angle

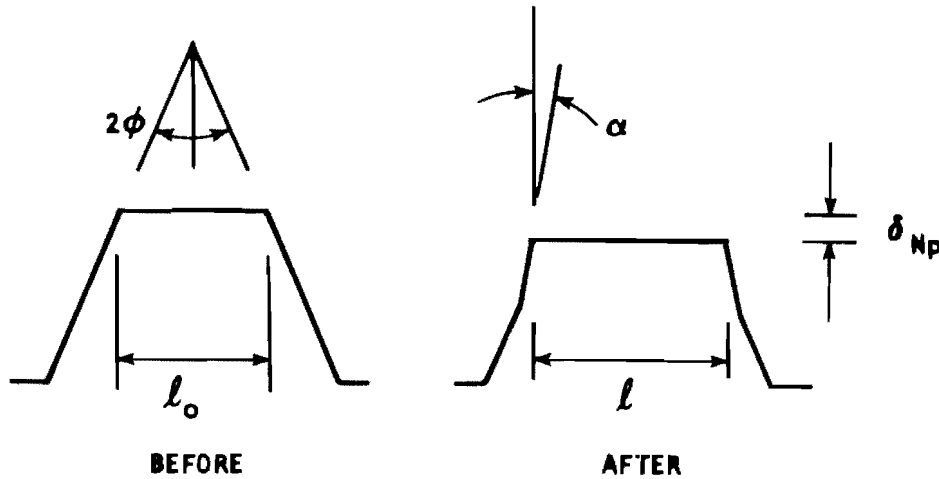
The preceding relationships for the wedge are based only on a normal load. Reference 8 presents the following data for a roller sliding on a plane (both elastic) under both normal and tangential loads.

Coefficient of Friction	0	1/12	1/9	1/6	1/3
Ratio of Octahedral Shearing Stress to Normal Stress	0.272	0.265	0.255	0.277	0.368

As the maximum octahedral shearing stress criteria for inelastic action is equivalent to the Huber-VonMises-Hencky method used in Ref. 1, the preceding data for P_y/S_0 may be modified to approximate the effect of the tangential load as follows:

$$\frac{P_y}{S_0} \cong \frac{0.272}{0.368} f(\phi) \cong 0.74 f(\phi) \quad (B-1)$$

Reference 9 presents data on the contact length of a rigid, perfectly plastic wedge deformed by a normal load. After modification of the equations to permit an initial blunting of the wedge, the equations become as listed below:



- l = contact length, inch
- δ_{Np} = normal plastic deformation, inch
- ϕ = wedge half angle ($26.6 \leq \phi < 90$), degrees
- α = angle of deformed wall to normal, degrees

$$l = l_0 + \frac{2(1 + \sin\alpha)}{\cos\alpha} \delta_{Np} \quad (B-2)$$

$$\tan\phi = \frac{(1 + \sin\alpha)^2}{\cos\alpha (2 + \sin\alpha)} \quad (B-3)$$

The trigonometric relationships in Eq. B-2 and B-3 are plotted in Fig. B-5 and B-6.

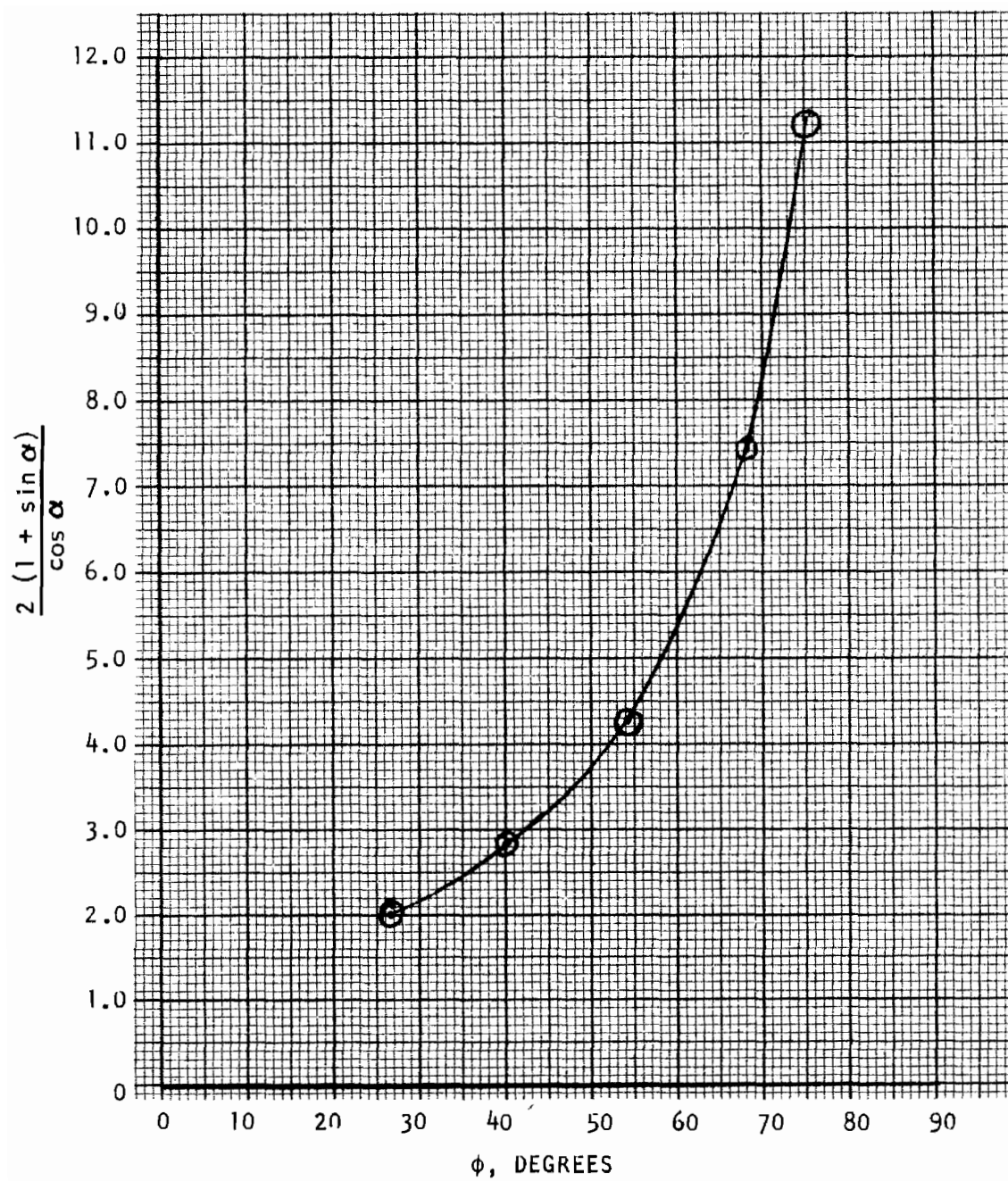


Figure B-5. Contact Length Function vs Wedge Angle

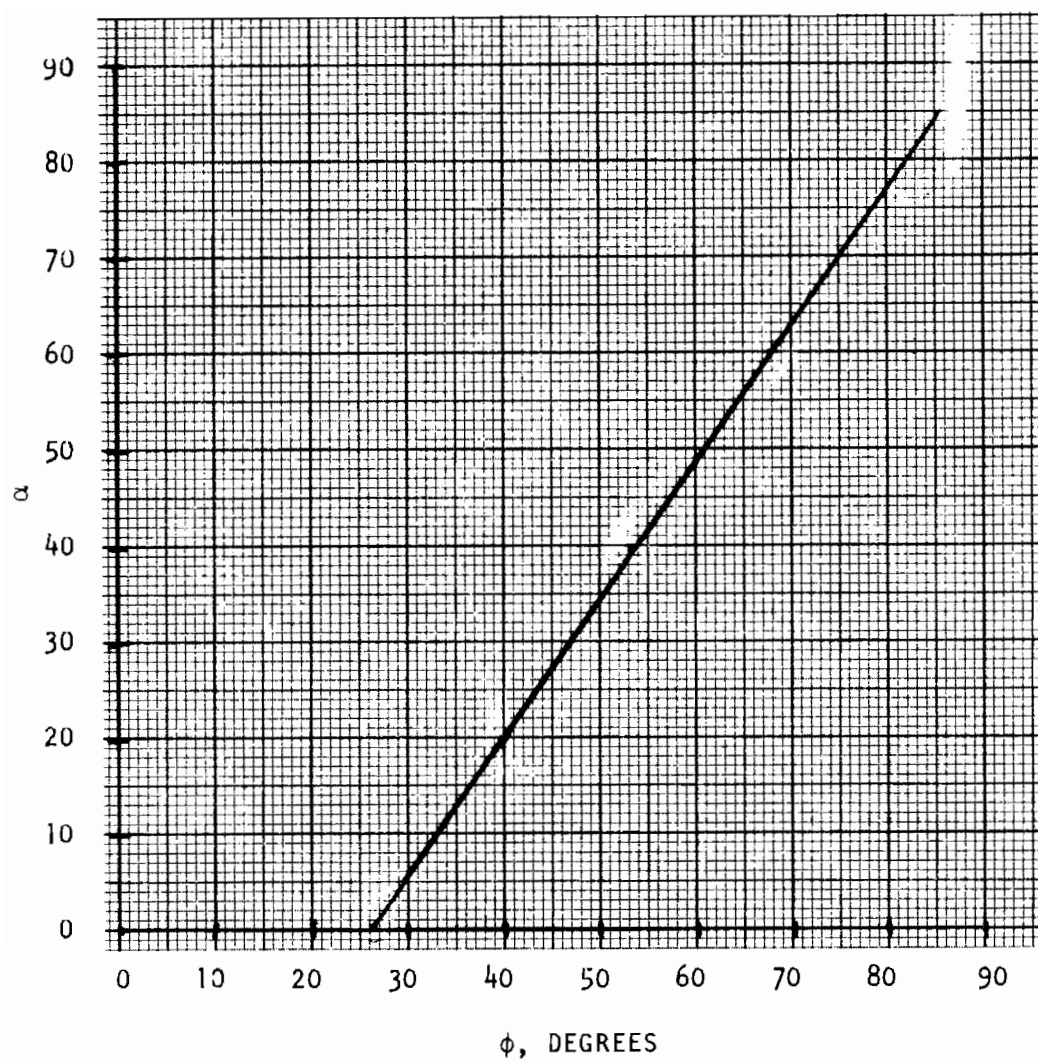
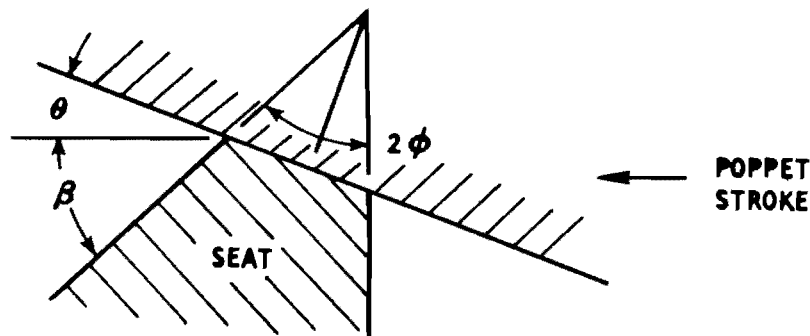


Figure B-6. Deformed Wall Angle vs Wedge Angle

A review of Fig. B-2 through B-5 indicates that a wedge angle between 26.5 and 60 degrees should be selected to obtain a reasonable deformation and contact length (ℓ).



For the general case

$$2\phi = 90^\circ - \beta$$

For a symmetrical wedge

$$\beta = 90^\circ - 2\theta$$

It is desirable to keep (θ) small to achieve maximum scrubbing during closure. With $\theta = 20^\circ$, $\beta = 50^\circ$, and $\phi = 20^\circ$ (symmetrical wedge), excessive deformation is required to generate sufficient contact length (ℓ).

Selecting $\theta = 20^\circ$ and $\beta = 20^\circ$ results in $\phi = 35^\circ$; thus, the wedge is unsymmetrical. It is assumed, however, that the criteria developed may be applied to an unsymmetrical wedge without gross error.

The following data were obtained from Ref. 10 for electrolytic, tough pitch copper (oxygen-free material has identical mechanical properties):

Condition	Yield Stress,* ksi	Tensile Stress, ksi	Rockwell F Hardness
Soft	10	32	40
1/8 Hard	28	36	60
1/4 Hard	30	38	70
1/2 Hard	36	42	84
Full Hard	45	50	90

*0.5 percent elongation; $\nu = 0.33$; $E = 17 \times 10^6$ psi

ELASTIC ANALYSIS

Elastic analysis of the cylindrical seat load-deflection is based on the following assumptions:

1. The actual meridional curve of the tube wall can be represented adequately by midlength expansion caused by internal pressure

and equations that describe tip angle and deflection under uniform end shear.

2. Elastic instability will not occur at the operating stress levels selected.
3. Uniform end shear may be approximated by a uniformly distributed load concentrated at the end.
4. The end support (poppet) is at an angle equal to that assumed by the loaded tube, hence, no end bending moments exist placing the tube outer wall in compression.

The following definitions, nomenclature, and equations have been abstracted from Ref. 2.

Definitions



Membrane Stresses:

S_1 = meridional stress, constant through wall
 S_2 = hoop stress, constant through wall

Discontinuity Stresses:

S'_1 = meridional bending stress, linear through wall
 S'_2 = hoop bending stress, linear through wall
 S_s = shear stress on circumferential sections, constant through wall

Sign Convention:

<u>Stress</u>	<u>Sign</u>	<u>Condition</u>
S_1	+	Tensile
S_2	+	Tensile
S'_1	+	Tensile on convex surface
S'_2	+	Tensile on convex surface

Superposition of stresses gives:

$$S_1 + |S'_1| = \text{maximum meridional}$$

$$S_2 + |S'_2| = \text{maximum hoop}$$

Nomenclature

S = stress, psi
 t = thickness, inch
 R = tube radius, inch
 p = pressure, psig
 ψ = change in wall slope at edge of tube, radians
 δ = radial deflection of tube end, inch
 V = transverse shear normal to wall, lb/in.
 M = bending moment, in.-lb/in.

$$D = \frac{Et^3}{12(1 - \nu^2)}, \text{ in.-lb}$$

$$\lambda = \left[\frac{3(1 - \nu^2)}{(Rt)^2} \right]^{1/4}, \frac{1}{\text{in.}}$$

x = distance from end of tube, inch
 E = modulus of elasticity, psi
 ν = Poisson's ratio

Equations

Case 1. Cylinder under uniform internal or external pressure:

$$S_2 = \frac{PR}{t}, \psi = 0$$

$$\delta = \frac{R}{E} (S_2 - \nu S_1)$$

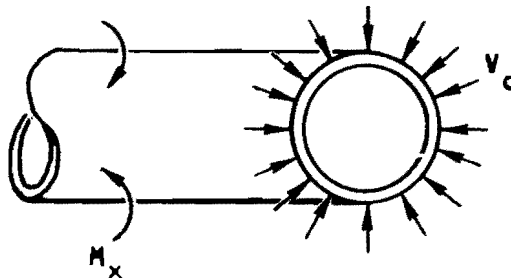
$$(S_1 = 0 \text{ from pressure})$$

For previously defined constants, these equations reduce to

$$S_2 = \frac{0.235p}{t}$$

$$\delta = 3.25 \times 10^{-9} \frac{p}{t} - 4.57 \times 10^{-9} S_1$$

Case 14. Cylinder under uniform end shear (length greater than $6/\lambda$):



$$\begin{aligned}
M_x &= \frac{V_o}{\lambda} e^{-\lambda x} \sin \lambda x \\
S'_1 &= \frac{6 M_x}{t^2}, \quad S'_{1(\max)} = \frac{1.932 V_o}{\lambda t^2} \text{ at } x = \frac{\pi}{4\lambda} \\
S'_2 &= \nu S'_1, \quad S_s = \frac{V}{t} \\
S_2 &= \frac{-2 V_o \lambda R}{t} e^{-\lambda x} \cos \lambda x \\
\delta &= \frac{-V_o}{2D \lambda^3}, \quad \psi = \frac{-V_o}{2D \lambda^2}
\end{aligned}$$

For previously defined constants, these equations reduce to

$$\begin{aligned}
|S_2 \pm S'_2|_{\max} &\cong |S_2| \\
S'_1 &= \frac{0.733 V_o}{t^{1.5}} (\max) \\
S_2 &= \frac{1.24 V_o}{t^{1.5}} (\max) \\
\delta &= 1.72 \times 10^{-8} \frac{V_o}{t^{1.5}} \\
\psi &= \lambda \delta \\
S_s &= \frac{V_o}{t}
\end{aligned}$$

ELASTIC-PLASTIC ANALYSIS

This analysis combines the results of the wedge plastic flow and elastic analyses to predict the seat land width and associated loads. For this analysis it is assumed that maximum pressure = 1500 psig and axial load is sufficient to put the poppet on the seat stop.

Nomenclature

- F = force, lb/in.
- p = pressure, psig
- θ = poppet half angle, degrees
- μ = coefficient of friction
- δ = seat deformation and deflection, inch

Δx = poppet motion (axial), inch
 Δy = poppet motion (radial), inch
 ΔN = poppet motion (normal), inch
 K = constants evaluated in Table B-1

Subscripts.

a = applied force
 R = reaction force
 x = axial
 y = radial
 N = normal
 t = tangential
 e = elastic
 p = plastic

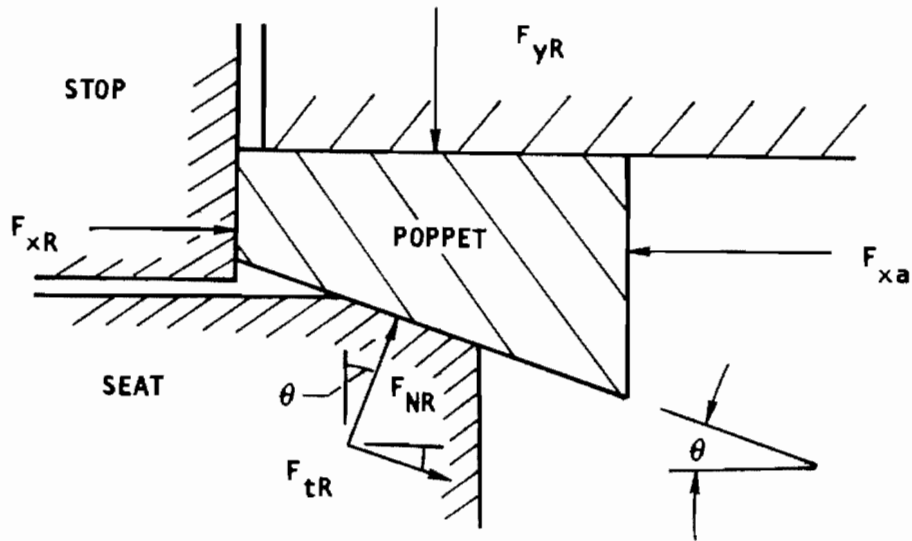
TABLE B-1

LIST OF CONSTANTS

Symbol	Value	Definition
K_1	3.25×10^{-9}	R^2/E
K_2	4.57×10^{-9}	$R \nu/E$
K_3	1.72×10^{-8}	$(2 D \lambda^3)^{-1}$
K_4	0.837	$\cos\theta - \mu \sin\theta$
K_5	0.624	$\sin\theta + \mu \cos\theta$
K_6	0.342	$\sin\theta$
K_7	0.364	$\tan\theta$
K_8	0.940	$\cos\theta$
K_9	1.125	$0.74 f(\phi)$
K_{10}	0.733	$1.932/\lambda t^{1/2}$
K_{11}	0.235	R
K_{12}	1.24	$2(\lambda t^{1/2}) R$

NOTE: $\lambda t^{1/2} = 2.64$ with $\nu = 0.33$

Poppet-Seat Force Balance



Force balance equations are given by

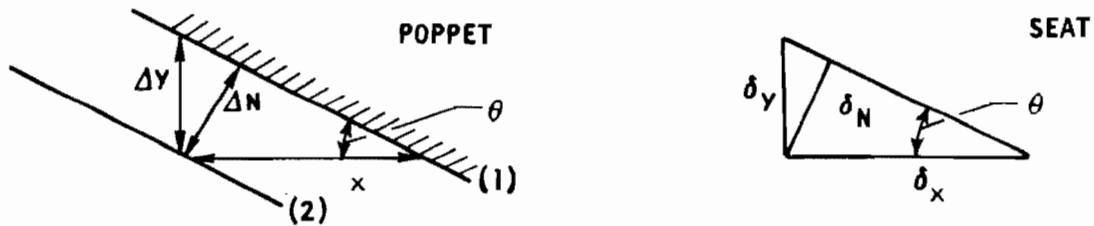
$$F_{NR} (\cos\theta - \mu \sin\theta) = F_{yR} \quad (B-4)$$

$$F_{NR} (\sin\theta + \mu \cos\theta) = F_{xa} - F_{xR} \quad (B-5)$$

where

$$F_{tR} = \mu F_{NR}$$

Poppet Motion and Seat Deflection

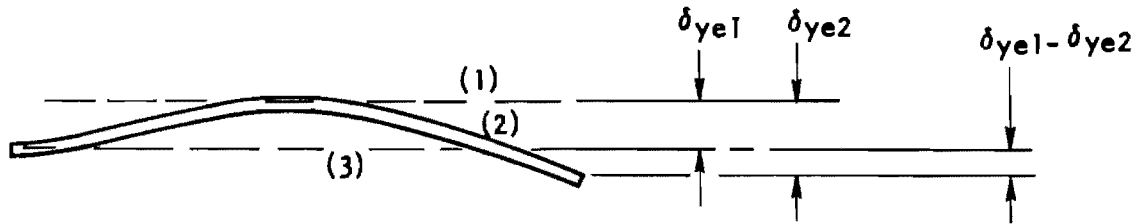


As the poppet moves (Δx) from (1) to (2), the seat deforms and deflects (δ_x). By assuming the deformed and deflected seat conforms to the contour of the rigid poppet and neglecting the angle of the deflected tube (ψ), the following related seat deflections are produced:

$$\left. \begin{aligned} \delta_N &= \delta_x \sin\theta, & \Delta N &= \delta_N \\ \delta_y &= \delta_x \tan\theta, & \Delta y &= \delta_y \\ \delta_N &= \delta_y \cos\theta, & \Delta x &= \delta_x \end{aligned} \right\} \quad (B-6)$$

Tube Elastic Deflection

Elastic tube deflections are shown schematically below:



where

- (1) = tube deflection from internal pressure and compressive load from poppet (δ_{ye1})
- (2) = meridional curve of loaded tube end deflection (δ_{ye2}) resulting from poppet radial load
- (3) = centerline of tube without pressure or load

Combining equations and constants from Table B-1 gives

$$\begin{aligned} \delta_{ye1} &= K_1 \frac{P}{t} - K_2 S_1 \\ S_1 &= (F_{xa} - F_{xR})/t \quad (\text{compressive}) \\ \delta_{ye1} &= K_1 \frac{P}{t} + K_2 (F_{xa} - F_{xR})/t \\ \delta_{ye2} &= K_3 \frac{V_o}{t^{1.5}} \\ V_o &= F_{yR} \\ \delta_{ye2} &= K_3 \frac{F_{yR}}{t^{1.5}} \end{aligned} \quad (B-7)$$

$$\delta_{ye2} = K_3 \frac{F_{yR}}{t^{1.5}} \quad (B-8)$$

As seat deformation is assumed perfectly plastic and the poppet is against the stop

$$\delta_{ye1} - \delta_{ye2} = \delta_{ye} \quad (B-9)$$

and (δ_{ye}) is constant regardless of load or pressure.

With $\theta = 20^\circ$, $\mu = 0.3$, Eq. B-4, B-5, and B-6 become

$$\left. \begin{aligned} K_4 F_{NR} &= F_{yR} \\ K_5 F_{NR} &= F_{xa} - F_{xR} \\ \delta_N &= K_6 \delta_x \\ \delta_y &= K_7 \delta_x \\ \delta_N &= K_8 \delta_y \end{aligned} \right\} \quad (B-10)$$

From Eq. B-7, B-8, and B-9

$$\delta_{ye} = \frac{1}{t} \left[K_1 p + \frac{K_2 K_5}{K_4} F_{yR} - \frac{K_3 F_{yR}}{\sqrt{t}} \right]$$

With $t \ll 1.0$

$$\begin{aligned} \frac{K_3}{\sqrt{t}} &\gg \frac{K_2 K_5}{K_4} \\ \delta_{ye} &\approx \frac{1}{t} K_1 p - \frac{K_3 F_{yR}}{\sqrt{t}} \end{aligned} \quad (B-11)$$

Evaluating (δ_{ye}) at $p(\max)$ and $F_{yR}(\max)$, the latter corresponding to $F_{xa} - F_{xR}(\max)$ yields

$$F_{yR} = \frac{t^{1.5}}{K_3} \left(\mp \delta_{ye} + \frac{K_1 p}{t} \right) \quad (B-12)$$

Pressure-derived seat stress data are obtained directly from Eq. B-12.

Plastically Deformed Seat

From the plastic analysis

$$\begin{aligned} \frac{P}{S_0} &= K_9 = (0.74)(1.52) \text{ with } P_y = \frac{F_{NR}}{\ell}, \text{ then} \\ \ell &= \frac{F_{NR}}{K_9 S_0} \end{aligned} \quad (B-13)$$

From Eq. B-10 and B-13

$$\frac{F_{xa} - F_x}{\ell} = K_5 K_9 S_0$$

The load required to produce a given (ℓ) varies linearly with S_0 (tensile yield strength) for fixed θ , β , and hence ϕ .

Tube Wall Stresses

The seat must withstand the stresses resulting from maximum poppet load (poppet against the stop) and internal pressure (1500 psig proof); these stresses are given by

$$S_1 + S'_1 = \frac{F_{xa} - F_{xR}}{t} + K_{10} \frac{V_o}{t^{1.5}}$$

$$S_1 = \frac{F_{xa} - F_{xR}}{t}$$

$$S_2 = K_{11} \frac{p}{t} - K_{12} \frac{V_o}{t^{1.5}}$$

$$S_s = \frac{V_o}{t}$$

With $V_o = F_{yR}$ and Eq. B-10, $F_{ax} - F_{xR} = \frac{K_5}{K_4} F_{yR}$, the above becomes

$$S_1 + S'_1 = \frac{K_5 F_{yR}}{K_4 t} + K_{10} \frac{F_{yR}}{t^{1.5}} \quad (B-14)$$

$$S_2 = K_{11} \frac{p}{t} - K_{12} \frac{F_{yR}}{t^{1.5}} \quad (B-15)$$

$$S_s = \frac{F_{yR}}{t} \quad (B-16)$$

With $t \ll 1.0$, S_2 and $S_1 + S'_1 > S_s$.

As the tube is relatively thick walled, S_2 and $S_1 + S'_1 \rightarrow S_0$ without buckling. Therefore, at maximum load and pressure

$$S_0 = \frac{K_5 F_{yR}}{K_4 t} + \frac{K_{10} F_{yR}}{t^{1.5}} \quad (B-17)$$

Seat Land Length

From Eq. B-10 and B-13,

$$\ell = \frac{F_{yR}}{K_4 K_9 S_0}$$

Combining with Eq. B-17 yields

$$\ell = \frac{t^{1.5}}{K_5 K_9 \left(\sqrt{t} + K_{10} \frac{K_4}{K_5} \right)}$$

Numerical solution with $R = 0.235$ inch yields the following:

<u>t, inch</u>	<u>ℓ, inch</u>	<u>R/t</u>
0.010	0.00131	23.5
0.020	0.00355	11.7
0.030	0.00641	7.85

Solution for larger (t) is not valid as stress equations require $R/t > 10$.

From Eq. B-10 and B-13, the required force is

$$F_{xa} - F_{xR} = K_5 K_9 S_0 \ell$$

Using annealed copper with $S_0 = 10,000$ psi and $\ell = 0.00641$ inch gives $F_{xa} - F_{xR} = 45$ lb/in. From Eq. B-10, $F_{yR} = 60.4$ lb/in.

The resulting hoop stress at $p = 1500$ psig from Eq. B-15 is $S_2 = 2650$ psi compressive. The shear stress from Eq. B-16 is $S_s = 2010$ psi.

Deflections and Deformation

From Eq. B-2 and Fig. B-5 at $\phi = 35^\circ$

$$\delta_{NP} = \frac{\ell - \ell_0}{2.45}$$

Selecting $\ell_0 = 0.001$ gives $\delta_{NP} = 0.00221$ inch. From Eq. B-11 with $p = 1500$ psig and $F_{yR} = 60.4$ pounds (maximum values with the poppet on the stop), $\delta_{ye} = -3.72 \times 10^{-5}$ inch (minus sign indicates radial squeeze. From Eq. B-10, $\delta_{xp} = 0.00647$ inch, $\delta_{xe} = 0.000102$ inch, and $\Delta x = 0.00657$ inch.

Seat Stress

From Eq. B-12 with $p = 0$, $F_{yR} = 11.25 \text{ lb/in.}$ From Eq. B-10, $F_{xa} - F_{xR} = 8.39 \text{ lb/in.}$ This load places the poppet against the stop. From Eq. B-10, $F_{NR} = 13.4 \text{ lb/in.}$ The initial seat stress is then approximately

$$\frac{F_{NR}}{\ell_0} = \frac{13.4}{0.001} = 13,400 \text{ psi}$$

From Eq. B-1 and Fig. B-3, the stress required for yield initiation is $P_y = K_9 S_0 = 11,250 \text{ psi.}$ From Fig. B-4, the stress required for fully developed plastic flow is $1.9 P_y = 21,400 \text{ psi.}$ As the internal pressure is applied, the seat stress would reach

$$\frac{F_{NR}(\text{max})}{\ell_0}$$

or 72,000 psi if the seat did not deform. This is far more than the value of 21,400 psi required to obtain fully developed plastic flow.

Seat Elasticity

The seat elasticity (Δx_e) is the distance the poppet can travel and still touch the seat at zero load; it is given by

$$\Delta x_e = \frac{1}{K_7} \left(\tau \delta_{ye} + \frac{K_1 p}{t} \right)$$

with the results plotted in Fig. B-7.

Seat Stress vs Pressure and Load

From Eq. B-10 and B-12,

$$F_{NR} = \frac{t^{1.5}}{K_3 K_4} \left(\tau \delta_{ye} + \frac{K_1 p}{t} \right)$$

$$\frac{F_{NR}}{\ell} = \text{seat stress}$$

From Eq. B-10, $F_{xa} - F_{xR} = K_5 F_{NR}$ with the results plotted in Fig. B-8.

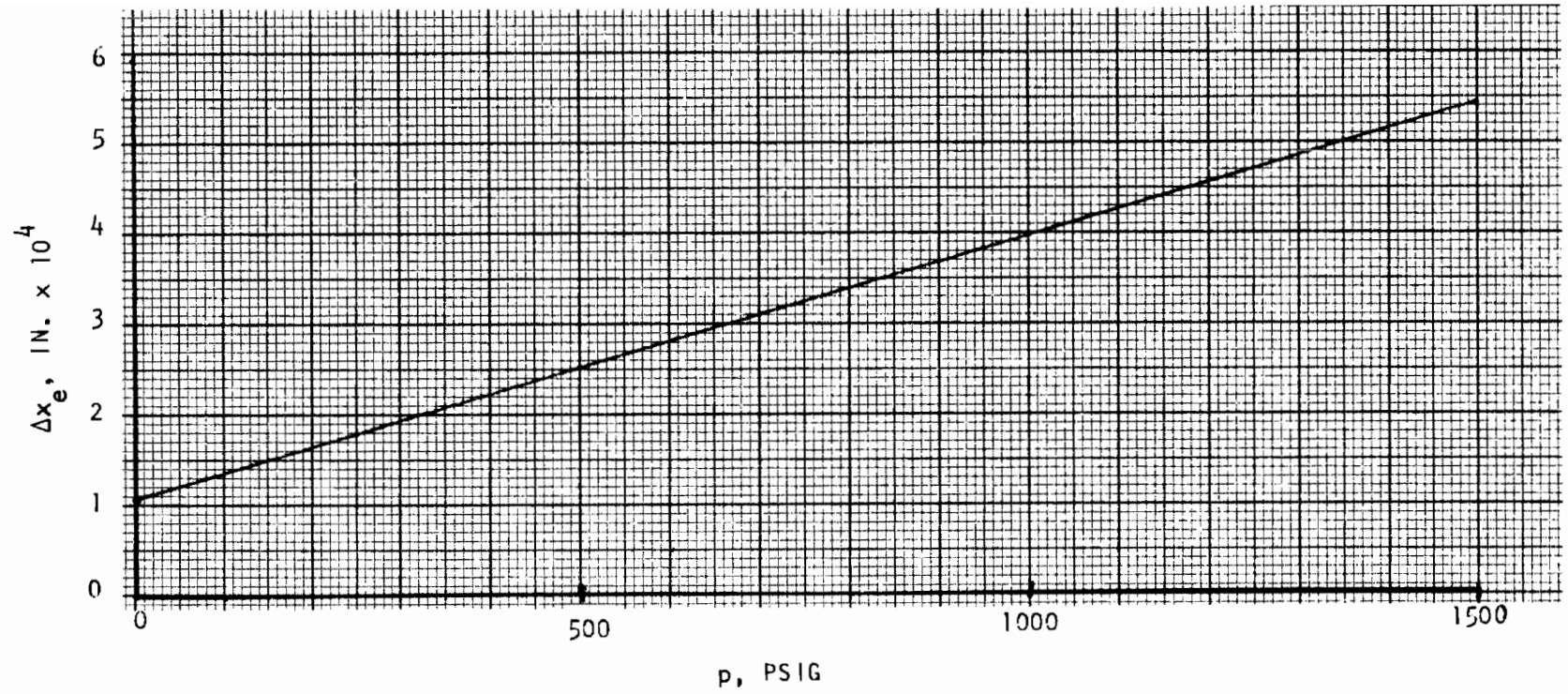


Figure B-7. Seat Elasticity vs Pressure

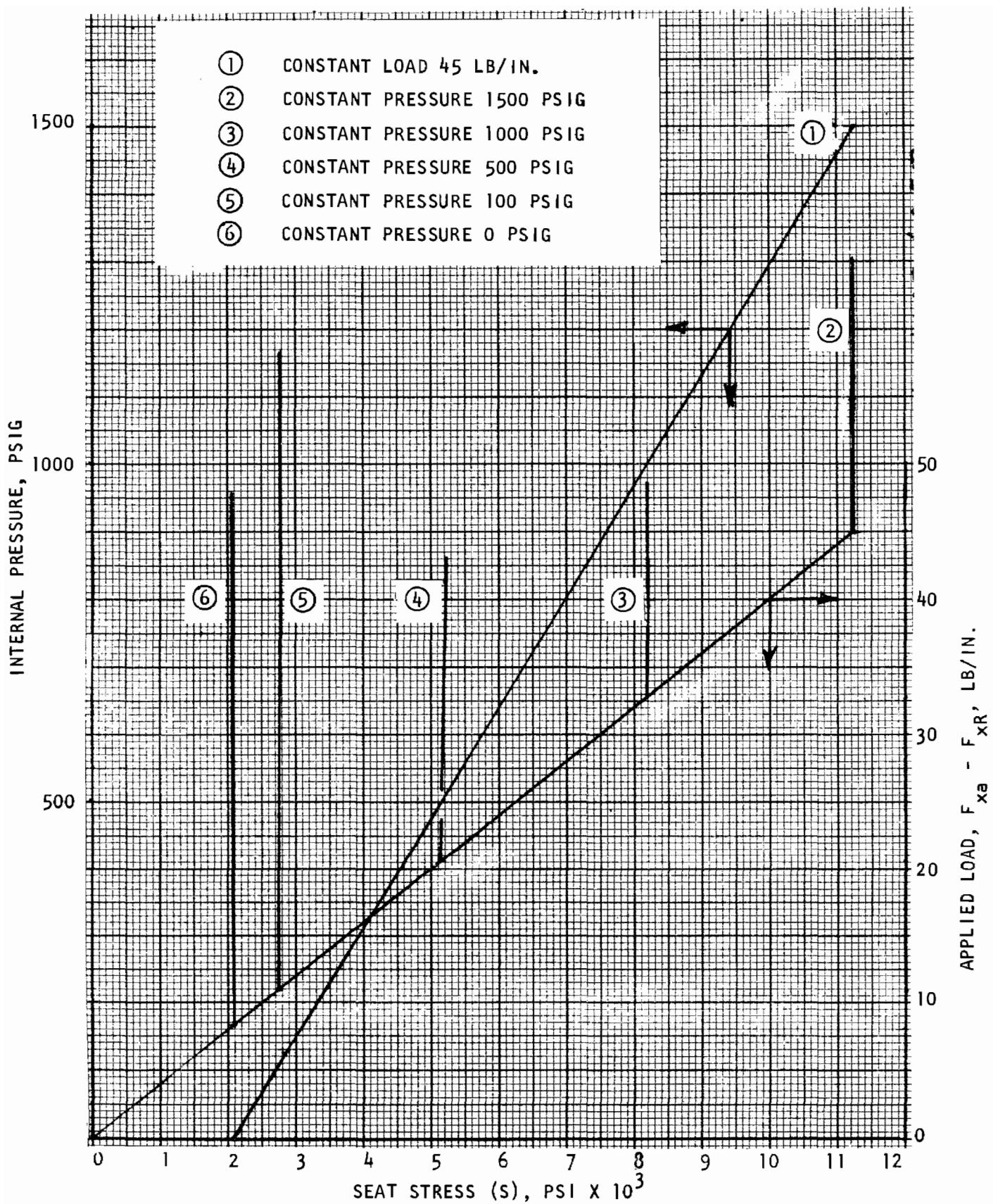


Figure B-8. Shear Seal Load Parameters

APPENDIX C

STATIC TEST FIXTURE

Experimental evaluation of poppet and seat sealing characteristics required test fixtures that did not introduce variables which could influence the seating parameters under observation. Basically this involved the precise location of sealing surfaces with a means for accurately loading them and measuring leakage as a function of that load. The test fixture used for static evaluation of contamination effects (static tester) was fabricated to provide this capability for the initial poppet and seat evaluation program (Ref. 11). Minor changes evolved during subsequent programs, however, the basic features remained unchanged.

In Phase II static testing, the static tester was used for on-seat evaluation of model surfaces, both with and without entrapped particulate matter. The tester provided for the establishment of control, clean-condition test model load-leakage data for comparison with subsequent information obtained with entrapped test particles. As an adjunct to these tests, particle envelopment loads and particle-surface deformation characteristics could be evaluated.

The following paragraphs describe salient features and the functional capability of the static tester. During Phase II tests, certain tester characteristics and limitations were uncovered and evaluated. These are discussed and their effect on output data is analyzed.

DESCRIPTION

A detailed description of static tester design criteria, assembly, check-out and developmental changes was reported in Ref. 3. The following is a reiteration of basic features as shown in the schematic (Fig. C-1) and detail static tester drawing (Fig. C-2).

Hydrostatic Bearing

The hydrostatic pressure-supported piston is the fundamental design feature of the static tester and permits essentially frictionless loading of test model surfaces. Fabricated with a 0.0002-inch diametral clearance, the aluminum oxide flame-plated piston constricts while the body expands with application of filtered (0.45 micron) gas pressure to form a 50-microinch tapered flow path from center to ends. Pressure gradient along these tapers provides a centering force capable of withstanding a 105-in.-lb moment about the piston center with 450 psig supply pressure (termed film pressure). To provide an additional centering load margin, film pressure of 600 psig was used for all testing.

As originally designed, the piston and test poppet were restrained from rotating by a flexure device attached to the tester body. Because exact-position poppet reassembly was not necessary (in fact, reorientation between tests was practiced), the piston was merely taped to the body to provide gross control of preferred position.

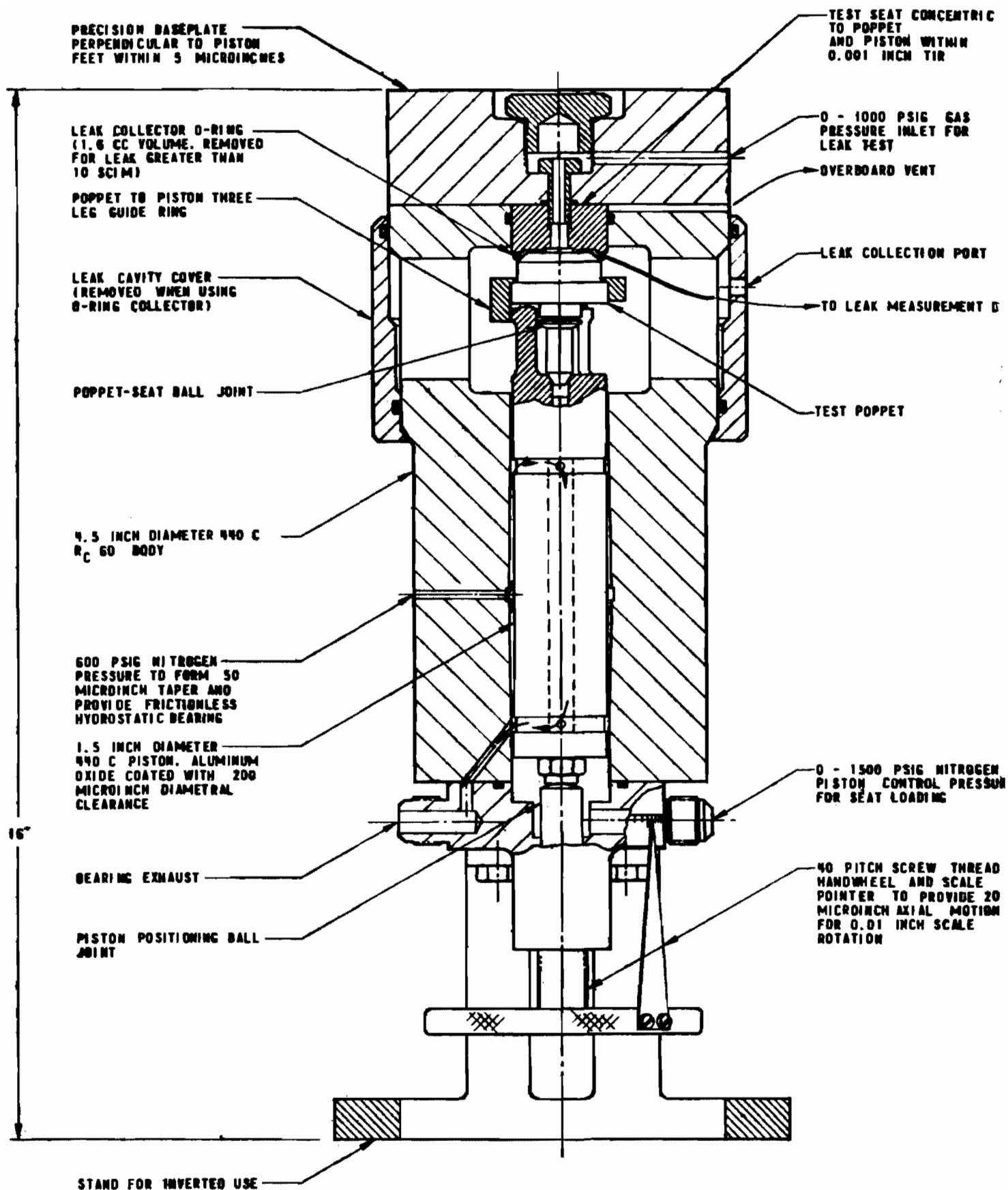
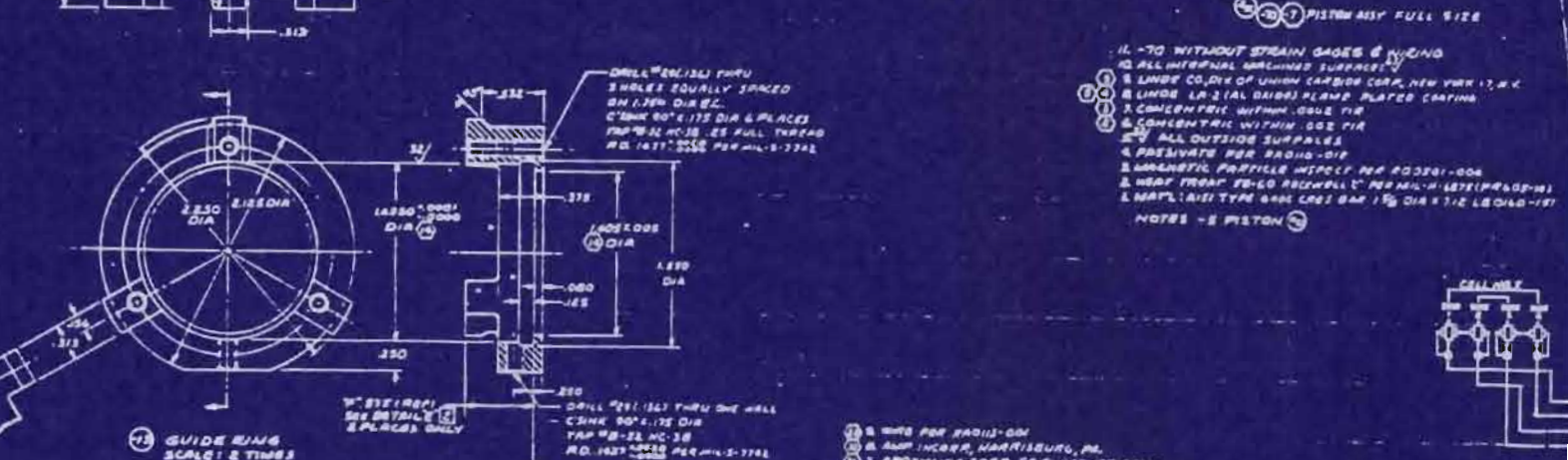
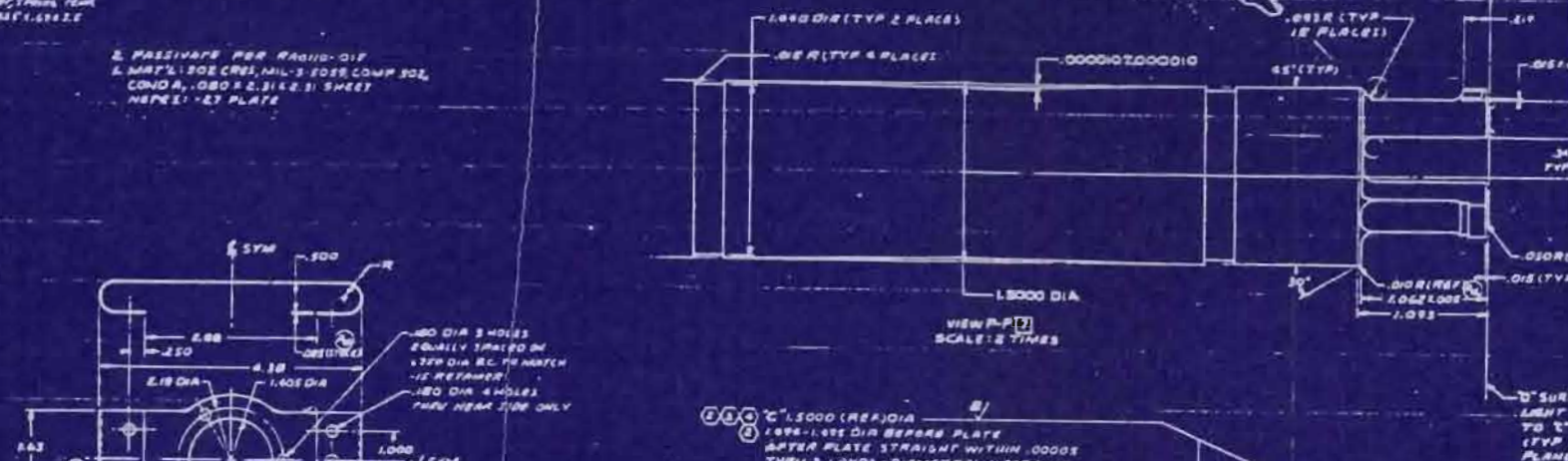
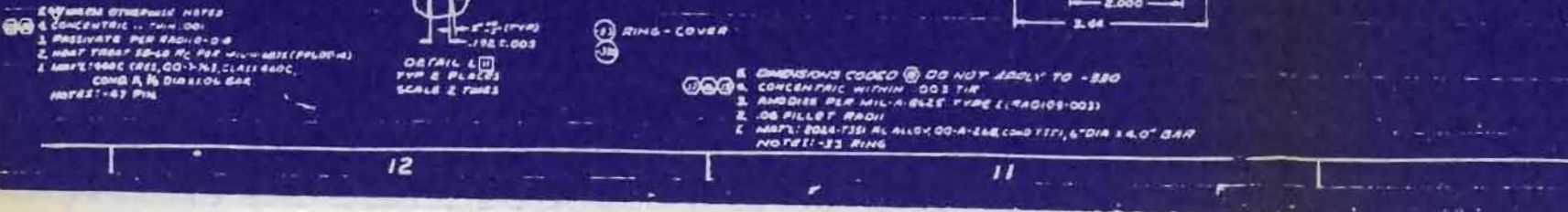
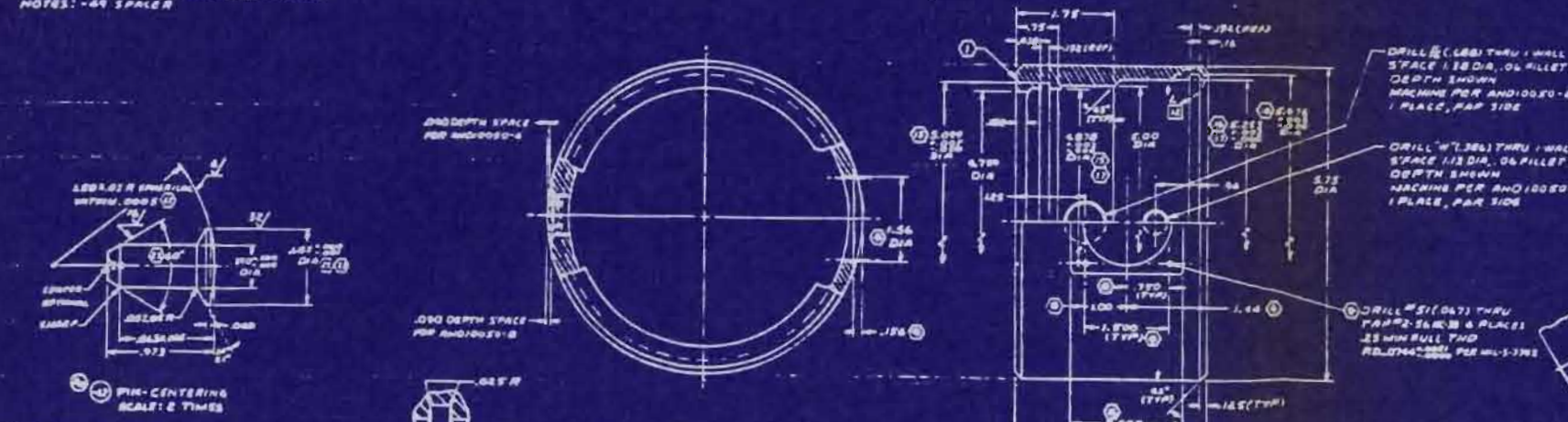
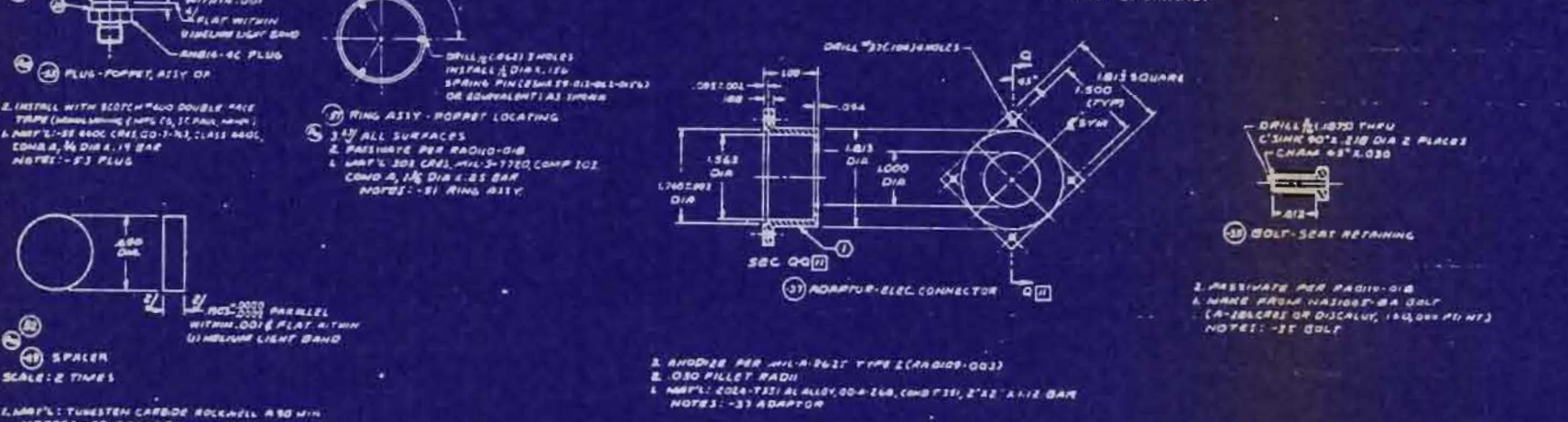
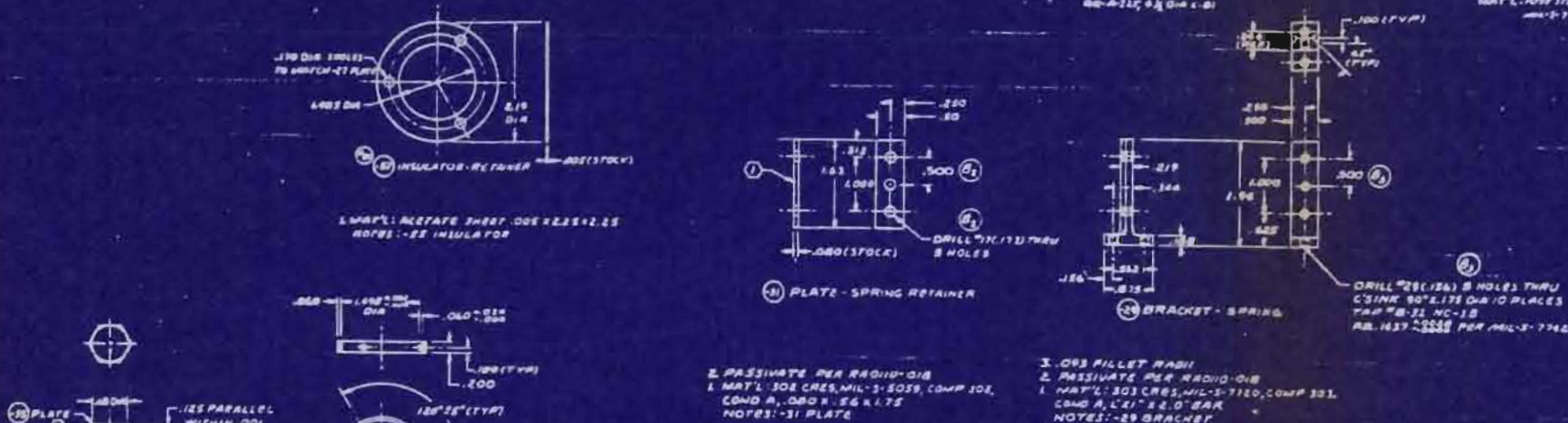
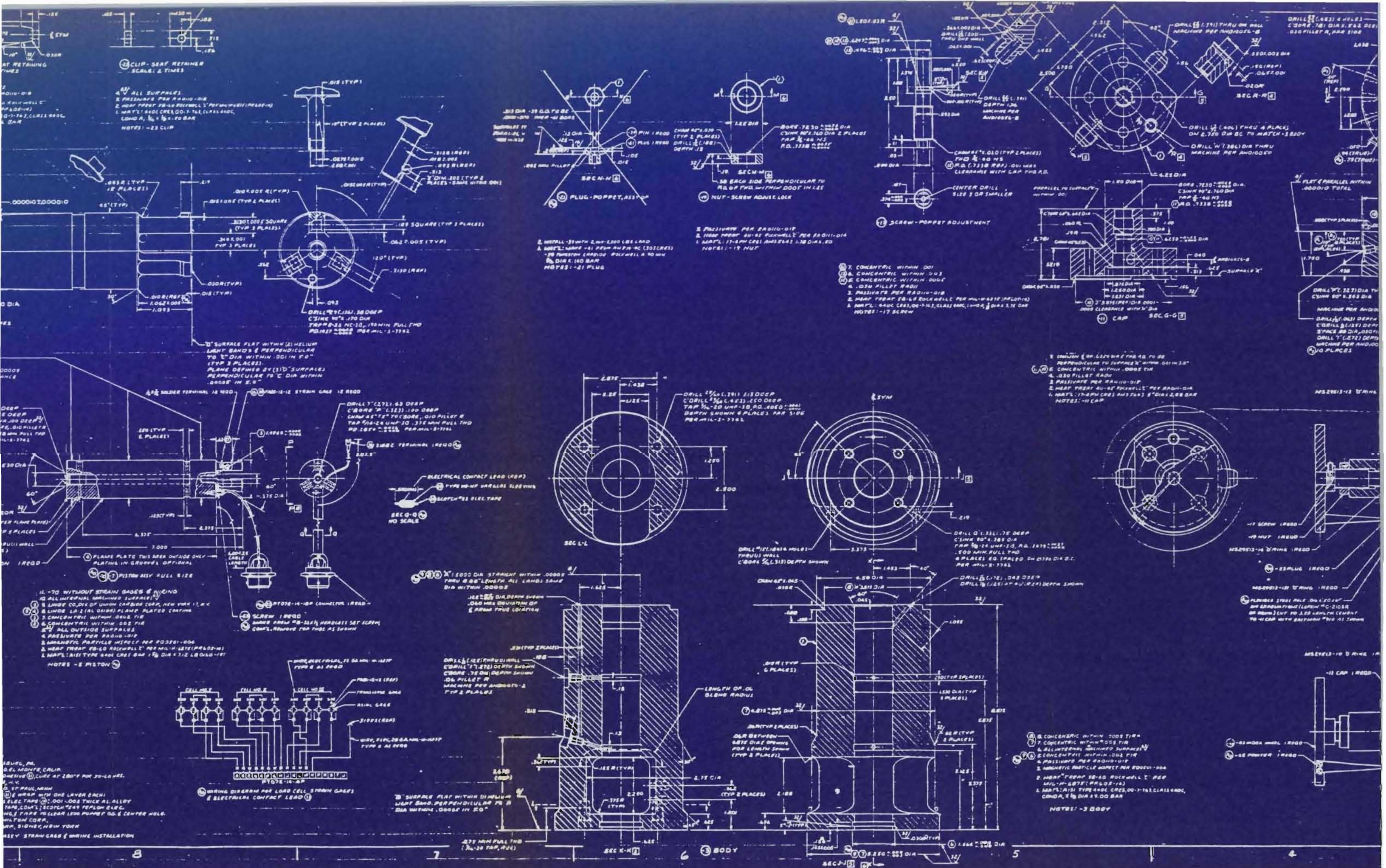


Figure C-1. Poppet and Seat Static Tester





Poppet and Seat Assembly

The static tester was designed to permit precision poppet and seat assembly within the limits of practical handling ease and access. Maximum diametral clearance between seat-body, poppet-guide ring, and guide ring-piston ranged from 0.0004 to 0.0006 inch. Combined with individual part concentricities, poppet and seat seating diameters under worst tolerance conditions could be misaligned a maximum of 0.00125 inch. Average eccentricity, however, is estimated to be less than 0.001 inch.

Tester construction dictated that the seat be installed first. The method of seat installation adopted for the static tester proved troublesome because of contamination problems. Wrench and nut wear particles were generated during seat bolt clamping, but installation of the clamping bolt cavity closure nut also introduced particulates into the inlet pressure flow path. A common seat clamping and inlet pressure bolt, such as employed on the dynamic tester (refer to Appendix F), would have minimized this problem.

Originally, the poppet was clamped into place using the guide ring. With the advent of ball joint loading, the tester was used in the inverted position shown in Fig. C-1 and the poppet was restrained only by the guide ring clearances. Thus the poppet was essentially free floating. The ball joint feature was adopted to permit testing to relatively low loads without the necessity for extraordinary parallelism control required of the clamped condition. (Out-of-parallel seating leakage is extremely load sensitive until full seat surface contact is achieved.) The ball joint was intended to permit no-load compliance of seating surfaces, thus excluding the influence of nonparallelism, either from detail parts or assembly contaminants. As subsequently described, however, facets of the ball joint design contributed to data error and negated some test results.

Leak Collection

Two methods of poppet-seat leakage collection were employed. For leakage greater than 10 scim, the tester cavity served as a collection chamber (cover installed) with flow directed from the cover port to leak-measurement devices. For lesser flowrates, particularly those in the 10^{-2} to 10^{-5} scim range, a leak volume-reducing ring was used; this took two forms. An O-ring, drilled for insertion of an 0.040-inch-diameter brass tube, was initially employed. Later tests used an aluminum leak-collector ring (Section III, Phase II Test Models) sealed to poppet and seat with centerpoint lubricant. Unlike the O-ring, the latter device produced no variable load input to system forces. Plastic tubing from both collector rings carried leakage flow to flowmeter or buret measuring devices.

Poppet and Seat Loading Capability

The piston control pressure cavity was designed for operation to 2500 psig. Thus, with the 1.50-inch-diameter piston, a gross pressure-area loading force of 4400 pounds maximum was available. The net seat force is reduced by the amount required to balance (1) inlet pressure-effective seat area force (nominally 181 pounds at 1000 psig inlet pressure) and (2) other opposing loads as subsequently described.

Axial Position Control

The handwheel with 40-pitch thread and ball joint contact provided poppet-seat gap control accurate to ± 2 microinches during off-seat tests in previous investigations. Aside from assembly and disassembly operations, its use in the subject effort was (1) providing a minimum-gap, off-seat positive stop for balance pressure measurements, and (2) relatively sensitive hand closure during particle deformation tests.

SEAT LOADING ANALYSIS

Much of the data on static particle loading effects depends on precise definition of a control or base leakage characteristic condition. In past programs a high degree of accuracy was repeatably demonstrated in correlation of balance pressure obtained from (1) test and (2) computation based upon dimensions and laminar flow pressure distribution across the seat land. With the flat poppet and seat, agreement within 0.5 percent was usual. These early tests were performed with the poppet clamped. An electrical signal from a microammeter was employed to precisely define contact. However, with introduction of the ball joint the electrical contact definition could not be used and balance pressure was interpreted from a pronounced leak change. Most balance pressure tests were performed with 300 psig inlet pressure and the test value compared against (P_{cb}) computed from measured effective area with agreement usually within 0.6 percent. Balance pressure for 1000 psig inlet pressure was then computed from these data.

The preceding results were assumed to prove the method and consequently balance pressures were computed for most static tests herein. However, initial attempts to establish control stress-leakage model data at low loads (down to 4 pounds) with 1000 psi inlet pressure indicated the presence of uncontrolled variables. The usual condition was one of high leakage at low loads, often accompanied by a "crossover" in the stress-leakage data. This was identified by greater leakage with decreasing load than at the corresponding initially increasing load point (Ref. 3, Test Models H, L, and M). Initial attempts at correcting this condition involved variation in assembly and cleaning procedures and model refinishing since it was assumed that contaminants or "nodules" caused high leakage. Tests with particles, however, revealed that a relatively large amount of surface upset apparently could be enveloped following particle removal without significant effect. An eccentric load hypothesis was then developed which was eventually proved to be the primary cause of high leakage and crossover phenomena.

The purpose of this analysis is to first present basic seat-loading equations and from these analytically relate potential load error limits applicable to past and current test model data. The error analysis is presented in two parts:

1. Axial load error (E_p) caused by balance pressure measurement and 0.1 percent Heise pressure gage error. (This was the only significant error recognized in previous programs.)

2. Torque load error (E_e) caused by eccentricity between the ball joint point-of-contact and seat land pressure-area axis.

These analyses are supported by correlating test model data followed by a summary of test model data validity for this and previous programs.

Static Axial Force Balance

Previous program efforts displayed actual model leakage data in terms of a stress-leakage plot. The common parameter stress term was usually based on the projected land area and thus represented an apparent (average) stress rather than seal contact pressure. In most cases, this procedure has been followed herein.

General Force Balance Equation. The following expressions were used to compute apparent seat stress from the control pressure-piston area loading for the inverted static tester:

$$\sum F = 0 = P_c A_p - P_1 A_e - W - F_o - S A_s$$

and

$$S \equiv \frac{F}{A_s}$$

where

$$A_e \equiv \frac{\pi}{4} D_e^2 = \frac{\pi}{4} (D_s + \frac{L}{3})^2 = \text{effective seating area for flat plate, laminar flow pressure distribution, sq in. (Ref. 3).}$$

(For the standard flat model, $D_s = 0.470$ inch, $L = 0.03$ inch, and $A_e = 0.181$ sq in.)

A_p = static tester piston area, 1.767 sq in.

A_s = flat seat land normal projected area, sq in. (for standard flat model $A_s = 0.0433$ sq in.)

D_e = effective seat diameter, inches

D_s = mean seat diameter, inches

F = seat force, pounds

F_o = leak collector O-ring force, 3.5 ± 0.7 pounds

L = flat seat land width, inches

P_1 = seat inlet pressure, psig

P_c = piston control pressure, psig

S = apparent seat stress, psi

W = piston assembly weight, variable with poppet material and retaining method, pounds

Balance Pressure. To compute seat stress, the control pressure required to nullify extraneous forces must first be established. This was done directly by a balance pressure test or calculated indirectly. For the

balance pressure test, the piston was advanced by handwheel control until a maximum poppet-seat gap of about 50 microinches was established. Inlet pressure and sufficient control pressure to ensure closure were applied. Control pressure was then reduced until an abrupt inlet pressure decrease or leakage increase (into the audible range) occurred as the poppet unseated; this was defined as P_c balance pressure (P_{cb}).

As was noted, however, balance pressure was usually computed. Balance pressure is defined from the force balance equation for zero seat stress as

$$P_{cb} \equiv \frac{P_1 A_e + W + F_o}{A_p} \quad (S = 0)$$

Seat Stress. Seat stress (S) is related to the increase of control pressure above the balance point ($P_{c\Delta}$). Thus,

$$S = \frac{(P_{cb} + P_{c\Delta}) A_p - (P_1 A_e + W + F_o)}{A_s}$$

Combining these expressions gives

$$S = \frac{P_{c\Delta} A_p}{A_s}$$

Seat Stress Error. Seat stress error results from an error in balance pressure measurement (even if calculated) and accumulated gage errors. The balance pressure error is given by

$$\Delta P_{cb} = \frac{\Delta P_1 A_e + \Delta F_o}{A_p} + P_{cbe}$$

where Δ preceding the term denotes a "change in"; other terms are estimated as follows:

$$\Delta F_o = \pm 0.7 \text{ pound}$$

$$\Delta P_1 = \begin{array}{l} \pm 0.1 \text{ psi gage error (0.1 percent 1000 psi)} \\ \pm 0.1 \text{ psi reading error} \\ \pm 1.0 \text{ psi allowed setting variation} \end{array}$$

$$P_{cbe} = \begin{array}{l} \pm 0.6 \text{ psi gage error (0.1 percent 600 psi)} \\ \pm 0.1 \text{ psi reading error} \\ \pm 0.2 \text{ psi test point interpretation error} \end{array}$$

The rms average of these errors indicates a probable balance pressure error for the standard model ($A_e/A_p = 0.1024$) of ± 0.766 psi. This error is included with the preceding seat stress equation to arrive at the seat stress percentage error defined as

$$E_g = \frac{\Delta S}{S} = \frac{\Delta F}{F} = \frac{(\Delta P_{c\Delta} + \Delta P_{cb}) A_p + \Delta P_l A_e + \Delta F_o}{SA_s}$$

where

$$\Delta P_{c\Delta} = \begin{matrix} \pm 0.6 \text{ psi gage error in excess of initial } P_{cbe} \\ \pm 0.1 \text{ psi reading error} \end{matrix}$$

and other terms as defined for (ΔP_{cb}) above. The rms average of these errors indicates an additive force error of ± 2.04 pounds or ± 46.0 psi for the standard model; corresponding percentage errors are tabulated below:

<u>S,</u> <u>psi</u>	<u>$\pm E_g$,</u> <u>percent</u>
100	46.0
300	15.3
1000	4.60
3000	1.53

Eccentric Load Analysis

Eccentricity (e) between the ball joint contact and seat land axis results in a torque being applied to the poppet. This produces a nonsymmetrical load distribution and requires an increase in balance pressure. Because most static test balance pressures were computed from model inspection data, the net effect is a potential loss in seat load. This error is independent of the preceding gage error.

Figure C-3 is a pictorial schematic of the assembled standard flat poppet and seat. While generally to scale, certain features have been exaggerated to show pertinent dimensions. This schematic includes the free body diagram of significant forces acting on the poppet and related dimensional terms.

Eccentricity (e) is derived from tolerances and clearance, particularly the clearance allowed between the piston legs and ball joint QD, which allows misalignment of the ball joint load axis. Because the ball joint spherical radius (R_B) is larger than the swing radius (R_p), the contact point "U" moves opposite to the direction of motion. A large spherical radius (R_B) was necessary to meet loading requirements. This radius was never directly measured and it is hypothesized that a potentially much larger effective radius may have been caused by overstress in past program testing (Ref. 11, Model E loaded to 4280 pounds compared with ball joint computed yield load of about 2000 pounds). Thus, misalignment of the ball joint as shown would

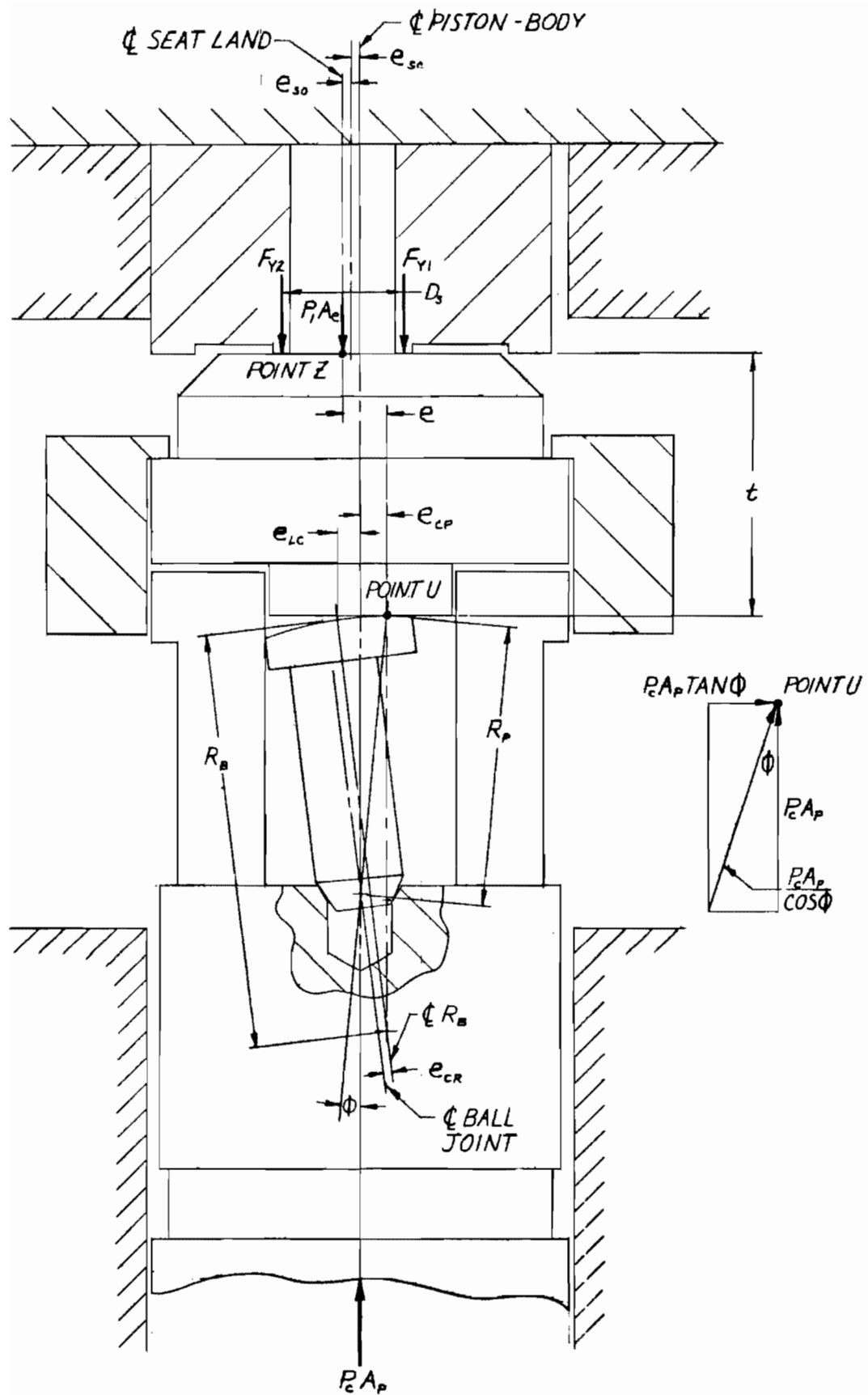


Figure C-3. Flat Poppet and Seat Eccentric Load Schematic

result in much greater eccentricity than indicated by the specified dimensions. Consequently, this analysis explores two cases; the first is for maximum eccentricity and $R_B = 1.5$ inches as designed, and the second the same except $R_B = 5.0$ inches.

Eccentricity Data. Nomenclature and specific data (from Fig. C-2 and C-3) are as follows:

$$\begin{aligned} e_{CR} &= 0.001 \text{ inch} \\ e_{SO} &= 0.00025 \text{ inch} \\ e_{SC} &= 0.00025 \text{ inch} \\ e_{LC} &= 0.004 \text{ inch (computed from 0.002 inch radial clearance)} \end{aligned}$$

Point "U" eccentricity is given by

$$e_{CP} = e_{LC} \left(\frac{R_B}{R_P} - 1 \right)$$

Total eccentricity (e) is the sum of (e_{CR}), (e_{SC}) and (e_{CP}), and is tabulated below with (e_{CP}) versus R_B for $R_P = 0.900$ inch.

R_B , inch	e_{CP} , inch	e , inch
1.5	0.00267	0.0042
5.0	0.0182	0.0197

Force and Moment Analysis. A final seat force equation involving eccentric load error is derived from a sum of forces along the piston axis and sum of moments about point "Z" (Fig. C-3) as follows:

$$\begin{aligned} \sum F_{axis} &= 0 = P_c A_p - P_1 A_e - F_{y1} - F_{y2} \\ F_e &= F_{y1} + F_{y2} = (P_{cb} + P_{c\Delta}) A_p - P_1 A_e \end{aligned} \quad (C-1)$$

$$\sum M_z = 0 = F_{y1} (D_s/2) - F_{y2} (D_s/2) - P_c A_p t \tan \phi - P_c A_e e$$

where $\tan \phi = e/R_P$

$$F_{y1} - F_{y2} = (P_{cb} + P_{c\Delta}) A_p \beta \quad (C-2)$$

$$\text{where } \beta = \frac{2e}{D_s} \left(\frac{t}{R_P} + 1 \right)$$

As previously noted, seat load error is the loss in load because of eccentric loading. This results from the use of computed balance pressures based on axial force balance. However, had balance pressure tests been performed with each model, there is no assurance that the control condition so defined would be repeated upon reassembly of the poppet for particle testing since ball joint position was random. Leakage is predominantly affected by the minimum load. Any overload because of decrease of eccentricity at low apparent loads would have much less effect on the data than corresponding load loss caused by eccentricity introduced on reassembly. Consequently, only load loss is considered in the error analysis.

Balance pressure condition is defined as

$$P_{c\Delta} = 0 = F_{y2}$$

and

$$F_{y1} \equiv F_b$$

Combination with Eq. C-1 and C-2 gives eccentric load total seat force

$$F_e = F_{y1} + F_{y2} = \frac{P_1 A_e}{\frac{1}{\beta} - 1} + P_{c\Delta} A_p$$

and seat force error

$$F_b = \frac{P_1 A_e}{\frac{1}{\beta} - 1}$$

As before, percentage error in apparent seat stress is

$$E_e = \frac{\Delta S}{S} = \frac{\Delta F}{F} = \frac{F_b}{F} = \frac{P_1 A}{\left(\frac{1}{\beta} - 1\right) S A_s}$$

Computed seat stress errors for the standard flat model are shown in Table C-1.

Summary of Seat Stress Error Analyses

The results of the preceding two seat stress error analyses are illustrated in Fig. C-4 ($P_1 = 300$ psig) and C-5 ($P_1 = 1000$ psig) for two typical slopes identified as "true curves." Constant gage error ($E_g S$) is added (\pm) to the true curve. Eccentric load error ($F_b = E_e S$) is added to the upper gage error curve to indicate the maximum computed error caused by load loss. Care must be exercised in interpreting these curves. A point on an error curve represents the apparent stress believed to have been applied at a measured leakage rate, whereas the true curve reflects the effective stress (relative to leakage) that was actually applied. This, then explains the high, low stress leakage phenomena.

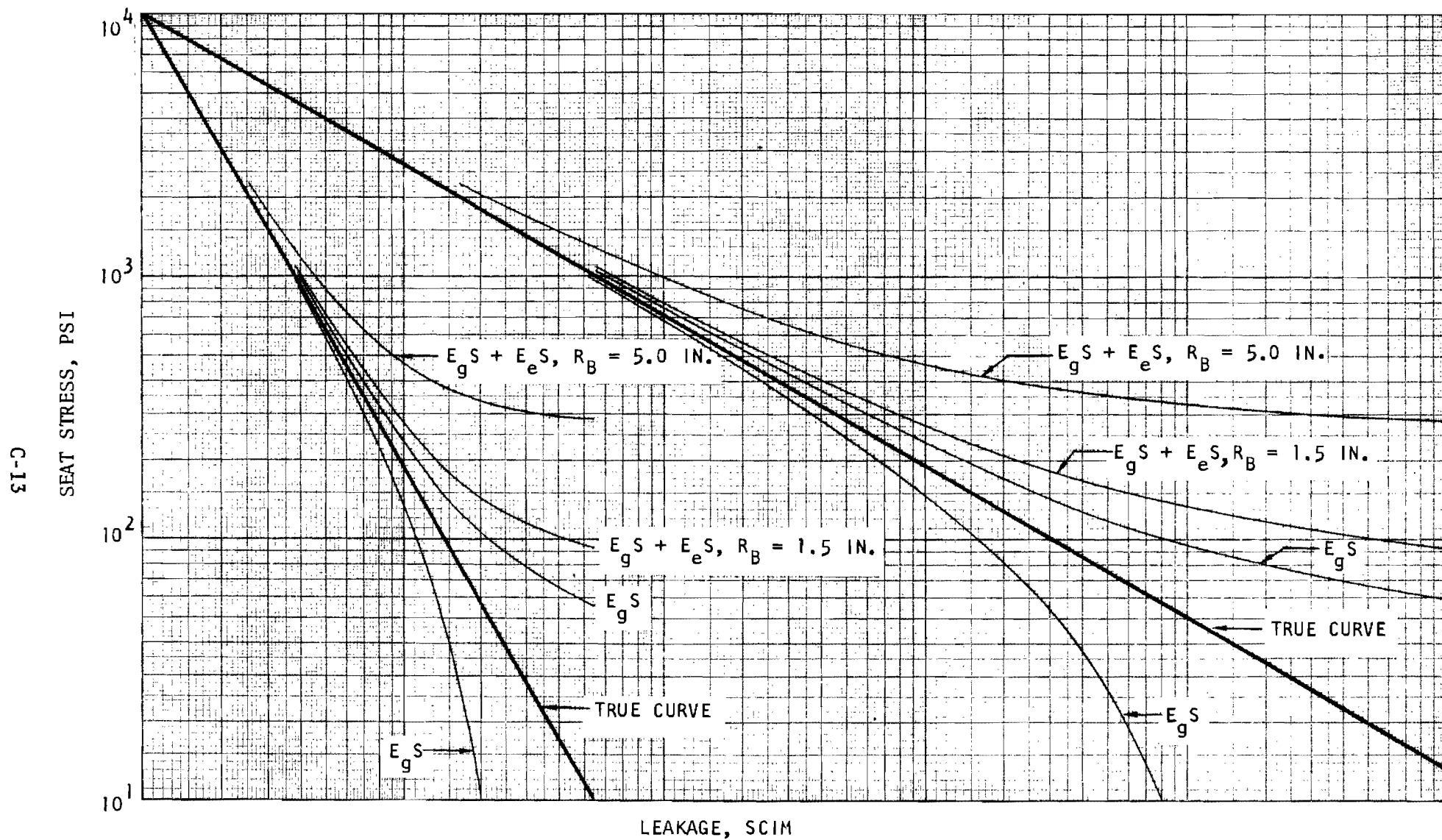


Figure C-4. Error Band, Typical Stress-Leakage Curves at 300 Psig Inlet Pressure

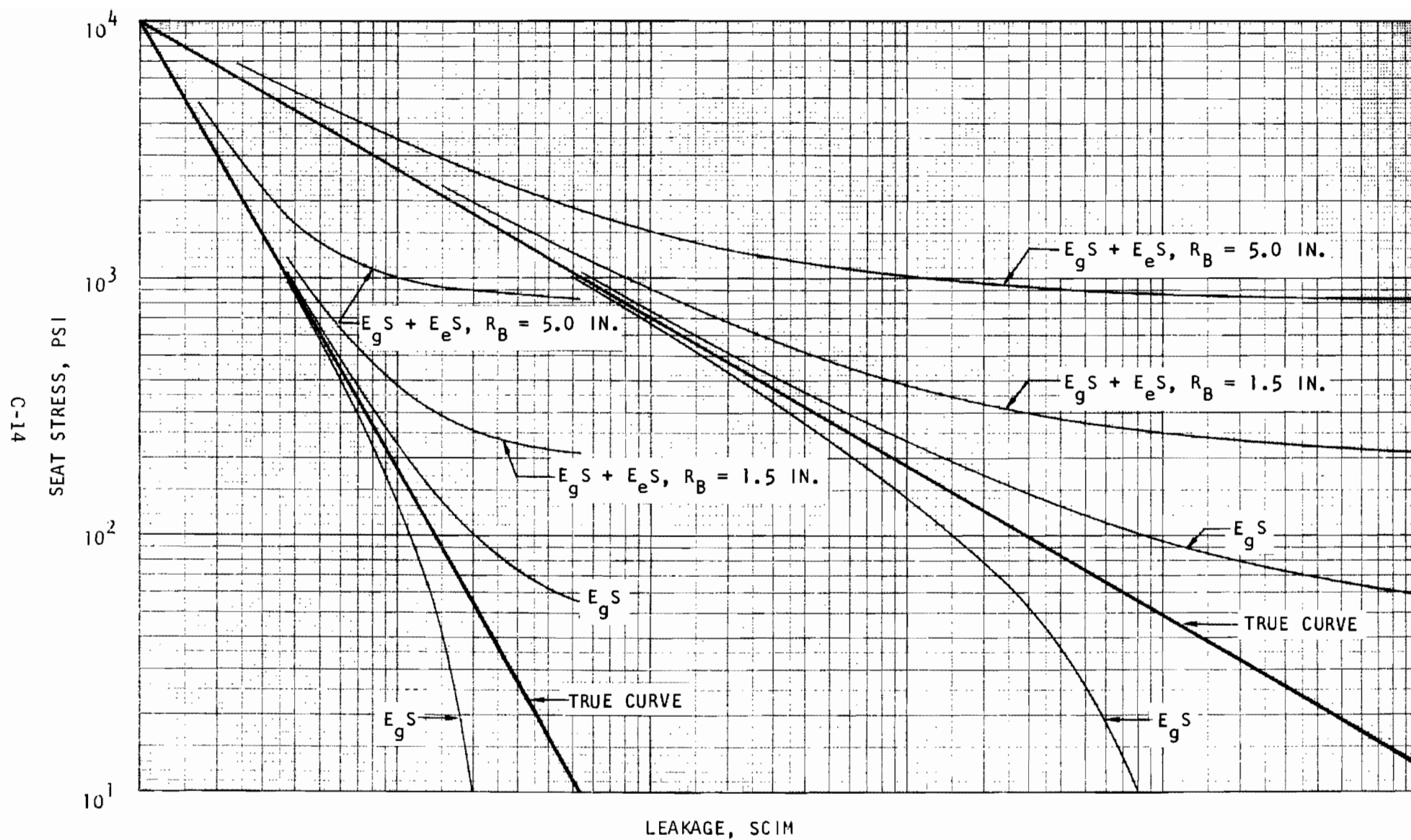


Figure C-5. Error Band, Typical Stress-Leakage Curves at 1000 Psig Inlet Pressure

TABLE C-1

FLAT MODEL SEAT STRESS ERROR BECAUSE OF ECCENTRIC LOADING
Percent Error (E_e) Versus (P_1) and (S)

P_1 , psig	S, psi			
	100	300	1000	3000
Case 1: $R_B = 1.5$ inches, $e = 0.0042$ inch				
30	4.65	1.55	0.465	0.155
100	15.5	5.17	1.55	0.517
300	46.5	15.5	4.65	1.55
1000	155.0	46.5	15.5	5.17
Case 2: $R_B = 5.0$ inches, $e = 0.0182$ inch				
30	23.1	7.70	2.31	0.77
100	77.0	25.5	7.70	2.55
300	231.0	77.0	23.1	7.70
1000	770.0	231.0	77.0	23.1

Model 128 Correlating Test Data

Flat 440C test model 128 was refinished for eccentric load testing. Since the static particle testing effort was completed these tests were performed to (1) support the eccentric load hypothesis and (2) indicate the effect of a 0.001-inch shim wrapped around the ball joint OD used in later Phase II static tests (from model 119 on). Pertinent seat inspection data for this model is listed below:

Total L = 0.0282 inch
 Flat L = 0.0258 inch
 $D_s = 0.4685$ inch (flat L)
 $A_s = 0.03795$ inch² (flat L)
 $A_e = 0.1788$ inch²

Stress-leakage results are summarized in Fig. C-6 (note that the stress scale matches that of Fig. C-4 and C-5 but is shifted a factor of 10 lower than normal test model data curves). These data are based on computed balance pressures (P_{cb}) for the 300- and 1000-psig inlet pressure test

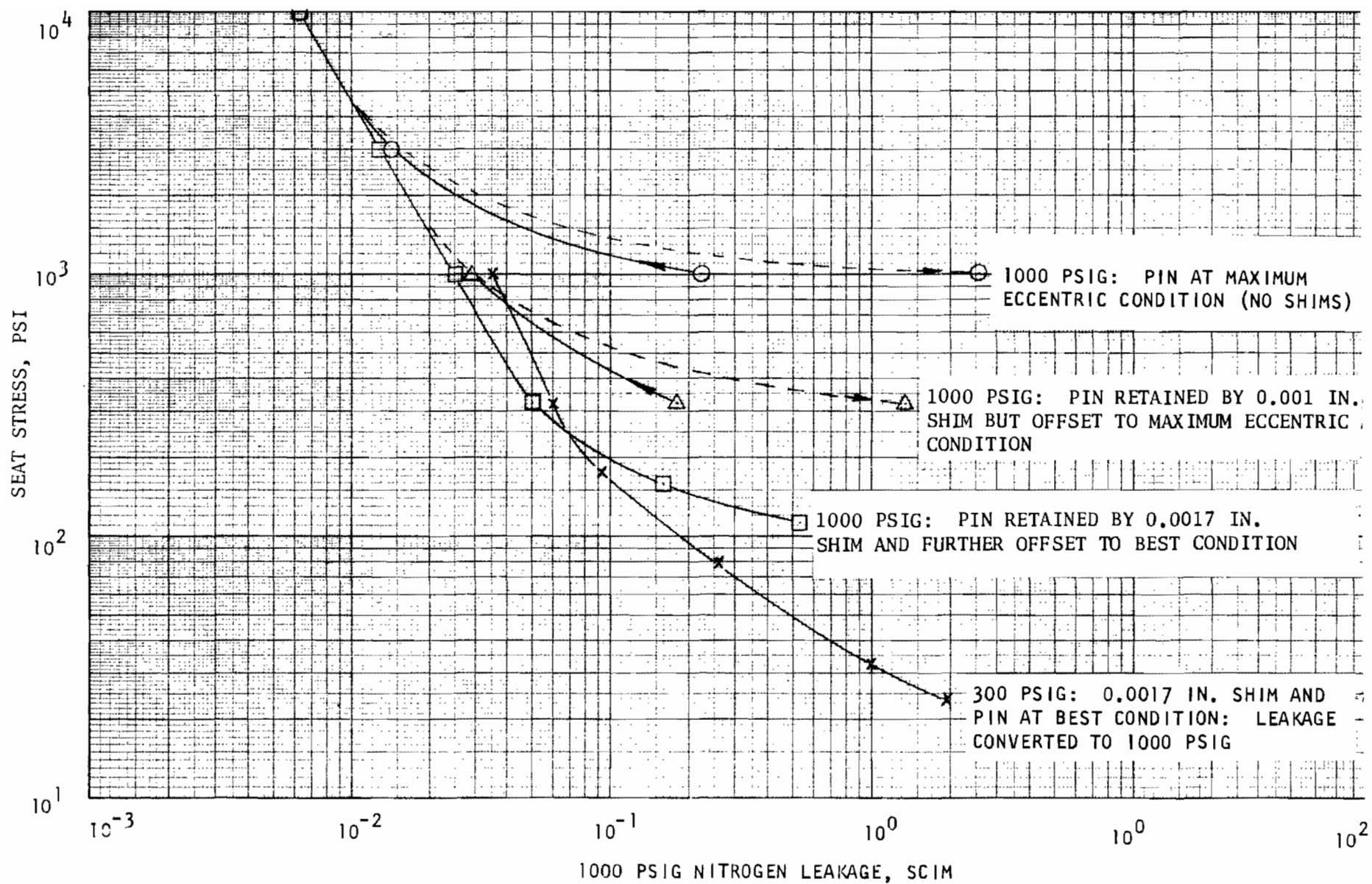


Figure C-6. Model 128 Summary of Eccentric Loading Tests Data Taken Under Noted Inlet Pressure and Ball Joint Pin Conditions

conditions. Maximum eccentricity was obtained by pushing the ball joint to an extreme position between the piston legs. Minimum eccentricity was obtained with a 0.0017-inch shim wrapped around the ball joint OD with trial adjustment to a minimum leakage condition. The carbide button spacer between the ball joint and poppet was also shimmed concentric. The presumed optimum condition most closely representing the "true curve" is reflected by the 300-psig inlet pressure test. Failure of the 0.0017-inch-shimmed 1000-psig test to follow this curve indicates that some eccentricity was present under best conditions. The worst condition compares closely with the computed worst condition curves of Fig. C-5 for $R_B = 5.0$ inches.

Balance pressure tests were performed with the 0.0017-inch shim at $P_1 = 300$ and 1000 psig. The results are tabulated below:

P_1 , psig	P_{cb} , psig	
	Computed With $A_e = 0.1788 \text{ inch}^2$	Test
300	32.3	32.5
1000	103.1	104.5

The greater error in (P_{cb}) with increased inlet pressure substantiates that some eccentricity was still present. Since verification of curve characteristics was the primary test objective, no further investigation was undertaken. However, balance pressure tests performed subsequently on dynamic test model 127 using the 0.0017-inch shim indicated agreement between computed and test balance pressure within 0.1 psi. The above error of 1.4 psi in (P_{cb}) with model 128 is probably near the maximum and indicates that the stress curve of Fig. C-6 (squares) should be reduced by 65 psi. This places the 1000-psi curve almost directly on the corresponding 300-psi curve.

Seat Loading Error Effect on Model Data

Review of previous program model data (Ref. 3), static model test results obtained in this program, and the preceding analyses have led to the following conclusions relative to the loading error effect on model static stress-leakage data.

1. With ball joint unshimmed, the validity of leakage data below 2000 psi apparent stress (about 76 pounds load) with $P_1 = 1000$ psi is questionable. Data indicating extreme sensitivity to stress (i.e., small $\Delta S/\Delta Q$) are likely influenced by eccentricity error (see models L_f and H_f in Ref. 3). Data which do not indicate substantial change in slope from a higher stress level may be valid to lower stress levels than 2000 psi as shown by model M_{f_1} of Ref. 3 and some models described herein.

2. Unshimmed data obtained with $P_1 = 300$ psig are considered valid to 600 psi apparent stress.
3. Static model test data obtained herein using a 0.001-inch shim are considered valid to between 1000- and 600-psi stress with $P_1 = 1000$ psig. As above, a flat slope is indicative of minimal eccentricity effect.
4. The crossover phenomena is not fully understood but likely derives from frictional effects that apparently reduce the effective seat load following high loading. This may be related to piston twist within the 0.0002-inch clearance caused by the misaligned ball joint. Crossover was negligible with 0.001-inch shim concentric loading.

APPENDIX D

LEAKAGE MEASUREMENT

Leakage, as a function of seat load, was the basic parameter used to evaluate test model performance. Consequently, accurate and repeatable measurement of this parameter was a necessary adjunct to proper interpretation of model test results. Numerous methods (and variations) of leakage measurement are known (Ref. 12). However, the reliability, repeatability, and accuracy achieved in previous programs with specific ball-float rotameters (0.1 scim and greater) and a leveling buret procedure below 0.1 scim dictated these devices should be used again.

ROTAMETERS

Pyrex ball-float rotameters were used to measure leakage flow from 0.1 scim to the maximum encountered (approximately 300 scim). These devices were calibrated with the conventional bubble-under and leveling buret methods subsequently described. Calibration precision was on the order of ± 2 percent, with an overall accuracy better than ± 5 percent.

Of particular interest is the long-term repeatability and precision exhibited by the Brooks tube number R-2-15-AAA used for Phase II static testing. This tube had also been used in the previous program where, over a 2-year time span, periodic calibrations indicated a repeatability error of less than 0.01 scim from 0.02 scim to full scale (3.6 scim). Recalibration for the subject program, some 3-1/2 years after the original calibration indicated that the same level of accuracy was still evident (less than 3.5-percent deviation over the full range). This tube was subsequently used to calibrate a similar Brooks tube used for leakage measurements during Phase II and III dynamic testing. In numerous cases throughout the program, both Brooks tubes were checked against buret measurements when the occasion permitted, and no significant deviation was noted.

BURET SYSTEM

Of the two positive-displacement systems evaluated in previous programs, the first was the conventional method of introducing a leak through water at the base of an inverted buret to displace a column of water. This proved satisfactory and accurate for larger flows; however, leakage rates less than 0.1 scim required small-bore tubes to obtain readings in a reasonable time and, when used in the above manner, large gas bubbles tended to stick at the base of the tube. Reducing the diameter of the gas bubbles by a small-exit orifice helped to attain the measurement, but this caused back pressure on the leak which had to be overcome before a stable reading could be taken. Thus, the bubble-under buret method was only used for calibration of rotameters at flowrates greater than 1.0 scim.

The leveling bulb buret method, which overcame these difficulties, was successfully employed for low-rate leakage testing. The gas leak was introduced at the top of the buret via 52 inches of 0.038-inch-ID plastic tubing, rather than bubbling it through the water. A leveling bottle connected to the base of the buret provided control of both the level and internal pressure after introducing the leak. By dropping the height of the bottle to match (within approximately 0.06-inch negative head) the level in the buret as the leak volume increased, the pressure differential in the system was made negligibly small. However, in measuring small leaks, it was noted that slight positive or negative pressure differentials could cause extraneous leakage resulting in large errors. Therefore, the system was always leak checked by sealing off the inlet pressure and purposely creating up to a 1-foot negative head so that the buret level could be observed for change which would indicate an external leak. Figures D-1 and D-2 illustrate the leveling bulb system setup and a Brooks tube.

Examination of the flow equations that correct for water head, vapor pressure, and ambient conditions for the conventional and leveling bottle systems show the advantage of the second method in requiring fewer corrections. These expressions assume a constant run temperature and pressure.

Conventional:

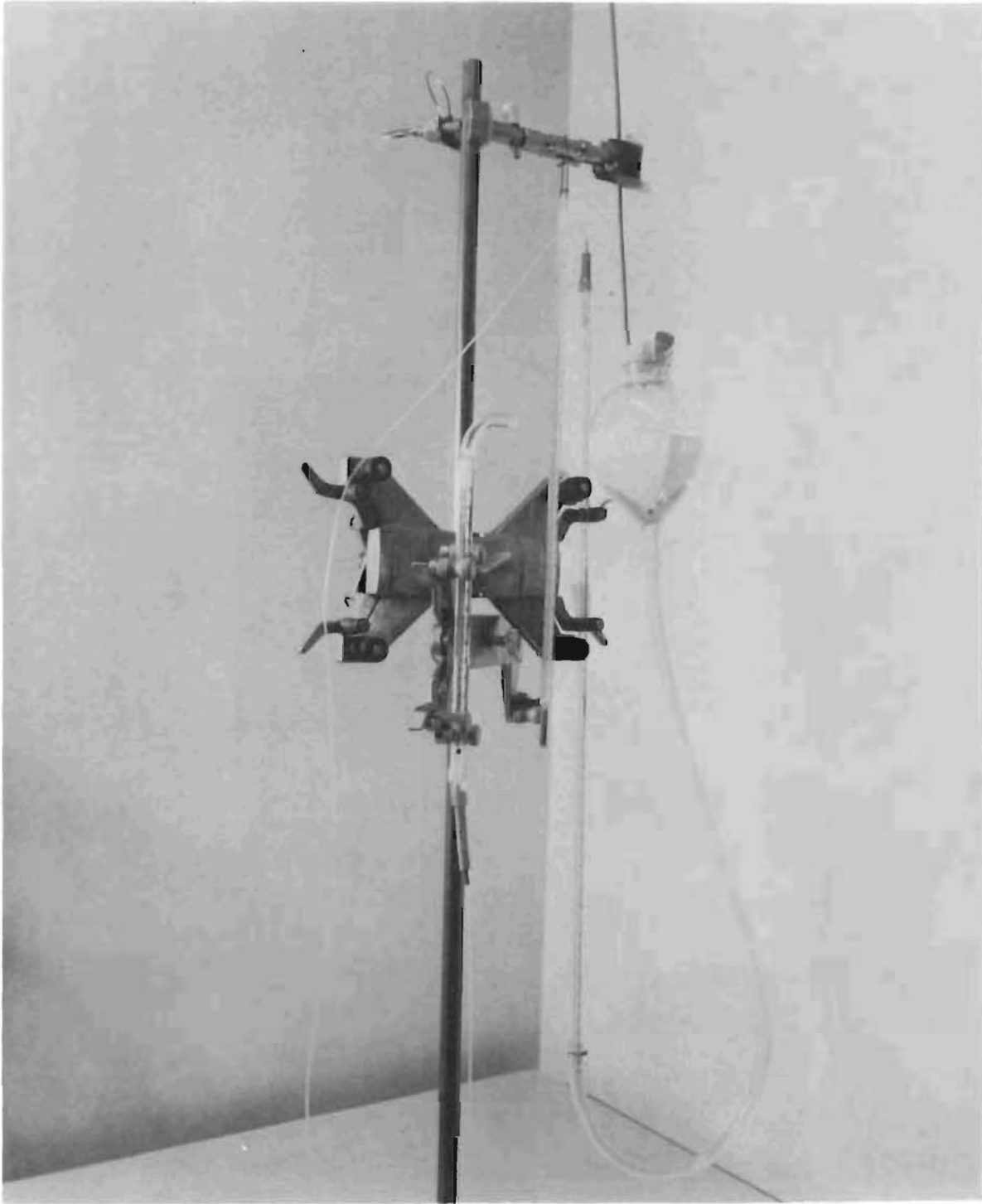
$$Q_s = \frac{3.66 T_s}{T t P_s} \left[\rho_L V_1 (h_1 - h_2) + \Delta V (P_a - \rho_L h_2 - P_v) \right]$$

Leveling:

$$Q_s = \frac{3.66 \Delta V (P_a - P_v) T_s}{T t P_s}$$

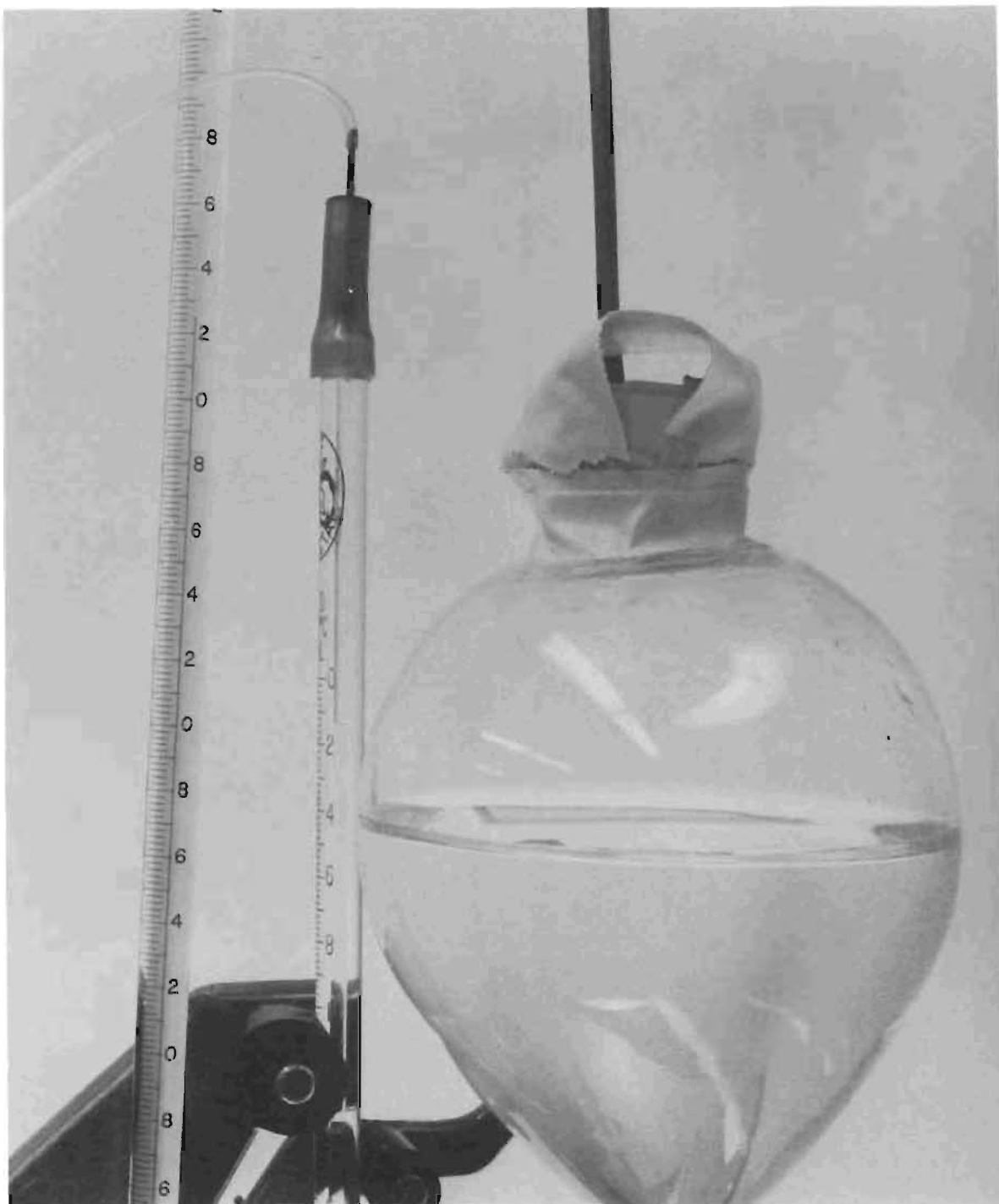
where

- h = water level head, inches
- P_a = atmospheric pressure, psia
- P_s = standard atmospheric pressure, psia
- P_v = vapor pressure of water at temperature, psia
- Q_v = leakage, scim
- t = time, seconds
- T = gas temperature (assumed equal to water temperature), R
- T_s = standard atmospheric temperature, R
- V₁ = initial volume in buret, cc
- ρ_L = liquid density (with water used) lb/in.³
- ΔV = change in volume as a result of leakage, cc



6AL42-11/6/69-C1J

Figure D-1. Leveling Bulb Leak Measurement Setup and
Low-Range Rotameter Tube



6AL42-11/6/69-C1K

Figure D-2. Leveling Bulb and 1-Milliliter Buret

Buret Flow Measurement Errors

The ultimate use of the flow data is to allow comparison of the performance capabilities of various seating configurations. Because the range of data spans several orders of magnitude, great accuracy is not required. However, consistency of point-to-point data and repeat hysteresis loops dictated the need for reasonable precision, i.e., about ± 2 percent. To meet these requirements, the following measurement errors were evaluated.

Volumetric. Where leakage values were greater than 10^{-3} scim, volume and time errors were made small by obtaining suitably large buret displacements over a sufficient time interval. These intervals ranged from a minimum of 30 seconds to several minutes. When leakage was measured between 10^{-3} and 10^{-5} scim, a minimum volume of 0.01 cc was displaced from the 1.0-milliliter buret (five 0.002 cc divisions). Because burets have precision bore tubes, the significant source of error is in the reading accuracy of the displaced water levels at start and stop. For the minimum leak of 10^{-5} , the length of displaced water was 0.200 inch which, for an estimated $h = 0.02$ inch (± 0.01 at each level), results in a maximum error of 10 percent. (The \pm is dropped as an error is assumed to deviate from the perfect reading.)

Leveling. Errors in leveling cause the volume of gas being leaked into, as well as the leak volume, to be at a pressure other than atmospheric. Leveling errors stem from two sources:

1. Capillary action results in a differential height between the tube and bulb level. Variations in this height differential (due to film contamination of the glass) over a given span will result in pressure changes during a test run if a constant capillary height is assumed. This error was nullified by calibration over a specific span. (Thorough detergent cleaning of the tubes usually eliminated any noticeable error.)
2. Basic comparison reading errors of the levels in the bulb and buret

The equation for leakage error caused by pressure variations from variable head is:

$$\text{Error} = \frac{\rho_L \Delta h (V_L + \Delta V + V_1)}{(P_a - P_v + \rho_L \Delta h) \Delta V}$$

where (Δh) is the leveling head error, and (V_L) is the total leakage volume external from the buret. This relation indicates that within visual leveling capabilities there is a minimum leak volume (ΔV) that can be measured for a given error and total volume ($V_L + V_1$). For the 23-cu in. volume enclosed by the static tester cover, the minimum leak volume (ΔV) for a 5-percent error (0.02 inch Δh reading error assumed) is 0.023 cu in. or 0.38 cc. Thus, for a 1-minute test, the minimum rate

for this large volume is 0.023 scim, or 1/1000 of the total volume. The volume of the collecting ring system, external to the buret, was less than 0.1 cu in.; thus, for a 50- percent error, only 1×10^{-4} cu in. or 0.00164 cc leakage need be captured. This minimum volume was increased to 0.01 cc to compensate for reading and temperature errors. With this volume, it was concluded that basic leveling errors had negligible effect on leak measurement accuracy compared with other errors.

Temperature. Variations in air temperature surrounding the external leak volume and buret induced indeterminate changes in the final leak volume. Consequently, where timed runs were long for low leakage, a thermometer was located next to the tube to measure any temperature change. The equation for leakage error caused by a change in system temperature is:

$$\text{Error} = \frac{V_L \Delta T}{\Delta V T}$$

Where (ΔT) is the temperature variation, and (T) is the mean absolute temperature. Because temperature errors occurred only for long-duration runs involving low leakage, only the low-volume system was affected. Temperature variations were estimated to be generally less than 1.0 R. Consequently, for a minimum leak of 0.01 cc (6.1×10^{-4} cu in.), maximum leak volume of 0.1 cu in. and mean temperature of 530 R, the maximum (calculated) error in leakage is 31 percent. For most measurements, the leakage volume was sufficiently large and time short enough so that temperature error was less than 5 percent.

Summary of Errors

From the previous discussion, it is evident that an accuracy of better than ± 5 percent was probable for leakage values down to 10^{-3} scim. It should be noted that had human errors resulted in even a 10-percent deviation, little effect would be noted in the data presentation (i.e., stress-leakage plots) which can only be read to about this level. Between 10^{-3} and 10^{-5} scim, the possible error increases from the 5-percent level to a predicted 41 percent. Numerous repeats of data points did indicate, however, better precision than this, usually ± 10 to ± 30 percent. Overall data presentation accuracy was improved by simultaneously reducing and plotting stress-leakage data during test; thus, nonrepeat points or those appearing in error could be rerun if required.

APPENDIX E

STATIC TEST SYSTEM AND MODEL TEST PROCEDURES

The test system and procedures used in Phase II static testing generally paralleled those formerly established and reported in Ref. 3. The particle deformation parameter, however, necessitated some procedural changes and innovations. In addition, problem areas were encountered, which resulted in evolutionary improvements to former standard operations.

TEST SYSTEM

The static test system consisted of film, control, and inlet pressure supplies required for the static tester function of loading pressurized seating surfaces. Figures E-1 and E-2 schematically and pictorially illustrate the test setup. Dry gaseous nitrogen (MIL-N-6011) at room temperature was used for leak testing and tester control functions. The critical filtration requirements of inlet and film pressure supplies were served by 0.45-micron (absolute) membrane filters, while a 5-micron wire-mesh filter was used for control pressure.

Conventional bottle regulators (Hoke and Airco; e.g., Fig. E2) were used to control 2200-psig bottle gas to the 0 to 1500-psig test pressure levels. These devices, used in low-flow applications, provided exceptional pressure stability (within 0.2 psig for relatively long duration) and sensitive control. Response was enhanced by the addition of external downstream bleed flow.

Several types of pressure gages were used, depending on the function and accuracy required. Film pressure, for example, was set directly from the regulator gage since a nominal 150-psig margin was used and extreme accuracy was not essential (see Appendix C, Static Test Fixture). Critical control and inlet pressures were measured with 0.1-percent accurate Heise gages, which were temperature compensated and had zero reset capabilities. For control pressures greater than 600 psig, the Heise (P_C) gage was isolated and a 0.25-percent, 1500-psig-range Ashcroft gage was used.

The static test system was set up in a clean (but not cleanliness-monitored) air-conditioned room with temperature controlled at 70 ± 1 F. Local temperature adjacent to the tester and leak measurement system was monitored with a thermometer.

The possibility of floor-transmitted shock and vibration influence on test results was considered. Consequently, rubber vibration damping pads were placed under the tester stand and bench legs. This effectively isolated the tester from vibration input.

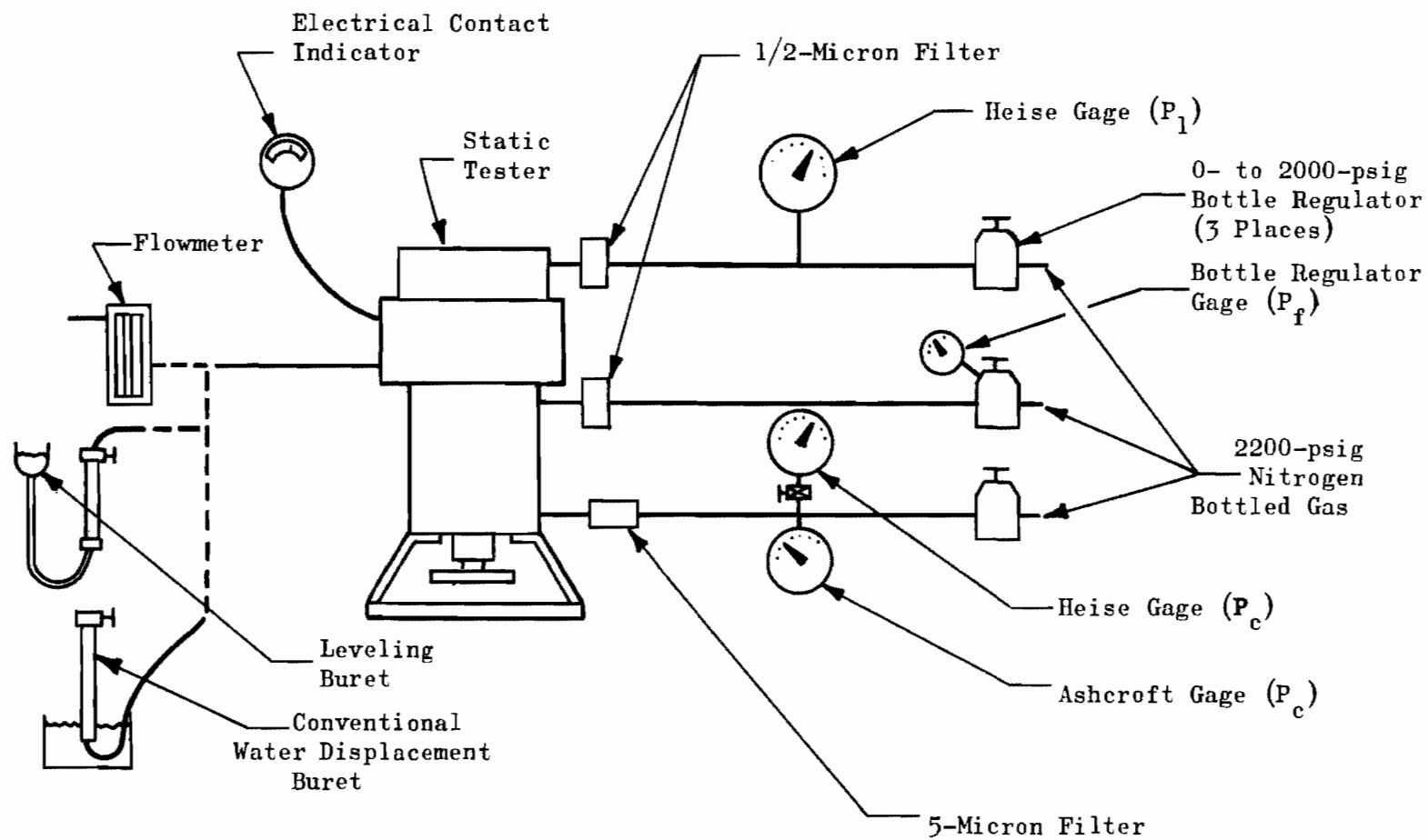
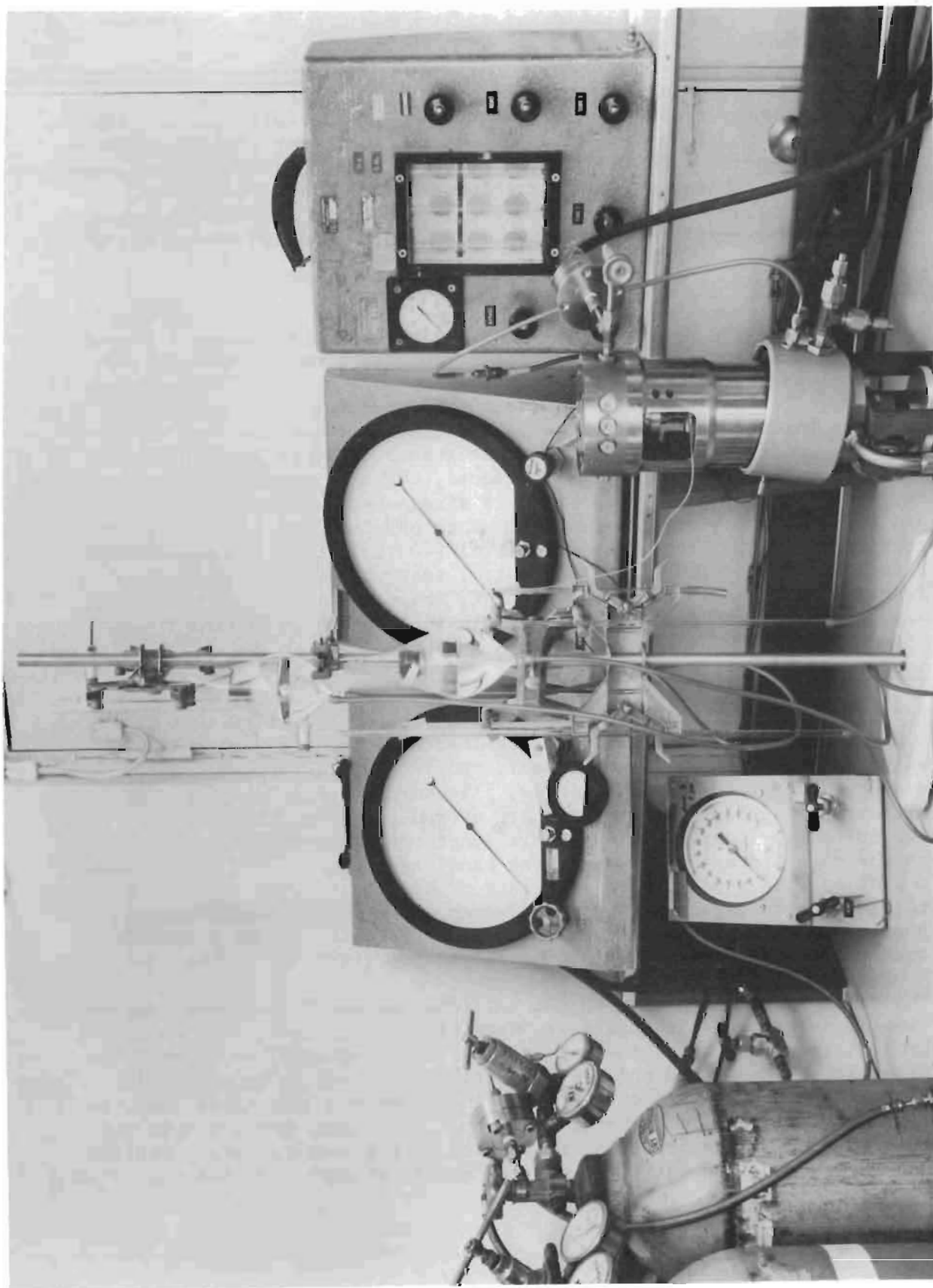


Figure E-1. Static Test Setup Schematic



6AD41-2/16/66-CLG

Figure E-2. Static Test Setup

TEST PROCEDURES

Model Cleaning

Poppet and seat models were inspected for appropriate dimensional and surface roughness requirements, then cleaned and installed in the tester. After several model tests, it was determined that, for optimum cleanliness, model surfaces could not be wiped, or touched in any manner. Thus, they were sonic cleaned in hot trichloroethylene, vapor degreased, cooled in a clean container, and directly assembled with filtered gas blowoff used as required to remove contaminants acquired during assembly.

Stress-Leakage Test

Test model sealing capabilities were determined by performing a stress (load)-vs-leakage test, where leakage resulting from incremental increasing and decreasing loads was measured. The test was initiated by applying a control pressure of 5 to 10 psig greater than the balance value to ensure positive closure load while inlet pressure was subsequently applied. This gave a pretest stress cycle of about 4500 psi. Next, to minimize any hysteresis effects, three 30,000-psi stress loops were initially applied, followed by a stress-leakage test to 30,000 psi and return. When the potential influence of eccentric loading was recognized, maximum stress during initial (control) data acquisition was limited to 3000 psi. After the control test, the poppet was removed from the tester for particle placement, while the still-installed seat was protected from contamination by closing the tester cover.

Test Particle Placement

Particle placement was accomplished with a handling system that utilized a magnetic base surface gage (spring-loaded rocker arm with setscrew adjustment for arm vertical motion), and the interference microscope with X-Y micrometer-adjusted table. The surface gage was placed on the microscope baseplate so that the arm overhung the X-Y table and was under the objective lens (100X). A short length of brass tubing was cemented to the gage arm as a receptacle for handling probes. After some experimentation with steel and brass, glass probes, heat drawn from pyrex tubing to, in some cases, less than 0.0002-inch diameter, were selected for particle handling. For optimum pickup and release, it was determined that probe tip diameters should be one-to-two times that of the particle.

The test poppet was placed on the X-Y table adjacent to a gage block of similar height on which particles were placed. The particles were brought into view by table micrometer screw adjustment, an appropriate size particle selected and electrostatically picked up by vertically depressing the probe to contact it. The probe was then raised and the table moved laterally to bring the poppet into view; the particle was then lowered and deposited at the center of the seating land. This sequence was repeated until the desired number of particles had been placed

equidistant around the land circumference. With the calibrated reticle system in the interference microscope, particle sizing accuracy was estimated at ± 2 microns.

Particle Stress-Leakage Test

Following particle placement, the seating surface was 100-percent inspected for deposited airborne contaminants which, when noted, were removed with the handling probe. The poppet was then reassembled into the tester for stress-leakage testing in the particle-contaminated condition. Several procedural variations were utilized for this phase of the test. (The tabulated test procedure sequence concluding this appendix relates specific test models with procedural changes.)

Early models used the O-ring leak collector ring (blocked open for initial leakages when greater than 3.5 scim). Poppet and seat closure was effected by gradual application of control pressure after the interface had been brought to within about 0.010 inch by handwheel closure. Subsequent models, after particles were occasionally dislodged during the initial sequence, used the aluminum leak collector ring (Fig.III-6) and closure by handwheel operation until contact. With the latter procedure, the variable and potential poppet-cocking O-ring load was eliminated along with possible impact closure associated with control pressure application and nonuniform O-ring deformation. Tests of handwheel sensitivity (or "feel") indicated that a closure load of less than 10 pounds could be detected.

Once closure contact was established, incremental control and inlet pressure increases were sequentially applied (or "juggled") until operating pressure levels were attained. In the pressure juggling operation, apparent seat stress was initially held within 100 to 300 psi for all particle sizes so that the first stress-leakage data point could be acquired in the 300-psi stress region. After recognition of the eccentric load problem, it was suspected that early particle loss problems were caused by reduction of seating loads to much less than 100 psi, with particles literally blown off the seating surface by leakage flow due to clamshell opening. With concentric loading, 15-micron particles were tested as low as 300-psi stress, but first data points were increased to 1000 psi for 30-micron particles and 3000 psi for the 60-micron size.

For models tested prior to the utilization of concentric ball joint loading, inlet pressures of 30 or 100 psig were used for initial leak points with inlet pressure subsequently increased to 300 or 1000 psig as leakage decreased. With the inauguration of concentric loading, all tests were performed at 1000 psig inlet pressure. Maximum particle deformation stress was determined by conformance of the stress-leakage characteristic with that of the control condition, but did not exceed 30,000 psi.

After stress-leakage testing with entrapped particles, both poppet and seat were removed from the tester for inspection and particle removal. Following these operations, the test parts were recleaned and installed in the static tester with seating surfaces reoriented (rotated) about 10 degrees. A stress-leakage test was performed to indicate the effect of particle-caused damage on the model sealing capabilities. During testing, it was determined that finishing numerous models having the same surface characteristics and thus, near identical stress-leakage performance, was impractical. It was further determined that residual effects after particle removal were minimal. Therefore, successively larger particles were tested using the same model, thus effectively minimizing surface characteristic influence. In these cases, the post-particle removal stress-leakage test also provided the control data reference from which subsequent entrapped particle data could be assessed.

Test Procedure and Sequence Summary

As the preceding paragraphs have indicated, significant procedural changes evolved during Phase II static testing. These changes, as they applied to the static test sequence of operations and the family of models static tested with particles, are summarized in the following tabulation:

<u>Test Procedure Sequence</u>	<u>Procedure Comments</u>	<u>Models Involved</u>
1. Clean	Ultrasonic clean, vapor degrease, wipe off	102-108
	Ultrasonic clean, vapor degrease, blow off	112-125
2. Assemble in tester	O-ring leak collector	102-108
	Aluminum leak collector	112-125
	Eccentric ball joint	102-118
	Concentric ball joint	119-125
3. Control stress- leakage test at 1000-psig inlet pressure	Three 30,000-psi prestress loops, 30,000-psi maximum test stress	102-112
	Three 3000-psi prestress loops, 3000-psi maximum test stress	118-125
4. Remove poppet, add particles, reassemble		102-125
5. Initiate seating surface-particle contact	With control pressure	102-108
	With handwheel	112-125

<u>Test Procedure Sequence</u>	<u>Procedure Comments</u>	<u>Models Involved</u>
6. Adjust operating pressures (P_1 and P_C)	30- to 1000-psig inlet pressure 1000-psig inlet pressure	102-108 112-125
7. Stress-leakage test	To conformance	102-125
8. Remove particles, inspect model, and reclean		102-125
9. Reassemble model in tester, 10-degree reorientation	Assembly conditions same as in Item 2	102-125
10. Stress-leakage test	Three 30,000-psi prestress loops, 30,000-psi maximum test stress After 15-micron particles: 2500-psi maximum prestress, first test loop to 3000-psi, three prestress loops to 10,000-psi, and final 10,000-psi test loop After 30-micron particles: 9000-psi maximum prestress, first test loop to 10,000 psi, three prestress loops to 30,000 psi, and final 30,000-psi test loop	102-112 118-125

APPENDIX F

DYNAMIC TEST FIXTURE

The dynamic test fixture (dynamic tester) was developed during the previous program (Ref. 3) for cycle-impact evaluation of poppet and seat test models. It was similar to the static tester in the use of the hydrostatic bearing concept and other general features and could be used for static testing. However, it employed additional features for controlled load and impact velocity testing with built-in instrumentation.

The dynamic tester was modified for liquid service to permit model cycling in controlled contamination environments for the subject program. The alterations involved addition of flushing flow and drain ports, with emphasis on minimizing particle traps and promoting drainage and did not significantly affect basic capabilities. In addition to its cycling function, the tester was used to evaluate effects of cycles on test models through static stress-leakage testing.

DESCRIPTION

As with the static test fixture, a detailed discussion of the dynamic tester is presented in Ref. 3. Features of particular importance to the subject program are illustrated in Fig. F-1 and described in the following paragraphs. Figure F-2 shows tester assembly and detail parts.

Hydrostatic Bearing

Dynamic tester hydrostatic bearing design and characteristics were virtually identical with that of the static tester, except that a smaller (50 micro-inch) diametral clearance was used. A film pressure of 600-psig Freon TF was used to promote bearing flushing and for compatibility with the dynamic test system.

Formerly, a flexure assembly connected the piston to the body to prevent rotation during cycling with a leaf spring providing bias force. The flexure also permitted precise poppet realignment after removal for inspection. Because the flexure assembly had numerous crevices which formed potential particle traps, a modification in this area was made prior to liquid operation. As shown in Fig. F-1, a combined flexure-bias spring provided for antirotation and piston return. While not as rigid as the earlier flexure, this arrangement did prevent piston rotation while cycling. Bolt hole clearances in the new spring, however, precluded precise realignment of a test poppet once the spring, or poppet had been disassembled. As the spring could not be stroked enough to permit installation of a leak collection device, it was removed for stress-leakage testing. A majority of cycle tests were thus performed with model surfaces reoriented after each stress-leakage test. As subsequently discussed, this problem was ultimately resolved with latter Phase III models.

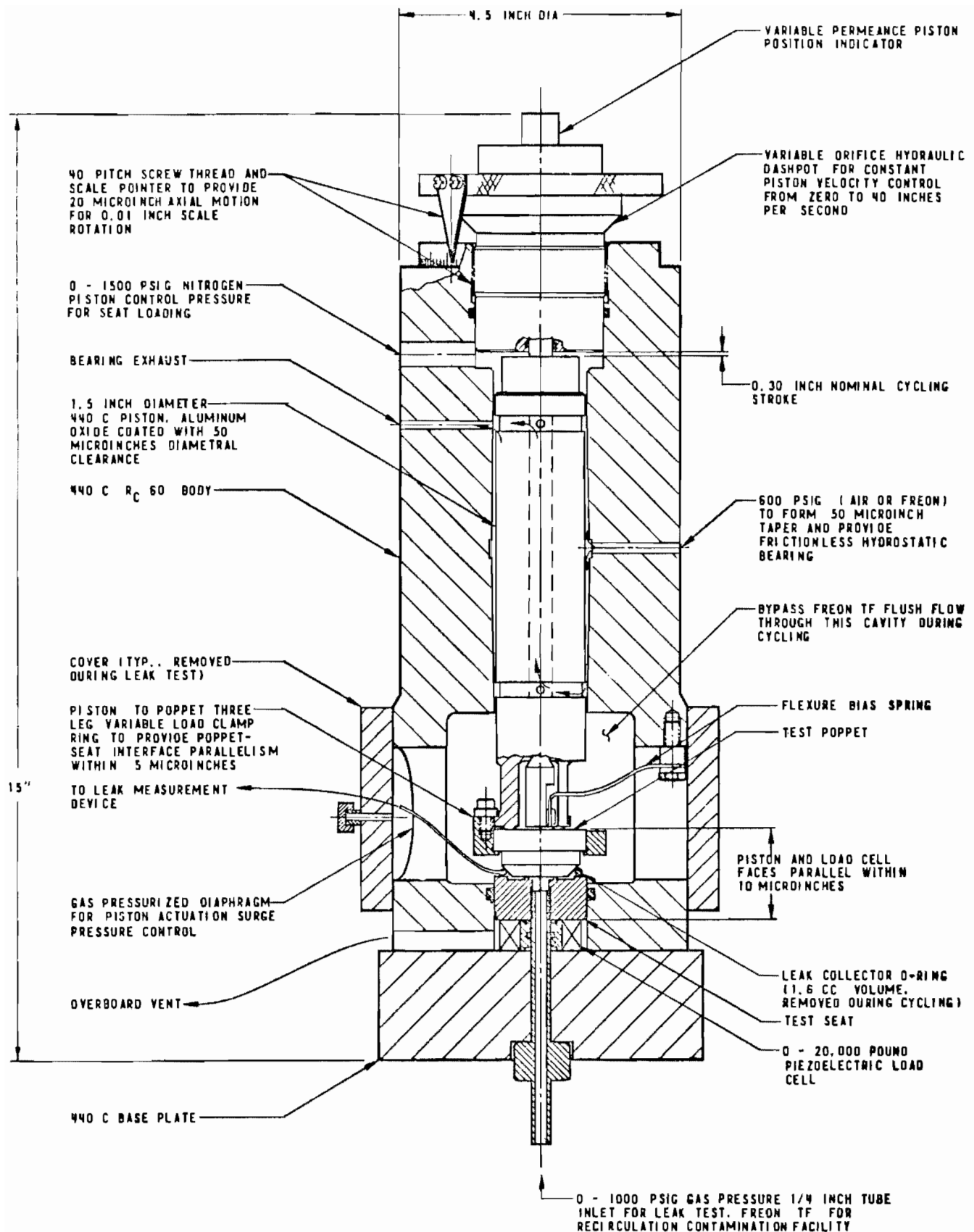
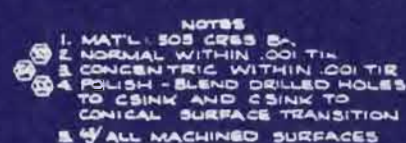
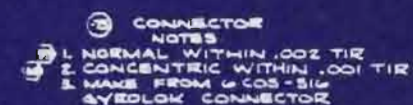
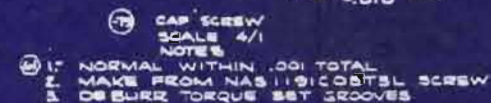
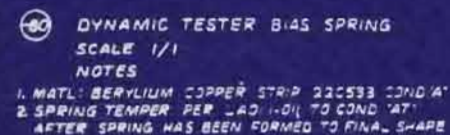
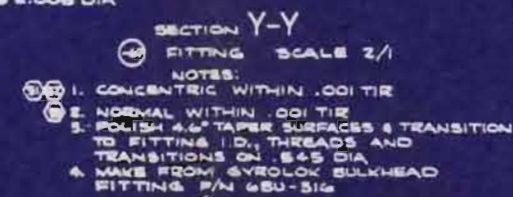
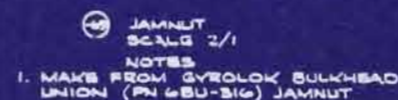
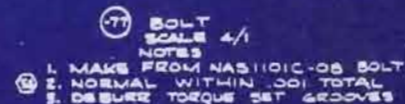


Figure F-1. Poppet and Seat Dynamic Tester



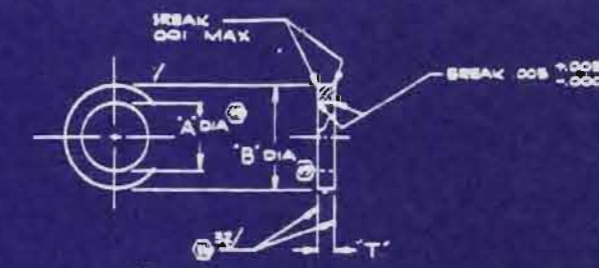
Technical drawing of a hexagonal nut. The side view shows a hexagonal shape with a central hole. Dimensions include a top width of 3/4, a 45° chamfer, a central hole diameter of .620, a hole depth of .010, and a bottom thickness of .000 DIA. The end view shows a regular hexagon with concentric circles representing the hole.

Technical drawing of a shaft assembly. The drawing includes a side view and a cross-sectional view. Key dimensions and features are labeled:

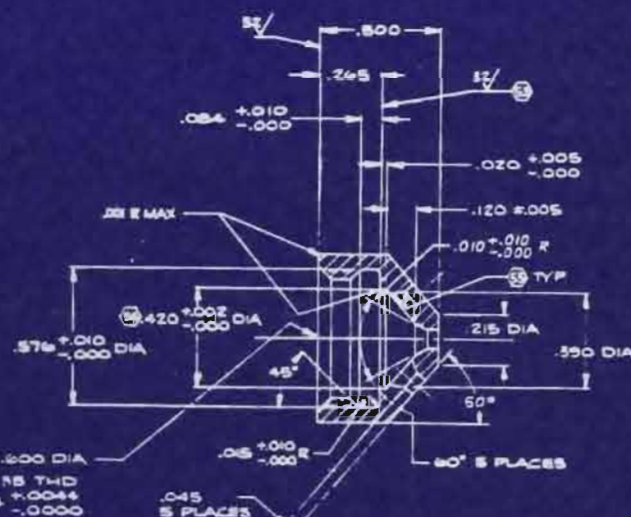
- Shaft diameter: $.545 \pm .000$ DIA (REF)
- Shaft length: $4.000 \pm .005$
- Keyway width: $.25 \pm .010 \pm .000$
- Keyway depth: $.010$
- Keyway radius: $.010 R$
- Shaft taper: 4.6°
- Shaft chamfer: 45° CHAM TO $.485 \pm .000$ DIA
- Nut diameter: $.524 \pm .000$ DIA (REF)
- Nut length: $.455 \pm .005$ DIA (REF)
- Washer diameter: $.485 \pm .000$ DIA
- Washer thickness: $.010$
- Assembly length: $4.455 \pm .005$ DIA (REF)
- Assembly radius: $.001 R$ MAX

NOTES:

1. CONCENTRIC WITHIN .001 TIR
2. NORMAL WITHIN .001 TIR
3. POLISH 4-6° TAPER SURFACES & TRANSITION TO FITTING I.D. THREADS AND TRANSITIONS ON .545 DIA
4. MAKE FROM SYVELOK BULKHEAD FITTING P/N 680-516



C-SWASHER
 SCALE: 6/1
 OTES:
 1. MATL IS CRSS BAR
 2. CONCENTRIC WITH .005 TIR
 3. PARALL WITHIN .0002 TOTAL



Technical drawing of a mechanical part showing two views: a side view and a top view.

Side View Dimensions:

- Top surface: $.010 +.040 / -.000 R$
- Vertical edge: $.050 +.030 / -.000$ TYP Z PLACES
- Chamfer: 45°
- Feature on side: $.035 \pm .005$

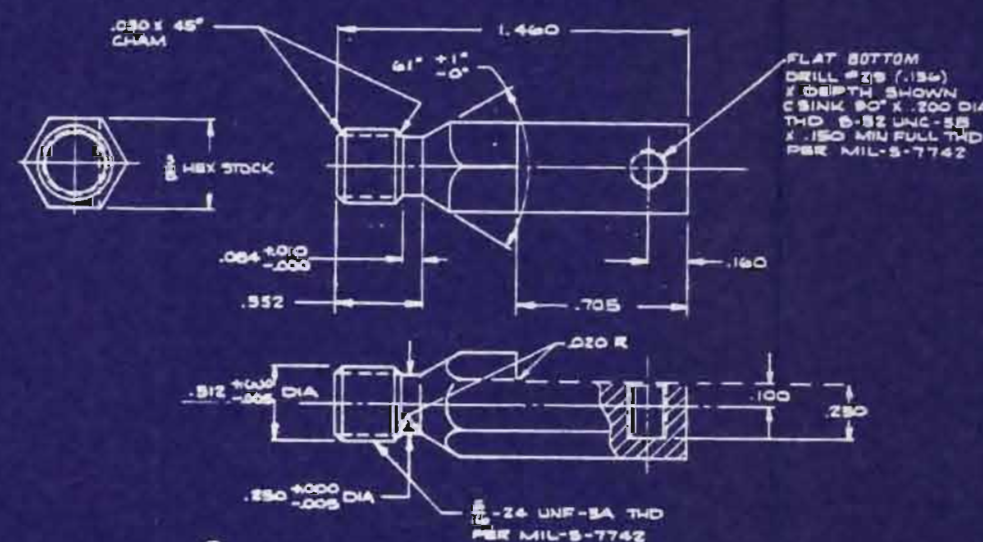
Top View Dimensions:

- Overall diameter: $.076 +.002 / -.001$ DIA
- Central hole: \varnothing
- Four smaller holes: \varnothing

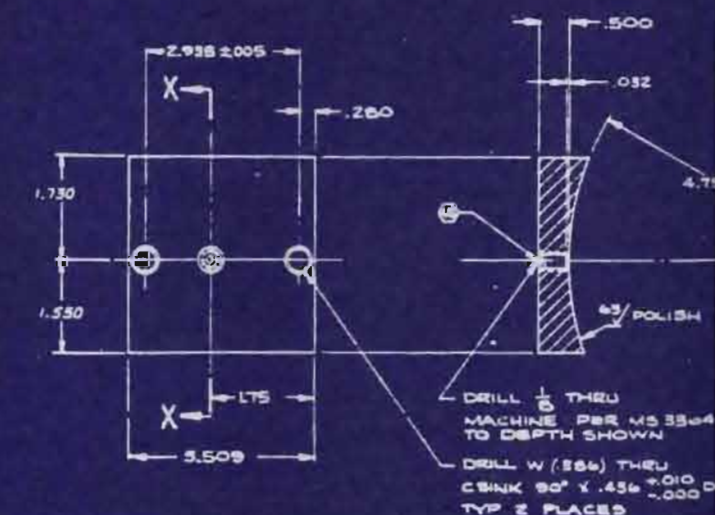
Note: THRU PLACES BREAK EXTERNAL CORNERS .001 MAX

NOTES

1. MATL: 303 CRSS B.
2. NORMAL WITHIN .001 TI
3. CONCENTRIC WITHIN .001 TI
4. POLISH - BLEND DRILLED HOLES TO CSINK AND CSINK TO CONICAL SURFACE TRANSITION
5. $\frac{1}{4}$ ALL MACHINED SURFACES

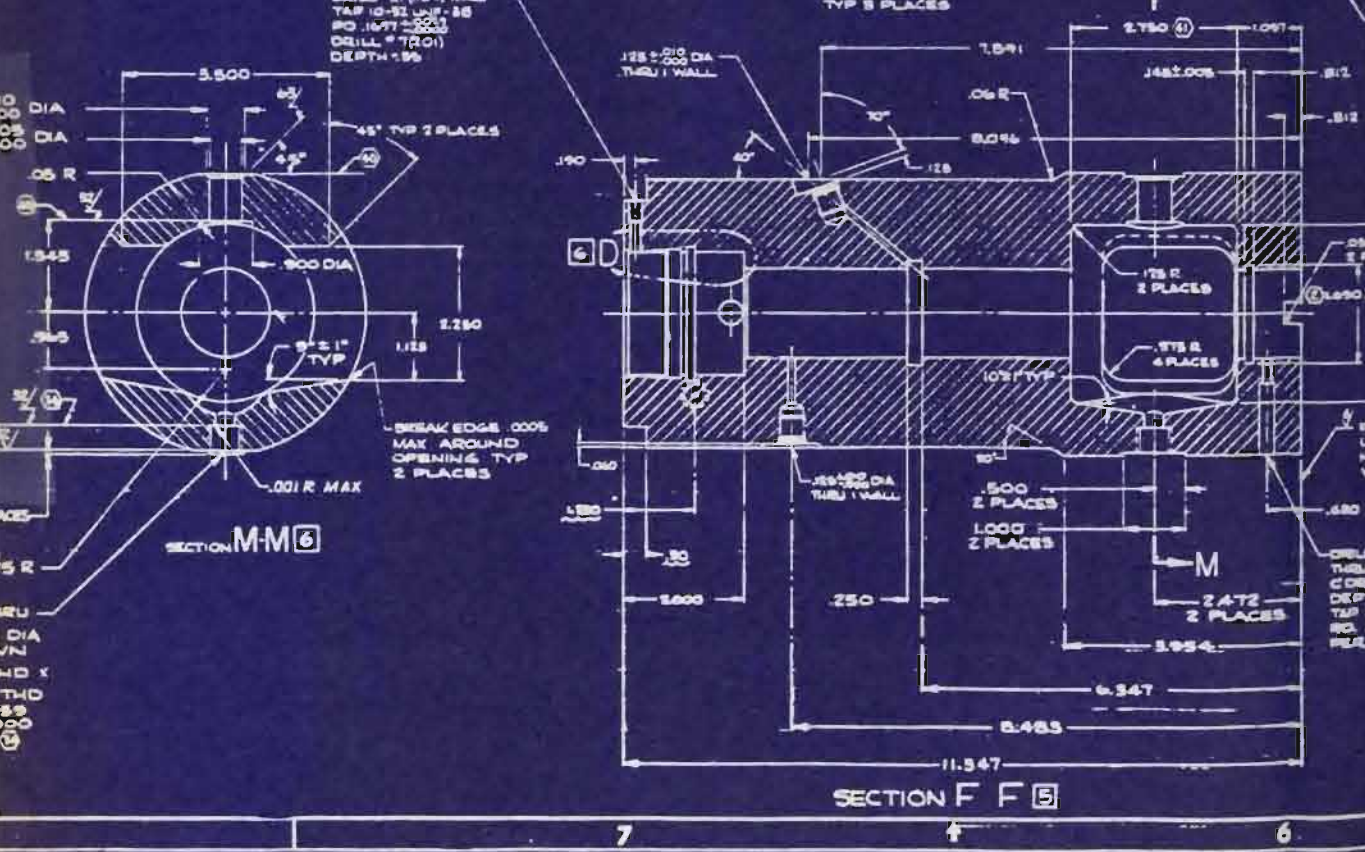
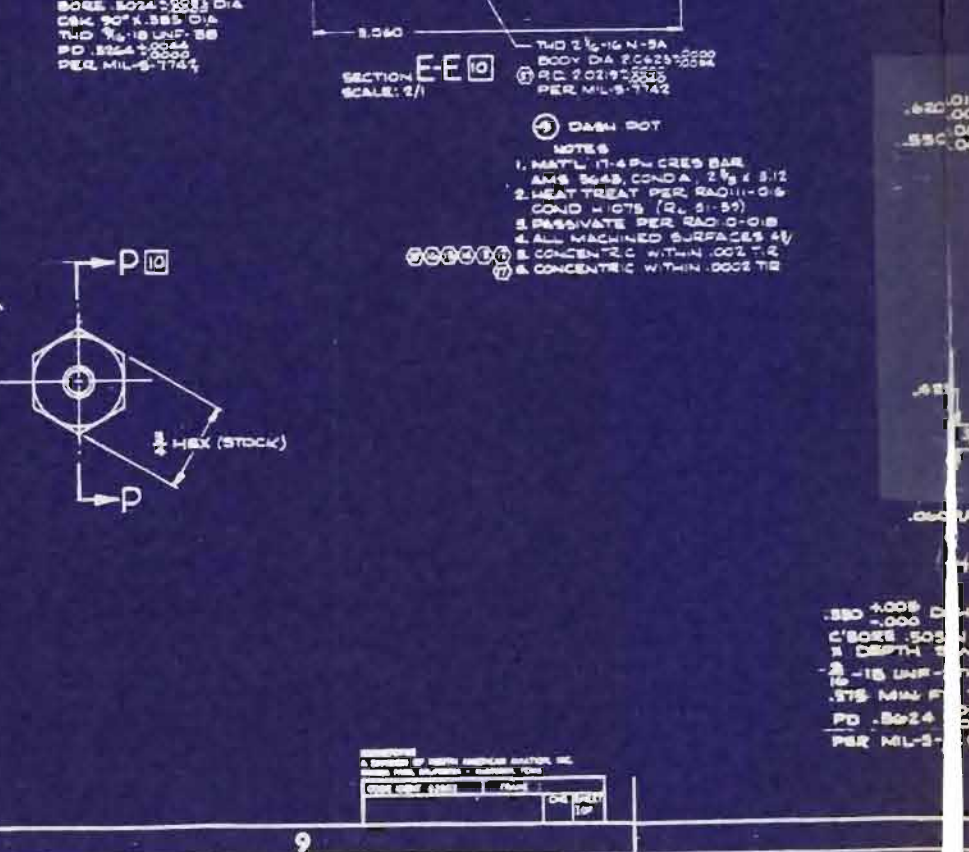
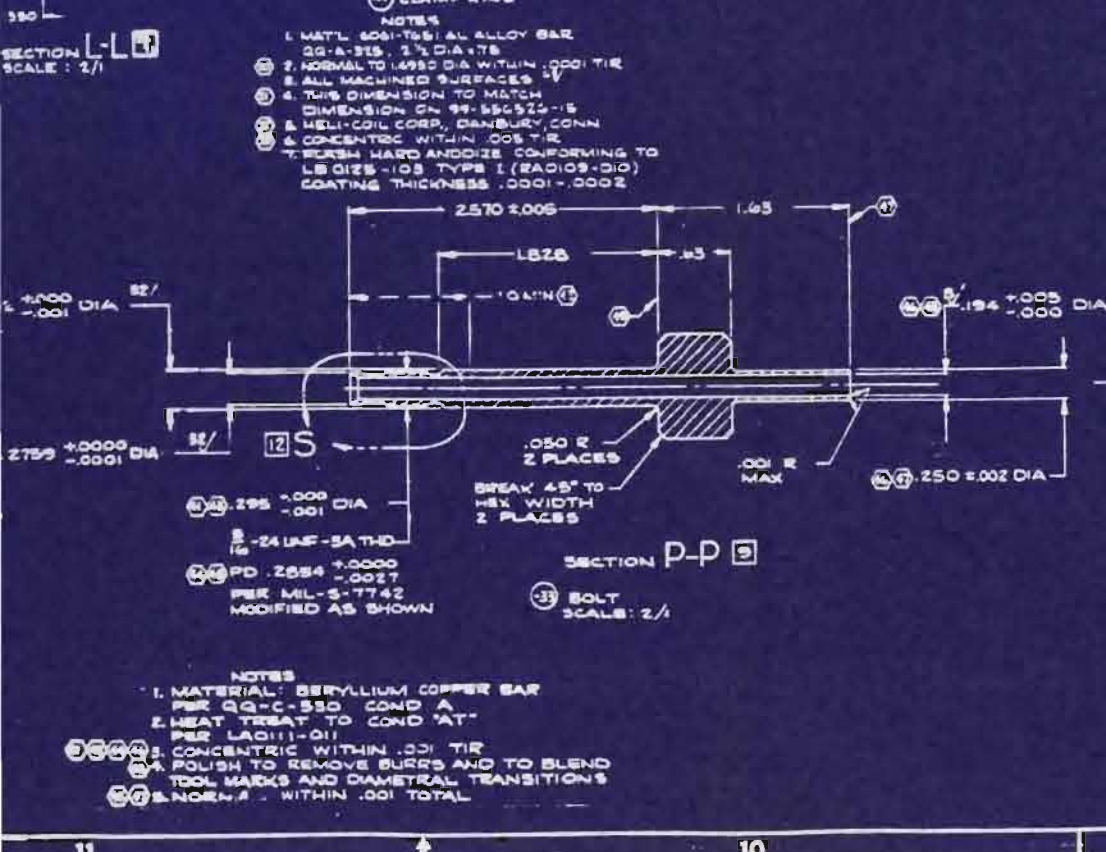
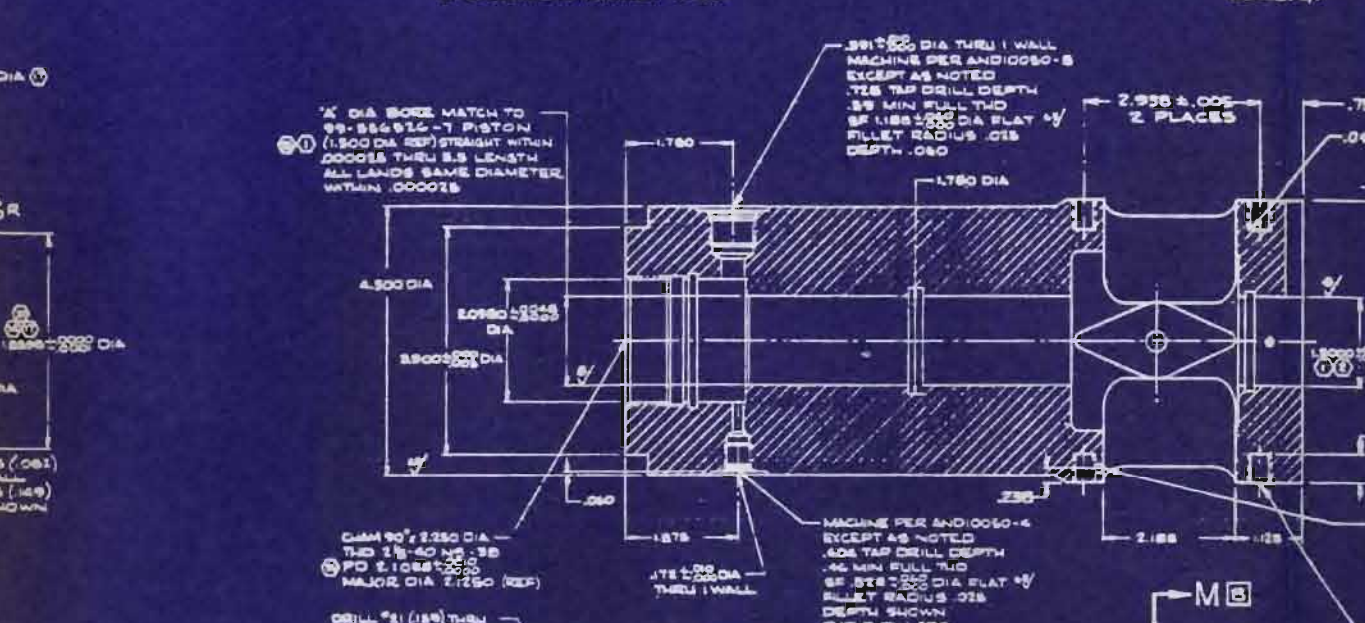
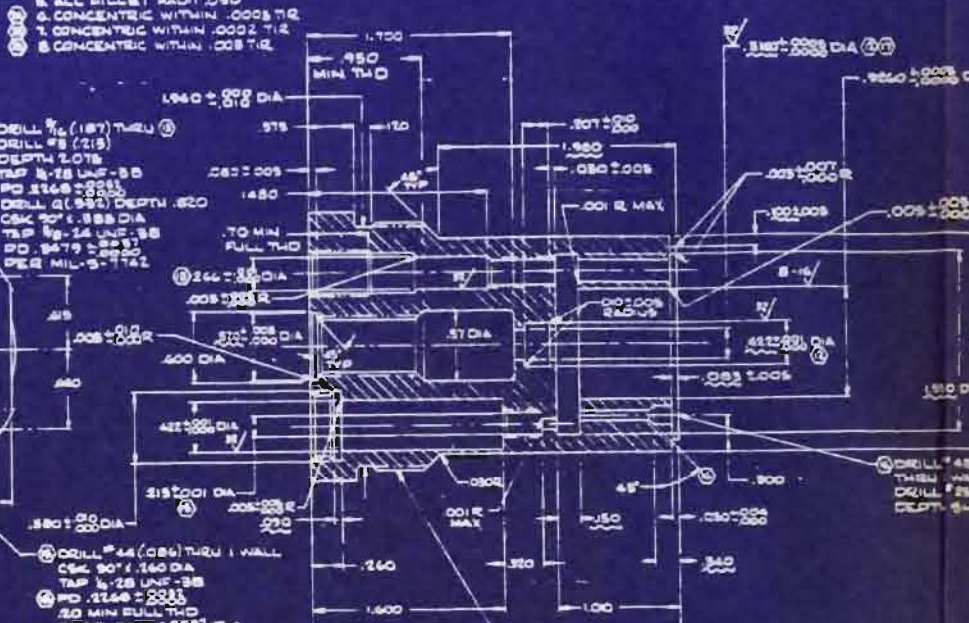
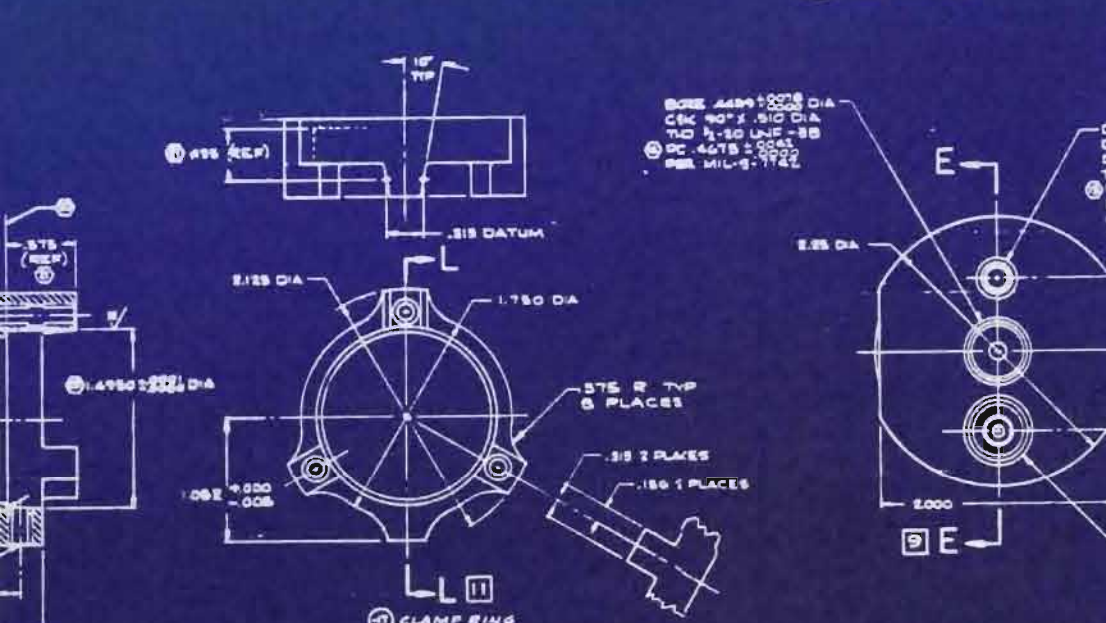
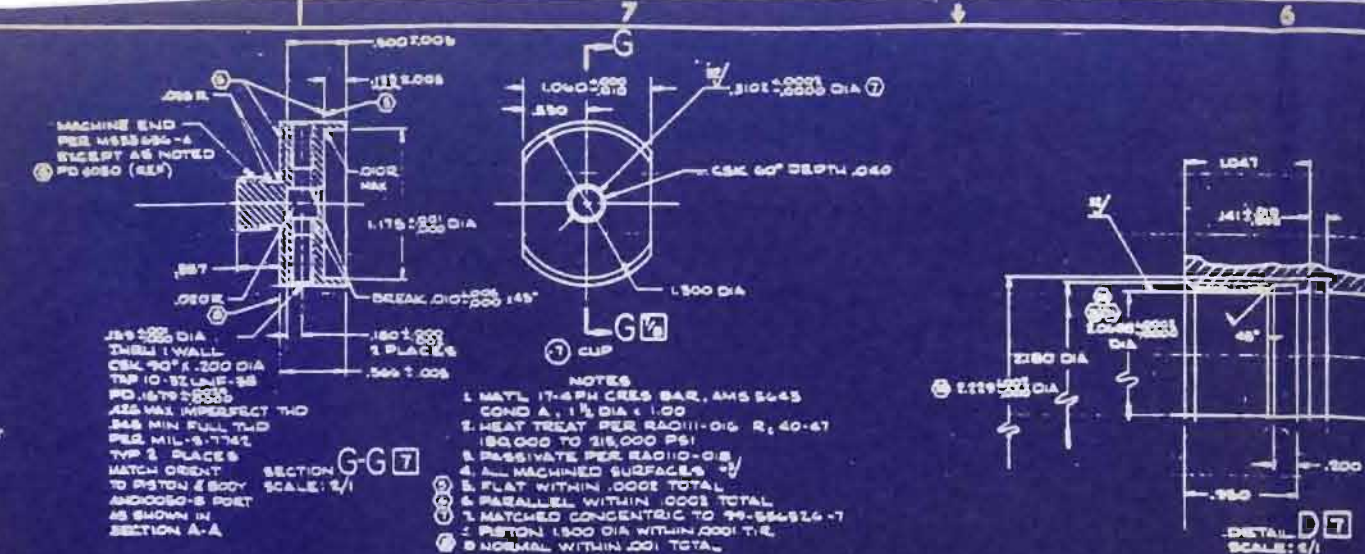
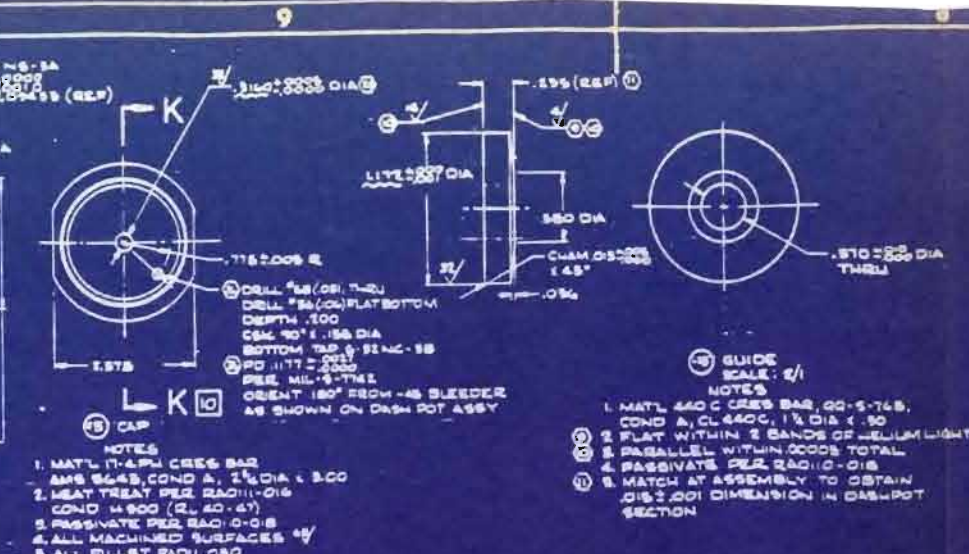
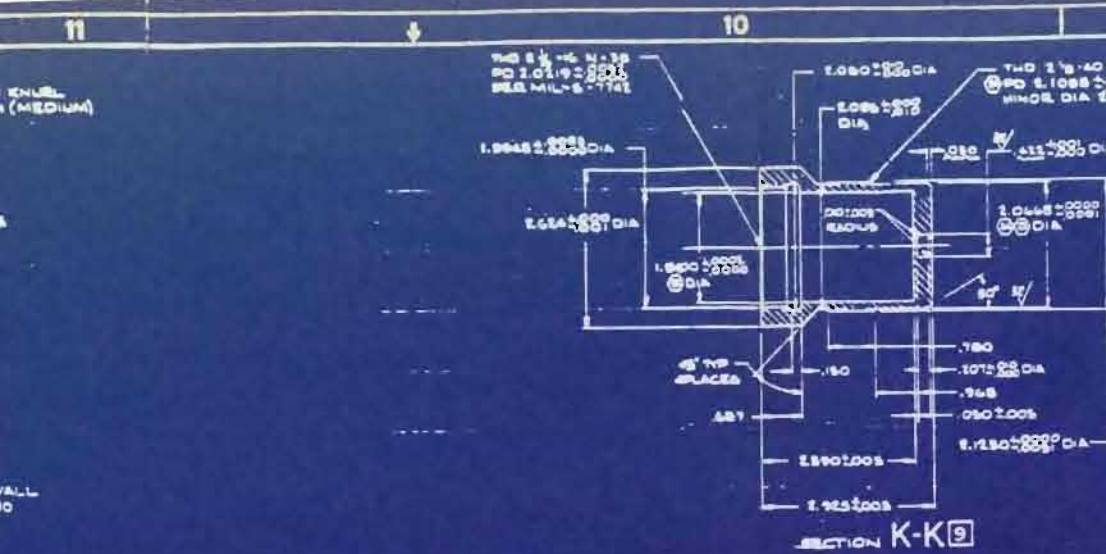


NOTES:
1. MATL: 17-4 PH CRES BAR
AMS 5643 COND A
2. HEAT TREAT TO COND H-900
(Rc 40-47) PER RA0111-016
3. $\frac{1}{2}$ ALL MACHINED SURFACES



NOTES:
1. MAT'L: 17-4 PH CRSS BAR
PER AMS 5643 COND A
2. HEAT TREAT TO COND H-300
(Rc 40-47) PER RA0111-016
3. BREAK EDGES .010 T.O.D
- .000
4. INSTALLATION OF THIS PORT
IS OPTIONAL





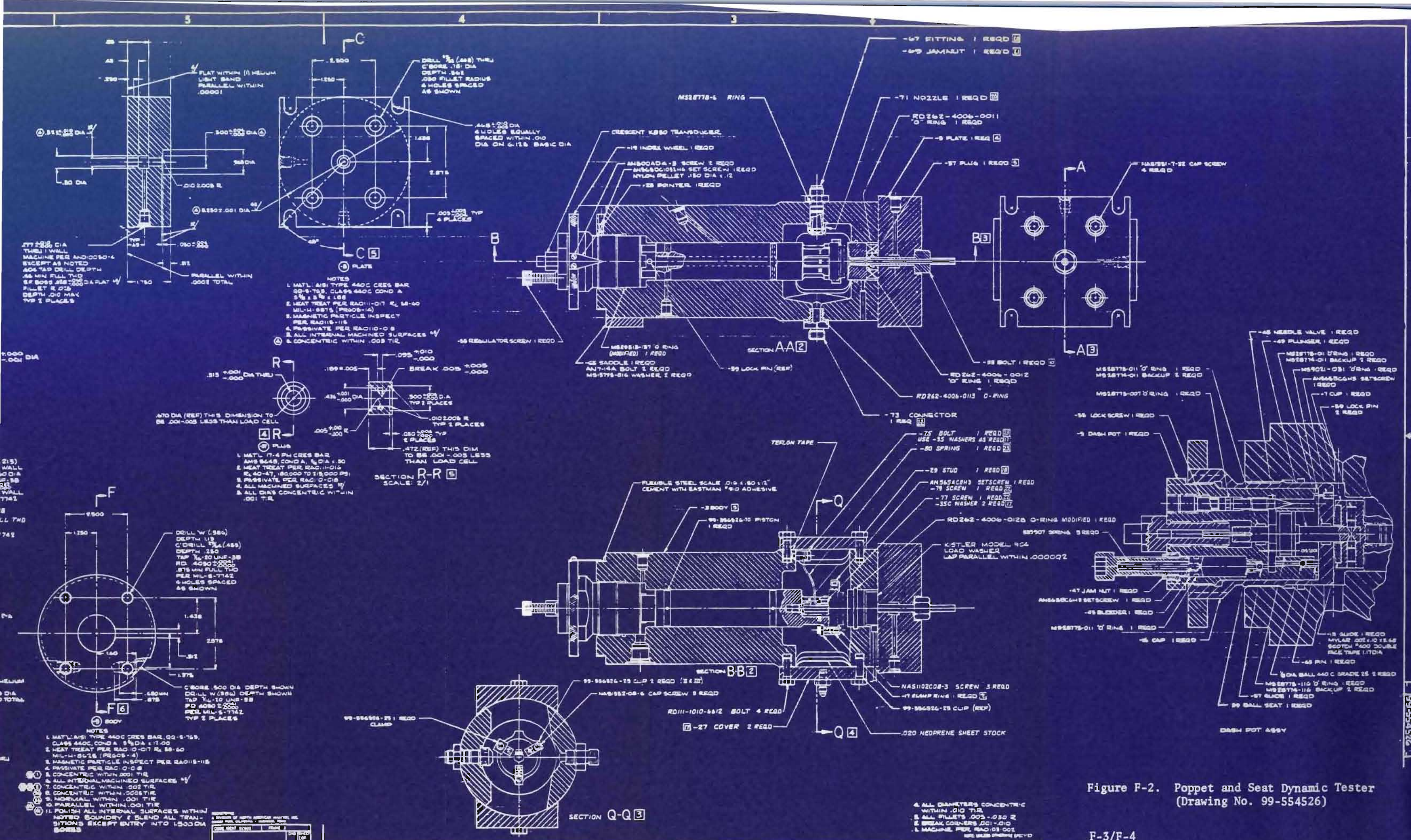


Figure F-2. Poppet and Seat Dynamic Tester
(Drawing No. 99-554526)

F-3/F-4

Poppet and Seat Assembly

With the dynamic tester mounted in a horizontal position, poppet and seat assembly posed no problems. The seat was installed first with 200 pounds bolt load, followed by the poppet and clamp ring. With the latter part engaged on the piston legs, the poppet was safely retained while the three mounting clips were attached. Clip screw torque was ultimately adjusted to improve poppet-seat parallelism, but with initial Phase II models assembly torque was approximately 10 inch-pounds. Even with subsequent readjustment to lesser values (one or two screws) there was no significant post-cycle evidence of poppet-piston interfacial motion or wear.

Concentricity and clearance values and tolerances were the same as for the static tester. Radial misalignment of poppet and seat lands was estimated to be less than 0.001 inch.

Test Model Parallelism

With clamped condition assembly, the effect of model and tester out-of-parallelism was notable. In the previous program, model poppet and seat surfaces were fabricated parallel within 10 microinches (each) at the 0.470-inch mean seating diameter. Piston leg mounting pads were parallel to the seat mounting face (load cell) within 10 microinches. Following model assembly, an electrical contact test versus leakage check (described in later paragraphs) was made to indicate the net equivalent parallel plate gap when the poppet and seat interfaces made first contact. Twenty-five microinches was established as the maximum allowable for this test. Models failing to meet this requirement were disassembled, cleaned, and reassembled on the assumption that contaminants or improper assembly procedure was the cause of poor assembly parallelism. Models passing the arbitrary assembly test were accepted, even though the effect of out-of-parallelism was generally apparent with leakage change extremely load-sensitive (small $\Delta S/\Delta Q$) up to about 2000-psi seat stress. A characteristic stress-leakage curve for an out-of-parallel model thus indicated large reduction (with load) of leakage to the 1000-psi stress region followed by a relatively abrupt slope change where further leakage reduction was much less affected by applied load.

In the subject program, it was discovered that dynamic test model interfacial out-of-parallelism could be significantly reduced by discrete adjustment of the clamp ring screw loads. The model was loaded slightly above the balance pressure level (1000-psig inlet pressure) until leakage could be monitored on the 0.1- to 4.0-scim nitrogen flowmeter. Axial finger load was then applied to each screw in turn, and the effect on leakage noted. The system was depressurized, seating surfaces separated, and screw torques adjusted in the direction indicated by the test to reduce leakage. This procedure was repeated until no further improvement could be achieved and the stress-leakage test was then performed. As will be noted in the sections describing test results, model out-of-parallelism effects above the 1000-psi stress level were nullified, and in most cases, were minimal well below 1000 psi.

The probable degree of nonparallelism, which could be accommodated by clamp ring adjustment, was demonstrated with Test Model 601 (described in Section VII, Phase III Model Tests). This model initially exhibited a poor stress-leakage characteristic with nonparallelism influence evident up to 5000- to 6000-psi stress, even after adjustment capabilities had been exhausted. Parallelism inspection revealed this model had been incompletely finished with a net out-of-parallelism at the 0.470-inch mean diameter of 23 microinches. After refinishing to 7-microinches net deviation, adjustment was readily accomplished and negligible parallelism effect at 500 psi was noted. Except for this model, all flat model surfaces in the subject program were parallel within 12 microinches, and all could be adjusted to produce relatively flat stress-leakage curves. Thus, it is estimated that the parallelism deviation limit, beyond which reasonable dynamic tester adjustment is impractical, is about 15 microinches. Because previous program models were all parallel within 20 microinches maximum, it follows that many of those models might have been improved by the aforementioned adjustment procedure (particularly those models in which screw torques were inadvertently set to increase an out-of-parallel condition).

Cycle and Velocity Control

For model cycling, piston control pressure was applied and vented through a three-way solenoid valve actuated by an automatic cycler. Except for one model configuration, a common control pressure was used for all models and impact velocity-load was controlled by the hydraulic dashpot.

Dashpot design details were described in Ref. 3. It is a variable-orifice device with integral position transducer and is attached to the piston with a connecting shaft. Reservoir pressure is maintained at approximately 200 psig by a spring-loaded piston. For this reason, control pressure during cycling was maintained at a lesser pressure to prevent gas leakage into the dashpot. (In the case of static tests, the reservoir piston spring was overridden by an adjustment screw to increase dashpot pressure to that of specific control pressures applied.)

During the previous program, the dashpot body galled in its housing during assembly preventing disassembly for cleaning and inspection purposes. Since it was possible to refill and air bleed the device without disassembly, this operation was performed prior to initiation of the subject program tests and no dashpot problems occurred. A phenomenon involving the dashpot and position transducer was noted, however.

Impact velocity was computed from the time-piston displacement relationship obtained from oscilloscope readout data. It was observed that impact load rose to a peak value prior to completion of poppet travel, generally with the poppet apparently about 0.003 inch off-seat. It was theorized that the premature load rise was caused by compressive expulsion of seating interface fluid, or a "squeeze film."

The phenomenon was evaluated by comparing both air and liquid impact cycle characteristics; it occurred in both cases. Investigations ultimately revealed that piston actuation force (control pressure) and the dynamically generated dashpot pressure opposing it during piston travel caused transient elastic stretching of the dashpot-piston connecting shaft. The position transducer moving slug, attached to the low pressure end of the dashpot shaft, thus reflected reduced displacement until piston travel stopped

(impact). With dashpot dynamic pressure decay and shaft springback (toward the poppet end of the piston), the slug gave indication of continuing piston motion.

Liquid Flow Adaptation

As shown in Fig. F-2, the dynamic tester incorporated two liquid flow inlet ports and a single drain. Inlet fluid for the test poppet and seat flowed through a combination inlet fitting and seat clamping bolt which provided a clean flow path. After exiting past the poppet, this fluid combined with flush flow introduced through a nozzle at the top of the horizontal tester cavity and discharged through a low-point drain port.

Access hole ledges and the bottom of the tester cavity were sloped to promote free particle flow and drainage. Optimum nozzle position adjustment was established during preliminary tests to minimize residual particles on cavity surfaces after filtered cleanup flow operations. (Surfaces were also polished to reduce particle adhesion tendencies.)

Both nozzle and drain fittings were designed for butt contact with the tester and had 0.001-inch maximum corner radii to minimize particle trapping crevices. Similarly, the inlet fitting bolt had 0.0003-inch maximum diametral clearance with the model seat bores.

The former cylindrical access hole cover was replaced with two separate covers bolted to the tester body and sealed with Teflon tape. Access hole exterior corner radii were less than 0.0005 inch and the tape was trimmed tangent to the hole edge to minimize particle entrapment in this area.

During much of Phase II dynamic testing, an apparent seat load rise to about 200 pounds, just prior to impact, was noted. This condition is shown in Fig. F-3 where, with elapsed time running from left to right, the rising trace represents load cell output. The second (decending) trace indicates piston position and shows relatively constant velocity was not attained until this poppet was about 0.015 inch off-seat.

This phenomenon was initially attributed to a squeeze film effect associated with interfacial fluid expulsion. Ultimately, it was determined as the indication of tester cavity pressure rise caused by piston-displaced fluid. The tester drain capacity was exceeded by the additional transient flowrate and cavity pressure increased accordingly. (For the 1.5-inch OD seat less seat area, 200 pound load is equivalent to 126 psig.) Also, piston velocity was limited by tester pressure and was not fully dashpot controlled.

To alleviate the problem, a surge-suppressing diaphragm was added to the tester. This diaphragm, or bladder, was edge glued to one tester cover (clamped to the body with cover assembly) and pressurized on the order of 1 to 2 psig prior to each liquid test. This produced a bladder volume much greater than that displaced by the piston stroke. Transient cavity pressure was, therefore, prevented from exceeding that of the inlet seat as indicated by the Fig. F-4 load trace of approximately 10 pounds, or 5.5 psig. Prior to this installation, reverse seat flow occurred and affected test particle distribution. As the position trace of Fig. F-4 indicates, dashpot control of piston velocity was also improved.

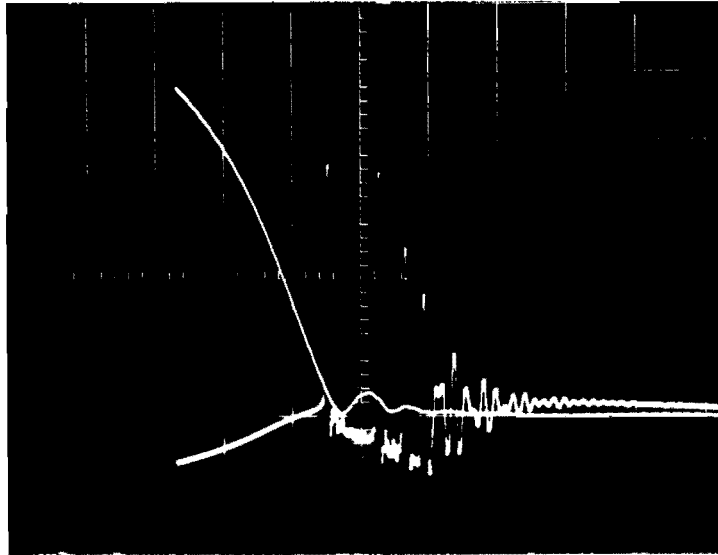


Figure F-3. Load and Displacement Traces Prior to Tester Bladder Installation (0.002 sec/div; 200 lb/div; 0.005 in./div)

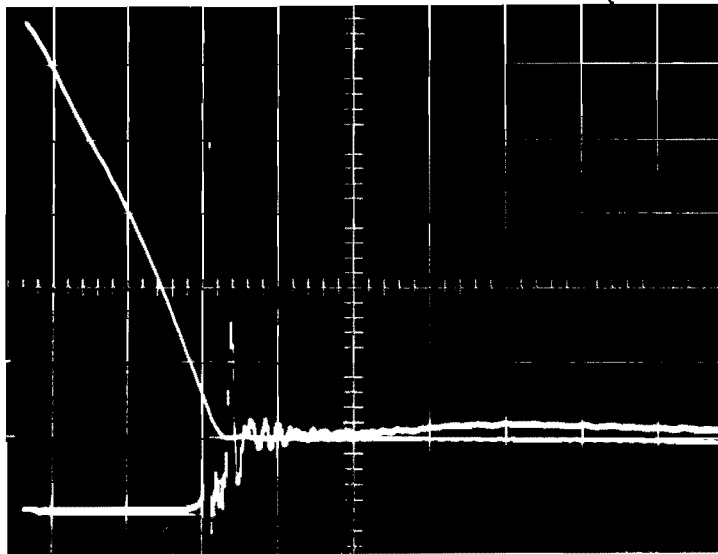


Figure F-4. Load and Displacement Traces After Tester Bladder Installation (0.002 sec/div; 200 lb/div; 0.005 in./div)

Leak Collection

As with the static tester, gross and limited range leak collection provisions were available on the dynamic tester. Leakage in excess of about 5 scim was collected in the tester cavity (covers installed) and directed to the flowmeter via the drain port and the subsequently described discharge valve. For lesser flows, the O-ring, formerly used for static test leakage collection, was employed. With the spherical seat test model, an aluminum leak collector ring was used.

As previously noted, removal of the bias spring precluded precise realignment of the poppet and seat. With the hard seating surfaces this posed no problem, because reoriented testing was desired to obtain worst condition residual effects. However, later Phase III tests using soft metal flat seats revealed secondary surface damage from reoriented embedded particles. Consequently, these later dynamic tests were performed without bias spring removal. This was accomplished by installing the leak collection O-ring stretched onto the 1.313-inch poppet diameter. Following this, the bias spring was installed (fixing poppet-seat alignment). By rolling the O-ring into the wedge-shaped poppet and seat gap, stress-leakage tests could be performed. Subsequently, the O-ring was rolled back onto the poppet for cycling. Tests showed that short term (1 to 2 hours) exposure to Freon TF in the stretched condition produced no significant O-ring permanent set and that cyclic operation did not dislodge the O-ring. This approach was first employed with Model 504. A balance pressure check to establish combined spring and O-ring deflection forces was mandatory for each model because of variations in spring position (poppet and seat over-all length) and high spring rate. Secondly, because the poppet had to be removed to inspect sealing surfaces (or at least the spring disengaged to permit adequate poppet retraction for viewing), only one test series per model could be performed without reorientation.

Poppet and Seat Loading Capability

The dynamic tester produced two types of loads, static and dynamic. Static loads for stress-leakage testing were generated by control pressure acting over the net piston area. With a 1500-psig (maximum) control pressure, gross static loads up to 2500 pounds were available.

Dynamic (impact) load capability was basically a function of mass, spring rate, and impact velocity and far exceeded test needs. In the previous program, impact loads up to 6000 pounds were recorded. For the subject program, peak dynamic loading was generally in the 600- to 800-pound range and never exceeded 1500 pounds. Dynamic loads were measured with a 20,000-pound piezoelectric load cell and charge amplifier system with oscilloscope-photographic readout. As described in Ref. 3, this system, calibrated with piston pressure-area loading, could resolve loads as low as 50 pounds and overall accuracy was within 5 percent. Dynamic loads measured by the load cell were proved in the previous program to accurately reflect actual seat interface loads. This was accomplished with a correlation of digital computer dynamic analysis and test data.

Axial Position Control

The dashpot housing was designed with a 40-pitch thread and handwheel for axial position control. This feature was used both for accurate stroke adjustment and for gaging purposes when determining plastic strain characteristics of specific test models.

In conjunction with screw thread position control, an electrical contact (EC) indicator was used to detect poppet and seat contact. This device incorporated a microammeter, battery, and suitable resistors to give a 7-microampere short-circuit current, suitable for contact recognition, but insufficient to cause visible (500X) pitting.

As described in Ref. 3, the piston and dashpot shaft were electrically isolated from the tester body. By connecting the EC meter between poppet and seat, and advancing the handwheel, zero gap position could be established within 20 microinches. With the handwheel pointer and body scale for reference, cycle stroke was then readily set within ± 0.0001 inch. With magnified pointer-scale viewing, even more precise adjustment would have been possible had it been considered necessary.

As previously noted, a position transducer was built into the dashpot for dynamic position measurement. This device was calibrated at the extreme limits established by basic stroke measurement setup and was monitored by oscilloscope and photographic readout. Previous program calibration of transducer linearity and oscilloscope basic and parallax errors indicated that determination of piston velocity from the displacement-time relationship was accurate within 5 percent.

SEAT LOADING ANALYSIS

With clamped poppet, the analysis of seat loading reduces to a simple axial balance of all forces. Seat loading error is derived from variation in axial loading parameters similar to the static tester but without eccentric load error.

General Force Balance Equation

A general force balance equation is defined below which includes all terms. For different modes of operation, various terms will drop out. Summation of the axial forces gives:

$$\sum F = 0 = P_c (A_p - A_r) - P_t (A_p - A_e) - P_l A_e - F_f - F_o - F_B - S A_s$$

and

$$S \equiv \frac{F}{A_s}$$

where

$$A_e \equiv \frac{\pi}{4} D_e^2 = \frac{\pi}{4} (D_s + \frac{1}{3} L)^2 = \text{effective seating area for flat plate laminar flow pressure distribution, sq in. (Ref. 3)}$$

A_p = dynamic tester piston area 1.762 sq in.

A_r = dashpot rod area, 0.0756 sq in.

A_s = flat seat land normal projected area, sq in.

D_e = effective seat diameter, inches

D_s = mean seat diameter, inches

F = seat force, pounds

F_B = bias flexure spring force, constant on assembly between 30 and 40 pounds

F_f = dashpot O-ring friction, ± 2 pounds

F_o = leak collector O-ring force, 3.5 ± 0.7 pounds

L = flat seat land width, inch

P_1 = seat inlet pressure, 100, 300, or 1000 psig for gas leak testing; 21.0-psig total pressure with poppet closed at standard Freon TF flows

P_c = piston control pressure, variable for gas leak testing; 169 psig for flat model cycle test

P_t = tester cavity pressure, zero during stress-leak testing; 4.0 psig with poppet on seat at standard flow conditions

S = apparent seat stress, psi

Stress-Leakage Testing

Balance Pressure. Similar to the static tester, a balance pressure (P_{cb}) that cancelled all forces was determined prior to gas leakage test. This was accomplished both analytically and by test, depending upon the model configuration. Verification of theoretical and test balance pressure was obtained early in Phase II (flat 440C dynamic test Model 120). In this case, balance pressure was determined from sharp leakage change at $P_1 = 1000$ psig with only P_1 and P_c as variables (dashpot, bias spring, etc., disconnected). From measurements, P_{cb} was computed at 101.9 psig compared with test results of 102.0 ± 0.2 psig. Additional tests performed at $P_1 = 0$ and 1000 psig with the dashpot and other devices installed indicated their respective load inputs as defined in the preceding nomenclature list.

For stress-leakage testing, balance pressure is defined by $S = 0$ and thus,

$$P_{cb} = \frac{P_1 A_e + F_f + F_o + F_B}{A_p - A_r}$$

Seat Stress. Seat stress (S) is computed from the net increase of control pressure above the balance point ($P_{c\Delta}$); thus,

$$S = \frac{(P_{cb} + P_{c\Delta}) (A_p - A_r) - (P_l A_e + F_f + F_o + F_B)}{A_s}$$

which reduces to

$$S = \frac{P_{c\Delta} (A_p - A_r)}{A_s}$$

Seat Stress Error. Seat stress error in the dynamic tester resulted from the same variables identified for the static test (except eccentricity). The additional loading variable of dashpot friction (± 2 pounds) is relatively insignificant for flat model seat stress above 1000 psi. Moreover, with very low load testing, the friction effect was nearly cancelled by repetitive balance pressure measurements. Consequently, percentage stress errors and error band curves (Fig. C-4 and C-5 for E S) established for the static tester are considered representative of dynamic tester data.

Cycle Testing

Static seat stress during cycle testing in Freon TF is computed from the force balance equation, as follows:

$$S = \frac{P_c (A_p - A_r) - P_t (A_p - A_e) - P_l A_e - F_f - F_B}{A_s}$$

For the standard flat model (defined in static tester, Appendix C) and 169 psig (P_c) control pressure, the indicated static stress is 5370 psi or 238 pounds (Nominal net $P_c = 141$ psig).

APPENDIX G

DYNAMIC TEST SYSTEM AND MODEL TEST PROCEDURES

The most difficult aspects of testing valve seating are (1) recognition of significant variables, and (2) designing a test system in which these variables can be isolated, controlled, and thus quantitatively assessed. The previously described dynamic tester provided precise control of the myriad valve seat leakage variables. The purpose of the dynamic test system was to provide a controlled fluid contamination environment for poppet and seat models cycled in the dynamic tester. By comparison of clean control data in the form of visual inspection and seating load (stress) versus leakage before and after cycling, the effects of a known contaminant environment could be determined.

From the Phase I Survey (Ref. 4), the following two candidate methods for obtaining a controlled fluid contamination level emerged:

1. A pump or pressure blowdown system in which a concentrated contaminant slurry is injected downstream of a filter directly to the test model poppet and seat. A clean, trap-free flow section would be required only between the injector and test model.
2. A pump recirculation system in which the entire system is designed for low contaminant generation (background) and is free of traps to maintain a steady state particle flow.

At first glance, the injection method appeared to be the simplest approach and had been employed by others with limited success (Ref. 4). Further study of each method, however, led to the conclusion that the requirement for steady fluid flow with constant particle concentration over a period of hours would best be met by the recirculation system. This was based on the conservation of expensive classified test particles and the anticipated mechanical difficulties associated with steady flow particle injection. The major obstacle anticipated in the recirculation system was pump seal contamination.

General design objectives established for the system were as follows:

1. Steady-state clean flow for 2 hours.
2. Steady-state particle flow for 2 hours.
3. Automatic particle counting with continuous pitot sampling.
4. Seat particle flow diverted from higher flow mainstream which would be unaffected by test model cycling.
5. System flows to be free from pulsations, compatible with basic test model flow area and of sufficient velocity to maintain particle flow.

6. Standard flows and line resistances to be established such that all valves are wide open during unfiltered operation (i.e., no valve throttling).
7. Existing commercial components to be used with minimum modification to achieve a configuration free of particle traps.
8. Hard lines and butt-joint connections.
9. Valving to provide bypass filter flow for cleanup and alternate 1000-psig gaseous nitrogen pressure feed to the test model.
10. Test particle size 10 to 300 microns.
11. System installation in class 100,000 clean room with availability of associated cleaning, flushing, and particle counting equipment.

An overall system performance goal was to quantitatively reconcile particle input-output in terms of (1) weight input, (2) sample data, (3) fluid and particle velocities, and (4) percent of weight input extracted. These data would thereby provide understanding of changing particle counts as a function of (1) time, (2) filtration, and (3) test model cycling.

Freon TF was a natural choice for a system fluid because of its solvent action, filterability, nontoxicity, and high evaporative rate (118 F boiling point). Close proximity of a high-pressure Freon TF blowdown system provided a ready fluid source and additional high flow capability. TF is a registered trademark of the DuPont Co.)

The dynamic test system which finally evolved resulted from study and analysis of many commercial pumps, valves, and fittings. It was considered desirable to have all joints and connections such that there were no re-entry dead cavities, nor any shoulders presented to on-coming flow exceeding 0.004 inch (100 microns). Also carefully evaluated was the particle counter which was found to be absolutely essential in system development and subsequent poppet and seat testing. Final selection of system hardware and necessary design modifications resulted in many compromises. Some of these contributed to system performance limitations. Because of the many unknowns in controlled particle flow and measurement, a period of development and attendant modification was necessary to achieve satisfactory operation. This was followed by system calibration, performance evaluation, and development of standard operating procedures for poppet and seat model tests.

GENERAL DESCRIPTION AND OPERATION

A schematic of the dynamic test system is shown in Fig. G-1 with associated instrumentation defined in the block diagram of Fig. G-2. Relative size and position of components have been portrayed to closely represent the actual system and thus facilitate detail examination of system photographs. The system was built around a 4- by 8-foot table in a class 100,000 clean room which also contained the controls and flow section of a 600-psi Freon TF flow bench. Main portions of the system are shown by Fig. G-3 (central), G-4 (bottom), G-5 (right front), and G-6 (right end). Closeup photographs are shown by Fig. G-7 (sample system),

G-8 (Varidrive-pump), G-9 (tester front), G-10 (tester end), and G-11 (HIAC particle counter). Drawings of special hardware fabricated for the system are detailed in Fig. G-12 through G-23 which are cross-referenced in the schematic (Fig. G-1).

Major parts of the system are discussed in the order of flow circuits, hardware, and instrumentation as follows:

Main Flow Circuits

Filter Flow Circuits

Sample Flow Circuits

Subsidiary Circuits

Reservoir

Pump

Valves

Lines and Fittings

Diverter and Samplers

Sample Flow Manifold

Membrane Filters

Pressure Gages

Flow Indicators

Particle Counter

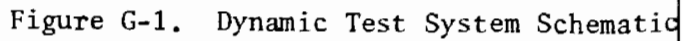
Auxiliary Instrumentation

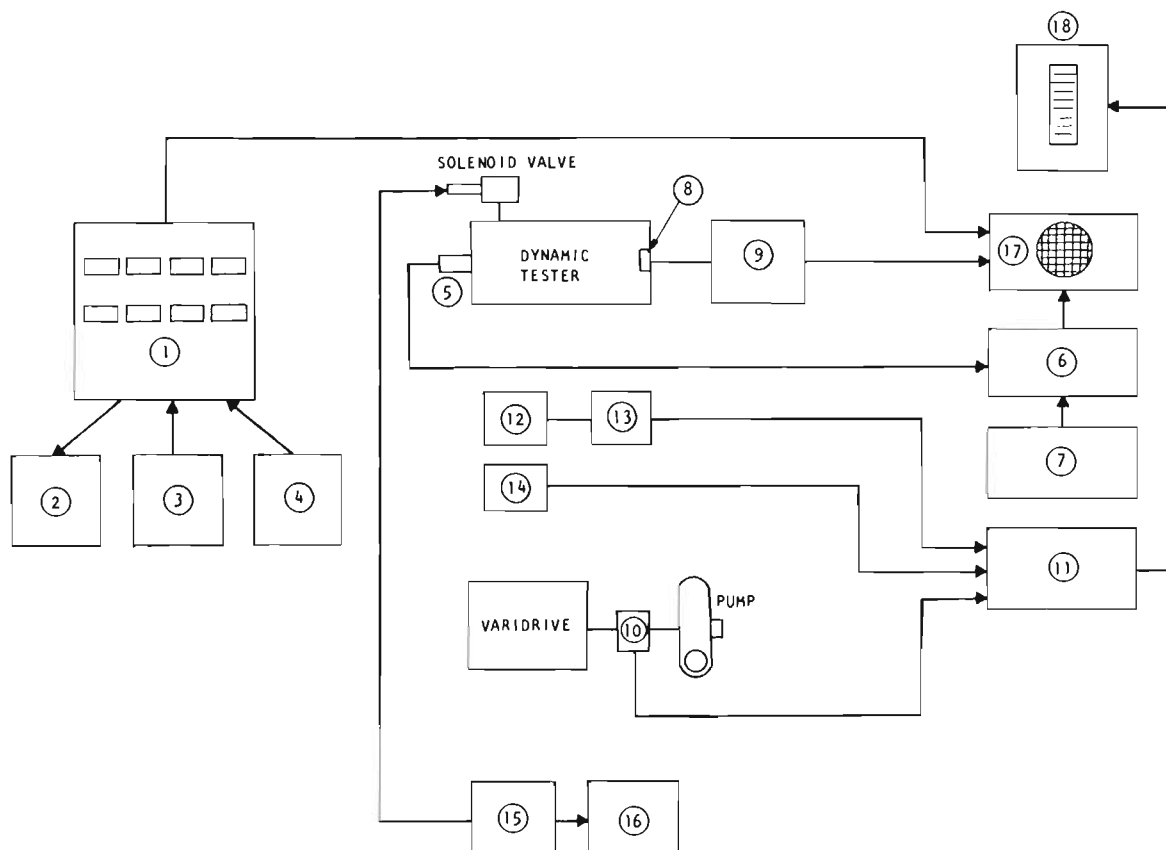
Main Flow Circuits

The main flow loop, designated by system flow (Q_s), consisted of a 3/8-inch CRES line which carried fluid from a centrifugal pump (Fig. G-8) to a pitot tube flow diverter (Fig. G-7) where 20 percent of main flow (Q_s) was diverted for seat flow (Q_b). The main line continued to the tester cavity, housing the test poppet and seat (Fig. G-10), where its discharge through a five-hole shower head served to flush this area. Main and seat bypass flows recombined inside the tester cavity and returned to a conical reservoir (Fig. G-6) to close the loop.

The purpose of the 20-percent diverted (Q_b) flow was to maintain a fairly constant main stream particle flow during cycling when (Q_b) seat flow was interrupted. In this fashion, it was expected (and subsequently proved) that a uniform concentration of particles could be extracted via the diverter for seat cycle testing.

The objective of wide open valves under standard flow conditions was achieved by adjusting line resistances. This was accomplished by crimping the 3/8-inch line upstream of VNI, as shown by Fig. G-10. The dynamic tester could be isolated from the liquid system by three valves, V3, V4,

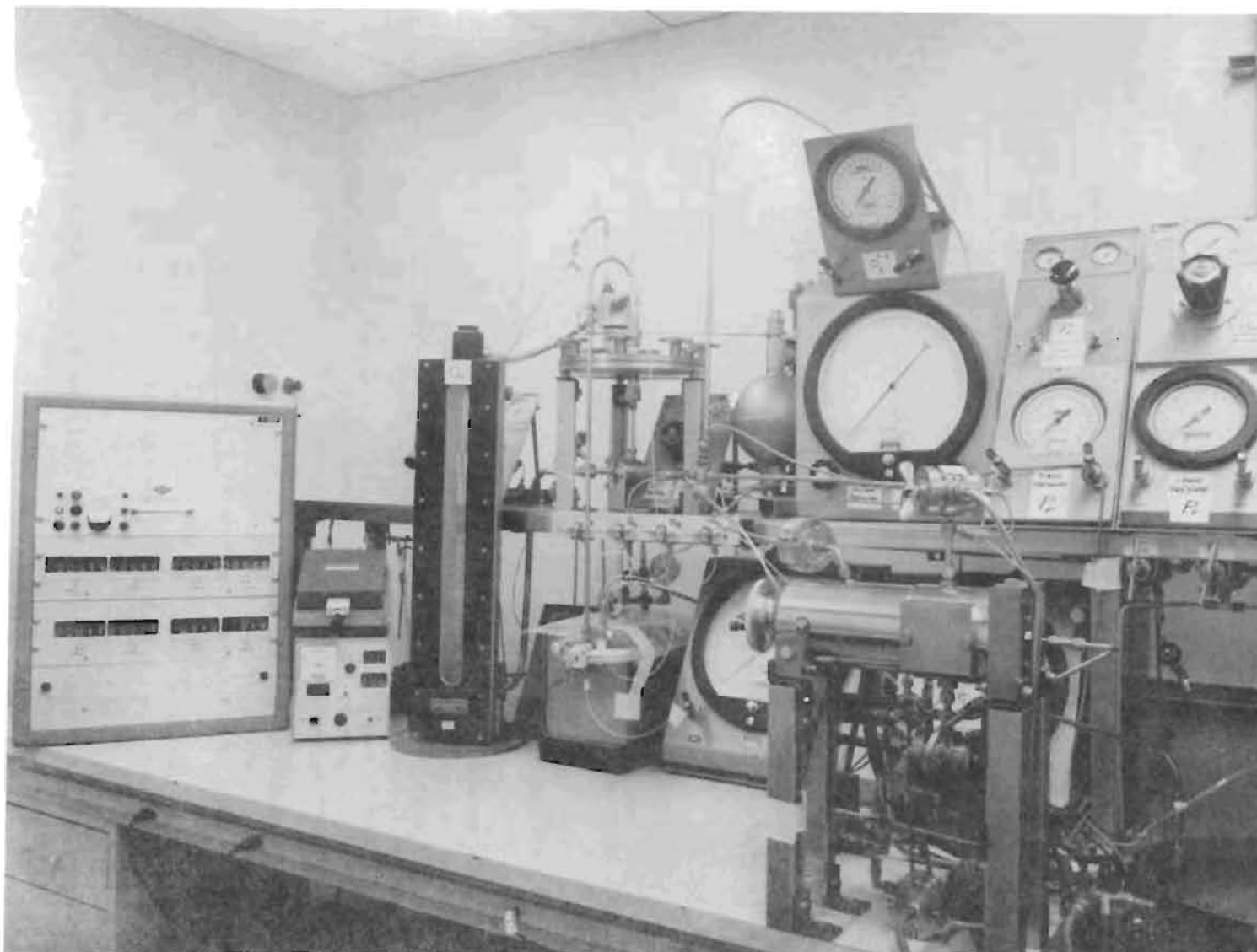




INSTRUMENTATION BLOCK DIAGRAM LEGEND

- 1 HIAC (HIGH ACCURACY PRODUCTS CORP.) AUTOMATIC PARTICLE COUNTER MODEL PC-20, S/N 2; EIGHT CHANNEL VISUAL READOUT; CONTROL, AND CALIBRATION SECTIONS
- 2 HIAC TAPE PRINTER
- 3 HIAC AUTOMATIC SAMPLING AND PRINTOUT (ASPO) SECTION
- 4 HIAC PARTICLE SENSOR SECTION, MODEL C-300 MICROCELL
- 5 POPPET POSITION INDICATOR, CRESCENT ENGINEERING AND RESEARCH CO. VARIABLE PERMEANCE LINEAR TRANSDUCER, MODEL KB-50.
- 6 3KC CARRIER-AMPLIFIER, CONSOLIDATED ELECTRONICS CORP., TYPE 1-113B
- 7 OSCILLATOR-POWER SUPPLY, CONSOLIDATED ELECTRONICS CORP., TYPE 2-105A
- 8 PIEZOELECTRIC LOAD WASHER, KISTLER INSTRUMENT CORP., MODEL 904, 0 TO 20,000 POUNDS RANGE
- 9 CHARGE AMPLIFIER, KISTLER MODEL 568
- 10 SIX-POLE PROXIMITY RPM TRANSDUCER, ELECTRO 3030-HTAN
- 11 THREE-CHANNEL FLOW PULSE CONVERTER, WAUGH ENGINEERING CO., MODEL FR-213
- 12 FLOWMETER (Q_s), FISCHER AND PORTER TURBINE TYPE 1/2-10 MODEL 15430, 0.2 TO 6.5 GPM, 0.3 PERCENT PRECISION CALIBRATION
- 13 FLOWMETER OSCILLATOR-PREAMPLIFIER, MODEL 55 GE2239X
- 14 FLOWMETER (Q_B), WAUGH ENGINEERING CORP. MODEL FL-6S, 0.1 TO 1.0 GPM
- 15 ELECTRONIC CYCLER (20VOC), SEPARATELY VARIABLE ON-OFF PERIODS
- 16 CYCLE COUNTER
- 17 DUAL BEAM OSCILLOSCOPE, TEKTRONIX INC., MODEL 502A
- 18 VERICAL SCALE DRUM INDICATOR, BROWN ELECTRONIK, 500 DIVISIONS FULL SCALE

Figure G-2. Dynamic Test System Instrumentation Block Diagram



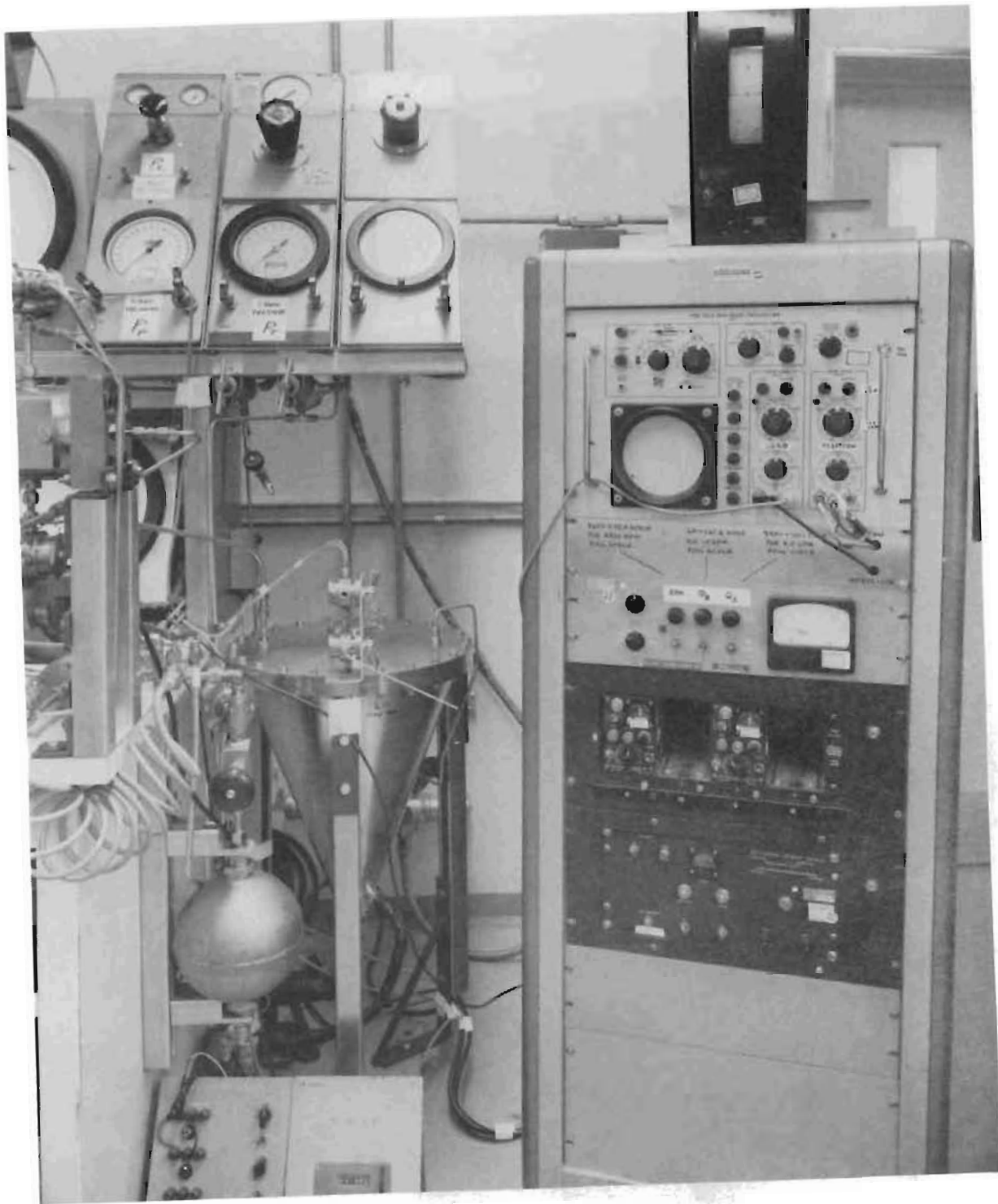
6AL42-11/6/69-C1E

Figure G-3. Dynamic Test System Setup (Central)



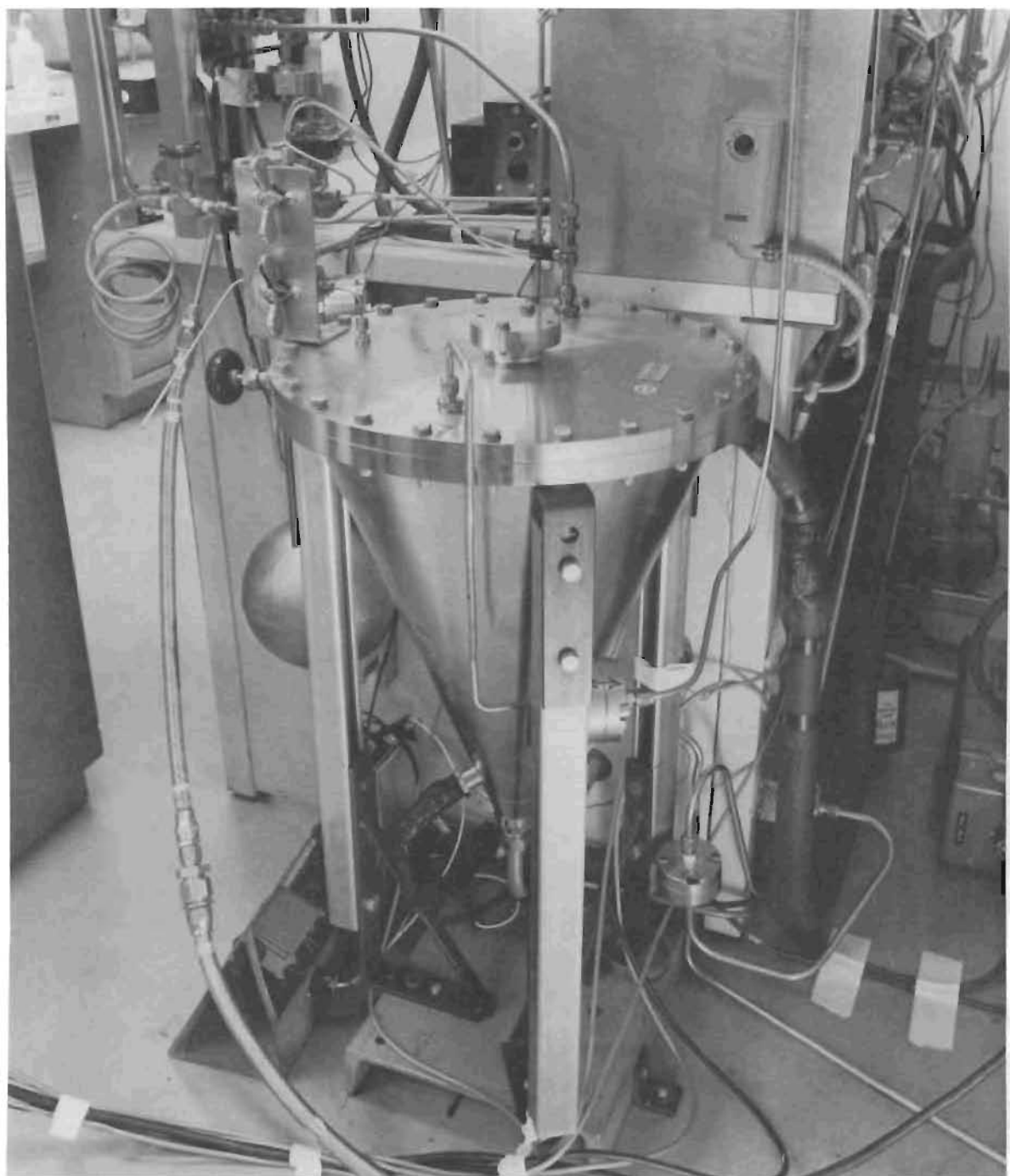
6AL42-11/6/69-C1C

Figure G-4. Dynamic Test System Setup (Bottom)



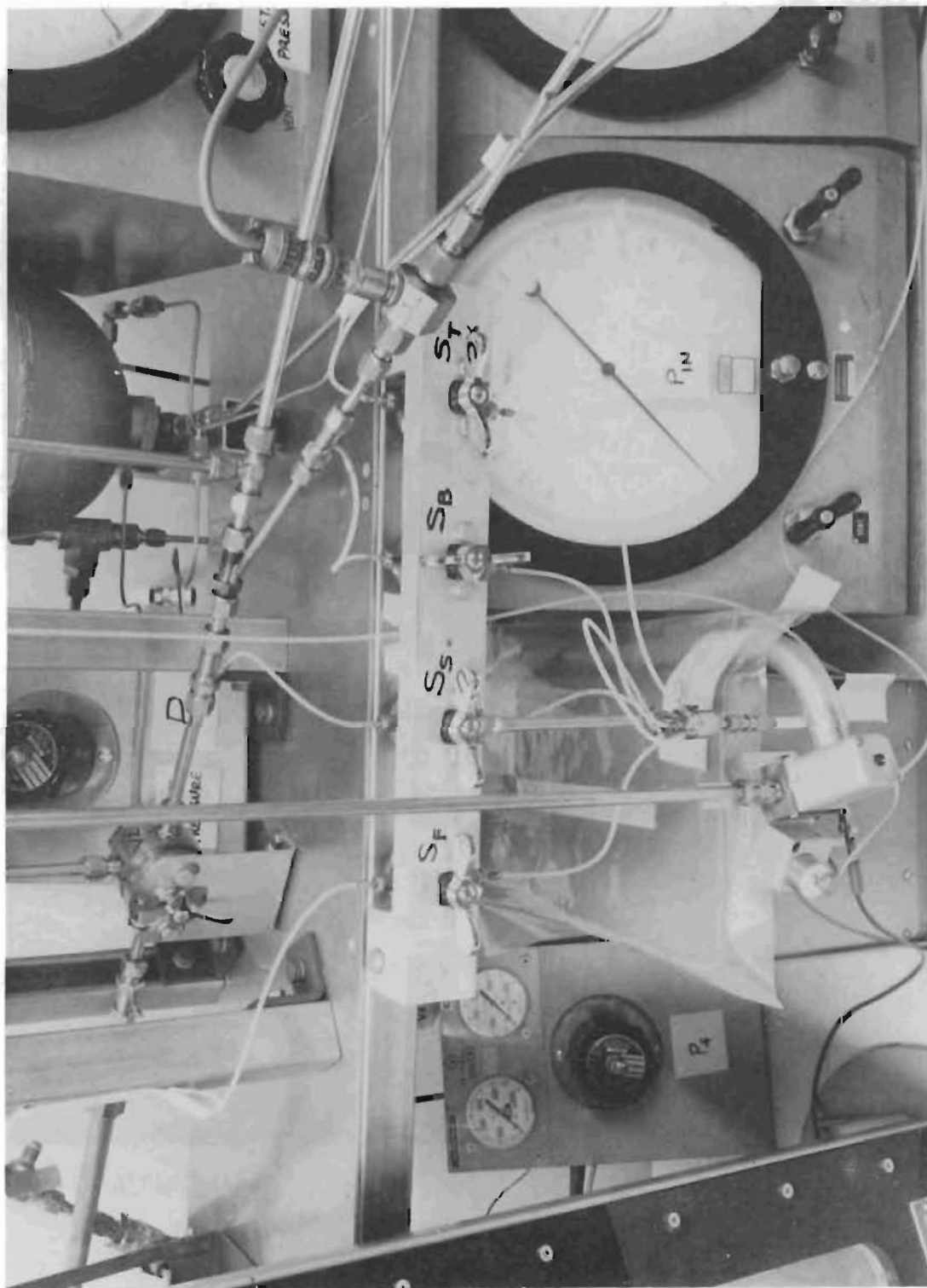
6AL42-11/6/69-C1G

Figure G-5. Dynamic Test System Setup (Right Front)



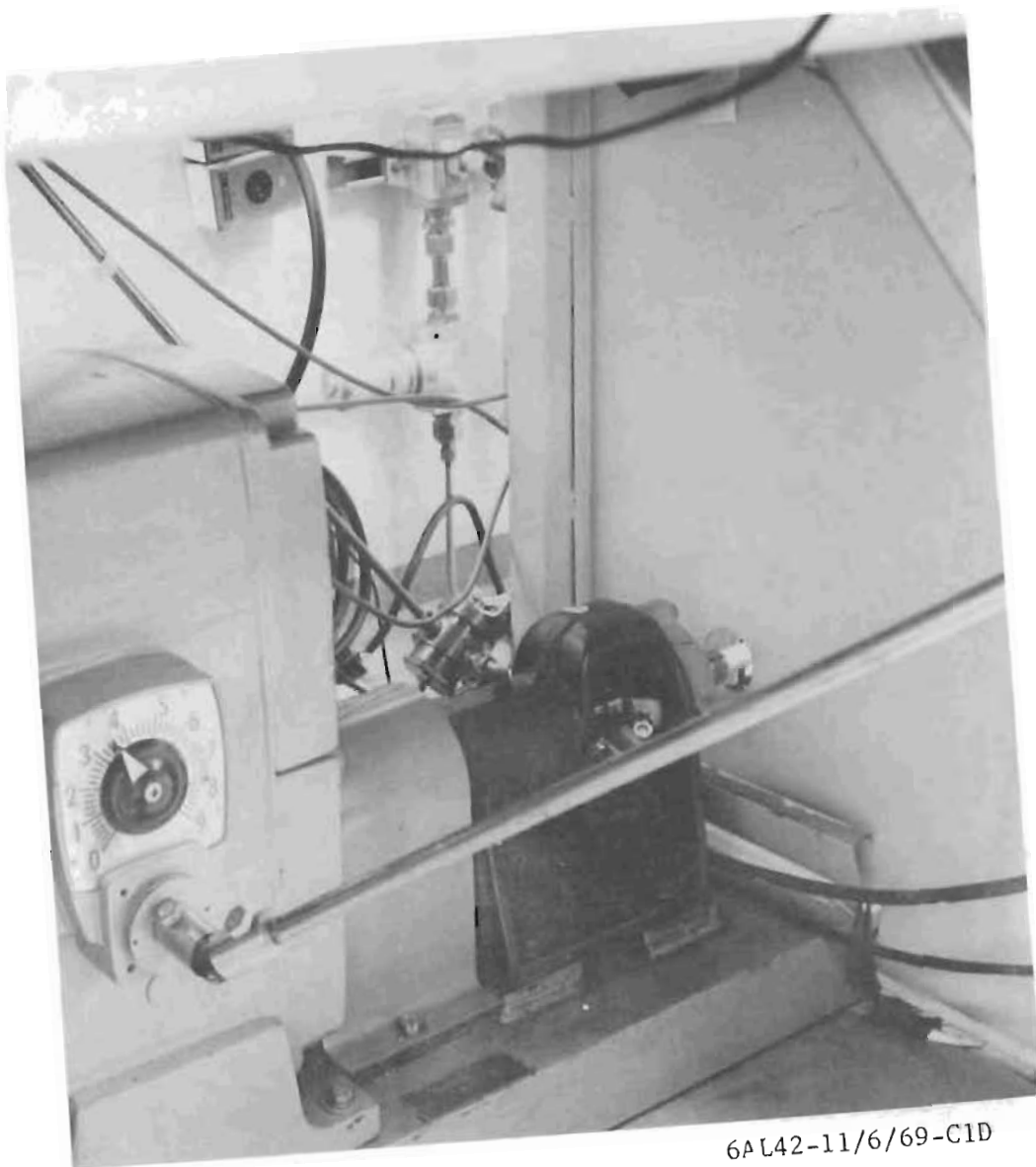
6AL42-11/6/69-C1M

Figure G-6. Dynamic Test System Setup (Right End)



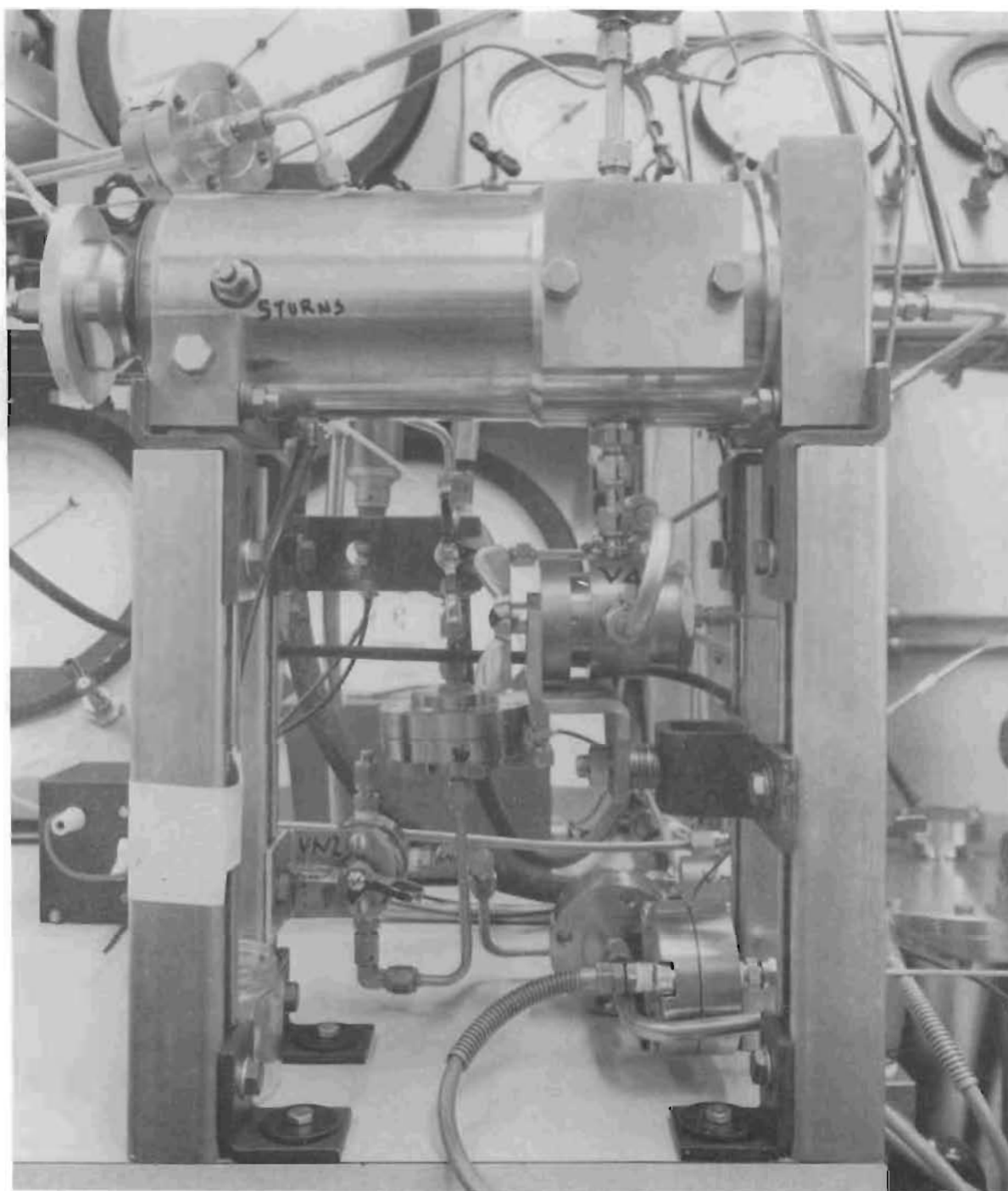
6AL42-11/6/69-C1B

Figure G-7. Sample System



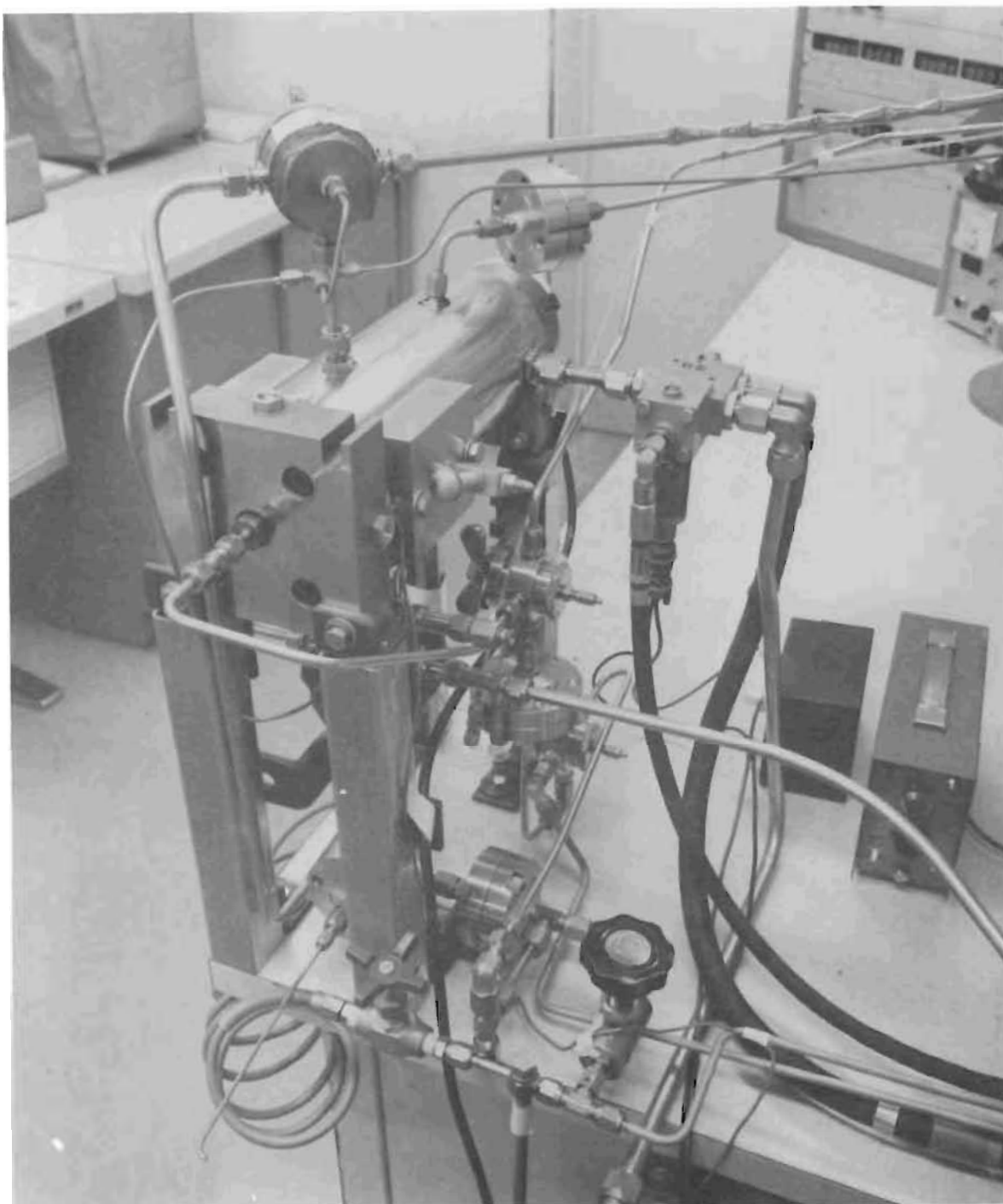
6AL42-11/6/69-C1D

Figure G-8. Varidrive Pump



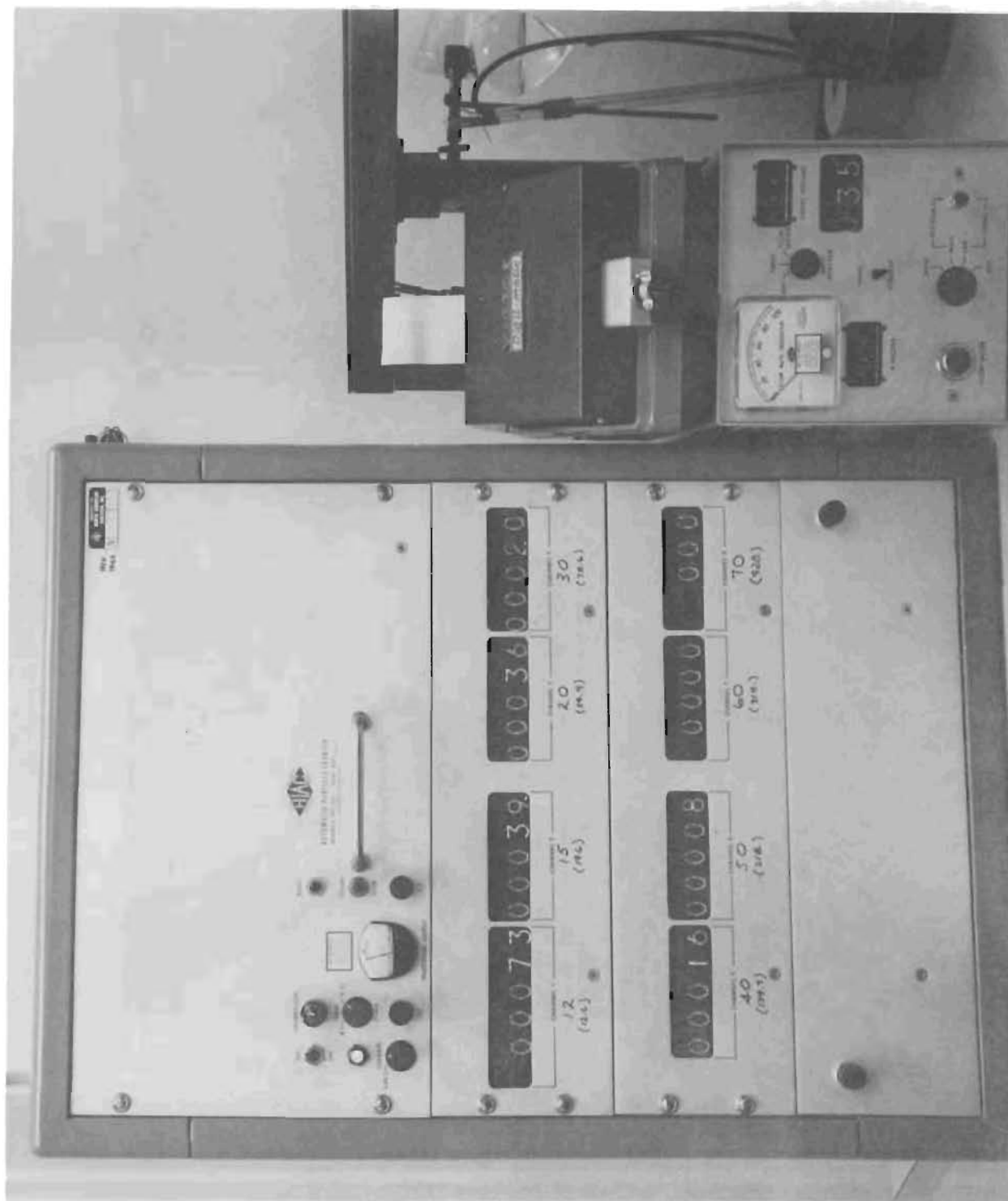
6AL42-11/6/69-C1N

Figure G-9. Dynamic Tester Front



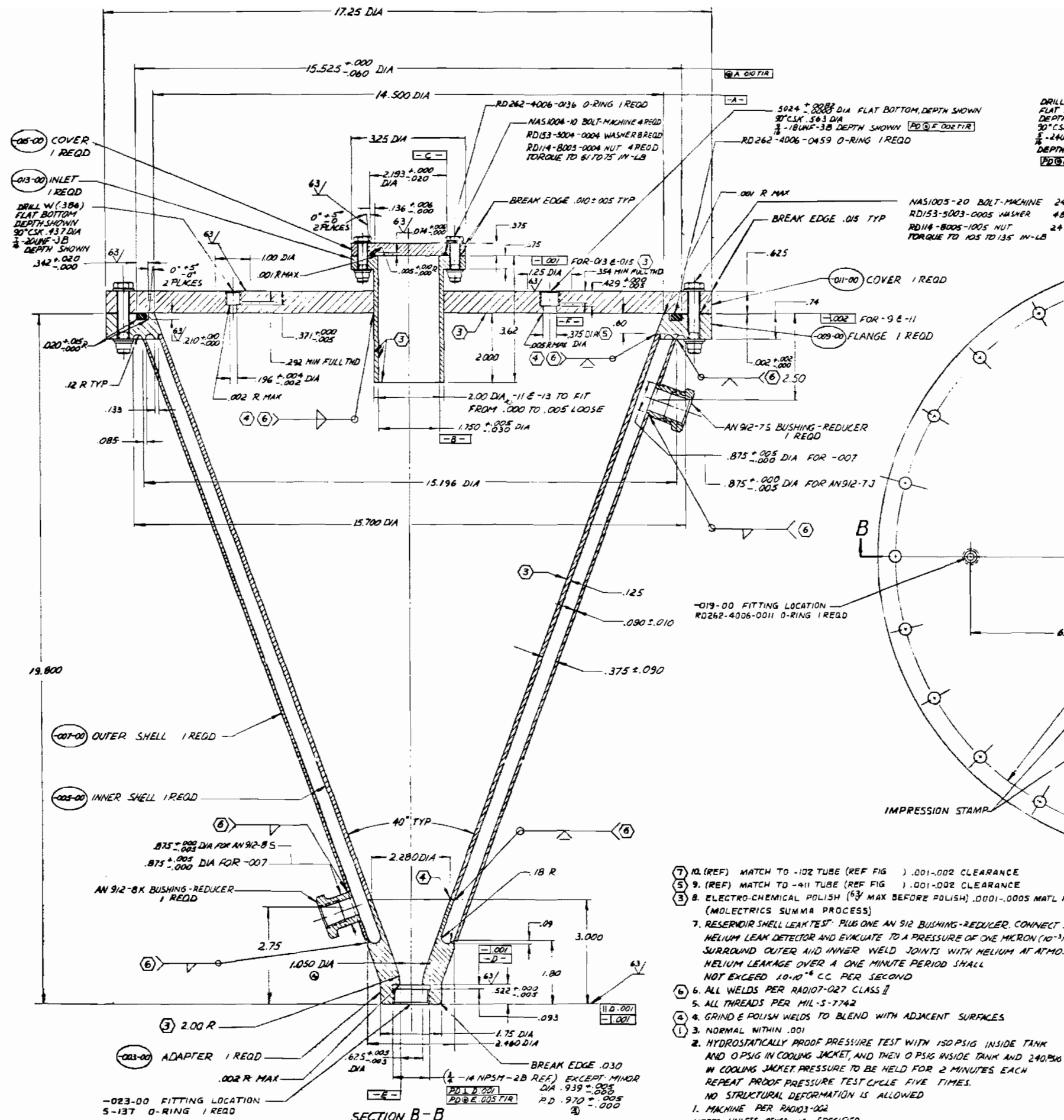
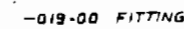
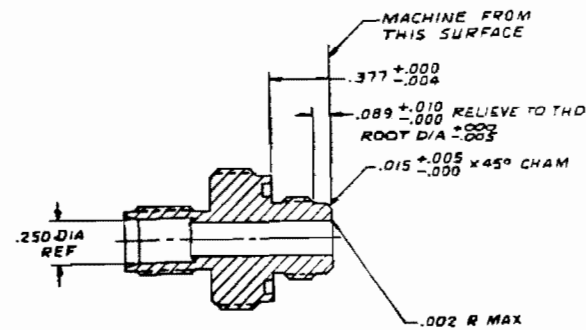
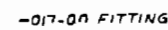
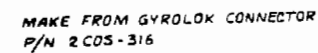
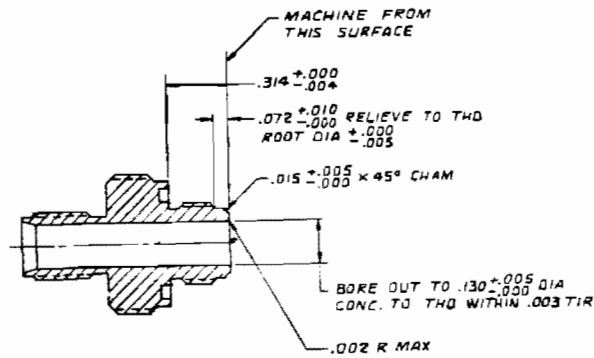
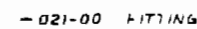
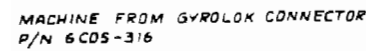
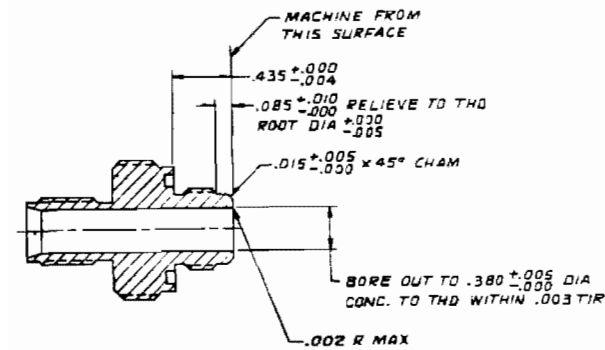
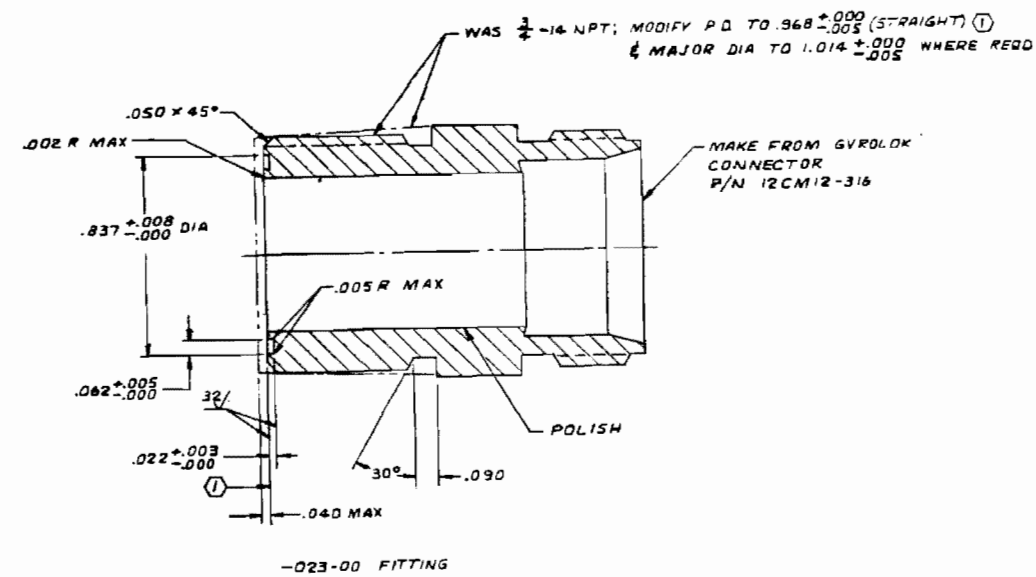
6AL42-11/6/69-C1H

Figure G-10. Dynamic Tester End



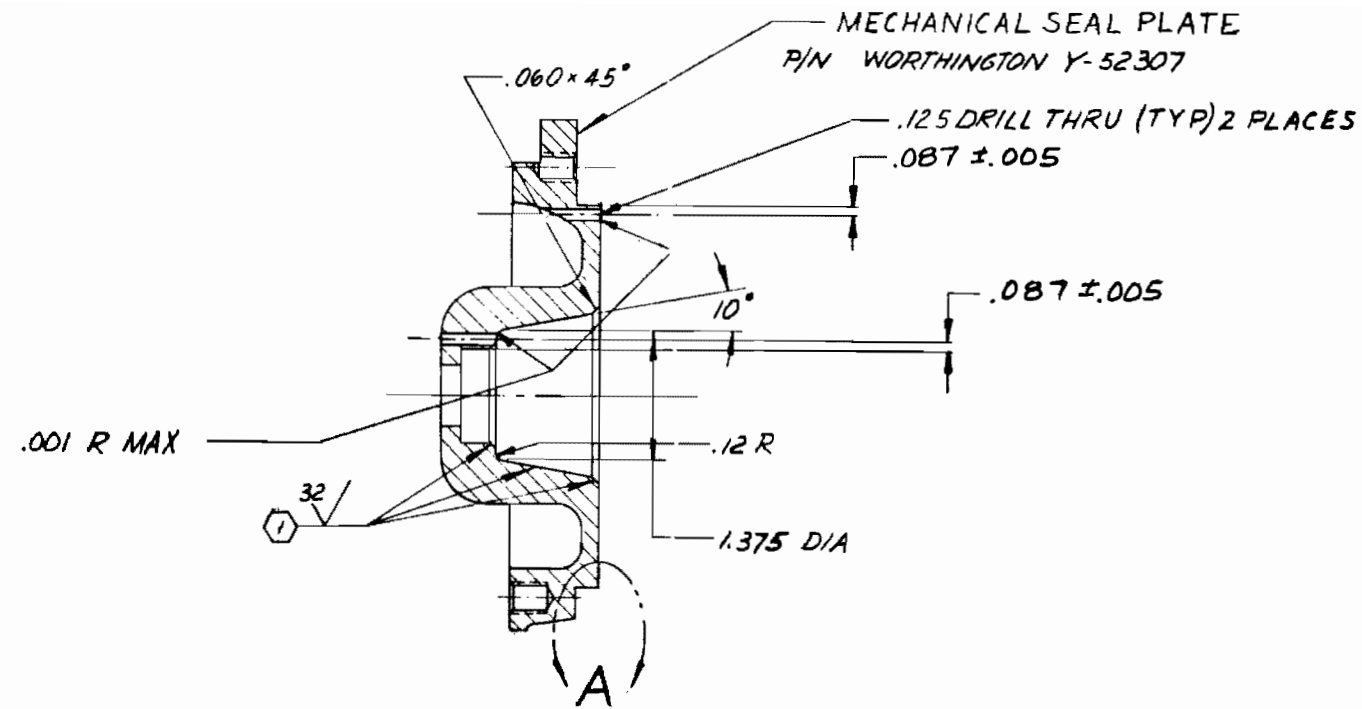
6AL42-11/6 /69-CIF

Figure G-11. HIAC Particle Counter



- ⑦ 12. (REF) MATCH TO -102 TUBE (REF FIG) .001-.002 CLEARANCE
 - ⑤ 9. (REF) MATCH TO -411 TUBE (REF FIG) .001-.002 CLEARANCE
 - ③ 8. ELECTRO-CHEMICAL POLISH (63% MAX BEFORE POLISH) .0001-.0005 MATL. (MOLECTRICS SUMMA PROCESS)
 7. RESERVOIR SELL LEAK TEST: PLUG ONE AN 912 BUSHING-REDUCER. CONNECT HELIUM LEAK DETECTOR AND EVACUATE TO A PRESSURE OF ONE MICRON (10^{-3}). SURROUND OUTER AND INNER WELD JOINTS WITH HELIUM AT ATM. HELIUM LEAKAGE OVER A ONE MINUTE PERIOD SHALL NOT EXCEED $10 \cdot 10^{-6}$ CC PER SECOND
 - ⑥ 6. ALL WELDS PER RAD107-027 CLASS II
 5. ALL THREADS PER MIL-S-7742
 - ④ 4. GRIND & POLISH WELDS TO BLEND WITH ADJACENT SURFACES
 - ③ 3. NORMAL WITHIN .001
 2. HYDROSTATICALLY PROOF PRESSURE TEST WITH 150 PSIG INSIDE TANK AND 0 PSIG IN COOLING JACKET, AND THEN 0 PSIG INSIDE TANK AND 240 PSIG IN COOLING JACKET. PRESSURE TO BE HELD FOR 2 MINUTES EACH REPEAT PROOF PRESSURE TEST CYCLE FIVE TIMES.
NO STRUCTURAL DEFORMATION IS ALLOWED
 1. MACHINE PER RAD103-002
- NOTES UNLESS OTHERWISE SPECIFIED

- STUFFING BOX SEAL PLATE
P/N WORTHINGTON Y-52973



5 $\pm .005$
- .000
32/1

MACHINE TO CLEANUP FACE
WITH MINIMUM MATERIAL
REMOVAL

0050 $\pm .0000$
- .0002 DIA

32/1

.001 R MAX

-- WELD TO BUILDUP PRIOR TO MACHINING
CARPENTER 20 CB OR EQUIVALENT MAT'L

040 MIN

OR BOTH STUFFING BOX PLATES)

2. XX $\pm .03$, .XXX $\pm .010$
① 1. POLISH AFTER MACHINING

NOTE: UNLESS OTHERWISE SPECIFIED

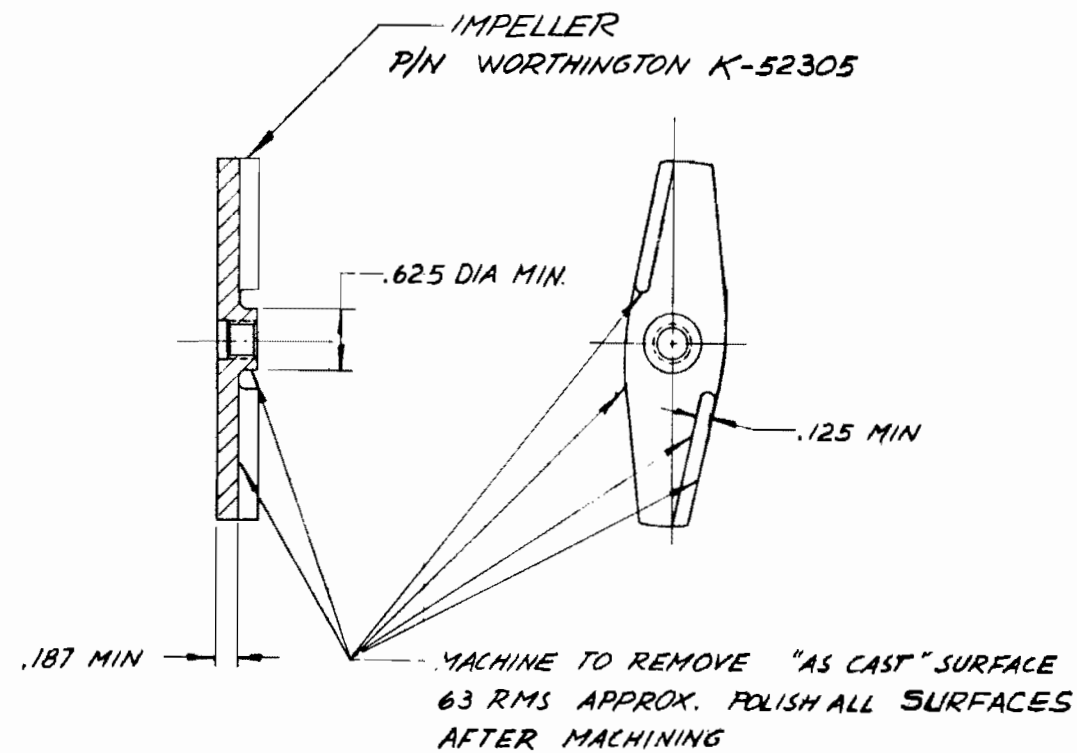
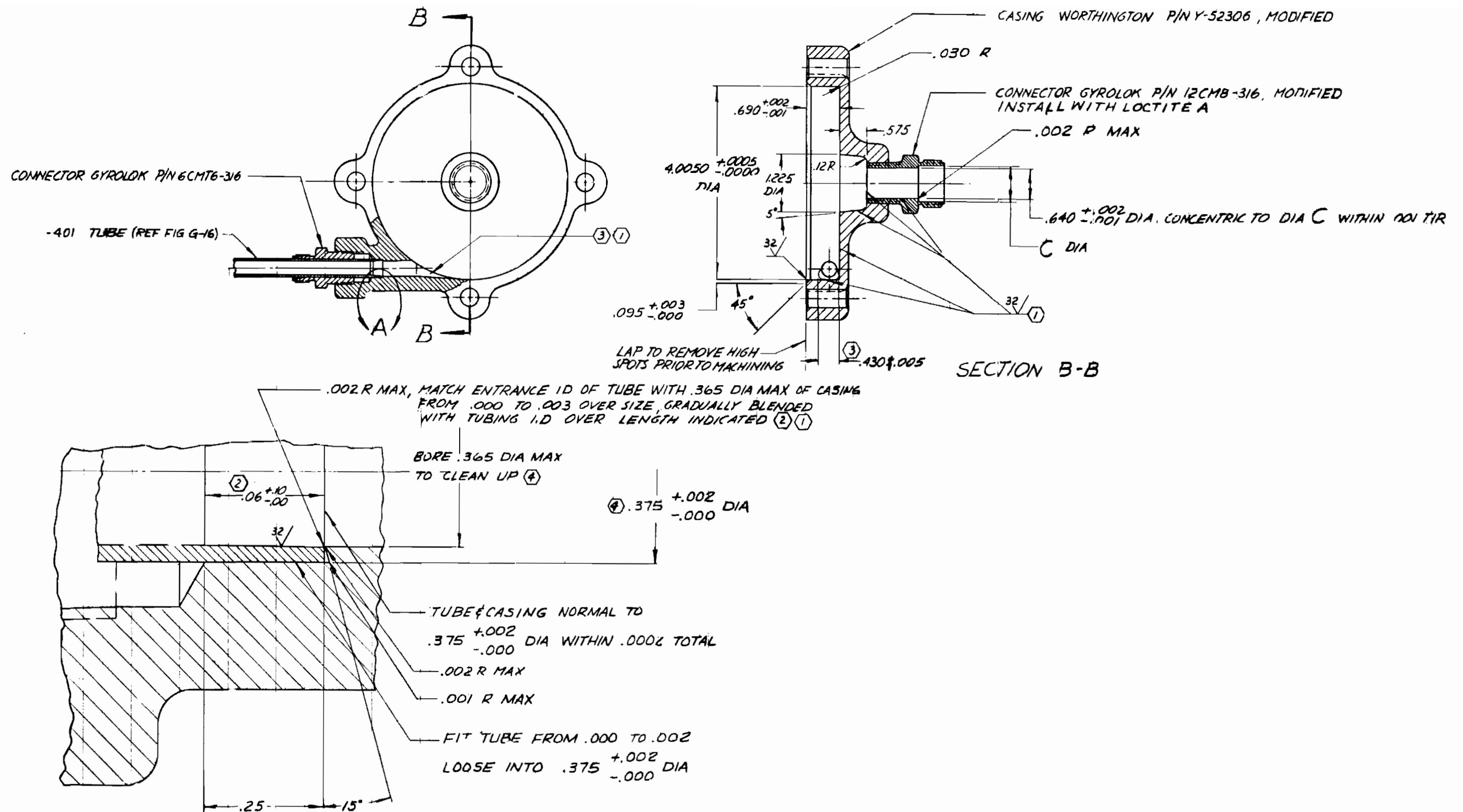
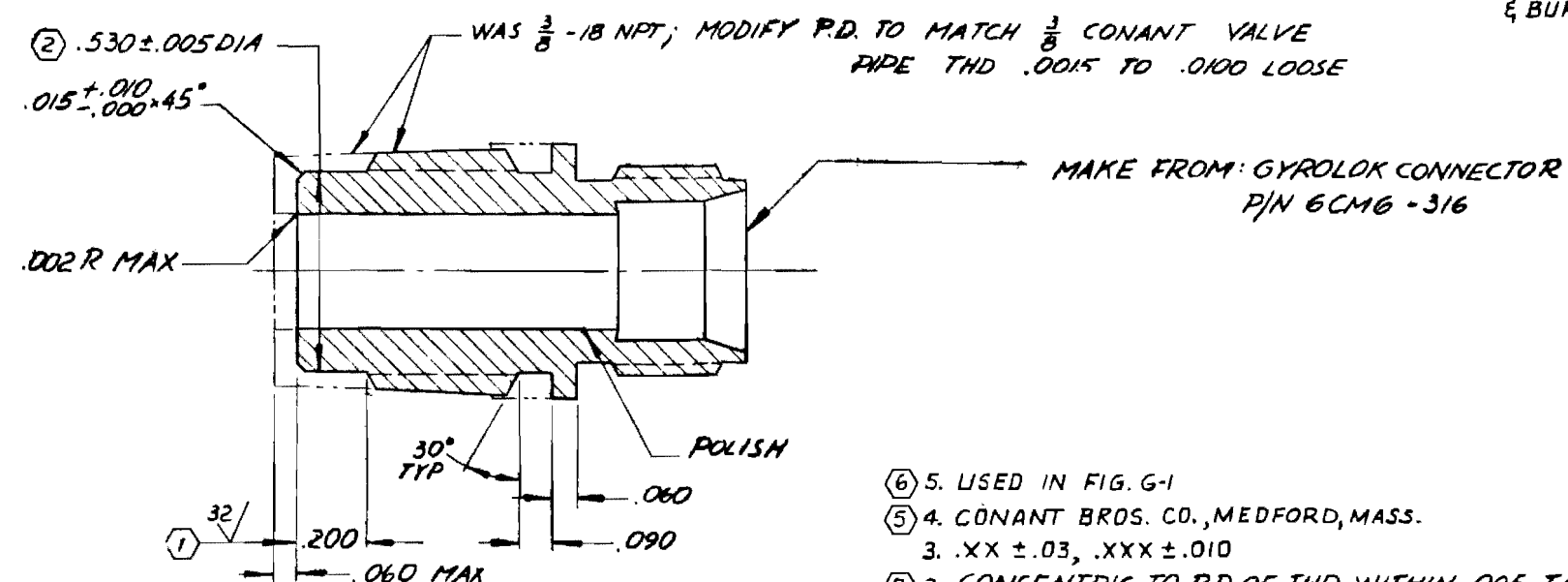
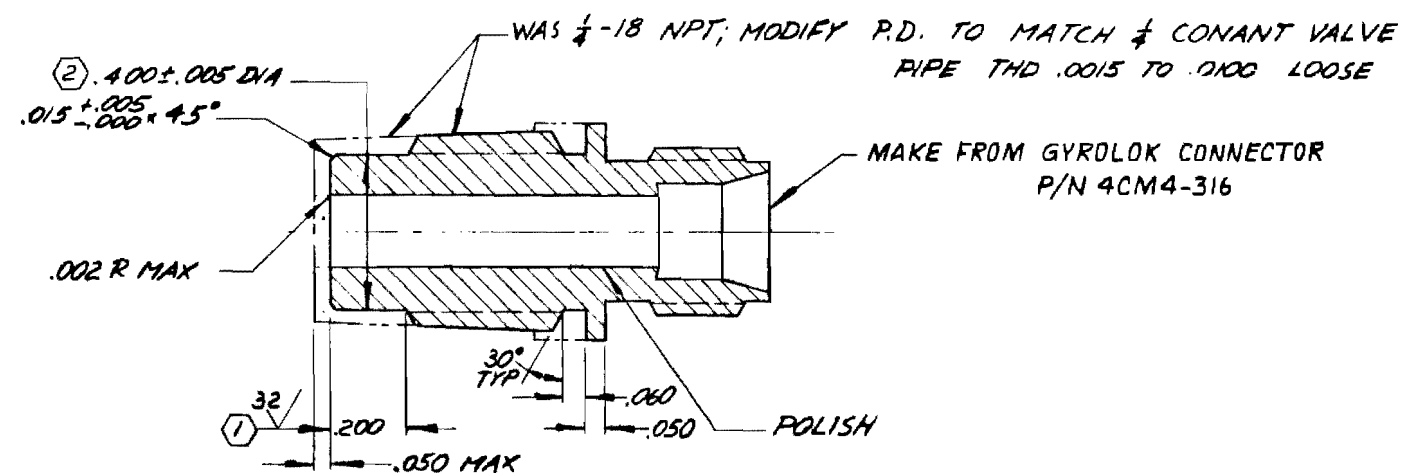
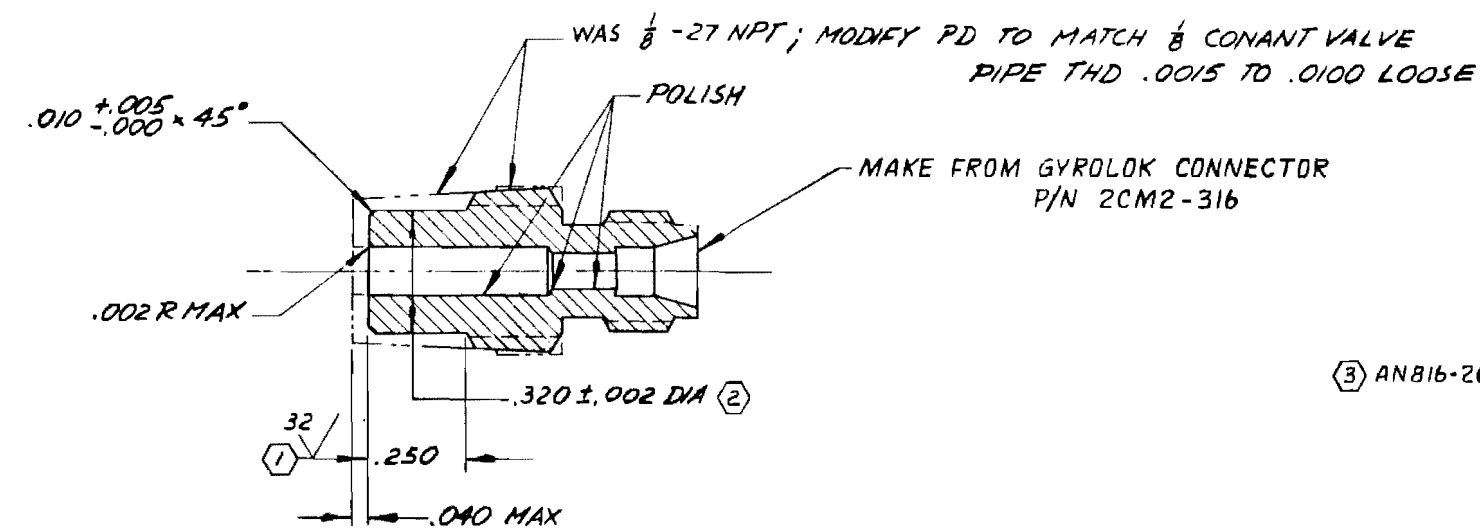


Figure G-13. Pump Plate and Impeller
Modifications (Sketch
No. 6096)



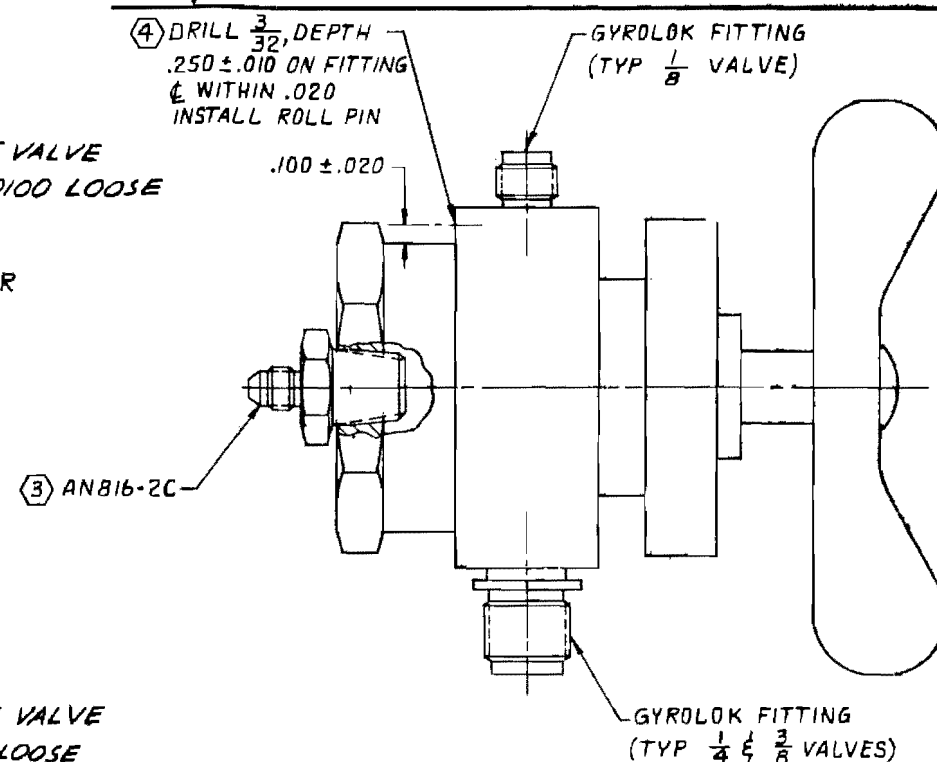
5. .XX ±.03, .XXX ±.010
4. BREAK CORNERS .005^{+.005}/_{-.000}
- (4) 3. CONCENTRIC WITHIN .001 TIR
- (3) 2. BLEND .365 DIA MAX WITH 4.0050 DIA, APPROX. AS SHOWN
- (1) 1. POLISH AFTER MACHINING
- NOTE: UNLESS OTHERWISE SPECIFIED

Figure G-14. Pump Inlet Casing Modifications
(Sketch No. 6094)



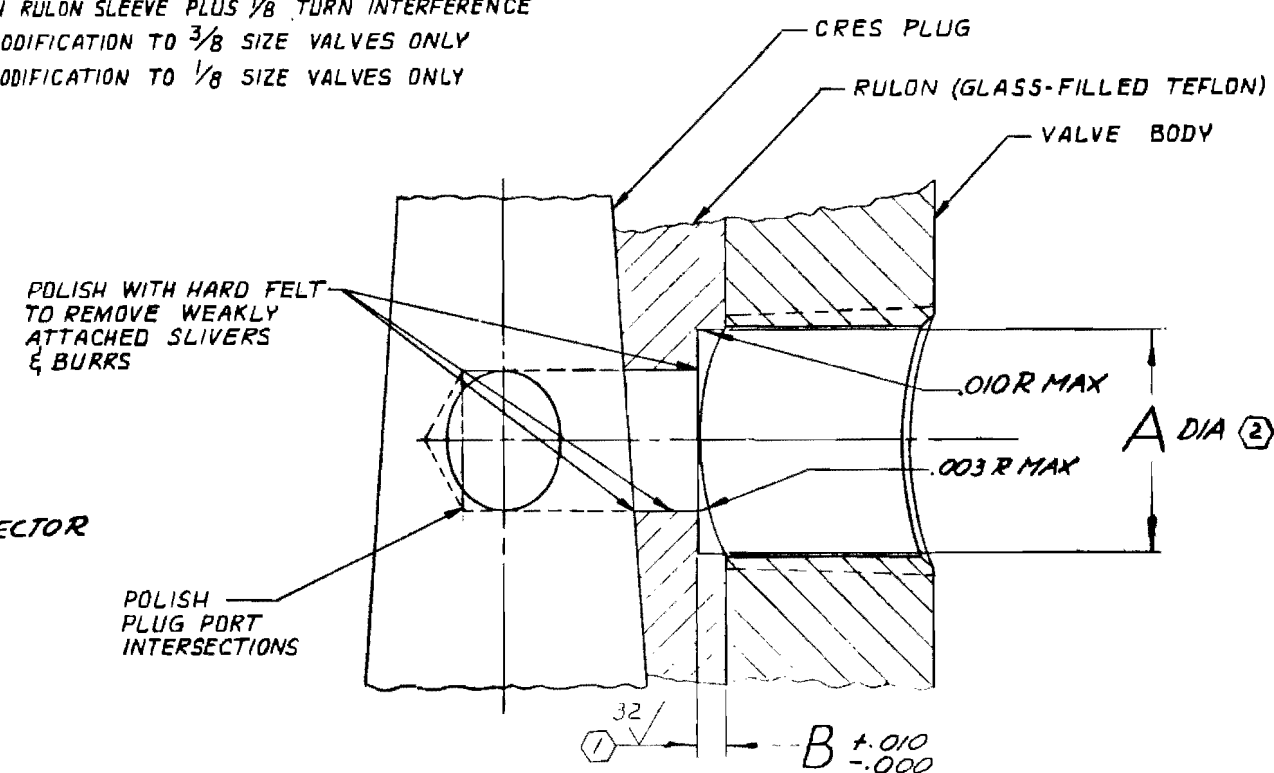
- (6) 5. USED IN FIG. G-1
- (5) 4. CONANT BROS. CO., MEDFORD, MASS.
3. XX \pm .03, XXX \pm .010
- (2) 2. CONCENTRIC TO P.D. OF THD WITHIN .005 TIR AT MMC
- (1) 1. NORMAL TO P.D. OF THD WITHIN .001 TIR

NOTE: UNLESS OTHERWISE SPECIFIED



TYPICAL VALVE ASSEMBLY

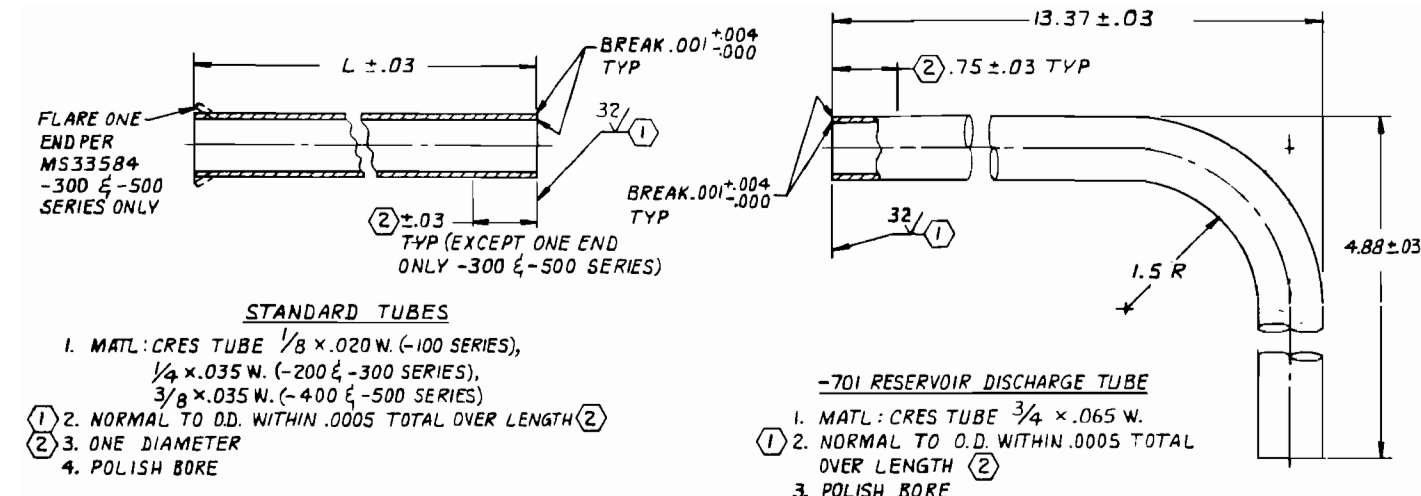
1. P/N $\frac{1}{8}$ BR2TSL SHUTOFF VALVES TO BE CROSS DRILLED WITH 2 PORTS ONLY, 180 DEGREES APART
2. INSTALL GYROLOK FITTINGS WITH LOCTITE "A" & BOTTOM FITTING ON RULON SLEEVE PLUS $\frac{1}{8}$ TURN INTERFERENCE
- (3) 3. MODIFICATION TO $\frac{3}{8}$ SIZE VALVES ONLY
- (4) 4. MODIFICATION TO $\frac{1}{8}$ SIZE VALVES ONLY



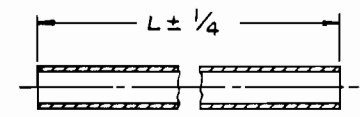
VALVE DESCRIPTION & MODIFICATION DIMENSIONS

(5) P/N	TUBE SIZE	MATL	SCHEMATIC DESIGNATION	(6) A DIA	3
BR2TSL	$\frac{1}{8}$	BRASS	VS4, VS5, VS6, VS7, VS8, VS9, VS10	.335 \pm .005	.03
BR2TSL	$\frac{1}{8}$	BRASS	VS6	.335 \pm .005	.03
2316	$\frac{1}{4}$	CRES	VN1, VN2	.430 \pm .010	.05
BR2TSL	$\frac{3}{8}$	BRASS	V3, V4	.560 \pm .010	.06
BR4TSL	$\frac{3}{8}$	BRASS	V1, V2	.560 \pm .010	.06

Figure G-15. Fitting and Valve Modifications (Sketch No. 6098)



DASH NO.	L
101	1 1/4
102	9
103	9
201	15 3/4
301	1 15/16
302	27 1/16
303	1 3/16
401	6 7/16
402	2 1/2
403	4 3/8
404	1 3/4
405	1 23/32
406	32 3/8
407	2 7/8
408	1 3/4
409	1 3/4
410	24
411	9 1/2
412	26
501	40 3/16
502	19 13/16
503	2 1/8
504	4 3/16
505	76



SAMPLE TUBES

1. MATL: AWG 12 x .015W TEFLON SLEEVING (REF. 1150B, .085 I.D.)

DASH NO.	L
801	15 5/8
802	5 3/4
803	5 1/8
804	7 1/8
805	5 1/8
806	9 7/8
807	7 5/8
808	10 1/4
809	43 5/8
810	37 5/8
811	19 1/8

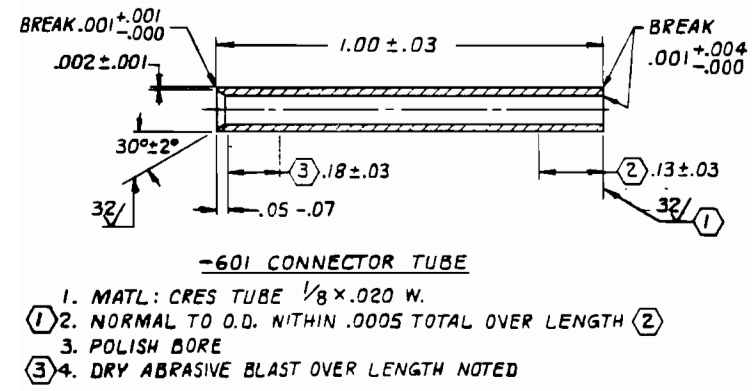


Figure G-16. Dynamic Test System Tubing

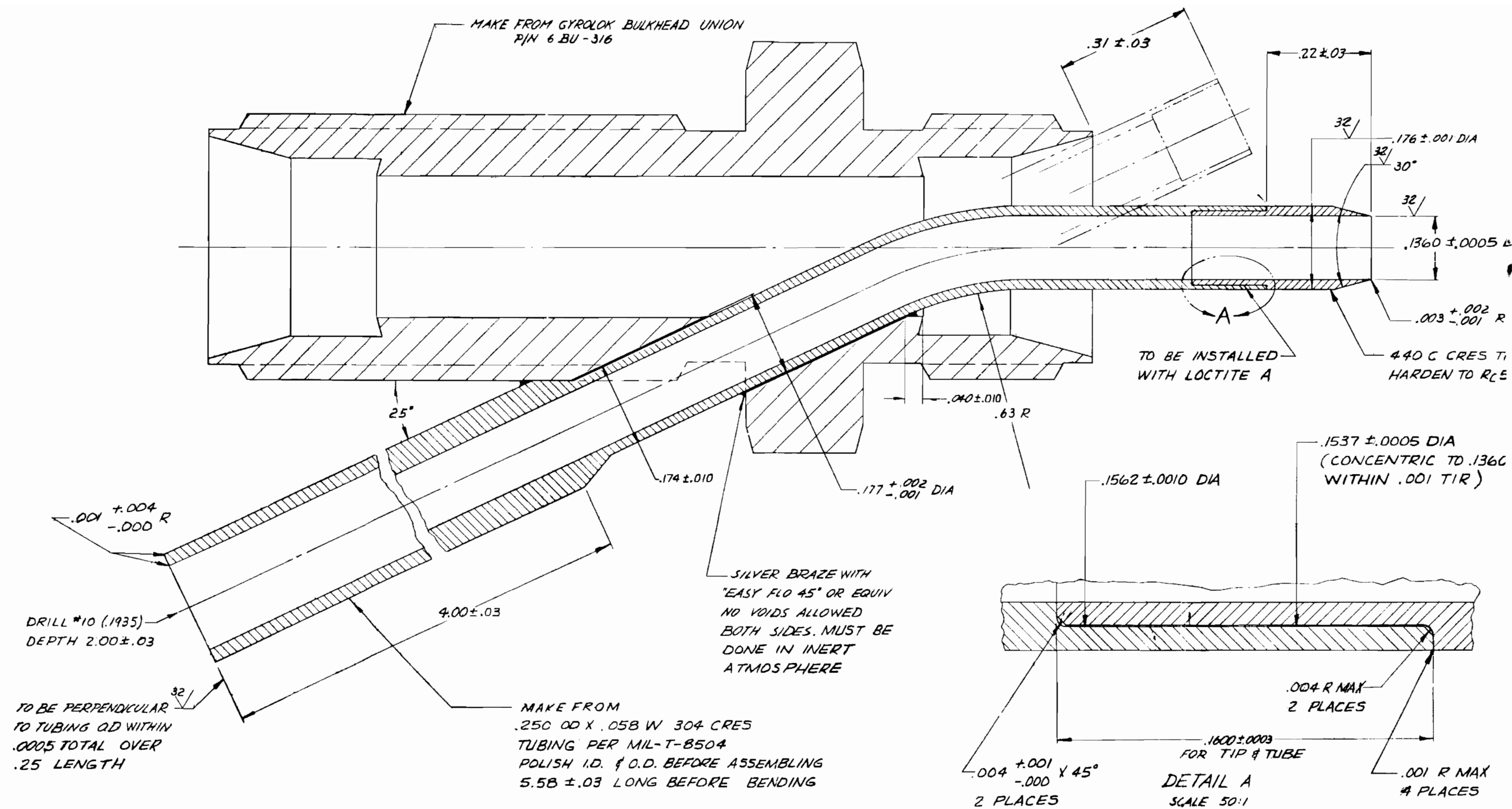


Figure G-17. Diverter Assembly
(Sketch No. 6092)

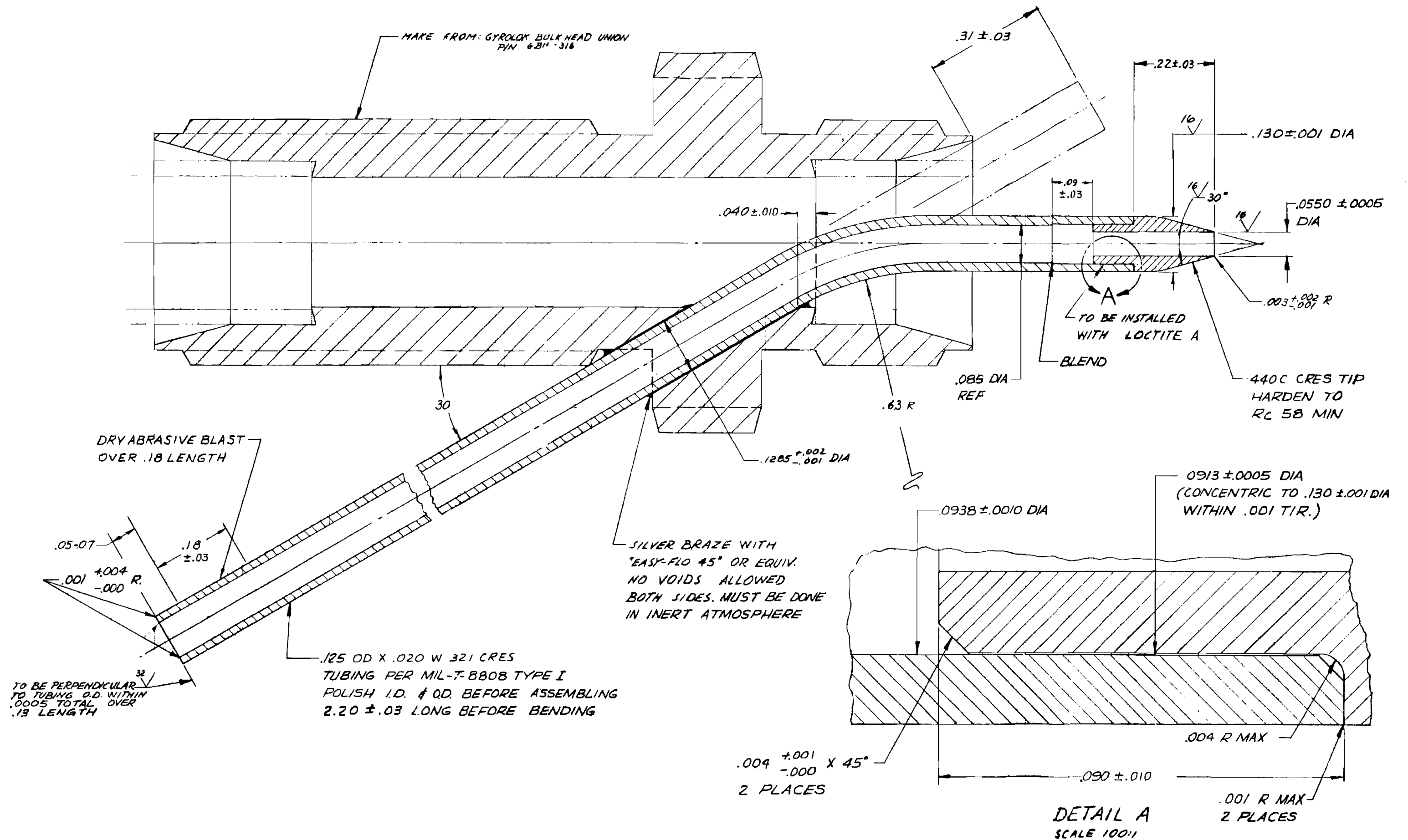


Figure G-18. 3/8 Sampler Assembly
(Sketch No. 6091)

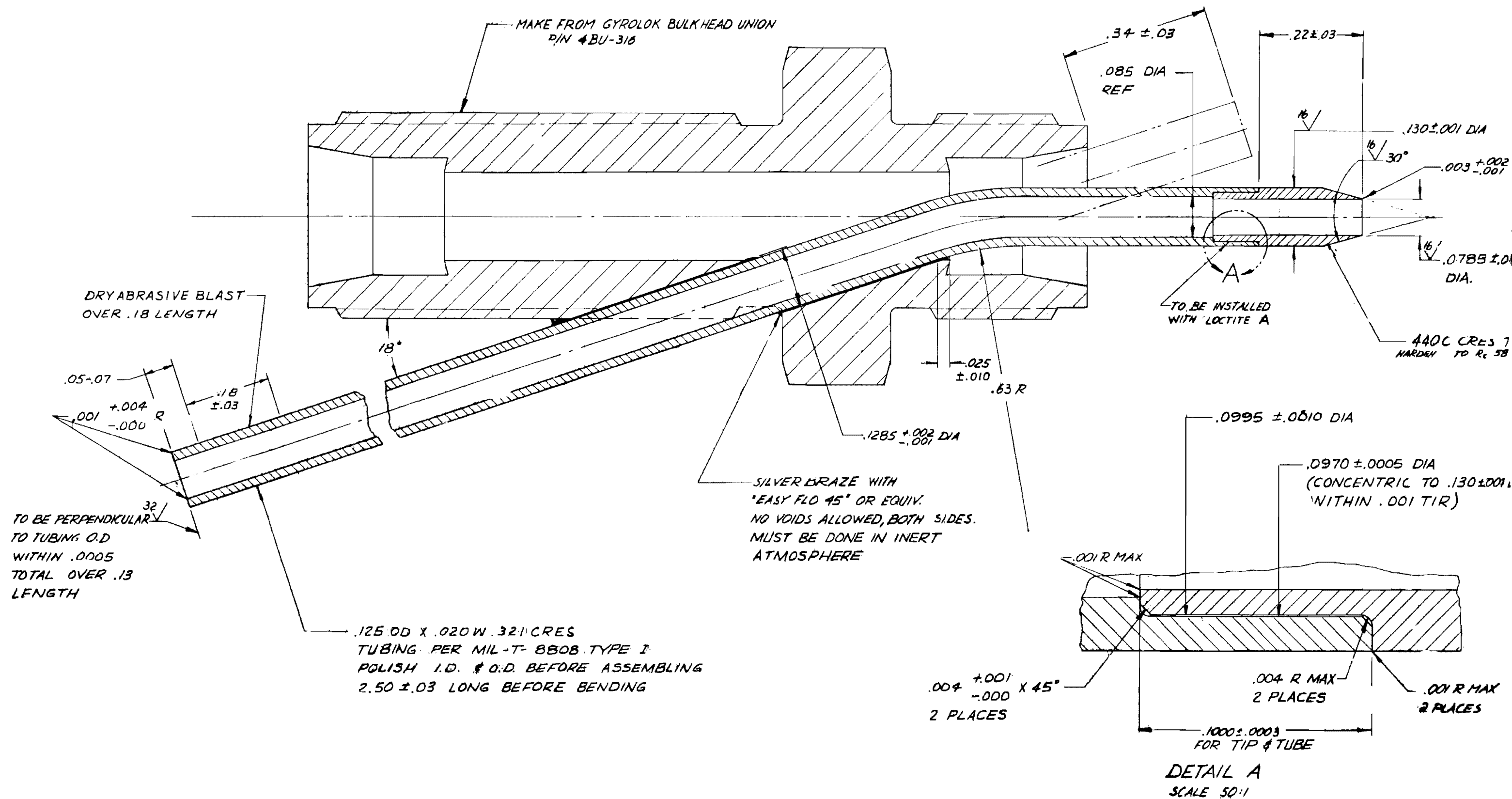
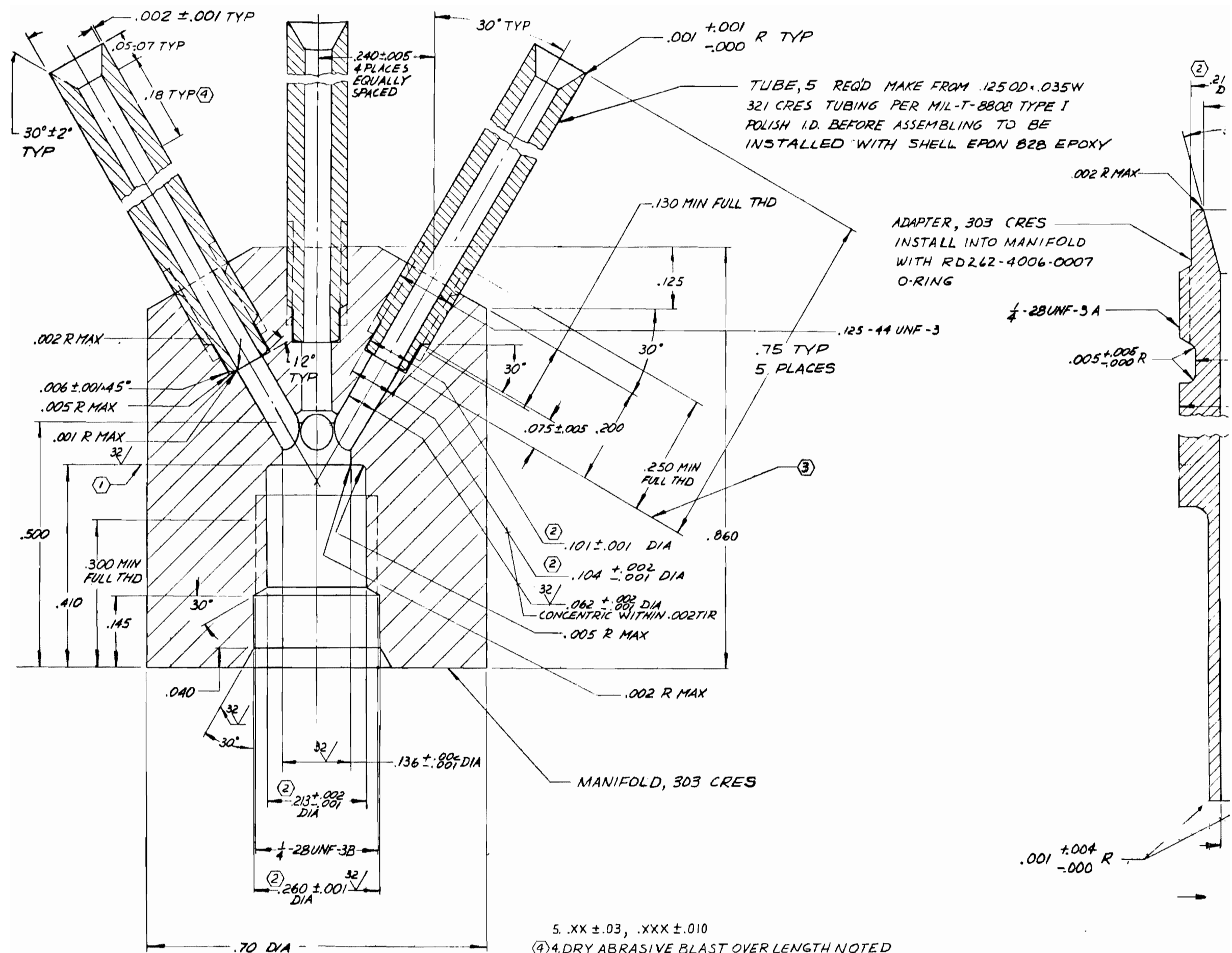


Figure G-19, 1/4-Sampler Assembly
(Sketch No. 6091)



5. XX ± .03, .XXX ± .010
- (4) 4. DRY ABRASIVE BLAST OVER LENGTH NOTED
- (3) 3. NORMAL TO THREAD WITHIN .003 TOTAL
- (2) 2. CONCENTRIC TO P.D. OF THD WITHIN .001 TIR AT MMC
- (1) 1. NORMAL TO THREAD WITHIN .0002 TOTAL
- NOTE: UNLESS OTHERWISE SPECIFIED

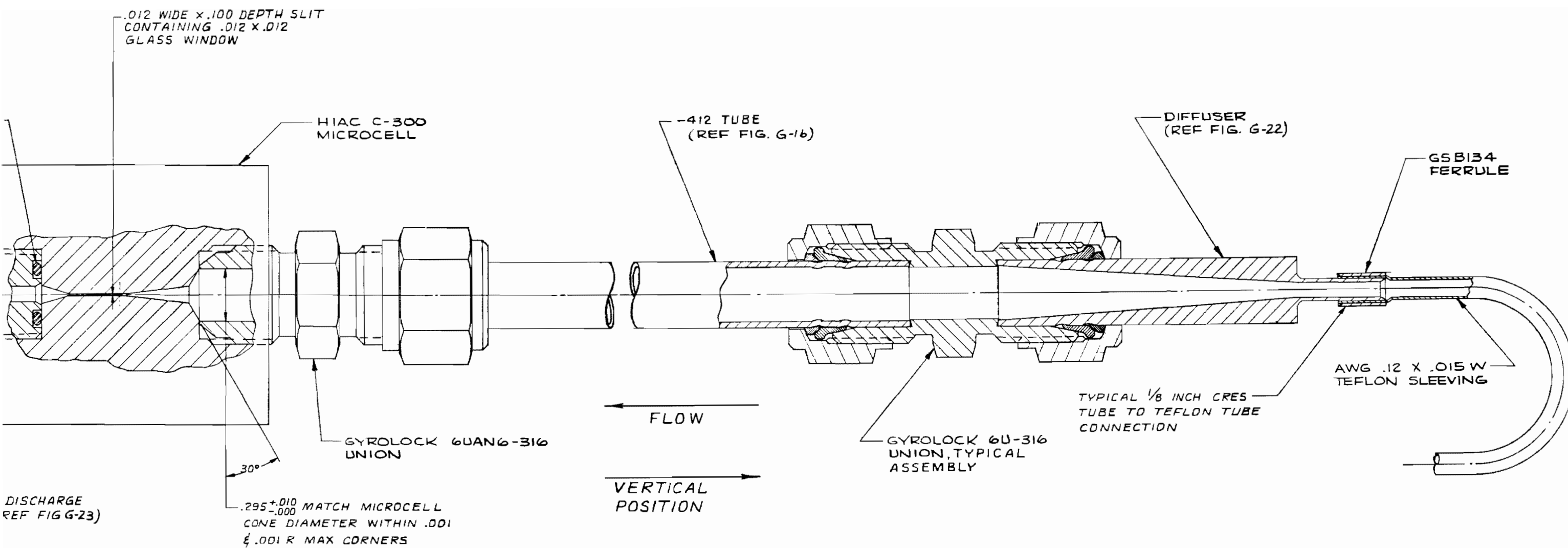
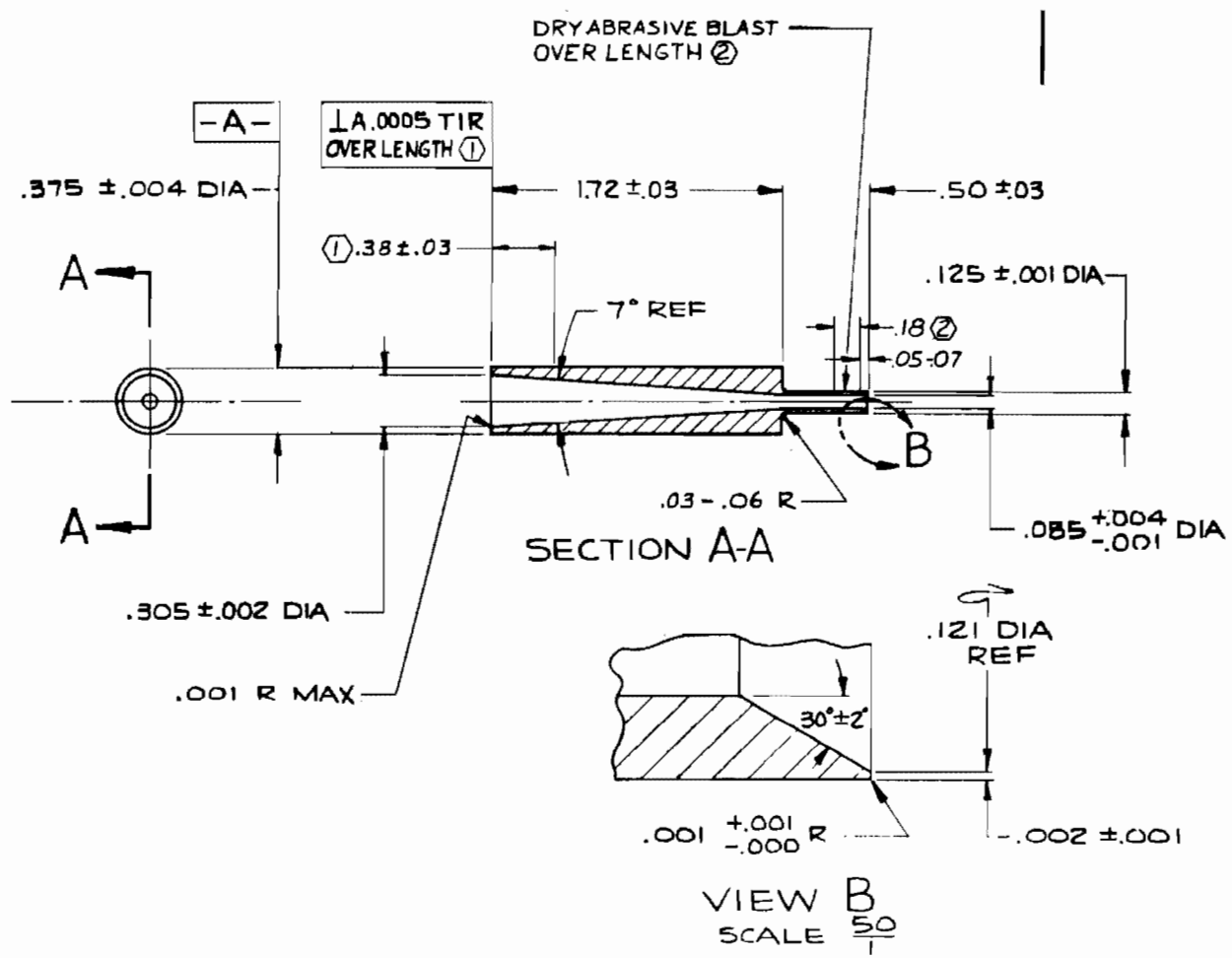


Figure G-21. HIAC Microcell Feed Assembly



3. MATL: 303 CRES BAR
2. BREAK CORNERS .010 MAX
1. \sqrt{R} SURFACE ROUGHNESS

NOTE: UNLESS OTHERWISE SPECIFIED

Figure G-22. HIAC Inlet Diffuser (Sketch No. 6189)

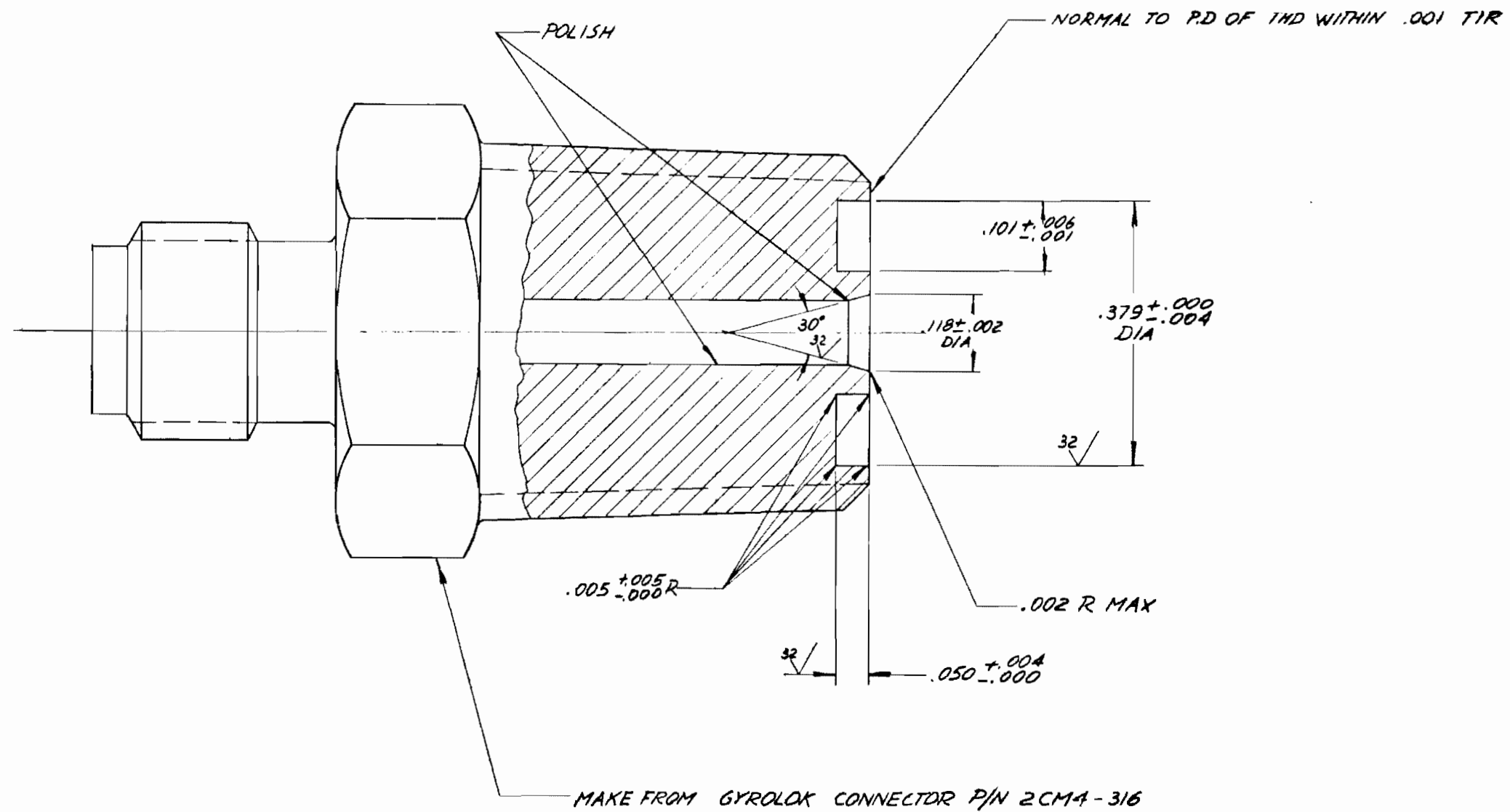


Figure G-23. HIAC Microcell Discharge Fitting (Sketch No. 6095)

and VN1. Valve V3 provided alternate connection of the tester cavity to a low-pressure nitrogen purge supply or point "A" for tank fill. With valves V3 and VN1 switched from the position shown in Fig. G-1, connection of a Freon TF flow bench 3/4-inch line to point "A" allowed both for tank fill and back flushing the two 3-micron, 47-mm membrane filter elements in these circuits. For additional high-flow flushing of these circuit elements and the tester, valve V4 was rotated with discharge (point "B") connected to the Freon TF flow bench 3/4-inch return line. The fill method resulted from development tests which showed that the cavity between valve VN1 and the adjacent 3-micron, 47-mm filter was inadequately cleaned, being exposed only to low volume gas flow. Moreover, this valve proved to be marginal for the required 1000-psig nitrogen service and consequently generated contamination which had to be periodically flushed out.

Filter Flow Circuits

Main flow (Q_s) could be diverted into two separate filter circuits via four-way rotary plug hand valves. The first, located immediately downstream of the pump (Fig. G-6), contained a 47-mm membrane used for foreign contaminant analysis of total flow. The second filter circuit (shown in the upper left of G-1 and also in Fig. G-3) was the main system flow filtration loop (filter bank). Line size downstream of the filter inlet sampler (S_f) was 3/4-inch, directing flow to a large glass tube rotameter and then to a cartridge paper filter followed by the final 293-mm membrane element.

Sample Flow Circuits

The sample flow circuits were designed to extract and direct, through 1/8-inch CRES and Teflon lines (Fig. G-7), a representative sample of fluid from various locations to the microcell for particle analysis. The analysis was automatically performed by the HIAC electronic particle counter on samples singularly selected by sample valves (e.g., VS_b). From the microcell, sample flow was directed back to the reservoir, passing through the full-open throttle valve and three-way diverter valve (Fig. G-5). The latter valve allowed taking overboard samples for microscopic analysis and flowrate calibration.

Three pitot tube samplers were located in the system. The tube inlets were sized so that sample extraction flow velocity was equal to line approach velocity at the standard flowrates defined in Fig. G-1. Two 3/8-inch line samplers provided data on fluid contamination immediately upstream and downstream of the main system filter circuit. The third (1/4-inch line) sampler extracted fluid directed to the test poppet and seat. A fourth sampler was initially provided downstream of the tester (from sample valve VS_t) but was later replaced with a straight union.

Subsidiary Circuits

These circuits provided support and function fluids to the dynamic tester. Referring to the schematic (Fig. G-1), these included the following:

1. P_C piston control nitrogen pressure through a 1/2-inch, three-way solenoid valve. The 200-cu in. volume ensured repeatable impact velocity during cycling.
2. P_P nitrogen purge supply for tester cavity purging and also supply for a manual blowoff probe. This latter item was used to purge the poppets and seats, as required, prior to assembly and also purge the tester cavity.
3. Tester Freon TF film pressure and HIAC microcell cooling purge.
4. P_1 tester nitrogen inlet supply pressure through VN2 and VN1.
5. Rotary plug hand valve Freon TF end cavity pressure.

Reservoir

The purpose of the reservoir (Fig. G-12) was to provide sufficient surface area to allow for necessary Freon TF cooling. The conical shape ensured free particle flow, and associated fittings were bottomed to avoid cracks. The reservoir was designed for pressurized operation, but this system feature was later found unnecessary and the reservoir was vented to atmosphere. Access to the fluid for particle insertion was through the 2-inch center hole tube which also established a consistent fill level. Both sample and main system return flows were directed through swage-type fittings which allowed the tubing ends to be submerged as shown by Fig. G-1. Reservoir vortex action could be controlled by rotating the bent 3/8-inch discharge tube (-411).

Pumps

Requirements of steady flow and contaminant insensitivity eliminated turbine, diaphragm, piston, gear and flexible tube pumps, leaving the shaft seal as the critical component in a centrifugal pump. External bearings and lack of internal low-velocity cavities were design requirements in addition to smooth internal surface finish for cleanability and stainless-steel construction. The following centrifugal pumps were evaluated:

1. Crane Chempump (seal-less chemical pump)--too complex and expensive; bearings in fluid.
2. Ladish Tri-Flow (sanitary pump)--too large and only mechanical seal.
3. Heinicke (stainless)--too large and only mechanical seal.
4. Rheinlutte (chemical pump)--too large and complex.
5. Eastern (industrial)--bronze and requires 2 stages; therefore, complex.

6. ECO Engineering--3/8-inch pipe, single-stage, open-face six blade impeller with mechanical seal.
7. Worthington (stainless)--3/8-inch pipe, single-stage, open-face two blade impeller with packing or mechanical seal.

Sanitary pumps were close to meeting most requirements; however, such large volume centrifugal pumps have reported pressure instability and excessive heating of the pumped fluid when they are run at low flow (near shutoff). Fluid velocity would also be low in some areas of large volume pumps; therefore, they were considered unsuitable.

Two 3/8-inch pipe size stainless-steel Worthington pumps were obtained for evaluation in the system. One pump incorporated a mechanical seal assembly consisting of a stationary ceramic face seal ring and compounded carbon rotor seal ring. The second (backup) pump had a conventional stuffing box. Each pump required extensive rework to preclude contaminant traps. This consisted of (1) remachining to remove rough cast surfaces and provide a tight fit between seal plate and casing, and (2) incorporation of swage-type tube fittings.

The mechanical seal pump was initially evaluated during system development. It proved to be exceptionally clean providing unfiltered flow (following system cleanup) in which no counts greater than 10 microns per liter were registered by the counter. Furthermore, the mechanical seal was unaffected by the HA particles then used. Unfortunately, dynamic action between the impeller and large seal cavity (Fig. G-13) resulted in complete separation of HA particles from system fluid within less than 1 hour. It was never proved whether the particles were being whirled within the cavity or were merely being pushed back toward the seal by circulation. Retention of particles in this cavity was proved by (1) induced cavitation which caused particles to be reintroduced into the flow stream, and (2) by stopping the system after apparent particle loss, draining system fluid, and disassembling the pump wherein the particles were observed. A 1/8-inch line was placed between the discharge and seal cavity in the seal plate (Fig. G-13) in an attempt to flush out particles. Prior to interconnecting the line, static pressures were measured at standard flow ($Q_s = 2.44$ gpm) as follows:

Discharge hole = 30.8 psig

Seal hole = 3.3 psig

Pump inlet = 1.6 psig

These pressures indicated an approximate flush flow potential of 0.5 gpm. Particle tests indicated slight improvement as a result of flushing. The ΔP of 1.7 psi between the seal and inlet indicated substantial flow between these points which helped explain the separating tendency of this pump design.

The stuffing box packing seal pump was then evaluated for clean flow operation and ability to pump fluid with HA particles. The packing seal of "Blue African Asbestos" was the antithesis of "clean", being composed of unoriented, compacted asbestos fibers and some lubricant having the appearance of Teflon and graphite particles. It was therefore initially planned that a new seal design would be necessary. Teflon lip seals and hydrostatic bearing were considered. Pump operation proved surprisingly clean, and after the previous experience including several other major setbacks the apparent steady-state particle flow represented a breakthrough. The pump was used in this configuration throughout the remainder of the program without further modification. It proved, however, to be the major source of background contamination in cycle testing. As shown later, this contaminant did not have significant effect on any but the later Phase III test models. Increased background level in later testing was believed caused by breaking down of the packing material after hundreds of hours of operation.

Valves

All valves for the system were required to have straight through flow and an absolute minimum of traps. Known commercial valve manufacturers of small Teflon sealed ball and plug valves were therefore investigated. These included Whitey, Republic, Conant, Hoke, Jamesbury, Dragon, Contromatics, and Jenkins. The usual ball valve was not suitable because the flow passage is connected to the stem cavity in the closed position. This reduced candidate valves to Republic, Conant, and Whitey. Of the three, the Whitey valve appeared the cleanest, especially with Swagelok fittings. The valve was made only in a 1/4-inch two-way configuration which severely limited its application. The Republic and Conant valves were both of tapered stop-cock design. Although available with AN male fittings, the Republic valve was rated only to 50 psi because of a solid Teflon plug. The solid plug also could cold flow which would offset the flow holes. On the other hand, the Conant valve had been used to 1000 psi in a 1/4-inch pipe size because it incorporated a thin Teflon sleeve and stainless-steel rotor. It was, however, available only with pipe fittings. Since 1/8-, 1/4-, and 3/8-inch valves of two-, three-, and four-way function were required for up to 100-psi operation, the Conant valve was selected. Special adaptor fittings were necessary to convert from pipe to tubing fittings. These and other modifications are detailed in Fig. G-15.

These valves probably constituted the major source of particle traps in the system. This was believed a result of substantial differences in fitting, Teflon, and rotor hole diameters. There were also large chamfers (0.03 inch) on the internal side of the Teflon sleeve and CRES plug ports to allow for rotary overlap. With the fitting modifications shown, it was necessary to provide end pressure to the 3/8-inch valves to obtain a seal because of apparent distortion of the narrow Teflon seal land between ports.

During system development, it was determined that valve operation occasionally produced a high background. The contaminant was traced to wear of the filled Teflon valve sleeves. Disassembly of V3 revealed a Teflon "skin" or loose wear film on the CRES rotor plug which contained a myriad of glass rods about 12 microns in diameter and 45 to 60 microns long. The Teflon sleeve also had a generally "hairy" appearance in small wear areas as compared with the highly polished glaze over the remainder of the surface. It was assumed that the other valves were similar. No repairs were made and the valve was reassembled and put back into the system. By operating all valves during filtered flow, the wear film was apparently reduced and background usually was negligible. Because of the narrow size range of the glass rods, this contaminant was easily recognized from the HIAC readings around 20 microns. This problem made it necessary to limit valve operations during the dynamic tests.

Additional modifications to the two high pressure valves (VN1 and VN2) were required. Following system flow calibration it was found that (Q_B) flow dropped by several percent. It was determined that high pressure nitrogen was locked up at the ends of the valve rotors over an elapsed time of several days. This had extruded the rotor through the Teflon sleeve, producing a mismatch in flow holes. The problem was corrected by grooving the Teflon sleeve between the high pressure port and the sleeve end so that reduction of inlet pressure also vented the valve end cavity. The problem did not appear with normal usage because the 1000-psig pressure was only applied for a short period, usually less than 1 hour.

A clean, high-pressure multiport plug valve design was considered for the system but this was beyond the program scope. Nevertheless, the requirement exists for this type of a valve.

Lines and Fittings

Considerable effort was expended in reviewing methods of joining lines to result in minimum particle traps. Various forms of flanges, flareless and AN type fittings, brazed sleeves and the like were considered. Flanges of sufficient precision would prove prohibitively expensive, brazed joints could contaminate the system and, further, make it rather inflexible. The standard fitting would have intolerable gaps and rework of fittings and tubing to provide a reasonably streamlined joint would also be expensive. Even with rework, the likelihood of the AN-type joints being perfectly aligned was remote, thus resulting in gaps caused by angularly displaced conical surfaces.

Flareless fittings appeared to be the best compromise and several types were evaluated. The tube is inserted into the fitting to butt against an internal shoulder. With the coupling nut tightened, ferrules plastically deform the tube to grip it; in the process the tube expands to provide a slight interference fit in the fitting bore. With this interference, subsequent reassembly requires reasonable good tube and fitting alignment. This alignment in conjunction with the tube-to-fitting butt joint provides for a minimum particle trap at the joint.

Informal tests of several fittings indicated the internal butt joint may not be bottomed hence an annular particle trap results. The Gyrolok, however, employs a reverse angle at the shoulder and swaging produced considerable axial load which causes visible plastic deformation of the tube end and the assurance of a gap-free joint. For this reason the Gyrolok design was selected.

To provide maximum initial and subsequent flushing cleanliness, all 1/4- and 3/8-inch tubing bores were polished using wood dowels and paper wads coated with 900 grit aluminum oxide compound. In this lathe operation, tube ends were faced off with sharp corners to insure a butt joint seal, as detailed in Fig. G-16.

Assembly of 1/4- and 3/8-inch CRES tubes in the system was accomplished by first mocking up the system with aluminum tubing from which accurate lengths were determined. Straight CRES tubes were cut and polished and then bent to match the aluminum tubes. A firm butt joint at each connection was made by assembling first one end of the tube to lock the ferrules in place and then this connection was removed and the other end was swaged. Both connections were then made and the next tube was assembled. As initially designed, the sample system had 1/8-inch OD, thick wall CRES lines throughout. (Subsequent vibration problems with the HIAC, described later, led to adoption of Teflon lines up and downstream of the microcell.) Because of the small bore, these tubes were lapped with drill rod and 900-grit compound instead of being polished as with the larger sizes. During system "clean" testing for background, various areas of the system were hammered to loosen particles. Initial impacts on these 1/8-inch lines produced several hundred thousand particles between 10 and 300 microns. Although most loosely adhered large particles were initially dislodged, it was apparent from repeated impacts producing 5,000 to 10,000 particles that a severe contamination problem existed. A membrane sample revealed red and black particulates which were determined to be rust and iron scale. These were assumed to have originated from the previous lapping process which involved carbon steel. Hydrofluoric acid descaling was attempted which resulted in unacceptable pitting of most internal surfaces.

The entire sample system (including samplers and manifold) was then remade using short CRES tubes (which could be wood dowel polished) interconnected with Teflon lines. Connections were made by heat expanding the Teflon tubing over the CRES tubes which were locally sand blasted to provide a nonslip surface (Fig. G-16). Electrical sleeving ferrules were then pressed over the joint to ensure a tight seal. These connections were tested to 100 psig without pullout or visible leakage. A typical assembly of all tubing connections is illustrated in Fig. G-21.

Diverter and Samplers

These devices, shown in Fig. G-17, G-18 and G-19, were designed to extract "representative" samples of fluid from various parts of the system. The probe tip inside diameters were sized to provide an extraction flow velocity (under standard flow conditions) that was equal to the line approach velocity. The probe tips were fabricated of hardened 440C CRES to ensure that the leading edges remained sharp and also to preclude possible particle erosion.

Sample Flow Manifold

The purpose of this device was to allow smooth transition of multiple sample flow paths to a common line feeding the HIAC counter. As shown in Fig. G-20, this was accomplished without traps by vertical positioning of the five tube manifold feed lines. Particles from a single flowing line thus were not forced back up other closed feed lines.

Membrane Filters

Membrane filters were used throughout the system. These elements produced a continuous fluid cleanliness level well below the 10-micron sensitivity of the HIAC counter for many days of operation. Both the 293-mm main system and 47-mm analytical filter elements had only downstream support. All other filters were backed up on both sides. After numerous breakages of the 293-mm element and several attempts at precluding this event by various operating procedures, the problem was solved by using a nylon-reinforced element and a thick prefilter pad.

The main circuit analytical filter was used to perform particle input-output recovery experiments later described. Although the system was designed with the objective of having no internally generated contamination, such was not the case as noted. Consequently, this filter was also used to examine the total system generated contaminants. To avoid breaking the element during valve V1 switching, it was necessary to slow the pump before this operation. It was also necessary to predrain attached lines (disconnected at V1) in proper sequence to avoid disturbing contaminants distributed on the pad.

Pressure Gages

All pressure measurements were made with bourdon tube gages as specified in Fig. G-1. The main system pressure gage (P_S) was of the internal bleed type which allowed complete filling of this line. The feed line and tee (Fig. G-3 and G-7) were designed to preclude trapping particles in the gage. The primary purpose of this gage was to provide one of the basic criteria used to define and monitor standard flow conditions. Along with (P_F) it also provided indication of filter ΔP , but this did not change significantly throughout the test program.

Flow Indicators

Main system flow (Q_s) was indicated by an extended range turbine meter and associated readout equipment (Fig. G-2). This meter was independently calibrated by displacement-time with an overall calibration precision of 0.3 percent. Upon installation in the system, it was used to calibrate both the (Q_b) turbine meter readout and the filter circuit rotameter. For (Q_b) meter calibration, valves were closed so that all (Q_s) flow passed through (Q_b) meter. The filter circuit rotameter was included in the system to ensure flow measurement capability if subsequent particle tests proved detrimental to turbine meter function. Comparison of (Q_s) turbine meter flow at 2.44 gpm and that computed from the rotameter scale reading using the manufacturer's constants indicated agreement within 1 percent. Additional direct volumetric calibration of (Q_b) meter output during sampler calibrations indicated similar accuracy.

As typically shown by (Q_b) meter in Fig. G-7, it was necessary to reduce larger male AN fittings to system line size with special external threaded fittings. The previously noted (Q_s) meter calibration was made with these fittings in place and in a 3/8-inch line to duplicate system plumbing. These meter fittings are the only flared-tube-type connections in the main (unfiltered) flow circuit. Along with the meters, they undoubtedly contained a number of traps contributing to particle loss described later.

Sample flow was initially indicated by a small paddle wheel turbine meter. This meter verified that switching VS6 from reservoir to over-board did not change the sample flowrate. Having minute ball bearings, it clogged so often that it was replaced (after system calibration was completed) with an 1/8-inch tube connection (-810 tube in Fig. G-1). This was crimped to produce equivalent flow resistance and thus allow valve VS5 to be left wide open under standard conditions. Sample flow was thereafter monitored by a combination of system pressure (P_s) and time-volume measurement.

Particle Counter

The instrumentation heart of the dynamic system was the automatic particle counter. This instrument provided steady-state and transient data on background and artificial contaminant (particle) concentration. Its various component sections were comprised of a particle sensor (microcell, Fig. G-7), electronic counter (Fig. G-11), and associated sampling and printout equipment.

The most important item of the particle counter was the microcell. This unit consisted of an assembly forming a narrow slit in the flow direction (Fig. G-21). Sample flow was thus accelerated to a high velocity through this section so that individual particles would be widely spaced.* A 0.012-inch-square glass window placed perpendicular to, and precisely fitting the flow section narrow width (within 0.0001 inch), formed the

*Computed average spacing for most dynamic tests was greater than 5 inches; see Fig. 10.

path for collimating a light beam from a tungsten lamp. The light passed through the fluid, a second larger window, and onto a multiplier phototube. Each particle, as it passed the window, interrupted a portion of the light beam according to its size. This caused a proportional voltage pulse (ΔE) from the phototube. These voltage pulses were tallied by the counter's eight counting circuits (channels) with sensitivity thresholds preset to desired size ranges.

Standard signals for pulse calibration were provided within the counter system to permit periodic checking of channel threshold settings to within ± 5 percent of particle size.

Data were obtained both visually and by automatic printout. Depending upon the type of data desired, the counter could be set to record particle size distribution as the total count greater than individual channel settings or the differential count between settings. This simplified data reduction and allowed visual tally of one channel for short time evaluation.

The automatic sampling unit provided automatic stop-start inputs to the counter by preset volume. The volume could be totalized from flowrate measured on a time basis from 60 cycle line voltage or pulses from the sample flow turbine meter. Removal of the sample flowmeter required use of the time basis. This posed no problem because flowrate proved consistent within 2 percent.

In usual operation at 300 ccm, the sample volume was set to produce an eight channel data printout at either 100 or 1000 cc. At this sample flowrate, the counting operation thus required 20 or 200 seconds. Following 10.7 seconds for printout, the counting cycle was automatically restarted. A continuous tape of steady-state particle count data was thereby obtained for precise time intervals. However, no data were obtained during printing.

Theory of Operation and Calibration. The information in Fig. G-24 was taken from the operating manual for the PC-20 counter.

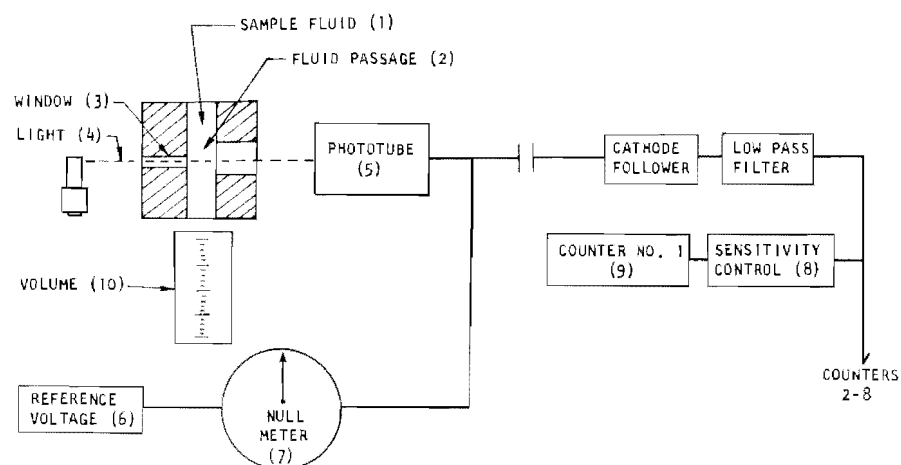


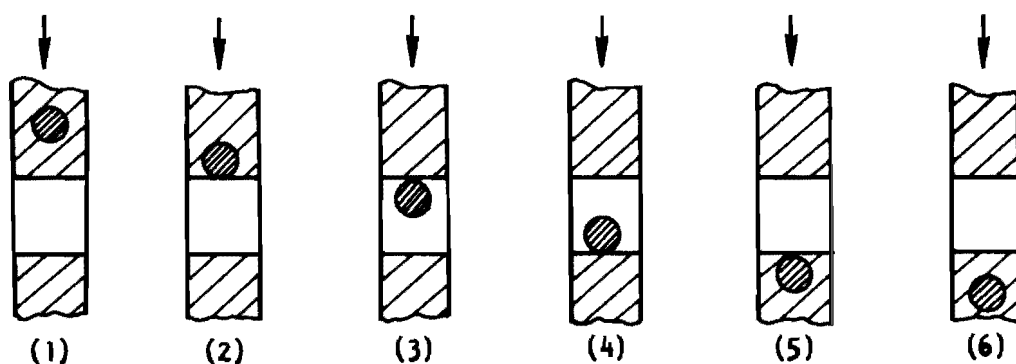
Figure G-24. HIAC Counter Schematic

Sample fluid (1) flows through the fluid passage (2) in a stream so small that foreign particles in the fluid pass the window (3) one by one. Light (4) is collimated by the long tunnel-shaped window into a parallel beam. This beam is directed through the fluid stream onto a phototube (5) at the opposite side. The light intensity is adjusted to create a base phototube output voltage (V_p) equal to a standard reference voltage (6), as indicated when the null meter (7) is balanced in center scale.

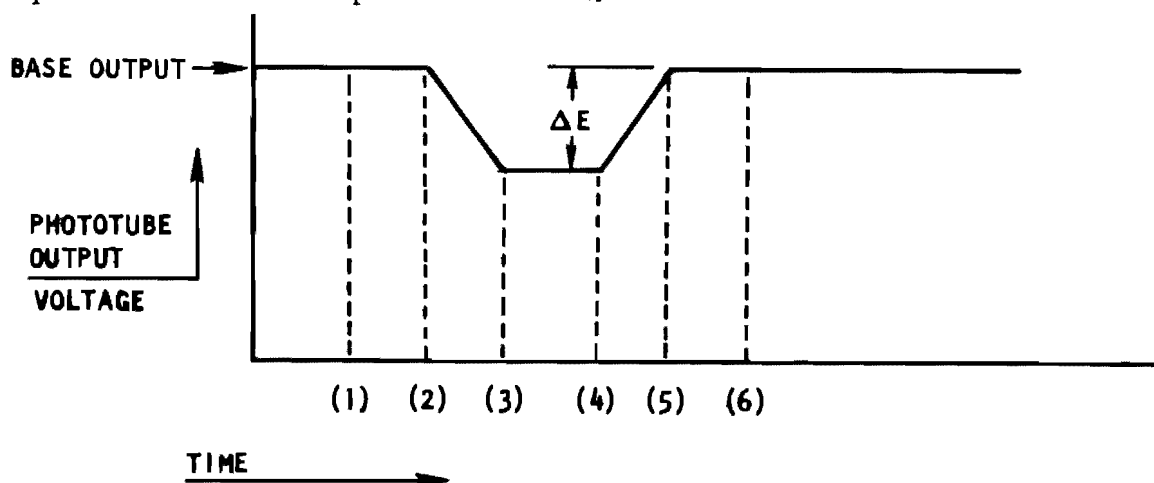
Whenever a particle passes the window, a portion of the light beam is interrupted. This causes a momentary change in the output signal from the phototube which is proportional to the size of the particle passing through the light beam. This signal change (ΔE) is then sent to the counter sensitivity controls (8) which have been preset to various thresholds for simultaneous counting of eight size ranges. Each particle is then tallied according to its size on the electronic counters (9). The sample volume is measured (10) so that the result can be reported as the number of particles (in each size range) in a given volume of fluid.

A block diagram of the Model PC-20 system is shown in Fig. G-25.

Particle Sizing. A parallel beam of light formed by the window to an exact size is directed through the fluid stream and onto a phototube. The following sketch shows a beam of light (as seen by the phototube) as a particle approaches, passes through, and leaves the window.



Phototube output voltage is plotted against time below for the preceding particle in the six positions shown.



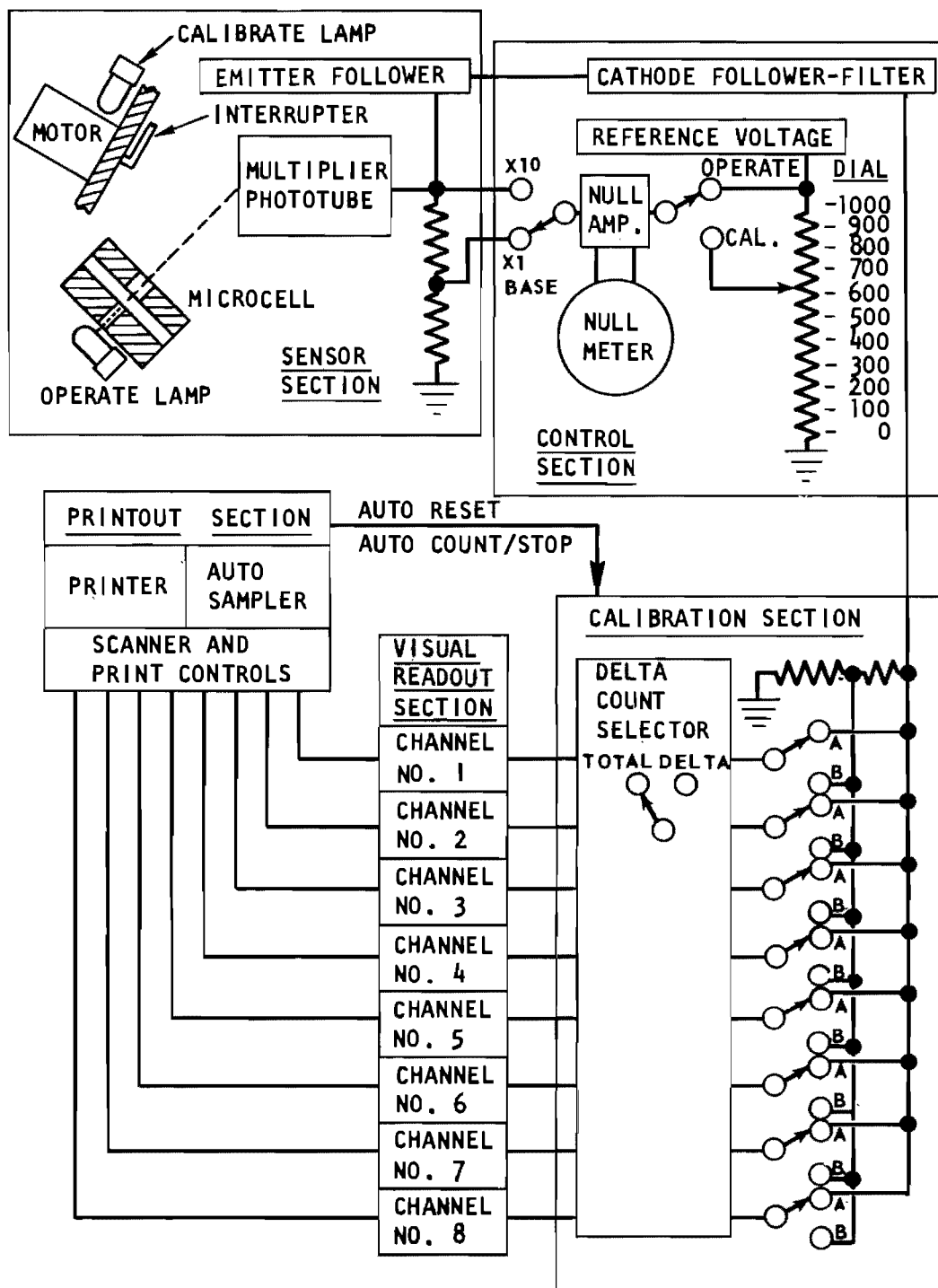
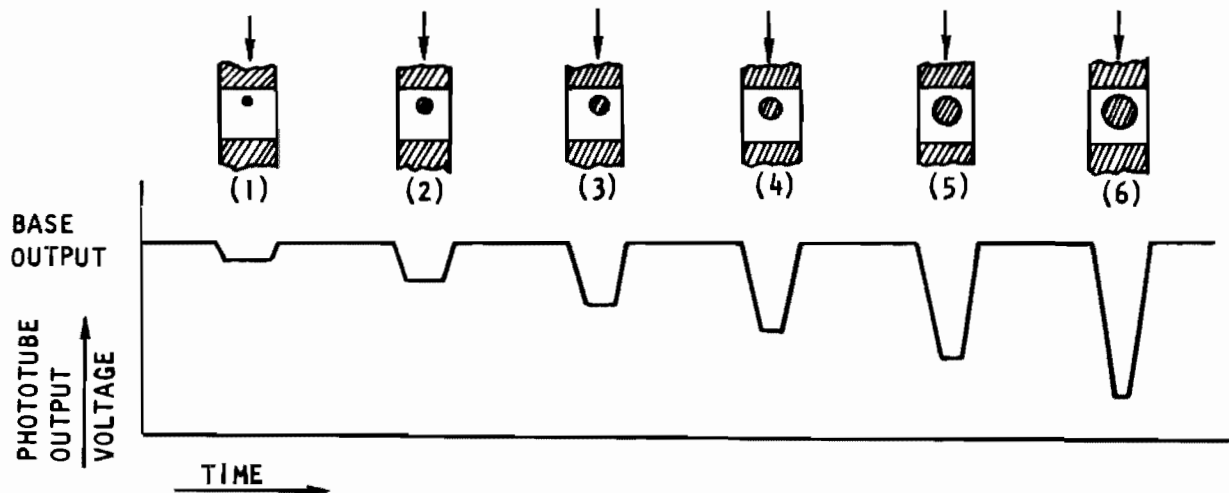


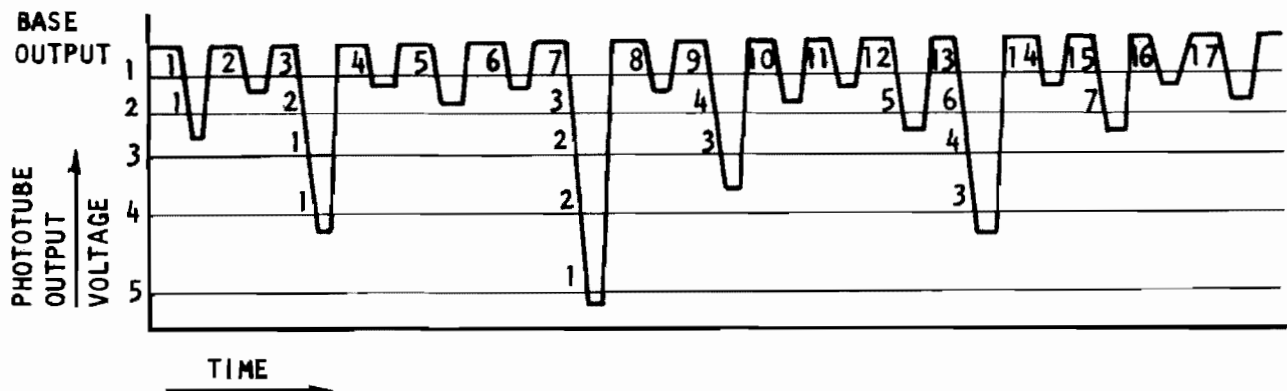
Figure G-25. Block Diagram of Model PC-20 System

As long as the fluid is free from foreign particles, the output of the phototube remains constant. Whenever a particle passes the window, a change in base output occurs (ΔE). The larger the particle is, the more light it will block out, and the greater will be the amplitude (ΔE) of the signal change.

The following sketch shows particles of different sizes passing through the window and the corresponding changes in phototube output signal.



Each electronic counter can be adjusted to a different threshold, as shown in the following plot. Any particle that blocks out sufficient light to cause the phototube output to drop below the threshold setting of any counter will cause that counter to register one count. Thus, the particles



causing the pulses shown would be counted by the various counters as indicated. The final readings would be:

Counter No. 1	17
Counter No. 2	7
Counter No. 3	4
Counter No. 4	3
Counter No. 5	1

The number of particles and their distribution by size within the ranges set on the counters is therefore determined.

Because voltage pulses representing particle areas are established on a proportional basis, a shift in base output voltage during operation (indicated by null meter) will result in a particle area size error equal to the percentage change in this voltage. A ± 2 division null meter shift corresponds to approximately $\pm 1\frac{1}{2}$ percent error in particle sizing.

Calibration. Standard signals for accurate calibration are provided with the system shown in Fig. G-26. This is the same system as shown for operation in Fig. G-24, except that the calibrate light is used to simulate particle size, and pulses are generated with the interrupter disk driven by an electric motor.

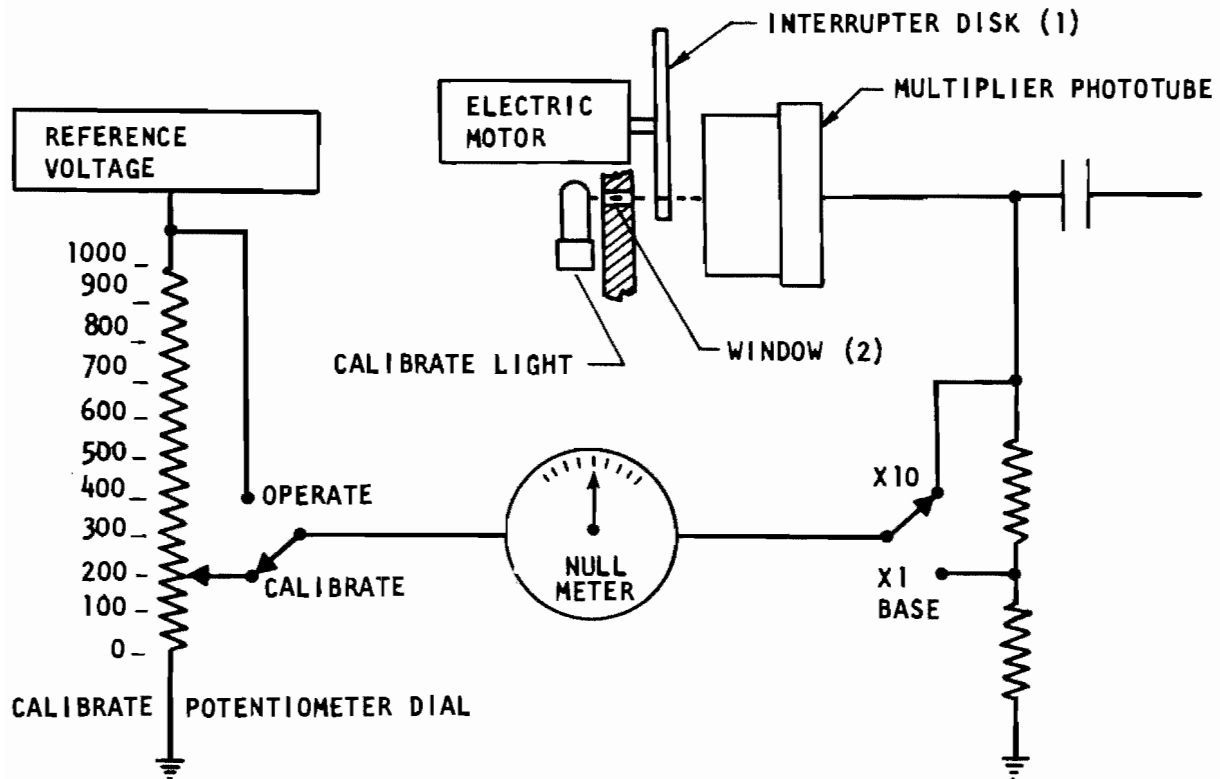
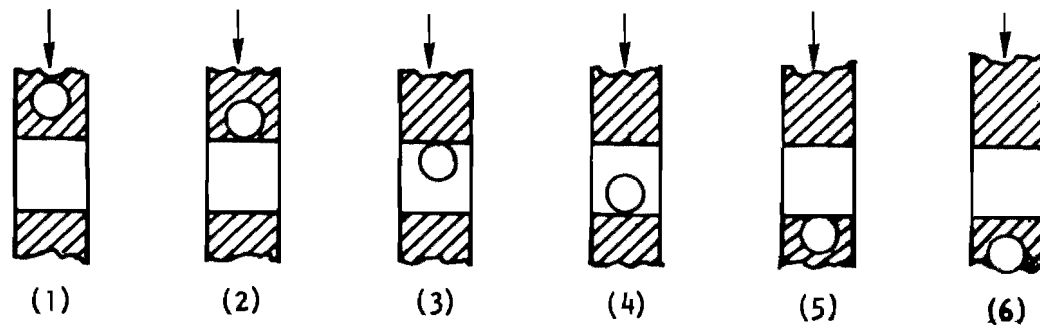


Figure G-26. Calibration Schematic

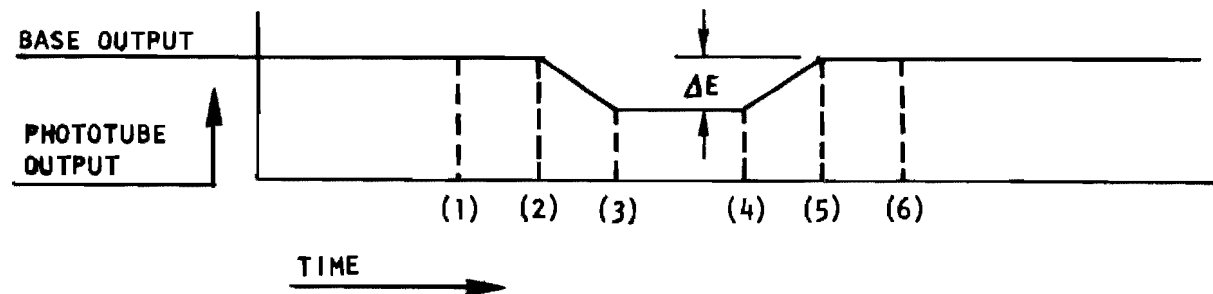
For calibration purposes, standard particles are considered to be circles with size designated by diameter. The window (3), shown in Fig. G-24, is fabricated to exact tolerances so that its area is accurately known. Thus, the percent of light that will be blocked out by any given standard particle can be precisely calculated. This, then, gives the percent change in phototube base output (ΔE) that will be caused by a particle of a given size.

The calibrate potentiometer dial provides 1000 increments for selecting any percent of the base operating voltage. For example, to simulate a particle that blocks out 10 percent of the light, the calibrate potentiometer is set at 100. The light intensity is then adjusted to balance the null meter so that it is then equivalent to 10 percent of the normal base light intensity. The transparent interrupter disk (1) has an opaque radial line scribed on it which is slightly wider than the window (2) through which the calibrate light is shining. For each revolution of the interrupter disk, therefore, this light is completely blocked out once. This is equivalent to blocking out 10 percent of the base light during operation. A momentary signal change from the phototube (ΔE) is thus generated equal to 10 percent of the base output.

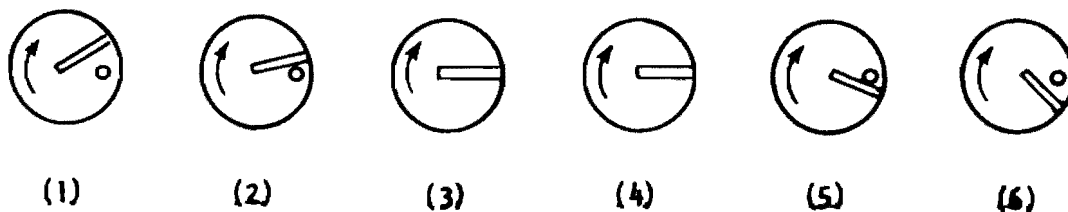
Following is a brief comparison between a pulse generated by a particle during operation and one generated by the calibrator.



A particle in the fluid stream is shown above as it passes through the window. The plot below shows the resulting pulse which occurs in the phototube output voltage.



The calibrator disk is shown below in six positions corresponding to the same six positions of the particle.



The circle on the right side of the interrupter disk represents the calibrate window. If the calibrate light intensity is adjusted to create a phototube output voltage of amplitude (ΔE), then the pulse caused by completely blocking this light will be the same as shown in the preceding plot for the particle in the fluid stream. Thus, a method is provided to simulate any particle blocking out from zero to 100 percent of the window area. (It should be noted, however, that this calibration procedure establishes counter sensitivity settings and is not a substitute for a specific particle size calibration as subsequently described.)

Signal Output and Calibration Dial Settings. From the preceding, the change in base output voltage (pulse signal) versus particle area is given by:

$$\Delta E = \frac{A_p}{A_w} R E$$

where

$$A_p = \text{particle area} = \frac{\pi}{4} D_p^2$$

$$A_w = \text{window area (3000 square microns)}$$

$$D_p = \text{Particle equivalent diameter, microns}$$

$$E = \text{phototube base output voltage } (\approx 56 \text{ vdc})$$

$$\Delta E = \text{change in phototube base output voltage, i.e., pulse signal}$$

$$R = \text{pulse ratio (phototube efficiency)}$$

Values of (ΔE) measured from phototube output base signal during calibration are tabulated below:

D_p , microns	E , mv
10	47
12	68
15	103
20	185

Because pulse signals are related to proportional blocking of the microcell window by a voltage ratio maintained constant by null meter, theoretical calibration settings are independent of these voltages; theoretical settings for spheres are as follows:

X 10 Scale for Size to 100-Micron Diameter

$$S_{10} = \frac{10^4 A_p}{A_w}$$

X 1 Scale for Size Greater Than 100-Micron Diameter

$$S_1 = \frac{10^3 A_p}{A_w}$$

Final settings used in model testing with HB particles are shown (parenthesized) in Fig. G-11 for particle size from 12 to 70 microns.

HIAC Development. It was apparent from the Phase I Survey (Ref. 4) that the dynamic system was a unique application of the HIAC particle counter. Previous experience with most liquid particle counters was in analysis of bottle specimens of hydraulic oil. Consequently, successful utilization of the particle counter within the system (i.e., on line) required a period of development to define suitable compromises between the HIAC instrument and the system.

With the system nonoperating, the counter base signal noise level was measured at 35 to 40 millivolts. System operation with hard lines to the sensor resulted in spurious counting in channels up to 50 microns due to vibration (probably of the operation lamp filament). Isolating the sensor with Teflon lines and foam pad (Fig. G-7) partially reduced the noise.

A more subtle problem was revealed by variation in base signal noise level (oscilloscope monitored) with cycling of the refrigeration unit. During Freon TF cooling, the noise level would increase; it would then decrease as the fluid was heated from pumping. A significant temperature differential existed between the Freon TF and the microcell flow passage and window which was heated by the base lamp. It was hypothesized that nonuniform feed geometry, high flow velocity, and heat transfer all combined in varying amounts to produce a fluctuating boundary layer and refractive index which caused excessive signal noise.

Adding to this noise level were ground voltages and electrical fields from the Varidrive and refrigeration motors. A secondary noise input was occasional gross variation in line voltage which caused base signal bounce and counting in channels up to 20 microns.

Because all of the above variables occurred randomly and sometimes simultaneously, considerable experimentation was required to isolate and reduce their effect. Aside from the vibration problem, which was almost entirely solved as noted, the following action was taken to arrive at the final system defined herein.

Fluid Turbulence. Multiple changes were necessary to correct this problem. Tests indicated a flow reduction would be helpful, but this required redefinition of system flows and/or sample pitot pickups. Final solution resulted from the following:

1. Sample flow was introduced to the microcell through a 7-degree diffuser (Fig. G-22) followed by 26 inches of straight 3/8-inch tubing.
2. The original straight slot microcell was reworked to streamline inlet flow to the window via a polished, 120-degree, cone shaped transition from the round to slot shape (Fig. G-21).
3. The microcell was cooled by the GN₂ purge system (Fig. G-7).

Shorter lengths of 3/8-inch microcell feed tubing were evaluated, including direct installation of the diffuser into the microcell fitting. With only a small temperature differential between the fluid and microcell, satisfactory operation was achieved. This solution, however, would have required extensive rework of the operate lamp and, also, precision temperature control. Due to the low laminar flow velocity within this tube, significant time existed between sample extraction and counting of a specific particle (about 1 minute average). Thus, the overall sample system and counter output data response was quite slow. This effect is discussed later.

Electrical Noise. This problem was minimized by: (1) rotating the phototube to a minimum noise position, and (2) applying ground cables to various locations.

Base Signal Level. The phototube base signal noise level was monitored with an oscilloscope during critical runs to ensure a stable signal and noise bandwidth less than the smallest channel trigger level. During initial tests, channel 1 was set at 10 microns, but over one-half of the 100cc run data involved excessive noise. For later tests, channel 1 was set for 12 microns with very little noise interference.

Auxiliary Instrumentation

This equipment functioned without any problems and consisted of: (1) pump rpm transducer, (2) cycler-counter used in cycle testing, (3) tester position and load transducers (Appendix F), and (4) dual beam oscilloscope and drum indicator readout instruments.

SYSTEM CALIBRATION AND PARTICLE MEASUREMENTS

The purpose of system calibration was to establish standard operating conditions and the capability of the sampling and measuring system to define particle concentration in (Q_b) seat flow. This required individual calibration of the HIAC counter and (S_b) sampler. Concurrent with this task, precise size distributions for HA, SB, and HB particles were obtained by microscopic measurement and from the calibrated HIAC readings. A weight-frequency correlation of HA particles also was performed to verify particle composition and specific system performance characteristics. Specialized techniques required for direct particle handling and sample preparation were developed.

In usual system operation, particle counts were continuously recorded by the HIAC printer. Each event which potentially affected counts or associated data was recorded on a data pad and the corresponding count tape printout as an "item number." Individual particle counts were thus retrieved by date and item number. Specific counts following an item number count are designated by additive number (e.g., 29+3) in data presented herein.

Standard Operating Conditions

These conditions were obtained by adjusting pump rpm and line resistance. Basic flowrates were analytically defined to suit required flow velocities and fixed-area parameters. Minimum pump rpm was desirable to reduce audible noise, vibration, and pressure fluctuations. Also, the pump rpm could not be at a system vibration resonance point because of the HIAC sensor sensitivity to mechanical vibration. Final conditions evolved by trial and were obtained by multiple crimping the 3/8-inch line downstream of (P_s) gage and the 1/4-inch line downstream of (Q_b) flowmeter. Just enough line resistance was added to obtain standard flowrates (within ± 2 percent) with all valves wide open to fixed stops. The test model open seat flow area was much larger than the feed area and, therefore, the effect on flow distribution from variations in model geometry was negligible.

During calibration, (Q_b) flow, system pressure (P_s), and (Q_{sb}) sample flow (via 1-percent meter subsequently removed) were frequently checked. Minor adjustments were made in rpm as required to maintain standard flows within ± 2 percent (indicated Q_b flow setting sensitivity was ± 0.25 percent). It was determined that little, if any, adjustments were necessary as the Varidrive unit proved exceptionally stable. Pumping produced about ± 0.2 -psi fluctuation in the undamped (P_s) gage. Q_b and other flows varied by ± 1 percent due to heating and cooling (70 to 78 F) of the Freon TF. Adjustments for this change were not made.

Parameters for standard operating conditions are listed in Table G-1.

TABLE G-1

DYNAMIC TEST SYSTEM STANDARD
OPERATING CONDITION PARAMETERS

Flow Location (Temperature = 74 ± 4 F)	Flowrate, gpm	Flow Area, A			Velocity, ft/sec $V = \frac{0.32Q}{A}$
		Line or Pitot	ID, in.	A, in. ²	
Main Flow (Q_s)	2.44	3/4	0.620	0.302	2.58
		3/8	0.305	0.0731	10.7
Diverter Flow ($Q_s + Q_{s_b}$)	0.488	Pitot	0.136	0.0145	10.8
		1/4	0.194	0.0296	5.29
Seat Flow (Q_b)	0.409	1/4	0.180	0.0254	6.15
Sample Flow (Q_{s_b})	0.0793	S_f & S_s	0.0550	0.00238	10.7
		S_b	0.078	0.00478	5.31
		1/8	0.085	0.00568	4.47
		3/8	0.305	0.00731	0.347
		(C300 microcell)		0.0012	21.1
<u>Pressure Versus Pump Rpm</u> Bypassing Filter: $P_s = 18.7$ psig at 2930 rpm Through Filter: $P_F = 24.6$ psig, $P_s = 18.7$ at 3260 rpm $\Delta P = 7.9$ psig					

Membrane Sampling, Preparation, and Counting

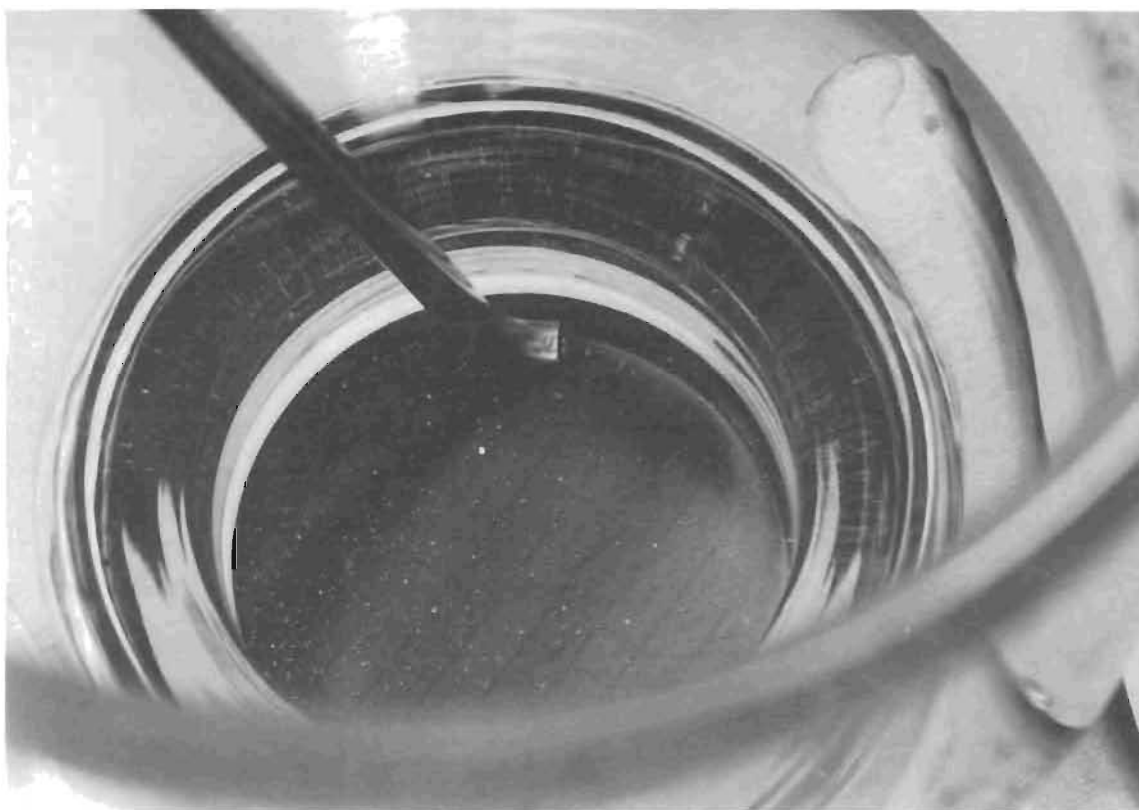
HIAC counter and sampler calibration was based on microscopic analysis of sampled particles for comparison with other data. Methods for obtaining and evaluating such samples accurately were developed. S_b and full-flow (Q_b) samples were taken directly into the Millipore apparatus. Background runs, in which each operation was performed with "clean" fluid, established that the preparation operations (glassware and membrane cleaning, etc.) did not add significantly to the final sampled fluid results. This task was performed repeatedly with extreme care. In no case were there more than 10 particles on the element greater than 10 microns, and these were dust and/or skin and were not counted.

Initial tests indicated that after fluid evacuation the nickel balls were not evenly distributed on the membrane surface. Significant quantities collected at the funnel ID periphery and these were not totally dislodged by swirling the fluid during evacuation. A clean 1/8-inch probe was inserted into the funnel through which 0.45-micron, filtered Freon TF flush flow was directed at the funnel periphery. The particles were easily moved to the center of the filter element (Fig. G-27) which facilitated subsequent counting.

Because of static charge effects and gravity, the balls were propelled from, and rolled off, the membrane with even the slightest amount of handling. A method of glass slide mounting was then developed in which clean slides were placed on both sides of the membrane and held together with a capillary film of fast-drying cement at the edges. The slides thus physically clamped the balls in place for viewing. The problem of static charges repelling particles during removal from the Millipore apparatus was eliminated by placing the top slide on the Freon TF-wetted filter element prior to removal from the fritted base. The entire apparatus was inverted and then the element and slide were simultaneously removed while holding the element in place on the slide. The backing slide was then installed and, after drying, the assembly was cemented in place. Typical slides are shown in Fig. G-28. The entire slide was previewed with low magnification and an ink boundary was placed around grouped particles to reduce counting time at higher magnifications. The right-hand slide was a special preparation for weight reconciliation discussed later.

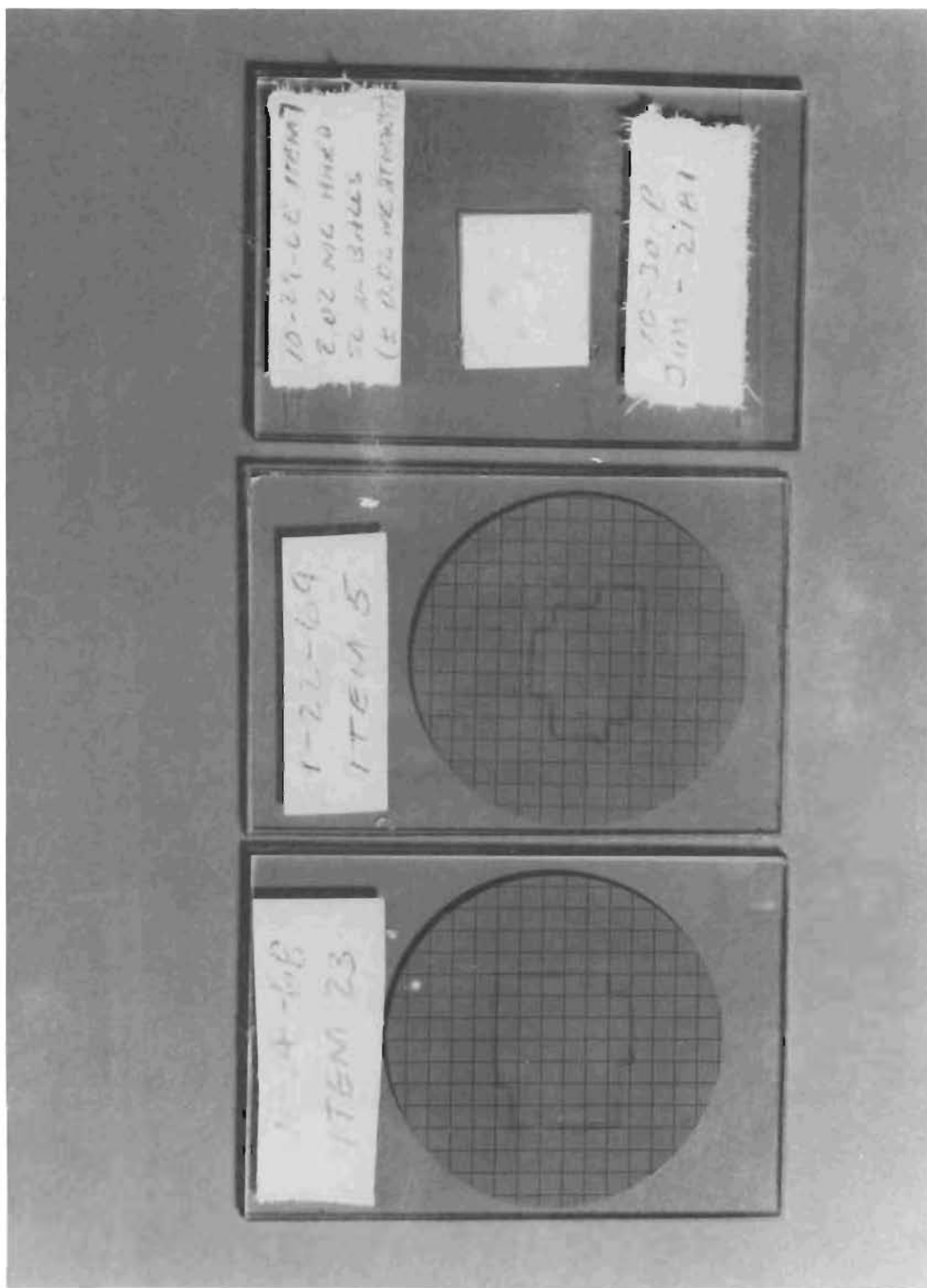
Microscopic analysis of the prepared samples was performed at three magnifications. For size distribution data, 200X was employed with microscope reticle divisions equal to 7.5 microns. For quantity analysis only, 100X, 60X, and 40X magnifications were usually used.

Due to the importance of these measurements, the program principal investigators performed all counts. Although exceedingly tedious, the lack of significant background and sphericity and color contrast of the nickel particles rendered counting simple and straight forward. With very bright side lighting, the particles appeared a brilliant gold on the purple Millipore filter membrane. At 200X, particle size discrimination was



6AL42-11/6/69-C1I

Figure G-27. Particle-Centering Method



6AL42-11/6/69-C1A

Figure G-28. Typical Glass Slide Mounts

within ± 2 microns. However, each particle was not directly measured, but was counted within a 7.5-micron size range by visual comparison between particle diameter and the microscope reticle divisions. Consequently, sizing error of ± 3 microns or greater, especially with egg-shaped particles, was probable. All slides were totally counted. As this required multiple-stage advancements, double counting was avoided by precise reticle reference to minute flaws or "identifiers" in the element surface.

In the final analysis, accuracy must be determined by comparison with a standard. The microscope reticle was calibrated with a precision-graduate-stage micrometer and further comparisons were made with small hole gages. Visual measurement capability was demonstrated to be within ± 3 microns. Nevertheless, particle sizing was by visual estimate and thus subject to bias error. The degree of this error can be seen from comparison of two independent counts of the same slide (to be presented) which indicated a mean particle size difference of 1 and 3 microns. It is concluded that overall visual measurement accuracy was within ± 5 percent of size or ± 3 microns for specific particles. Multiple measurements probably reduced this error somewhat.

HIAC Calibration

The HIAC particle counter was evaluated for both total count and size discrimination with HA and SB particles. For these and subsequent (S_b) sampler tests, the HIAC channel size settings were established from the previously defined theoretical particle-to-window area ratios. The technique employed was to obtain stable repetitive readings from sampler (S_b) per 100 cc. At 300 cc/min, a printout each 30.7 seconds was obtained (10.7-second print time). A 100- or 300-cc sample was taken directly into the Millipore filter apparatus by: (1) turning VS6 sample diverter valve overboard, (2) setting the HIAC automatic sampling and printout unit (ASPO) to totalize 100 or 300 cc, and (3) collecting the sample throughout the ASPO cycle. Flow time between the microcell window and Millipore is computed as 1.3 seconds. Thus, for a 60-second run, the collected sample represented all but about 2 percent of the particle flow tallied by the counter (or 6 percent for a 20-second 100-cc run). This error was negligible as particle counting was steady. Total volume accuracy was a function of the HIAC paddle wheel flowmeter (within ± 1 percent) and timing error of about 0.2 second at start and stop. Overall error was less than ± 2 percent.

HA Particles. Three 300-cc samples were taken for calibration with HA particles. One sample was counted and sized at 200X to define HIAC channel setting accuracy. The data taken for this sample are shown in Table G-2. Because of different size ranges, the data are best analyzed by the log-normal plot of Fig. G-29. As indicated, the geometric mean count size from the three independent counts is 58 microns by HIAC and 60 and 61 microns by visual sizing; the HIAC total count was 3.8 percent lower than visual. This could be due to some duplicate visual counting.

TABLE G-2

HIAC CALIBRATION WITH HA PARTICLES

(Microscopic count and sizing at 200X vs HIAC count
for Item 41, 10-23-68; 300-cc

S_b sample at 300 cc/min; see Fig. G-29)

Microscopic Count						
Lower Size of Range (d_i), microns	J. W. Lewellen \odot			G. F. Tellier Δ		
	n_i	$\sum n_i$ $>d_i$	$\% \sum n_i$ $>d_i$	n_i	$\sum n_i$ $>d_i$	$\% \sum n_i$ $>d_i$
37.5	0	245	100	0	246	100
45.0	22	245	100	13	246	100
52.5	81	223	90.9	103	233	94.7
60.0	108	142	58.0	111	130	52.8
67.5	28	34	13.9	18	19	7.6
75.0	4	6	2.5	1	1	0.4
>82.5	2	2	0.8	0	0	0
$\sum n_i = 245$ $\sum n_i = 246$ $= 81.7/100 \text{ cc}$ $= 82.0/100 \text{ cc}$ $\sigma_g = \frac{61.0}{55.0} = 1.11$ $\sigma_g = \frac{60.0}{55.0} = 1.08$						
HIAC Count for 300 cc \square						
40	0	236	100			
45	9	236	100			
50	53	227	96.2			
55	83	174	73.8			
60	67	91	38.6			
65	23	24	10.2			
70	1	1	0.4			
>75	0	0				
$\sum n_i = 236$ $= 78.7/100 \text{ cc}$ $\sigma_g = \frac{58.0}{53.3} = 1.09$						

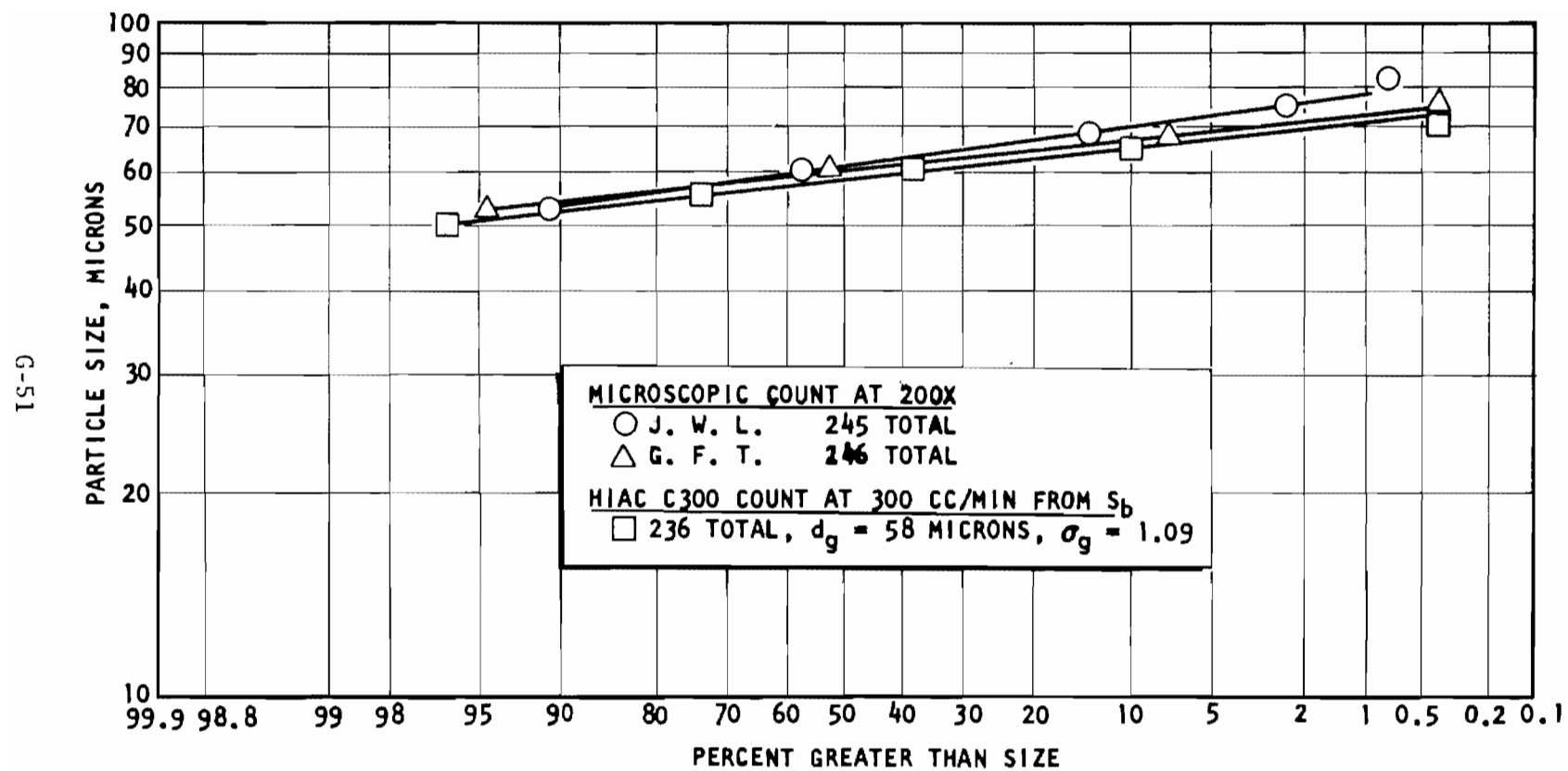


Figure G-29. HIAC-Visual Count Comparison for HA Particles

Analysis of the two additional HIAC calibration samples was performed on a count-only basis. Comparison data, as shown in Table G-3, indicate count differences of 0.3, 3.8, and 1.9 percent for all three tests.

SB Particles. Three 100-cc samples were taken and visually counted in eight size ranges at 200X magnification. The data and comparison with simultaneously recorded HIAC counts is shown in Table G-4. A numerical count-only at 100X magnification further verified the total size count. Size distribution data reduced in Table G-4 is plotted in Fig. G-30a, b, and c. The geometric standard deviation (σ_g , which is the ratio of the 50-percent geometric mean and 84-percent size) is recorded in Table G-4 from the data of Fig. G-30. These data and plots show nearly identical sizing between the visual and HIAC counts with an overall average diameter of 33 microns indicated for the SB particles. The slightly larger size distribution indicated by microscopic count may possibly be attributed to the larger sizing of a small percentage of odd-shaped particles which present maximum area on the membrane but, very likely, a lesser area for light blockage to the counter.

Summary. It is concluded that for the HA and SB particle sizes, the particle counter size discrimination was within the limits of accuracy defined herein for the microscopic method, i.e., ± 5 percent. It was further concluded that for the concentrations examined (up to 3700 particles/liter) the counter does tally particles individually and with some undefined, but small, error due to occasional simultaneous passage of more than one particle. Average visual-HIAC count difference was less than 5 percent. It is emphasized, however, that the subject counter is a complex electronic instrument dependent on precise control of numerous voltages and current flows in conjunction with output from a light-sensitive multiplier phototube. Consequently, periodic size calibration should be performed with specific particles in addition to calibration of the counter sensitivity settings as previously described.

TABLE G-3

HIAC FREQUENCY CALIBRATION WITH HA PARTICLES

HIAC C300 Calibration; 300 cc at 300 cc/min								% Count Differential
Test Date, 1968	Item No.	Microscopic Count				HIAC Count		
		J. W. Lewellen		G. F. Tellier				
		Σn_i	Σn_i^* per 100 cc	Σn_i	Σn_i^* per 100 cc	Σn_i	Σn_i^* per 100 cc	
10-23	33	298	99.3	--	--	297	99.0	0.3
10-23	41	245	81.8	246	82.0	236	78.7	3.8
10-24	21	263	87.6	--	--	268	89.3	1.9

*Greater than 40 microns

TABLE G-4

HIAC CALIBRATION WITH S_b PARTICLES

(Microscopic Count and Sizing at 200X vs HIAC Count for Item 11;
1-21-69, and Items 4 and 5; 1-22-69; 100 cc S_b Sample
at 300 cc/min; See Fig. G-30a, b, c)

Item 11: Total Count Only at 100X by J. W. Lewellen = 325								
Scope Count by J. W. Lewellen ☉				HIAC Count ☐				% Count Differential
Lower d _i , microns	n _i	Σ n _i >d _i	% Σ n _i >d _i	Lower d _i , microns	n _i	Σ n _i >d _i	% Σ n _i >d _i	
7.5	1	326	100	12	1	307	100	
15.0	6	325	99.6	15	3	306	99.7	
22.5	131	319	97.8	20	142	303	98.7	
30.0	101	188	57.6	30	123	161	52.4	
37.5	55	87	26.7	40	36	38	12.4	
45.0	27	32	9.8	50	1	2	0.7	
52.5	5	5	1.5	60	1	1	0.3	
60.0	0	0	0	70	0	0	0	
Σ n _i = 326, σ _g = $\frac{31.4}{24.0}$ = 1.31				Σ n _i = 307, σ _g = $\frac{30.3}{24.0}$ = 1.26				5.9
Item 4: Total Count Only at 100X by J. W. Lewellen = 386								
7.5	3	395	100	12	1	371	100	
15.0	5	392	99.2	15	2	370	99.7	
22.5	110	387	97.9	20	108	368	99.2	
30.0	119	277	70.1	30	163	260	70.1	
37.5	92	158	40.0	40	88	97	26.2	
45.0	50	66	16.7	50	9	9	2.4	
52.5	5	16	4.1	60	0	0	0	
60.0	11	11	2.8	70	0	0	0	
Σ n _i = 395, σ _g = $\frac{34.7}{26.4}$ = 1.32				Σ n _i = 371, σ _g = $\frac{34.1}{26.8}$ = 1.27				4.0

TABLE G-4
(Concluded)

Item 5: Total Count Only at 100X by J. W. Lewellen = 220								
Scope Count by J. W. Lewellen				HIAC Count				% Count Differential
Lower d_i , microns	n_i	Σn_i > d_i	% Σn_i > d_i	Lower d_i , microns	n_i	Σn_i > d_i	% Σn_i > d_i	
7.5	1	217	100	12	1	218	100	
15.0	4	216	99.5	15	2	217	99.5	
22.5	77	212	97.6	20	68	215	98.6	
30.0	68	135	62.2	30	106	147	67.4	
37.5	42	67	30.8	40	38	41	18.8	
45.0	22	25	11.5	50	3	3	1.4	
52.5	3	3	1.4	60	0	0	0	
60.0	0	0	0	70	0	0	0	
$\Sigma n_i = 217, \sigma_g = \frac{32.3}{25.0} = 1.29$				$\Sigma n_i = 218, \sigma_g = \frac{33.0}{26.7} = 1.24$				0.9
Average mean particle size: HIAC = 32.5 microns, Visual = 32.8 microns								

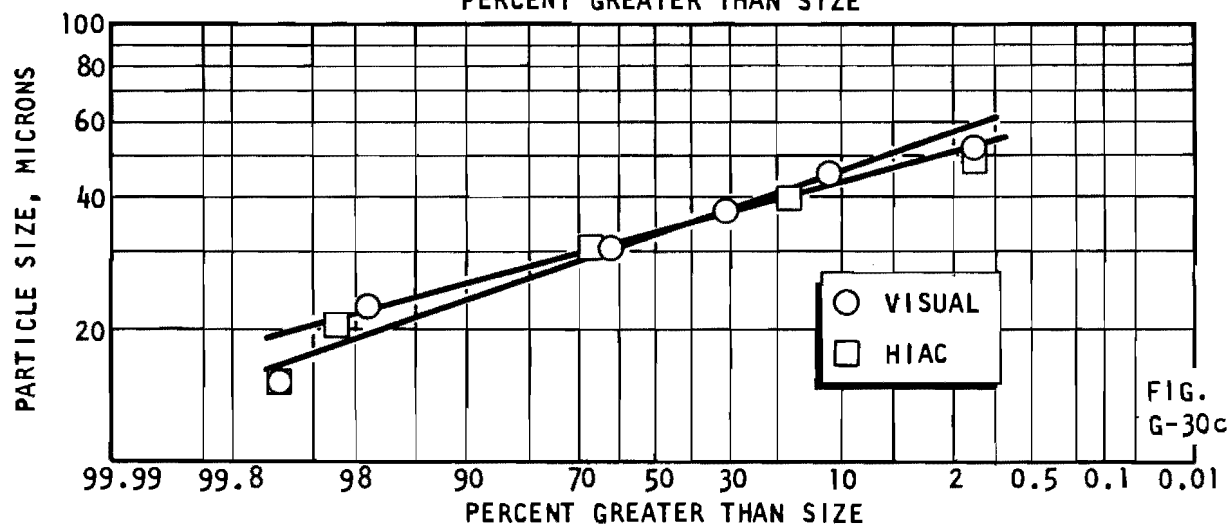
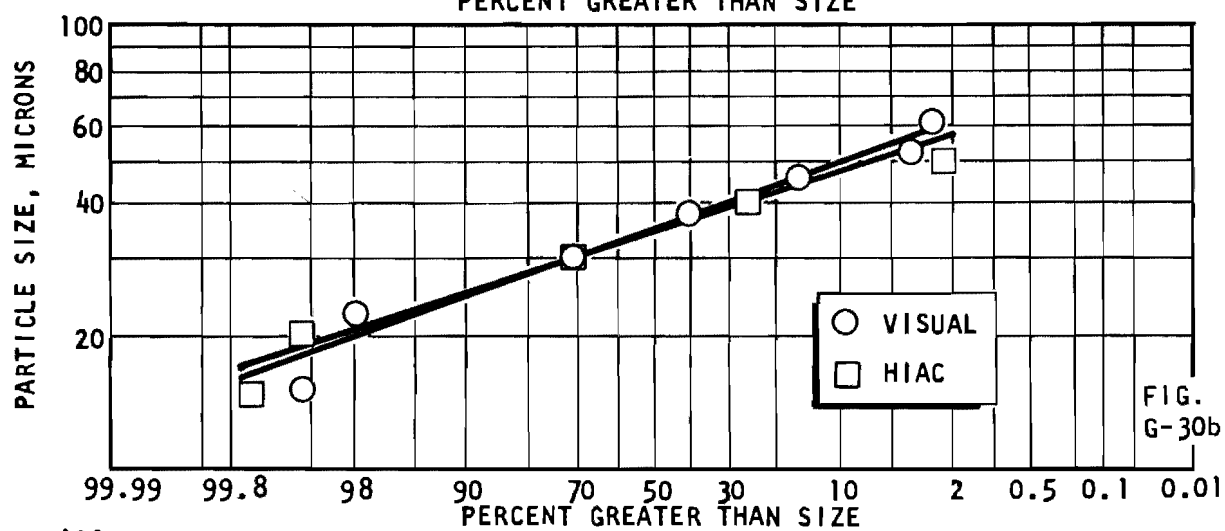
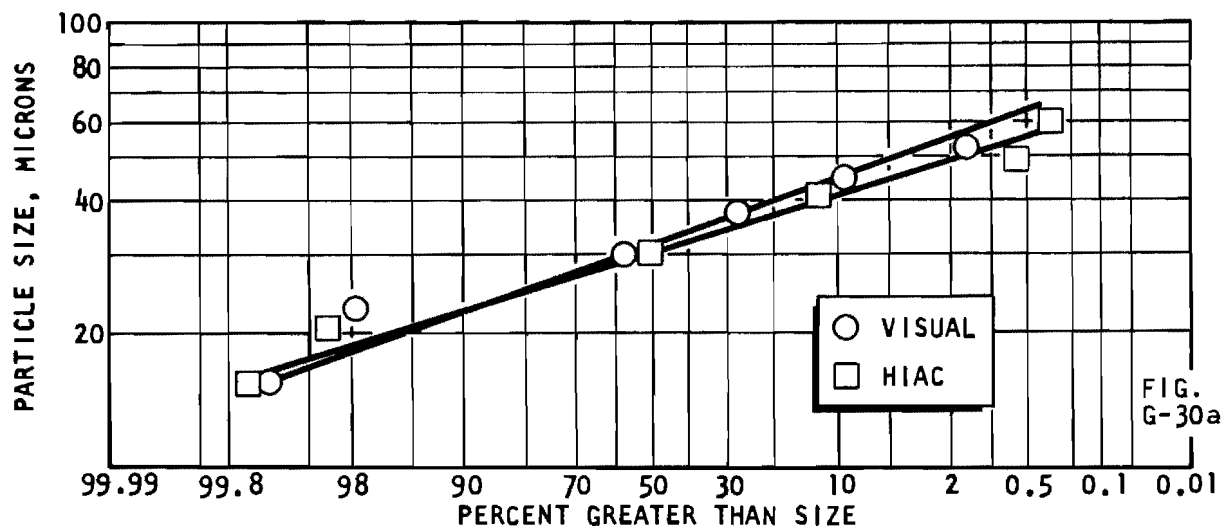


Figure G-30. HIAC-Visual Count Comparison for SB Particles

Sampler Calibration

Calibration of the (S_b) sampler was performed by comparing the particle count obtained from the full-flow (Q_b) line with the proportional (S_b) count. By replacing the line between VN1 and the cycle tester seat with a combination crimped hard line (for standard flows) and flexible nylon tube, all flow to the poppet and seat was directed overboard. The seat inlet was capped off. During steady-state running, the nylon line was placed in the tank inlet. A 10-second calibration sample (258 cc at 0.409 gpm) was obtained by switching flow from the nylon line between tank inlet to a Millipore filter funnel (Fig. G-31). Simultaneous with taking this sample, (S_b) pitot flow at 300 cc/min was counted by the HIAC. Prior to actual sampling, (Q_b) flowrate was calibrated to be within ± 1 percent of standard (0.409 gpm) with a 1550-cc volume (60 second run). Overall, 10-second sample volume error is estimated at ± 5 percent.

HA Particles. Two samples were taken for analysis along with the simultaneously recorded HIAC printout per 100 cc from (S_b). One of these samples, counted for size distribution at 200X magnification, is shown in Table G-5, with the distribution plotted in Fig. G-32.

Comparison data shown in Table G-6 indicate that (S_b) sampler extracted between 75.1 and 90.5 percent of the full-line particle flow concentration (82.8-percent average). These percentages were established by averaging the HIAC (S_b) readings as shown. This is based on the assumption of uniform (Q_b) particle flow and slightly fluctuating (S_b) particle flow as indicated by the counter data. As discussed later, laminar flow through the HIAC inlet tube disperses particles extracted via the pitot tube due to the parabolic velocity profile. Because of this and differing flow velocities, it is not possible to compare precisely the exact percentage of particles extracted over the 10-second calibrate period. Another possible error for these runs is a slight variation between pitot inlet and line velocities. This variable was previously examined and found to be significant for 10-percent velocity differences. These results indicated the need for additional tests.

Prior to further calibration tests, the counter was reset for intended model cycle tests with HA particles. Typical "clean" operation following 20 minutes of unfiltered operation produced the following count from (S_b) per 1000 cc.

<u>Channel</u>	<u>Range, microns</u>	<u>Count</u>
1	10 to 12	25
2	12 to 15	15
3	15 to 20	5
4	20 to 30	7
5	30 to 50	1
6	50 to 80	1
7	80 to 120	0
8	> 120	0



6AL42-11/6/69-C1L

Figure G-31. Sampler Calibration Technique

TABLE G-5

 S_b SAMPLER SIZE-FREQUENCY CALIBRATION WITH HA PARTICLES

(Microscopic count at 200X of item 29, 10-23-68, full Q_b (0.409 gpm) flow for 10 sec (258 cc) vs HIAC recorded S_b sample count average of three readings per 100 cc; see Fig. G-32)

Lower Size of Range d_i , microns	Microscopic Count					
	J. W. Lewellen \odot			G. F. Tellier Δ		
	n_i	Σn_i > d_i	% Σn_i > d_i	n_i	Σn_i > d_i	% Σn_i > d_i
37.5	1	391	100	0	384	100
45.0	9	390	99.9	9	384	100
52.5	109	381	97.4	135	375	97.7
60.0	171	272	69.7	197	240	62.5
67.5	79	101	25.9	37	43	11.2
75.0	13	22	5.6	5	6	1.6
> 82.5	<u>9</u>	9	2.8	<u>1</u>	1	0.3
$\Sigma n_i = 391$ $\Sigma n_i = 384$ $= 152/100 \text{ cc}$ $= 149/100 \text{ cc}$ $\sigma_g = \frac{63.0}{56.4} = 1.12$ $\sigma_g = \frac{61.0}{56.4} = 1.08$						
	HIAC Count for 100 cc			Avg		
	Item 29	Item 29 + 1	Item 29 + 2			
10	6	5	-			
12	6	6	4			
15	2	3	1			
20	0	2	1			
30	6	6	4	5.3		
50	109	109	103	107.		
80	0	1	0	0.3		
> 120	0	0	0	0.		
				<u>112.6</u>	$\cong 113/100 \text{ cc}$	

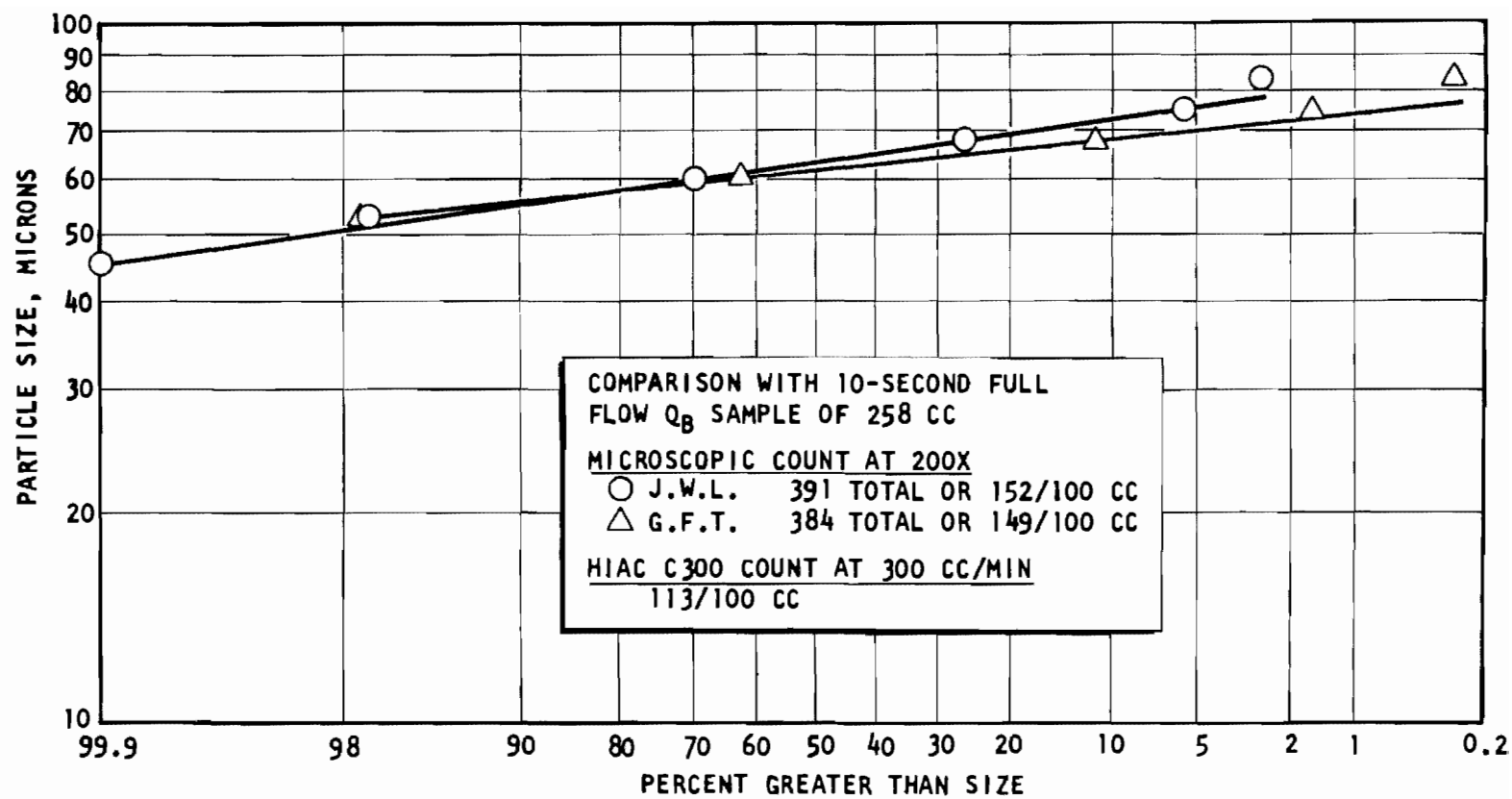


Figure G-32. S_b Sampler Flow HA Particle Distribution

TABLE G-6

 S_b SAMPLER FREQUENCY CALIBRATION COMPARISON WITH HA PARTICLES

Test Date, 1968	Item No.	Microscope Count				HIAC S _b	% HIAC Microscope
		J. W. Lewellen		G. F. Tellier		Count ②	
		Σ n _i	Σ n _i ① per 100 cc	Σ n _i	Σ n _i ① per 100 cc	Σ n _i ① per 100 cc	
258 cc at 0.409 gpm							
10-23	26	378	147	379	147	133 ③	90.5
10-23	29	391	152	384	149	113 ④	75.1

① Greater than 40 microns.

② Average of noted item HIAC count plus following two 100 cc samples over 1-1/2-minute period.

③ Ten 100-cc reading average (five before item 26 and 5 after item 26, including 26) = 137 with $\sigma = 13.2$.

④ Same as (3) for item 29 = 118 with $\sigma = 10.2$.

In preparation for additional (S_b) calibration, 25.6 mg of HA particles were added to the system. Three full-flow samples were taken from the nylon bypass line via VN1 at 0.409 gpm for 10 seconds. Summary of the count data, averages, and microscopic count comparison is shown in Tables G-7 and G-8. As indicated, the overall average for the five calibration runs is 81.7 percent (S_b sampler extraction percentage of line concentration). It is evident from these data that the particle flowrate is not uniform and, therefore, a precise calibration (i.e., within a few percent) is not possible. However, for the test purpose, the HA particle flow uniformity is considered excellent.

SB Particles. (S_b) pitot sampler calibration was performed for the SB particles as with HA particles. Four 10-second full-flow samples of 258 cc were taken directly onto a 47-mm membrane, redistributed with the hand nozzle, mounted between glass slides, and numerically only counted. With HA particles, there was only a small difference between an average of three 100 cc totalized HIAC counts, and a similar average of ten 100 cc counts of five readings before and after taking the sample (see Table G-6). This was due to nearly uniform particle flow. Consequently, the three 100-cc reading average was employed. However, SB particle count per 100 cc varied by up to 2/1 between consecutive readings, and the 1000-cc average obtained from ten 100-cc printouts was used to indicate an average concentration. Results from these tests are shown in Table G-9. Except for one sample, the ratio of HIAC to total sample count generally agreed with that obtained with the HA particles, i.e., 82 percent.

Cyclic concentration and gradual reduction in concentration observed during these tests was caused by the entrapment of magnetized SB particles within the 440C cycle tester and flowmeters. During tester inspection, a significant number of particles were observed at almost all 90-degree joints within the tester. The system could not be adequately cleaned because particles were being released at intermittent intervals. As previously noted, the HIAC sample flowmeter had to be removed from the system. Disassembly revealed many particles within the miniature ball bearing and magnetically attached to the paddle wheel edges. Similar problems occurred with the (Q_b) turbine meter although it had journal bearings. Observation of the system (Q_s) high-sensitivity, extended-range turbine meter indicated no particle adherence or entrapment, possibly due to higher flow velocities and/or lower magnetic level.

A final test of SB particle flow characteristics was performed with a carefully demagnetized system. Flowmeters, removable tester detail parts, wrenches involved in assembly, poppet and seat, and the SB particles used were demagnetized. As with previous tests, however, an unacceptable cyclic flow condition resulted. Examination of the SB particles used indicated they had become permanently magnetized and would agglomerate into strings and batches. Apparently, the relatively massive tester and flowmeters could not be adequately demagnetized with the equipment used and were the primary magnetic sources. In view of these results, all later program tests were performed with the nonmagnetic hard (H series) particles which were determined to flow uniformly throughout the system.

TABLE G-7

HIAC S_b SAMPLER CALIBRATION WITH HA PARTICLES

(Data represent HIAC count from $S_b/100$ cc; each item represents 20-second run at 300 cc/min with 10.7 printout time; items 20, 23, and 27 taken 11/14/68, and 26 and 29 on 10/23/68)

Item	HIAC Channel and Size Range, microns								Σ Channel 5 \rightarrow 8
	1 10-12	2 12-15	3 15-20	4 20-30	5 30-50	6 50-80	7 80-120	8 120	
20	-	23	8	4	9	259	1	0	269
20+1	-	21	12	6	14	260	0	0	274
20+2	39	22	6	5	6	235	0	0	<u>241</u>
Avg = $784/3 = 261/100$ cc									784
23	41	17	11	6	11	241	0	0	252
23+1	-	31	10	8	7	250	1	0	258
23+2	40	21	16	6	5	249	0	0	<u>254</u>
Avg = $764/3 = 255/100$ cc									764
27	50	21	13	7	11	261	0	0	272
27+1	57	19	4	9	13	227	0	0	240
27+2	-	25	12	7	9	237	0	0	<u>246</u>
Avg = $758/3 = 253/100$ cc									758
26	-	3	3	3	6	137	0	0	143
26+1	6	4	1	2	5	120	0	0	125
26+2	-	5	4	0	0	132	0	0	<u>132</u>
Avg = $400/3 = 133/100$ cc									
29	6	6	2	0	6	109	0	0	115
29+1	5	6	3	2	6	109	1	0	116
29+2	-	4	1	1	5	105	0	0	<u>110</u>
Avg = $341/3 = 113/100$ cc									341

TABLE G-8

 S_b SAMPLER CALIBRATION DATA SUMMARY FOR HA PARTICLES

(Microscope data and comparison with HIAC S_b data from Table G-7; microscope data from full Q_b (0.409 gpm) flow for 10 seconds; 258 cc)

Item	Microscopic Count Data						HIAC Avg From Table G-7	% HIAC Scope
	J. W. Lewellen		G. F. Tellier		Avg Σn_i	Σn_i per 100 cc		
	Mag.	Σn_i	Mag.	Σn_i				
20	40	799	40	807				
			100	804	802	311	261	83.9
23	40	852	100	857	854	331	255	76.8
27	40	800	100	805				
	100	801			<u>803</u>	311	253	81.4
					(2459)			
26	40	378	40	379	378	147	133	90.5
29	200	391	200	384	387	149	113	<u>75.8</u>
								408.4
Overall Avg = 408.4/5 = 81.7 Percent								
σ = 5.3 Percent								

TABLE G-9

HIAC S_b SAMPLER FREQUENCY CALIBRATION WITH SB PARTICLES

(Data Summary Comparison of Microscopically Counted,
Full-Flow Q_b (0.409 gpm), 10-Second Sample With
10-Item 100-cc HIAC Count Average (5 Before, 5 After)
Over 5.1-Minute Period)

Date, 1969	Item No.	Visual Count Data at 100X by J. W. Lewellen		HIAC S_b Average per 100 cc	% HIAC Microscope
		Σn_i per 258 cc	Σn_i per 100 cc		
1-8	10	522	202	175.0	86.6
1-8	13	261	101	81.0	80.1
1-8	16	240	93	57.0	61.3
1-22	6	991	384	322.0	83.8
<p>Average S_b Sampler Calibration Factor (Except Item 16) for SB (33 Micron Mean Diameter) Particles = $(86.6 + 80.1 + 83.8)/3 = 83.5$ percent.</p> <p>Previous S_b Calibration With 61-Micron Mean Diameter HA Particles was 82 Percent Therefore, Assume Same Factor for 30- to 60-Micron Particles.</p>					

S_s Versus S_b. Comparison of average (S_s) and (S_b) HA particle counts per 1000-cc sample indicated that (S_s) count was 92.4 percent of the (S_b) count.

Summary. The preceding results show that the HIAC sample indication of (Q_b) flow particle concentration was about 82 percent of full line concentration. Variation of this factor was within ± 8 percent. Combined with the previously noted 5-percent counting error (± 2.5 percent) gives an overall counting error of about ± 10 percent. From these limited data, it seems reasonable that the large majority of particle concentrations specified for the dynamic tests are within this limit.

HB Particle Flow and Distribution

In comparison with SB particles, HB particle flow was quite uniform, similar to the HA particles. Eleven minutes after inserting 20.4-mg HB particles into the system, the count had stabilized. The average count greater than 20 microns for ten 100-cc sample printouts (20-second sample at 300 cc/min plus 10.7 seconds print time) taken from (S_b) sampler was 644 with a standard deviation (σ) of 27.4. Similarly, (S_s) sampler gave a 10-sample average of 638 and (σ) of 21.8.

It was demonstrated from the previous HIAC calibration with SB particles that the instrument accurately sized and counted the nominal 30-micron particles. It was also shown in HA particle calibration that the (S_b) or (S_s) samplers did not discriminate particle size (at least for this narrow size range) because the mean size visually determined from (S_b) pitot and full-flow samples was essentially the same.

Consequently, measurement of HB particle size-frequency distribution was done using the HIAC counter. Counts were taken less than one-half hour from inserting particles into a clean system. Background count was less than 1 percent of stabilized total count greater than 12 microns. Counts from three particle insertions were used to determine the mean particle size; the data are shown in Table G-10. (The lower size range was increased from the previously used 10 to 12 microns because of recurrent HIAC noise problems.) Figure G-33 displays the plotted data and, as shown, good repeatability is indicated. The geometric mean particle size (d_g) for the HB particles is 32 microns with a geometric standard deviation (σ_g) of 1.25. This is nearly the same as the SB particles.

In view of the preceding results with SB and HB particle flow and dynamic model tests later discussed, it was decided to perform all further tests using HB particles.

Particle Size and Weight Analysis

To assist correlation between weight input, theoretical concentration, and quantity counted, a small quantity of HA particles was dispersed on a pre-weighed piece of Scotch mending tape approximately 3/4 in. sq and bordered

TABLE G-10

HB PARTICLE DISTRIBUTION FROM HIAC DATA

(HIAC distribution measurements of HB particles based on HIAC calibration with SB particles; n_i count per 1000-cc reading; see Fig. G-33*)

Test Item No.	Date, 1969	Particle Weight, mg	Lower d_i , microns	n_i	$\sum_{>d_i} n_i$	$\% \sum_{>d_i} n_i$
23 ⊙	2-7	20.4	12	59	5978	100.00
			15	62	5919	99.01
			20	1798	5857	97.98
			30	2846	4059	67.90
			40	1075	1213	20.29
			50	135	138	2.26
			60	3	3	0.05
			70	0	0	0
				$\sum n_i = 5978$		
15 △	2-12	4.8	12	22	1580	100.00
			15	21	1558	98.60
			20	582	1537	97.28
			30	675	955	60.44
			40	241	280	17.72
			50	38	39	2.41
			60	1	1	0.06
			70	0	0	0
				$\sum n_i = 1580$		
5 □	2-14	6.9	12	19	2473	100.00
			15	30	2454	99.23
			20	979	2424	98.02
			30	1081	1445	60.03
			40	326	364	14.72
			50	36	38	1.54
			60	2	2	0.08
			70	0	0	0
				$\sum n_i = 2473$		

*From Fig. G-33: $d_g = 32 \mu$
 $\sigma_g = 32.4/26.0 = 1.25$

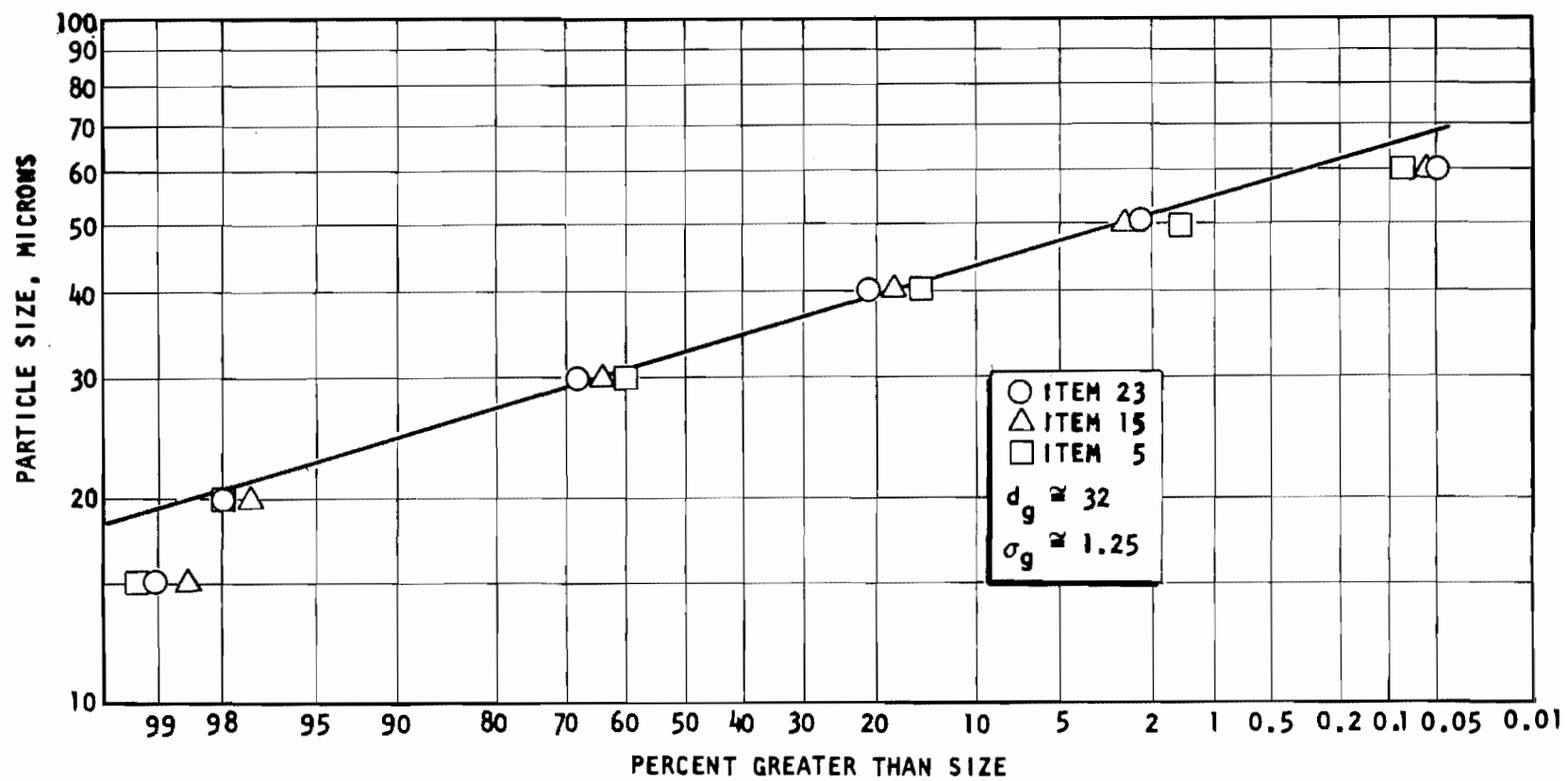


Figure G-33. HB Particle Size Distribution

with cellophane. After weighing, the tape and particles were mounted between glass slides (Fig. G-28) and counted. The net particle weight was measured on a Cahn Electrobalance as 2.02 ± 0.02 mg. Particles were counted at 200X magnification without sizing. A count of 2181 was obtained.

Based on the theoretical density for the HA particles computed from reported chemical composition, the computed mean volume diameter is 60.3 microns compared with the HIAC measured mean of 58 microns. These results essentially verify the theoretical concentration and, thus, prove the number versus weight amount of particles being placed into the system.

SYSTEM PERFORMANCE

The previous calibration tests and particle experiments led to a partial understanding of system characteristics and performance. However, it was not understood why concentration would change with flowrate, and steady-state particle counts could not be reconciled with weight input. Also in question was the steady decrease in concentration with operation. Answers to these questions were necessary before dynamic tests could be performed with confidence.

Particle Flow Velocity

To help explain the overall system operation and relationship between particle quantity input and HIAC counts, several particle velocity tests were performed. These consisted of: (1) high-velocity line tests, (2) HIAC inlet tube influence, and (3) particle flow velocity through entire system.

High-Velocity Lines. Approximately 2 mg of HA particles were placed just downstream of V1 3-micron filter holder (no element or backup screen) while the system was operating in a clean mode with flow through the filter bank and sampling from (S_f) Pump speed had been adjusted so that on switching the analytical filter circuit in via V1, standard flows would be established. For this test, the HIAC laminar flow inlet tube was removed with the diffuser placed at the microcell. The average flow time computed from actual line sizes from the filter to the HIAC microcell was 2.54 seconds. Two test runs were made timing the interval from snapping V1 open to first counts; 2.50 seconds were obtained in each. Two additional runs were made recording channel 5 (50 to 80 microns) count each 2 seconds with the following results:

<u>Time, seconds</u>	<u>Counts</u>	
	<u>Run 1</u>	<u>Run 2</u>
0	0	0
2.5	46	73
4.5	51	78
6.5	55	81
8.5	56	81
60.	56	81

These data show that the suddenly injected particles traveled as a "cloud" at essentially the line velocity (10.7 ft/sec in the 3/8 line and 4.47 ft/sec in sampler lines).

HIAC Inlet Tube. The preceding test was repeated with the HIAC inlet tube in place. Initial counts occurred in 5.5 seconds. A total S_f count of 52 was recorded in 120 seconds with the median (26) passing the counter in 56 seconds. This indicates that the average particle velocity for the 25.1-inch-length tube was 0.467 inch/sec. Count rate in percent of total particles counted per second is plotted versus time in Fig. G-34 (triangles). This plot shows an initial high count rate presumed to be caused by a cluster of particles following the higher velocity streamlines near the center of the tube.

From the previous test, the flow time attributable to the inlet tube is the data read less the 3/8-inch line flow of 2.5 seconds. This gives 3.0 seconds for the fastest particle and about 2 minutes for the slowest. For laminar flow, the maximum velocity is twice the average of 4.17 inch/sec or 8.34 inch/sec. Thus the fluid travel time at the center of the 25.1-inch inlet tube is 3.0 seconds, which correlates with the above. The computed falling velocity of 60-micron nickel spheres is about 1.0 inch/sec in Freon TF, indicating a maximum travel time down the tube of 25 seconds. The fluid velocity 60 microns from the wall is computed as 0.022 inch/sec which is small compared with the falling velocity. The 2-minute time for all particles to pass the tube is probably caused by particles rolling and sliding down the tube wall. The consequence of the above is that the HIAC reading is merely a representation of the particle concentration actually extracted by the sampler pitot. It is undoubtedly a good representation because the particles used have a narrow size range and the particle flow in and out is identical for steady flow. However, if particles within the tube tended to separate into faster or slower streamlines by size, the output distribution (which would be counted) would be different from that sampled. Also, changes in flowrate would have a pronounced effect on instantaneous counts, as has been observed.

Further insight into concentration in low-velocity areas was obtained in tests performed to measure the static particle concentration trapped in the HIAC inlet tube. The test was performed with the system operating steady state, bypassing the filter bank, and with continuous readings from (S_b) per 100 cc. Sampling valves VS5 followed by VS_b were closed, trapping fluid in between. The counter was reset and counting initiated simultaneously with opening VS5 and the fifth manifold inlet, which allowed the HIAC inlet tube volume to fully drain into the tank at about 90 cc/min.

In two tests, the particle concentration from the recorded count for the 32.1-cc inlet tube was about 6 times the steady-state run count at 300 cc/min. Based on the average particle and fluid velocities of 0.467 and 4.17 inch/sec, respectively, the computed concentration increase is 8.93/1. The difference might be due to the few seconds delay between VS5 valve shutoff and count initiation, wherein a percentage of the particles settled out. Nonetheless, the effect of greatly increased concentration was observed and explained as above.

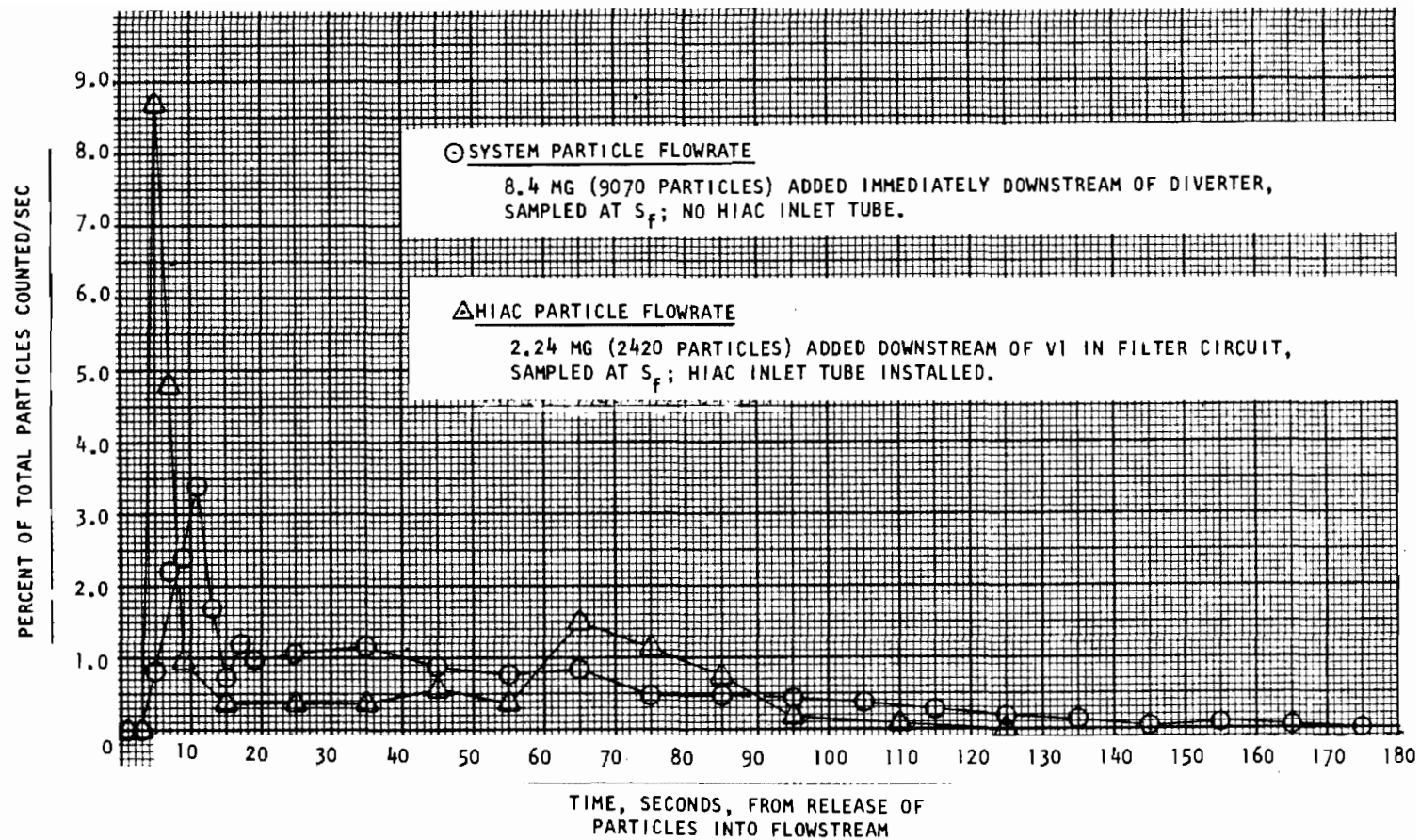


Figure G-34. HA Particle Flowrate Characteristics

System. To determine the flow characteristic of particles throughout the system, HA particles were inserted into a clean system at the Heise gage (P_S) tee. The HIAC inlet tube was removed from the system so that the count versus time would be essentially that resulting from the tester and tank. The sequence of events was as follows:

1. Obtain clean system flow (2.44 gpm) through filter bank as sensed by (S_f).
2. Shut down pump and, during 5-second coastdown, switch V2, V1 (filter removed and ports capped), V4 and VS_f . This traps fluid at gage tee and retains fluid in filter bank.
3. Open tee cap and insert 8.4-mg HA particles; cap tee.
4. Switch V2 (filter bank in); open V1 and VS_f .
5. Start pump and bring to previous rpm.
6. Switch VS_6 sample diverter to overboard flow.
7. Snap open V4 under tester and manually record channel 6 (50 to 80 microns) count each 2 seconds, as sampled by (S_f) at 300 cc/min.

The results of the above test sequence produced an initial count between 4 and 6 seconds. A total of 205 particles was counted over a continuous 180-second period with the average quantity (103) passed in 42 seconds. A plot of particle flowrate versus time is shown in Fig. G-34 (circles). It can be seen that, in the recirculation mode (bypassing the filter bank) some particles will make multiple loops compared with others. Furthermore, sampled flow particles experience an additional delay of about 1 minute. The net effect of the above is to constantly disperse and mix the total population.

Particle Count Reconciliation

Why doesn't the sample particle count equal the weight concentration input? A partial answer to this question has been given above. These data also provide the facts necessary to build a fairly strong hypothesis of particle flow within the system. Considering the analogy between HIAC inlet tube, tester cavity, and reservoir wherein fluid surface velocities are very low, it is believed that observed "low" sample concentration resulted from a high concentration in these low-velocity areas caused by particles falling out (particularly in the tank) onto these surfaces and, from there, moving very slowly toward the exit.

This explanation is supported by two other observed "phenomena." During operation, wherein the system was bypassing the filter bank and a steady-state count from (S_b) was being recorded, the reservoir inlet tube jet was rotated from its position normal to the reservoir axis to a tangential direction creating a vortex. Between the vortex and the normal positions, the steady-state sampled fluid count was varied up to 2/1.

Within 19 minutes from inserting 25.9 mg of HA particles into the reservoir, (S_b) counts per 1000 cc (30 to 80 microns) averaged about 1450 p/l. The 25.9 mg corresponds to a theoretical concentration of 27,200 particles, or $27,200/13.9 = 1960$ p/l. Considering the vortex effect and previous factors, it is reasonably certain that concentration variations were caused by low particle flow velocity in the reservoir.

The second "phenomenon" was the marked increase and decrease in sample concentration with similar changes in sample and system flowrate. It is believed that the effect primarily resulted from changes in tank turbulence and/or vortex agitation, which influenced particle movement through the reservoir.

Several particle recovery tests were performed to reconcile particle weight input-output. The usual result was 80 to 90 percent. In a final attempt to recover a larger percentage, 52.0 mg of HA particles were added to the clean system. Within 5 minutes, the (S_b) count had stabilized to 7400 p/l. After 17 minutes of steady operation, the analytical filter was switched in for 10 minutes at standard flows. The recovered particle weight was 47.9 mg, or 92.2 percent. Subsequent system operation at maximum flow with several stops to allow particles to "settle out" produced a cumulative (S_b) count of 342 p/l, corresponding to $342/7400 \times 52.0 = 2.4$ mg. The total weight accounted for is thus 50.3 mg, or 96.7 percent of that inserted. It is interesting to note that the concept of theoretical concentration based on quantity added, with respect to system total volume of 13.9 liters, bears little relationship to the dynamic concentration. Based on the above recovery, it can be assumed that the 7400 count for (S_b) per 1000 cc very nearly represented the total 52.0 mg of particles inserted. This corresponds to a total input of 54,100 particles, or a theoretical concentration of 3890 p/l. Applying the (S_b) calibration results, the actual flowing concentration was $7400/0.82 = 9000$ p/l, a factor of 2.3 times greater than theoretical. As previously demonstrated, this is due to the tank wall flow. It is, therefore, reasonably certain that the upper half of the tank fluid was almost free of particles.

Throughout a 1000-cycle model test, a decrease in particle concentration was typical. This gradual decrease in concentration was never pinpointed to any one component, although valve disassembly did reveal a few particles. It is hypothesized that "lost particles" became lodged in the various low-velocity trap areas within the system. If these areas were absent, the system could be cleaned free of particles within a few minutes; however, up to 1 hour was usually required. This is more easily visualized by considering the following:

1. A typical 1000 p/l loss corresponds to about 6000 particles
2. Distributed in 100 traps = 60 particles/trap
3. This number of HB particles would cover about 0.01-in. sq and, thus, would be barely visible.

TEST PROCEDURES

Dynamic evaluation of a given test model involved a sequence of several individual tests and associated operations. Generally, at least three static or stress-leakage tests were performed to: (1) define fundamental model performance capability (thus, an acceptance test), and (2) assess performance changes, if any, after clean and particle-laden fluid cycles. The clean cycle test provided a stabilization or, in some cases, a wear-in function from which a datum postcyclic sealing capability was established. Finally, cycling with a known particle population provided impact (hit frequency) data and, by the concluding stress-leakage test, a measure of sealing degradation caused by particle encounters or entrapments.

The following paragraphs describe pertinent features of these test procedures together with dynamic test system operation requirements and sequences.

Assembly and Static Testing

Test model surfaces were precleaned by high-pressure flushing with 3-micron, filtered flow bench Freon TF. After assembly, and prior to initial closure, a gas purge via VN1 and VN2 was established through the seat, and sealing surfaces were flushed with 0.45-micron filtered Freon TF from a pressurized bottle. This was followed by manual gas purging of model and adjacent surfaces. With these cleaning procedures, no assembly-incurred contamination problems were encountered.

Assembly and stroke adjustment procedures followed cleaning, as described in Appendix F. Virtually all testing was performed with the dashpot connected, using the O-ring leak collector. Preliminary testing established bias loads associated with these devices which were considered in the calculation of balance pressure as analyzed in Appendix F. Except for the later oriented-position tests of Phase III, the bias spring was not installed until the conclusion of the stress-leakage test and, thus, was not a factor in balance pressure computation. On those occasions when the spring was installed, balance pressure was directly measured prior to each stress-leakage test.

After assembly, stroke adjustment and final cleaning operations were completed, the leak collector O-ring was installed, and the parallelism adjustment sequence described in Appendix F was performed. The stress-leakage test followed which (except for the shear seal models) was standardized at 10,000-psi maximum apparent seat stress (about 440 pounds) loops. With the acquisition of satisfactory stress-leakage data, the O-ring was removed, bias spring installed, and the tester covers attached in preparation for cycle tests. (During later Phase III dynamic tests, the O-ring remained with the poppet during cycling.)

Cycle Test

Model cycling required consideration of impact loads, velocity, cycle rates, clean and particle cycling characteristics, and particle monitoring procedures as follows.

Impact Level. Previous cycle testing (Ref. 3) indicated that flat 440C models, cycled 10,000 times in an essentially contaminant-free nitrogen environment at an impact stress of 25,000 psi, evidenced no notable change in surface structure or sealing capability. Because the cycle testing phase of the subject program was intended as means of evaluation contaminant-caused effects, uninfluenced by basic cycle parameters, a similar impact level was targeted. Initially, however, the piston pumping tester cavity surge pressure (Appendix F) limited impact velocity and stress to approximately 7 inches per second and 20,000 psi, respectively. As this reduction was not particularly significant, similar impact values were employed even after the surge-reducing bladder was added to the tester.

Impact Velocity. Impact velocity was recorded from oscilloscope photos of position for the stroke between about 0.013 and 0.003 inch of impact. As noted in Appendix F, dashpot dynamic effects occurred at about 0.003 inch off-seat.

Cycle Rate. The cycle rate was based on requirements that: (1) the system flows return to a full steady-state condition between each cycle, and (2) the entire line fluid volume between the diverter and seat be replaced with new fluid prior to the next impact. The first condition was obtained quite rapidly; however, based on the seat feed line minimum velocity of 5.2 ft/sec, a period of 0.97 second was required to refill the line. Observation of the impact traces indicated that the full impact cycle required less than 10 ms; therefore, the ON cycle time was set at 0.07 second and the OFF time at 1.93 seconds, for a total cyclic rate of 30 cpm. A routine 1000-cycle test then took about 33 minutes.

Clean Cycles. As initially conceived, the clean cycle test was to establish model sealing degradation tendencies after exposure to background contamination typical of that expected during particle cycles. Thus, the system was precleaned, until no more than 10 counts greater than 12 microns per 1000 cc were recorded, switched to the unfiltered mode, and 1000 cycles accumulated. After several such tests, it was determined that sealing performance at elevated stress tended to improve with cycles and the influence of any generated or loosened contaminants encountered was negligible. Therefore, subsequent clean cycles were performed in the filtered flow mode. This still permitted acquisition of stabilized postcycle performance data while providing system cleaning in preparation for the subsequent test with particles.

Particle Cycles. For particle cycles, the system was precleaned as before to ensure removal of contaminants introduced during stress-leakage testing. Test particles were then added to the system via the reservoir access tube.

At first, particles were added on a weight basis from computations of weight-frequency conversion for concentration levels desired. The weighing step was soon eliminated as volume selection proficiency developed and the test concentration was achieved within 10 percent with the first measure added.

System particle concentration was monitored via sampler (S_b) per 100 cc during stabilization which took approximately 10 minutes. The HIAC was operated in the total mode and concentration was based on total counts greater than a given size. For the predominantly used HB particle size, channel 3 (greater than 20 microns) readout was used. This value was corrected by the 82-percent sampler efficiency factor previously discussed. After reasonably stable readings were established for 100-cc samples, final concentration was recorded on a 1000-cc (S_b) sample basis with up to three readings taken to ensure repeatability. Particle cycling was then begun.

Particle concentration was periodically monitored during the cycle test. When early tests indicated that population reduction with time occurred relatively slowly, total count checks (1000 cc) were taken after 100, 200, 500, and 1000 cycles. The counts so obtained were averaged and weighted on a frequency or cycle basis to best represent the particle concentration (C_n) presented to the test model for each cycle. The average C_n is given by:

$$C_n = \frac{\sum_{i=1}^I f_i C_{ni}}{f}$$

with nomenclature defined in the following tabular example of typical data reduction.

Number of Cycles, f	Recorded C_n	Cycle Increment, f_i	Incremental Average Concentration C_{ni}	$f_i C_{ni}$
0	3500	0	3500	0
100	3312	100	$\frac{3500 + 3312}{2}$	340,600
200	3270	100	$\frac{3312 + 3270}{2}$	329,100
500	3104	300	$\frac{3270 + 3104}{2}$	956,100
1000	3071	500	$\frac{3104 + 3071}{2}$	1,544,000
				$\sum f_i C_{ni} = 3,169,800$

$$C_n = \frac{\sum f_i C_{ni}}{f} = \frac{3,169,800}{1000} \cong 3170 \text{ particles/liter}$$

Applying the (S_b) correction factor of 82 percent gives the final particle concentration value as

$$C_n = \frac{3170}{0.82} = 3866 \text{ particles/liter}$$

Operational Sequence

Through preliminary investigations and accumulated experience, model dynamic testing evolved to the following typical sequence of operations:

1. Instrumentation and system setup
2. Poppet and seat assembly
3. Manual cleaning
4. Stress-leakage test
5. 1000 clean cycles
6. Stress-leakage test
7. 1000 particle cycles
8. Stress-leakage test
9. Disassemble and inspect

Detail system operating procedures to accomplish the preceding events follows for the standard flat model. Note that, with Phase II and initial Phase III models, the poppet-to-seat rotational alignment was changed (reoriented) with each cycle test because of the need to remove the bias spring to install the leak collector O-ring. For latter Phase III models, poppet-seat orientation was maintained throughout the entire dynamic test series (see Appendix F).

A. Instrumentation and System Setup

1. Turn on all instrumentation equipment 1/2 hour prior to data acquisition or recording.
2. Verify 50-psig Freon TF actuation pressure to V1 through V4.
3. During periods of HIAC operation with sample flow, GN₂ cooling purge to the microcell light bulb is set at 160 psig on No. 80 orifice. This may be continued for 1/2-hour (or less) periods of no sample flow; but, for longer periods the microcell light is shut off (X10 setting) along with the purge.

B. Assembly--tester switched out of liquid circuit via V3, V4, and VN1. VN2 switched to inlet pressure circuit.

1. Assemble poppet and seat. Torque seat to 200 pounds as indicated by load cell.
2. Raise film pressure to 600 psig.
3. Set stroke (usually 0.030 inch).
4. Flush-clean model sealing surfaces with 0.45-micron filtered Freon TF from pressurized bottle and purge dry using manual blowoff probe.

C. Stress-Leakage Testing

1. Back out piston via dashpot 10 turns and place leak-collecting O-ring between poppet and seat. Return poppet to 0.03-inch stroke position (bias spring installed with latter Phase III models).
2. Open three-way solenoid valve and raise P_C to balance pressure (about 110 psig).
3. Connect leak collector O-ring via 52 inches of 0.038-ID plastic tubing to buret leveling system and verify leak collector seal with 1-foot water vacuum ($P_1 = 0$).
4. Reconnect plastic tubing to AAA Brooks pyrex ball leak meter (4-scim GN_2 full scale).
5. Raise P_1 to establish meter midrange leak (800 to 950 psig).
6. Gently apply finger axial seating load to each of the three clamp ring screws and observe leak decrease. A significant difference indicates out-of-parallel assembly, which may be corrected by appropriate torque adjustment. This must be done by trial and with poppet and seat separated until optimum adjustment (minimum leakage) is achieved.
7. Raise P_C to the equivalent of 300-psi seat stress (about 7.0-psi P_C above computed balance pressure), and P_1 to 1000 psig; block leak collector O-ring open and perform balance pressure test.
8. Record leakage for increasing and decreasing apparent seat stresses of 500, 1000, 2000, 5000, and 10,000 psi. Plot data as obtained to verify consistency; add data points as required. (At P_C pressures above 169 psig, the dashpot reservoir pressure must be commensurately increased to preclude nitrogen leakage into dashpot.)
9. Reduce P_1 to zero.
10. Switch VN2 to Freon fill and purge position.
11. Reduce P_C to zero.
12. Remove leak collector O-ring and install bias spring with stroke at 0.03 inch (this step deleted with latter Phase III models).
13. Bolt on tester covers.

D. Switching Tester to Freon System and Precleaning

1. Switch V4 to reservoir and VN2 to liquid purge position.
2. Top off reservoir from flow bench (Point A) through 3-micron purge and VN1 inlet filters as required. Remove fill line and cap port A.

3. Switch VN1 then V3 to liquid system.
4. Start pump to a system pressure (P_s) of about 1 psig and start refrigeration unit.
5. Switch in filter bank via V2 and open VS5 and VS_b (VS6 switched to reservoir).
6. Increase pump speed to 4500 rpm and adjust VS5 to produce 300 cc/min sample flow through HIAC C-300 microcell. Observe count, particularly in 12- to 30-micron ranges which should drop to zero per 100 cc within two 1000-cc sample printouts (7 minutes). Counts beyond this time may be caused by broken 293-mm membrane.
7. Operate system for sufficient time to reduce S_f count greater than 12 microns per 100 cc to zero. This should be less than 10 minutes because system was left clean from the previous test and major source of contamination to be removed is from assembly and previous stress-leakage test. The tester is now ready for clean and particle cycle testing.

E. Switching Tester Out of Freon Circuit After Cycle Testing

1. Switch to S_b and close VS5.
2. Reduce pump speed to produce P_s of about 1 psig.
3. Switch out filter bank via V2.
4. Stop pump and refrigeration.
5. Raise purge pressure to VA1 to 50 to 60 psig.
6. Switch V3 and VN1 together to purge position.
7. Open VA1 to cause gentle bubbling in tank, then switch V4 overboard.
8. Open VA1 fully to purge tester interior for 30 seconds.
9. Close VA1 and switch VN2 to GN₂ inlet position. Reduce purge pressure to zero.
10. Raise inlet pressure to audibly purge seat inlet for 30 seconds. Reduce inlet pressure to zero. The tester is now ready for GN₂ testing.

F. Ultraclean Background or Particle Cycle Testing

1. Switch in tester and preclean as in D1-D7.
2. With VN2 in Freon purge position, raise P_1 to 100 psig.
3. Switch VN1 to purge position and VN2 to GN₂ inlet position. This flows about 0.2-scfm GN₂ into tester cavity and serves to clean this area. Purge for 30 seconds with exhaust from tank cover.
4. Switch back VN2 then VN1 and reduce P_1 to zero.

5. Upon obtaining zero count greater than 12 microns per 100 cc from S_f , cycle tester 100 times.
6. Switch out filter tank as in items E1-E3.
7. Increase pump speed to 4500 rpm for one 1000-cc S_b sample printout (3.5 min at 300 cc/in.), switch filter bank back in by reducing speed, and then return to 4500 rpm.
8. Switch to S_f and observe system count. Upon obtaining zero count greater than 12 microns per 100 cc, switch to S_b . For background or particle tests only, switch out filter bank by reducing pump speed. Ultraclean tests are performed with flow through filter bank.
9. Increase pump speed to give standard flows ($Q_s = 2.44$ gpm, $Q_b = 0.409$ gpm, $Q_{sb} = 300$ cm) and observe S_b count per 1000 cc. If total count greater than 12 microns is zero for ultraclean tests or less than 10 for background or particle tests, proceed; if not, repeat items F7-F9.
10. Perform 1000 cycles with $P_c = 169$ psig at 30 cpm (0.07 sec ON, 1.93 sec OFF) and obtain noncyclic S_b count per 1000 cc at 0, 100, 200, 500, and 1000 cycles. Observe oscilloscope impact and position traces during cycling for proper operation and obtain photos as required.
11. Reduce pump speed, switch in filter bank (after background or particle tests) and increase to 4500 rpm.
12. Switch to S_f and observe for zero count greater than 12 microns per 100 cc.
13. Switch tester out of liquid system as in items E1-E10; perform stress-leakage test per items C1-C4, and C7-13 and clean up per items F1-F9.
14. Introduce particles into tank via cover.
15. Upon stable count in proper size ranges, proceed with cycle test as in item F10 above.
16. Clean system and perform stress-leakage test per items F11, F12, E1-E10, C1-C4, and C7-C9. Item F12 may require up to 2 hours to complete.
17. Remove leak collector O-ring and reduce piston film pressure to zero. Remove poppet and seat from tester and inspect. Obtain interference photomicrographs of surface texture and damage as required to correlate with stress-leakage results.

APPENDIX H

HELICAL VANE TESTS

A series of tests was performed on several helical vanes in the dynamic test system (Appendix G) to determine particle separation potential. These tests were preceded by a brief evaluation of reverse pitot flow which proved relatively ineffectual in HB particle separation capability, with between 3 and 5/1 particle concentration reduction at standard dynamic test system flowrates (Fig. G-1).

The vane tests were performed with pitot sampler S_b reading the true line concentration and a second pitot S_x (with 0.0667-inch probe ID) providing concentration data downstream of the vane. The discharge was passed through Q_b meter, a backpressure restriction line, and directly into the tank cover via plastic tubing.

Numerous tests were performed to determine: (1) the necessary vane length, (2) optimum distance between vane and S_x pitot tip, and (3) preferred helix angle for the standard seat Q_b flow of 0.409 gpm. Additionally, sample flow was varied to produce pitot feed velocities above and below line velocity. This was determined to have only a minor effect on concentration; therefore, the tests were performed with S_b and S_x sample flowrates of 300 and 200 cc/min, respectively, which were near constant velocity. Final test results and conclusions are as follows:

1. Of the two helix angles tested (0.75- and 0.55-inch pitch), the shorter pitch provided much greater decrease in concentration (up to 100 p/l). This was the shortest pitch helix that could be fabricated without helix distortion.
2. Vane length is relatively unimportant because particle separation takes place downstream of the vane. There was evidence that particles were mixed inside the vane. It was shown that results from one turn were slightly better than from four turns.
3. Helix vane positions from contacting to 1-1/2 inches from the pitot were tested at 1/4-inch intervals and $\pm 1/16$ at the optimum position of 11/16 inch. Good particle separation occurred between 1/2- and 1-inch gaps.
4. Final concentration reduction of HB particles per liter was as follows:

Particle Size Range, microns	S_b Upstream (U) Count	S_x Downstream (D) Count	Ratio (U/D)
12 to 15	668	319	2.1
15 to 20	661	201	3.3
20 to 30	7,594	60	130.
30 to 40	15,287	18	850.
40 to 50	3,409	3	1100.
50 to 60	571	3	190.
60 to 70	50	1	50.
>70	2	0	--

Tests with high concentrations of larger HA particles showed much greater ratios than above, but this was misleading because some large particles did enter the downstream pitot even at low concentrations as shown. This may have been due to particles shaking loose from the nominal 0.0005-inch vane-to-tube ID clearance, which would thus have a relatively low velocity.

5. A Freon TF flow- ΔP test of the optimum vane (1-1/4-inch long, in 0.194-inch ID tubing) indicated a tare ΔP of 0.65 psi at 0.409 gpm.

APPENDIX I

FLAT-GROOVED COPPER SEAT FABRICATION AND INSPECTION

Specialized fabrication and inspection techniques were developed in arriving at the final, flat-grooved copper seat configuration (Fig. VI-5). Basic problems resolved were land width uniformity and burr control. Development, detail machining setup and final processing and inspection is described in the following pages.

FABRICATION EXPERIMENTS

A brief review of the literature was undertaken to gather information pertinent to lathe turning copper. Other than the usual generalities, however, little was gained leading to production of very fine finishes. Direct experimentation using carbide tooling and a Hardinge lathe was then performed.

Five grooved sealing lands were fabricated to identify problems prior to undertaking a final design. The initial two parts were plunge cut in one pass with a 30-degree included angle carbide tool to a depth of 0.0056 inch. This produced peaks with a 0.0030-inch pitch. Three additional parts were then turned with a 60-degree tool to produce the same 0.0030-inch pitch. The initial part was plunge cut in a single pass and the remaining parts were produced with multiple passes to increasing depth. This latter method was found necessary to avoid lateral plastic flow of the previously cut (and unsupported) wedge.

Surface lapping, polishing, cleaning, and microscopic inspection of these parts led to the following observations:

1. To maintain uniform wedge form, a multiple-pass cut method must be used.
2. Plunge cutting produces a circumferential burr 0.0003- to 0.0005-inch wide at each land crest, which must be removed by lapping. The burr problem could possibly be minimized or eliminated by compound-angle cutting wherein previously cut wedge burrs are shaved by subsequent cuts.
3. Overall groove tolerance control is nominally ± 0.0001 inch with ± 0.0002 inch as a maximum limit.
4. Groove cleaning is a problem because even sonic cavitation capable of removing burrs could not remove particles at the groove base.
5. Common carbide tool sharpening procedures are based on significantly deeper cuts than required with the grooved seat. Observations of several tools, diamond lapped with a conventional oscillating disk, revealed cracks and chips on the cutting edge up to 0.0005 inch. Use of fine diamond reduced these flaws to about 0.0002 inch. Edge wear of this tool after cutting one part (eight grooves) was about 0.0002 inch.

6. With proper control of final lapping and polishing procedures, a crest land width of less than 0.0003 inch was obtained.
7. Measurement of land crest flatness and parallelism must be accomplished optically. A part with 0.001-inch wide lands was passed under a Johansson Mikrokator comparator set at minimum load (1 ounce). The 1/8-inch ball produced deep scratches and grooves across the land. A flatness and parallelism measurement technique using the interference microscope with an optical flat was devised and compared with two gage blocks differing by 50 micro-inches. The results using white light interference bands indicated measurement repeatability within ± 2 microinches. Additional refinements of this technique are described later.

FABRICATION DEVELOPMENT

The preceding experiments led to the conclusion that groove pitch should be increased to 0.0060 inch to be commensurate with the ± 0.0001 -inch groove tolerance. Initial seat fabrication attempts also led to the problems of excessive crest burr and tool wear. A brief exploration of tool material, cutting angles, edge sharpening, and cutting speed was then undertaken in machining 14 sample seat surface pieces. From these data, seat detail parts suitable for leak testing were then fabricated in accordance with Fig. VI-5.

Setup

All machining was performed on a Hardinge tool room lathe using a 0.0001-inch dial indicator for groove depth control, and the cross-feed lead screw dial for radial pitch control (Fig. I-1).

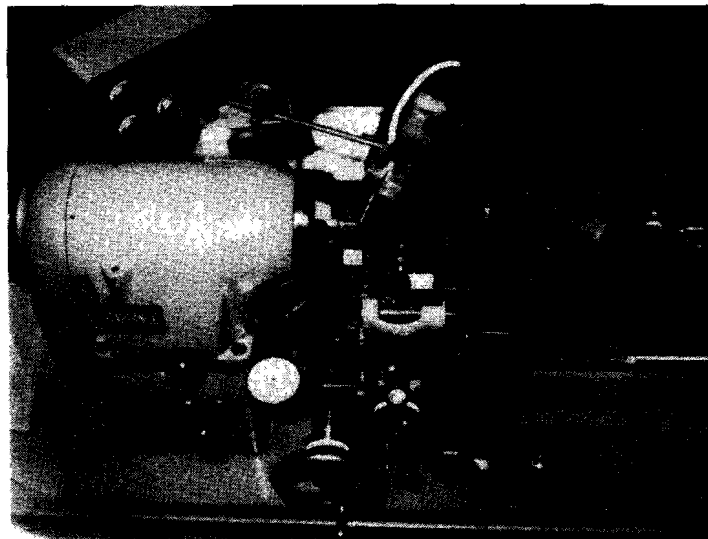


Figure I-1. Lathe Setup

Consideration of additional complexity and tolerance attendant with compound cutting resulted in the decision to remain with the form tool plunge cutting technique. A 40-power microscope was mounted on the lathe at about 20 degrees from the vertical, parallel with the centerline looking at the seat ID and tool face. A 500-watt fiber optic light, located approximately 1/4 inch from the tool tip, provided sufficient light to position the 0.0001-inch tool tip radius within 0.0001 inch of the 0.4320 seat bore corner. This initial alignment established a "zero" for subsequent cuts. Plunge feed was by hand at a rate of about 0.001 inch per second.

Sample Surface Fabrication Experiments

All 14 of the sample seat surfaces were cut to a final depth of 0.0057 inch in five passes of increasing depth to minimize land radial plastic flow and, of course, burr formation; these were 0.003, 0.0045, 0.0049, 0.0057, and 0.0057 inch (free pass). Kerosene was used as a cutting fluid. This resulted in crest intersections at nominally 0.0005 inch below the original surface. Six tools were employed to cut these surfaces, as shown below:

Tool No.	Material	Lap Finish Compound, microns	Side Clearance Angle, degrees	Top Back Rake Angle, degrees
1	HSS	3	10	10
2	WC883	3	10	10
3	WC883	3	15	10
4	WC883	3	20	10
5	WC883	1	20	10
6	WC883	3	10	20

General criteria of acceptability determined in cutting with these tools are as follows:

1. Lack of chatter
2. Surface finish
3. Crest burr
4. Crest radial pushover (measured from contact between work and tool at a depth dimension less than previous pass cut)
5. Tool wear and/or fracture

The one piece cut with the high-speed steel (HSS) tool indicated excessive burr and tool wear. All further pieces were cut with tungsten carbide (WC) tools. In general, tools 4 and 5 produced minimum pushover and the best surfaces, but still with significant crest burrs. Lapping sample surfaces proved difficult with light compound because other land material had to be removed before making contact with the crests.

Tool number 5 was used in an attempt to obtain a cutting edge free from the typical 0.0001- to 0.0002-inch crumbled edge observed on all carbide tools. A special carbide lap was prepared for the oscillating lap wheel and the tool edges lapped with 0- to 2-micron diamond compound. Although of some benefit, it was concluded that the conventional lap procedure was a limiting factor in producing intersecting tool surface finishes with less than 0.0001-inch edge crumble.

Several pieces were cut at 200 and 1300 rpm using tool number 4 to compare with the 650-rpm cutting speed employed for all other pieces. The burr results indicated that 650 rpm cutting speed was best.

Seat Fabrication

The first three seat details were turned on Phase II flat copper seats using tool number 5. Lapping was necessary to remove crest burrs but was difficult because the crests were initially below the outer land. Use of 1- to 5-micron diamond on cast iron, copper, and WC laps proved unsatisfactory because of poor surface finish and occasional deep gouges cut in the land crests. After cutting the first part, it was decided to cut above the surface and, thus, to a defined land width. As a result, parts 2 and 3 were successfully made with almost no burr. Because the surface was on one plane, a wet slurry lapping technique using only 0- to 1/4-micron diamond water-soluble compound with alcohol on a 5-microinch crowned 3-inch OD carbide lap gave a suitable finish while removing crest edge burrs. Prior to placing a new seat on the lap, it was preconditioned with a scrap seat blank, which also ensured a clean surface.

Part 4 revealed a tool wear problem which resulted from cutting to specific dial-indicated depths. As proved later, about 0.0003 inch was worn from the tool cutting edge. Because the work was initially faced off with the 60-degree form tool, tip wear of about 0.0005 inch resulted in a zero shift by the same amount and, thus, below-surface cutting. Because only three good parts had been made (with compensation for wear in No. 2 and 3), it was concluded that a reduced cutting angle was necessary to provide more tool life. Accordingly, the previous 15 degree tool (No. 3) was lapped with 0 to 2-micron diamond to produce 0.010- to 0.020-inch-wide, side-cutting lands at 10 degrees. Observation of above parts being cut at 40X revealed negligible edge pushover, and it was concluded that shallow cuts and unnecessary rubbing attendant with free passes was contributing to tool wear. Accordingly, part No. 6 was made in only three passes at depths of 0.003, 0.0044 and 0.0049 inch. The last pass depth of 0.0049 inch was 0.0002 inch less than that required to produce sharp crests at 0.0060-inch pitch.

FINAL SEAT FABRICATION

With solution of tool life and seat land crest lapping problems, 25 seat parts were fabricated from full hard (R_F 90) copper bar stock. A five-tool box turret on a Hardinge tool room lathe was used to fabricate a part without removal from the lathe (Fig. I-2). The turning procedure

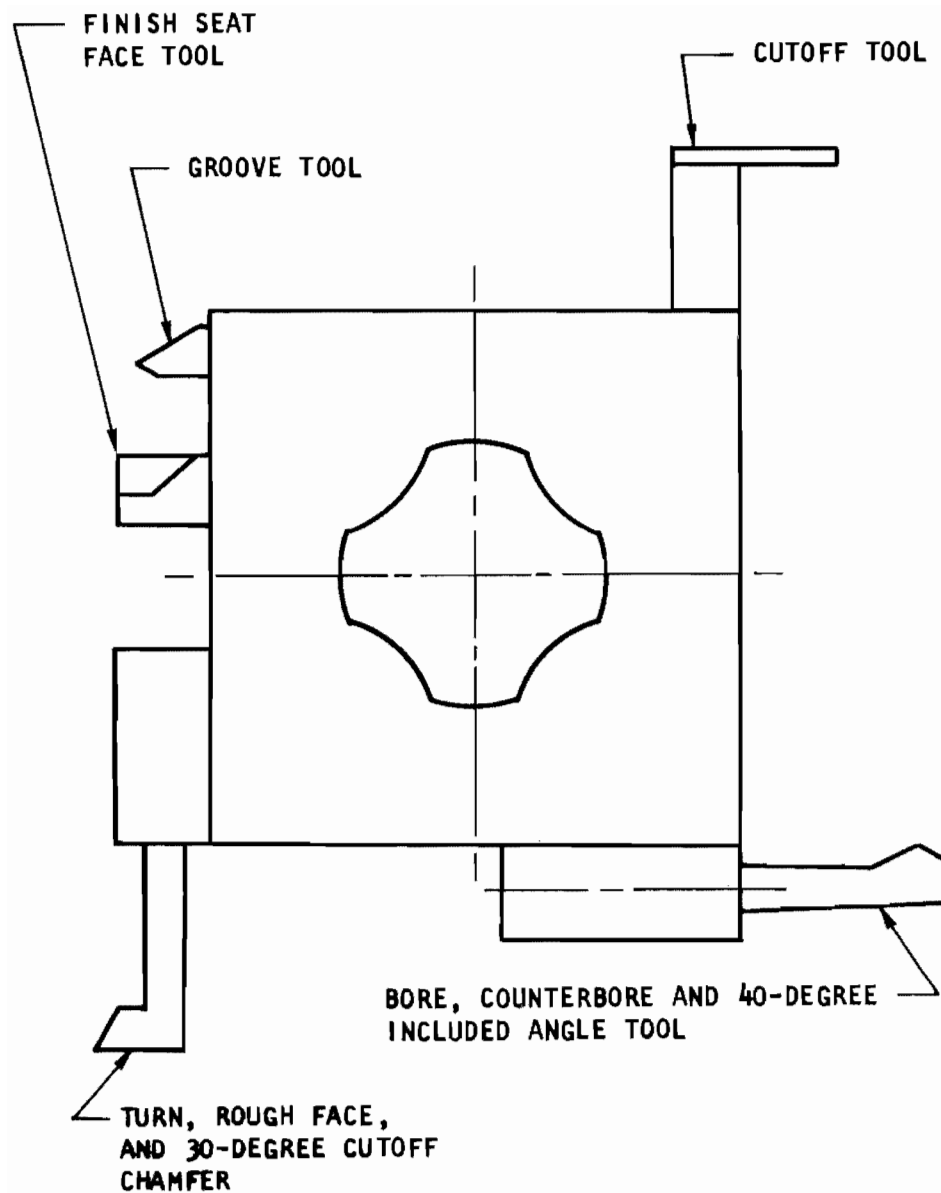


Figure I-2. Top View of Box Turret Tooling

required about 2 hours per part. This procedure and specialized optical inspection techniques are defined in the following paragraphs.

Turning Procedure

Each part was turned from the following instructions:

1. Extend 5/8-inch OD copper bar from collet 7/8 inch.
2. Counterdrill and drill 0.348-inch hole 1-1/2-inch deep at 800 rpm.
3. Rough face at 1100 rpm, leaving 0.00300 to finish turn face.
4. Rough-cutoff at 650 rpm to within 0.05 inch of bore and 0.0030 inch of length.
5. Turn OD 0.005 inch oversize at 1100 rpm.
6. Bore hole 0.005 inch undersize at 1100 rpm.
7. Conterbore to size in three passes with 0.01 inch last pass at 370 rpm; plunge 40-degree included angle.
8. Finish-bore through hole at 1100 rpm.
9. Finish-turn OD and 30-degree chamfer at 1100 rpm.
10. Finish-turn seat face at 1100 rpm, removing 0.00300 inch with extra slow cross feed.
11. Groove seat face per detail (Fig. VI-5).
12. Use soft balsa wood and 0- to 1/4-micron diamond to deburr face at 650 rpm for approximately 6 seconds.
13. Finish cutoff at 650 rpm.
14. Place part in cylindrical container with cotton.

Inspection and Final Lapping

Due to the grooved seat's extremely delicate surface profile, it was necessary to perform all flatness and parallelism inspection using white light interference with the interference microscope at 100X and 200X. With plain flat surfaces, this proved to be a simple procedure; but, with the very narrow grooved lands, several difficulties had to be resolved. A subtle error was uncovered when it was noted that the central black interference band had a gradation of color across the field of vision varying from purple to black to purple. This gradation also varied with band orientation, i.e., vertical, horizontal, etc. With bands in the usual horizontal position, a slight amount of black was visible on colored bands above and below, and to the left and right of the central black band. With continuous surfaces, this never created a problem; however, with the grooved surface, assessment of land OD duboff proved difficult to follow. The problem was corrected by squaring the micrometer stage base with internal optics using shims. All bands then had the same color across the field regardless of orientation.

As noted in model test, the sealing lands did not remain perfectly flat following the forming operation at 15,000-psi apparent stress. When combined with an out-of-parallel condition, assessment of the band deviations appeared formidable. To form a basis for measurement, a flat, but out-of-parallel, seat holder (Fig. VI-4) was used to indicate measurement precision. This part had a 1-1/2-inch OD and 3/4-inch thickness, and opposing surfaces flat within 1 microinch around a 1-inch diameter, but was out of parallel 47 microinches at the same diameter. Using an optical flat as a bearing datum base, the seat holder was rotated on this base against a V block under the interference microscope at 100X to measure changes in absolute height. This was accomplished in 45-degree increments at the 1-inch diameter. Light-band spacing was established as two reticle divisions (0.008 inch) per band with each (green light) band representing 10.6 microinches height change. Reading error and repeatability was estimated as ± 0.2 division per reading or about ± 2 microinches for the total differential. This error was primarily from overall height shifts caused by dust and other contaminants between the seat holder and optical flat base.

Runout of a flat, out-of-parallel datum surface will generate a sine wave on a linear trace; thus, comparison of the recorded data against this mathematical curve having the same peak-to-valley height (h), is an indication of measurement precision. These data are shown in the following tabulation. Each point was repeated several times from various locations and the data averaged.

Location Corrected to High Point (θ), degrees (± 2)	Measured Deviation From High Point, microinches	Datum Surface Differential,* microinches	Error,** microinches
0	0.0	0.0	0.0
20	0.5	1.4	0.7
65	12.7	13.5	0.8
110	31.8	31.3	-0.5
155	46.1	44.4	-1.7
180	46.6	46.6 = h	0.0
200	46.1	45.2	-0.9
245	33.4	33.2	-0.2
290	15.9	15.3	-0.6
335	2.1	2.2	0.1

$$*\Delta = \frac{h}{2} (1 - \cos \theta)$$

**The indicated error of +0.8 to -1.7 microinches is within reading resolution, repeatability, and overall flatness.

Finish seat lapping was performed as previously described to a final condition. Flatness across the outer land diameter was within several microinches. The seat base was then lapped to bring this surface into a parallel condition with the finished seat face.* Preliminary optical parallelism

*This proved troublesome because cutoff formed a convex surface. This could have been avoided by finish facing the seat base concave and parallel within 0.00005 inch with a sixth lathe tool. Upon cutoff, the part would be reversed and the center core chamfered to remove the ridge. The face would thus be flat, and only minor burr removal would be necessary.

measurements were made directly on the seat tube. Final parallelism measurements were obtained with the seat locked in the holder with a 5/16 bolt and nut. This assembly was then wrung to a blank spherical poppet retainer (Fig. III-4, -6 part lapped parallel within 10 microinches), which was used as a base fixture for rotation or sliding on the optical flat.

REFERENCES

1. Fruedenthal, A. M.: The Inelastic Behavior of Engineering Materials and Structures, John Wiley and Sons, New York, N.Y., 1950.
2. Roark, R. J.: Formulas for Stress and Strain, fourth edition, McGraw-Hill Book Co., New York, N.Y., 1965.
3. Tellier, G. F.: Poppet and Seat Design Data for Aerospace Valves, AFRPL-TR-66-147, Rocketdyne, a division of North American Rockwell Corporation, Canoga Park, California, July 1966.
4. Tellier, G. F., et al.: Survey of Contamination in Rocket Propulsion Fluid Systems, AFRPL-TR-67-290, Rocketdyne, a division of North American Rockwell Corporation, Canoga Park, California, November 1967.
5. Beard, K. L., et al.: Liquid-Fluorine Shutoff Valve Development, AFRPL-TR-68-3, The J. C. Carter Co., Costa Mesa, California, January 1968.
6. Dixon, W. J., Massey, F. J.: Introduction to Statistical Analysis, McGraw-Hill Book Co., New York, N.Y., 1957.
7. Robertson, W. H.: Tables of the Binomial Distribution Function for Small Values of P, SCR-143, TID-4500, Sandia Corp., January 1960.
8. Seely, F. B., Smith, J.O.: Advanced Mechanics of Materials, second edition, John Wiley and Sons, Inc., New York, N.Y., 1952.
9. Ling, F. F.: "Some Factors Influencing the Area-Load Characteristics for Semi-Smooth Contiguous Surfaces Under Static Loading." Transactions of the ASME, July 1958.
10. Metals Properties, ASME Handbook, McGraw-Hill Book Co., New York, N.Y., first edition, 1954.
11. RPL-TDR-64-68, Rocket Engine Valve Poppet and Seat Design Data, Rocketdyne, a division of North American Rockwell Corporation, Canoga Park, California, May 1964.
12. Howell, G. W., Weathers, T. M.: Aerospace Fluid Component Designers Handbook, RPL-TDR-64-25 (Vol. II) TRW Systems Group, TRW Inc., Redondo Beach, California, Revision C, November 1968.

DISTRIBUTION LIST

AFRPL (RPRPD) ATTN: Jack Hartley Edwards, CA 93523	1	Air Force Avionics Laboratory AFAL Wright-Patterson AFB OH 45433 AFAL WPAFB OHIO	1
AFRPL ATTN: Technical Library Edwards, CA 93523	1	Air Force Flight Dynamics Laboratory AFFDL Wright-Patterson AFB OH 45433	1
Air Force Rocket Propulsion Lab ATTN: RPG Edwards CA 93523	1	Commander Air Flight Dynamics Laboratory Flight Control Division	1
AFRPL (RPM) Edwards, California 93523	1	Attn: V. R. Schmitt FDCL, Wright-Patterson Air Force Base Dayton, Ohio 45433	
AFRPL (RPC) Edwards, California 93523	1	Air Force Aero-Propulsion Laboratory AFAPL	1
AFRPL (RPCCA) Attn: Lt. James C. Chigleri Edwards, California 93523	1	Wright-Patterson AFB OH45433 AFAPL WPAFB OHIO	
AFFTC (PSD) Attn: Technical Library Edwards AFB, California 93523	1	AFML ATTN: MAAE Wright-Patterson AFB OH 45433	1
Air Force Systems Command Director of Laboratories Attn: SCTSP Andrews AFB, Wash. DC 20331	1	AF Office of Scientific Research ATTN: SREP 1400 Wilson Blvd. Arlington VA 22209	1
Hq. AFSC (SCTR) Andrews Air Force Base Washington, D.C. 20331	1	SAMSO ATTN: Lt. Cambell (SSUJE) AF Unit Post Office Los Angeles CA 90045	1
RTD (RTNP) Bolling AFB Washington, D.C. 20332	1	SMAMA (SMMQQLA) Attn: Robert Martin McClellan AFB, Sacramento, CA 95652	1
Air Force Office of Scientific Research Attn: SREP, Dr. J.F. Masi Washington, D.C. 20333	1	Rome Air Development Center RADC Griffiss AFB NY 13440 RADC GRIFFISS AFB NY	1
Foreign Technology Division ATTN: TDBTL Wright-Patterson AFB OH 45433	1	Arnold Engineering Development Center AEDC Arnold AFSTN 37389 AEDC ARNOLD AFS TENN	1

AIR FORCE ARMAMENT LABORATORY AFATL Eglin AFB FL32542 AFATL EGLIN AFB FLA	1	Bureau of Naval Weapons Department of the Navy Attn: RRRE-6 Washington, D.C. 20360	1
United States Air Force Epidemiological Lab USAFEL Lackland AFB TX78236 USAFEL LACKLAND AFB TEX	1	Bureau of Naval Weapons Department of the Navy Attn: DLI-3 Washington, D.C. 20360	1
Office of Research Analysis (OAR) ATTN: RRRT Holloman AFB NM 98330	1	Naval Ordnance Sys Comd ATTN: ORD-9132 Tech. Library WASH DC 20360	1
Air Force Weapons Laboratory AFWL Kirkland AFB NM 87117	1	Commanding Officer Office of Naval Research 1030 E. Green Street Pasadena, CA 91101	1
Defense Documentation Center ATTN: TSR Cameron Station, Bldg 5 Alexandria VA 22314	20	Commander US Naval Missile Center Attn: Technical Library Point Mugu CA 93041	1
National Bureau of Standards ATTN: Library Boulder CO80302	1	Naval Missile Center ATTN: Code 5632.2, TECH LIBRARY Point Mugu CA 93041	1
Defense Research and Engineering Pentagon 3D1065 Attn: Propulsion Technology Washington DC 20301	1	Naval Weapons Center ATTN: Code 753-Tech Library China Lake CA 93555	1
Central Intelligence Agency ATTN: DRS/ ADD-Standard Dist. Washington DC 20505	1	Commander (Code 753) Naval Weapons Center Attn: Technical Library China Lake, CA 93557	1
Department of the Navy Office of Naval Research Attn: Code 429 Washington, DC 20360	1	Commanding Officer U S Naval Propellant Plant ATTN: Technical Library Indian Head MD 20640	1
Naval Air Systems Comd. ATTN: AIR-6042, Tech. Library Washington DC 20360	1	Picatinny Arsenal Scientific & Tech Info Br Attn: SMUPA-VA6, Librarian Dover NJ 07801	1
Bureau of Naval Weapons Department of the Navy Attn: RMMP-2 Washington, D.C. 20360	1	Commanding Officer U S Naval Underwater Ordnance Stn Attn: W. W. Bartlett Newport RI 02844	1

Army Missile Command
Redstone Scientific Info Center
ATTN: Chief, Document Section
Redstone Arsenal AL 35809

White Sands Missile Range
ATTN: Technical Library
White Sands MR NM 88002

ArmyResearch Office
ATTN: CRD-AA-IP
Box DM, Duke Station
Durham NC 27706

Commanding Officer
Frankford Arsenal
Attn: Propellant and Explosives
Section, 1331
Philadelphia PA 19137

NASA
ATTN: Code RPS, R.W. Ziem
Washington DC 20546

NASA
Kennedy Space Center
ATTN: Library-ATS-132C
Kennedy Space Center FL 32899

NASA
John F. Kennedy Space Center
ATTN: R.E. Corman
Dir for Support Operations
C. Hoppesch
Quality Control
Kennedy Space Center FL 32899

NASA Scientific & Tech Info
Facility
ATTN: SAF/DL, ACQ Division
P.O. Box 33
College Park MD 20740

NASA
Goddard Space Flight Center
ATTN: Library, Code 252
Greenbelt MD 20771

1 Natl Aeronautics & Space Administration 1
Attn: B R Gantz
Propulsion Engineering Office
Code R.G.
Drawer M
1 White Sands Test Facility
Los Cruces NM 88001

NASA 3
1 Lewis Research Center
ATTN: Librarian
L. Gordon
R. Grey
21000 Brookpark Road
1 Cleveland OH 44135

NASA 2
Manned Spacecraft Center
ATTN: Library/Code BM6
J. Capps
1 Houston TX 77058

NASA 1
1 Langley Research Center
Attn: Librarian
Langley Station
Hampton VA 23565

Aerojet-General Corp 1
2 Attn: Tech Library
P.O. Box 296
Azusa CA 91702

Aerojet-General Corporation 1
Attn: T. R. Wallace
Supervisor Engrg.
Azusa CA 91702

1 Aerojet-General Corporation 1
Attn: Library
11711 South Woodruff Avenue
Downey CA 90241

1 Aerojet-General Corp 1
Attn: Tech Info Center
Group 8678, Bldg 2015A
P.O. Box 15847
Sacramento CA 95813

Aerojet-General Corp Attn: H. Goldthorpe P.O. Box 1947 Sacramento CA 95813	1	The Boeing Company Aerospace Division Attn: Ruth E. Peerenboom, Library Process Sup (1190) P.O. Box 3707 Seattle WA 98124	1
Aerojet-General Corp Attn: J.M. Norris, Mgr. Quality Control P.O. Box 15847 Sacramento CA 95813	1	The Boeing Company Wichita Division Attn: Dr. Roger Tucker 3801 South Oliver Wichita KS 67210	1
Bell Aerosystems Company ATTN: Dr. W. Connor P.O. Box 1 Buffalo NY 13240	1	The Boeing Company Attn: W.V. Newman (M/S R S27) P.O. Box 1079 Wash DC 20013	1
Bell Aerosystems Company Attn: H.A. Ferullo Chief Engr., Rockets Buffalo NY 13240	1	Chrysler Corporation Space Division Attn: N E Hildebrandt Propulsion & Vehicle Engrg. Materials Group P.O. Box 29200 New Orleans LA 70129	1
Bell Aerosystems Co. ATTN: Technical Library P.O. Box 1 Buffalo NY 13240	1	Curtiss-Wright Corp ATTN: W W Frank Caldwell NJ 07006	1
The Bendix Corporation Bendix-Pacific Division Attn: Boublas M. Longyear, Jr. Chief Engineer North Hollywood CA 91600	1	Philco-Ford Corporation Aeronutronic Division Attn: H L Podell Newport Beach CA 92663	1
Bendix Corporation Bendix Filter Division Attn: F. W. Cole Chief Project Engineer 434 W. Twelve Mile Rd P.O. Box 135 Madison Heights MI 48071	1	Philco-Ford Corporation Aeronutronic Division Attn: Tech Info Svcs-Acquisitions Ford Road Newport Beach CA 92663	1
The Boeing Co Space Division, Aerospace Group Attn: P.J. Helberg, Director Space Research and Development P.O. Box 3868 Seattle, Washington 98124	1	General Dynamics Corporation Attn: Library P O Box 2507 Pomona CA 91766	1
The Boeing Company Attn: Aerospace Library-8K-38 P O Box 3999 Seattle WA 98124	1	General Dynamics/Fort Worth Attn: Library P O Box 747 Fort Worth TX 76101	1

General Dynamics/Convair Attn: Mr. L. M. Nelson Dept 984-20 P. O. Box 1129 San Diego CA 92112	1	Grumman Aircraft Engineering Corp Attn: H S Marx I M Program Contamination Control Manager Bethpage L I NY 11100	1
General Dynamics/Convair Attn: M. C. Miyaji P.O. Box 1128 San Diego CA 92112	1	Grumman Aircraft Engineering Corp ATTN: Library Bethpage, Long Island NY 11714	1
General Dynamics/Convair Attn: G. L. Hansen, Vice Pres. & Program Director Dept 950-0 Atlas & Centaur P.O. Box 1128 San Diego CA 92112	1	Hughes Aircraft Company Aerospace Group Space Systems Division Attn: H Di Cristina Senior Staff Engr. Propulsion Dept P O Box 90919, Airport Station Los Angeles CA 90009	1
General Dynamics, Convair Division Lindbergh Field Plant Attn: R. J. Okonski Mail Zone 597-00 P.O. Box 1950 San Diego CA 92112	1	Hughes Aircraft Company Attn: Library Aerospace Group Space Systems Division Culver City CA 90230	1
General Dynamics/Convair Library & Info Services P.O. Box 12009 San Diego CA 92112	1	Lockheed Missiles & Space Co Attn: Tech Info Ctr. 50-14 3251 Hanover St Palo Alto CA 94304	1
General Dynamics/Convair Attn: W. Roberts P.O. Box 12009 San Diego CA 92112	2	Lockheed Propulsion Co Attn: Library P O Box 111 Redlands 92373	1
General Electric Company Attn: J A Bain General Engineering Laboratory Schenectady NY 12300	1	Lockheed Missiles & Space Co Attn: I. Altman P O Box 504 Sunnyvale CA 94088	1
General Electric Company Apollo Support Department Attn: C. Day P O Box 2500 Daytona Beach FL 32015	1	Lockheed Missiles & Space Co Attn: J. Guill 1111 Lockheed Way Sunnyvale CA 93087	1
General Electric Company Attn: Acquisitions Bldg 4, Rm 109 Daytona Beach FL 32015	1	Lockheed Missiles & Space Co Propulsion Engineering Division D55-11 1111 Lockheed Way Sunnyvale CA 93087	1

Lockheed Missiles & Space Co Attn: R G Gavlak Resident Manager Vandenberg AFB Space Systems Vandenberg AFB CA 93437	1	McDonnell Douglas Astronautics Co Western Division Attn: Library A2-260 3000 Ocean Park Blvd Santa Monica CA 90405	1
LTV Astronautics Division Attn: Library P O Box 6267 Dallas TX 75222	1	McDonnell-Douglas Astronautics Company - Western Division 3000 Ocean Park Blvd. Santa Monica CA 90405 Attn: P W Van Horn H D Samuel D R Walker J W Orr	4
The Marquardt Corporation Attn: H. Wichmann, Mgr Components Engrg Rocket Systems Division 16555 Saticoy Street Van Nuys CA 91409	1	McDonnell Aircraft Corporation Attn: Library P O Box 516 St. Louis MO 63166	1
Marquardt Corporation Attn: Library P O Box 2014, South Annex Van Nuys CA 91409	1	Minneapolis-Honeywell Regulator Co Aeronautical Division Attn: Mario Cardullo, Engrg. 2600 Ridgeway Rd. Minneapolis MN 55424	1
Martin Company Attn: D. Murphy Denver Division Denver CO 80201	1	Minneapolis-Honeywell Regulator Co Valve Division 300 Gommers Drive Fort Washington PA	1
Martin Company Denver Division Attn: M. Piccone P O Box 179 Denver CO 80201	1	Minnesota Mining & Mfg Co Attn: Code 0013 R & D Via: H C Zeman, Security Administrator 900 Bust Avenue St. Paul MN 55106	1
McDonnell-Douglas Corp Missile and Space Systems Division Development Engineering Attn: J. W. Thomas, Director Design Technology 2560 Walnut Ave Culver City, California	1	North American Rockwell Rocketdyne Division Attn: Library Dept 086-306 6633 Canoga Avenue Canoga Park CA 91304	1
McDonnell-Douglas Corp Missile & Space Systems Division Astropower Laboratory Attn: W D English 2121 Campus Drive Newport Beach CA 92663	1	North American Rockwell Space & Information Systems Division Attn: Tech Info Ctr 096-722 12214 Lakewood Blvd Downey CA 90241	1

Northrop Carolina, Incorporated Attn: Library P O Box 3049 Asheville NC 28802	1	NASA Marshall Space Flight Center Attn: H G Paul, Chief Propulsion Division Propulsion & Vehicle Engrg. Lab. Huntsville, Alabama 35812	1
Olin Mathieson Chemical Corp Main Control Room Attn: Asst. Librarian 275 Winchester Ave New Haven CT 06511	1	Thiokol Chemical Corporation Elkton Division Attn: Tech Info Center Elkton MD 21921	1
Olin Mathieson Chemical Corp Attn: Research Library P O Drawer G Marion IL 62959	1	Thiokol Chemical Corporation Wasatch Division Attn: Technical Library Brigham City UT 84302	1
Rocket Research Corporation 520 South Portland Street Seattle WA 98108	1	TRW Systems, Inc. Attn: T. Weathers One Space Park Redondo Beach CA 90277	1
Rocket Research Corporation Attn: Technical Library York Center Willow Road at N E 116th St. Redmond WA 98052	1	Thompson Ramo Wooldridge, Inc. Thompson Products Valve Division Attn: J M Cherrie, Mgr Product Engrg. 1455 East 185th Street Cleveland OH 44110	1
Rohm and Haas Company Redstone Arsenal Research Div Attn: Tech. Librarian Huntsville AL 35807	1	United Aircraft Corporation Division of United Aircraft Corporation Attn: L. J. Weber Windsor Locks, Conn 06906	1
Thiokol Chemical Corporation Huntsville Division Attn: Technical Library Huntsville AL 35807	1	United Aircraft Corporation Pratt & Whitney Aircraft Division Florida Research and Development Center Attn: E. F. Esmeier Fuel Control Project Engr. P O Box 2691 West Palm Beach FL 33402	1
Thiokol Chemical Corporation Alpha Division, Huntsville Plant Attn: Technical Director Huntsville, AL 35807	1	United Aircraft Corporation Pratt & Whitney Aircraft Division Attn: Head Librarian P O Box 2691 West Palm Beach FL 33402	1
AFML (MAAE) Wright-Patterson AFB OH 45433	1	United Aircraft Corporation Pratt & Whitney Aircraft Division Attn: Head Librarian P O Box 2691 West Palm Beach FL 33402	1
NASA Attn: Office of Technical Information & Educational Programs, Code ELT Washington DC 20546	1	United Aircraft Corporation United Technology Center Attn: Tech. Librarian P O Box 358 Sunnyvale CA 94088	1

Adel Products Division General Metals Attn: B R Teree Chief Engineer 10777 Vanowen Street Burbank CA 91502	1	Benbow Mfg. Corp. Attn: Frank Aikins, Chief Engr. 11920 Jefferson Blvd. Culver City CA	1
Aeroprojects, Inc. Attn: C D McKinney 310 East Rosedale Avenue West Chester PA 19380	1	Calmec Mfg. Corporation 5825 District Boulevard Los Angeles CA 90022	1
Aeroquip Corporation Attn: E. Robert Steinert Ch. Aircraft Devel. Engr. Jackson MI 49200	1	J C Carter Co. 671 W 17th Street Costa Mesa CA 92627	1
Aircraft Porous Media, Inc. Sub. Pall Corp Attn: J. Farris 30 Sea Cliff Avenue Glen Cove, New York 11542	1	Cermarc Corporation Attn: J. Buckingham John Winzen 343 Glasgow Avenue Inglewood CA 90301	2
AiResearch Manufacturing Co. of Arizona Attn: A. D. Stromme M/S3570 402 South 36th Street Phoenix AR 85034	1	Clary Dynamics Attn: George F. Eas, Chief Engr. 408 Junipero Street San Gabriel CA 91776	1
Garrett Corporation AiResearch Mfg. Div. Attn: Tech. Library 9851 Sepulveda Blvd Los Angeles CA 90009	1	Conoflow Corporation Attn: A J Hanseen Chief Engineer 2100 Arch Street Philadelphia PA 19103	1
The Annin Company Attn: R. D. Randall Chief Engineer P O Box 22081 Los Angeles CA 90022		Consolidated Controls Corp Attn: James A McBride Chief Engineer 750 S. Isis Avenue Inglewood CA 90304	1
Applied Power Industries, Inc. Fluid Power Group Attn: G. R. Koeppel Pewaukee WI 53072	1	Cryogenic Engineering Company Attn: M. M. Reynolds Vice President, Sales 200 West 48th Avenue Denver CO 80216	1
Atlantic Research Corporation Attn: Security Office for Library Shirley Highway and Edsall Road Alexandria VA 22314	1	Eckel Valve Company Attn: H. Sutter 1425 First Street San Fernando CA 91340	1
		Engineering Physics Company 12721 Twinbrook Parkway Rockville MD 20852	1

Fairchild-Hiller, Stratos Division Attn: Library 1800 Rosecrans Avenue Manhattan Beach CA 90277	1	Walter Kidde Company Attn: Technical Info. Office 675 Main Street Belleville NJ 08102	1
Fox Valve Development Co., Inc. Attn: Mr. Zola Fox #2 Great Meadow Lane Hackensack NJ 07601	1	Arthur D. Little, Inc. Attn: Tech. Library 20 Acron Park Cambridge MA 02140	1
Frebank Company Attn: Director of Engrg. 711 West Broadway Glendale CA 91204	1	Hydraulic Research Attn: R. T. Banfield 2835 No. Naomi St. Burbank CA	1
Futurecraft Corporation Attn: Murry Chilcoat Chief Engineer 15430 Proctor Avenue Industry CA	1	Paul L. Magill 600 S. Spring Los Altos CA 94022	1
Giannini Controls Corporation Attn: Library 1600 S. Mountain Ave. Duarte CA 91010	1	Marotta Valve Corp Attn: Jon Janozur 2215 Standard Ave. Santa Ana CA 92707	1
Hannifin Pneumatic Division Attn: Z. J. Lansky, Mgr. 500 S. Wolf Road Des Plaines IL 60018	1	Micro Surface Engr. Co. 1560 East Slauson Ave Los Angeles CA 90011	1
Homestead Valve Manufacturing Co. Jenny Division Attn: D. M. Simmons, Jr. Chief Engineer Corapolis PA 15108	1	Moog Servoncontrols, Inc. Attn: W. Thayer Proner Airport East Aurora NY 14052	1
Hydro-Aire Division of Crane Co. 3000 Winona Avenue Burbank CA 91504	1	National Waterlift Co. Attn: Library 2220 Palmer Ave. Kalamazoo MI	1
Jamesbury Corporation 640 Lincoln Street Worcester MA 01605	1	National Water Lift Co. Attn: D. Bauer 1301 E. El Segundo Blvd. El Segundo CA 90245	1
James, Pond and Clark 2128 East Foothill Blvd. Pasadena CA 91107	1	Parker Aircraft Co. Attn: E. W. Cassaday K. Bragg 5827 West Century Blvd. Los Angeles CA 90045	2

Parker-Hannifin Corp. Attn: J. Mohler 17325 Euclid Ave. Cleveland OH 44112	1	Weston Hydraulics Limited 7500 Tyrone Avenue Van Nuys CA 91405	1
Pyronetics Attn: Mr. Bartrum 11973 Slauson Santa Fe Springs CA 90670	1	West Coast Hydraulics Co., Inc. Attn: W. J. Makusay, Pres. 7222 Hinds Ave. North Hollywood CA 91605	1
Randall Engineering Corp Attn: R. Oberbeck 5933 Bowcroft St. Los Angeles CA 90016	1	Whittaker Controls Division Attn: Vern Smith Telecomputing Corp. 915 North Citrus Ave. Los Angeles CA 90038	1
Robertshaw Controls Company Attn: J. F. Tobias Santa Ana Freeway at Euclid Ave. Anaheim CA 92704	1	Whittaker Corp - Controls Division Attn: Library 13035 Saticoy St. North Hollywood CA 91605	1
Royal Industries Attn: W. R. Brown 20401 E. Dyer Santa Ana CA 92700	1	Aerospace Corporation Attn: Tech. Info Ctr. Doc. Group P O Box 95085 Los Angeles CA 90045	1
Sterer Engrg. & Mfg. Co. 4690 Colorado Blvd. Los Angeles CA 90039	1	Aerospace Corp. Attn: Library P O Box 1308 San Bernardino CA 92402	1
Sage Engineering & Valve Co. Attn: Mike Crim P O Box 19217 Houston TX 77024	1	Arnold Eng. Development Cen. Attn: AEOIM Air Force Systems Command Tullahoma TN 37389	1
Valcor Engineering Co. Attn: A. L. LaMastra 365 Carnegie Avenue Kenilworth NJ 07033	1	ARO, INC. Arnold Engrg. Dev. Cen. Attn: Dr. B. H. Boethert Chief Scientist	1
Wallace O. Leonard, Inc. 373 Fair Oaks Ave. Pasadena CA 91103	1	Arnold AF Station TN 37389	
The Weatherhead Company Attn: Richard C. Acker, Development Engr. 300 E. 31st. Street Cleveland OH 44108	1	ARO, Inc. Attn: Tech. Documents Library Arnold AF Station TN 37389	1
		AEDC (ARO, Inc.) Attn: J. R. McCabe Chem. Laboratory Chem. & Metallurgical Br. Engr. Support Facility ESF-CM Arnold Air Force Station Tullahoma TN 37389	1

Battelle Memorial Institute Attn: Report Library, Rm 6A 505 King Avenue Columbus OH 43201	1	American Cyanamid Co. 1937 W. Main St. Stamford CT 06902	1
Battelle Memorial Institute Attn: T. M. Trainer 505 King Ave. Columbus OH 43201	1	Allied Chem. Corp. Industrial Chemicals Div. Attn: J A Smith, Tech. Serv. P O Box 405 Morristown NJ 07960	1
Chemical Propulsion Info. Agcy. Applied Physics Lab - JHU 8621 Georgia Ave. Silver Spring MD 20910	1	Gallery Chemical Co. Attn: Document Control Research & Development Gallery PA 16024	1
ITT Jennings Division Attn: Mr. Don Nolte Mfg. & Process Engrg. 970 McLaughlin Ave. San Jose CA 95116	1	Dow Chemical Co. Scientific Projects Lab. Attn: Dr. R. S. Karpuik Bldg. 1710 Midland MI 48641	1
ITT Research Institute Technology Center Attn: C. K. Hersh, Chemistry Div. Chicago IL 60616	1	DuPont Company Eastern Division Attn: Report Clerk, A. R. Steward Gibbstown NJ 08027	1
ITT Research Institute Attn: Dr. A. Lieberman Document Library 10 West 35th St. Chicago IL 60616	2	Esso Research & Engineering Co. Process Research Division Attn: Dr. J. R. Lovett Linden NJ 07036	1
Institute for Defense Analyses Attn: Classified Library 400 Army-Navy Drive Arlington VA 22202	1	Ethyl Corporation P O Box 3091 Baton Rouge LA 70805	1
Jet Propulsion Laboratory Propulsion Division Attn: R. Weiner L. R. Toth 4800 Oak Grove Drive Pasadena CA 91103	1	Hercules Inc. Attn: C. Sausaman Asst. Tech. Super. P O Box 116 Hercules CA 94547	1
California Inst. of Technology Jet Propulsion Lab. Attn: Library, TDS 4800 Oak Grove Dr. Pasadena CA 91103	1	Hercules, Inc. Research Center Attn: Tech. Info. Cen. Wilmington DE 19899	1
Stanford Research Institute Document Center for Propulsion Sciences 333 Ravenswood Ave. Menlo Park CA 94025	1	Hercules, Inc. Allegany Ballistics Laboratory Attn: Tech. Library P.O. Box 210 Cumberland MD 21502	1

Hynes Chemical Research Corp. 308 Bon Air Avenue Durham NC 27704	1
Pennsalt Chemicals Corp. Technological Center Attn: Security Officer 900 First Avenue King of Prussia PA 19406	1
Shell Oil Co. Shell Development Co. Div. Attn: Technical Files 1400 53rd Street Emeryville CA 94608	1
University of Denver Denver Research Institute Attn: Security Officer P O Box 10127 Denver CO 80210	1
Oklahoma State University School of Mechanical Engr. Attn: Dr. E. C. Fitch Stillwater OK	1
Purdue University Attn: M. J. Zucrow B. A. Reese Lafayette IN 47907	2
University of Utah, College of Engr. Attn: Prof. M. L. Williams 1400 E. Second South Salt Lake City UT 84112	1

UNCLASSIFIED

Security Classification

DOCUMENT CONTROL DATA - R & D

(Security classification of title, body of abstract and indexing annotation must be entered when the overall report is classified)

1. ORIGINATING ACTIVITY (Corporate author) Rocketdyne, a Division of North American Rockwell Corporation, 6633 Canoga Avenue, Canoga Park, California 91304		2a. REPORT SECURITY CLASSIFICATION UNCLASSIFIED	
		2b. GROUP	
3. REPORT TITLE Poppet and Seat Design Criteria for Contaminant-Particle Resistance			
4. DESCRIPTIVE NOTES (Type of report and inclusive dates) Final Report (April 1967-January 1970)			
5. AUTHOR(S) (First name, middle initial, last name) Rocketdyne Engineering			
6. REPORT DATE April 1970	7a. TOTAL NO. OF PAGES 390	7b. NO. OF REFS 12	
8a. CONTRACT OR GRANT NO. F04611-67-C-0085	9a. ORIGINATOR'S REPORT NUMBER(S) R-8126		
b. PROJECT NO. 3058			
c. Task 305802	9b. OTHER REPORT NO(S) (Any other numbers that may be assigned this report) AFRPL-TR-70-1		
d.			
10. DISTRIBUTION STATEMENT Approved for public release—Distribution unlimited. Auth.: AFRPL letter dated 29 Sep 71. Ref: TAB 72-15.			
11. SUPPLEMENTARY NOTES		12. SPONSORING MILITARY ACTIVITY AFRPL AFSC Edwards, California	
13. ABSTRACT This final report describes analytical and experimental investigations to establish design criteria for reliable metal-to-metal poppet and seat sealing in contaminated fluid environments. Static evaluation of standard flat 440C models (0.470-inch seat diameter, 0.03-inch land) with placed hard (R _c 62-67) and soft (R _c 17-21) spherical metal particles defined envelopment closure loads and stress-leakage change characteristics. The control condition was nominally 0.01-scim nitrogen leakage at 1000 psig and 40-pound seat load. Envelopment loads, defined by leakage increase less than 10 times control, were determined to be nearly proportional to the particle diameter squared. The 30-micron diameter constituted an approximate upper size limit for the 0.03-inch land, with about 46 pounds required to envelope one to three equally spaced particles. Larger particles created a radial channel leak path necessitating substantial load increase to effect closure. Dynamic tests of four closure configurations in a recirculation liquid system containing a precisely controlled concentration of hard spherical metal particles provided correlation of impact frequency predictions based on a binomial analysis of concentration, cycles, and theoretical seat sampling volume. A hard poppet on soft seat combination was capable of sealing with larger particles entrapped. The particle avoidance concept was investigated experimentally and is a potentially fruitful approach to particle resistance. The flat groove copper seat was most capable of sustaining numerous particle impacts with minimal leakage increase at low loading. These results established hitherto unknown fundamental data but, also, emphasized the need for additional effort in gathering parametric data on particle effects parameters (size, hardness, land width) and impact frequency influences for the more promising closure designs.			

DD FORM 1473
1 NOV 65UNCLASSIFIED
Security Classification

14	KEY WORDS	LINK A		LINK B		LINK C	
		ROLE	WT	ROLE	WT	ROLE	WT
	Valve Poppets and Seats Valve Seating Analyses Valve Seat Impact Tests Leakage (gases) Analyses, Measurements, and Tests Surface Texture and Finishing Interference, Optical Surface Inspection Contamination Effects on Sealing Contaminant-Resistant Poppets and Seats Particle Flow in Fluid Systems Particle Entrapment Probability Entrapped Particle and Surface Deformation Particle Size, Distribution, and Calibration						